MOLECULAR AND CELLULAR PHYSIOLOGY OF GAMETES IN DOMESTIC AND WILD ANIMAL MODELS

EDITED BY: Andreina Cesari, Ana Josefa Soler and Silvina Perez-Martinez

PUBLISHED IN: Frontiers in Cell and Developmental Biology

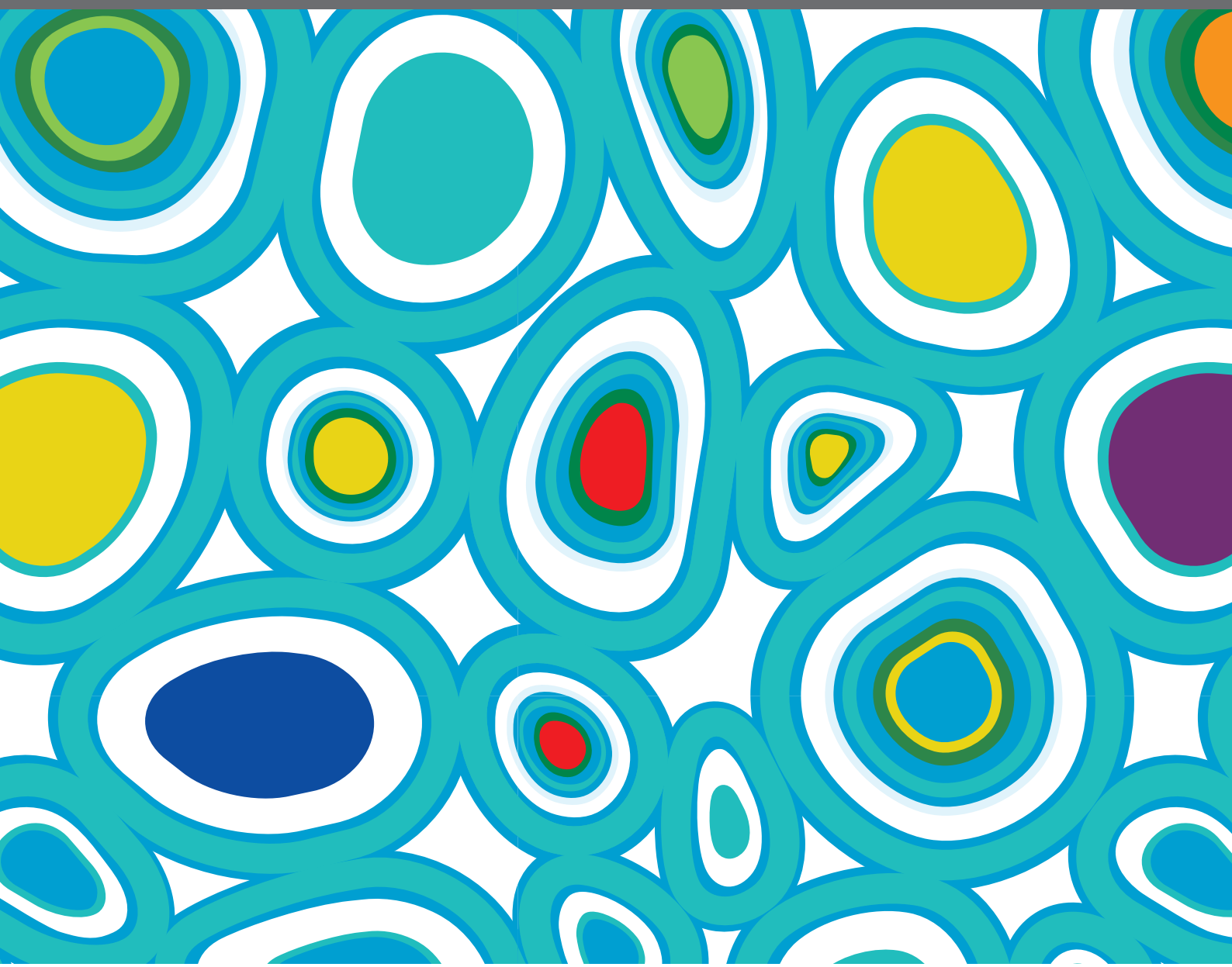

frontiers Research Topics

ISSN 1664-8714
ISBN 978-2-88976-965-0
DOI 10.3389/978-2-88976-965-0

About Frontiers

Frontiers is more than just an open-access publisher of scholarly articles: it is a pioneering approach to the world of academia, radically improving the way scholarly research is managed. The grand vision of Frontiers is a world where all people have an equal opportunity to seek, share and generate knowledge. Frontiers provides immediate and permanent online open access to all its publications, but this alone is not enough to realize our grand goals.

Frontiers Journal Series

The Frontiers Journal Series is a multi-tier and interdisciplinary set of open-access, online journals, promising a paradigm shift from the current review, selection and dissemination processes in academic publishing. All Frontiers journals are driven by researchers for researchers; therefore, they constitute a service to the scholarly community. At the same time, the Frontiers Journal Series operates on a revolutionary invention, the tiered publishing system, initially addressing specific communities of scholars, and gradually climbing up to broader public understanding, thus serving the interests of the lay society, too.

Dedication to Quality

Each Frontiers article is a landmark of the highest quality, thanks to genuinely collaborative interactions between authors and review editors, who include some of the world's best academicians. Research must be certified by peers before entering a stream of knowledge that may eventually reach the public - and shape society; therefore, Frontiers only applies the most rigorous and unbiased reviews.
Frontiers revolutionizes research publishing by freely delivering the most outstanding research, evaluated with no bias from both the academic and social point of view. By applying the most advanced information technologies, Frontiers is catapulting scholarly publishing into a new generation.

What are Frontiers Research Topics?

Frontiers Research Topics are very popular trademarks of the Frontiers Journals Series: they are collections of at least ten articles, all centered on a particular subject. With their unique mix of varied contributions from Original Research to Review Articles, Frontiers Research Topics unify the most influential researchers, the latest key findings and historical advances in a hot research area! Find out more on how to host your own Frontiers Research Topic or contribute to one as an author by contacting the Frontiers Editorial Office: frontiersin.org/about/contact

MOLECULAR AND CELLULAR PHYSIOLOGY OF GAMETES IN DOMESTIC AND WILD ANIMAL MODELS

Topic Editors:
Andreina Cesari, Consejo Nacional de Investigaciones Científicas y Técnicas (CONICET), Argentina
Ana Josefa Soler, University of Castilla-La Mancha, Spain
Silvina Perez-Martinez, CONICET Centro de Estudios Farmacológicos y Botánicos (CEFYBO), Argentina

Citation: Cesari, A., Soler, A. J., Perez-Martinez, S., eds. (2022). Molecular and Cellular Physiology of Gametes in Domestic and Wild Animal Models. Lausanne: Frontiers Media SA. doi: 10.3389/978-2-88976-965-0

Table of Contents

frontiers in Cell and Developmental Biology

EDITORIAL
published: 03 December 2021
doi: 10.3389/fcell.2021.805036

Editorial: Molecular and Cellular Physiology of Gametes in Domestic and Wild Animal Models

Silvina Perez-Martinez[1], *Ana Josefa Soler*[2] *and Andreina Cesari*[3]*

[1]Centro de Estudios Farmacológicos y Botánicos (CEFYBO UBA/CONICET), Buenos Aires, Argentina, [2]IREC (UCLM-CSIC-JCCM), ETSIAM Campus Universitario, Albacete, Spain, [3]Instituto de Investigaciones Biologicas (IIB CONICET/UNMdP), Mar del Plata, Argentina

Keywords: sperm, oocyte, seminal plasma, embryo, development, wild animals, domestic animals

Editorial on the Research Topic

Molecular and Cellular Physiology of Gametes in Domestic and Wild Animal Models

Gamete physiology contributes not only to the zygote formation but also to early embryo development. In mammals, most of the knowledge has been acquired from research on the murine and human models. This topic fills the information gap related to the effect of male and female microenvironments over sperm physiology from different species and offers critical and new insights into the molecular mechanism of gametes' maturation to acquire fertilizing competence in wild and domestic animals.

It includes 16 original research articles divided into three Research Topic: 1) oocyte maturation; 2) sperm fertilizing ability in response to female reproductive environment, and 3) molecular evaluation of seminal plasma related to sperm quality.

1) Oogenesis has been studied in mammalian and non-mammalian organisms, however to date, the mouse has been the most studied model. Knowledge of how conserved or distinctive are both nuclear and epigenetic molecular mechanisms of oocyte maturation and development in farm and wild animals would help to delineate complex molecular mechanisms and identify major genes and proteins involved.

In this direction, nuclear proteins such as chromatin and ribosomal binding proteins have been identified as conserved molecular actors. Here, Chavez et al. identify nuclear BRD2 and NPM1 as novel factors that contribute to oocyte meiotic competence in the domestic cat. By transfecting complex-oocyte-cumulus with specific antibodies against these proteins they showed that BRD2 and NPM11 inhibited *in vitro* fertilization and oocytes were arrested at the germinal vesicle (GV) stage. Other nuclear proteins are known to interact with the kinetochore during the spindle formation controlling chromosome segregation during meiosis. Unlike rodents, mares have prolonged reproductive scenes and it is shown that three spindle related mRNAs are downregulated during aging: Mps1, Spc25 and AurkC (Rizzo et al.). Moreover, after pharmacological inhibition of MPS1 kinase, MII oocytes from aged mares showed a higher incidence of spindle abnormalities while AURKC inhibition severely impaired microtubule organization and spindle formation in all oocytes, irrespective of mare age. On the other hand, non-nuclear proteins have been also found to be implicated in spindle organization during oocyte maturation. In sheep, Han et al. showed that CLTC is localized in the oocytes spindle after GV break-down. Knockdown of the membrane protein CLTC by morpholino injection into GV oocytes disrupted spindle assembly and chromosome alignment, accompanied by impaired first polar body emission and altered early embryo development.

Regarding extracellular factors, the dialog between the oocyte and surrounding granulosa/cumulus cells operates through cytoplasmic projections-gap-junctions and through soluble molecules with specific receptors. Idrees et al. explores a novel role for a SHP2-ERa complex in the nucleus of bovine cumulus cells. The SHP2/ERa complex is highly expressed in the cumulus cells

OPEN ACCESS

Edited and reviewed by:
Philipp Kaldis,
Lund University, Sweden

***Correspondence:**
Andreina Cesari
acesari@mdp.edu.ar

Specialty section:
This article was submitted to Cell Growth and Division, a section of the journal Frontiers in Cell and Developmental Biology

Received: *29 October 2021*
Accepted: *08 November 2021*
Published: *03 December 2021*

Citation:
Perez-Martinez S, Soler AJ and Cesari A (2021) Editorial: Molecular and Cellular Physiology of Gametes in Domestic and Wild Animal Models. Front. Cell Dev. Biol. 9:805036. doi: 10.3389/fcell.2021.805036

of immature oocytes (GV) and reduced in the cumulus cells of mature oocytes (MII). They showed that the formation of a SHP2/ERa complex promotes NPPC and NPR2 transcription (genes related to meiotic arrest) and that meiotic resumption controlled by FSH or growth factors, restricts SHP2-ERa interaction by promoting its extrusion from the nucleus.

In targeted species for the productive sector, successful *in vitro* oocyte maturation is required for *in vitro* embryo production. These biotechnologies produce cellular stress and one of the main mechanisms is associated with the endoplasmic reticulum (ER). Pioltine et al. provide insight into the role of TUDCA (tauroursodeoxycholic acid) in relieving ER stress by decreasing reactive oxygen species (ROS) production in bovine oocytes. This bile acid acts as a potent chemical chaperone and increases the abundance of transcripts related to antioxidant activity in bovine oocytes (CAT, GPX1, and HMOX1) and embryos (GPX1 and PRDX3). In contrast to other mammals, oocytes of dogs and foxes are ovulated at the GV stage and undergo meiotic maturation within the oviduct (Viveiros and De la Fuente, 2019). For this reason, *in vitro* maturation to MII is not successful and most oocytes degenerate. The work by Duque Rodriguez et al. addresses the supplementation of media with BSA and fetal bovine serum in the presence of insulin-transferrin-selenium. Insulin promotes the absorption of nutrients, while transferrin and selenium are antioxidants. They found a condition that increased the proportion of oocytes at the MII stage, with a higher integrity of the cytoplasmic membrane and lower ROS levels.

These last three works underline the *in vivo* and *in vitro* effects of environmental factors on oocyte and embryo quality.

2) Sperm exposure to the female reproductive tract leads them to constantly changing environments, from which they receive different chemical signals (Plant and Zeleznik, 2014). This set of inputs drives a series of signaling events that are essential for sperm capacitation, a process that confers spermatozoa the ability to fertilize an oocyte (Chang, 1951; Austin, 1952). After entering the female tract, spermatozoa find higher bicarbonate and calcium levels, whose influx activates cAMP-PKA pathway and increases tyrosine phosphorylation downstream, thus hyperactivating sperm motility. This ion flow through the sperm plasma membrane triggers lipid reorganization, cholesterol efflux, and consequently, membrane hyperpolarization that increases its fusogenicity. Exposure to the female reproductive tract involves a major challenge to sperm ability to adapt to drastic osmolality variations. In this sense, the results presented from Delgado-Bermudez et al. showed the essential role of aquaporins in osmoregulation in order to maintain sperm motility and lipid architecture during sperm capacitation. They also found that aquaporins might have a relevant role in sperm signaling pathways involved in acrosome reaction in pigs.

On the other hand, ROS are essential for processes like capacitation, hyperactivation, acrosome reaction, and sperm-oocyte fusion, although an excess can be detrimental to these processes. In ovine, reproduction has a marked seasonality controlled by melatonin secretion from the pineal gland. Miguel-Jimenez et al. described how melatonin, also presented in the reproductive fluids, directly affects ram sperm functionality and exerts an antioxidant role, decreasing oxidative stress, by modulating NOX5 activity during capacitation.

About fifty percent of male subfertility diagnosis is idiopathic and is usually associated with genetic abnormalities or protein dysfunction, which are not detectable through the conventional spermiogram. Recent studies have evidenced the essential role of antioxidant enzymes, such as GSTP, in sperm protection against oxidative stress and preservation of sperm function and fertilizing ability. Llavanera et al. found that the dissociation of the GSTP1–JNK heterocomplex results in the activation of JNK and significantly declines sperm viability, motility, mitochondrial activity and plasma membrane stability. This study evaluated the function of this heterocomplex in pig sperm physiology.

Many sperm-specific proteins and their underlying molecular activation mechanisms involved in sperm physiology of most vertebrates still remain unknown. As transcription and translation are highly limited in sperm, proteins are key molecules defining their function, making proteomic approaches one of the most adequate methods to investigate sperm fertilizing ability. In particular, the molecular basis of male fertility in chickens is still unexplored. Here, Carvalho et al. identified 57 proteins related to fertility in meat-type roosters. These proteins were involved in various molecular pathways including flagellum integrity and movement, mitochondrial function, sperm maturation, and storage in the female tract as well as oocyte–sperm interaction. This relevant study about avian reproduction may impact future work on bird fertility and conservation of species.

Spermatozoa are highly differentiated cells that present their chromatin mainly condensed in protamines to protect genetic information from damaging agents, facilitating the delivery of an intact genetic material to the future embryo. This topic includes a study that describes species-specific differences in the decondensation capacity of sperm DNA, and especially in DNA condensation type around protamine 1 and protamine 2 or only protamine 1 (Ribas-Maynous et al.).

Here are also shown results related to the expression and the regulation of circRNAs in sheep testis. Li et al. elucidated for the first time, circRNA dynamic expression patterns across three reproductive stages in postnatal sheep testes, They also described circRNA-associated miRNA-gene network implicated in testicular function such as spermatogenesis, germ cell development, blood-testis barrier and cell cycle/meiosis. These gene tools could be helpful for providing new insights into the molecular mechanism of ovine testis function.

3) The extracellular environment determines gamete physiology. In the case of the male gamete there are two different natural milieus contributing to intracellular changes: the seminal plasma (SP) and the female fluids. SP interchanges molecules with spermatozoa that promote their acquisition of fertilizing ability. In addition, proteins from reproductive fluids interact with the sperm proteome and differ among species. This topic includes two works related to enzymes and metabolites from pig SP. Llavanera et al.used a RMN analysis finding 23 metabolites categorized as: amino acids, saccharides, salts,

alcohols/other organic compounds. To look for potential biomarkers, they search for associations between those molecules and breed, fresh sperm quality/functionality parameters and resilience to liquid storage. They found that only fumarate followed a breed-dependent behavior, while they could associate metabolite patterns from all the categories with specific sperm parameters. Delgado-Bermúdez et al. characterize AKR1B1 from pig SP, a NADPH-dependent enzyme involved in fructose production. They found higher concentrations of AKR1B1 in the post sperm-rich fraction of SP and it was detected in most boar male reproductive tissues. This enzyme was not related to sperm quality/functionality or to the sperm ability to withstand liquid storage.

Little information concerning reproductive features is available in the case of aquatic animals like cetaceans. Furthermore, the importance of studying this animal model is under enormous anthropogenic pressure as a result of commercial overfishing, incidental captures in fisheries and habitat degradation. Indeed, many cetacean species are threatened or in danger of extinction. The work developed by Fuentes-Albero et al. is the first characterization of the proteome in cetacean sperm and SP, which could be an important contribution to future research into new biomarkers, the analysis of conservation capacity, or possible additional applications in the field of assisted reproductive technologies.

Post-thaw sperm quality is quite different among animal species as a result of their different sensitivity to freezing and thawing. The low survival rate of cryopreserved sperm is associated with structural and functional alterations. In this sense, the low sterol/phospholipid ratio of ram sperm membranes has been identified as one of the most significant factors determining their low tolerance to cold temperatures. Recently, Carro et al. (2020) found a positive effect on membrane biophysical properties in ram sperm adding cholesterol and desmosterol into sperm extenders prior to cryopreservation. In this topic, these authors (Carro et al.) studied the role of cholesterol and desmosterol in ram sperm functionality and fertility, proposing the benefit of the incorporation of desmosterol as a strategy to improve fertility outcome.

The works presented in this topic provide meaningful information on studying molecular and cellular processes that give fertilizing competence in spermatozoa and oocytes of non-murine or non-human animals. These findings also contribute to the knowledge of new insight into molecular mechanisms to develop biotechnological tools for improving domestic animal production and for the conservation of biodiversity of wild species.

AUTHOR CONTRIBUTIONS

SP-M, AC, and AV drafted and further revised the manuscript. All authors listed have read this editorial and approved it for publication.

ACKNOWLEDGMENTS

As Research Topic editors we would like to express our sincere thanks to all authors and referees for their valuable contributions, which made it possible for us to compile this interesting Research Topic on Molecular and Cellular Physiology of Gametes in Domestic and Wild Animal Models.

REFERENCES

Austin, C. R. (1952). The 'Capacitation' of the Mammalian Sperm. *Nature* 170 (4321), 326. doi:10.1038/170326a0

Carro, M. D. L. M., Peñalva, D. A., Antollini, S. S., Hozbor, F. A., and Buschiazzo, J. (2020). Cholesterol and Desmosterol Incorporation into Ram Sperm Membrane before Cryopreservation: Effects on Membrane Biophysical Properties and Sperm Quality. *Biochim. Biophys. Acta (Bba) - Biomembranes* 1862 (9), 183357. doi:10.1016/j.bbamem.2020.183357

Chang, M. C. (1951). Fertilizing Capacity of Spermatozoa Deposited into the Fallopian Tubes. *Nature* 168, 697–698. doi:10.1038/168697b0

Plant, T., and Zeleznik, A. (2014). "Knobil and Neill's Physiology of Reproduction Physiology of Reproduction," in *Section I: Section I. Gametes, Fertilization and Embryogenesis*. Editors T. Plant and A. Zeleznik. 4th Edition. doi:10.1016/C2011-1-07288-0

Viveiros, M. M., and De La Fuente, R. (2019). "Regulation of Mammalian Oocyte Maturation," in *Chapter 11 - Regulation of Mammalian Oocyte Maturation (165-180), the Ovary*. Editors P. C. K. Leung and E. Y. Adashi. Third Edition (Academic Press), 165–180. doi:10.1016/B978-0-12-813209-8.00011-X

Conflict of Interest: The authors declare that the research was conducted in the absence of any commercial or financial relationships that could be construed as a potential conflict of interest.

frontiers in Cell and Developmental Biology

ORIGINAL RESEARCH
published: 22 January 2021
doi: 10.3389/fcell.2020.611503

SHP2 Nuclear/Cytoplasmic Trafficking in Granulosa Cells Is Essential for Oocyte Meiotic Resumption and Maturation

*Muhammad Idrees[1], Vikas Kumar[2], Myeong-Don Joo[1], Niaz Ali[3], Keun-Woo Lee[2] and Il-Keun Kong[1,4]**

[1] Division of Applied Life Science (BK21 Four), Institute of Agriculture and Life Science (IALS), Gyeongsang National University, Jinju, South Korea, [2] Division of Applied Life Science, Department of Bio and Medical Big Data (BK21 Four), Research Institute of Natural Science (RINS), Gyeongsang National University (GNU), Jinju, South Korea, [3] Institute of Basic Medical Sciences, Khybar Medical University, Peshawar, Pakistan, [4] The King Kong Corp. Ltd., Gyeongsang National University, Jinju, South Korea

OPEN ACCESS

Edited by:
Karin Lykke-Hartmann,
Aarhus University, Denmark

Reviewed by:
Lucie Němcová,
Academy of Sciences of the Czech Republic (ASCR), Czechia
Wang Chao,
China Agricultural University, China

***Correspondence:**
Il-Keun Kong
ikong7900@gmail.com

Specialty section:
This article was submitted to Cell Growth and Division, a section of the journal Frontiers in Cell and Developmental Biology

Received: 30 September 2020
Accepted: 30 November 2020
Published: 22 January 2021

Citation:
Idrees M, Kumar V, Joo M-D, Ali N, Lee K-W and Kong I-K (2021) SHP2 Nuclear/Cytoplasmic Trafficking in Granulosa Cells Is Essential for Oocyte Meiotic Resumption and Maturation. Front. Cell Dev. Biol. 8:611503. doi: 10.3389/fcell.2020.611503

Src-homology-2-containing phosphotyrosine phosphatase (SHP2), a classic cytoplasmic protein and a major regulator of receptor tyrosine kinases and G protein-coupled receptors, plays a significant role in preimplantation embryo development. In this study, we deciphered the role of SHP2 in the somatic compartment of oocytes during meiotic maturation. SHP2 showed nuclear/cytoplasmic localization in bovine cumulus and human granulosa (COV434) cells. Follicle-stimulating hormone (FSH) treatment significantly enhanced cytoplasmic SHP2 localization, in contrast to the E_2 treatment, which augmented nuclear localization. Enhanced cytoplasmic SHP2 was found to negatively regulate the expression of the ERα-transcribed *NPPC* and *NPR2* mRNAs, which are vital for oocyte meiotic arrest. The co-immunoprecipitation results revealed the presence of the SHP2/ERα complex in the germinal vesicle-stage cumulus–oocyte complexes, and this complex significantly decreased with the progression of meiotic maturation. The complex formation between ERα and SHP2 was also confirmed by using a series of computational modeling methods. To verify the correlation between SHP2 and *NPPC*/*NPR2*, SHP2 was knocked down *via* RNA interference, and *NPPC* and *NPR2* mRNAs were analyzed in the control, E_2, and FSH-stimulated COV434 cells. Furthermore, phenyl hydrazonopyrazolone sulfonate 1, a site-directed inhibitor of active SHP2, showed no significant effect on the ERα-transcribed *NPPC* and *NPR2* mRNAs. Taken together, these findings support a novel nuclear/cytoplasmic role of SHP2 in oocyte meiotic resumption and maturation.

Keywords: granulosa cells, SHP2, ER-α, Nppc/Npr2, ERK1/2, COV434 cell line, protein-protein docking, molecular dynamics simulations

INTRODUCTION

In mammals, dormant oocytes surrounded by somatic cells enter meiotic cell division during embryonic development and meiotic arrest during the first meiotic prophase (MI) stage for a prolonged period (Guo et al., 2018). The communication between the oocyte and its surrounding somatic cells (including theca, mural granulosa, and cumulus cells) is critical for maintaining this stage, as meiosis inhibitory signals pass from somatic cells to oocytes *via* gap junctions. Several molecular mechanisms in somatic cells work together to preclude the activation of meiotic-progression-related machinery in oocytes (Zhang et al., 2010). The estradiol (E_2)–estrogen receptor (ER) system is one of the mechanisms of oocyte meiotic arrest maintained by granulosa cells (Liu et al., 2017). E_2, a steroid hormone, is a critical regulator of oocyte meiotic arrest and exerts its effects by binding to ERα and ERβ (Lubahn et al., 1993). Ligand-activated ERα regulates the transcription of natriuretic peptide type C (*NPPC*) and natriuretic peptide receptor 2 (*NPR2*) by directly binding to their promoter regions and enhancing their expression in granulosa cells (Liu et al., 2017). The *NPPC* and *NPR2* genes further regulate the production of cyclic guanosine monophosphate in granulosa cells, which then enters the oocyte *via* gap junctions, inhibit phosphodiesterase 3A-induced cyclic adenosine monophosphate degradation, and maintain oocyte meiotic arrest (Zhang et al., 2010; Kiyosu et al., 2012; Wigglesworth et al., 2013).

Follicle-stimulating hormone (FSH), a negative feedback regulator of ERα, controls folliculogenesis by stimulating the granulosa cells of early antral follicles (Glidewell-Kenney et al., 2008; El-Hayek et al., 2014). FSH transduces its signals *via* the FSH-specific G protein-coupled receptor (FSHR), depending on intracellular effectors (Casarini and Crepieux, 2019). By activating mitogen-activated protein kinase (MAPK)/extracellular signal-regulated kinase (ERK) and AKT (protein kinase B) signaling pathways, FSH induces the proliferation and differentiation of granulosa cells to a pre-ovulatory phenotype (El-Hayek et al., 2014; Donaubauer et al., 2016). FSH requires several proteins to transduce its signaling in granulosa cells, and SHP2 has been identified to play a key role in FSH signaling (Donaubauer et al., 2016). SHP2, a main regulating component of receptor tyrosine kinases (RTKs) and G protein coupled receptors (GPCRs), shows ubiquitous expression and has multiple functions (Qu, 2002; Zhang et al., 2004; Furcht et al., 2014). Evidence has shown that SHP2 is critical for numerous reproductive tissues (Hu et al., 2015, 2017; Ran et al., 2017; Idrees et al., 2019b, 2020; Kim et al., 2019). By interacting with the transmembrane adaptor proteins, SHP2 induces the sustained activation of the rat sarcoma (RAS) and ERK1/2 signaling pathway, which is essential for oocyte meiotic maturation and ovulation (Fan and Sun, 2004; Dance et al., 2008; Fan et al., 2009). In addition to folliculogenesis, SHP2 is important for embryonic development, as indicated by SHP2-knockout embryos which exhibit inner cell mass death and failure to yield trophoblast stem cells (Saxton et al., 1997; Yang et al., 2006).

The primary function of SHP2 is to positively affect the intracellular signaling of RTKs and GPCRs in the cytoplasm, but unconventional nuclear localization of SHP2 has also been identified by several studies (Jakob et al., 2008; Li et al., 2014; Ran et al., 2017). The nucleus-localized SHP2 is essential for the activity of several nuclear proteins, such as nuclear SHP2, which retain telomerase reverse transcriptase in the nucleus for telomere lengthening (Jakob et al., 2008). SHP2 is required for signal transducer and activator of transcription 5 nuclear translocation and transcriptional activity (Chughtai et al., 2002). ERα, an essential protein for fertility, also requires nuclear SHP2 for DNA binding, as SHP2 enhances the Src kinase-mediated tyrosine phosphorylation of ERα in the uterus and facilitates its binding to the progesterone promoter region (Ran et al., 2017). Cytoplasmic SHP2 and extra-nuclear ERα also form a complex and significantly affect mitogen-activated protein (MAP) kinases and AKT signaling (Levin, 2009; Li et al., 2014).

In this study, we identified a novel role of SHP2 in association with ERα and FSH in mammalian oocyte meiotic resumption. Our results provide an experimental proof that SHP2 exists in complex with ERα in the nucleus of human granulosa and bovine cumulus cells. Progression in bovine oocyte meiotic maturation significantly reduced the SHP2/ERα complex. The FSH-mediated stimulation of cultured granulosa cells also reduced the SHP2/ERα complex as compared to E_2 treatment that markedly enhanced it. Furthermore, FSH increases the cytoplasmic localization of SHP2, and this may be due to FSHR-induced signaling in granulosa cells. Moreover, the E_2 activation of ERα not only enhanced the mRNA expression of *NPPC* and *NPR2* but also increased the nuclear localization of SHP2. The functional role of SHP2 in oocyte-surrounding somatic cells and its significance in oocyte maturation have never been studied. Thus, the elucidation of the SHP2 mechanism could provide a potential therapeutic target in the treatment of infertility.

MATERIALS AND METHODS

The study was conducted in full compliance with the Gyeongsang National University Institute of Animal Care Committee (GNU-130902-A0059). Most of the chemicals and reagents were obtained from Sigma-Aldrich (St. Louis, MO, USA), unless otherwise noted.

Experiment Procedures

Experiment 1

To understand the role of SHP2 in the somatic compartment of oocytes, bovine ovary-derived cumulus–oocyte complexes (COCs) were used to culture cumulus cells. Primary bovine cumulus cells were separated from pre-ovulatory follicles and cultured in α-MEM media. FSH (20 ng/ml) and epidermal growth factor (EGF 25 ng/ml) were used to stimulate the cultured cumulus cells. Phenyl hydrazonopyrazolone sulfonate 1 (PHPS1) (5 μM) was used for COCs and cultured cumulus cells according to our previous study (Idrees et al., 2019b). Samples from various stages of bovine oocytes were used to

examine the SHP2/ERα complex *via* co-immunoprecipitation (co-IP) and immunofluorescence.

Experiment 2

To analyze the SHP2/ERα complex in granulosa cells, COV434 human granulosa cell line was used, and co-IP was used to detect complex formation. 3-(4,5-Dimethylthiazol-2-yl)-2,5-diphenyltetrazolium bromide (MTT) assay showed that the least effective concentration of PHPS1 in the COV434 cell line was 3 μM. For FSH and E_2, the same effective concentrations were used as those in a previous study that used the COV434 cell line (Liu et al., 2017). SHP2 was knocked down using small interfering RNA (siRNA, 10 nM). The expression of ERα was examined *via* immunofluorescence, and its transcribed genes (*NPPC* and *NPR2*) were analyzed *via* quantitative real-time polymerase chain reaction (RT-qPCR).

COC Collection and *in vitro* Maturation

Local abattoir-derived bovine ovaries were transported to the laboratory within 2 h after dissection. COCs with follicle diameter ranging from 3 to 6 mm and with a minimum of three layers of cumulus cells were collected according to a previously described protocol (Idrees et al., 2019b). In brief, ovaries were washed with Dulbecco's phosphate-buffered saline (D-PBS), and COCs were aspirated using 18-gauge disposable needles attached to a vacuum pump. The follicular medium was diluted using TL-HEPES [10 mM HEPES (H-6147), 2 mM calcium chloride (C-7902), 3.2 mM potassium chloride (P-5405), 0.5 mM magnesium chloride (M-2393), 10 mM sodium lactate, 2 mM sodium bicarbonate (S-5761), 114 mM sodium chloride (S-5886), 0.34 mM sodium bisphosphate (S-5011), 1 μl/ml phenol red, 100 IU/ml penicillin, and 0.1 mg/ml streptomycin]. A stereomicroscope was used to collect COCs with a minimum of three uniform layers. The retrieved GV-stage oocytes, along with cumulus cells in groups of 40–50, were cultured in 700 μl of TCM199 media (Invitrogen Corp., Carlsbad, CA, USA) supplemented with 10% (v/v) fetal bovine serum (FBS; Gibco BRL, Life Technologies, Grand Island, NY, USA, cat. 16000-044), 10 ng/ml EGF, 10 μg/ml FSH, 1 μg/ml ostradiol-17β, 0.6 mM cysteine, and 0.2 mM sodium pyruvate (Gibco BRL, Life Technologies, Grand Island, NY, USA, cat. 11360-070). Incubator conditions were set to 38.5°C and 5% CO_2 for 22–24 h.

In vitro Fertilization and Embryo Culture

In vitro-matured (MII) COCs were co-cultured with frozen–thawed bovine sperm of already proven fertility (Idrees et al., 2019a). The sperm straw was thawed at 37.0°C for 1 min and diluted in D-PBS. Subsequently, the sperm suspension was centrifuged at 750 × *g* for 5 min at room temperature, and the pellet was re-suspended in 500 μl of heparin (20 μg/ml) diluted in *in vitro* fertilization (IVF) medium [Tyrode's lactate solution supplemented with 6 mg/ml bovine serum albumin (BSA), 22 μg/ml sodium pyruvate, 100 IU/ml penicillin, and 0.1 mg/ml streptomycin]. The heparin-diluted sperm suspension was incubated at 38.5°C and 5% CO_2 for 15 min to facilitate capacitation. Subsequently, the sperm suspension was diluted in IVF medium to a final density of 1.0–2.0 × 10^6 sperms/ml and co-cultured with mature oocytes for 20 h. On the next day, the cumulus cells were removed from the presumed zygotes by vortexing for 3 min and cultured in SOF-BE1 medium supplemented with 5 μg/ml insulin, 5 μg/ml transferrin, 5 ng/ml sodium selenite (cat. 11074547001), 4 mg/ml fatty-acid-free BSA, and 100 ng/ml EGF. The presumed zygotes were cultured for 8 days, with one-time media replacement after 3 days.

RNA Extraction and Reverse Transcription Quantitative PCR

To generate cDNA, mRNA was extracted from samples using the Dynabeads mRNA Direct Kit (Dynal AS, Oslo, Norway) according to the manufacturer's protocol and as previously described (Idrees et al., 2019b). The concentration of the purified mRNA was determined spectroscopically (NANO DROP 2000c Thermo Fisher Scientific) at 260 nm. Superscript III reverse transcriptase (iScript® cDNA Synthesis Kit from Bio-Rad Laboratories Hercules, CA, USA) was used to reverse-transcribe the first-strand cDNA. The PCR primers were designed using the Primer3 (v. 0.4.0) software of the National Center for Biotechnology Information nucleotide database. A CFX98 instrument (Bio-Rad Laboratories) was used to quantify the transcription levels. The reaction was carried out in a final volume of 10 μl, comprising 3 μl diluted cDNA, 1X iQ SYBR Green Super mix (iQ SYBR Green Super Mix Kit, Bio-Rad Laboratories, cat. 170-8882 Laboratories Hercules, CA, USA), and 0.2 mM each of forward and reverse primers. The samples were processed in triplicate according to the manufacturer's guidelines. The relative gene expression was calculated using the threshold $^{\Delta\Delta}$C(t) method. The *GAPDH* gene was used as an endogenous control and for the normalization of the expressed data. The primers and the PCR conditions for each gene are given in **Supplementary Table 4**.

H_2DCFDA Staining for Reactive Oxygen Species

To measure the reactive oxygen level (ROS) level, 2,7-di-chloro-di-hydro-fluorescein di-acetate (H2DCFDA, cat. #D6883) staining was performed according to a previously described protocol (Idrees et al., 2019a). In brief, the MII stage live oocytes were incubated in PBS containing 10 nM H2DCFDA for 30 min at 38.5°C and 5% CO_2. After that, the samples were washed thrice with PBS and examined under an epifluorescence microscope (Olympus IX71) under 490-nm excitation and 525-nm emission filters.

Cells and Cell Culture

Primary Bovine Cumulus Cell Culture

Bovine cumulus cells obtained from 3–6-mm COCs were cultured in previously described media and conditions (Baufeld and Vanselow, 2013). In brief, cumulus cells were collected immediately after COC isolation and denuded by recurrent pipetting through a narrow pipette. The collected cumulus cells were cultured on collagen-coated 24-well-plates with 1.25 × 10^5 viable cells per well. The serum free α-MEM medium was supplemented with HEPES (20 mM), BSA (0.1%), sodium bicarbonate (0.084%), sodium selenite (4 ng/ml), transferrin

(5 μg/ml), insulin (10 ng/ml), androstenedione (2 μM), L-glutamine (2 mM), non-essential amino acids (1 mM), penicillin (100 IU), and streptomycin (0.1 mg/ml). FSH (20 ng/ml) and EGF (25 ng/ml) were also added to the culture medium to stimulate the cells.

COV434 Cell Culture, Treatment, and Transfection

The COV434 human granulosa cell line was kindly gifted by Professor Jeehyeon Bae (Chung-Ang University, Seoul, Republic of Korea). Cells were cultured in Dulbecco's modified Eagle's medium containing 1% penicillin–streptomycin and 10% FBS as previously described (Jin et al., 2016). The incubator conditions were set to 37.0°C and 5% CO_2 air. Cell treatment was performed using the MTT assay in accordance with the manufacturer's protocol (Sigma-Aldrich). In 96-well-plates, COV434 cells were cultured at a concentration of 0.8×10^4 cells per well, with 200 μl of media already contained per well. After growing the cells for 24 h, the medium was replaced with a fresh medium containing no or varying concentrations of PHPS1 and incubated for 24 h. Subsequently, the cells were incubated with MTT solution for 3 h. Thereafter, DMSO (100 μl) was added, and the plate was agitated for 20 min. A microplate scanning reader was used to measure absorbance at 550 to 570 nm (L1, value for viable cells) and 620 to 650 nm (L2, value for debris). The corrected absorbance (A = L1–L2) was used to calculate the number of viable/dead cells in each well for each group.

Lipofectamine™ RNAiMAX Transfection Reagent (Thermo Fisher Scientific, Waltham, MA USA cat #13778030) was used to transiently transfect the COV434 cell line. Briefly, lipofectamine was diluted in the Opti-MEM medium (Thermo Fisher Scientific, Inc.), and the transfection complexes were prepared by diluting the siRNAs (Santa Cruz products sc-37007 and sc-36488, respectively, Santa Cruz Biotechnology, St. Louis, MO, USA) in the Opti-MEM medium. The diluted siRNA was added to the diluted lipofectamine reagent and incubated for 20 min at room temperature. The transfection complexes were added to each well and incubated for 24 h, after which the medium was replaced with a fresh one. At 48 h after transfection, the cells were fixed (4% paraformaldehyde) or lysed for the examination of specific protein expression *via* immunoblotting or immunofluorescence.

Co-immunoprecipitation and Antibodies

To analyze the SHP2/ERα complex, co-immunoprecipitation was performed according to the manufacturer's protocol (Pierce Co-IP cat. 26149). The SHP2 antibody was used to pull down the protein complex. The SHP2/ERα complex levels in various samples were analyzed *via* western blotting. The following primary antibodies were used in this study: β-actin (Santa Cruz cat. sc-47778), SHP2 (Santa Cruz Biotechnology, USA cat. sc-271106), ERα (Abcam, Cambridge, Cambs, UK cat. ab3575), AKT (Cell Signaling technology cat. 9272), p-AKT (Cell Signaling, cat. 9271), p-ERK1/2 (Cell Signaling, cat. CST 9101S), ERK1/2 (Cell Signaling, cat. CST 9102S), FOXL2 (LifeSpan BioScience, Seattle, WA, USA cat. LS-B12865), SF1 (Abcam cat. ab168380), Wnt4 (Santa Cruz cat. sc-376279), octamer-binding transcription factor 4 (OCT4; Santa Cruz cat. Sc-8629), Caspase-3 (Santa Cruz cat. Sc-1225), p-Nf-Kb (Santa Cruz cat. Sc-271908), and p-mTOR (Abcam cat. ab84400). The secondary antibodies used in this study were mouse horseradish peroxidase (HRP; Amersham ECL cat. NA931), rabbit HRP (Amersham ECL cat. NA934), mouse-FITC (Santa Cruz cat. sc-516140), and rabbit-TRITC (Thermo Fisher Scientific, Waltham, MA, USA, cat. A16101).

Histological Analysis

Bovine ovaries collected from the local abattoir were washed with saline and stored at 4°C in 20% sucrose diluted in 1× PBS solution for 72 h. Thereafter, the ovaries were washed with saline and stored in 4% paraformaldehyde at 4°C for 72 h. The ovaries were placed in an optimal cutting temperature compound (Sakura Finetek Inc., Torrance, CA, USA) and stored at −80°C for a minimum of 24 h to make blocks, and 12-μm-thick sections were taken on probe-on plus charged slides (Fisher, Rock-ford, IL, USA) using a CM 3050C cryostat (Leica, Germany). The slides were stored at −80°C until further processing.

Immunofluorescence

For immunofluorescence, staining was performed according to a previously defined protocol (Idrees et al., 2019b). In brief, 4% (v/v) paraformaldehyde in 1 M PBS was used to fix the samples, which were preserved at 4°C for a minimum of 30 min to a prolonged period. On the staining day, the samples were washed twice in 0.3% polyvinyl alcohol in 1× PBS (PBS-PVA) and permeabilized with the proteinase K solution (0.1%) for 5 min. After washing twice with PBS-PVA for 5 min, the samples were incubated for 90 min in 5% blocking solution (BSA-PBS-PVA). Primary antibodies were applied to the samples and kept at 4°C overnight. On the next day, after washing twice with PVA-PBS for 10 min, the samples were incubated with secondary antibodies (FITC and TRITC) at room temperature for 90 min. For nuclear staining, 10 μg/ml 4,6-diamidino-2-phenylindole was applied for 5 min. Thereafter, the samples were washed thrice with PVA-PBS for 5 min, mounted with a fluorescent mounting medium, and covered with a slide cover. A confocal laser scanning microscope (Fluoview FV 1000, Olympus, Japan) was used to capture images. ImageJ analysis software (National Institutes of Health, Bethesda, MD, USA; https://imagej.nih.gov/ij) was used to measure the relative integrated density of the signals.

Immunoblotting

The samples [MII oocytes (100 per extract) or trypsinized cells] were washed with D-PBS and dissolved in PRO-PREP™ (iNtRON Biotechnology, Burlington, NJ, USA, cat. 17081). Subsequently, the samples were sonicated, and the cell lysate was centrifuged at 10,000 × *g* for 25 min at 4°C. The supernatant was collected and quantified using the Bradford assay (cat. 5000002 Laboratories Hercules, CA, USA), while the settled debris was discarded (Idrees et al., 2019a). Equal amounts of protein (10–20 μg) were fractionated by SDS-PAGE (10 and 12%) and then transferred to a polyvinylidene fluoride (PVDF) membrane (cat. GE 10600023; Sigma-Aldrich). The PVDF membrane was blocked with skimmed milk for 1 h and

incubated overnight with a primary antibody at 4°C in a two-dimensional shaker. Thereafter, it was incubated with HRP-conjugated secondary antibody at room temperature for 90 min. An enhanced chemiluminescence detection reagent (Pierce TM ECL Western Blotting Substrate, Thermo Fisher Scientific, Waltham, MA, USA) was used to detect bound antibodies. Protein ladders (Abcam, USA, cat. ab116029) were used to determine the molecular weights of the proteins. ImageJ software (National Institutes of Health, Bethesda, MD, USA; https://imagej.nih.gov/ij) was used to detect the optical densities of the bands on X-ray films (iNtRON, Biotechnology Inc., Burlington, NJ, USA).

Molecular Docking of ERα and SHP2

The 3D structural information on the binary complex of human ERα and SHP2 has not been reported yet; therefore, we performed a molecular docking study to gain an insight into the molecular-level interaction between ERα and SHP2. The ERα complex structure was not available in Protein Data Bank (PDB), but a recent study modeled a full-length structure of the ERα comprising the ligand-binding domain and DNA-binding domain, which is available in the Small-Angle Scattering Biological Data Bank (Valentini et al., 2015; Huang et al., 2018). For SHP2, an open conformation structure (PDB ID: 6CRF) was selected from the literature (LaRochelle et al., 2018) and downloaded from PDB (https://www.rcsb.org/). The structures of both proteins were prepared using a clean protein protocol and were further minimized using the Discovery Studio v2018 software (http://3dsbiovia.com/products/). Water molecules were removed, and hydrogen atoms were added. For molecular docking, we utilized HDOCK, the web server for protein–protein and protein–DNA/RNA docking (Yan et al., 2020). During molecular docking, ERα was used as a receptor and SHP2 as a ligand. Owing to the lack of structural information for the ERα and SHP2 complex, the docking simulation was performed with default parameters, without defining the binding site according to a previously established method (Selent et al., 2013). The HDOCK server uses a fast Fourier transform-based approach to sample all possible binding modes globally (Katchalski-Katzir et al., 1992). Additionally, all binding modes collected were reassessed with iterative-knowledge-based scoring functions (Yan et al., 2017).

Molecular Dynamic Simulation for the ERα and SHP2 Binary Complex

The prediction of the correct 3D binding mode for protein–protein interaction is extremely difficult, as protein-protein molecular docking studies have always been challenging. Therefore, to refine the docked ERα-SHP2 complex, we subjected the best docked structure to molecular dynamics (MD) simulations using GROMACS v2018.2 (Pronk et al., 2013). The topology parameters of the protein were prepared by the AMBER99SB-ILDN force field (Lindorff-Larsen et al., 2010). The binary complex was placed into a dodecahedron box, and the TIP3P water model was used for solvation. The system was neutralized by 18 Na^+ ions and subjected to an energy-minimization step with the steepest descent algorithm to avoid steric clashes and bad contacts. Subsequently, the energy-minimized system was subjected to equilibration in two phases. In the first phase, temperature balancing was performed under an NVT ensemble for 500 ps at 300 K while using a V-rescale thermostat (Bussi et al., 2007). In the second phase, pressure equilibration was achieved under the NPT ensemble for 500 ps at 1.0 bar using the Parrinello–Rahman barostat (Parrinello and Rahman, 1981). Each system was then subjected to 50 ns of production run. The particle mesh Ewald method was used to estimate the electrostatics of long-range interactions (Darden et al., 1993). During simulation, the bond lengths were restrained using the Linear Constrain Solver algorithm (Hess et al., 1997). The MD simulation results were analyzed using the visual molecular dynamics (Humphrey et al., 1996) and DS software programs. Additionally, the binding free energy calculations were performed with the molecular mechanics-generalized Born surface area (MM-GBSA) algorithm using an online webserver, Hawk Dock (Weng et al., 2019).

Statistical Analysis

At least three separate and independent experiments were performed to derive data, which were expressed as mean ± SEM. The western blotting bands and immunofluorescence images were analyzed using Graph Pad Prism 6 (Graph Pad Software, USA) and Image J software programs. *P*-values were calculated on the basis of one-way analysis of variance (ANOVA), followed by Student's *t*-test (significance: $^*p < 0.05$, $^{**}p < 0.01$, $^{***}p < 0.001$, and $^{****}p < 0.0001$).

RESULTS

SHP2 Expression in Ovarian Tissue and Dynamic Changes With Growth Factor Treatment in Cultured Bovine Granulosa Cells

To investigate the protein localization pattern of SHP2 in the somatic compartment of a follicle, we first performed the immunofluorescence staining of bovine ovarian sections with an SHP2-specific antibody (**Figures 1A,B**; Eppig and Handel, 2012). The results showed the protein expression of SHP2 in the granulosa cells of pre-ovulatory follicles and in the ovarian medulla. The localization pattern analysis revealed that SHP2 was evenly distributed between the nucleus and the cytosol. To analyze SHP2 localization in cumulus cells, the ovarian immature COCs were fixed and immunofluorescent-stained with the SHP2 antibody ($n = 20$ COCs per group) (**Figure 1C**). The results showed that SHP2 had a localization pattern similar to that identified in granulosa cells. To further confirm the nuclear localization of SHP2, pre-antral-follicle-derived bovine cumulus cells were cultured *in vitro*, and SHP2 was evaluated (**Figure 1D**; Georges et al., 2014). Although SHP2 is a main regulating component of growth factor receptor intracellular signaling, it showed unconventional nuclear localization in granulosa and cumulus cells. To examine the function of SHP2, cultured cumulus cells were treated with EGF and FSH, and samples were prepared for RT-qPCR (**Figure 1E**). The mRNA expression of

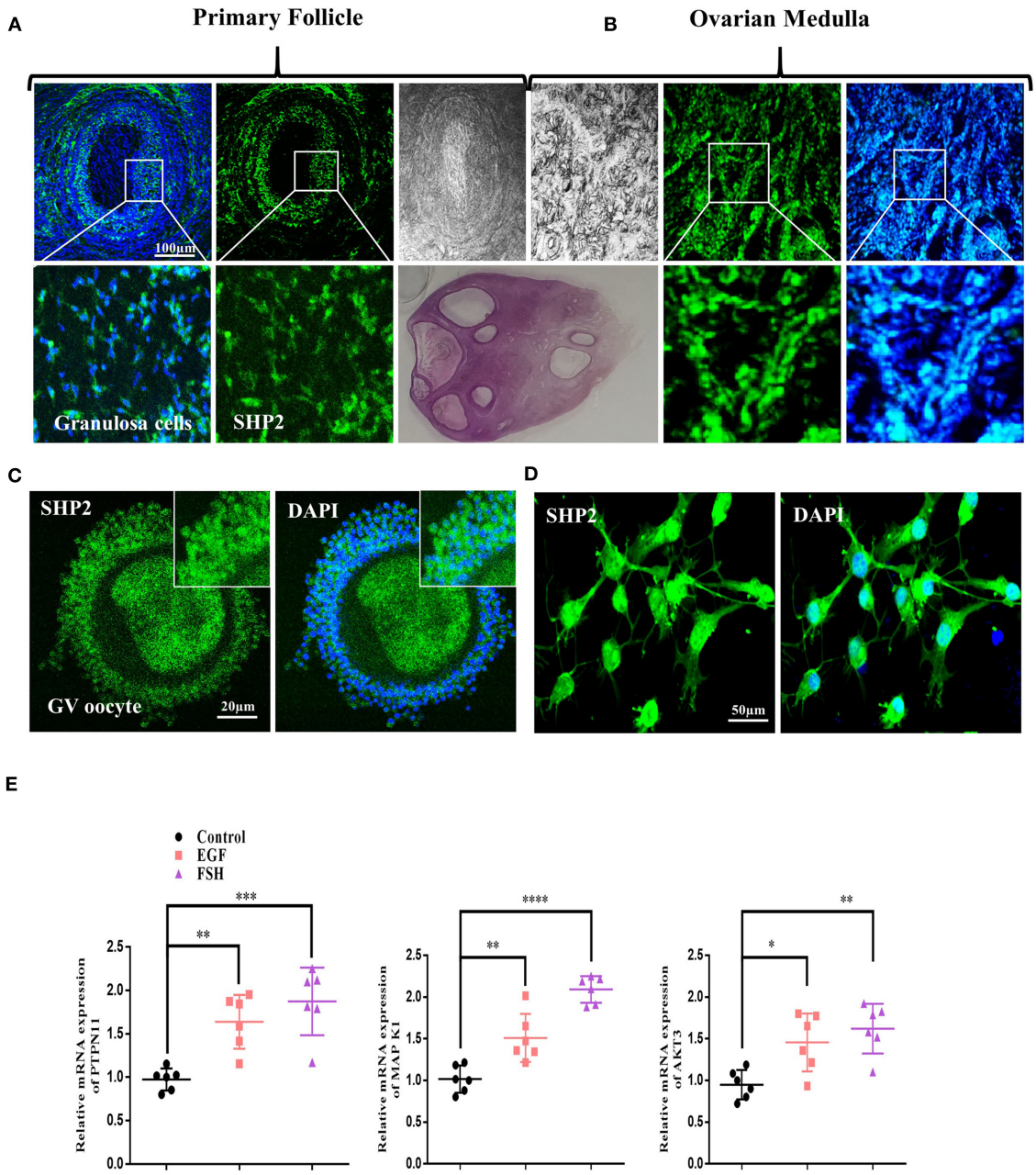

FIGURE 1 | Src-homology-2-containing phosphotyrosine phosphatase (SHP2) expression in bovine ovary and upregulation with follicle-stimulating hormone (FSH) or epidermal growth factor (EGF) treatment. **(A)** Representative images of SHP2 protein expression (green, fluorescein isothiocyanate) in bovine pre-ovulatory oocyte granulosa cells. **(B)** SHP2 protein expression in bovine ovarian medulla. The lower images are zoom-ins of the upper images. **(C)** SHP2 expression in the cumulus cells of bovine oocyte (germinal vesicle, GV). **(D)** SHP2 expression in cultured cumulus cells obtained from GV-stage oocytes. **(E)** Cultured cumulus cells treated with FSH or EGF and PTPN11 (*SHP2*), mitogen-activated protein kinase 1 (*MAPK1*), and protein kinase B (*AKT3*) genes analyzed *via* RT-qPCR (the experiment was repeated thrice, and data are shown as mean ± SEM. NS, not significant; $^{*}P < 0.05$; $^{**}P < 0.01$; $^{***}P < 0.001$; $^{****}P < 0.0001$.

protein tyrosine phosphatase N11 (*PTPN11* encoding protein SHP2) and *AKT3* genes was found to be statistically significant with EGF or FSH stimulation as compared to the control, while *MAP K1* was found to be very significant with FSH treatment ($n = 20$ per group; $^{*}p < 0.05$, $^{**}p < 0.01$, $^{****}p < 0.0001$). These findings indicate that SHP2 shows nuclear and cytoplasmic localization in bovine granulosa and cumulus cells. EGF or FSH treatment can upregulate *PTPN11* (SHP2) mRNA expression in cultured cumulus cells (Dance et al., 2008), but the function of the nucleus-localized SHP2 still needs exploration.

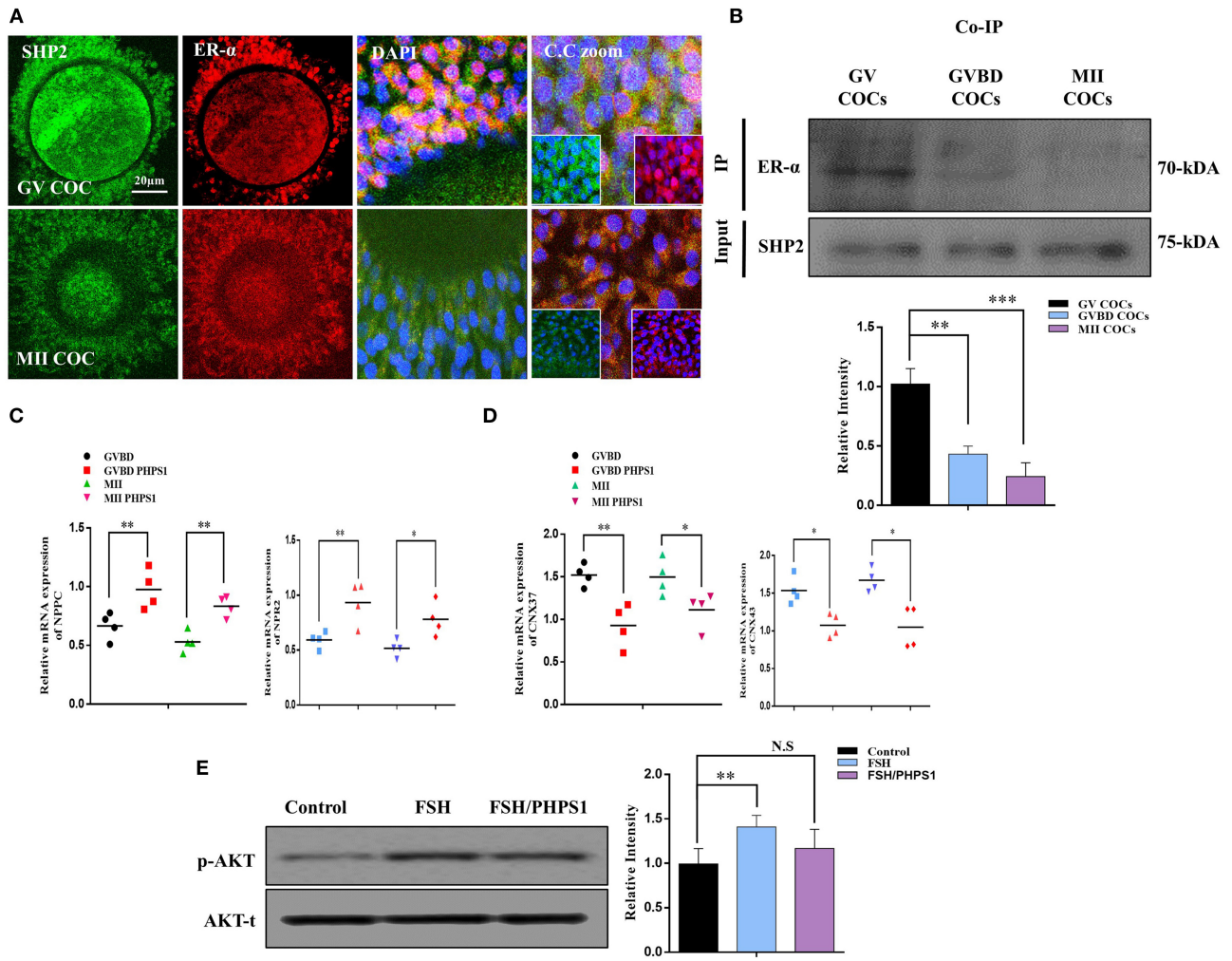

FIGURE 2 | Src-homology-2-containing phosphotyrosine phosphatase (SHP2)/estrogen receptor alpha (ERα) complex and ERα-dependent gene expression in cumulus cells. **(A)** SHP2 and ERα proteins analyzed in germinal vesicle (GV)- and MII-stage cumulus–oocyte complexes (COCs) *via* immunofluorescence. Both proteins showed nuclear localization and exited the nucleus with the progression of meiotic maturation. Data are expressed as means ± SEM. GV and MII COCs were immune-labeled with SHP2 (green) and ERα (red) and counterstained with 10 μg/ml 4′,6′-diamidino-2-phenylindole to visualize DNA (mean ± SEM). **(B)** Co-immunoprecipitation of SHP2 and ERα showed that both proteins form a complex at the GV COC stage, and the complex is significantly reduced with oocyte maturation. **(C)** Natriuretic peptide C (*NPPC*) and natriuretic peptide receptor 2 (*NPR2*) genes analyzed *via* RT-qPCR in GV, germinal vesicle breakdown (GVBD), and MII-stage COCs and compared with phenylhydrazonopyrazolone sulfonate 1 (PHPS1) treatment of GVBD- and MII-stage oocytes. **(D)** *CX37* and *CX43* genes analyzed *via* RT-qPCR in GVBD- and MII-stage COCs and compared with the PHPS1 treatment of GVBD- and MII-stage oocytes. **(E)** Cultured bovine granulosa cells were stimulated with follicle-stimulating hormone (FSH) and FSH plus PHPS1, and the p-AKT protein was analyzed along with total AKT. The experiments were repeated thrice, and data are shown as mean ± SEM. NS, not significant; $^{*}P < 0.05$; $^{**}P < 0.01$; $^{***}P < 0.001$; $^{****}P < 0.0001$.

SHP2 Forms a Complex With ERα in GV Oocyte Cumulus Cells and Is Involved in ERα Transcriptional Activity

ERα plays a key role in oocyte meiotic resumption and maturation, and several studies have identified the role of nuclear SHP2 in the transcriptional activity of ERα (Li et al., 2014; Ran et al., 2017). To analyze the interaction of SHP2 and ERα in the cumulus cells of GV- and MII-stage oocytes, we immunostained COCs with specific SHP2 and ERα antibodies (**Figure 2A**). At the GV stage, SHP2 and ERα were localized in the nucleus of cumulus cells, but at the MII stage, both proteins showed complete cytoplasmic localization. Few studies have identified that SHP2 forms a complex with ERα in the MCF7 and Ishikawa cell lines for activating signaling pathways and ERα transcription (Li et al., 2014; Ran et al., 2017). To understand the SHP2 and ERα behavior in cumulus and granulosa cells, samples were collected from ovary-retrieved immature COCs, 16-h cultured germinal vesicle breakdown (GVBD) COCs, and 22-h cultured mature (MII) COCs for the Co-IP of SHP2 and ERα proteins (**Figure 2B**). These data imply that SHP2 exists in complex with ERα in immature COCs, but the amount of complex becomes significantly reduced with the progression of

meiotic maturation. It was previously identified that ERα binds with the promoter regions of *NPPC* and *NPR2* in granulosa and cumulus cells and sustains oocyte meiotic arrest (Liu et al., 2017). Therefore, we applied PHPS1, a site-specific inhibitor of SHP2, to examine ERα transcriptional activity. Contrary to our expectations, the PHPS1-treated COCs showed a higher expression of *NPPC/NPR2* as compared to the control COCs, in which the expression of both genes was significantly reduced with meiotic progression ($n = 20$ per group; $^{*}P < 0.05$, $^{**}P < 0.01$; **Figure 2C**). To further confirm, we analyzed the expression of connexin-43 (CX43) and connexin-37 (CX37), as both genes are required for *NPPC/NPR2* signaling to mediate oocyte meiotic arrest (Richard and Baltz, 2014). The results indicated a significantly higher expression of both *CX37* and *CX43* in the control group than in the PHPS1-treated COCs (**Figure 2D**; $n = 20$ per group; $^{*}P < 0.05$, $^{**}P < 0.01$). FSH activates MAP kinases and AKT signaling in the cumulus cells of oocytes, which inhibit *NPPC/NPR2* (Tsuji et al., 2012; Wang et al., 2013), while SHP2 inhibition reduced FSH signaling in granulosa cells (Donaubauer et al., 2016). We found that FSH stimulation of cultured cumulus cells enhanced the expression of p-AKT protein, whereas the combined application of FSH and PHPS1 significantly reduced its expression ($^{*}P < 0.05$, $^{**}P < 0.01$; **Figure 2E**). All the above-mentioned results revealed that SHP2 exists in complex with ERα, and this complex shows a significant reduction with the progression of oocyte meiotic maturation. Unexpectedly, SHP2 inhibition had no significant effect on ERα transcriptional activity during COC meiotic maturation, but it can significantly reduce FSH intracellular signaling in cultured cumulus cells.

Cumulus Cell Cytoplasmic SHP2 Inhibition Deteriorates Oocyte Maturation and Embryo Development

SHP2 cytoplasmic localization is essential for FSH-induced activation of MAP kinases and AKT signaling, and PHPS1 inhibits active cytoplasmic SHP2 (Donaubauer et al., 2016; Idrees et al., 2019b). To analyze the effects of FSH signaling blockage *via* SHP2 inhibition on oocyte meiotic maturation, we treated immature COCs with PHPS1 and collected samples for immunofluorescence with the progression of meiotic stages [oocyte maturation percentage control $n = 172$ (84%) *vs*. PHPS1 $n = 185$ (58%), $n = 50$ per group, with four independent biological replicates] (**Figure 3A**). The PHPS1-treated COCs showed reduced cytoplasmic localization of SHP2 and ERα compared to the control, where both proteins were localized in the cytoplasm ($n = 30$ per group; $^{*}P < 0.01$). Next, we tested p-ERK1/2 and p-AKT signals in the MII oocytes (**Figure 3B**), as both proteins are essential for oocyte meiotic maturation and are downstream of SHP2 (Hatch and Capco, 2001; Andrade et al., 2017). We found a significant reduction in the p-ERK1/2 and p-AKT proteins in GVBD and MII oocytes treated with PHPS1 compared to control oocytes. Furthermore, the MII oocyte also showed a significant enhancement in ROS (**Supplementary Figure 1A**). Given the effects of SHP2 inhibition on oocyte quality, we speculated whether the loss of SHP2 would impair the development of subsequent embryos. To do this, we carried out IVF using control and SHP2-inhibited oocytes, and then zygotes were cultured in IVC media for 8 days to check the development. PHPS1 application reduced the embryo development by almost 50% [control $n = 143$ (39%) *vs*. PHPS1 $n = 108$ (21%)]. The SHP2-inhibited oocytes that developed to the blastocyst stage showed significantly high apoptosis as identified *via* nucleus-localized NF-kB and enhanced caspase-3 expression (**Figure 3C**). Furthermore, the developed blastocysts showed the reduced expression of OCT4 (**Supplementary Figure 1B**; Simmet et al., 2018). Moreover, SHP2 downstream proteins p-AKT and p-ERK1/2 showed a significant reduction with PHPS1 treatment as compared to the control littermates (**Supplementary Figure 1C**). These findings altogether suggest that SHP2-inhibited oocytes, in many cases, are unable to develop properly.

FSH Reduces SHP2/ERα Complex in Human Granulosa Cells (COV434)

To uncover the SHP2/ERα complex expression, localization, and involvement in human oocyte meiosis, we cultured an immortalized human granulosa cell line COV434 that exhibits the biological characteristics of normal human granulosa cells (Zhang et al., 2000). Granulosa cells were treated with PHPS1 at various concentrations, and 3.5 μM was selected as the least effective concentration *via* an MTT assay (**Figure 4A**). Thereafter, SHP2 and fork head box L2 (FOXL2, a surrogate marker of granulosa cells) antibodies were applied, and the results showed that SHP2 had a localization pattern similar to that previously detected in cultured bovine cumulus cells (**Figure 4B**; Georges et al., 2014). PHPS1 application to human granulosa cells had no noticeable effect on nucleus-localized SHP2. To analyze the effects of estradiol and FSH on SHP2 and ERα localization in granulosa cells, we applied E_2 (10.0 μM) and FSH and checked both proteins *via* immunofluorescence (**Figure 4C**). The results indicated that the application of E_2 highly localized SHP2 in the nucleus and that of FSH translocated it to the cytoplasm. To detect the SHP2/ERα complex in granulosa cells and determine the effects of E_2 and FSH on this complex, we performed a co-immunoprecipitation assay (**Figure 4D**). The SHP2/ERα complex was detected in the control group and was significantly enhanced with E_2, but the FSH treatment markedly reduced this complex in granulosa cells. The reduction in the SHP2/ERα complex caused by the FSH treatment might be due to FSH intracellular signaling in granulosa cells (Li et al., 2014). Therefore, the p-ERK1/2 and p-AKT proteins were analyzed *via* western blotting, and the results showed a high expression of these proteins in the presence of FSH as compared to the control and E_2-treated groups (**Figure 4E**). The above-mentioned results indicated that the SHP2 and ERα complex is present in human granulosa cells, and the FSH treatment can reduce the amount of this complex. Furthermore, E_2 acts in an opposite manner by enhancing the SHP2/ERα complex and reducing FSH-induced intracellular signaling in the COV434 cell line.

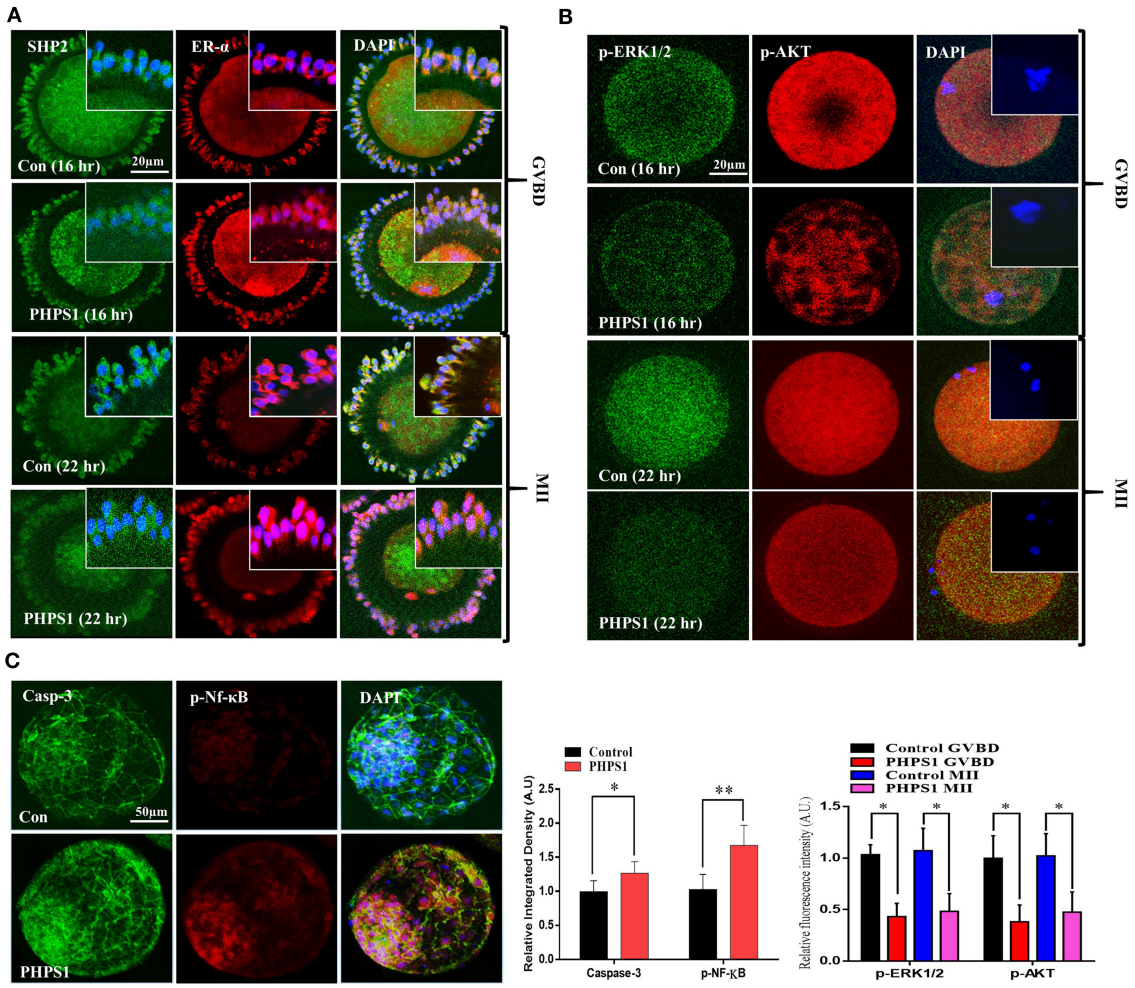

FIGURE 3 | Cumulus-cell cytoplasmic Src-homology-2-containing phosphotyrosine phosphatase (SHP2) inhibition deteriorates oocyte maturation and embryo development. **(A)** SHP2/ERα (GFP-labeled SHP2 and red fluorescent protein-labeled ERα) proteins analyzed *via* immunofluorescence in cumulus cells during germinal vesicle breakdown (GVBD) and MII stages of control cumulus–oocyte complexes (COCs) and phenylhydrazonopyrazolone sulfonate 1 (PHPS1)-treated COCs. **(B)** Representative images of p-ERK1/2 and p-AKT in GVBD- and MII-stage oocytes in the control and PHPS1-exposed groups. 4′,6′-Diamidino-2-phenylindole was used to stain the nucleus. **(C)** Immunofluorescence images of Caspase-3 and phosphorylated NF-Kb in control and PHPS1-treated bovine day 8 blastocysts. Qualitative analysis showed that PHPS1 treatment enhances p-NF-kB nuclear localization and enhances Caspase-3 expression. All experiments were repeated thrice, and data are shown as mean ± SEM. NS, not significant; $^{*}P < 0.05$; $^{**}P < 0.01$; $^{***}P < 0.001$.

Molecular Modeling Studies for Predicting the Binding Mode Between ERα and SHP2

To support our experimental findings, protein–protein docking studies were performed to determine the probable binding mode between human ERα and SHP2 proteins. For this purpose, protein–protein/DNA docking was performed using an online webserver, HDOCK. The 50 models generated were downloaded, and the binding modes of all models were then assessed by cluster analysis in Discovery Studio. The cluster analysis revealed that three different binding modes could be possible for ERα and SHP2. The best model with the lowest docking energy score from each cluster was selected and subjected to 50 ns of MD simulation (**Supplementary Table 1**). The stability of the entire complex structure during the simulation times was analyzed by examining the root mean square deviation (RMSD) of the protein backbone atoms. It was observed that the RMSD values of model 1 was significantly lower than those of model 2 and model 3 (**Figure 5A**), implying that the structure of model 1 was more stable than the others during the simulation times. Moreover, the binding free energy calculations using the MM-GBSA algorithm was performed to further predict the binding affinity. It was found that model 1 showed the lowest binding free energy score (−115.2 kcal/mol) among the three models (model 2, −72.47 kcal/mol; model 3, −70.44 kcal/mol)] (**Supplementary Table 2**). The MM-GBSA calculations also provide the contribution of each amino acid in the binding. In model 1, the key residues involved in complex formation were Trp484, Leu130, Thr688, Thr131, and His308 of ERα and Asn336, Trp248,

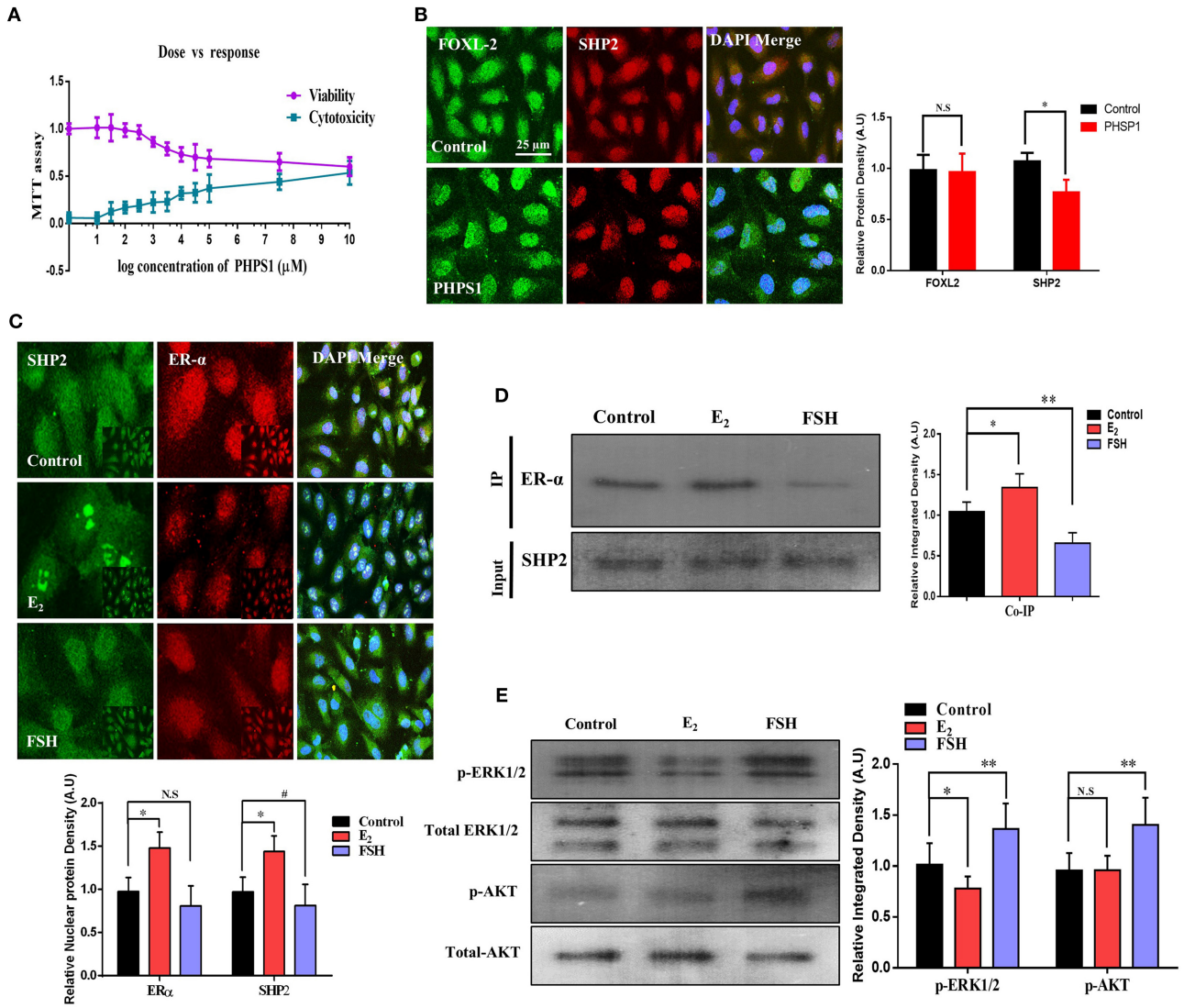

FIGURE 4 | Follicle-stimulating hormone (FSH) reduces the amount of SHP2/ERα complex in human granulosa cells (COV434). **(A)** To obtain the effective concentration of phenylhydrazonopyrazolone sulfonate 1 (PHPS1), an MTT assay was performed in COV434 cells, and 3 μM of PHPS1 was identified as the least effective concentration. **(B)** Immunofluorescence experiment of FoxL2 (green) and SHP2 (red) identified that SHP2 shows nuclear localization in COV434 cells, and PHPS1 had no effect on SHP2 nuclear localization. **(C)** FSH- and E_2-stimulated COV434 cells showed the differential localization of SHP2 and ERα after 24 h. Estradiol (E_2) significantly enhanced the nuclear localization of SHP2, while FSH significantly reduced its nuclear localization, compared to that in the control group. **(D)** Co-immunoprecipitation identified that SHP2 and ERα form a complex in COV434 cells, and E_2 or FSH treatments had a significant effect on this complex. **(E)** FSH augmented extracellular signal-regulated kinase (ERK) and AKT signaling in the COV434 cell line compared to that in the control and E_2-treated groups, wherein signaling was significantly reduced. The experiments were repeated thrice, and data are shown as mean ± SEM. NS, not significant; $^*P < 0.05$; $^{**}P < 0.01$; $^{***}P < 0.001$.

Gln506, Gln256, and Glu379 of SHP2 (**Figure 5B**). The per-residue contribution for ERα and SHP2 interaction was also calculated in model 2 and model 3 and is shown in **Supplementary Figures 2, 3**.

Furthermore, the binding mode for the ERα and SHP2 interaction was analyzed by calculating the average structure from the last 5 ns of the MD simulation trajectory for model 1, model 2, and model 3 (**Figure S3**). A detailed analysis revealed that, in model 1, the ERα and SHP2 complex was observed to form 24 hydrogen bonds, five electrostatic interactions, and five hydrophobic interactions (**Figures 5C,D**, **Supplementary Table 3**). The residues in chain A and chain B of ERα interact with the catalytic domain of SHP2 that has been reported to have a ligand-binding site ranging from 260 to 510 amino acids (Hellmuth et al., 2008). Model 1 displayed a higher number of molecular interactions in this region as compared to model 2 and model 3 (**Supplementary Table 3**). Finally, model 1 was selected as an ideal model for the ERα and SHP2 interaction

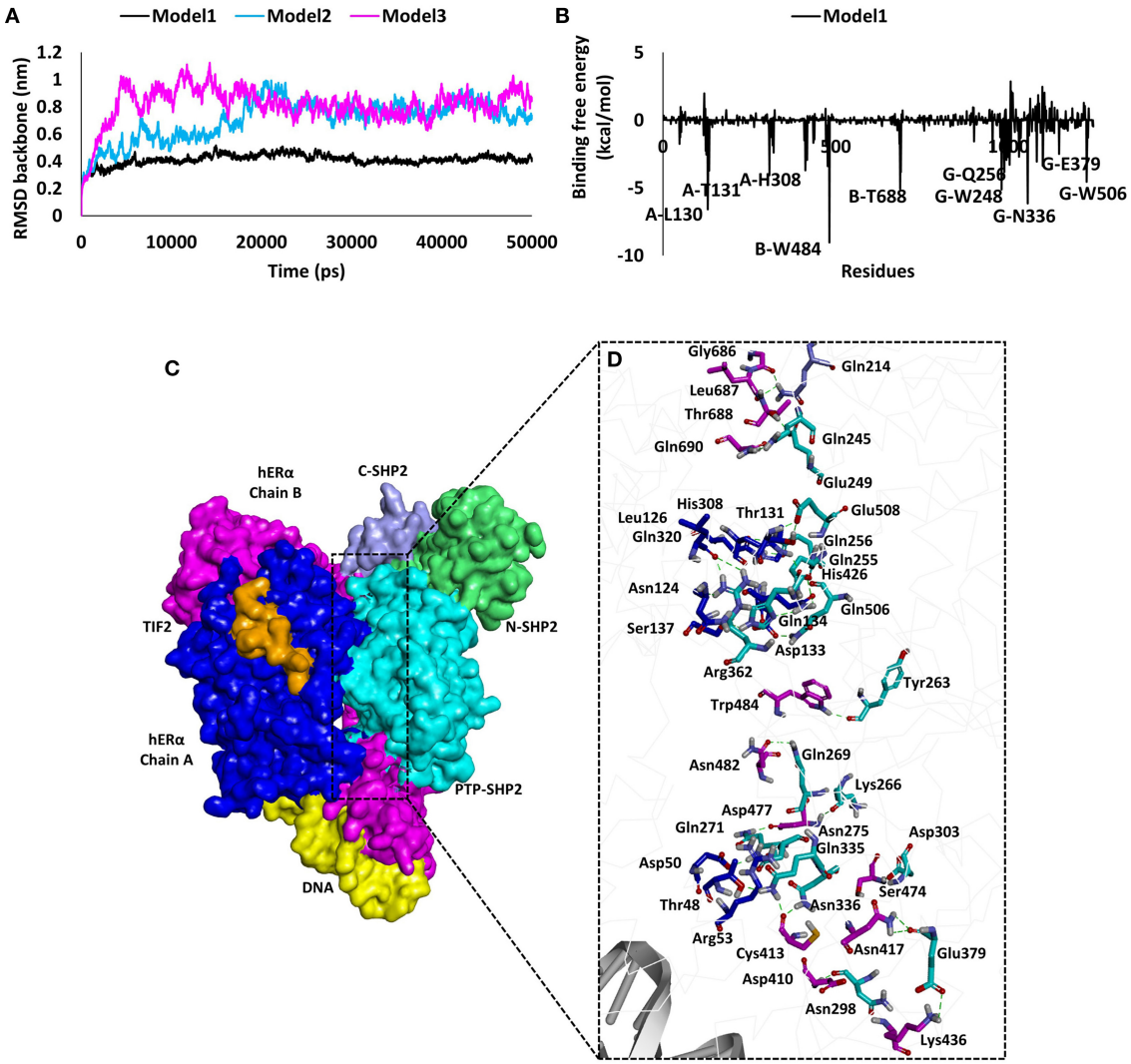

FIGURE 5 | Results of molecular modeling studies for predicting the binding mode between human ERα and SHP2. **(A)** The root mean square deviation values of the backbone atoms of ERα and SHP2 complexes during the molecular dynamics simulation times. **(B)** Decomposition of the molecular mechanics-generalized Born surface area energy for each amino acid of the binding surface from ERα and SHP2. The key interacting residues observed in ERα and SHP2 are highlighted. **(C)** Predicted binding mode of ERα and SHP2 complex in surface representation. ERα chain A is shown in blue, chain B in pink, TIF2 in orange, and DNA in yellow. The SHP2 protein domains are represented in purple (C-SHP2), green (N-SHP2), and cyan (PTP domain). **(D)** Enlarged view for the contact area between the two proteins. Interacting amino acids are shown in stick representation. The pink (chain B) and blue (chain A) sticks are from ERα, whereas the cyan (PTP domain) and purple (C-SHP2) sticks are from the SHP2 protein. The hydrogen bonds are shown as dashed green lines.

because of its stable RMSD throughout the simulation, the lowest binding free energy, and the highest number of interactions. Similar approaches for final model selection have also been used in previous studies (Selent et al., 2013; Ge et al., 2018; Wu et al., 2020).

SHP2 Knockdown Reduced ERα Transcription of *NPPC*/*NPR2* and Aromatase Activity of Human Granulosa Cells

To validate the direct link between the transcriptional activities of SHP2 and ERα in granulosa cells, we knocked down SHP2 *via* siRNA and verified it at the protein level ($^*P < 0.05$; **Figure 6A**). SHP2-knockdown cells were immunofluorescent-stained with ERα antibody, and the results showed a significant reduction in ERα nuclear localization (**Figure 6B**). E_2 and FSH have opposing regulatory effects on *NPPC*/*NPR2* genes in granulosa cells, and all of our above-mentioned results showed that SHP2 plays a role in the transcriptional activity of E_2 and in the intracellular signaling of FSH. To directly analyze SHP2 interactions with E_2 and FSH, the SHP2-knockdown granulosa cells were stimulated with E_2 and FSH, and the mRNA expression of *NPPC*/*NPR2* was quantified *via* RT-qPCR (**Figure 6C**) (Liu et al., 2017). E_2 application to granulosa cells had a significant effect on ERα transcriptional activity, while

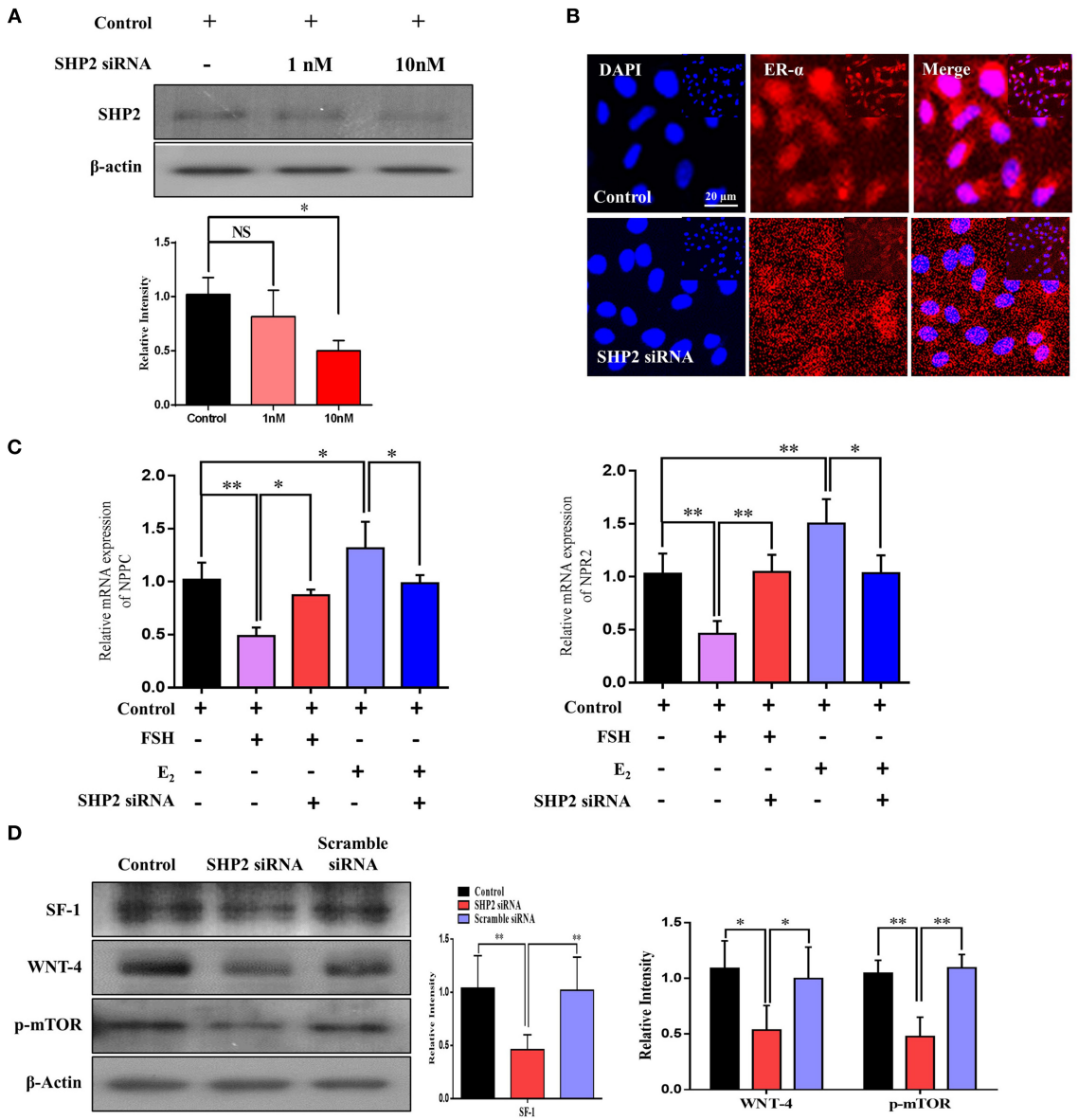

FIGURE 6 | Src-homology-2-containing phosphotyrosine phosphatase (SHP2) knockdown reduced estrogen receptor alpha (ERα) transcription of the NPPC and NPR2 genes and aromatase activity of granulosa cells. **(A)** SHP2 siRNA was applied to COV434 cell line, and SHP2 protein expression was analyzed *via* western blotting. **(B)** To check the localization of ERα, an immunofluorescence experiment was performed using SHP2-knockdown COV434 cells. The results suggest that ERα nuclear localization was significantly reduced with SHP2 knockdown. **(C)** NPPC/NPR2 mRNA expressions were analyzed in follicle-stimulating hormone- and E_2-stimulated SHP2-knockdown COV434 cell line. **(D)** To examine the effect of SHP2 knockdown on the functional activity of granulosa cells, the SF1, Wnt4, and p-mTOR proteins were analyzed *via* western blotting, and a significant reduction in all proteins was observed with SHP2 knockdown. β-Actin was used as the loading control for western blotting. Bands were quantified using ImageJ software, and the differences are represented by histograms. The experiments were repeated thrice, and data are shown as mean ± SEM. NS, not significant; $^{*}P < 0.05$; $^{**}P < 0.01$; $^{***}P < 0.001$.

SHP2 siRNA abrogated the E_2 stimulation of ERα and enhanced *NPPC*/*NPR2* mRNA expression (control *vs.* E_2 vs. E_2 + SHP2 siRNA; $^{*}P < 0.05$, $^{**}P < 0.01$). Furthermore, SHP2 knockdown interrupted FSH intracellular signaling-induced inhibition of *NPPC* and *NPR2* genes (control *vs.* FSH *vs.* FSH + SHP2 siRNA; $^{*}P < 0.05$, $^{**}P < 0.01$). Moreover, we examined the effect of SHP2 knockdown on the functional activities of granulosa cells, taking into account the potential interference with FSH signaling-mediated transcriptional factor activation. We found that SHP2 knockdown markedly reduced the steroidogenic factor-1 (SF1 encoded by the *NR5A1* gene) and β-catenin pathway protein wingless-type MMTV integration site family member 4 (Wnt4) proteins (**Figure 6D**) (control *vs.* siRNA *vs.* scramble siRNA; $^{*}P < 0.05$, $^{**}P < 0.01$). SF1 and Wnt4 are the

downstream transcriptional factors of FSH signaling that regulate the aromatase activity of granulosa cells (Parakh et al., 2006; Pelusi et al., 2008; Boyer et al., 2010). FSH was also found to activate the mammalian target of rapamycin complex 1 (mTOR), which is necessary for the transcription of several proteins related to follicular development (Alam et al., 2004). Collectively, these results suggest that SHP2 plays a dual role in the granulosa and cumulus cells of oocytes. SHP2 interacts with ERα for its transcriptional activity and transduces FSH signaling for meiotic resumption and maturation.

DISCUSSION

In this study, we identified a novel relationship between SHP2 and ERα in bovine cumulus and human granulosa cells. ERα, a transcriptional regulator of *NPPC* and *NPR2* genes in granulosa cells, interacts with SHP2 for its transcriptional activity. The SHP2/ERα complex is highly expressed in the cumulus cells of immature oocytes (GV stage) but is significantly reduced in the cumulus cells of mature oocytes (MII stage). Human immortalized granulosa cells (COV434) also express the SHP2/ERα complex, which shows a different expression with FSH or E_2 supplementation. Furthermore, SHP2 knockdown reduced the ERα-transcribed *NPPC* and *NPR2* genes in granulosa cells, but PHPS1-mediated SHP2 inhibition had no significant effect on the SHP2/ERα complex.

Intercommunication between the oocyte and its surrounding granulosa cells is critical for the production of a mature oocyte capable of fertilization, as these cells provide 85% of the nutrients, including growth factors, amino acids, and other energy sources, to the oocyte (Albertini et al., 2001; Eppig, 2001; Sugiura et al., 2005). Granulosa cells also play a vital role in oocyte meiotic arrest and resumption, two critical phenomena that determine the entire reproductive potential of females (Zhang et al., 2010). During the meiotic arrest or pre-ovulatory stage of ovarian follicles, granulosa cells maintain oocyte meiotic arrest by expressing NPPC and its receptor, NPR2. Several studies have recognized that the NPPC/NPR2 system is also essential for the morphological and genetic health of an oocyte (Zhang et al., 2015; Celik et al., 2019). A previous study stated that ERα is the upstream regulator of NPPC/NPR2 governing

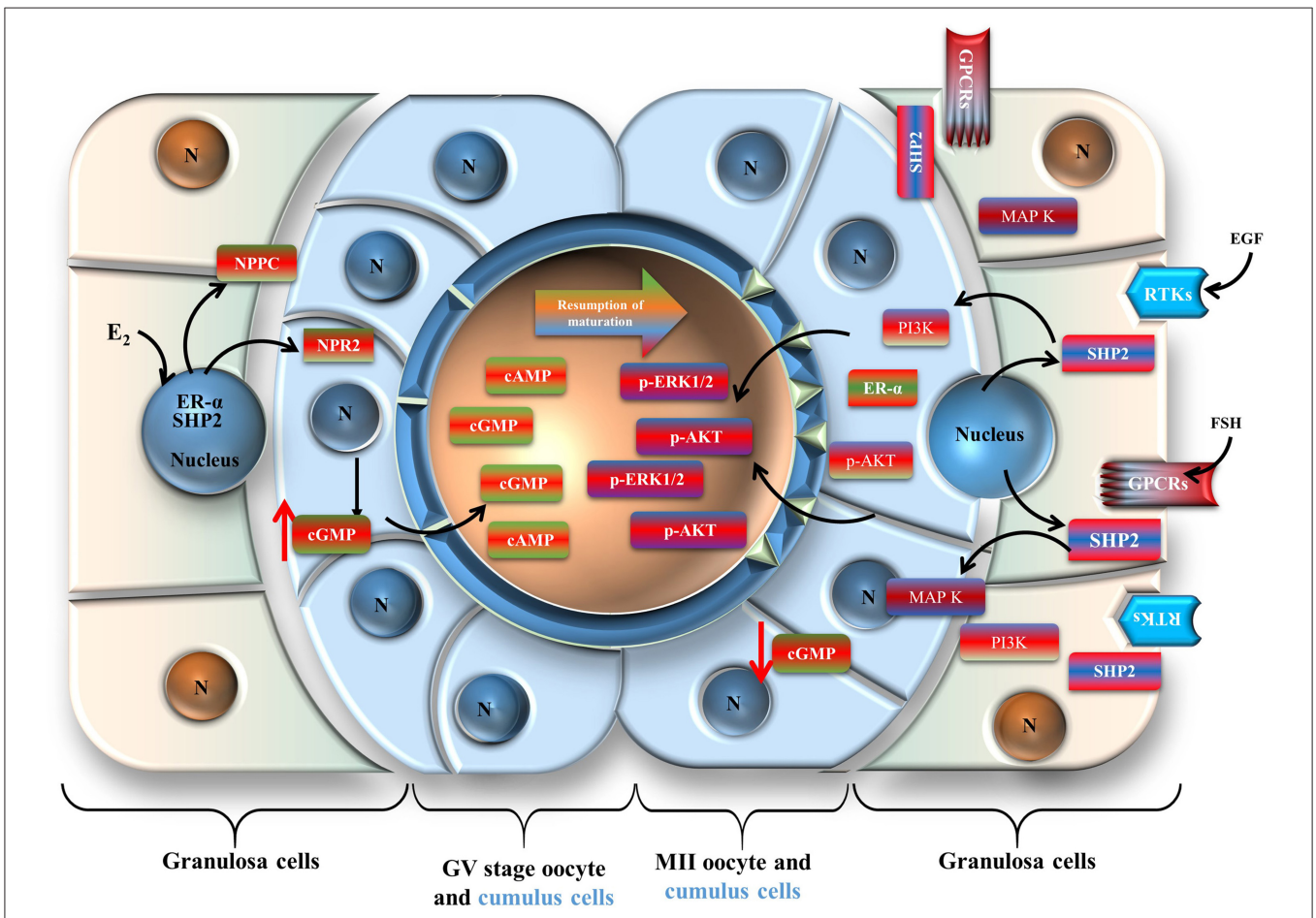

FIGURE 7 | Schematic presentation of the Src-homology-2-containing phosphotyrosine phosphatase regulation of oocyte meiotic maturation. Cumulus cells are shown in light blue, and granulosa cells are shown in reddish green.

oocyte meiotic arrest in granulosa cells (Liu et al., 2017). ERα is a ligand-activated transcription factor, and we found that it requires nucleus-localized SHP2 for the regulation of *NPPC* and *NPR2* genes in cumulus and granulosa cells. A previous study detected the ERα and SHP2 complex in breast tissues and confirmed its cytoplasmic localization and involvement in triggering MAP kinases and AKT signaling (Li et al., 2014). In our study, the co-immunoprecipitation analysis revealed that ERα forms a physiological complex with SHP2 in the cumulus cells of GV-stage oocytes, and this complex becomes significantly reduced with the progression of oocyte meiotic maturation *in vitro*. Furthermore, to determine the localization of ERα/SHP2 complex, we found that the cumulus cells of immature (GV) oocytes showed nuclear localization of the ERα/SHP2 complex, but those of mature (MII) oocytes showed cytoplasmic localization of both proteins. The nucleus-localized SHP2's role in ERα transcriptional activity has been previously identified in uterine tissues, but it dephosphorylates ERα and recruits it to the target gene without making a complex (Ran et al., 2017). We found a physiological complex of SHP2/ERα in granulosa cells, and the knockdown of SHP2 highly affected ERα-targeted *NPPC* and *NPR2* genes. Additionally, cultured granulosa cells (COV434) express the SHP2/ERα complex, and the FSH and E_2 stimulation of granulosa cells has significant effects on this complex.

To analyze the probable structure of the SHP2/ERα complex, we applied a series of computer modeling methods, including protein–protein molecular docking, molecular dynamic simulation, and MM-GBSA calculations, to identify the binding modes of ERα and SHP2. Similar approaches for protein–protein interaction or complex generation have been used in previous studies (Selent et al., 2013; Ge et al., 2018; Wu et al., 2020). Initially, 50 models of the SHP2/ERα complex were generated *via* the online webserver HDOCK. Subsequently, the cluster analysis in Discovery Studio revealed that three different binding modes could be possible for ERα and SHP2. We further applied MD simulations to select the best model for the interaction between SHP2 and ERα. Based on the RMSD values, binding free energies, and key residue interaction numbers, model 1 was selected as the most probable candidate for the SHP2/ERα complex with DNA. In our wet lab data, we found that PHPS1, a site-directed inhibitor of SHP2, has no substantial effects on SHP2 nuclear localization and its involvement with ERα transcriptional activity (Hellmuth et al., 2008). After observing the key residues that are involved in ERα (Leu130, Thr131, His308, Trp484, and Thr688) and SHP2 (Trp248, Gln256, Asn336, Glu379, and Gln506) complex formation, we found that PHPS1 binds to SHP2 in a similar range (Hellmuth et al., 2008). Therefore, PHPS1 is unable to bind with SHP2 and inhibit its nuclear localization in cumulus and granulosa cells.

SHP2 not only interacts with ERα to regulate meiotic arrest, but it also transduces FSH receptor signaling in granulosa cells. SHP2 is a classic cytoplasmic protein, is a core component of growth factor and cytokine signal transduction, and is essential for oocyte maturation and embryo development (Saxton et al., 1997; Idrees et al., 2019b; Kim et al., 2019). SHP2 is mostly found in two states, an inactive or auto-inhibition state and an active state. During the inactive or auto-inhibition state, the N-terminal SH2 domain blocks the PTP domain, while in the active state, the SH2 domain binds to specific phosphotyrosine sites on the adaptor proteins of receptors (Hof et al., 1998; Neel et al., 2003). Active cytoplasmic SHP2 interacts with the transmembrane adaptor proteins of RTKs and GPCRs and activates MAP kinases, cell cycle controller p34 (CDC2), and PI3K/AKT signaling, which are involved in oocyte GVBD and meiotic progression (Wehrend and Meinecke, 2001; Lin et al., 2009). SHP2 plays a critical role in FSH receptor-induced ERK1/2 and PI3K/AKT signaling in granulosa cells (Donaubauer et al., 2016). In our study, we found significantly enhanced SHP2 cytoplasmic localization during *in vitro* oocyte maturation or with the cells (cumulus or granulosa) exposed to FSH. It may be possible that, during LH surge, SHP2 move toward the cytoplasm and transduce FSH signaling in granulosa cells (**Figure 7**), but this mechanism of SHP2 needs further verification in *in vivo* animal models. Furthermore, SHP2 knockdown significantly affected FSHR signaling, targeting downstream transcriptional factors such as SF1, Wnt4, and p-mTOR, which regulate the aromatase activity of granulosa cells and play a key role in follicular development (Alam et al., 2004; Parakh et al., 2006; Pelusi et al., 2008; Boyer et al., 2010).

CONCLUSION

Taken together, our findings clearly demonstrate that nuclear SHP2 is involved in ERα transcriptional activity for the promotion of *NPPC* and *NPR2* genes related to oocyte meiotic arrest. Furthermore, FSH or growth factors restrict SHP2 interaction with ERα by promoting its export from the nucleus to transduce RTKs or GPCR-dependent signaling in oocyte somatic cells during meiotic resumption. These findings could contribute to opening new avenues of research to understand the process of oocyte meiosis in the mammalian ovary.

DATA AVAILABILITY STATEMENT

The original contributions generated for the study are included in the article/supplementary material, further inquiries can be directed to the corresponding author/s.

ETHICS STATEMENT

The animal study was reviewed and approved by All experiments, including surgical procedures, were approved by the Gyeongsang National University Institute of Animal Care Committee (GNU-130902-A0059).

AUTHOR CONTRIBUTIONS

MI designed the research and analyzed the data. MI and VK performed the research, M-DJ provided reagents and helped in the experiments. MI, VK, and NA wrote the paper. K-WL and I-KK reviewed the paper and supervised the study. All authors contributed to the article and approved the submitted version.

FUNDING

This work was partly supported by the National Research Foundation of Korea (NRF), a grant funded by the Korean government (MSIT; Grant No. 2020R1A2C2006614), Korea Institute of Planning, a scholarship from the BK21 Four Program, the Bio & Medical Technology Development Program of the National Research Foundation (NRF), and fund granted by the Korean government (MSIT) (Grant No. NRF-2018M3A9A70-57263).

ACKNOWLEDGMENTS

We thank Prof. Jeehyeon Bae (Chung-Ang University, Seoul, Republic of Korea) for giving us the COV434 cell line.

SUPPLEMENTARY MATERIAL

The Supplementary Material for this article can be found online at: https://www.frontiersin.org/articles/10.3389/fcell.2020.611503/full#supplementary-material

REFERENCES

Alam, H., Maizels, E. T., Park, Y., Ghaey, S., Feiger, Z. J., Chandel, N. S., et al. (2004). Follicle-stimulating hormone activation of hypoxia-inducible factor-1 by the phosphatidylinositol 3-kinase/AKT/Ras homolog enriched in brain (Rheb)/mammalian target of rapamycin (mTOR) pathway is necessary for induction of select protein markers of follicular differentiation. *J. Biol. Chem.* 279, 19431–19440. doi: 10.1074/jbc.M401235200

Albertini, D. F., Combelles, C. M., Benecchi, E., and Carabatsos, M. J. (2001). Cellular basis for paracrine regulation of ovarian follicle development. *Reproduction* 121, 647–653. doi: 10.1530/rep.0.1210647

Andrade, G. M., da Silveira, J. C., Perrini, C., Del Collado, M., Gebremedhn, S., Tesfaye, D., et al. (2017). The role of the PI3K-Akt signaling pathway in the developmental competence of bovine oocytes. *PLoS ONE* 12:e0185045. doi: 10.1371/journal.pone.0185045

Baufeld, A., and Vanselow, J. (2013). Increasing cell plating density mimics an early post-LH stage in cultured bovine granulosa cells. *Cell Tissue Res.* 354, 869–880. doi: 10.1007/s00441-013-1712-9

Boyer, A., Lapointe, E., Zheng, X., Cowan, R. G., Li, H., Quirk, S. M., et al. (2010). WNT4 is required for normal ovarian follicle development and female fertility. *FASEB J.* 24, 3010–3025. doi: 10.1096/fj.09-145789

Bussi, G., Donadio, D., and Parrinello, M. (2007). Canonical sampling through velocity rescaling. *J. Chem. Phys.* 126:014101. doi: 10.1063/1.2408420

Casarini, L., and Crepieux, P. (2019). Molecular mechanisms of action of FSH. *Front. Endocrinol.* 10, 305. doi: 10.3389/fendo.2019.00305

Celik, O., Celik, N., Ugur, K., Hatirnaz, S., Celik, S., Muderris, I. I., et al. (2019). Nppc/Npr2/cGMP signaling cascade maintains oocyte developmental capacity. *Cell. Mol. Biol.* 65, 83–89.

Chughtai, N., Schimchowitsch, S., Lebrun, J. J., and Ali, S. (2002). Prolactin induces SHP-2 association with Stat5, nuclear translocation, and binding to the beta-casein gene promoter in mammary cells. *J. Biol. Chem.* 277, 31107–31114. doi: 10.1074/jbc.M200156200

Dance, M., Montagner, A., Salles, J. P., Yart, A., and Raynal, P. (2008). The molecular functions of Shp2 in the ras/mitogen-activated protein kinase (ERK1/2) pathway. *Cell. Signal* 20, 453–459. doi: 10.1016/j.cellsig.2007.10.002

Darden, T., York, D., and Pedersen, L. (1993). Particle mesh Ewald: an N log (N) method for Ewald sums in large systems. *J. Chem. Phys.* 98, 10089–10092.

Donaubauer, E. M., Law, N. C., and Hunzicker-Dunn, M. E. (2016). Follicle-stimulating hormone (FSH)-dependent regulation of extracellular regulated kinase (ERK) phosphorylation by the mitogen-activated protein (MAP) kinase phosphatase MKP3. *J. Biol. Chem.* 291, 19701–19712. doi: 10.1074/jbc.M116.733972

El-Hayek, S., Demeestere, I., and Clarke, H. J. (2014). Follicle-stimulating hormone regulates expression and activity of epidermal growth factor receptor in the murine ovarian follicle. *Proc. Natl. Acad. Sci. U.S.A.* 111, 16778–16783. doi: 10.1073/pnas.1414648111

Eppig, J. J. (2001). Oocyte control of ovarian follicular development and function in mammals. *Reproduction* 122, 829–838. doi: 10.1530/rep.0.1220829

Eppig, J. J., and Handel, M. A. (2012). Origins of granulosa cells clarified and complexified by waves. *Biol. Reprod.* 86:34. doi: 10.1095/biolreprod.111.096651

Fan, H. Y., Liu, Z., Shimada, M., Sterneck, E., Johnson, P. F., Hedrick, S. M., et al. (2009). MAPK3/1 (ERK1/2) in ovarian granulosa cells are essential for female fertility. *Science* 324, 938–941. doi: 10.1126/science.1171396

Fan, H. Y., and Sun, Q. Y. (2004). Involvement of mitogen-activated protein kinase cascade during oocyte maturation and fertilization in mammals. *Biol. Reprod.* 70, 535–547. doi: 10.1095/biolreprod.103.022830

Furcht, C. M., Buonato, J. M., Skuli, N., Mathew, L. K., Munoz Rojas, A. R., Simon, M. C., et al. (2014). Multivariate signaling regulation by SHP2 differentially controls proliferation and therapeutic response in glioma cells. *J. Cell Sci.* 127 (Pt. 16), 3555–3567. doi: 10.1242/jcs.150862

Ge, X., Mandava, C. S., Lind, C., Aqvist, J., and Sanyal, S. (2018). Complementary charge-based interaction between the ribosomal-stalk protein L7/12 and IF2 is the key to rapid subunit association. *Proc. Natl. Acad. Sci. U.S.A.* 115, 4649–4654. doi: 10.1073/pnas.1802001115

Georges, A., Auguste, A., Bessiere, L., Vanet, A., Todeschini, A. L., and Veitia, R. A. (2014). FOXL2: a central transcription factor of the ovary. *J. Mol. Endocrinol.* 52, R17–33. doi: 10.1530/JME-13-0159

Glidewell-Kenney, C., Weiss, J., Hurley, L. A., Levine, J. E., and Jameson, J. L. (2008). Estrogen receptor alpha signaling pathways differentially regulate gonadotropin subunit gene expression and serum follicle-stimulating hormone in the female mouse. *Endocrinology* 149, 4168–4176. doi: 10.1210/en.2007-1807

Guo, J., Zhang, T., Guo, Y., Sun, T., Li, H., Zhang, X., et al. (2018). Oocyte stage-specific effects of MTOR determine granulosa cell fate and oocyte quality in mice. *Proc. Natl. Acad. Sci. U.S.A.* 115, E5326–E5333. doi: 10.1073/pnas.1800352115

Hatch, K. R., and Capco, D. G. (2001). Colocalization of CaM KII and MAP kinase on architectural elements of the mouse egg: potentiation of MAP kinase activity by CaM KII. *Mol. Reprod. Dev.* 58, 69–77. doi: 10.1002/1098-2795(200101)58:1<69::AID-MRD10>3.0.CO;2-O

Hellmuth, K., Grosskopf, S., Lum, C. T., Wurtele, M., Roder, N., von Kries, J. P., et al. (2008). Specific inhibitors of the protein tyrosine phosphatase Shp2 identified by high-throughput docking. *Proc. Natl. Acad. Sci. U.S.A.* 105, 7275–7280. doi: 10.1073/pnas.0710468105

Hess, B., Bekker, H., Berendsen, H. J., and Fraaije, J. G. (1997). LINCS: a linear constraint solver for molecular simulations. *J. Comput. Chem.* 18, 1463–1472.

Hof, P., Pluskey, S., Dhe-Paganon, S., Eck, M. J., and Shoelson, S. E. (1998). Crystal structure of the tyrosine phosphatase SHP-2. *Cell* 92, 441–450. doi: 10.1016/s0092-8674(00)80938-1

Hu, X., Tang, Z., Li, Y., Liu, W., Zhang, S., Wang, B., et al. (2015). Deletion of the tyrosine phosphatase Shp2 in sertoli cells causes infertility in mice. *Sci. Rep.* 5:12982. doi: 10.1038/srep12982

Hu, Z., Li, J., Gao, Q., Wei, S., and Yang, B. (2017). SHP2 overexpression enhances the invasion and metastasis of ovarian cancer *in vitro* and *in vivo*. *Onco. Targets. Ther.* 10, 3881–3891. doi: 10.2147/OTT.S138833

Huang, W., Peng, Y., Kiselar, J., Zhao, X., Albaqami, A., Mendez, D., et al. (2018). Multidomain architecture of estrogen receptor reveals interfacial cross-talk between its DNA-binding and ligand-binding domains. *Nat. Commun.* 9:3520. doi: 10.1038/s41467-018-06034-2

Humphrey, W., Dalke, A., and Schulten, K. (1996). VMD: visual molecular dynamics. *J. Mol. Graph* 14, 27–38. doi: 10.1016/0263-7855(96)00018-5

Idrees, M., Oh, S. H., Muhammad, T., El-Sheikh, M., Song, S. H., Lee, K. L., et al. (2020). Growth factors, and cytokines; understanding the role of tyrosine phosphatase SHP2 in gametogenesis and early embryo development. *Cells* 9:1798. doi: 10.3390/cells9081798

Idrees, M., Xu, L., El Sheikh, M., Sidrat, T., Song, S. H., Joo, M. D., et al. (2019a). The PPARdelta agonist GW501516 improves lipolytic/lipogenic balance

through CPT1 and PEPCK during the development of pre-implantation bovine embryos. *Int. J. Mol. Sci.* 20:6066. doi: 10.3390/ijms20236066

Idrees, M., Xu, L., Song, S. H., Joo, M. D., Lee, K. L., Muhammad, T., et al. (2019b). PTPN11 (SHP2) is indispensable for growth factors and cytokine signal transduction during bovine oocyte maturation and blastocyst development. *Cells* 8:1272. doi: 10.3390/cells8101272

Jakob, S., Schroeder, P., Lukosz, M., Buchner, N., Spyridopoulos, I., Altschmied, J., et al. (2008). Nuclear protein tyrosine phosphatase Shp-2 is one important negative regulator of nuclear export of telomerase reverse transcriptase. *J. Biol. Chem.* 283, 33155–33161. doi: 10.1074/jbc.M805138200

Jin, H., Won, M., Park, S. E., Lee, S., Park, M., and Bae, J. (2016). FOXL2 is an essential activator of SF-1-induced transcriptional regulation of anti-mullerian hormone in human granulosa cells. *PLoS ONE* 11:e0159112. doi: 10.1371/journal.pone.0159112

Katchalski-Katzir, E., Shariv, I., Eisenstein, M., Friesem, A. A., Aflalo, C., and Vakser, I. A. (1992). Molecular surface recognition: determination of geometric fit between proteins and their ligands by correlation techniques. *Proc. Natl. Acad. Sci. U.S.A.* 89, 2195–2199. doi: 10.1073/pnas.89.6.2195

Kim, K. H., Kim, E. Y., Ko, J. J., and Lee, K. A. (2019). Gas6 is a reciprocal regulator of mitophagy during mammalian oocyte maturation. *Sci. Rep.* 9:10343. doi: 10.1038/s41598-019-46459-3

Kiyosu, C., Tsuji, T., Yamada, K., Kajita, S., and Kunieda, T. (2012). NPPC/NPR2 signaling is essential for oocyte meiotic arrest and cumulus oophorus formation during follicular development in the mouse ovary. *Reproduction* 144, 187–193. doi: 10.1530/REP-12-0050

LaRochelle, J. R., Fodor, M., Vemulapalli, V., Mohseni, M., Wang, P., Stams, T., et al. (2018). Structural reorganization of SHP2 by oncogenic mutations and implications for oncoprotein resistance to allosteric inhibition. *Nat. Commun.* 9:4508. doi: 10.1038/s41467-018-06823-9

Levin, E. R. (2009). Plasma membrane estrogen receptors. *Trends Endocrinol. Metab.* 20, 477–482. doi: 10.1016/j.tem.2009.06.009

Li, J., Kang, Y., Wei, L., Liu, W., Tian, Y., Chen, B., et al. (2014). Tyrosine phosphatase Shp2 mediates the estrogen biological action in breast cancer via interaction with the estrogen extranuclear receptor. *PLoS ONE* 9:e102847. doi: 10.1371/journal.pone.0102847

Lin, Y. H., Hwang, J. L., Seow, K. M., Huang, L. W., Chen, H. J., and Tzeng, C. R. (2009). Effects of growth factors and granulosa cell co-culture on *in-vitro* maturation of oocytes. *Reprod. Biomed. Online* 19, 165–170. doi: 10.1016/s1472-6483(10)60068-5

Lindorff-Larsen, K., Piana, S., Palmo, K., Maragakis, P., Klepeis, J. L., Dror, R. O., et al. (2010). Improved side-chain torsion potentials for the Amber ff99SB protein force field. *Proteins* 78, 1950–1958. doi: 10.1002/prot.22711

Liu, W., Xin, Q., Wang, X., Wang, S., Wang, H., Zhang, W., et al. (2017). Estrogen receptors in granulosa cells govern meiotic resumption of pre-ovulatory oocytes in mammals. *Cell Death Dis.* 8:e2662. doi: 10.1038/cddis.2017.8

Lubahn, D. B., Moyer, J. S., Golding, T. S., Couse, J. F., Korach, K. S., and Smithies, O. (1993). Alteration of reproductive function but not prenatal sexual development after insertional disruption of the mouse estrogen receptor gene. *Proc. Natl. Acad. Sci. U.S.A.* 90, 11162–11166. doi: 10.1073/pnas.90.23.11162

Neel, B. G., Gu, H., and Pao, L. (2003). The 'Shp'ing news: SH2 domain-containing tyrosine phosphatases in cell signaling. *Trends Biochem. Sci.* 28, 284–293. doi: 10.1016/S0968-0004(03)00091-4

Parakh, T. N., Hernandez, J. A., Grammer, J. C., Weck, J., Hunzicker-Dunn, M., Zeleznik, A. J., et al. (2006). Follicle-stimulating hormone/cAMP regulation of aromatase gene expression requires beta-catenin. *Proc. Natl. Acad. Sci. U.S.A.* 103, 12435–12440. doi: 10.1073/pnas.0603006103

Parrinello, M., and Rahman, A. (1981). Polymorphic transitions in single crystals: a new molecular dynamics method. *J. Appl. Phys.* 52, 7182–7190.

Pelusi, C., Ikeda, Y., Zubair, M., and Parker, K. L. (2008). Impaired follicle development and infertility in female mice lacking steroidogenic factor 1 in ovarian granulosa cells. *Biol. Reprod.* 79, 1074–1083. doi: 10.1095/biolreprod.108.069435

Pronk, S., Pall, S., Schulz, R., Larsson, P., Bjelkmar, P., Apostolov, R., et al. (2013). GROMACS 4.5: a high-throughput and highly parallel open source molecular simulation toolkit. *Bioinformatics* 29, 845–854. doi: 10.1093/bioinformatics/btt055

Qu, C. K. (2002). Role of the SHP-2 tyrosine phosphatase in cytokine-induced signaling and cellular response. *Biochim. Biophys. Acta* 1592, 297–301. doi: 10.1016/s0167-4889(02)00322-1

Ran, H., Kong, S., Zhang, S., Cheng, J., Zhou, C., He, B., et al. (2017). Nuclear Shp2 directs normal embryo implantation via facilitating the ERalpha tyrosine phosphorylation by the Src kinase. *Proc. Natl. Acad. Sci. U.S.A.* 114, 4816–4821. doi: 10.1073/pnas.1700978114

Richard, S., and Baltz, J. M. (2014). Prophase I arrest of mouse oocytes mediated by natriuretic peptide precursor C requires GJA1 (connexin-43) and GJA4 (connexin-37) gap junctions in the antral follicle and cumulus-oocyte complex. *Biol. Reprod.* 90:137. doi: 10.1095/biolreprod.114.118505

Saxton, T. M., Henkemeyer, M., Gasca, S., Shen, R., Rossi, D. J., Shalaby, F., et al. (1997). Abnormal mesoderm patterning in mouse embryos mutant for the SH2 tyrosine phosphatase Shp-2. *EMBO J.* 16, 2352–2364. doi: 10.1093/emboj/16.9.2352

Selent, J., Kaczor, A. A., Guixa-Gonzalez, R., Carrio, P., Pastor, M., and Obiol-Pardo, C. (2013). Rational design of the survivin/CDK4 complex by combining protein-protein docking and molecular dynamics simulations. *J. Mol. Model* 19, 1507–1514. doi: 10.1007/s00894-012-1705-8

Simmet, K., Zakhartchenko, V., Philippou-Massier, J., Blum, H., Klymiuk, N., and Wolf, E. (2018). OCT4/POU5F1 is required for NANOG expression in bovine blastocysts. *Proc. Natl. Acad. Sci. U.S.A.* 115, 2770–2775. doi: 10.1073/pnas.1718833115

Sugiura, K., Pendola, F. L., and Eppig, J. J. (2005). Oocyte control of metabolic cooperativity between oocytes and companion granulosa cells: energy metabolism. *Dev. Biol.* 279, 20–30. doi: 10.1016/j.ydbio.2004.11.027

Tsuji, T., Kiyosu, C., Akiyama, K., and Kunieda, T. (2012). CNP/NPR2 signaling maintains oocyte meiotic arrest in early antral follicles and is suppressed by EGFR-mediated signaling in preovulatory follicles. *Mol. Reprod. Dev.* 79, 795–802. doi: 10.1002/mrd.22114

Valentini, E., Kikhney, A. G., Previtali, G., Jeffries, C. M., and Svergun, D. I. (2015). SASBDB, a repository for biological small-angle scattering data. *Nucleic Acids Res.* 43 (Database issue), D357–363. doi: 10.1093/nar/gku1047

Wang, Y., Kong, N., Li, N., Hao, X., Wei, K., Xiang, X., et al. (2013). Epidermal growth factor receptor signaling-dependent calcium elevation in cumulus cells is required for NPR2 inhibition and meiotic resumption in mouse oocytes. *Endocrinology* 154, 3401–3409. doi: 10.1210/en.2013-1133

Wehrend, A., and Meinecke, B. (2001). Kinetics of meiotic progression, M-phase promoting factor (MPF) and mitogen-activated protein kinase (MAP kinase) activities during *in vitro* maturation of porcine and bovine oocytes: species specific differences in the length of the meiotic stages. *Anim. Reprod. Sci.* 66, 175–184. doi: 10.1016/s0378-4320(01)00094-x

Weng, G., Wang, E., Wang, Z., Liu, H., Zhu, F., Li, D., et al. (2019). HawkDock: a web server to predict and analyze the protein-protein complex based on computational docking and MM/GBSA. *Nucleic Acids Res.* 47, W322–W330. doi: 10.1093/nar/gkz397

Wigglesworth, K., Lee, K. B., O'Brien, M. J., Peng, J., Matzuk, M. M., and Eppig, J. J. (2013). Bidirectional communication between oocytes and ovarian follicular somatic cells is required for meiotic arrest of mammalian oocytes. *Proc. Natl. Acad. Sci. U.S.A.* 110, E3723–3729. doi: 10.1073/pnas.1314829110

Wu, H., Wang, Y., Zhang, Y., Xu, F., Chen, J., Duan, L., et al. (2020). Breaking the vicious loop between inflammation, oxidative stress and coagulation, a novel anti-thrombus insight of nattokinase by inhibiting LPS-induced inflammation and oxidative stress. *Redox Biol.* 32:101500. doi: 10.1016/j.redox.2020.101500

Yan, Y., Tao, H., He, J., and Huang, S. Y. (2020). The HDOCK server for integrated protein-protein docking. *Nat. Protoc.* 15, 1829–1852. doi: 10.1038/s41596-020-0312-x

Yan, Y., Wen, Z., Wang, X., and Huang, S. Y. (2017). Addressing recent docking challenges: a hybrid strategy to integrate template-based and free protein-protein docking. *Proteins* 85, 497–512. doi: 10.1002/prot.25234

Yang, W., Klaman, L. D., Chen, B., Araki, T., Harada, H., Thomas, S. M., et al. (2006). An Shp2/SFK/Ras/Erk signaling pathway controls trophoblast stem cell survival. *Dev. Cell* 10, 317–327. doi: 10.1016/j.devcel.2006.01.002

Zhang, H., Vollmer, M., De Geyter, M., Litzistorf, Y., Ladewig, A., Durrenberger, M., et al. (2000). Characterization of an immortalized human granulosa

cell line (COV434). *Mol. Hum. Reprod.* 6, 146–153. doi: 10.1093/molehr/6.2.146

Zhang, J., Wei, Q., Cai, J., Zhao, X., and Ma, B. (2015). Effect of C-type natriuretic peptide on maturation and developmental competence of goat oocytes matured *in vitro*. *PLoS ONE* 10:e0132318. doi: 10.1371/journal.pone.0132318

Zhang, M., Su, Y. Q., Sugiura, K., Xia, G., and Eppig, J. J. (2010). Granulosa cell ligand NPPC and its receptor NPR2 maintain meiotic arrest in mouse oocytes. *Science* 330, 366–369. doi: 10.1126/science.1193573

Zhang, S. Q., Yang, W., Kontaridis, M. I., Bivona, T. G., Wen, G., Araki, T., et al. (2004). Shp2 regulates SRC family kinase activity and Ras/Erk activation by controlling Csk recruitment. *Mol. Cell* 13, 341–355. doi: 10.1016/s1097-2765(04)00050-4

Conflict of Interest: I-KK was employed by company The King Kong Corp. Ltd.

The remaining authors declare that the research was conducted in the absence of any commercial or financial relationships that could be construed as a potential conflict of interest.

frontiers in Cell and Developmental Biology

ORIGINAL RESEARCH
published: 19 February 2021
doi: 10.3389/fcell.2021.623852

Treatment of *in vitro*-Matured Bovine Oocytes With Tauroursodeoxycholic Acid Modulates the Oxidative Stress Signaling Pathway

Elisa Mariano Pioltine[1], Camila Bortoliero Costa[1], Laís Barbosa Latorraca[2], Fernanda Fagali Franchi[1], Priscila Helena dos Santos[1], Gisele Zoccal Mingoti[3], Fabíola Freitas de Paula-Lopes[2] and Marcelo Fábio Gouveia Nogueira[1,4]**

[1] Multi-user Laboratory of Phytomedicines Pharmacology, and Biotechnology (PhitoPharmaTec), Institute of Biosciences, Department of Pharmacology, São Paulo State University, Botucatu, Brazil, [2] Department of Biological Sciences, Federal University of São Paulo, Diadema, Brazil, [3] School of Veterinary Medicine, Department of Production and Animal Health, São Paulo State University, Araçatuba, Brazil, [4] Laboratory of Embryonic Micromanipulation, School of Sciences and Languages, Department of Biological Sciences, São Paulo State University, Assis, Brazil

OPEN ACCESS

Edited by:
Ana Josefa Soler, University of Castilla-La Mancha, Spain

Reviewed by:
Satoshi Kishigami, University of Yamanashi, Japan
Tetsuya Tani, Kindai University, Japan

***Correspondence:**
Elisa Mariano Pioltine
elisapioltine@hotmail.com
Marcelo Fábio Gouveia Nogueira
marcelo.fabio@unesp.br

Specialty section:
This article was submitted to Cell Growth and Division, a section of the journal Frontiers in Cell and Developmental Biology

Received: *30 October 2020*
Accepted: *01 February 2021*
Published: *19 February 2021*

Citation:
Pioltine EM, Costa CB, Barbosa Latorraca L, Franchi FF, dos Santos PH, Mingoti GZ, Paula-Lopes FF and Nogueira MFG (2021) Treatment of in vitro-Matured Bovine Oocytes With Tauroursodeoxycholic Acid Modulates the Oxidative Stress Signaling Pathway. Front. Cell Dev. Biol. 9:623852. doi: 10.3389/fcell.2021.623852

In several species, oocyte and embryo competence are improved by the addition of endoplasmic reticulum (ER) stress inhibitors to *in vitro* maturation (IVM) medium and/or *in vitro* culture (IVC) medium. This study aimed to evaluate the effects of three concentrations of tauroursodeoxycholic acid (TUDCA; 50, 200, and 1,000 μM), a chemical chaperone for relieving ER stress, during IVM of bovine cumulus–oocyte complexes (COCs) for 24 h. Treated oocytes were analyzed for nuclear maturation, reactive oxygen species (ROS) production, mitochondrial activity, and abundance of target transcripts. In addition, the number of pronuclei in oocytes was evaluated after 18–20 h of insemination, and the rates of blastocyst and hatched blastocyst formation were evaluated after 7 and 8/9 days of culture, respectively. We further evaluated the transcript abundance of embryonic quality markers. Our findings showed that supplementation of IVM medium with 200 μM of TUDCA decreased ROS production and increased abundance of transcripts related to antioxidant activity in oocytes (*CAT*, *GPX1*, and *HMOX1*) and embryos (*GPX1* and *PRDX3*). Interestingly, high concentration of TUDCA (1,000 μM) was toxic to oocytes, reducing the nuclear maturation rate, decreasing mitochondrial activity, and increasing the abundance of ER stress (*HSPA5*) and cellular apoptosis (*CASP3* and *CD40*) related transcripts. The results of this study suggest that treatment with 200 μM of TUDCA is associated with a greater resistance to oxidative stress and indirectly with ER stress relief in bovine oocytes.

Keywords: oocyte, *in vitro* maturation, TUDCA, endoplasmic reticulum stress, oxidative stress, cattle

INTRODUCTION

In vitro maturation (IVM) is one of the main restrictive steps in the optimization of *in vitro* production (IVP). During IVM, oocytes acquire the intrinsic capacity for gradual development until activation of the embryonic genome after fertilization (Ferreira et al., 2009; Gilchrist, 2011).

However, previous studies have indicated that *in vitro* conditions in which oocytes are exposed to a variety of cellular stresses contribute to the greater incidence of loss of competence in *in vitro*

developed embryo compared with that in embryos derived *in vivo* (Latham, 2016; Del Collado et al., 2017). Response to exogenous stress is a vital part of cellular physiology and it is increasingly becoming apparent that one of the main mechanisms involved in initiating the cellular response to a variety of exogenous stressors is associated with the endoplasmic reticulum (ER; Guzel et al., 2017). ER is an important organelle responsible for protein folding, transport and synthesis, trafficking, metabolism of lipids, and cellular Ca^{2+} storage (Groenendyk and Michalak, 2005; Hetz, 2012). *In vitro*, however, the ER microenvironment can be disturbed due to Ca^{2+} depletion, hypoxia, and N-terminal glycosylation dysfunction, causing ER stress (Hetz, 2012). ER stress is triggered when misfolded or unfolded proteins accumulate in the lumen of the ER. As a pro-survival response, unfolded protein response (UPR) alleviates the accumulation of unfolded proteins and restores ER function (Schröder and Kaufman, 2005). However, when ER stress exceeds its threshold, cellular damages such as apoptosis, degeneration, and carcinogenesis ensue (Olzmann et al., 2013; Yoon et al., 2014).

It is worth mentioning that oxidative stress and reactive oxygen species (ROS) generation are key to ER stress and not just consequences of its induction (Bhandary et al., 2012; Yoon et al., 2014). In addition, the exacerbated increase in ROS levels resulting from ER stress can cause the amplification of mitochondrial ROS and, consequently, the activation of pro-apoptotic signaling pathways (Sutton-McDowall et al., 2016; Fan and Simmen, 2019).

To relieve ER stress, ER stress inhibitors are added to the culture media. Tauroursodeoxycholic acid (TUDCA), a bile acid that acts as a potent chemical chaperone (Xie et al., 2002; Cortez and Sim, 2014), has been used to alleviate ER stress during *in vitro* oocyte maturation and/or embryo development (Song et al., 2011; Kim et al., 2012; Zhang et al., 2012; Yoon et al., 2014; Zhao et al., 2015; Mochizuki et al., 2018). Although the exact chaperoning mechanism of TUDCA is still unclear, it has been shown to prevent UPR malfunction and ameliorate ER stress in various cell types (Xie et al., 2002; Miller et al., 2007; Lee et al., 2010; Seyhun et al., 2011). However, little is known about the mechanism of TUDCA activity and its effects on *in vitro*-matured bovine oocytes.

We hypothesized that IVM of bovine oocytes supplemented with TUDCA could relieve the ER stress caused by the *in vitro* environment. Thus, we proposed a model to improve oocyte maturation and, consequently, fertilization and *in vitro* embryonic development.

Therefore, the aim of this study was to evaluate the effect of different TUDCA concentrations on *in vitro* oocyte maturation and the quality, polyspermy, and *in vitro* blastocyst development in cattle.

MATERIALS AND METHODS

All chemicals used in this study were purchased from Sigma–Aldrich (St. Louis, MO, United States) unless otherwise indicated.

Experimental Design

Tauroursodeoxycholic acid (Selleckchem, Houston, TX, United States) was dissolved in sterile distilled water to prepare a 100 mM stock solution that was stored at −80°C. This stock solution was freshly diluted with IVM media to obtain 50 μM (T50), 200 μM (T200), and 1,000 μM (T1000) solutions of TUDCA (Kim et al., 2012; Zhang et al., 2012; Mochizuki et al., 2018; **Figure 1**). In all experiments, we included the control group (without TUDCA). The first series of experiments aimed to evaluate the influences of control, T50, T200, and T1000 TUDCA on the following oocyte quality parameters during IVM of bovine oocytes: nuclear maturation (experiment 1), ROS production (experiment 2), mitochondrial activity (experiment 3), and the abundance of target transcripts in oocytes (experiment 4). Other experiments aimed to evaluate the influence of supplementation with control, T50, and T200 TUDCA during IVM on fertilization and embryonic development, particularly on pronucleus formation in presumptive zygotes (experiment 5), developmental competence of embryos (experiment 6), and transcript abundance of embryonic quality markers (experiment 7).

In vitro Maturation

Bovine ovaries, from *Bos taurus indicus* and its crossbreeds, were obtained from a commercial abattoir located in Assis (São Paulo state, Brazil; latitude: 22°36'38.78' S and longitude: 50°26′53.54″ W). These ovaries were transported to the laboratory in sterile saline (0.9% NaCl) at 37°C for 30 min at maximum. *Cumulus*–oocyte complexes (COCs) were collected by the aspiration of follicles with 3–8 mm diameter (Botigelli et al., 2018). After sedimentation, COCs were recovered and selected using a stereomicroscope. Only COCs with a homogeneous cytoplasm and a compact multilayer of *cumulus* cells were used (grades 1 and 2; Seneda et al., 2001). COCs were washed and transferred to 500 μL drops of maturation medium (10 μL/COCs) in a four-well plate consisting of TCM199 with Earle salts and supplemented with 0.1 IU/mL rhFSH (Gonal-f, Merck Serono, Rockland, MA, United States), 0.22 mg/mL sodium pyruvate, 75 μg/mL amikacin, 4 mg/mL bovine serum albumin (BSA), and increasing concentrations of TUDCA according to the experimental design previously described (section "Experimental Design"). All experiments had a control group. COCs were incubated at 38.5°C in humidified air with 5% CO_2 for 24 h.

In vitro Fertilization and Culture

In experiments where *in vitro* fertilization (IVF) and *in vitro* culture (IVC) were performed, groups of 25 COCs were transferred to 90 μL drops of Tyrode albumin lactate pyruvate (TALP) supplemented with fatty-acid-free BSA (6 mg/mL), pyruvate (0.22 mg/mL), amikacin (75 μg/mL), heparin (30 μg/mL), and PHE (20 μM penicillamine, 10 μM hypotaurine, and 1 μM epinephrine). Oocytes were inseminated with frozen-thawed semen from a single sample of a Nelore breed bull. Spermatozoa were selected using the Select SPERM (Botupharma Animal Biotechnology, Botucatu, São Paulo, Brazil) method, and the concentration was adjusted to 1×10^6

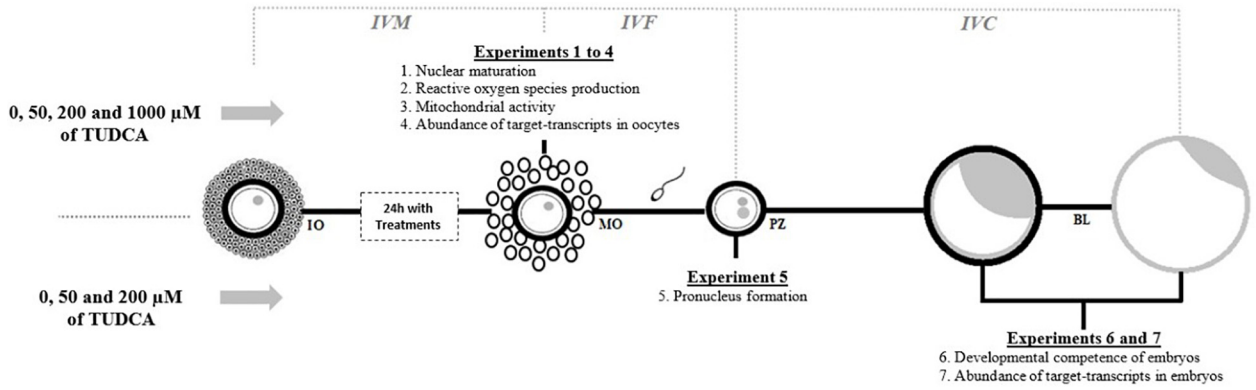

FIGURE 1 | Illustrative experimental design. IVM, *in vitro* maturation; IVF, *in vitro* fertilization; IVC, *in vitro* culture; IO, immature oocyte; MO, mature oocyte; PZ, presumptive zygote; BL, blastocyst and hatched blastocyst.

spermatozoa/mL. Oocytes and spermatozoa were co-incubated under the same conditions as during IVM, and the day of insemination was designated as Day 0. At 18–20 h post-insemination, presumptive zygotes were denuded from *cumulus* cells and transferred to 500 µL drops of SOF medium (synthetic oviduct fluid; 10 µL/zygotes) in a four-well plate, supplemented with pyruvate (0.22 µg/mL), amikacin (75 µg/mL), 2.5% v/v fetal calf serum, and BSA (5 mg/mL). Subsequently, the oocytes and spermatozoa were cultivated under physiological oxygen tension (5%) and high humidity in small sealed plastic bags with a gas mixture containing 5% O_2, 5% CO_2, and 90% N_2 (based on Vajta et al., 1997) in an incubator at 38.5°C. In all experiments, the culture was maintained for 9 days after insemination until the hatching stage of the embryos. Blastocyst and hatched blastocyst formation rates were assessed as the proportions of observed structures on days 7 and 8/9, respectively, based on the number of COCs used in IVM.

Nuclear Staining

Nuclear staining was used in two studies. COCs (Experiment 1) and presumptive zygotes (Experiment 5) were collected after 24 h of IVM and 18–20 h of IVF, respectively, and then vortexed in wash medium for 2 min. Denuded oocytes and presumptive zygotes were fixed in 4% (v/v) paraformaldehyde for 30 min in a humidifier chamber at room temperature (RT), incubated with 5 µg/µL Hoechst 33342 for 30 min at RT, and transferred to Poly-L-lysine-coated slides mounted with a coverslip. The oocytes and presumptive zygotes were analyzed using an epifluorescence inverted microscope (Eclipse Ti-E, Nikon, Japan) with A4 filter (emission 420 nm and excitation 330–385 nm). Nuclear maturation was graded into two categories: immature oocytes (germinal vesicle stage and metaphase I without first polar body) and mature oocytes [metaphase II (MII) with primary polar body; Ghaffari Novin et al., 2015]. Pronucleus formation was graded into three categories: (1) unfertilized oocytes with a single pronucleus in the ooplasm, (2) fertilized oocytes with two pronuclei in the ooplasm, and (3) polyspermic oocytes with more than two pronuclei in the ooplasm (Zhao et al., 2018).

Evaluation of Reactive Oxygen Species and Mitochondrial Activity

For Experiments 2 and 3, the same staining protocol was performed and the details of each one are provided in the text below. COCs were collected at 0 and 24 h of IVM and vortexed in wash medium for 2 min. The denuded oocytes were separately incubated in 5 µM Cell Rox Green (Life Technologies, Foster City, CA, United States) or 0.5 µM Mito Track Red CMX ROS (Invitrogen, Ltd.) for 30 min in a humidifier chamber at 38.5°C or RT, depending on the purpose of the study. Then, the oocytes were fixed in 4% (v/v) paraformaldehyde for 15 min in a humidifier chamber at RT and transferred to Poly-L-lysine-coated slides mounted with a coverslip. In the staining, fixation, and slide mounting processes, oocytes were washed three times in phosphate-buffered saline (PBS) containing 1 mg/mL polyvinylpyrrolidone (PVP). Oocytes were analyzed using an epifluorescence microscope (Eclipse Ti-E, Nikon) equipped with an L5 filter (emission 519 nm and excitation 495 nm) for ROS detection and with N21 filter (emission 615 nm and excitation 587 nm) for mitochondrial evaluation. In both experiments, a digital camera attached to the microscope was used to acquire images and the fluorescent pixel intensity value of the total area of each oocyte was measured using a freehand tool to delimitate the cytoplasm of each oocyte (ImageJ software[1]). Background fluorescence was subtracted from each image before fluorescence measurement and quantification (Rodrigues et al., 2016; Ispada et al., 2018).

Relative Quantitation of Target-Transcripts: Reverse Transcription Quantitative Polymerase Chain Reaction (RT-qPCR)

RNA Isolation and Reverse Transcription

Total RNA from oocytes and blastocysts was extracted using the PicoPure RNA Isolation kit (Life Technologies, Foster City, CA, United States) following the manufacturer's

[1]https://imagej.nih.gov/ij/index.html

protocol. Extracted RNA was stored at −80°C until further analysis by qPCR. RNA concentration was quantified using a spectrophotometer (Nanodrop, Thermo Fisher Scientific, Waltham, MA, United States).

For each sample, we used a pool of 20 oocytes and a pool of three blastocysts for reverse transcription. cDNA synthesis was performed using a High Capacity Reverse Transcription kit (Applied Biosystems, Foster City, CA, United States), following the manufacturer's instructions. All samples were treated with DNase according to the manufacturer's instructions before reverse transcription.

Pre-amplification and qPCR

Gene expression analyses of bovine oocytes and blastocysts were performed independently using Applied Biosystems™ TaqMan® Assays specific for *B. taurus* and based on Fontes et al. (2020). A total of 86 target genes were analyzed (**Supplementary Table S1** describing all the genes and their signaling pathways). Prior to qPCR thermal cycling, each sample was subjected to sequence-specific preamplification process as follows: 1.25 μL assay mix (TaqMan® Assay was pooled to a final concentration of 0.2× for each of the 96 assays), 2.5 μL TaqMan PreAmp Master Mix (Applied Biosystems, #4391128), and 1.25 μL cDNA (5 ng/μL). The reactions were activated at 95°C for 10 min, followed by denaturation at 95°C for 15 s, annealing, and amplification at 60°C for 4 min for 14 cycles. These preamplified products were diluted fivefold (oocyte and embryos) prior to RT-qPCR analysis.

Assays and preamplified samples were transferred to an integrated fluidic circuit plate. For gene expression analysis, the sample solution preparation consisted of 2.25 μL cDNA (preamplified products), 2.5 μL of TaqMan Universal PCR Master Mix (2×, Applied Biosystems), and 0.25 μL of 20× GE Sample Loading Reagent (Fluidigm, South San Francisco, CA, United States); the assay solution included 2.5 μL 20× TaqMan Gene Expression Assay (Applied Biosystems) and 2.5 μL of 2× Assay Loading Reagent (Fluidigm). The 96.96 Dynamic Array™ Integrated Fluidic Circuits (Fluidigm) chip was used for data collection. After priming, the chip was loaded with 5 μL each of the assay solution and each sample solution and loaded into an automated controller that prepares the nanoliter-scale reactions.

The qPCR thermal cycling was performed in the Biomark HD System (Fluidigm) using the protocol TaqMan GE 96 × 96 Standard, which involved one stage of Thermal Mix (50°C for 2 min, 70°C for 20 min, and 25°C for 10 min) followed by a hot start stage (50°C for 2 min and 95°C for 10 min), 40 cycles of denaturation (95°C for 15 s), primer annealing, and extension (both at 60°C for 60 s).

Statistical Analysis

The fluorescence intensity data for ROS detection and mitochondrial activity were compared using the non-parametric Kruskal–Wallis test and Dunn's *post hoc* test. Data on nuclear maturation rate, sperm penetration rate, and the rates of formation of blastocysts and hatched blastocysts were arcsines transformed and subjected to analysis of variance, and the means were compared using Tukey's *post hoc* test. The normality of data was assessed using the Shapiro–Wilk and Bartlett tests. The results are presented as the mean ± standard error of the mean (SEM) or median, and first and third interquartile intervals based on data normality. Quantitative PCR data were assessed using the ΔC_q values relative to the geometric mean of the best reference genes among the 96-gene set, i.e., *HPRT1*, *PPIA*, and *HPRT1* (Experiment 4) and *GAPDH*, *HPRT1*, and *PPIA* (Experiment 7). Fold-changes were calculated using the $2^{-\Delta\Delta Cq}$ method. All analyses were performed using JMP software (SAS Institute, Cary, NC, United States). Moderate statistical significance was determined based on $0.01 < P\text{-value} \leq 0.06$, while strong significance was considered when $P\text{-value} \leq 0.01$.

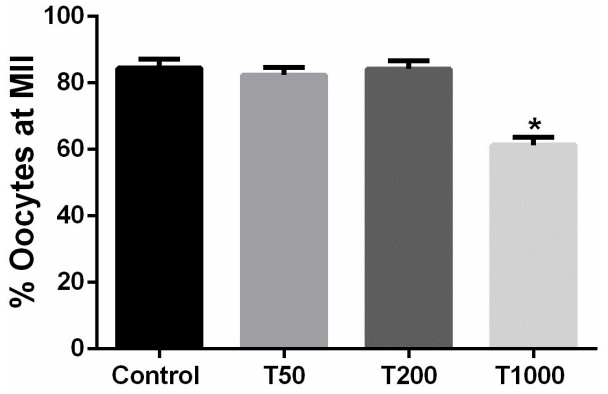

FIGURE 2 | Effect of TUDCA concentrations on the proportion of oocytes that reached the MII stage during IVM. Results are represented by means ± SEM of five replicates using 87–110 COCs/treatment. The bar marked with asterisk differs significantly ($P \leq 0.06$). Control, 0 μM TUDCA; T50, 50 μM TUDCA; T200, 200 μM TUDCA; T1000, 1,000 μM TUDCA.

RESULTS

The Effect of TUDCA on Oocyte Nuclear Maturation During IVM

After 24 h of IVM, the proportion of oocytes that reached MII was similar among the Control, T50, and T200 groups (**Figure 2**). However, the T1000 group exhibited decrease ($P = 0.002$) in the proportion of oocytes in MII compared to those in the other groups, with or without TUDCA treatment.

The Effect of TUDCA on Oocyte ROS Production During IVM

After 24 h of IVM, the T200 group exhibited decreased ROS production ($P = 0.001$) compared to the other groups, with or without TUDCA treatment. There was no difference in ROS levels among the control, T50, and T1000 groups. Furthermore, immature oocytes were not significantly different from mature oocytes (**Figure 3**).

The Effect of TUDCA on Oocyte Mitochondrial Activity During IVM

After 24 h of IVM, there was no difference in mitochondrial activity among the Control, T50, and T200 groups. However,

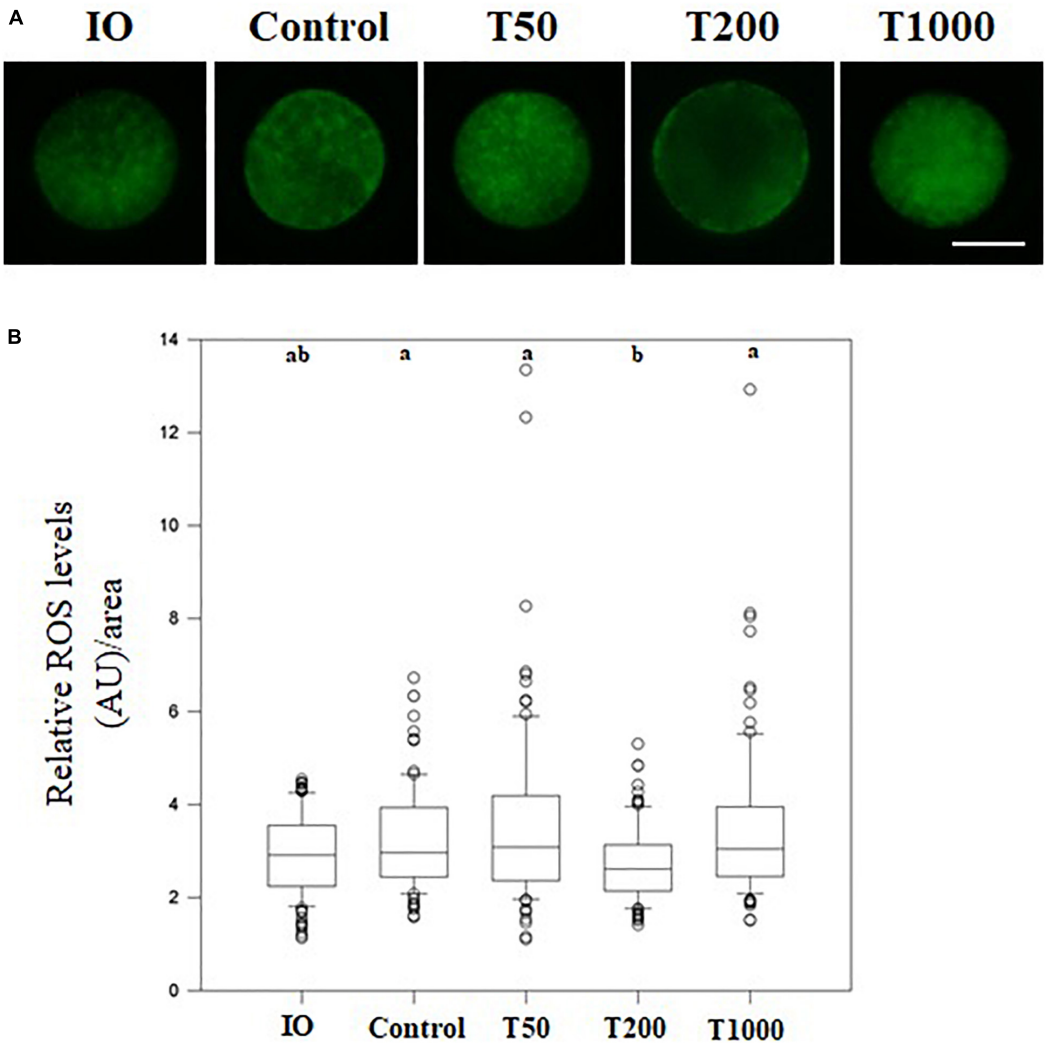

FIGURE 3 | Intracellular ROS levels in oocytes matured *in vitro* in the presence of increasing TUDCA concentrations. **(A)** Representative photomicrographs of bovine oocytes stained with Cell Rox Green for ROS semi-quantitative quantification. Bar = 50 μm. **(B)** Results are presented as the median and first and third interquartile interval of five replicates using 87–95 COCs/treatment. Different letters in each box represent significant differences ($P \leq 0.06$). IO, immature oocyte; Control, 0 μM TUDCA; T50, 50 μM TUDCA; T200, 200 μM TUDCA; T1000, 1,000 μM TUDCA.

the T1000 group showed decreased ($P = 0.001$) mitochondrial activity compared to the other groups, with or without TUDCA treatment. In addition, when matured oocytes were compared to immature oocytes (no IVM, i.e., oocytes just after being retrieved from ovarian follicles), treatments with 200 and 1,000 μM of TUDCA significantly reduced mitochondrial activity in the matured oocyte ($P = 0.001$; **Figure 4**).

The Effect of TUDCA on the Abundance of Target-Transcripts in Oocytes During IVM

Transcript abundance of six genes in oocytes was significantly affected after TUDCA treatment (**Figure 5**). All the others target transcripts analyzed (**Supplementary Table S1**) did not differ in a statistically significant way. Compared with the Control group, transcript abundance was upregulated in the T50, T200, and T1000 groups, according to each gene evaluated. Among the differentially expressed genes, there were transcripts related to ER stress (*HSPA5*) and oxidative stress, in which the T1000 group was upregulated; response to cellular stress (*CAT*, *GPX1*, and *HMOX1*) was upregulated in the group treated with 200 μm of TUDCA; and apoptosis (*CASP3* and *CD40*), which the T1000 group was upregulated (**Figure 5**).

The Effect of TUDCA Supplementation During IVM on Pronucleus Formation in Presumptive Zygotes and Developmental Competence of Embryos

A total of 237 oocytes were evaluated (79, 74, and 84 oocytes, respectively, for the Control, T50, and T200 groups). The rates

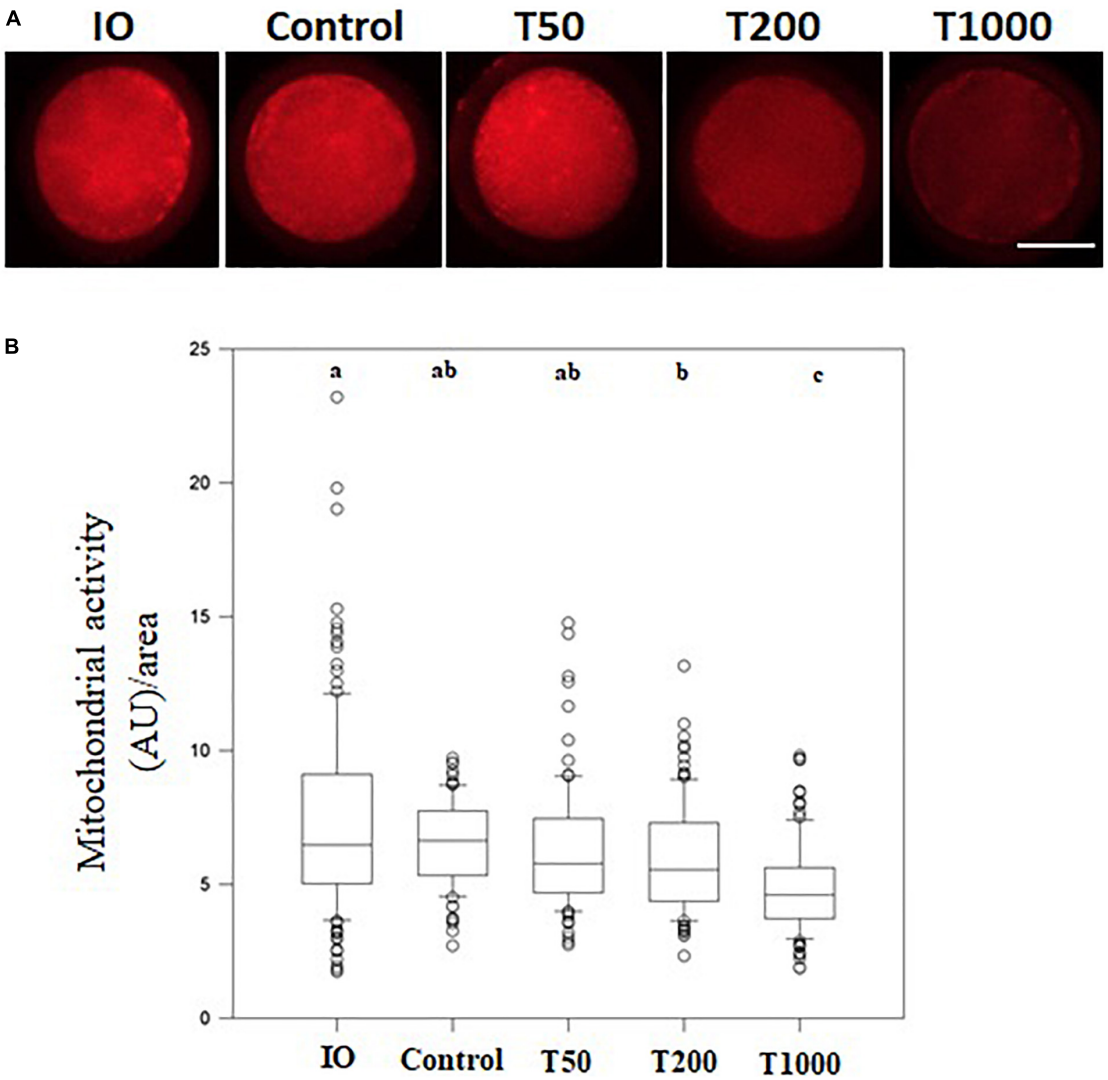

FIGURE 4 | Mitochondrial activity in oocytes matured *in vitro* in the presence of increasing TUDCA concentrations. **(A)** Representative photomicrographs of bovine oocytes stained with Mito Track Red CMX ROS for mitochondrial activity semi-quantitative quantification. Bar = 50 μm. **(B)** Results are presented as the median and first and third interquartile interval of five replicates using 87–105 COCs/treatment. Different letters in each box represent significant differences ($P \leq 0.06$). IO, immature oocyte; Control, 0 μM TUDCA; T50, 50 μM TUDCA; T200, 200 μM TUDCA; T1000, 1,000 μM TUDCA.

of pronucleus formation in the oocytes with one, two, or more pronuclei were not statistically different among the Control, T50, and T200 groups ($P = 0.79$; **Table 1**). There was no significant difference in the rates of formation of blastocysts ($P = 0.14$; **Table 2**) and hatched blastocysts on days 7 and 8/9, respectively, after fertilization ($P = 0.96$; **Table 2**).

The Effect of TUDCA Supplementation During IVM on Transcript Abundance of Embryonic Quality Markers

Transcript abundances of four genes were significantly affected in blastocysts after TUDCA treatment during IVM (**Figure 6**). All the others target transcripts analyzed (**Supplementary Table S1**) did not differ in a statistically significant way. Compared with the control group, transcript abundances of embryonic quality markers were upregulated in the T50 and T200 groups. Among the differentially expressed genes, there were transcripts related to oxidative stress and response to cellular stress (*GPX1* and *PRDX3*), that were upregulated in the T200 group; metabolism (*AGPAT9*) being upregulated in T50 and T200 groups; and pluripotency and cell differentiation (*OCT4*) with higher relative abundance in T200 (**Figure 6**).

DISCUSSION

Overproduction and accumulation of ROS overloads the antioxidant defense mechanism, resulting in cellular damage called oxidative stress (Menezo et al., 2016). There is an intimate

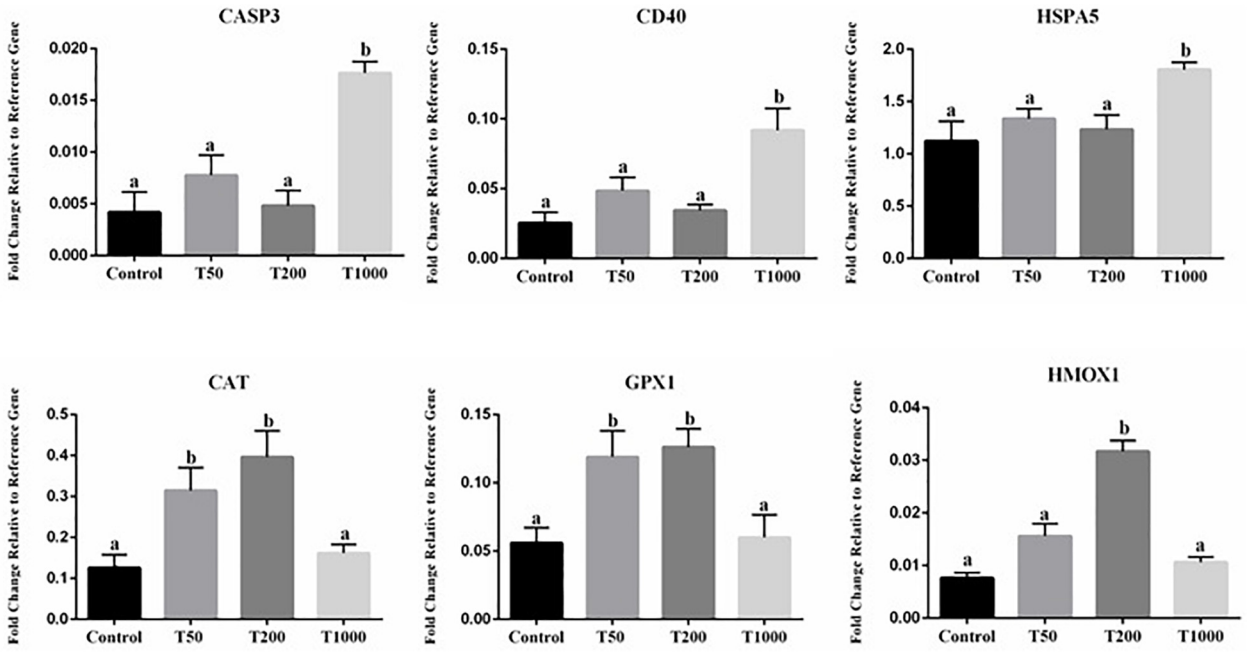

FIGURE 5 | Effect of TUDCA concentrations on differential gene expression in oocyte during IVM. Data represent the fold change in level of expression relative to the reference gene. Results are represented by least-squares means ± SEM of five replicates using 100 COCs/treatment. Different letters in each bar represent significant differences ($P \leq 0.06$). Control, 0 μM TUDCA; T50, 50 μM TUDCA; T200, 200 μM TUDCA; T1000, 1,000 μM TUDCA.

relation between ER stress and oxidative stress (Stadtman et al., 2002; Plaisance et al., 2016). Based on this relationship, the present study demonstrated that supplementing the IVM medium with TUDCA may relieve ER stress by decreasing ROS production in the oocyte and increasing the abundance of transcripts related to antioxidant activity in bovine oocytes and embryos developed *in vitro*.

Although ER is a key organelle involved in protein and lipid synthesis (Groenendyk and Michalak, 2005; Hetz, 2012), it is sensitive to disturbances in cellular homeostasis and can be triggered by different types of stresses (Latham, 2016), such as oxidative stress (Malhotra and Kaufman, 2007; Yoon et al., 2014). Such imbalance in cellular homeostasis leads to the accumulation of malformed proteins, activating ER stress and impairing cell function (Olzmann et al., 2013; Ghemrawi et al., 2018). In several species, it has been observed that ER stress is present during *in vitro* embryo production (Song et al., 2011; Kim et al., 2012; Zhang et al., 2012; Yoon et al., 2014; Zhao et al., 2015; Mochizuki et al., 2018), reducing oocyte competence and impairing embryonic development. In this study, we investigated the effects of supplementing IVM with different TUDCA concentrations during bovine oocyte maturation under *in vitro* environmental stress. Based on previous reports (Song et al., 2011; Kim et al., 2012; Zhang et al., 2012; Yoon et al., 2014; Zhao et al., 2015; Mochizuki et al., 2018), we propose a method to relieve ER stress in oocytes through treatment with TUDCA, reinforcing that ER stress is present in *in vitro*-matured oocytes.

Previous studies have demonstrated that TUDCA has potential therapeutic benefits on various models of many diseases, and its therapeutic effects are mainly attributed to its ability for relieving ER stress (Lee et al., 2010; Kusaczuk, 2019). In addition, it has been discovered that TUDCA reduces oxidative stress, suppresses apoptosis, and decreases inflammation in many *in vitro* models (Rodrigues et al., 1998; Schoemaker et al., 2004; Yoon et al., 2014; Rosa et al., 2017; Kim et al., 2019), thus

TABLE 1 | Pronuclei formation in Control, T50, and T200 groups.

	Control	T50	T200	*P*
Total number of oocytes	79	74	84	
Unfertilized oocytes rate (%; mean ± SEM)[a]	19.43 ± 1.42	20.36 ± 4.10	17.07 ± 2.97	**0.79**
Fertilized oocytes rate (%; mean ± SEM)[a]	74.68 ± 2.12	75.61 ± 3.34	77.19 ± 1.04	**0.76**
Polyspermic oocytes rate (%; mean ± SEM)[a]	5.89 ± 2.49	4.03 ± 2.80	5.74 ± 2.44	**0.86**

[a] *Total pronuclei/presumptive zygote. Number of replicates: 5. Control, 0 μM of TUDCA; T50, 50 μM of TUDCA; T200, 200 μM of TUDCA. Bold value indicates non significant (NS).*

TABLE 2 | Embryo production in Control, T50, and T200 groups.

	Control	T50	T200	*P*
Total number of oocytes	223	224	218	
Blastocyst formation rate (%; mean ± SEM)[a]	37.79 ± 0.85	43.10 ± 2.00	42.04 ± 2.32	**0.14**
Hatched blastocyst formation rate (%; mean ± SEM)[b]	37.49 ± 6.01	38.07 ± 6.61	35.60 ± 3.62	**0.96**

[a] *Total blastocysts/total oocyte—from D7.*
[b] *Total hatched blastocysts/total blastocysts—from D8 and D9. Number of replicates: 5. Control, 0 μM TUDCA; T50, 50 μM TUDCA; T200, 200 μM TUDCA. Bold value indicates non significant (NS).*

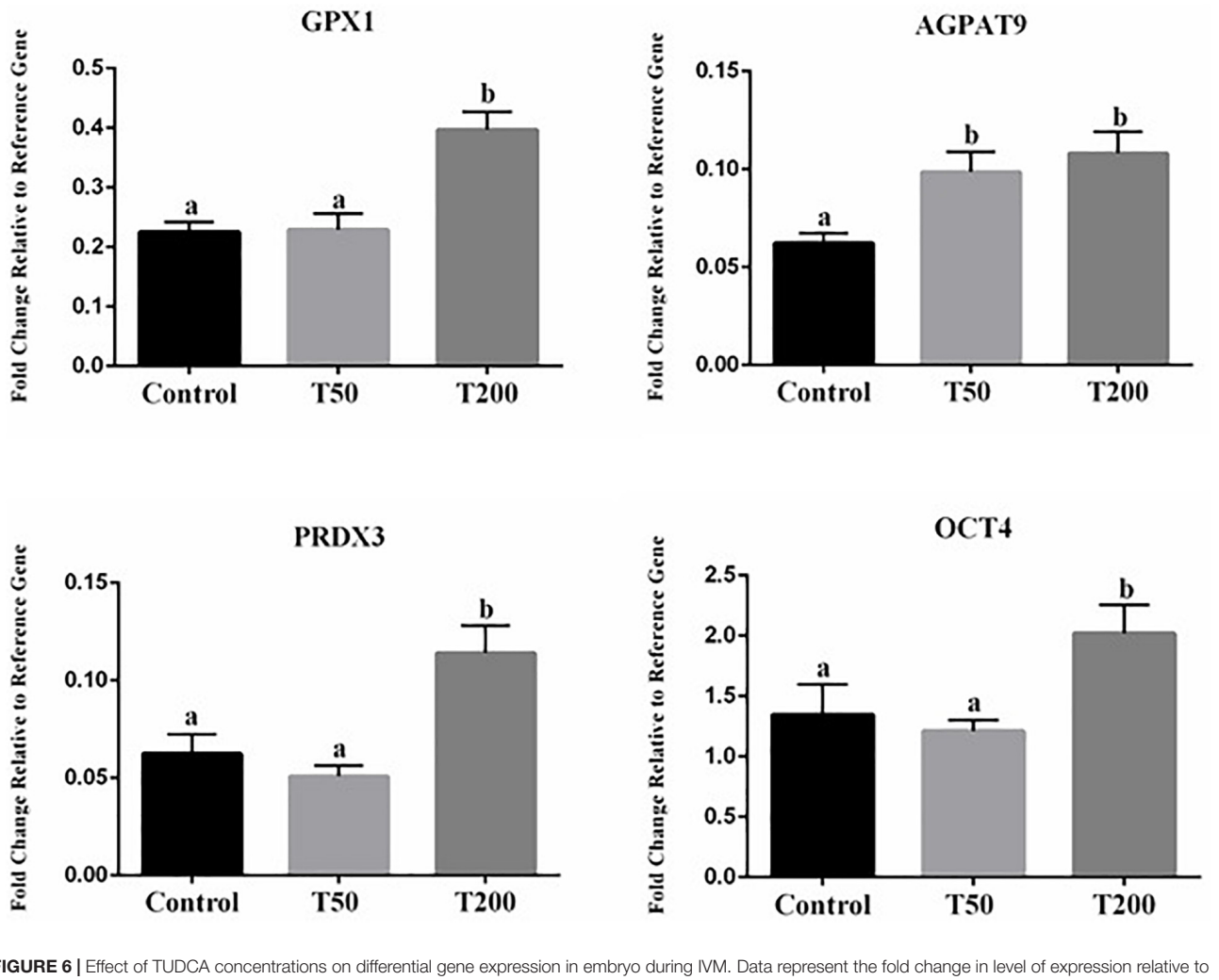

FIGURE 6 | Effect of TUDCA concentrations on differential gene expression in embryo during IVM. Data represent the fold change in level of expression relative to reference gene. Results are represented as least-squares means ± SEM of five replicates using 218–224 COCs/treatment. Different letters in each bar represent significant differences ($P \leq 0.06$). Control, 0 μM TUDCA; T50, 50 μM TUDCA; T200, 200 μM TUDCA.

demonstrating its antioxidant activity. Since oxidative stress can cause reduction–oxidation (redox) imbalance and trigger ER stress (Malhotra and Kaufman, 2007; Yoon et al., 2014), thereby increasing the excessive production of ROS and exacerbating oxidative stress (Malhotra and Kaufman, 2007; Yoon et al., 2014), we evaluated the function of TUDCA in modulating ROS levels in oocytes. During IVM, ROS levels were significantly decreased in COCs treated with 200 μM TUDCA compared to those in the control. Recently, a study has shown that 100 μM TUDCA supplementation reduces ROS production in bovine oocytes, which is in line with the findings of the present study (Khatun et al., 2020). In pigs, the use of 50 μM TUDCA during IVM reduced the ROS levels in oocytes (Zhang et al., 2012). Collectively, the data suggest that the mechanism of action of TUDCA in oocytes during IVM may be highly influenced by the species/subspecies, the tested concentration, and the *in vitro* conditions that the oocytes are subjected to, thus explaining the different results of previous studies and our present study.

However, regardless of species and cell type, most studies have reported potential reduction in ROS levels due to TUDCA treatment (Rodrigues et al., 1998; Yoon et al., 2014; Yun et al., 2018), corroborating our findings.

Although the mechanistic details of TUDCA activity in the ER stress pathway have not been fully elucidated, previous studies have ascribed the beneficial role of this drug to suppression of UPR pathways (Kusaczuk, 2019), thus improving protein folding and reducing the expression of ER stress markers in several cell types (Xie et al., 2002; Seyhun et al., 2011; Kusaczuk, 2019). Based on this information, the abundances of transcripts related to oocyte and embryonic competence after oocyte maturation with TUDCA treatment were evaluated. In oocytes, a significant increase in the abundances of *CAT* and *GPX1* mRNAs was observed in the T50 and T200 groups, while *HMOX1* mRNAs was increased in the T200 group when compared with those in the control. The relative abundances of *CAT*, *GPX1*, and *HMOX1* mRNAs are related to the antioxidant defense mechanism, which is important for maintaining cellular homeostasis in cases of high ROS levels (Combelles et al., 2009; Di Emidio et al., 2014). Balance between ROS production and antioxidant cell defense mechanisms is essential during IVM; otherwise, oxidative stress could cause cell damage and apoptosis (Remião et al., 2016; Gad et al., 2018; Nie et al., 2020). Furthermore, in the embryo, a significant increase in the abundances of *GPX1*, *PRDX3*, and *OCT4* mRNAs was observed in the T200 group compared with those in the control. Moreover, the T200 group exhibited upregulation of genes related to the antioxidant mechanism, in addition to that of genes involved in cellular pluripotency. Similar to *GPX1*, *PRDX3* plays an important role in oocyte maturation and embryonic development (Gad et al., 2018; Pereira et al., 2018; Camargo et al., 2019). OCT4, encoded by the *POU5F1* gene, is a key component of the pluripotency regulatory network (Wu and Schöler, 2014). OCT4 is postulated to play a critical role in defining totipotency and inducing pluripotency during embryonic development (Wu and Schöler, 2014; Daigneault et al., 2018), and is essential for the retention of pluripotency in the inner cell mass and epiblast. We also found that the AGPAT9 isoform, a key regulator of lipid accumulation in adipocytes (Bunel et al., 2015), was upregulated in the T50 and T200 groups, suggesting that it can influence the highest lipid droplet content in the embryo.

In parallel with our findings, other experimental studies have reported beneficial effects of TUDCA as an antioxidant (Moreira et al., 2017; Rosa et al., 2017; Daruich et al., 2019). The function of TUDCA in relieving oxidative stress has been demonstrated through the high expression of NRF2, DJ-1, and the antioxidant enzymes heme oxygenase-1 (HO-1) and glutathione peroxidase (GPx) in the human neuroblastoma cell line SH-SY5Y (Moreira et al., 2017), and by the reduction of high ROS levels in various cell types (Rodrigues et al., 1998; Yoon et al., 2014; Yun et al., 2018).

Surprisingly, in contrast with the effects observed so far, 1,000 μM TUDCA was apparently toxic to bovine oocytes during IVM. Remarkable increases in the expression of the apoptosis markers CASP3 and CD40 and the ER stress marker HSPA5 were observed in oocytes of the T1000 group when compared to those of the control. HSPA5 is an important molecular chaperone that activates UPR pathways in response to ER stress (Hetz, 2012; Olzmann et al., 2013). High expression of HSPA5 is associated with low oocyte competence (Wu et al., 2012; Park et al., 2018). In addition, increased *HSPA5* mRNA abundance is associated with cell apoptosis in cases of severe ER stress, which could promote the expression of pro-apoptotic genes (Xie et al., 2002; Szegezdi et al., 2003, 2006), such as Caspase-3 (Xie et al., 2002). Similar to *CASP3*, positive regulation of *CD40* in oocytes is associated with low competence and death of the oocyte (Tatone et al., 2006; Pang et al., 2018).

Thus, we hypothesize that high concentrations of TUDCA can activate the classic mitochondrial apoptosis pathway. Previous reports have shown that severe ER stress can interfere with mitochondrial activity, contributing to the decoupling of oxidative phosphorylation, reduction of mitochondrial membrane potential, matrix swelling, and subsequent release of various apoptotic factors, including cytochrome C and effector caspases that lead to cellular apoptosis (Berridge, 2002). These effects on mitochondria demonstrate the importance of balancing the flow of Ca^{2+} between these organelles (Bentov et al., 2011; Wu et al., 2012), because imbalance in one of them, such as ER stress, can severely affect the other. In mice, it was observed that mitochondrial dysfunction in oocytes can be mitigated by treatment of ER stress, such as through the use of Salubrinal (an ER stress inhibitor) in IVM (Wu et al., 2012). Contrary to this report but complementing the gene expression results, the T1000 group showed decreased mitochondrial activity compared to the control group, suggesting that high concentration of TUDCA may activate ER stress and mitochondrial apoptotic pathways.

Reported studies in available literature indicate that increased mitochondrial activity is necessary for nuclear maturation and completion of meiosis II (Picton et al., 1998; Tarazona et al., 2006). In the T1000 group, the nuclear maturation rate decreased in comparison to that in the control group, corroborating that high concentration of TUDCA is harmful for *in vitro*-matured bovine oocytes. The detrimental effect of 1,000 μM TUDCA on bovine oocytes under IVM has not been previously reported.

Although treatments with 50 and 200 μM TUDCA were beneficial for IVM, nuclear maturation and mitochondrial activity did not differ from those in the control. Possibly, during ER stress, TUDCA (at optimal concentrations) has a preventive effect in the early stages of apoptosis that do not involve mitochondria, as suggested by previous studies that did not observe beneficial effects of TUDCA on mitochondrial activity (Xie et al., 2002).

As already mentioned, balancing calcium oscillations is of great importance for maintaining cellular communication (Whitaker, 2006; Wu et al., 2012). In mammals, calcium oscillation is a feature of fertilization and plays a central role in activating development. The calcium required for these oscillations is mainly derived from the ER, wherein it accumulates in clumps in the microvillar subcortex during oocyte maturation (Whitaker, 2006). ER migration to the cortex plays an important role in making the ER competent for generating calcium oscillations during oocyte maturation

(Ducibella and Fissore, 2008). However, in stressful situations, ER distribution is altered, and calcium oscillations are impaired, making sperm penetration difficult (Ajduk et al., 2008). In our study, the addition of TUDCA to the maturation medium was not able to modulate oocyte fertilization, as demonstrated by the pronuclei number. Likewise, when we evaluated embryonic development, the formation rates of blastocyst and hatched blastocyst on days 7 and 8/9 of culture, respectively, were not statistically different among the groups. A previous study reported that the addition of 10, 100, and 1,000 μM TUDCA during IVM of cumulus free oocytes did not increase fertilization and blastocyst formation rate when compared to those in the control group (Mochizuki et al., 2018). The mechanism behind the apparent decoupling of the effect of TUDCA on fertilization and blastocyst formation rates, which was observed despite the detection of beneficial markers (ER and oxidative stress mitigation), is unclear. The release of oscillatory calcium waves by spermatozoa phospholipase during fertilization (Ajduk et al., 2008; Ducibella and Fissore, 2008) only partially relies on a non-stressed ER. The ability of ER to supply calcium may be retained in the early stages of ER stress, and an alternative calcium source theoretically explains the observed decoupling. Moreover, the absence of effect (at least statistically) on blastocyst production could be attributed to the absence of beneficial TUDCA effect at the end of maturation after 7–9 days of embryo culture without TUDCA. A possible way to assess this possibility is to conjugate a TUDCA treatment both on IVM and IVC.

Although TUDCA treatment had no effect on the gene expression reported in ER stress, both in the oocyte and in the embryo, we cannot rule out its possible effect in relieving ER stress. Yoon et al. (2014) demonstrated that embryo development *in vitro* depended on the orchestration between ROS and ER stress. Similarly, our results demonstrated that oocyte treatment with 200 μM TUDCA, a supposed ER stress inhibitor, reduced ROS production and positively regulated the transcripts related to the antioxidant system. Moreover, the *in vitro* conditions used in this study (i.e., low O_2 tension) were not strong enough to exert the TUDCA effect. A functional proof (i.e., pregnancy rate) can elucidate whether TUDCA effectively improves *in vitro* embryo production. Unlike our work, Khatun et al. (2020) observed that the addition of 100 μM of TUDCA to the maturation medium significantly decreased the expression of ER stress-related genes in bovine COCs (*GRP78*/*BIP*, *PERK*, *ATF4*, *IER1*, *XBP1*, and *CHOP*). However, we cannot make a direct comparison of these findings with our results, since the subspecies, protocol, and concentration of TUDCA (100 μM) investigated in that work were different from the experimental model proposed in the present work. Moreover, while Khatun et al. (2020) investigated gene expression in the COCs, our work evaluated specifically the relative abundance of target transcripts from oocytes.

In summary, TUDCA concentration was demonstrated to be decisive for the increase/decrease of *in vitro*-matured oocyte competence in our experimental model that used *B. taurus indicus* oocytes. The use of 200 μM TUDCA during IVM is suggested to be beneficial for relieving ER stress in oocytes through antioxidant effects. In contrast, supplementation with 1,000 μM TUDCA during IVM was detrimental to the development of oocytes and activated ER stress and mitochondrial apoptosis pathways. This study is just the second to report the action of TUDCA during IVM in bovine oocytes (Khatun et al., 2020); however, further studies are needed to confirm its possible influence on bovine subspecies, oxygen tension during incubation, and effect on the pregnancy rate of embryos produced.

DATA AVAILABILITY STATEMENT

The raw data supporting the conclusions of this article will be made available by the authors, without undue reservation.

ETHICS STATEMENT

Ethical review and approval was not required for the animal study because the use of bovine ovaries from a commercial abattoir in Brazil does not require a previous approval of an ethical committee.

AUTHOR CONTRIBUTIONS

EP contributed to the conception and design of the study, collected and analyzed data, and wrote the manuscript. CC performed most of the experiments and analyzed the data. FF and PS performed RNA extraction and reverse transcription for cDNA of samples subjected to gene expression analysis. LB contributed to data analysis. GM and FP-L provided technical support and critically revised the manuscript. MN contributed to the conceptualization and design of the entire study and supervised and contributed to critical revision and intellectual input to the manuscript. All authors have read and approved the final manuscript.

FUNDING

This work received financial support from grant #2012/50533-2, São Paulo Research Foundation (FAPESP). This study was financed in part by the Coordenação de Aperfeiçoamento de Pessoal de Nível Superior—Brasil (CAPES)—Finance Code 001.

ACKNOWLEDGMENTS

The authors would like to thank Professor Luiz Claudio Di Stasi, the Coordinator of the Multi-user Laboratory of Phytomedicines, Pharmacology, and Biotechnology (FitoFarmaTec) for allowing the use of this facility during the present study.

SUPPLEMENTARY MATERIAL

The Supplementary Material for this article can be found online at: https://www.frontiersin.org/articles/10.3389/fcell.2021.623852/full#supplementary-material

REFERENCES

Ajduk, A., Małagocki, A., and Maleszewski, M. (2008). Cytoplasmic maturation of mammalian oocytes: development of a mechanism responsible for sperm-induced Ca^{2+} oscillations. *Reprod. Biol.* 8, 3–22. doi: 10.1016/s1642-431x(12)60001-1

Bentov, Y., Yavorska, T., Esfandiari, N., Jurisicova, A., and Casper, R. F. (2011). The contribution of mitochondrial function to reproductive aging. *J. Assist. Reprod. Genet.* 28, 773–783. doi: 10.1007/s10815-011-9588-7

Berridge, M. J. (2002). The endoplasmic reticulum: a multifunctional signaling organelle. *Cell Calcium* 32, 235–249. doi: 10.1016/s0143416002001823

Bhandary, B., Marahatta, A., Kim, H. R., and Chae, H. J. (2012). An involvement of oxidative stress in endoplasmic reticulum stress and its associated diseases. *Int. J. Mol. Sci.* 14, 434–456. doi: 10.3390/ijms14010434

Botigelli, R. C., Razza, E. M., Pioltine, E. M., Fontes, P. K., Schwarz, K. R. L., Leal, C. L. V., et al. (2018). Supplementing in vitro embryo production media by NPPC and sildenafil affect the cytoplasmic lipid content and gene expression of bovine cumulus-oocyte complexes and embryos. *Reprod. Biol.* 18, 66–75. doi: 10.1016/j.repbio.2018.01.004

Bunel, A., Jorssen, E. P., Merckx, E., Leroy, J. L., Bols, P. E., and Sirard, M. A. (2015). Individual bovine in vitro embryo production and cumulus cell transcriptomic analysis to distinguish cumulus-oocyte complexes with high or low developmental potential. *Theriogenology* 83, 228–237. doi: 10.1016/j.theriogenology.2014.09.019

Camargo, L. S. A., Munk, M., Sales, J. N., Wohlres-Viana, S., Quintão, C. C. R., and Viana, J. H. M. (2019). Differential gene expression between in vivo and in vitro maturation: a comparative study with bovine oocytes derived from the same donor pool. *JBRA Assist. Reprod.* 23, 7–14. doi: 10.5935/1518-0557.20180084

Combelles, C. M., Gupta, S., and Agarwal, A. (2009). Could oxidative stress influence the in-vitro maturation of oocytes? *Reprod. Biomed. Online* 18, 864–880. doi: 10.1016/s1472-6483(10)60038-7

Cortez, L., and Sim, V. (2014). The therapeutic potential of chemical chaperones in protein folding diseases. *Prion* 8, 197–202. doi: 10.4161/pri.28938

Daigneault, B. W., Rajput, S., Smith, G. W., and Ross, P. J. (2018). Embryonic POU5F1 is required for expanded bovine blastocyst formation. *Sci. Rep.* 8:7753. doi: 10.1038/s41598-018-25964-x

Daruich, A., Picard, E., Boatright, J. H., and Behar-Cohen, F. (2019). Review: the bile acids urso- and tauroursodeoxycholic acid as neuroprotective therapies in retinal disease. *Mol. Vis.* 25, 610–624.

Del Collado, M., da Silveira, J. C., Oliveira, M. L. F., Alves, B. M. S. M., Simas, R. C., Godoy, A. T., et al. (2017). In vitro maturation impacts cumulus–oocyte complex metabolism and stress in cattle. *Reproduction* 154, 881–893. doi: 10.1530/REP-17-0134

Di Emidio, G., Falone, S., Vitti, M., D'Alessandro, A. M., Vento, M., Di Pietro, C., et al. (2014). SIRT1 signalling protects mouse oocytes against oxidative stress and is deregulated during aging. *Hum. Reprod.* 29, 2006–2017. doi: 10.1093/humrep/deu160

Ducibella, T., and Fissore, R. (2008). The roles of Ca2+, downstream protein kinases, and oscillatory signaling in regulating fertilization and the activation of development. *Dev. Biol.* 315, 257–279. doi: 10.1016/j.ydbio.2007.12.012

Fan, Y., and Simmen, T. (2019). Mechanistic connections between endoplasmic reticulum (ER) redox control and mitochondrial metabolism. *Cells* 8:1071. doi: 10.3390/cells8091071

Ferreira, E. M., Vireque, A. A., Adona, P. R., Meirelles, F. V., Ferriani, R. A., and Navarro, P. A. D. (2009). Cytoplasmic maturation of bovine oocytes: structural and biochemical modifications and acquisition of developmental competence. *Theriogenology* 71, 836–848. doi: 10.1016/j.theriogenology.2008.10.023

Fontes, P. K., Castilho, A. C. S., Razza, E. M., and Nogueira, M. F. G. (2020). Bona fide gene expression analysis of samples from the bovine reproductive system by microfluidic platform. *Anal. Biochem.* 596:113641. doi: 10.1016/j.ab.2020.113641

Gad, A., Abu Hamed, S., Khalifa, M., Amin, A., El-Sayed, A., Swiefy, S. A., et al. (2018). Retinoic acid improves maturation rate and upregulates the expression of antioxidant-related genes in in vitro matured buffalo (*Bubalus bubalis*) oocytes. *Int. J. Vet. Sci. Med.* 6, 279–285. doi: 10.1016/j.ijvsm.2018.09.003

Ghaffari Novin, M., Noruzinia, M., Allahveisi, A., Saremi, A., Fadaei Fathabadi, F., Mastery Farahani, R., et al. (2015). Comparison of mitochondrial-related transcriptional levels of TFAM, NRF1 and MT-CO1 genes in single human oocytes at various stages of the oocyte maturation. *Iran. Biomed. J.* 19, 23–28. doi: 10.6091/ibj.1400.2015

Ghemrawi, R., Battaglia-Hsu, S. F., and Arnold, C. (2018). Endoplasmic reticulum stress in metabolic disorders. *Cells* 7:63. doi: 10.3390/cells7060063

Gilchrist, R. B. (2011). Recent insights into oocyte–follicle cell interactions provide opportunities for the development of new approaches to in vitro maturation. *Reprod. Fertil. Dev.* 23, 23–31. doi: 10.1071/RD10225

Groenendyk, J., and Michalak, M. (2005). Endoplasmic reticulum quality control and apoptosis. *Acta Biochim. Pol.* 52, 381–395. doi: 10.18388/abp.2005-3451

Guzel, E., Arlier, S., Guzeloglu-Kayisli, O., Tabak, M. S., Ekiz, T., Semerci, N., et al. (2017). Endoplasmic reticulum stress and homeostasis in reproductive physiology and pathology. *Int. J. Mol. Sci.* 18:792. doi: 10.3390/ijms18040792

Hetz, C. (2012). The unfolded protein response: controlling cell fate decisions under ER stress and beyond. *Nat. Rev. Mol. Cell Biol.* 13, 89–102. doi: 10.1038/nrm3270

Ispada, J., Rodrigues, T. A., Risolia, P. H. B., Lima, R. S., Gonçalves, D. R., Rettori, D., et al. (2018). Astaxanthin counteracts the effects of heat shock on the maturation of bovine oocytes. *Reprod. Fertil. Dev.* 30, 1169–1179. doi: 10.1071/RD17271

Khatun, H., Wada, Y., Konno, T., Tatemoto, H., and Yamanaka, K. I. (2020). Endoplasmic reticulum stress attenuation promotes bovine oocyte maturation in vitro. *Reproduction* 159, 361–370. doi: 10.1530/REP-19-0492

Kim, J. S., Song, B. S., Lee, K. S., Kim, D. H., Kim, S. U., Choo, Y. K., et al. (2012). Tauroursodeoxycholic acid enhances the pre-implantation embryo development by reducing apoptosis in pigs. *Reprod. Domest. Anim.* 47, 791–798. doi: 10.1111/j.1439-0531.2011.01969.x

Kim, S. J., Ko, W. K., Heo, D. N., Lee, S. J., Lee, D., Heo, M., et al. (2019). Anti-neuroinflammatory gold nanocomplex loading ursodeoxycholic acid following spinal cord injury. *Chem. Eng. J.* 375:122088. doi: 10.1016/j.cej.2019.122088

Kusaczuk, M. (2019). Tauroursodeoxycholate—bile acid with chaperoning activity: molecular and cellular effects and therapeutic perspectives. *Cells* 8:1471. doi: 10.3390/cells8121471

Latham, K. E. (2016). Stress signaling in mammalian oocytes and embryos: a basis for intervention and improvement of outcomes. *Cell Tissue Res.* 363, 159–167. doi: 10.1007/s00441-015-2124-9

Lee, Y. Y., Hong, S. H., Lee, Y. J., Chung, S. S., Jung, H. S., Park, S. G., et al. (2010). Tauroursodeoxycholate (TUDCA), chemical chaperone, enhances function of islets by reducing ER stress. *Biochem. Biophys. Res. Commun.* 397, 735–739. doi: 10.1016/j.bbrc.2010.06.022

Malhotra, J. D., and Kaufman, R. J. (2007). Endoplasmic reticulum stress and oxidative stress: a vicious cycle or a double-edged sword? *Antioxid. Redox Signal.* 9, 2277–2293. doi: 10.1089/ars.2007.1782

Menezo, Y. J., Silvestris, E., Dale, B., and Elder, K. (2016). Oxidative stress and alterations in DNA methylation: two sides of the same coin in reproduction. *Reprod. Biomed. Online* 33, 668–683. doi: 10.1016/j.rbmo.2016.09.006

Miller, S. D., Greene, C. M., McLean, C., Lawless, M. W., Taggart, C. C., O'Neill, S. J., et al. (2007). Tauroursodeoxycholic acid inhibits apoptosis induced by Z alpha−1 antitrypsin via inhibition of bad. *Hepatology* 46, 496–503. doi: 10.1002/hep.21689

Mochizuki, M., Miyagi, K., and Kishigami, S. (2018). Optimizing treatment of tauroursodeoxycholic acid to improve embryonic development after in vitro maturation of cumulus-free oocytes in mice. *PLoS One* 13:e0202962. doi: 10.1371/journal.pone.0202962

Moreira, S., Fonseca, I., Nunes, M. J., Rosa, A., Lemos, L., Rodrigues, E., et al. (2017). Nrf2 activation by tauroursodeoxycholic acid in experimental models of Parkinson's disease. *Exp. Neurol.* 295, 77–87. doi: 10.1016/j.expneurol.2017.05.009

Nie, J., Yan, K., Sui, L., Zhang, H., Zhang, H., Yang, X., et al. (2020). Mogroside V improves porcine oocyte in vitro maturation and subsequent embryonic development. *Theriogenology* 141, 35–40. doi: 10.1016/j.theriogenology.2019.09.010

Olzmann, J. A., Kopito, R. R., and Christianson, J. C. (2013). The mammalian endoplasmic reticulum-associated degradation system. *Cold Spring Harb. Perspect. Biol.* 5:a013185. doi: 10.1101/cshperspect.a013185

Pang, Y., Zhao, S., Sun, Y., Jiang, X., Hao, H., Du, W., et al. (2018). Protective effects of melatonin on the in vitro developmental competence of bovine oocytes. *Anim. Sci. J.* 89, 648–660. doi: 10.1111/asj.12970

Park, H. J., Park, J. Y., Kim, J. W., Yang, S. G., Jung, J. M., Kim, M. J., et al. (2018). Melatonin improves the meiotic maturation of porcine oocytes by reducing endoplasmic reticulum stress during in vitro maturation. *J. Pineal Res.* 64:e12458. doi: 10.1111/jpi.12458

Pereira, B. A., Zangeronimo, M. G., Castillo-Martín, M., Gadani, B., Chaves, B. R., Rodríguez-Gil, J. E., et al. (2018). Supplementing maturation medium with insulin growth factor I and vitrification-warming solutions with reduced glutathione enhances survival rates and development ability of in vitro matured vitrified-warmed pig oocytes. *Front. Physiol.* 9:1894. doi: 10.3389/fphys.2018.01894

Picton, H., Briggs, D., and Gosden, R. (1998). The molecular basis of oocyte growth and development. *Mol. Cell. Endocrinol.* 145, 27–37. doi: 10.1016/s0303-7207(98)00166-x

Plaisance, V., Brajkovic, S., Tenenbaum, M., Favre, D., Ezanno, H., Bonnefond, A., et al. (2016). Endoplasmic reticulum stress links oxidative stress to impaired pancreatic beta-cell function caused by human oxidized LDL. *PLoS One* 11:e0163046. doi: 10.1371/journal.pone.0163046

Remião, M. H., Lucas, C. G., Domingues, W. B., Silveira, T., Barther, N. N., Komninou, E. R., et al. (2016). Melatonin delivery by nanocapsules during in vitro bovine oocyte maturation decreased the reactive oxygen species of oocytes and embryos. *Reprod. Toxicol.* 63, 70–81. doi: 10.1016/j.reprotox.2016.05.016

Rodrigues, C. M., Fan, G., Wong, P. Y., Kren, B. T., and Steer, C. J. (1998). Ursodeoxycholic acid may inhibit deoxycholic acid-induced apoptosis by modulating mitochondrial transmembrane potential and reactive oxygen species production. *Mol. Med.* 4, 165–178. doi: 10.1007/BF03401914

Rodrigues, T. A., Ispada, J., Risolia, P. H., Rodrigues, M. T., Lima, R. S., Assumpção, M. E., et al. (2016). Thermoprotective effect of insulin-like growth factor 1 on in vitro matured bovine oocyte exposed to heat shock. *Theriogenology* 86, 2028–2039. doi: 10.1016/j.theriogenology.2016.06.023

Rosa, A. I., Fonseca, I., Nunes, M. J., Moreira, S., Rodrigues, E., Carvalho, A. N., et al. (2017). Novel insights into the antioxidant role of tauroursodeoxycholic acid in experimental models of Parkinson's disease. *Biochim. Biophys. Acta Mol. Basis Dis.* 1863, 2171–2181. doi: 10.1016/j.bbadis.2017.06.004

Schoemaker, M. H., Conde de la Rosa, L., Buist-Homan, M., Vrenken, T. E., Havinga, R., Poelstra, K., et al. (2004). Tauroursodeoxycholic acid protects rat hepatocytes from bile acid-induced apoptosis via activation of survival pathways. *Hepatology* 39, 1563–1573. doi: 10.1002/hep.20246

Schröder, M., and Kaufman, R. J. (2005). The mammalian unfolded protein response. *Annu. Rev. Biochem.* 74, 739–789. doi: 10.1146/annurev.biochem.73.011303.074134

Seneda, M. M., Esper, C. R., Garcia, J. M., de Oliveira, J. A., and Vantini, R. (2001). Relationship between follicle size and ultrasound-guided transvaginal oocyte recovery. *Anim. Reprod. Sci.* 67, 37–43. doi: 10.1016/s0378-4320(01)00113-0

Seyhun, E., Malo, A., Schäfer, C., Moskaluk, C. A., Hoffmann, R. T., Göke, B., et al. (2011). Tauroursodeoxycholic acid reduces endoplasmic reticulum stress, acinar cell damage, and systemic inflammation in acute pancreatitis. *Am. J. Physiol. Gastrointest. Liver Physiol.* 301, G773–G782. doi: 10.1152/ajpgi.00483.2010

Song, B. S., Kim, J. S., Yoon, S. B., Lee, K. S., Koo, D. B., Lee, D. S., et al. (2011). Inactivated Sendai-virus-mediated fusion improves early development of cloned bovine embryos by avoiding endoplasmic-reticulum-stress-associated apoptosis. *Reprod. Fertil. Dev.* 23, 826–836. doi: 10.1071/RD10194

Stadtman, E. R., Moskovitz, J., Berlett, B. S., and Levine, R. L. (2002). Cyclic oxidation and reduction of protein methionine residues is an important antioxidant mechanism. *Mol. Cell Biochem.* 234, 3–9. doi: 10.1007/978-1-4615-1087-1_1

Sutton-McDowall, M. L., Wu, L. L., Purdey, M., Abell, A. D., Goldys, E. M., MacMillan, K. L., et al. (2016). Nonesterified fatty acid-induced endoplasmic reticulum stress in cattle cumulus oocyte complexes alters cell metabolism and developmental competence. *Biol. Reprod.* 94:23. doi: 10.1095/biolreprod.115.131862

Szegezdi, E., Fitzgerald, U., and Samali, A. (2003). Caspase-12 and ER-stress-mediated apoptosis—The story so far. *Ann. N. Y. Acad. Sci.* 1010, 186–194. doi: 10.1196/annals.1299.032

Szegezdi, E., Logue, S. E., Gorman, A. M., and Samali, A. (2006). Mediators of endoplasmic reticulum stress-induced apoptosis. *EMBO Rep.* 7, 880–885. doi: 10.1038/sj.embor.7400779

Tarazona, A. M., Rodríguez, J. I., Restrepo, L. F., and Olivera-Angel, M. (2006). Mitochondrial activity, distribution and segregation in bovine oocytes and in embryos produced in vitro. *Reprod. Domest. Anim.* 41, 5–11. doi: 10.1111/j.1439-0531.2006.00615.x

Tatone, C., Carbone, M. C., Gallo, R., Delle Monache, S., Di Cola, M., Alesse, E., et al. (2006). Age-associated changes in mouse oocytes during postovulatory in vitro culture: possible role for meiotic kinases and survival factor BCL2. *Biol. Reprod.* 74, 395–402. doi: 10.1095/biolreprod.105.046169

Vajta, G., Holm, P., Greve, T., and Callesen, H. (1997). The submarine incubation system, a new tool for in vitro embryo culture: a technique report. *Theriogenology* 48, 1379–1385. doi: 10.1016/S0093-691X(97)00379-8

Whitaker, M. (2006). Calcium at fertilization and in early development: VIII. calcium signals in eggs and embryos. *Physiol. Rev.* 86, 69–89.

Wu, G., and Schöler, H. R. (2014). Role of Oct4 in the early embryo development. *Cell Regen.* 3, 7. doi: 10.1186/2045-9769-3-7

Wu, L. L., Russell, D. L., Norman, R. J., and Robker, R. L. (2012). Endoplasmic reticulum (ER) stress in cumulus-oocyte complexes impairs pentraxin-3 secretion, mitochondrial membrane potential ($\Delta\Psi$m), and embryo development. *Mol. Endocrinol.* 26, 562–573. doi: 10.1210/me.2011-1362

Xie, Q., Khaoustov, V. I., Chung, C. C., Sohn, J., Krishnan, B., Lewis, D. E., et al. (2002). Effect of tauroursodeoxycholic acid on endoplasmic reticulum stress–induced caspase-12 activation. *Hepatology* 36, 592–601. doi: 10.1053/jhep.2002.35441

Yoon, S. B., Choi, S. A., Sim, B. W., Kim, J. S., Mun, S. E., Jeong, P. S., et al. (2014). Developmental competence of bovine early embryos depends on the coupled response between oxidative and endoplasmic reticulum stress. *Biol. Reprod.* 90:104. doi: 10.1095/biolreprod.113.113480

Yun, S. P., Yoon, Y. M., Lee, J. H., Kook, M., Han, Y. S., Jung, S. K., et al. (2018). Tauroursodeoxycholic acid protects against the effects of P-cresol-induced reactive oxygen species via the expression of cellular prion protein. *Int. J. Mol. Sci.* 19:352. doi: 10.3390/ijms19020352

Zhang, J. Y., Diao, Y. F., Oqani, R. K., Han, R. X., and Jin, D. I. (2012). Effect of endoplasmic reticulum stress on porcine oocyte maturation and parthenogenetic embryonic development in vitro. *Biol. Reprod.* 86:128. doi: 10.1095/biolreprod.111.095059

Zhao, N., Liu, X. J., Li, J. T., Zhang, L., Fu, Y., Zhang, Y. J., et al. (2015). Endoplasmic reticulum stress inhibition is a valid therapeutic strategy in vitrifying oocytes. *Cryobiology* 70, 48–52. doi: 10.1016/j.cryobiol.2014.12.001

Zhao, X. M., Wang, N., Hao, H. S., Li, C. Y., Zhao, Y. H., Yan, C. L., et al. (2018). Melatonin improves the fertilization capacity and developmental ability of bovine oocytes by regulating cytoplasmic maturation events. *J. Pineal Res.* 64:e12445. doi: 10.1111/jpi.12445

Conflict of Interest: The authors declare that the research was conducted in the absence of any commercial or financial relationships that could be construed as a potential conflict of interest.

frontiers in Cell and Developmental Biology

ORIGINAL RESEARCH
published: 25 February 2021
doi: 10.3389/fcell.2021.609311

Clathrin Heavy Chain 1 Plays Essential Roles During Oocyte Meiotic Spindle Formation and Early Embryonic Development in Sheep

Zhe Han†, Xin Hao†, Cheng-Jie Zhou†, Jun Wang†, Xin Wen, Xing-Yue Wang, De-Jian Zhang and Cheng-Guang Liang**

State Key Laboratory of Reproductive Regulation and Breeding of Grassland Livestock, School of Life Sciences, Inner Mongolia University, Hohhot, China

OPEN ACCESS

Edited by:
Andreina Cesari, Consejo Nacional de Investigaciones Científicas y Técnicas (CONICET), Argentina

Reviewed by:
Paula Stein, National Institute of Environmental Health Sciences (NIEHS), United States
Claudia Baumann, University of Georgia, United States

***Correspondence:**
De-Jian Zhang
zhangdejian00@163.com
Cheng-Guang Liang
liangcg@imu.edu.cn

† These authors have contributed equally to this work

Specialty section:
This article was submitted to Cell Growth and Division, a section of the journal Frontiers in Cell and Developmental Biology

Received: *23 September 2020*
Accepted: *28 January 2021*
Published: *25 February 2021*

Citation:
Han Z, Hao X, Zhou C-J, Wang J, Wen X, Wang X-Y, Zhang D-J and Liang C-G (2021) Clathrin Heavy Chain 1 Plays Essential Roles During Oocyte Meiotic Spindle Formation and Early Embryonic Development in Sheep. Front. Cell Dev. Biol. 9:609311. doi: 10.3389/fcell.2021.609311

As a major protein of the polyhedral coat of coated pits and vesicles, clathrin molecules have been shown to play a stabilization role for kinetochore fibers of the mitotic spindle by acting as inter-microtubule bridges. Clathrin heavy chain 1 (CLTC), the basic subunit of the clathrin coat, plays vital roles in both spindle assembly and chromosome congression during somatic-cell mitosis. However, its function in oocyte meiotic maturation and early embryo development in mammals, especially in domesticated animals, has not been fully investigated. In this study, the expression profiles and functional roles of CLTC in sheep oocytes were investigated. Our results showed that the expression of CLTC was maintained at a high level from the germinal vesicle (GV) stage to metaphase II stage and that CLTC was distributed diffusely in the cytoplasm of cells at interphase, from the GV stage to the blastocyst stage. After GV breakdown (GVBD), CLTC co-localized with beta-tubulin during metaphase. Oocyte treatments with taxol, nocodazole, or cold did not affect CLTC expression levels but led to disorders of its distribution. Functional impairment of CLTC by specific morpholino injections in GV-stage oocytes led to disruptions in spindle assembly and chromosomal alignment, accompanied by impaired first polar body (PB1) emissions. In addition, knockdown of CLTC before parthenogenetic activation disrupted spindle formation and impaired early embryo development. Taken together, the results demonstrate that CLTC plays a vital role in sheep oocyte maturation via the regulation of spindle dynamics and an essential role during early embryo development.

Keywords: CLTC, spindle assembly, chromosome congression, oocyte, early embryo development

INTRODUCTION

Successful oocyte maturation and early embryo development depend on correct spindle formation and chromosome separation during cell division (Duan and Sun, 2019; Radonova et al., 2019). Similar to somatic cells, the oocyte meiotic spindle is mainly composed of microtubules (MTs), and spindle organization depends on the activities of numerous MT-associated proteins (Xu et al., 2012; Petry, 2016; Namgoong and Kim, 2018). Well-organized spindles are responsible for maintaining

correct chromosome alignment and separation during meiosis I and meiosis II (Dumont and Desai, 2012). Conversely, most oocyte aneuploidy is caused by chromosome segregation errors during meiotic divisions, leading to embryo development failures or neonatal defects (Webster and Schuh, 2017; Mogessie et al., 2018).

Clathrin, a major protein component of the cytoplasmic face of intracellular organelles, is composed of three heavy chains and three light chains (Kirchhausen and Harrison, 1981; Fotin et al., 2004; Royle and Lagnado, 2006). During interphase, clathrin is involved in the intracellular trafficking of receptors and the endocytosis of a variety of macromolecules (Kirchhausen, 2000; Fielding and Royle, 2013; He et al., 2017). During mitosis, clathrin molecules stabilize kinetochore fibers of the mitotic spindle by acting as inter-MT bridges and promote chromosome congression in somatic cells (Booth et al., 2011; Cheeseman et al., 2011; Rao et al., 2016). Clathrin has been shown to interact directly with the spindle through the N-terminal domain of clathrin heavy chain 1 (CLTC) (Royle and Lagnado, 2006). Through the recruitment of the phosphorylated form of transforming acidic coiled coil 3 (TACC3) and colonic and hepatic tumor overexpressed gene (ch-TOG), CLTC forms a complex known as an inter-MT bridge (Fu et al., 2010; Booth et al., 2011), which has been shown to stabilize the MTs of the mitotic spindle (Lin et al., 2010). In addition, CLTC has been shown to interact with sorting nexin 9 (SNX9) to stabilize the kinetochore fibers of the mitotic spindle (Ma et al., 2013). Centrosome positioning in *Caenorhabditis elegans* embryos has also been shown to be regulated by CLTC (Spiro et al., 2014).

For meiosis, meiotic spindle-associated clathrin was initially shown in mouse metaphase II (MII) oocytes (Maro et al., 1985). Our previous mouse oocyte studies have shown that CLTC plays important roles in both spindle assembly and chromosome congression by interacting with cytoskeleton-associated protein 5 (CKAP5) (Han et al., 2010; Zhao et al., 2013; Lu et al., 2017). In porcine oocytes, clathrin has been shown to be crucial for stabilizing the metaphase spindle (Holzenspies et al., 2010). Although roles for CLTC in oocyte spindle formation and chromosome congression have been well studied in both mouse and porcine models, it remains unclear if CLTC affects oocyte maturation and embryo development via similar mechanisms in artiodactyl animals such as sheep, as significant differences exist between artiodactyl and rodent oocytes. For example, sheep oocytes are larger (∼120 μm in diameter) than mouse oocytes (∼70–80 μm in diameter) (Kim et al., 2004; Cotterill et al., 2013). In sheep, oocyte maturation time (from follicle release to stage MII) requires 22–24 h, much longer than that required for mouse oocytes (Wang et al., 2018, 2019). This longer maturation process in sheep oocytes also requires more MT stability to regulate chromosomal separations and may be affected by the existence of an undefined microtubular network observed in some goat MII oocytes (Velilla et al., 2005). Therefore, further investigations are warranted to determine if sheep and mouse oocytes share the same CLTC-regulated mechanisms for spindle formation and chromosome separation. Here, to further fundamental knowledge of domesticated animal reproduction, we report the expression and function of CLTC during sheep oocyte maturation and early embryo development.

MATERIALS AND METHODS

Ethics Statement

All study procedures were performed according to the National Research Council Guide for the Care and Use of Laboratory Animals and were approved by the Ethics Committee of Inner Mongolia University (Approval number: SYXK 2014-0002).

Cumulus–Oocyte Complex Collection and *in vitro* Maturation

Sheep ovaries were obtained from a local slaughterhouse and transported to the laboratory in saline solution (0.9% w/v) at 37°C within 2 h after slaughter. Mature follicles (2- to 6-mm diameters) were cut to release the cumulus–oocyte complexes (COCs) into cell culture dishes (Biosharp, Beijing, China) containing pre-warmed HEPES-buffered TCM-199 (11150059, Thermo Fisher Scientific, Waltham, MA, United States) supplemented with 50 IU/ml of heparin (H32020612, Wanbang Biopharma, Jiangsu, China). Only COCs with intact cumulus cell masses were selected for *in vitro* maturation (IVM). COCs were washed and cultured in oocyte maturation medium [TCM-199 supplemented with 0.02 IU/ml of follicle-stimulating hormone (FSH; F2293, Sigma-Aldrich, St. Louis, MO, United States), 1.0 IU/ml of luteinizing hormone (LH; L6420, Sigma-Aldrich), 0.1 μg/ml of β-estradiol (E2, E2758, Sigma-Aldrich), 0.22 mg/ml of sodium pyruvate (P4562, Sigma-Aldrich), 10% fetal bovine serum (FBS; 16000-044, Thermo Fisher Scientific), and 1% penicillin–streptomycin (15140122, Thermo Fisher Scientific)]. Fully grown germinal vesicle (GV)-stage oocytes were cultured in a humidified atmosphere of 5% CO_2 at 38.5°C for 24 h.

Parthenogenetic Activation and *in vitro* Embryo Development

Cumulus cells from matured COCs were peeled off by gentle pipetting in HEPES-buffered TCM-199 supplemented with 0.3 mg/ml of hyaluronidase (H3506, Sigma-Aldrich). Subsequently, denuded oocytes were activated using a potent Ca^{2+} ionophore (5 μM of ionomycin, C7522, Sigma-Aldrich) for 5 min and rapidly transferred to culture medium containing 2 mM of 6-(dimethylamino) purine (6-DMAP; D2629, Sigma-Aldrich) for 3.5 h. After activation, the parthenogenetic embryos were washed three times and transferred into synthetic oviduct fluid medium [119.2 mM of NaCl (S5886, Sigma-Aldrich), 7.9 mM of KCl (P5405, Sigma-Aldrich), 1.3 mM of KH_2PO_4 (P5655, Sigma-Aldrich), 0.8 mM of $MgSO_4{\cdot}7H_2O$ (M1880, Sigma-Aldrich), 0.66 μl/ml of Na-lactate (L7900, Sigma-Aldrich), 25.0 mM of $NaHCO_3$ (S5761, Sigma-Aldrich), 0.7 mM of sodium pyruvate, and 1.8 mM of $CaCl_2{\cdot}2H_2O$ (C7902, Sigma-Aldrich)] supplemented with 29.2 μg/ml of L-glutamine (G8540, Sigma-Aldrich), 0.5 mg/ml of inositol (I7508, Sigma-Aldrich), 6 mg/ml of bovine serum albumin (BSA; A3311, Sigma-Aldrich),

30 μl/ml of essential amino acid (B6766, Sigma-Aldrich), and 10 μl/ml of MEM non-essential amino acid solution (M7145, Sigma-Aldrich). Embryos were cultured at 38.5°C in a humidified atmosphere of 5% CO_2 for 48 h. The embryos were then transferred and cultured for 5 days in synthetic oviduct fluid medium supplemented with 29.2 μg/ml of L-glutamine, 0.5 mg/ml inositol, 4% FBS, 30 μl/ml of essential amino acid, and 10 μl/ml of MEM non-essential amino acid solution. Embryos were assessed for developmental stages at days 1, 2, 3, 4, and 5 to calculate two-cell, four-cell, morula, and blastocyst percentages, respectively. For the developmental rates for all embryos, the number of MII oocytes subjected to parthenogenetic activation was used as the denominator.

Immunofluorescence

Oocytes or embryos were fixed in 4% paraformaldehyde (157-8, Electron Microscopy Sciences, Hatfield, PA, United States) for 30 min at room temperature. Samples were permeabilized with 1% Triton X-100 (T8532, Sigma-Aldrich) overnight at 37°C and blocked with 2% BSA for 1 h at room temperature. Next, the samples were incubated with primary antibodies against CLTC (rabbit polyclonal, 1:1,000, ab21679, Abcam, Cambridge, United Kingdom) and beta-tubulin (mouse monoclonal, 1:2,000, ab44928, Abcam) overnight at 4°C. The samples were then incubated with rhodamine-conjugated donkey anti-rabbit IgG (1:300, 711-025-152, Jackson ImmunoResearch Laboratories, West Grove, PA, United States) or Dylight^{TM} 488-conjugated AffiniPure donkey anti-mouse IgG (1:800, 715-485-150, Jackson ImmunoResearch Laboratories) for 1 h at 37°C. DNA was stained using 5 μg/ml of 4′,6-diamidino-2-phenylindole (DAPI; 236276, Roche, Mannheim, German) at room temperature. Finally, specimens were mounted on glass slides and observed using a confocal laser scanning microscope (A1R, Nikon, Tokyo, Japan).

Immunoblotting

Immunoblotting was conducted as previously described (Zhou et al., 2019). Briefly, a rabbit polyclonal anti-CLTC (1:1,000, Abcam) or a mouse monoclonal anti-beta-actin (1:100, sc-69879, Santa Cruz Biotechnology, Dallas, TX, United States) was used as a primary antibody. Bands on membranes were detected using an Enhanced Chemiluminescence Detection Kit (32106, Thermo Fisher Scientific), and images were captured using a Tanon-5200 imaging system (Tanon, Shanghai, China).

Drug Treatments

For taxol treatment, 5 mM of taxol (T7191, Sigma-Aldrich) stock in dimethyl sulfoxide (DMSO; D5879, Sigma-Aldrich) solution was diluted with TCM-199 to a final concentration of 25 μM. Oocytes at metaphase I (MI) and MII stages were treated with taxol for 80 min and then fixed for immunostaining or collected for immunoblotting. The control group contained DMSO at the same concentration as the 25 μM of taxol treatment group. For nocodazole treatment, 10 mg/ml of nocodazole (M1404, Sigma-Aldrich) in DMSO solution was diluted with TCM-199 to a final concentration of 20 μg/ml. Oocytes at MI and MII stages were treated with nocodazole for 50 min and then collected for immunostaining or immunoblotting. The control group contained DMSO at the same concentration as the 20 μg/ml nocodazole treatment group.

Cold-Mediated Microtubule Depolymerization Assay

A cold-mediated MT depolymerization assay was performed by placing oocytes in oocyte maturation medium at 4°C for 1 h. Some oocytes were randomly selected and immediately collected for immunostaining or immunoblotting. Others were placed in oocyte maturation medium at 38.5°C in a humidified atmosphere of 5% CO_2 for 30 min as a rescue treatment and then collected for immunostaining or immunoblotting.

Morpholino Microinjections

Based on the sequence of CLTC in sheep (Ensembl: ENSOARG00000013249), *CLTC* morpholino (MO) (5′-TCT GAC TCC ATA GTC AAG GTA CTG A-3′) was designed and synthesized (Gene Tools, Philomath, OR, United States). Ten-picoliter volumes of either *CLTC*-MO or negative control-MO (5′-CCT CTT ACC TCA GTT ACA ATT TAT A-3′), both at concentrations of 2 mM, were microinjected into the cytoplasm of GV-stage oocytes in HEPES-buffered TCM-199 supplemented with 10 μM of milrinone (M4659, Sigma-Aldrich). After the microinjections, the oocytes were incubated for 20 h in oocyte maturation medium with 10 μM of milrinone to allow sufficient time for MO blocking of maternal mRNA. The oocytes were then washed three times and cultured for 24 h in oocyte maturation medium without milrinone to facilitate oocyte maturation.

For the CLTC translational block experiments in sheep embryos, 10 pl of 2 mM *CLTC*-MO or control-MO was injected into mature oocytes. After the microinjections, the oocytes were incubated for 30 min in oocyte maturation medium and then subjected to parthenogenetic activation.

Statistical Analyses

Data are shown as means ± standard deviations (SD) from at least three replicates of each experiment. Statistical comparisons were made using two-tailed Student's *t*-tests for absolute values and were calculated using Microsoft Excel software. The percentages for early embryo development (two-cell, four-cell, eight-cell, morula, and blastocyst stages) were compared using chi-squared tests (Microsoft Excel software). $P < 0.05$ values were considered statistically significant.

RESULTS

Expression and Subcellular Localization of Clathrin Heavy Chain 1 During Sheep Oocyte Meiotic Maturation and Early Embryo Development

Clathrin heavy chain 1 protein expression and subcellular localization during sheep oocyte meiotic maturation were examined by immunoblotting and immunofluorescence staining, respectively. The CLTC antibody used in our previous mouse study was also used in the current study. However, whether this

antibody is specific and sensitive enough to label CLTC in sheep oocytes has not yet been demonstrated. To validate this antibody in sheep oocytes, sheep and mouse oocyte lysates were loaded onto the same gel to compare labeled bands. Lysate from 20 sheep oocytes or 60 mouse oocytes were loaded in the corresponding lanes. We found that the single bands from both sheep and mouse oocyte extracts had the same molecular weight, and we matched the molecular weight (∼180 kDa) of the corresponding antigen. The immunoblotting analysis showed that CLTC was highly expressed in the GV, GV breakdown (GVBD), MI, and MII stages. Due to the bigger size of the oocytes in sheep, higher levels of beta-actin were expressed in sheep oocytes than that in mice (**Figure 1A**). We also determined that CLTC in mouse and sheep shared 99.8% protein sequence identity (data not shown). Combined with the immunoblotting results that CLTC was expressed in GV-stage oocytes (**Figure 1A**), this suggests that CLTC was distributed evenly throughout the GV stage cytoplasm. After the GVBD stage, CLTC was found to be concentrated around the chromosomes in the spindle area and co-localized with tubulin at the MI and MII stages (**Figure 1B**). Briefly, CLTC may be functionally associated with tubulin during sheep oocyte meiosis. After parthenogenetic activation, embryos developed to late one-cell, two-cell, four-cell, eight-cell, and blastocyst stages. Again, CLTC redistributed evenly within the cytoplasm during interphase for each embryo stages. However, focal accumulations of CLTC in both two-cell and four-cell embryos (in addition to diffuse cytoplasmic staining) were also observed. Similar to its localization in MII-stage oocytes, accumulations of CLTC in the mitotic spindles of metaphase one-cell-stage embryos were also observed, illustrating a similar potential role for CLTC in both meiosis and mitosis (**Figures 1B,C**).

Microtubule-Dependent Localization of Clathrin Heavy Chain 1 During Meiosis

To further investigate the correlation between CLTC and MTs, we used the spindle-perturbing drugs taxol and nocodazole to treat sheep oocytes at both MI and MII stages. The immunoblotting results showed that taxol and nocodazole did not affect the amount of CLTC at the MI (**Figure 2A**) or MII stage (**Figure 2B**). However, analysis of the immunofluorescence staining revealed that MTs were overpolymerized and formed larger spindles after

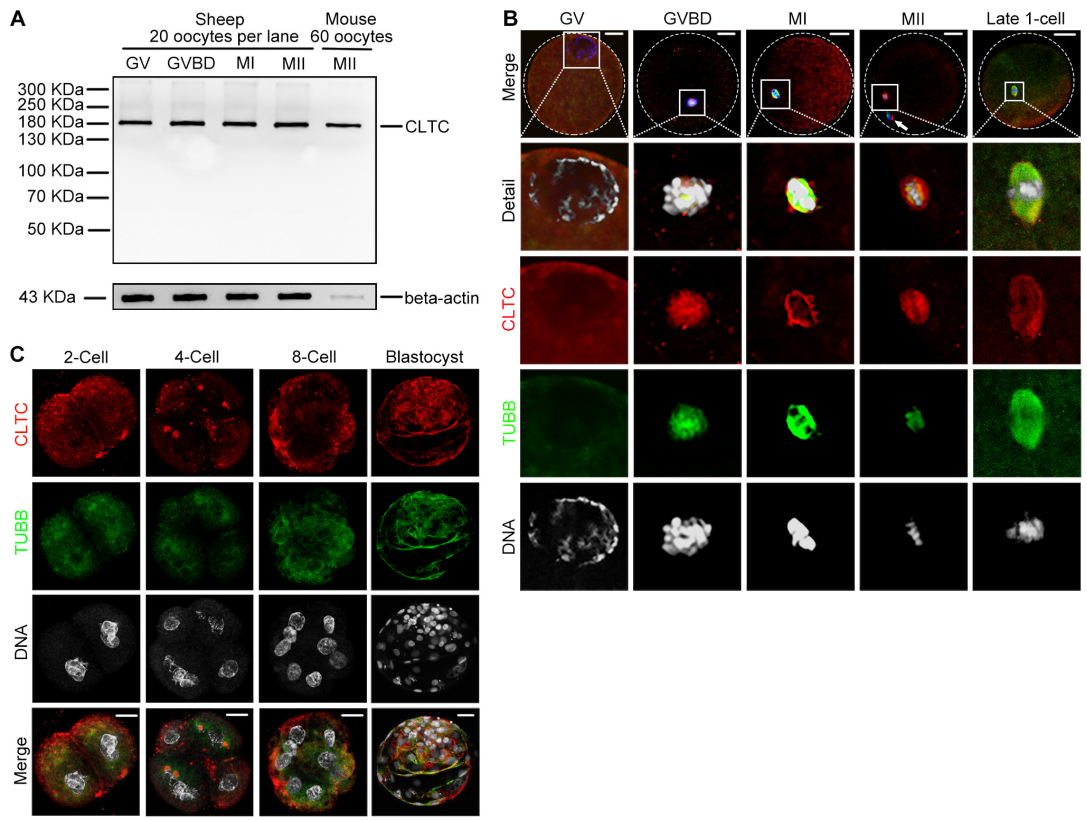

FIGURE 1 | Expression and subcellular localization of CLTC during sheep oocyte meiotic maturation and early embryonic development. **(A)** Immunoblotting analysis of CLTC in sheep oocytes during different stages of maturation (GV, GVBD, MI, and MII) and in mouse oocytes at MII stage. Lysate from 20 sheep oocytes or 60 mouse oocytes was loaded in the corresponding lanes. Beta-actin was used as a loading control. Oocyte samples were collected after being cultured for 0, 8, 12, and 24 h to reach the stages of GV, GVBD, MI, and MII, respectively. **(B,C)** Subcellular localizations of CLTC at each stage of oocyte and early embryonic development were detected by immunofluorescence staining. Slides were examined using a confocal microscope. White arrow indicates a polar body. Red, CLTC; green, TUBB; blue, DNA. Scale bar = 20 μm. CLTC, clathrin heavy chain 1; GV, germinal vesicle; GVBD, germinal vesicle breakdown; MI, metaphase I; MII, metaphase II.

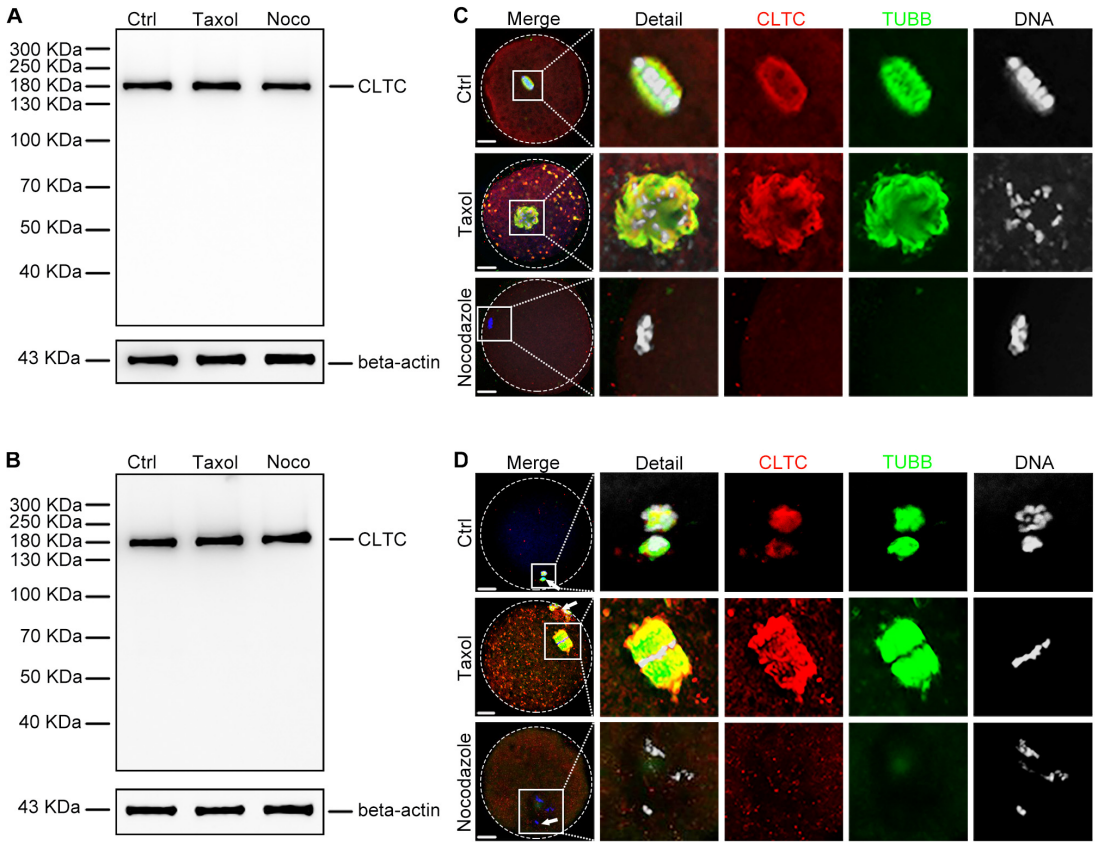

FIGURE 2 | Expression and localization of CLTC in metaphase oocytes treated with either taxol or nocodazole. **(A)** Immunoblotting analysis of CLTC from MI-stage oocytes after treatment with taxol or nocodazole. Beta-actin was used as a loading control. Noco, nocodazole. **(B)** Immunoblotting analysis of CLTC from MII-stage oocytes after treatment with either taxol or nocodazole. Beta-actin was used as a loading control. Noco, nocodazole. **(C)** Subcellular localizations of CLTC in MI-stage oocytes after treatment with either taxol or nocodazole were detected by immunofluorescence staining, respectively. Slides were examined using a confocal microscope. Red, CLTC; green, TUBB; blue, DNA. Scale bar = 20 μm. **(D)** Subcellular localizations of CLTC in MII-stage oocytes after treatment with either taxol or nocodazole were detected by immunofluorescence staining, respectively. Slides were examined using a confocal microscope. White arrows indicate polar bodies. Red, CLTC; green, TUBB; blue, DNA. Scale bar = 20 μm. CLTC, clathrin heavy chain 1; MI, metaphase I; MII, metaphase II.

taxol treatment, and many asters appeared in the cytoplasm of both MI- (**Figure 2C**) and MII-stage oocytes (**Figure 2D**). Similar distribution and localization of CLTC were also seen in the cytoplasm (**Figures 2C,D**). In contrast, when sheep MI and MII oocytes were treated with nocodazole to induce MT depolymerization, the immunofluorescence results showed completely depolymerized MTs. In addition, CLTC localization was also dispersed within the cytoplasm (**Figures 2C,D**). These results suggested that CLTC is involved in MT depolymerization and polymerization.

The cold-mediated MT depolymerization assay was used to assess the relationship between CLTC and MTs. Sheep oocytes were placed in a cold environment (4°C) to depolymerize MII-stage MTs and then re-incubated for 30 min at 38.5°C. Immunoblotting results showed that the expression level of CLTC did not change after the cold and rescue treatments (**Figure 3A**). Immunofluorescence staining showed depolymerized MTs and dispersed CLTC in the cytoplasm after cold treatment (**Figure 3B**). After rescue treatment, depolymerized MTs reassembled into spindles and CLTC localization also appeared in spindle regions (**Figure 3B**). Thus, the subcellular localization of CLTC in sheep oocytes requires the involvement of the spindle in MII-stage oocytes.

Knockdown of Clathrin Heavy Chain 1 Affects Spindle Assembly and Chromosome Congression During Oocyte Maturation

To investigate the role of CLTC in sheep oocyte maturation, we microinjected *CLTC*-MO into sheep GV oocytes to knockdown CLTC expression. The immunoblotting results demonstrated that CLTC expression decreased by 56% in the *CLTC*-MO-injected group compared with the control group (**Figures 4A,B**). Consistently, the immunostaining showed that CLTC staining intensity was much lower in the *CLTC*-MO group compared with the control group (**Figure 4C**), demonstrating the efficiency of CLTC knockdown by MO injection. Compared with the control group, the percentage of first polar body (PB1)-extrusion oocytes in the *CLTC*-MO group was significantly lower ($P < 0.05$)

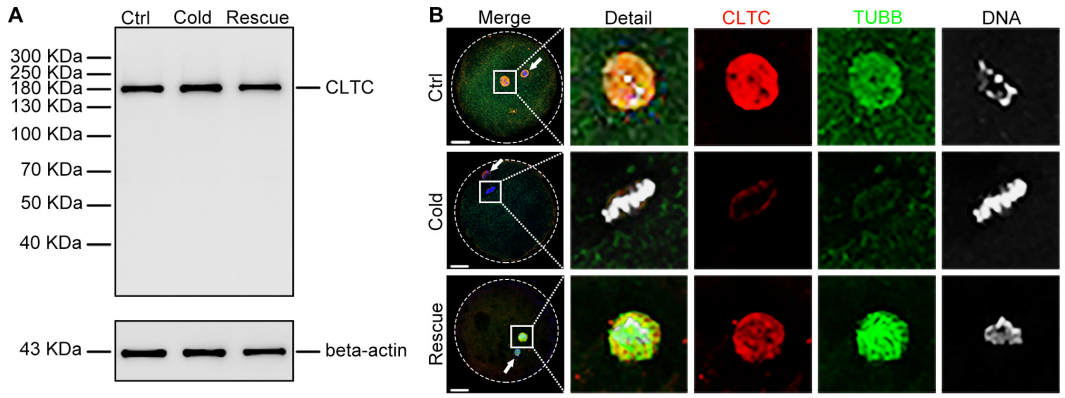

FIGURE 3 | Expression and localization of CLTC in MII oocytes after cold treatment. **(A)** Immunoblotting analysis of CLTC from MII-stage oocytes after cold or rescue treatment. Beta-actin was used as a loading control. **(B)** Subcellular localizations of CLTC in MII-stage oocytes after cold or rescue treatment were detected by immunofluorescence staining. Slides were examined using a confocal microscope. White arrows indicate polar bodies. Red, CLTC; green, TUBB; blue, DNA. Scale bar = 20 μm. CLTC, clathrin heavy chain 1; MII, metaphase II.

(**Figure 4D**). Moreover, severe spindle-assembly defects were also observed in the *CLTC*-MO group (**Figures 4E,F**). These spindle-assembly defects were categorized into three main types: type I failed to form spindle poles; type II exhibited residual beta-tubulin at the poles without kinetochore fibers; and type III could form a spindle, but it was multipolar (**Figure 4F**). The percentage of oocytes with abnormal spindles was much higher in the *CLTC*-MO group ($P < 0.01$) (**Figure 4E**). In addition, chromosome-congression defects (misaligned chromosomes) were also observed in the *CLTC*-MO group (**Figures 4F,G**), and the incidence misalignment was much higher after CLTC knockdown ($P < 0.01$) (**Figure 4G**). These results indicated that CLTC knockdown affected both spindle formation and chromosome congression during oocyte meiosis progression.

Knockdown of Clathrin Heavy Chain 1 Impairs Early Embryo Development in Sheep

To explore the functional role of CLTC in early embryo development in sheep, *CLTC*-MO was microinjected into sheep MII oocytes. The oocytes were then activated by parthenogenesis and cultured. We assessed the developmental rates of early embryos from the two-cell stage to the blastocyst stage. Embryos cultured for 24 h after parthenogenetic activation (during which *CLTC*-MO had an inhibitory effect) were collected for immunoblot analysis (**Figure 5A**). The immunoblot assessment showed that CLTC expression was significantly impaired by the specific MO injection (**Figures 5B,C**). In addition, immunofluorescence detection of CLTC in two-cell-stage embryos that undergoing cell division showed diminished staining in the CLTC-knockdown group. Consistently, chromosome alignment was also disturbed after CLTC impairment, illustrated by failures of metaphase plate formation (**Figure 5D**). In order to determine the effects of CLTC knockdown on the developmental procedure of both zygotic to embryo transition and the later embryo development, the number of MII-stage oocytes instead of two-cell was used as denominator to calculate the percent of embryo development to each stage. Unsurprisingly, disturbing CLTC function before the two-cell stage significantly reduced the formation of two-cell embryos ($P < 0.05$), four-cell embryos ($P < 0.01$), eight-cell embryos ($P < 0.01$), and morula embryos ($P < 0.01$) (**Figure 5E**). Approximately 13% of embryos in the control group were able to develop into blastocysts, whereas almost all of the embryos in the *CLTC*-MO group were arrested at various developmental stages; none of them progressed past the morula stage. After 5 days of culture, the blastocyst rate in the *CLTC*-MO group was significantly lower compared with the control group ($P < 0.001$) (**Figures 5E,F**). These results indicated that CLTC played a crucial role in the early embryo development of sheep.

DISCUSSION

Here, we assessed the expression profile of CLTC during oocyte maturation and early parthenogenetic embryo development in sheep. We also assessed the relationship between TUBB and CLTC, the functional role of CLTC in spindle formation and cell division, and the influence of spindle-perturbing drugs, cold treatment, and expression knockdown. Our results have shown that a lack of CLTC caused lower PB1 extrusion, spindle assembly defects, misaligned chromosomes, and impaired early embryo development, and we conclude that CLTC plays a vital role in spindle formation and chromosome congression to regulate the progression of oocyte meiosis and early embryo mitosis in sheep.

Clathrin is a cytosolic protein that mediates endocytosis through vesicular transport during interphase and has a vital role in stabilizing MT and chromosomal alignment during mitosis (Kirchhausen, 2000; Holzenspies et al., 2010; Fielding and Royle, 2013). Our previous studies in the mouse showed that CLTC played a key role in meiotic maturation by stabilizing metaphase spindle and chromosome congression through cooperation with CKAP5 (Zhao et al., 2013; Lu et al., 2017). The present study

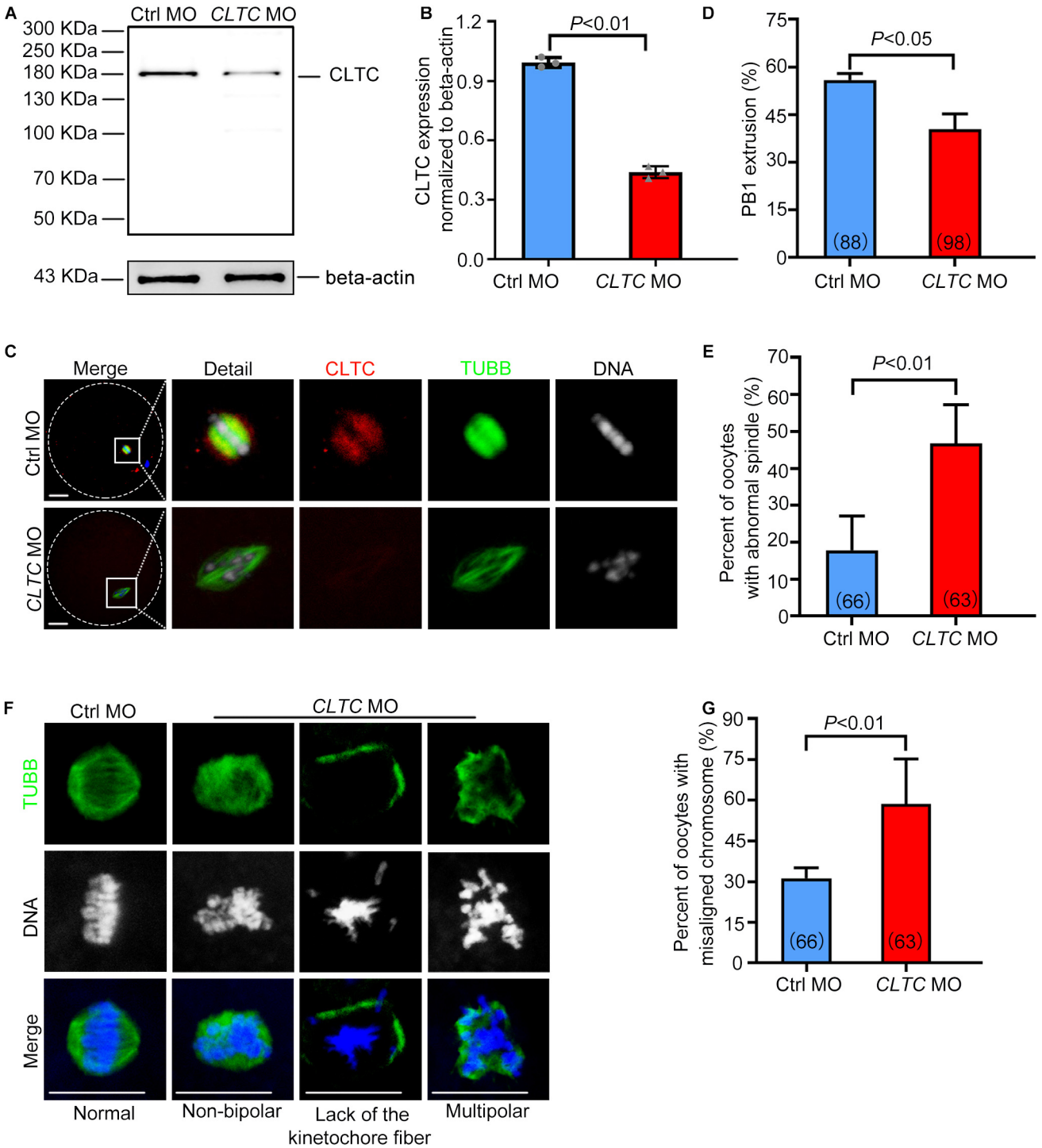

FIGURE 4 | CLTC knockdown in sheep oocytes induces spindle defects and misaligned chromosomes. **(A)** Immunoblotting of CLTC expression after either *CLTC*-MO or control-MO injections. Beta-actin was used as a loading control. **(B)** Band intensities (representing CLTC expression) were assessed using gray-level analyses after *CLTC*-MO or control-MO injections. **(C)** The CLTC, spindles, and DNA in MII-stage oocytes (control-MO and *CLTC*-MO groups) were stained with anti-CLTC (red), anti-tubulin (green), and DAPI (blue), respectively. Scale bar = 20 μm. **(D)** The percentage of oocytes demonstrating PB1 extrusion in the control-MO and *CLTC*-MO groups. **(E)** Percentages of oocytes with abnormal spindles in the control-MO and *CLTC*-MO groups. **(F)** Immunofluorescence staining of CLTC expression after *CLTC*-MO or control-MO injections. Green, TUBB; blue, DNA. Scale bar = 20 μm. **(G)** Percentages of oocytes with chromosome misalignments in the control-MO and *CLTC*-MO groups. Data are presented as mean ± SD from at least three independent experiments. $P < 0.05$ was considered statistically significant. CLTC, clathrin heavy chain 1; MO, morpholino; PB1, first polar body; DAPI, 4′,6-diamidino-2-phenylindole.

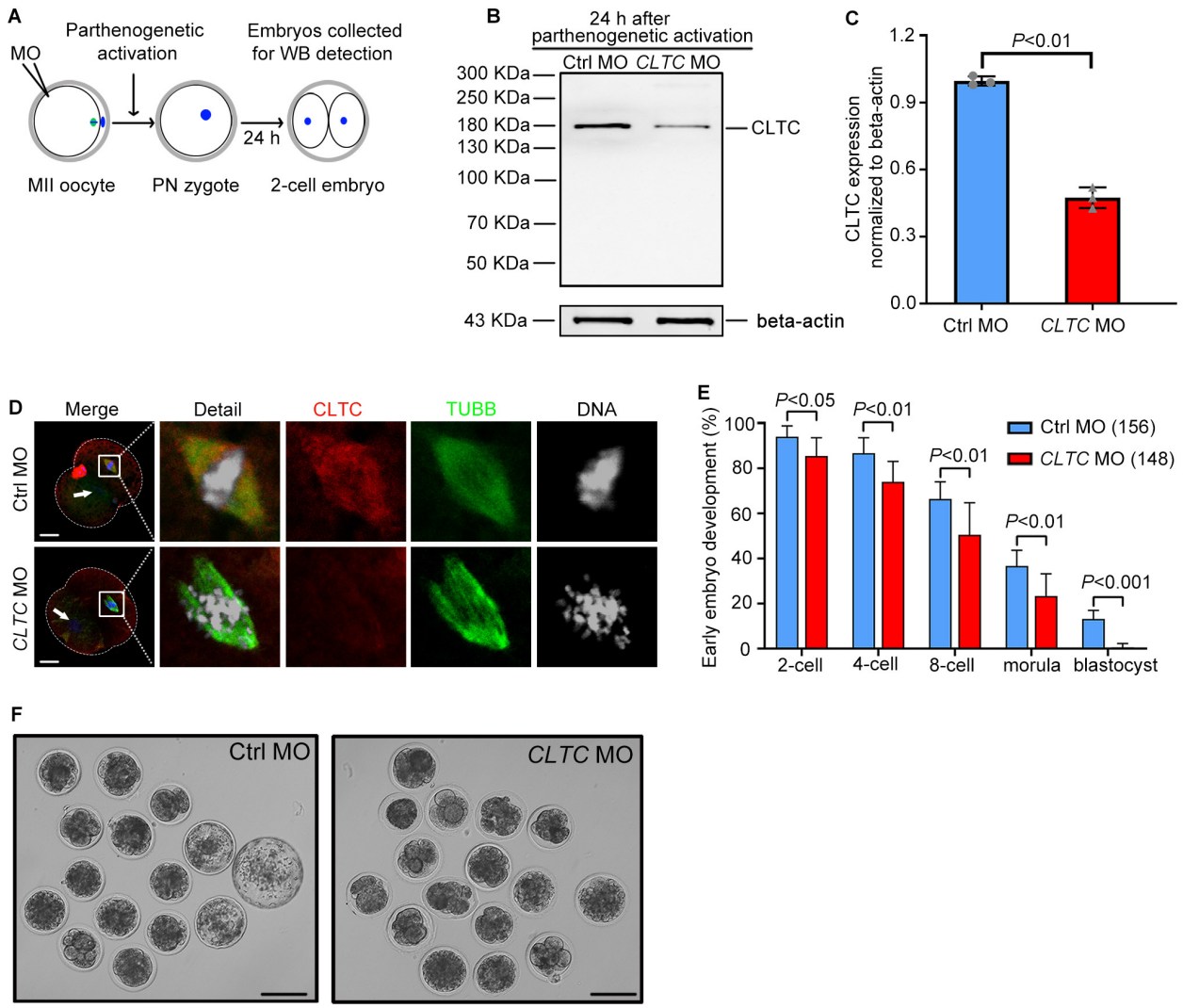

FIGURE 5 | MII-stage knockdown of CLTC impairs embryonic development. **(A)** Scheme for sample collections for immunoblotting analyses after MO injections into MII-stage oocytes. **(B)** CLTC-expression immunoblotting after *CLTC*-MO or control-MO injections into MII-stage sheep oocytes. Beta-actin was used as a loading control. **(C)** Band intensities (representing CLTC expression) were assessed using gray-level analyses after *CLTC*-MO or control-MO injections in MII-stage sheep oocytes. Data are presented as mean ± SD from three independent experiments. $P < 0.05$ was considered statistically significant. **(D)** The CLTC, spindles, and DNA in two-cell embryos from the control-MO and *CLTC*-MO groups were stained with anti-CLTC (red), anti-tubulin (green), and DAPI (blue), respectively. Scale bar = 20 μm. White arrows indicate the other blastomere nucleus. **(E)** MII-stage sheep oocytes were injected with either *CLTC*-MO or control-MO, and then the rate of early embryo developmental was measured. Data are presented as mean ± SD from eight independent repeats, and at least 12 MII oocytes were included for parthenogenetic activation in each group for each repeat. $P < 0.05$ was considered statistically significant. **(F)** Representative images of early embryos after *CLTC*-MO or control-MO injections. Scale bar = 100 μm. MII, metaphase II; CLTC, clathrin heavy chain 1; MO, morpholino; DAPI, 4′,6-diamidino-2-phenylindole.

is the first to report the necessity for CLTC during oocyte meiotic maturation and preimplantation embryo development in sheep. The oocyte expression of CLTC was maintained at a high level from the GV stage to the MII stage in sheep, which differs from our previous mouse results that CLTC expression was low at the GV stage and gradually increased to finally reach its highest level at the MII stage during oocyte meiotic maturation (Zhao et al., 2013). Oocyte maturation time in sheep required 22–24 h, considerably longer than the time required in mice (Wang et al., 2018, 2019); and as a result, more CLTC may be needed to regulate chromosomal separation during the longer maturation progress in sheep. In MII sheep oocytes, CLTC localized to the spindle, consistent with the results of our previous mouse study. The similar localization patterns of CLTC to the metaphase spindle areas of porcine, mouse, and sheep oocytes (Holzenspies et al., 2010; Zhao et al., 2013) indicate its fundamental functions in the spindle apparatus during oocyte meiosis. However, the colocalization between CLTC and tubulin appears to be only partial, with prominent extrusions at MI-stage spindle poles, which is different from our previous results (Zhao et al., 2013). In addition to diffuse cytoplasmic staining, we also found focal accumulations of CLTC at the plasma membrane

in the interphase two-cell and four-cell sheep embryos. This is probably due to CLTC participating in reassembly of the Golgi apparatus near the plasma membrane (Radulescu et al., 2007) and is required for postmitotic Golgi reformation (Radulescu and Shields, 2012). Additional studies need to be carried out to determine any differences in CLTC localization between mice and sheep during oocyte maturation and early embryo development.

The taxol, nocodazole, and cold-treatment experiments were designed to explore the relationship between CLTC and TUBB. Taxol is frequently used in MT-dynamics research because it stabilizes MTs as well as promotes non-spindle MT formations (Cao et al., 2018). Here, we observed that taxol treatment caused CLTC to form many cytoplasmic asters with MTs. It has been reported that the TACC3/ch-TOG/clathrin complex can stabilize the MTs of the mitotic spindle as inter-MT bridges and that ch-TOG is vital to MT aster assembly after taxol treatment (Dionne et al., 2000; Booth et al., 2011). The present results confirm that CLTC is involved in regulating MT assembly in sheep oocytes. After nocodazole treatment, CLTC localization was evenly dispersed in the cytoplasm with the collapse of the MI- and MII-stage spindles. However, CLTC expression was almost unchanged as assessed by immunoblotting, and similar results were seen in mouse oocytes (Zhao et al., 2013). Cold treatment has also been shown to accelerate MT depolymerization, and the results are similar to those of nocodazole treatment (Rieder, 1981). Interestingly, the depolymerized MTs reassembled into spindles, and CLTC localized to the spindle regions following rescue treatment. We therefore speculate that CLTC may participate in the regulation of MT assembly and that the subcellular localization of CLTC to spindles is dependent on intact MTs. The drug- and cold-treatment results provide further support for the role of CLTC in spindle and MT assembly in meiotic oocytes from sheep.

In order to further explore the functions of CLTC in sheep oocytes, CLTC expression was knocked down by a specific MO oligomer. This knockdown indicated that CLTC is indispensable for meiotic spindle assembly due to the larger proportion of abnormal spindles and a decreased polar body extrusion rate in the *CLTC*-MO group compared with the control group. We further discovered that chromosomes were not aligned properly at the spindle equator, and it is possible that CLTC in sheep, as previously demonstrated in mouse (Zhao et al., 2013), also assists with this crucial spindle process for correct chromosomal alignment at metaphase. Clathrin is a triskelion consisting of three heavy chains (each with an associated light chain), and the N-terminal domain of each leg can bind to the mitotic spindle (Halebian et al., 2017). A bridge hypothesis has been proposed whereby clathrin acts as a brace between two or three MTs within a kinetochore fiber to increase fiber stability during mitosis (Kirchhausen and Harrison, 1981; Royle et al., 2005; Royle and Lagnado, 2006). Clathrin recruits phosphorylated TACC3 and ch-TOG to form an inter-MT bridge (the TACC3/ch-TOG/clathrin complex) to stabilize kinetochore fibers and ensure proper spindle assembly and chromosome alignment (Royle et al., 2005; Booth et al., 2011). The removal of TACC3–ch-TOG–clathrin led to a decrease in spindle length and significant alterations in kinetochore dynamics (Cheeseman et al., 2013), and additional research (Ma et al., 2013) has shown that functional interactions between SNX9 and CLTC also stabilize mitotic-spindle kinetochore (K)-fibers to ensure both chromosomal alignment and segregation. The present results of CLTC knockdown in meiotic sheep oocytes are similar to those described for mouse oocytes and indicate that CLTC plays a functional role to regulate spindle formation and chromosome congression in oocyte meiotic maturation together with CKAP5 (Zhao et al., 2013; Lu et al., 2017). Accordingly, the significant PB1 reduction seen in the *CLTC*-MO group may have been to spindle assembly defects and abnormal chromosome separation caused by CLTC knockdown, suggesting its importance during oocyte maturation in sheep as well.

To further explore the functional role of CLTC in sheep early embryo development, *CLTC*-MO was microinjected into MII-stage sheep oocytes before parthenogenesis activation and being cultured to different embryonic stages. Similarly, *CLTC-MO* can be applied to sheep embryos for functional disturbance. Consistently, we observed disturbed chromosomal alignments and failures in metaphase-plate formations in 2-cell-stage embryos. We further found that early embryo development was impaired after CLTC knockdown in MII oocytes resulting in almost all of the *CLTC*-MO embryos showing arrested development and lower developmental rates compared with the control-MO group. Based on previous centrosome-positioning research showing that clathrin negatively regulated the pulling forces acting on centrosomes and spindle poles in one-cell *Caenorhabditis elegans* embryos and maintained proper tension of the acto-myosin cortex (Spiro et al., 2014), we speculate that the organization and tension of the actin–myosin cortex was also impaired by CLTC depletion during mitosis in sheep early embryo development, resulting in arrested maturation. Other studies have shown thicker metaphase plates in clathrin-depleted NRK cells and that centromeres did not organize on the mitotic spindle in an orderly manner (Royle et al., 2005). Consistent with our present observation of chromosomal scatter, clathrin knockdown was also shown to increase the incidence of misaligned chromosomes in metaphase-like cells and to destabilize kinetochore fibers, which led to defective chromosomal congression at the metaphase plate. Accordingly, we suggest that the CLTC regulatory mechanism in cell division at early embryo stages is similar to that for somatic mitotic cell division. Therefore, CLTC appears to be essential for early embryo development in sheep, but detailed mechanisms for its regulation of early embryo development remain to be elucidated.

In the present study, we have documented CLTC expression and localization during oocyte meiotic maturation and early embryo development in sheep. Taxol, nocodazole, and cold treatments were used to reveal the relationship between CLTC and TUBB. CLTC knockdown disrupted sheep oocyte meiotic spindle assembly and chromosomal alignment and impaired embryo-development potential. In conclusion, the results demonstrate that CLTC plays a vital role in regulating spindle assembly, chromosome congression during oocyte meiotic maturation, and early embryo developmental progression in sheep. In addition, this is one of few studies addressing the role of MT-associated proteins in oocytes and early embryo

development in domesticated animals, providing additional fundamental knowledge related to their reproduction.

DATA AVAILABILITY STATEMENT

The raw data supporting the conclusions of this article will be made available by the authors, without undue reservation.

ETHICS STATEMENT

The animal study was reviewed and approved by the Ethics Committee of Inner Mongolia University (Approval number: SYXK 2014-0002).

AUTHOR CONTRIBUTIONS

C-GL, D-JZ, ZH, XH, C-JZ, and JW conceived and designed the experiments and analyzed the data. ZH, XH, C-JZ, JW, XW, X-YW, D-JZ, and C-GL performed the experiments. ZH, XH, C-JZ, JW, and C-GL wrote the manuscript. All authors contributed to the article and approved the submitted version.

FUNDING

This work was supported by the NSF of China (31960158, 31871508, and 31671560 to C-GL and 31900596 to C-JZ), Major Projects of Natural Science Foundation of Inner Mongolia Autonomous Region (2019ZD09 to C-GL), Natural Science Foundation of Inner Mongolia Autonomous Region (2019BS03027 to C-JZ), Key Technology Research Plan Project of Inner Mongolia Autonomous Region (2019GG103 to C-GL), and Science and Technology Major Project of Inner Mongolia Autonomous Region of China to the State Key Laboratory of Reproductive Regulation and Breeding of Grassland Livestock (2020ZD0008 to C-GL).

REFERENCES

Booth, D. G., Hood, F. E., Prior, I. A., and Royle, S. J. (2011). A TACC3/ch-TOG/clathrin complex stabilises kinetochore fibres by inter-microtubule bridging. *EMBO J.* 30, 906–919. doi: 10.1038/emboj.2011.15

Cao, Y. N., Zheng, L. L., Wang, D., Liang, X. X., Gao, F., and Zhou, X. L. (2018). Recent advances in microtubule-stabilizing agents. *Eur. J. Med. Chem.* 143, 806–828. doi: 10.1016/j.ejmech.2017.11.062

Cheeseman, L. P., Booth, D. G., Hood, F. E., Prior, I. A., and Royle, S. J. (2011). Aurora a kinase activity is required for localization of TACC3/ch-TOG/clathrin inter-microtubule bridges. *Commun. Integr. Biol.* 4, 409–412. doi: 10.4161/cib.15250

Cheeseman, L. P., Harry, E. F., Mcainsh, A. D., Prior, I. A., and Royle, S. J. (2013). Specific removal of TACC3-ch-TOG-clathrin at metaphase deregulates kinetochore fiber tension. *J. Cell Sci.* 126, 2102–2113. doi: 10.1242/jcs.124834

Cotterill, M., Harris, S. E., Collado Fernandez, E., Lu, J., Huntriss, J. D., Campbell, B. K., et al. (2013). The activity and copy number of mitochondrial DNA in ovine oocytes throughout oogenesis in vivo and during oocyte maturation in vitro. *Mol. Hum. Reprod.* 19, 444–450. doi: 10.1093/molehr/gat013

Dionne, M. A., Sanchez, A., and Compton, D. A. (2000). ch-TOGp is required for microtubule aster formation in a mammalian mitotic extract. *J. Biol. Chem.* 275, 12346–12352. doi: 10.1074/jbc.275.16.12346

Duan, X., and Sun, S. C. (2019). Actin cytoskeleton dynamics in mammalian oocyte meiosis. *Biol. Reprod.* 100, 15–24. doi: 10.1093/biolre/ioy163

Dumont, J., and Desai, A. (2012). Acentrosomal spindle assembly and chromosome segregation during oocyte meiosis. *Trends Cell Biol.* 22, 241–249. doi: 10.1016/j.tcb.2012.02.007

Fielding, A. B., and Royle, S. J. (2013). Mitotic inhibition of clathrin-mediated endocytosis. *Cell Mol. Life. Sci.* 70, 3423–3433. doi: 10.1007/s00018-012-1250-8

Fotin, A., Cheng, Y., Sliz, P., Grigorieff, N., Harrison, S. C., Kirchhausen, T., et al. (2004). Molecular model for a complete clathrin lattice from electron cryomicroscopy. *Nature* 432, 573–579. doi: 10.1038/nature03079

Fu, W., Tao, W., Zheng, P., Fu, J., Bian, M., Jiang, Q., et al. (2010). Clathrin recruits phosphorylated TACC3 to spindle poles for bipolar spindle assembly and chromosome alignment. *J. Cell Sci.* 123, 3645–3651. doi: 10.1242/jcs.075911

Halebian, M., Morris, K., and Smith, C. (2017). Structure and assembly of clathrin cages. *Subcell Biochem.* 83, 551–567. doi: 10.1007/978-3-319-46503-6_20

Han, Z., Liang, C. G., Cheng, Y., Duan, X., Zhong, Z., Potireddy, S., et al. (2010). Oocyte spindle proteomics analysis leading to rescue of chromosome congression defects in cloned embryos. *J. Proteome Res.* 9, 6025–6032. doi: 10.1021/pr100827j

He, K., Marsland, R., Iii, Upadhyayula, S., Song, E., Dang, S., et al. (2017). Dynamics of phosphoinositide conversion in clathrin-mediated endocytic traffic. *Nature* 552, 410–414. doi: 10.1038/nature25146

Holzenspies, J. J., Roelen, B. A., Colenbrander, B., Romijn, R. A., Hemrika, W., Stoorvogel, W., et al. (2010). Clathrin is essential for meiotic spindle function in oocytes. *Reproduction* 140, 223–233. doi: 10.1530/rep-10-0045

Kim, D. H., Ko, D. S., Lee, H. C., Lee, H. J., Park, W. I., Kim, S. S., et al. (2004). Comparison of maturation, fertilization, development, and gene expression of mouse oocytes grown in vitro and in vivo. *J. Assist. Reprod. Genet.* 21, 233–240. doi: 10.1023/b:jarg.0000042008.83699.cc

Kirchhausen, T. (2000). Clathrin. *Annu. Rev. Biochem.* 69, 699–727.

Kirchhausen, T., and Harrison, S. C. (1981). Protein organization in clathrin trimers. *Cell* 23, 755–761. doi: 10.1016/0092-8674(81)90439-6

Lin, C. H., Hu, C. K., and Shih, H. M. (2010). Clathrin heavy chain mediates TACC3 targeting to mitotic spindles to ensure spindle stability. *J. Cell Biol.* 189, 1097–1105. doi: 10.1083/jcb.200911120

Lu, A., Zhou, C. J., Wang, D. H., Han, Z., Kong, X. W., Ma, Y. Z., et al. (2017). Cytoskeleton-associated protein 5 and clathrin heavy chain binding regulates spindle assembly in mouse oocytes. *Oncotarget* 8, 17491–17503. doi: 10.18632/oncotarget.15097

Ma, M. P., Robinson, P. J., and Chircop, M. (2013). Sorting nexin 9 recruits clathrin heavy chain to the mitotic spindle for chromosome alignment and segregation. *PLoS One* 8:e68387. doi: 10.1371/journal.pone.0068387

Maro, B., Johnson, M. H., Pickering, S. J., and Louvard, D. (1985). Changes in the distribution of membranous organelles during mouse early development. *J. Embryol. Exp. Morphol.* 90, 287–309.

Mogessie, B., Scheffler, K., and Schuh, M. (2018). Assembly and positioning of the oocyte meiotic spindle. *Annu. Rev. Cell Dev. Biol.* 34, 381–403. doi: 10.1146/annurev-cellbio-100616-060553

Namgoong, S., and Kim, N. H. (2018). Meiotic spindle formation in mammalian oocytes: implications for human infertility. *Biol. Reprod.* 98, 153–161. doi: 10.1093/biolre/iox145

Petry, S. (2016). Mechanisms of mitotic spindle assembly. *Annu. Rev. Biochem.* 85, 659–683. doi: 10.1146/annurev-biochem-060815-014528

Radonova, L., Svobodova, T., and Anger, M. (2019). Regulation of the cell cycle in early mammalian embryos and its clinical implications. *Int. J. Dev. Biol.* 63, 113–122. doi: 10.1387/ijdb.180400ma

Radulescu, A. E., and Shields, D. (2012). Clathrin is required for postmitotic Golgi reassembly. *FASEB J.* 26, 129–136. doi: 10.1096/fj.10-167684

Radulescu, A. E., Siddhanta, A., and Shields, D. (2007). A role for clathrin in reassembly of the Golgi apparatus. *Mol. Biol. Cell* 18, 94–105. doi: 10.1091/mbc.e06-06-0532

Rao, S. R., Flores-Rodriguez, N., Page, S. L., Wong, C., Robinson, P. J., and Chircop, M. (2016). The Clathrin-dependent spindle Proteome. *Mol. Cell. Proteomics* 15, 2537–2553. doi: 10.1074/mcp.m115.054809

Rieder, C. L. (1981). The structure of the cold-stable kinetochore fiber in metaphase PtK1 cells. *Chromosoma* 84, 145–158. doi: 10.1007/bf00293368

Royle, S. J., Bright, N. A., and Lagnado, L. (2005). Clathrin is required for the function of the mitotic spindle. *Nature* 434, 1152–1157. doi: 10.1038/nature03502

Royle, S. J., and Lagnado, L. (2006). Trimerisation is important for the function of clathrin at the mitotic spindle. *J. Cell Sci.* 119, 4071–4078. doi: 10.1242/jcs.03192

Spiro, Z., Thyagarajan, K., De Simone, A., Trager, S., Afshar, K., and Gonczy, P. (2014). Clathrin regulates centrosome positioning by promoting acto-myosin cortical tension in C. elegans embryos. *Development* 141, 2712–2723. doi: 10.1242/dev.107508

Velilla, E., Rodriguez-Gonzalez, E., Vidal, F., and Paramio, M. T. (2005). Microtubule and microfilament organization in immature, in vitro matured and in vitro fertilized prepubertal goat oocytes. *Zygote* 13, 155–165. doi: 10.1017/s0967199405003229

Wang, D. H., Ren, J., Zhou, C. J., Han, Z., Wang, L., and Liang, C. G. (2018). Supplementation with CTGF, SDF1, NGF, and HGF promotes ovine in vitro oocyte maturation and early embryo development. *Domest. Anim. Endocrinol.* 65, 38–48. doi: 10.1016/j.domaniend.2018.05.003

Wang, H. H., Zhang, Y., Tang, F., Pan, M. H., Wan, X., Li, X. H., et al. (2019). Rab23/Kif17 regulate meiotic progression in oocytes by modulating tubulin acetylation and actin dynamics. *Development* 146:dev171280. doi: 10.1242/dev.171280

Webster, A., and Schuh, M. (2017). Mechanisms of aneuploidy in human eggs. *Trends Cell Biol.* 27, 55–68. doi: 10.1016/j.tcb.2016.09.002

Xu, X. L., Ma, W., Zhu, Y. B., Wang, C., Wang, B. Y., An, N., et al. (2012). The microtubule-associated protein ASPM regulates spindle assembly and meiotic progression in mouse oocytes. *PLoS One* 7:e49303. doi: 10.1371/journal.pone.0049303

Zhao, J., Wang, L., Zhou, H. X., Liu, L., Lu, A., Li, G. P., et al. (2013). Clathrin heavy chain 1 is required for spindle assembly and chromosome congression in mouse oocytes. *Microsc. Microanal.* 19, 1364–1373. doi: 10.1017/s1431927613001943

Zhou, C. J., Wang, X. Y., Han, Z., Wang, D. H., Ma, Y. Z., and Liang, C. G. (2019). Loss of CENPF leads to developmental failure in mouse embryos. *Cell Cycle* 18, 2784–2799. doi: 10.1080/15384101.2019.1661173

Conflict of Interest: The authors declare that the research was conducted in the absence of any commercial or financial relationships that could be construed as a potential conflict of interest.

frontiers in Cell and Developmental Biology

ORIGINAL RESEARCH
published: 25 February 2021
doi: 10.3389/fcell.2021.627140

Deactivation of the JNK Pathway by GSTP1 Is Essential to Maintain Sperm Functionality

Marc Llavanera[1,2], Yentel Mateo-Otero[1,2], Ariadna Delgado-Bermúdez[1,2], Sandra Recuero[1,2], Samuel Olives[1,2], Isabel Barranco[1,2†] and Marc Yeste[1,2*†]*

[1] *Biotechnology of Animal and Human Reproduction (TechnoSperm), Institute of Food and Agricultural Technology, University of Girona, Girona, Spain,* [2] *Unit of Cell Biology, Department of Biology, Faculty of Sciences, University of Girona, Girona, Spain*

OPEN ACCESS

Edited by:
Ana Josefa Soler, University of Castilla–La Mancha, Spain

Reviewed by:
David Martin Hidalgo, University of Porto, Portugal
Olga Garcia-Alvarez, University of Castilla–La Mancha, Spain

****Correspondence:***
Isabel Barranco
isabel.barranco@udg.edu
Marc Yeste
marc.yeste@udg.edu

† These authors share senior authorship

Specialty section:
This article was submitted to Cell Growth and Division, a section of the journal Frontiers in Cell and Developmental Biology

Received: *08 November 2020*
Accepted: *22 January 2021*
Published: *25 February 2021*

Citation:
Llavanera M, Mateo-Otero Y, Delgado-Bermúdez A, Recuero S, Olives S, Barranco I and Yeste M (2021) Deactivation of the JNK Pathway by GSTP1 Is Essential to Maintain Sperm Functionality. Front. Cell Dev. Biol. 9:627140. doi: 10.3389/fcell.2021.627140

Fifty percent of male subfertility diagnosis is idiopathic and is usually associated with genetic abnormalities or protein dysfunction, which are not detectable through the conventional spermiogram. Glutathione *S*-transferases (GSTs) are antioxidant enzymes essential for preserving sperm function and maintaining fertilizing ability. However, while the role of GSTP1 in cell signaling regulation via the inhibition of c-Jun N-terminal kinases (JNK) has been enlightened in somatic cells, it has never been investigated in mammalian spermatozoa. In this regard, a comprehensive approach through immunoblotting, immunofluorescence, computer-assisted sperm assessment (CASA), and flow cytometry analysis was used to characterize the molecular role of the GSTP1–JNK heterocomplex in sperm physiology, using the pig as a model. Immunological assessments confirmed the presence and localization of GSTP1 in sperm cells. The pharmacological dissociation of the GSTP1–JNK heterocomplex resulted in the activation of JNK, which led to a significant decrease in sperm viability, motility, mitochondrial activity, and plasma membrane stability, as well as to an increase of intracellular superoxides. No effects in intracellular calcium levels and acrosome membrane integrity were observed. In conclusion, the present work has demonstrated, for the first time, the essential role of GSTP1 in deactivating JNK, which is crucial to maintain sperm function and has also set the grounds to understand the relevance of the GSTP1–JNK heterocomplex for the regulation of mammalian sperm physiology.

Keywords: ezatiostat, GSTP1-JNK heterocomplex, mitochondria, sperm functionality, mammalian sperm

INTRODUCTION

In humans, about 30–50% of fertilizations fail because of male subfertility problems, usually related to abnormal sperm count, motility, and/or morphology (Ghuman and Ramalingam, 2017). However, over 50% of male subfertility diagnosis is of unknown etiology, since no abnormalities are detected in conventional semen analysis (sperm count, motility, and morphology) (Ghuman and Ramalingam, 2017). These patients are diagnosed as normozoospermic subfertile men (i.e., male idiopathic subfertility). Male idiopathic subfertility has been associated with genetic abnormalities (Carrell et al., 2006) and low levels of sperm-specific proteins (Parent et al., 1999; Bracke et al., 2018). While the general processes of sperm maturation, capacitation, and fertilization are well

described, the underlying molecular mechanisms that take place in mammalian sperm cells remain mostly unknown (Klinovska et al., 2014). The origin of male idiopathic subfertility may be explained by molecular defects in these processes, since they are not detectable through the conventional spermiogram (Bracke et al., 2018). For this reason, characterization of signaling pathways and posttranslational modifications in mammalian sperm cells are of utmost interest for the andrology field.

Several studies reported the association between male idiopathic subfertility or infertility and some null genotypes of glutathione *S*-transferases (GSTs) (Aydos et al., 2009; Safarinejad et al., 2010; Vani et al., 2010; Tang et al., 2012; Kan et al., 2013; Lakpour et al., 2013; Song et al., 2013; Kolesnikova et al., 2017). Moreover, recent studies have evidenced the essential role of these antioxidant enzymes in sperm protection against oxidative stress and preservation of sperm function and fertilizing ability (Llavanera et al., 2019b, 2020). The first evidence of GST activity in mammalian sperm dates back to 1978 in murine species (Mukhtar et al., 1978), and the first report confirming the presence of the Pi class of GSTs (GSTP1) was published in 1998 in goat sperm (Gopalakrishnan et al., 1998). Since then, several proteomic profiling studies have identified GSTP1 in the sperm cells of a wide range of mammalian species, including humans (Wang et al., 2013), mice (Vicens et al., 2017), pigs (Pérez-Patino et al., 2019), cattle (Peddinti et al., 2008), and coatis (Rodrigues-Silva et al., 2018). In somatic cells, the main well-defined function of GSTP1 is cell signaling regulation via inhibition of the c-Jun N-terminal kinase (JNK)–C-Jun pathway (Adler et al., 1999; Wang et al., 2001; Turella et al., 2005). In non-stressed cells, GSTP1 is able to inhibit JNK kinase activity by blocking the JNK-binding site to C-Jun, forming a GSTP1–JNK heterocomplex. However, under cellular stress conditions, a GSTP1 aggregation followed by its dissociation from the heterocomplex leads to an increase in JNK activity (Adler et al., 1999; Wang et al., 2001; Turella et al., 2005). Recently, the JNK signaling cascade has been reported to be involved in sperm capacitation and apoptosis (Luna et al., 2017), which may undercover the role of GSTP1 in sperm physiology. However, the role of GSTP1 and the JNK–C-Jun pathway in mammalian sperm still remains unknown.

Ezatiostat or Terrapin 199 (TER) is a specific inhibitor of the GSTP1–JNK heterocomplex, used as an anticancer drug (Wu and Batist, 2013). After intracellular de-esterification, which is a process that commonly occurs in sperm cells (Griveau and Le Lannou, 1997), the active form of TER binds to GSTP1, blocking its JNK-binding site and, therefore, inhibiting the formation of the GSTP1–JNK heterocomplexes (Mathew et al., 2006). This inhibition enables JNK phosphorylation and activation of the subsequent pathway.

Along these lines, understanding the molecular role of the GSTP1–JNK heterocomplex in mammalian sperm physiology is much warranted. Herein, cell biology and immunological approaches were performed through pharmacologically inhibiting the formation of the GSTP1–JNK heterocomplex, prior to analyzing sperm quality and functionality parameters, the presence and localization of GSTP1, and the activation of JNK. Therefore, the present study aimed to investigate the function of this heterocomplex in mammalian sperm physiology, using the pig as a model, which has recently been stablished as a suitable animal model for research in human reproduction (Zigo et al., 2020). Accordingly, we hypothesized that the dissociation of the GSTP1–JNK heterocomplex, known to occur under cellular stress conditions, enhances the JNK signaling pathway and disrupts sperm physiology. The results obtained in this study can be used as a starting point for further investigations seeking the molecular basis of sperm dysfunction and may contribute to shedding light into the diagnosis of idiopathic male infertility.

MATERIALS AND METHODS

Reagents

Chemicals and reagents were purchased from Sigma-Aldrich (Saint Louis, MO, United States), unless otherwise indicated. TER was reconstituted in dimethyl sulfoxide (DMSO) to a stock solution of 64 mM. Fluorochromes [SYBR-14, propidium iodide (PI), merocyanine 540 (M540), Yo-Pro-1, 5,5′,6,6′-tetrachloro-1,1′,3,3′-tetraethyl-benzimidazolylcarbocyanine iodide (JC1), Fluo3-AM (Fluo3), hydroethidine (HE), and fluorescein-conjugated peanut agglutinin/PI (PNA)] were purchased from Life Technologies (Thermo Fisher Scientific, Carlsbad, CA, United States). SYBR-14, M540, Yo-Pro-1, JC1, Fluo3, and HE were reconstituted in DMSO, whereas PI and PNA were diluted in phosphate-buffered saline (PBS) 1X. Antibody against GSTP1 (ref. MBS3209038) was purchased from MyBioSource (San Diego, CA, United States), whereas phospho-JNK (Thr183/Tyr185) antibody (pJNK, ref. 4668S) was purchased from Cell Signaling Technology (Danvers, MA, United States). Secondary anti-rabbit (ref. P0448) and anti-mouse (ref. P0260) antibodies conjugated with horseradish peroxidase for immunoblotting analysis were purchased from Dako (Derkman A/S, Denmark), whereas the secondary anti-rabbit antibody conjugated with Alexa Fluor 488 for immunofluorescence analysis was purchased from Thermo Fisher Scientific (ref. A32731).

Animals and Ejaculates

Semen samples, commercially sold as pig artificial insemination (AI) seminal doses, were purchased from an authorized local AI center (Grup Gepork S.L., Masies de Roda, Spain) that followed ISO certification (ISO-9001:2008) and operates under commercial, standard conditions. Thirteen ejaculates (one ejaculate per boar, $n = 13$) from healthy and sexually mature Piétrain boars (1–3 years old) were collected using the gloved-hand method and diluted (33×10^6 sperm/ml) using a commercial extender (Vitasem LD, Magapor S.L., Zaragoza, Spain). Packed ejaculates were transported at 17°C to the laboratory within 4 h after ejaculation. Since seminal doses were purchased from the aforementioned farm and the authors of this study did not manipulate any animal, no authorization from the institutional ethics committee was required.

Experimental Design

All semen samples ($n = 13$) were split into three aliquots. The first aliquot was used to assess initial sperm quality

and functionality (control-0h). The second and third aliquots were liquid-stored at 17°C for 72 h in the presence of (i) 100 μM ezatiostat (TER-72h) and (ii) the same volume of DMSO, as a vehicle control group (control-72h). Concentration of TER was selected based on the results obtained from a preliminary concentration test performed in our laboratory (**Supplementary Figure 1**), whereas storage time was decided following practical application criteria, considering that sows are artificially inseminated (two to three times per estrus) with AI doses stored until 72 h at 17°C. After 72 h, both groups were incubated at 38°C for 1 h prior to their analysis. All assessments were performed at every time point (control-0h, control-72h, and TER-72 h). Sperm motility, viability, plasma membrane stability, mitochondrial activity, intracellular calcium levels, intracellular superoxide levels, and acrosome membrane integrity were determined to evaluate sperm quality and functionality. The presence and localization of GSTP1 were explored by immunoblotting and immunofluorescence analyses, respectively. Finally, the activation of the JNK pathway was evaluated through immunoblotting analysis of JNK tyrosine and threonine phosphorylation. Raw data of sperm quality and functionality parameters of all treatments and time points are available as a data set (**Supplementary Table 1**).

Sperm Motility Analysis

Sperm motility assessment was performed through a computer-assisted sperm analysis (CASA) system, using an Olympus BX41 microscope (Olympus, Tokyo, Japan) with a negative phase-contrast field (Olympus 10 × 0.30 PLAN objective, Olympus) connected to a personal computer containing the ISAS software (Integrated Sperm Analysis System V1.0, Proiser S.L., Valencia, Spain). Semen samples were incubated for 15 min at 38°C prior to motility assessment. Once incubated, 5 μl of each sample was examined in a prewarmed (38°C) Makler counting chamber (Sefi Medical Instruments, Haifa, Israel). Three technical replicates of at least 500 sperm per replicate were examined in each sample. Total motility (TMOT), progressive motility (PMOT), and average path velocity (VAP, μm/s) were used to evaluate sperm motility. A sperm cell was considered motile when VAP was ≥10 μm/s and progressively motile when the coefficient of straightness (STR) was ≥45%.

Flow Cytometric Assessments

Sperm viability, plasma membrane stability, mitochondrial activity, intracellular calcium levels, intracellular superoxide levels, and acrosome membrane integrity assessments were conducted using a Cell Laboratory QuantaSC cytometer (Beckman Coulter, Fullerton, CA, United States) equipped with an argon-ion laser (488 nm) set at a power of 22 mW. Semen samples were diluted (2×10^6 sperm/ml) in prewarmed PBS to a final volume of 600 μl prior to staining with the corresponding protocol. Sperm viability (SYBR-14/PI) (Garner and Johnson, 1995), plasma membrane stability (M540/Yo-Pro-1) (Rathi et al., 2001), mitochondrial membrane potential (MMP; JC1) (Ortega-Ferrusola et al., 2007), intracellular calcium levels (Fluo3/PI) (Harrison et al., 1993), intracellular superoxide levels (HE/Yo-Pro-1) (Guthrie and Welch, 2006), and acrosome membrane integrity (fluorescein-conjugated PNA/PI) (Nagy et al., 2003) were assessed. Extended flow cytometry protocols are described in **Supplementary File 1**.

The electronic volume (EV) gain, PMT voltages of optical filters (FL-1, FL-2, and FL-3), and fluorescence overlapping were set using unstained and single-stained samples of each fluorochrome. Flow rate, laser voltage, and sperm concentration were constant throughout the experiment. Sperm cells from debris events were distinguished using EV. Three technical replicates of at least 10,000 sperm per replicate were examined for each sample. As recommended by the International Society for Advancement of Cytometry (ISAC), Flowing Software (Ver. 2.5.1, University of Turku, Finland) was used to analyze flow cytometry data.

Immunofluorescence Analysis

Semen samples were diluted in PBS (3×10^6 sperm/ml) and fixed in 2% paraformaldehyde (Alfa Aesar, Haverhill, MA, United States) and washed twice. Two 150-μl aliquots of each sample were placed in an ethanol prerinsed slide and subsequently blocked and permeabilized for 40 min at room temperature (RT) with a blocking solution containing 0.25% (v:v) Triton X-100 and 3% (w:v) bovine serum albumin (BSA). Samples were incubated with anti-GSTP1 antibody (1:200, v:v) overnight, washed thrice, and subsequently incubated with an anti-rabbit antibody (1:400, v:v). In negative controls, the primary antibody was omitted. Then, 10 μl of Vectashield mounting medium containing 4,6-diamidino-2-phenylindole dihydrochloride (DAPI) was added prior to being covered and sealed with nail varnish. Finally, each sample was evaluated using a confocal laser scanning microscope (CLSM, Nikon A1R, Nikon Corp., Tokyo, Japan).

Immunoblotting Analysis

Semen samples were centrifuged twice (3,000 × *g* for 5 min), and the sperm pellets were resuspended in lysis buffer (xTractor™ buffer, Takara Bio, Kusatsu, Japan) following the manufacturer's instructions. Then, samples were centrifuged (10,000 × *g* for 20 min at 4°C), and the supernatants were assessed for total protein quantification using a detergent-compatible method (Bio-Rad, Hercules, CA, United States). Finally, samples were stored at −80°C until analysis.

Twenty micrograms of total protein was diluted (1:1, v:v) in Laemmli reducing buffer 4X (Bio-Rad) and heated at 95°C for 7 min prior to being loaded onto a 12% polyacrylamide gel (Mini-PROTEAN® TGX Stain-Free™ Precast Gels, Bio-Rad) and electrophoresed for 2 h at 120 V. Total protein was visualized using a G:BOX Chemi XL system (Syngene, Frederick, MD, United States). Mini-PROTEAN® TGX Stain-Free™ Precast Gels contain a trihalo compound that allows fluorescent detection of tryptophan residues. Thereafter, proteins from the gel were transferred onto polyvinylidene difluoride (PVDF) membranes using the Trans-Blot® Turbo™ (Bio-Rad). Transferred membranes were blocked using 5% BSA and incubated with the anti-GSTP1 (1:5,000, v:v) or anti-pJNK (1:2,000, v:v) antibodies for 1 h in agitation at RT. Next, membranes were rinsed thrice and incubated with the secondary

anti-rabbit antibody 1:10,000 (v:v) for GSTP1 and 1:4,000 (v:v) for pJNK. Then, membranes were washed five times, and bands were visualized through incubation with a chemiluminescent substrate (Immobilon^{TM} Western Detection Reagents, Millipore, United States) prior to scanning with G:BOX Chemi XL 1.4 (Syngene, India). Finally, membranes were stripped, and the process was repeated by replacing the primary antibody for the anti-α-tubulin antibody (1:100,000, v:v) and the secondary antibody for the anti-mouse antibody (1:150,000, v:v), as loading control and for normalization. In the pJNK assessment, Quantity One software package (Version 4.6.2, Bio-Rad) was used to quantify the bands of two technical replicates per sample, normalized using α -tubulin.

Statistical Analysis

Plotting and statistical analysis of the results were performed using GraphPad Prism v.8 (GraphPad Software, La Jolla, CA, United States) and IBM SPSS for Windows v. 25.0 (IBM Corp., Armonk, NY, United States). Each biological replicate was considered a statistical case, and data were checked for normal distribution (Shapiro–Wilk test) and homogeneity of variances (Levene test). Sperm quality and functionality parameters, as well as normalized pJNK relative levels, were compared between treatments (control-0h, control-72h, and TER-72h) using a one-way ANOVA followed by Tukey's multiple-comparison test. Data are shown as mean ± standard error of the mean (SEM). The level of significance was set at $p \leq 0.05$.

RESULTS

GSTP1 Is Present in Sperm Cells and Is Localized in the Principal and End Pieces of the Tail

The presence and localization of GSTP1 in sperm samples are presented in **Figures 1**, **2**. Immunoblotting analysis of GSTP1 (**Figure 1A**) showed a single band of ∼48 kDa in all samples, whereas anti-α-tubulin (**Figure 1B**) showed a ∼50 kDa band. In **Figure 2**, a GSTP1 signal was observed in the posterior region of the head and the middle, principal, and end pieces of the tail of control-0h samples. In control-72h and TER-72h samples, the GSTP1 signal was observed only in the equatorial subdomain of the head and in the principal and end pieces of the tail.

Inhibition of GSTP1–JNK Heterocomplex Formation by TER Induces Thr183 and Tyr185 Phosphorylation of JNK

Immunoblotting analysis of Thr183 and Tyr185 phosphorylation of JNK revealed a double-band pattern showing both p46 and p54 splicing variants of JNK (**Figure 3**). Anti-α-tubulin immunoblot showed a single band of ∼50 kDa, which corresponds to α-tubulin. Subsequent band quantification analysis of pJNK normalized using α-tubulin showed a significant increase ($p < 0.05$) in the relative levels of Thr183 and Tyr185 phosphorylation of the p46 splicing variant of JNK in TER-72h samples when compared to control-0h and control-72h samples. However, no effects of TER were observed in Thr183 and Tyr185 phosphorylation of the p54 splicing variant ($p > 0.05$).

Sperm Viability Is Reduced by TER-Induced JNK Phosphorylation

The percentage of viable sperm was higher ($p < 0.05$) in the semen samples of the control-0h group than in those of the TER-72h and control-72h groups (**Figure 4**). In addition, sperm viability was lower ($p < 0.05$) in the semen samples of the TER-72h group compared to those of the control-72h group.

Phosphorylation of JNK by the Inhibition of GSTP1–JNK Binding Impairs Sperm Motility

As shown in **Figure 5**, the percentage of total and progressive motile sperm was higher ($p < 0.05$) in the semen samples of the control-0h group than in those of the control-72h and TER-72h groups. However, VAP was lower ($p < 0.05$) in the semen samples of the TER-72h group compared to those of the control groups (0 and 72 h). Interestingly, total and progressive motility and VAP were significantly lower ($p < 0.05$) in the semen samples of the TER-72h group than in those of the control-72h group.

Mitochondrial Activity Is Significantly Reduced by JNK Phosphorylation by the Inhibition of GSTP1–JNK Binding

The assessment of MMP is presented in **Figure 6**. The percentage of sperm showing high MMP differed ($p < 0.05$) among the three groups, with the semen samples of the control-0h and TER-72h groups showing the highest and lowest percentages, respectively. Thus, a dramatic reduction in MMP was observed in the TER-72h group when compared to the control groups.

Sperm Plasma Membrane Is Highly Destabilized by the Inhibition of GSTP1–JNK Binding and Subsequent JNK Phosphorylation

As shown in **Figure 7**, sperm membrane stability was presented as the percentage of membrane-destabilized cells within the total viable sperm population. The percentage of viable sperm showing plasma membrane destabilization was higher ($p < 0.05$) in the semen samples of the TER-72h group than in those of the control groups (0 and 72 h). On the other hand, the plasma membrane stability of the semen samples did not differ between control groups ($p > 0.05$).

Intracellular Superoxide Levels Were Increased by the Phosphorylation of JNK

Figure 8 shows the relative E+ fluorescence intensity of the viable sperm population. No differences ($p > 0.05$) were observed in intracellular superoxide levels between semen samples of control groups (0 and 72 h). However, our results showed a significant increase ($p < 0.05$) in superoxide levels in semen samples of the TER-72h group compared to those of the control groups (0 and 72 h).

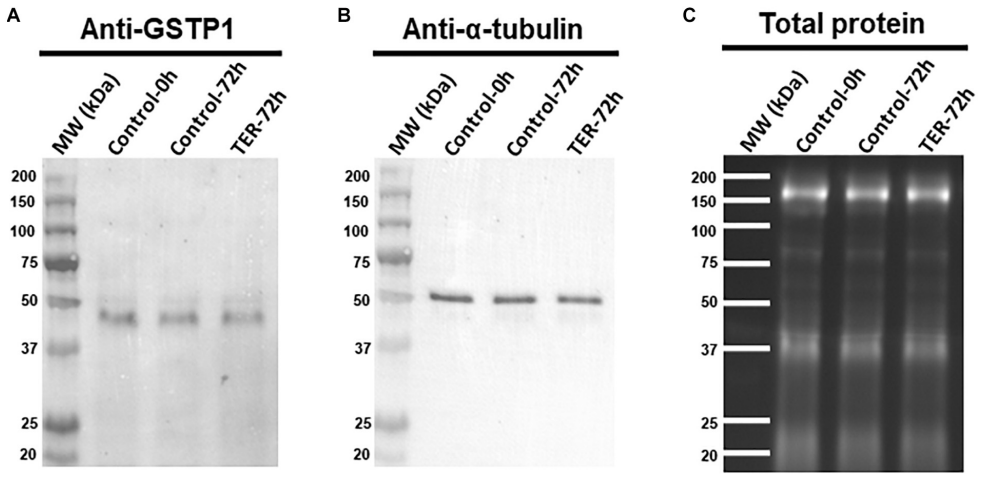

FIGURE 1 | Immunoblotting analysis of GSTP1. Pig sperm lysates were incubated with **(A)** anti-GSTP1 antibody, **(B)** anti-α-tubulin antibody, and **(C)** total protein bands. Lanes: MW (kDa), molecular weight; Control-0h, semen samples at 0 h of storage; Control-72h, vehicle control (dimethyl sulfoxide; DMSO) semen samples at 72 h of storage at 17°C; TER-72h, semen samples treated with 100 μM ezatiostat (TER) for 72 h of storage at 17°C. Alpha-tubulin (anti-tubulin) and TGX Stain-Free™ (total protein) were performed as complementary loading controls. These results are representative of three independent experiments (n = 3).

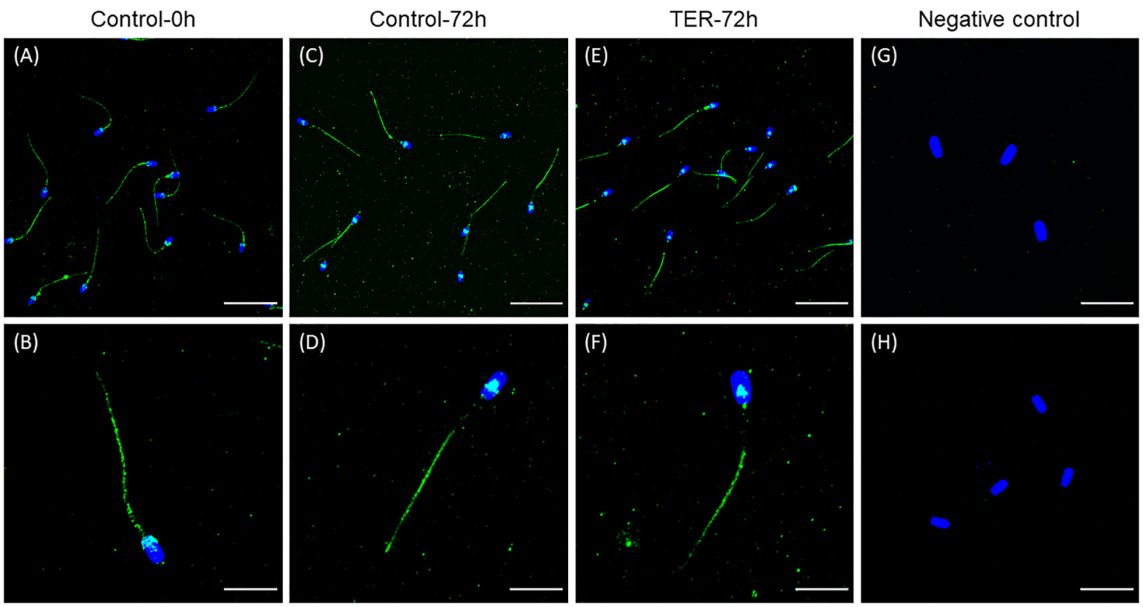

FIGURE 2 | Immunolocalization of GSTP1 in pig sperm. **(A,B)** Control-0h, semen samples at 0 h of storage. **(C,D)** Control-72h, vehicle control (dimethyl sulfoxide; DMSO) semen samples at 72 h of storage at 17°C. **(E,F)** TER-72h, semen samples treated with 100 μM ezatiostat (TER) for 72 h of storage at 17°C. **(G,H)** Negative control. The nucleus is shown in blue (DAPI), whereas GSTP1 is shown in green. Scale bars: **(A,C,E)**: 30 μm; **(B,D,F)**: 15 μm; **(G)**: 20 μm; **(H)**: 25 μm. These results are representative of three independent experiments (n = 3).

Sperm Intracellular Calcium Levels and Acrosome Membrane Integrity Are Not Affected by TER-Induced JNK Phosphorylation

The relative Fluo3 fluorescence intensity ($Fluo3^+$) of the viable sperm population (PI^-) is presented in **Figure 9**, whereas the percentage of viable sperm with an intact acrosome (PNA^-/PI^-) is shown in **Figure 10**. No differences ($p > 0.05$) in intracellular calcium nor acrosome membrane integrity was observed among groups.

DISCUSSION

Several studies have evidenced the essential role of GSTs as molecular regulators of mammalian sperm physiology and fertilizing capacity (Gopalakrishnan et al., 1998;

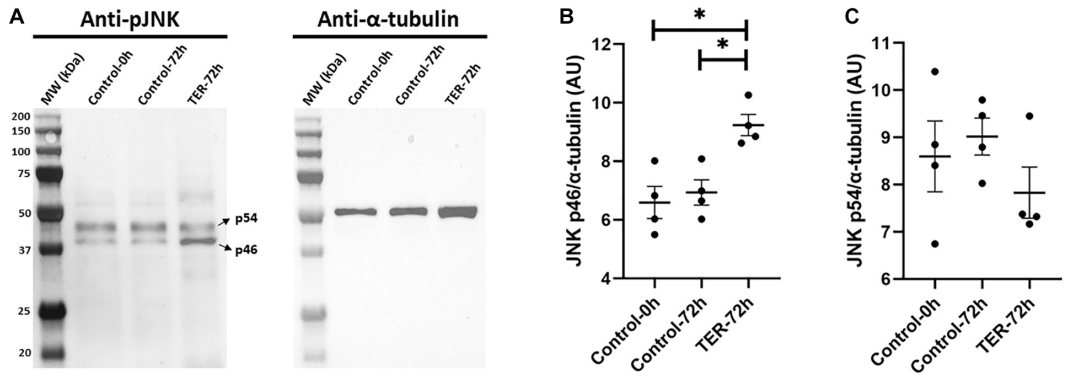

FIGURE 3 | (A) Immunoblotting of pig sperm lysate for pThr183 and pTyr185 of JNK (p46 and p54 splicing variants) and α-tubulin. Subsequent band intensity quantification and normalization of **(B)** p46 and **(C)** p54 splicing variants of JNK, normalized using α-tubulin, showed a significant increase in Thr183 and Tyr185 phosphorylation in the p46 variant ($p < 0.05$), but not in the p54 variant ($p > 0.05$), in TER-treated samples (TER-72h) compared to control samples (control-0h and control-72h). Lanes: MW (kDa), molecular weight; control-0h, semen samples at 0 h of storage; control-72h, vehicle control (dimethyl sulfoxide; DMSO) semen samples at 72 h of storage at 17°C; TER-72h, semen samples treated with 100 μM ezatiostat (TER) for 72 h of storage at 17°C. These results are representative of four independent experiments ($n = 4$). *$p \leq 0.05$.

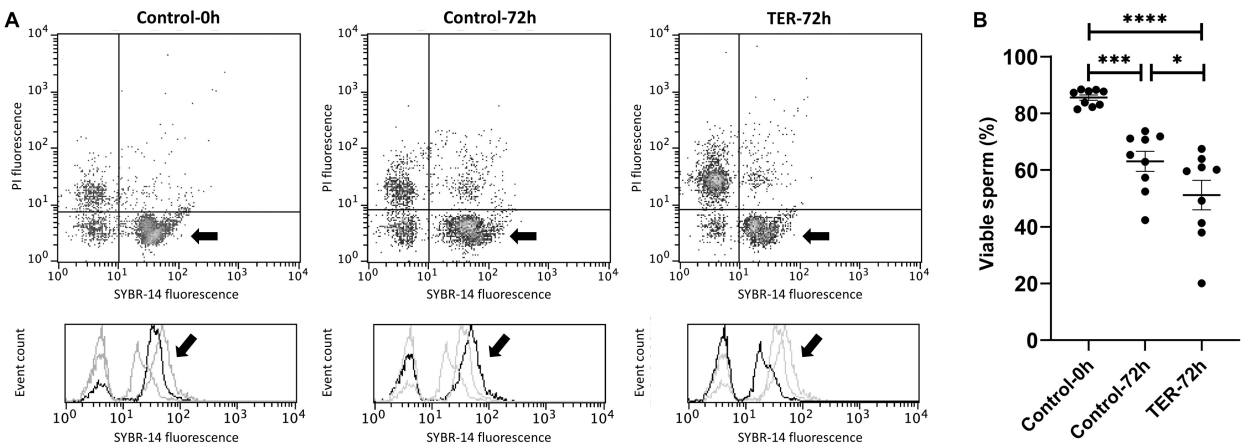

FIGURE 4 | Flow cytometry analysis of sperm viability. **(A)** Representative flow cytometry dot plots of propidium iodide (PI) and SYBR-14 fluorescence and histograms showing the event count of SYBR-14 fluorescence intensity of all treatments. Black arrows show the flow cytometry population selected for analysis represented in **(B)**. Dark gray lines in histograms show the event count of its corresponding treatment, whereas light gray lines show the event count of the remaining treatments. **(B)** Mean, standard error of the mean (SEM), and sample distribution of the percentage of viable sperm in all treatments. Control-0h, semen samples at 0 h of storage; Control-72h, vehicle control (dimethyl sulfoxide; DMSO) semen samples at 72 h of storage at 17°C; TER-72h, semen samples treated with 100 μM ezatiostat (TER) for 72 h of storage at 17°C. Sample size ($n = 9$). *$p \leq 0.05$; ***$p \leq 0.001$; ****$p \leq 0.0001$.

Aydos et al., 2009; Safarinejad et al., 2010; Vani et al., 2010; Tang et al., 2012; Kan et al., 2013; Lakpour et al., 2013; Song et al., 2013; Kolesnikova et al., 2017; Llavanera et al., 2019b, 2020). On the other hand, a recent study established JNK signaling cascade as a regulator of specific physiological parameters in sperm cells (Luna et al., 2017). In this regard, under physiological conditions, GSTP1 is a well-known regulator of the JNK singling pathway in somatic cells by inhibiting its kinase activity when forming a GSTP1–JNK heterocomplex (Adler et al., 1999; Turella et al., 2005). However, the effects of inhibiting GSTP1 upon JNK signaling regulation in male gametes have never been investigated. To the best of our knowledge, this is the first report uncovering the physiological role of JNK inhibited by GSTP1 in mammalian sperm physiology. To this end, a specific inhibitor of the GSTP1–JNK heterocomplex was used, leading to the subsequent activation of JNK.

While the presence of GSTP1 in the sperm was established by proteomic studies in several mammalian species such as human (Wang et al., 2013), murine (Vicens et al., 2017), porcine (Pérez-Patino et al., 2019), and bovine (Peddinti et al., 2008), its localization was determined for the first time in the present study. Immunoblotting analysis of the present study identified a single ∼48 kDa band corresponding to GSTP1. Although the molecular mass of GSTP1 is ∼24 kDa, it is known to exist intracellularly as homodimers (Okamura et al., 2015), which is likely to be responsible for the ∼48 kDa band found in immunoblots. Furthermore, immunofluorescence analysis found GSTP1 to be localized in the posterior region of the head and the middle,

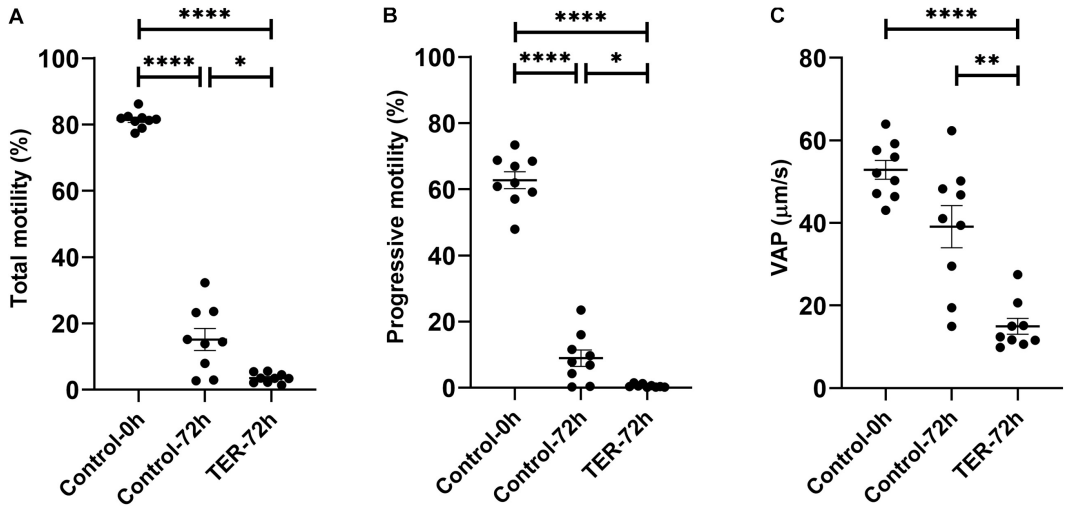

FIGURE 5 | Computer-assisted sperm analysis (CASA) of pig semen samples. Mean, standard error of the mean (SEM), and sample distribution of the percentage of **(A)** total motile sperm, **(B)** progressively motile sperm, and **(C)** average path velocity sperm (VAP; μm/s) in all treatments. Control-0h, semen samples at 0 h of storage; Control-72h, vehicle control (dimethyl sulfoxide; DMSO) semen samples at 72 h of storage at 17°C; TER-72h, semen samples treated with 100 μM ezatiostat (TER) for 72 h of storage at 17°C. Sample size (n = 9). *$p \leq 0.05$; **$p \leq 0.01$; ****$p \leq 0.0001$.

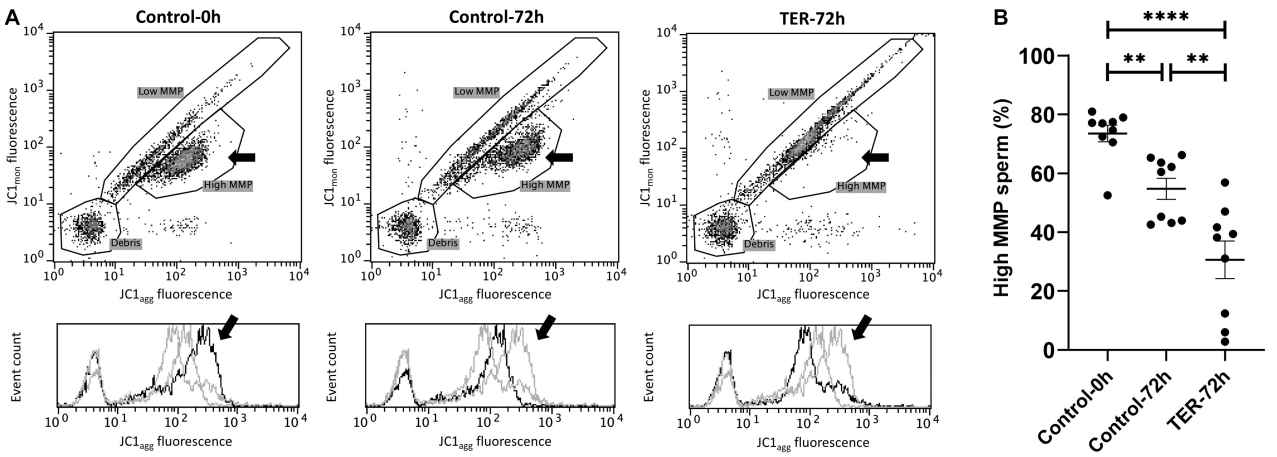

FIGURE 6 | Flow cytometry analysis of pig sperm mitochondrial activity. **(A)** Representative flow cytometry dot plots of JC1 monomers ($JC1_{mon}$) and JC1 aggregates ($JC1_{agg}$) fluorescence and histograms showing the event count of $JC1_{agg}$ fluorescence intensity of all treatments. Black arrows show the flow cytometry population selected for analysis represented in **(B)**. Dark gray lines in histograms show the event count of its corresponding treatment, whereas light gray lines show the event count of the remaining treatments. **(B)** Mean, standard error of the mean (SEM), and sample distribution of the percentage of high mitochondrial membrane potential (MMP) sperm in all treatments. Control-0h, semen samples at 0 h of storage; Control-72h, vehicle control (dimethyl sulfoxide; DMSO) semen samples at 72 h of storage at 17°C; TER-72h, semen samples treated with 100 μM ezatiostat (TER) for 72 h of storage at 17°C. Sample size (n = 9). **$p \leq 0.01$; ****$p \leq 0.0001$.

principal, and end pieces of the tail in fresh control samples. The localization pattern of GSTP1 in fresh samples was similar to that found for other GST family members such as GSTM3 in pig (Llavanera et al., 2020) and buffalo (Kumar et al., 2014) sperm, which is present in the entire sperm tail. Interestingly, liquid storage for 72 h rather than inhibition with TER was responsible for the alteration of the GSTP1 localization pattern. Contrary to fresh samples, GSTP1 was found to be localized in the equatorial subdomain of the head and the principal and end pieces of the tail. A similar modulation of the GSTP1 localization pattern due to liquid storage was observed in other GST family members such as GSTM3 (Llavanera et al., 2020). Contrary to that, GSTM3 was found to be relocalized to the middle piece during sperm cryopreservation (Llavanera et al., 2019a). According to the results of the present study, previous studies hypothesized that the GST localization pattern in the sperm tail and their relocalization from or to the middle piece during liquid storage or cryopreservation, respectively, could contribute to the explanation of their significant role in mitochondrial function, sperm motility, and membrane stability. Sperm GSTs are known to be membrane-anchored proteins, and thus, their localization is determined by membrane stability (Llavanera et al., 2019b).

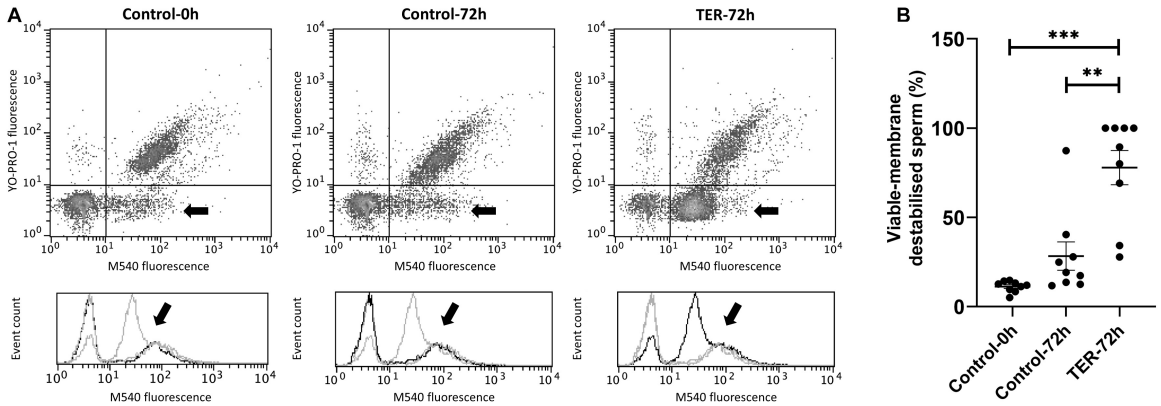

FIGURE 7 | Flow cytometry analysis of plasma sperm membrane stability. **(A)** Representative flow cytometry dot plots of Yo-Pro-1 and merocyanine (M540) fluorescence and histograms showing the event count of M540 fluorescence intensity of all treatments. Black arrows show the flow cytometry population selected for analysis represented in **(B)**. Dark gray lines in histograms show the event count of its corresponding treatment, whereas light gray lines show the event count of the remaining treatments. **(B)** Mean, standard error of the mean (SEM), and sample distribution of the percentage of membrane-destabilized cells within the total viable sperm population in all treatments. Control-0h, semen samples at 0 h of storage; Control-72h, vehicle control (dimethyl sulfoxide; DMSO) semen samples at 72 h of storage at 17°C; TER-72h, semen samples treated with 100 μM ezatiostat (TER) for 72 h of storage at 17°C. Sample size (n = 9). $^{**}p \leq 0.01$; $^{***}p \leq 0.001$.

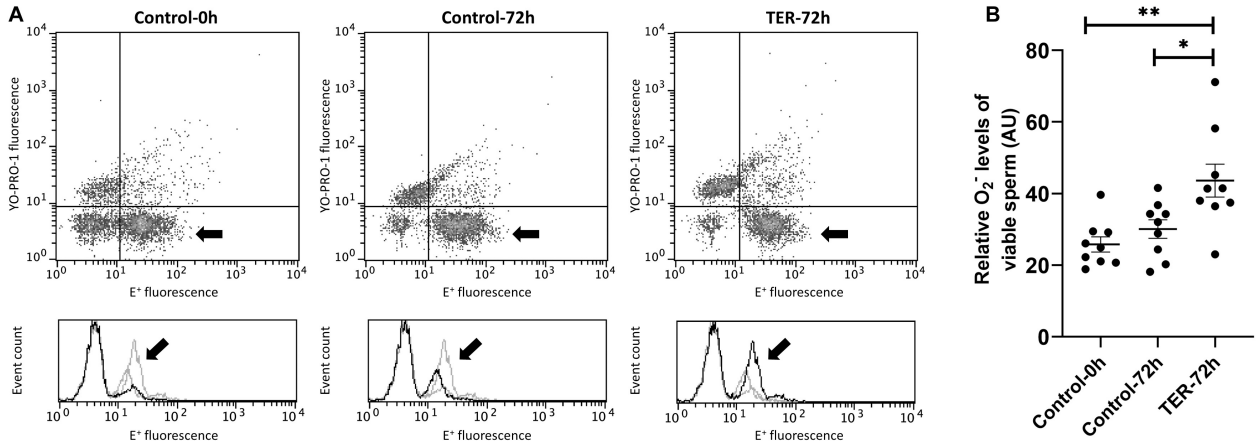

FIGURE 8 | Flow cytometry analysis of intracellular superoxide levels. **(A)** Representative flow cytometry dot plots of Yo-Pro-1 and ethidine (E^+) fluorescence and histograms showing the event count of E^+ fluorescence intensity of all treatments. Black arrows show the flow cytometry population selected for analysis represented in **(B)**. Dark gray lines in histograms show the event count of its corresponding treatment, whereas light gray lines show the event count of the remaining treatments. **(B)** Mean, standard error of the mean (SEM), and sample distribution of the relative E^+ fluorescence intensity of the viable sperm population in all treatments. Control-0h, semen samples at 0 h of storage; Control-72h, vehicle control (dimethyl sulfoxide; DMSO) semen samples at 72 h of storage at 17°C; TER-72h, semen samples treated with 100 μM ezatiostat (TER) for 72 h of storage at 17°C. Sample size (n = 9). $^{*}p \leq 0.05$; $^{**}p \leq 0.01$.

The loss of GSTP1 from the middle piece suggests stronger membrane destabilization of this region. In this regard, the loss of GSTP1 in the middle piece would indicate a major membrane destabilization of this region due to preservation in liquid storage.

As has been previously reported in the literature, the JNK activation is regulated by GSTP1 in somatic cells (Adler et al., 1999; Wang et al., 2001). However, there were no studies regarding this molecular interaction in mammalian sperm cells. Immunoblotting analysis of phospho-JNK reported herein showed an intensified tyrosine and threonine phosphorylation of this protein in TER-treated samples, a specific blocker of the JNK-binding site in GSTP1. It is widely known that mitogen-activated protein kinases (MAPKs; e.g., JNKs) are activated via a dual phosphorylation upon tyrosine and threonine residues (Lawler et al., 1998). Hence, our results evidence, for the first time in mammalian sperm, the role of the GSTP1–JNK heterocomplex as an inhibitor of JNK activation by preventing the dual phosphorylation of tyrosine and threonine residues.

An interesting physiological effect of the activation of JNK was the significant decrease in sperm mitochondrial activity, viability, and motility. Activation of JNK has been reported in the literature to be related to mitochondrial dysfunction and cell death in somatic cells (Aoki et al., 2002; Heslop et al., 2020). Admittedly, a study conducted in ram sperm (Luna et al., 2017) showed that phosphorylation of sperm JNK increased apoptotic-like changes and DNA damage as

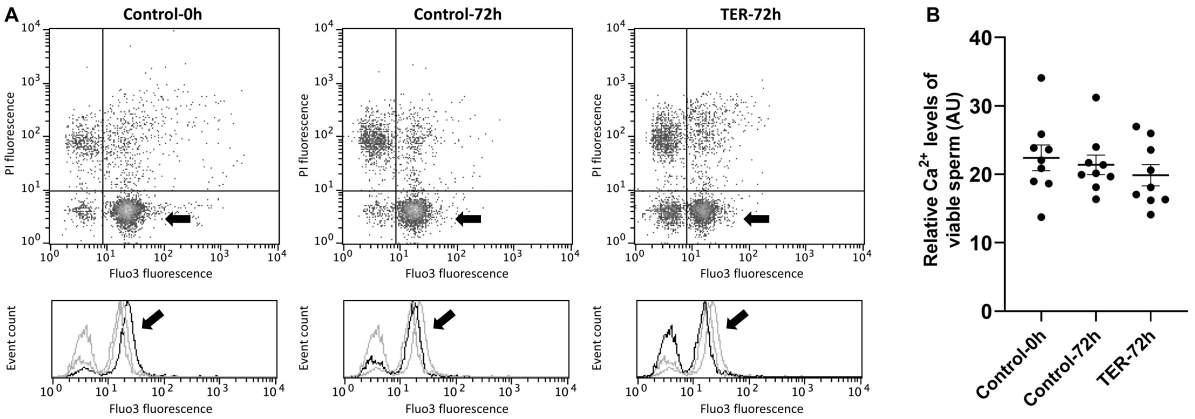

FIGURE 9 | Flow cytometry analysis of intracellular calcium levels. **(A)** Representative flow cytometry dot plots of propidium iodide (PI) and Fluo3-AM (Fluo3) fluorescence and histograms showing the event count of Fluo3 fluorescence intensity of all treatments. Black arrows show the flow cytometry population selected for analysis represented in **(B)**. Dark gray lines in histograms show the event count of its corresponding treatment, whereas light gray lines show the event count of the remaining treatments. **(B)** Mean, standard error of the mean (SEM), and sample distribution of the relative $Fluo3^{+}$ fluorescence intensity of the viable sperm population in all treatments. Control-0h, semen samples at 0 h of storage; Control-72h, vehicle control (dimethyl sulfoxide; DMSO) samples at 72 h of storage at 17°C; TER-72h, semen samples treated with 100 μM ezatiostat (TER) for 72 h of storage at 17°C. Sample size (n = 9). $p > 0.05$.

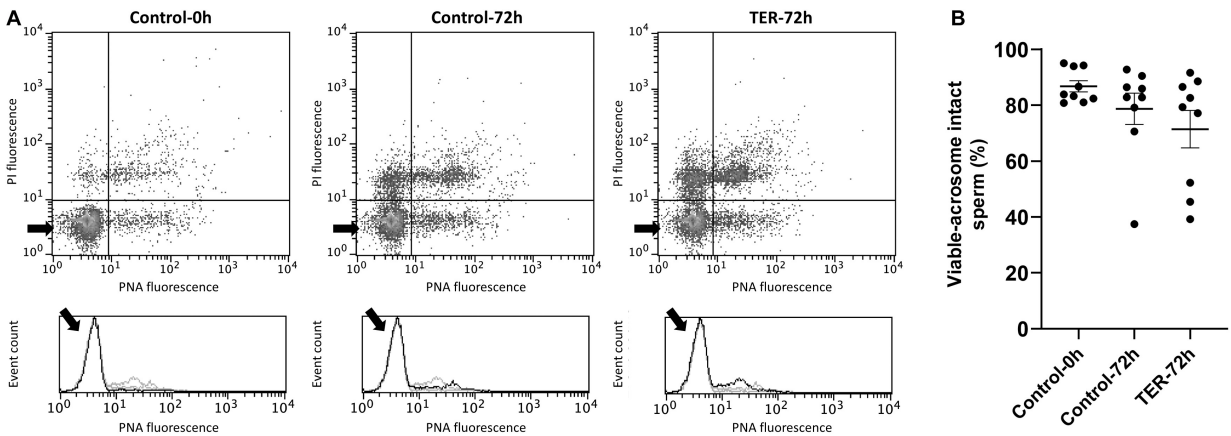

FIGURE 10 | Flow cytometry analysis of acrosome integrity. **(A)** Representative flow cytometry dot plots of propidium iodide (PI) and fluorescein-conjugated peanut agglutinin/propidium iodide (PNA) fluorescence and histograms showing the event count of PNA fluorescence intensity of all treatments. Black arrows show the flow cytometry population selected for analysis represented in **(B)**. Dark gray lines in histograms show the event count of its corresponding treatment, whereas light gray lines show the event count of the remaining treatments. **(B)** Mean, standard error of the mean (SEM), and sample distribution of the percentage of viable sperm with an intact acrosome in all treatments. Control-0h, semen samples at 0 h of storage; Control-72h, vehicle control (dimethyl sulfoxide; DMSO) semen samples at 72 h of storage at 17°C; TER-72h, semen samples treated with 100 μM ezatiostat (TER) for 72 h of storage at 17°C. Sample size (n = 9). $p > 0.05$.

well as capacitation-related events. These results would suggest that the GSTP1–JNK heterocomplex could prevent sperm to undergo early capacitation-related events or apoptotic-like changes during liquid storage. In this regard, the detrimental effects of JNK activation upon mitochondrial functionality in sperm cells showed herein are in agreement with the results reported in sperm and other cell types. Moreover, the reduction of mitochondrial activity is likely to be responsible for the loss of sperm motility, since mammalian sperm rely upon high levels of the adenosine triphosphate (ATP) required for axonemal dynein to drive sperm motility (Vívenes et al., 2009). Altogether, our findings suggest the role of the GSTP1–JNK heterocomplex in preserving sperm mitochondrial activity and subsequent viability and motility as well as in preventing capacitation-related events or apoptotic-like changes. Specific molecular mechanisms through which JNK activation may trigger sperm mitochondrial dysfunction in sperm cells remains to be determined. However, in somatic cells, JNK-mitochondrial SH3-domain binding protein 5 (SAB), a docking protein for JNK, has been suggested as a putative responsible for these processes, since it was found to lead to an intramitochondrial signal transduction pathway that impairs mitochondrial activity and enhances the production of reactive oxygen species (Win et al., 2018). In this regard, further investigations on the downstream effects of activated JNK upon mitochondrial activity should be performed.

Related to sperm mitochondrial dysfunction, the results of the present study showed an increase in intracellular superoxide levels triggered by the GSTP1–JNK heterocomplex dissociation and subsequent activation of JNK. Similar results were reported in somatic cells, where JNK activation was related to increased superoxide formation (Heslop et al., 2020). The main superoxide source in mammalian sperm cells is known to be the mitochondria, specifically, the electron transport chain (Storey, 2008; Brand, 2016). These results suggest that, in line with the previously mentioned results, the activation of JNK would lead to the disruption of the electron transport chain of sperm mitochondria. Moreover, previous studies in caprine and porcine evidenced the essential role of sperm GSTs in maintaining mitochondrial activity and physiological levels of reactive oxygen species (Hemachand and Shaha, 2003; Llavanera et al., 2020). Related with this, the results of the present study would indicate that the effects of GSTs upon sperm mitochondria would be mediated by a JNK signaling pathway. However, further research regarding the molecular mechanism of GSTs in regulating sperm mitochondrial function is required.

Our results showed that pharmacological dissociation of the GSTP1–JNK heterocomplex in sperm cells significantly impaired the stability of lipidic membranes, although it did not affect the acrosome membrane. Previous studies utilizing general GST inhibitors in goat and pig sperm reported high levels of plasma membrane damage and destabilization, although they did not find any effect on the acrosomal membrane (Gopalakrishnan and Shaha, 1998; Llavanera et al., 2020). These evidences reveal a significant role of these antioxidant enzymes on the stability of sperm plasma membrane but not on that of acrosome membrane. In accordance with the previously reported results, these findings could suggest a specific destabilization of the membranes located in the middle and principal pieces rather than from the sperm head, which could cause mitochondrial and motility impairment. However, the specific localization and molecular mechanisms by which GSTs are able to maintain membrane stability are currently unknown. The results of the present study shed some light on the mechanisms regulating destabilization of sperm membranes, suggesting that this process could be mediated by the activation of JNK signaling. However, the specific JNK downstream signaling proteins are yet to be determined. Uncovering the specific molecular signaling pathway through which sperm membrane stability is reduced is of utmost interest to develop new strategies for increasing sperm life span and quality.

Interestingly, although GSTP1–JNK dissociation caused severe mitochondrial damage and membrane destabilization in sperm cells, it did not have any effects upon intracellular calcium reservoirs. In this sense, previous studies in pig sperm showed that general GST inhibitors caused a significant increase in calcium levels, predominantly in the sperm middle piece (Llavanera et al., 2020). The present results suggested that, despite some specific GST classes being involved in the regulation of sperm calcium levels, the inhibition of GSTP1 upon JNK seems not to be related to calcium fluctuations. However, further research tackling calcium levels due to JNK activation should be performed in order to confirm this hypothesis.

In conclusion, immunological and cell biology analyses confirmed that, as schematized in **Figure 11**, the dissociation of the GSTP1–JNK heterocomplex results in the activation of JNK and significantly declines sperm viability, motility, mitochondrial activity, and plasma membrane stability and increased superoxide levels, without altering intracellular calcium

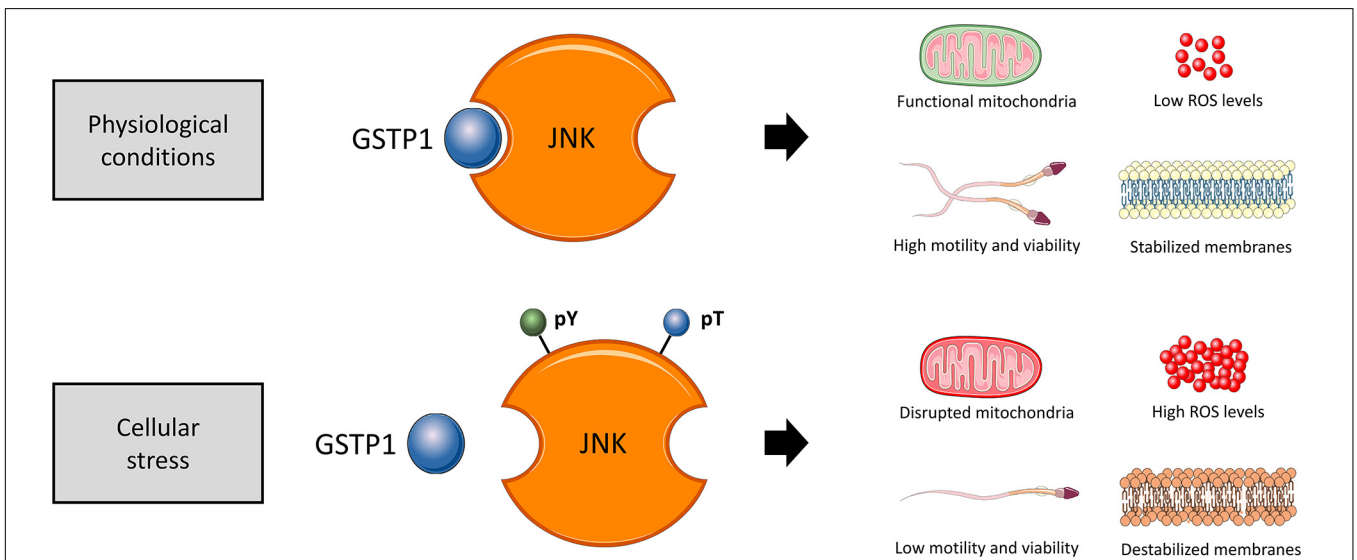

FIGURE 11 | Proposed diagram of the function of the GSTP1–JNK heterocomplex under physiological conditions and cellular stress in sperm cells. In physiological conditions, the GSTP1–JNK heterocomplex prevents JNK activation, maintaining sperm viability, motility, mitochondrial activity, and plasma membrane stability and increased superoxide levels. On the other hand, under cellular stress conditions, the GSTP1–JNK heterocomplex is dissociated, and thus, JNK is activated by tyrosine (pY) and threonine (pT) phosphorylation. The activation of JNK decreases sperm viability and motility, disrupts mitochondrial activity, causes plasma membrane destabilization, and increases intracellular superoxide levels.

levels and acrosome membrane integrity. Thus, the present study provides several evidences supporting the molecular role of JNK activation via dissociation of the GSTP1–JNK heterocomplex, uncovering the role of this protein in maintaining sperm functionality, especially with regard to the preservation of mitochondrial physiology. These findings set the grounds for understanding the relevance of GSTP1–JNK cell signaling regulation in mammalian sperm physiology.

DATA AVAILABILITY STATEMENT

The original contributions presented in the study are included in the article/**Supplementary Material**, further inquiries can be directed to the corresponding authors.

AUTHOR CONTRIBUTIONS

MY and ML: conceptualization and methodology. ML, SO, YM-O, AD-B, and SR: formal analysis and investigation. ML: writing-original draft preparation. MY and IB: writing-review and editing and supervision. MY: funding acquisition. All authors contributed to the article and approved the submitted version.

FUNDING

The authors acknowledged the support from the Ministry of Science, Innovation and Universities, Spain (RYC-2014-15581, AGL2017-88329-R, FJCI-2017-31689, and FPU18/00666), and Regional Government of Catalonia, Spain (2017-SGR-1229).

ACKNOWLEDGMENTS

The authors would like to thank the Technical Research Services (University of Girona) for their technical support. The authors would also like to thank the Servier Medical Art for their image bank used to create all figures.

SUPPLEMENTARY MATERIAL

The Supplementary Material for this article can be found online at: https://www.frontiersin.org/articles/10.3389/fcell.2021.627140/full#supplementary-material

Supplementary Figure 1 | Preliminary concentration test. Mean and standard error of the mean (SEM) of the percentage of **(A)** viable sperm, **(B)** total motile sperm, **(C)** viable-membrane destabilized sperm,and **(D)** high mitochondrial membrane potential (high MMP) sperm. Different ezatiostat (TER) concentrations (10 μM, 100 μM, and 1000 μM) were tested (TER 72h; light gray bars), and the same volume of DMSO was added to Control-72h samples as a vehicle control group (Control 72h; medium gray bars). Semen samples at 0 h of storage were also analyzed (Control 0h; dark gray bars). Sample size ($n = 3$). $^{*}p \leq 0.05$; $^{**}p \leq 0.01$. $^{***}p \leq 0.001$. A concentration of 10 μM of TER showed no effect on any sperm quality parameter compared to Control 0h and 72h samples ($p > 0.05$). Sperm samples treated with 100 μM showed a significant decrease in total sperm motility ($p < 0.001$) and MMP ($p < 0.01$), an increased sperm membrane destabilization ($p < 0.001$), and a minor but significant decrease in sperm viability ($p < 0.05$), compared to the Control 0h and 72h samples. Finally, samples treated with 1000 μM of TER showed significant ($p < 0.001$) detrimental effects upon all sperm quality parameters, especially on sperm viability, compared to the Control 0h and 72h samples. These results suggested that samples treated with 10 μM of TER did not exert any effect upon sperm physiology, whereas 1000 μM of TER caused cytotoxic effects on sperm and thus masking the physiological effects of the inhibitor upon sperm quality and functionality. Finally, samples treated with 100 μM of TER showed physiological effects upon sperm membranes, mitochondria, and motility without exerting critical cytotoxicity.

Supplementary Table 1 | Raw data. Raw data of sperm quality and functionality parameters of all treatments and time points. TMOT, percentage of total motile sperm; PMOT, percentage of progressively motile sperm; VAP, sperm average path velocity (μm/s); VIABILITY, percentage of viable sperm (SYBR-14^{+}/PI^{-}); M540, percentage of membrane-destabilized cells (M540^{+}) within the total viable sperm population (Yo-Pro-1^{-}); HE, relative fluorescence intensity of viable sperm with high levels of intracellular $O_2^{-\cdot}$ (E^{+}/PI^{-}); JC1, percentage of high mitochondrial membrane potential sperm ($\Delta\Psi$m) resulted from the orange-stained ($JC1_{agg}$) population; PNA, percentage of acrosome membrane-intact sperm (PNA-FITC^{-}) within the total viable sperm population (PI^{-}); FL3, relative Fluo3-AM fluorescence intensity of viable sperm with high levels of intracellular calcium (Fluo3-AM^{+}/PI^{-}); CNT 0h, semen samples at 0 h of storage; CNT 72h, vehicle control (dimethyl sulfoxide; DMSO) semen samples at 72 h of storage at 17°C; TER 72h, semen samples treated with 100 μM ezatiostat (TER) for 72 h of storage at 17°C.

Supplementary File 1 | Supplementary information for Materials and Methods.

REFERENCES

Adler, V., Yin, Z., Fuchs, S. Y., Benezra, M., Rosario, L., Tew, K. D., et al. (1999). Regulation of JNK signaling by GSTp. *EMBO J.* 18, 1321–1334.doi: 10.1093/emboj/18.5.1321

Aoki, H., Kang, P. M., Hampe, J., Yoshimura, K., Noma, T., Matsuzaki, M., et al. (2002). Direct activation of mitochondrial apoptosis machinery by c-Jun N-terminal kinase in adult cardiac myocytes. *J. Biol. Chem.* 277, 10244–10250. doi: 10.1074/jbc.M112355200

Aydos, S. E., Ph, D., Taspinar, M., Sc, M., Sunguroglu, A., and Ph, D. (2009). Association of CYP1A1 and glutathione S-transferase polymorphisms with male factor infertility. *Fertil. Steril.* 92, 541–547.doi: 10.1016/j.fertnstert.2008.07.017

Bracke, A., Peeters, K., Punjabi, U., Hoogewijs, D., and Dewilde, S. (2018). A search for molecular mechanisms underlying male idiopathic infertility. *Reprod. Biomed. Online* 36, 327–339. doi: 10.1016/j.rbmo.2017.12.005

Brand, M. D. (2016). Mitochondrial generation of superoxide and hydrogen peroxide as the source of mitochondrial redox signaling. *Free Radic. Biol. Med.* 100, 14–31. doi: 10.1016/j.freeradbiomed.2016.04.001

Carrell, D. T., De Jonge, C., and Lam, D. J. (2006). The genetics of male infertility: a field of study whose time is now. *J. Reprod. Syst.* 52, 269–274.doi: 10.1080/01485010500503603

Garner, D. L., and Johnson, L. A. (1995). Viability assessment of mammalian sperm using SYBR-14 and propidium iodide. *Biol. Reprod.* 53, 276–284.doi: 10.1095/biolreprod53.2.276

Ghuman, N., and Ramalingam, M. (2017). Male infertility. *Obstet. Gynaecol. Reprod. Med.* 28, 7–14. doi: 10.1016/j.ogrm.2017.10.007

Gopalakrishnan, B., Aravinda, S., Pawshe, C. H., Totey, S. M., Nagpal, S., and Salunke, D. M. (1998). Studies on glutathione S-transferase important for sperm function: evidence of catalytic activity-independent functions. *Biochem. J.* 329, 231–241.doi: 10.1042/bj3290231

Gopalakrishnan, B., and Shaha, C. (1998). Inhibition of sperm glutathione S-transferase leads to functional impairment

due to membrane damage. *FEBS Lett.* 422, 296–300. doi: 10.1016/S0014-5793(98)00032-5

Griveau, J. F., and Le Lannou, D. (1997). Reactive oxygen species and human spermatozoa: physiology and pathology. *Int. J. Androl.* 20, 61–69.doi: 10.1046/j.1365-2605.1997.00044.x

Guthrie, H. D., and Welch, G. R. (2006). Determination of intracellular reactive oxygen species and high mitochondrial membrane potential in Percoll-treated viable boar sperm using fluorescence-activated flow cytometry. *J. Anim. Sci.* 84, 2089–2100.doi: 10.2527/jas.2005-766

Harrison, R. A. P., Mairet, B., and Miller, N. G. A. (1993). Flow cytometric studies of bicarbonate-mediated Ca2+ influx in boar sperm populations. *Mol. Reprod. Dev.* 35, 197–208.doi: 10.1002/mrd.1080350214

Hemachand, T., and Shaha, C. (2003). Functional role of sperm surface glutathione S-transferases and extracellular glutathione in the haploid spermatozoa under oxidative stress. *FEBS Lett.* 538, 14–18. doi: 10.1016/S0014-5793(03)00103-0

Heslop, K. A., Rovini, A., Hunt, E. G., Fang, D., Morris, M. E., Christie, C. F., et al. (2020). JNK activation and translocation to mitochondria mediates mitochondrial dysfunction and cell death induced by VDAC opening and sorafenib in hepatocarcinoma cells. *Biochem. Pharmacol.* 171:113728.doi: 10.1016/j.bcp.2019.113728

Kan, H. P., Wu, F. L., Guo, W. B., Wang, Y. Z., Li, J. P., Huang, Y. Q., et al. (2013). Null genotypes of GSTM1 and GSTT1 contribute to male factor infertility risk: a meta-analysis. *Fertil. Steril.* 99, 690–696. doi: 10.1016/j.fertnstert.2012.10.037

Klinovska, K., Sebkova, N., and Dvorakova-Hortova, K. (2014). Sperm-egg fusion: a molecular enigma of mammalian reproduction. *Int. J. Mol. Sci.* 15, 10652–10668.doi: 10.3390/ijms150610652

Kolesnikova, L. I., Kurashova, N. A., Bairova, T. A., Dolgikh, M. I., Ershova, O. A., Dashiev, B. G., et al. (2017). Role of glutathione-S-transferase family genes in male infertility. *Bull. Exp. Biol. Med.* 163, 643–645.doi: 10.1007/s10517-017-3869-9

Kumar, R., Singh, V. K., and Atreja, S. K. (2014). Glutathione-S-transferase: role in buffalo (*Bubalus bubalis*) sperm capacitation and cryopreservation. *Theriogenology* 81, 587–598. doi: 10.1016/j.theriogenology.2013.11.012

Lakpour, N., Mirfeizollahi, A., Farivar, S., Akhondi, M. M., Hashemi, S. B., Amirjannati, N., et al. (2013). The association of seminal plasma antioxidant levels and sperm chromatin status with genetic variants of GSTM1 and GSTP1 (Ile105Val and Ala114Val) in infertile men with oligoasthenoteratozoospermia. *Dis. Markers* 34, 205–210.doi: 10.3233/DMA-120954

Lawler, S., Fleming, Y., Goedert, M., and Cohen, P. (1998). Synergistic activation of SAPK1/JNK1 by two MAP kinase kinases in vitro. *Curr. Biol.* 8, 1387–1391.doi: 10.1016/s0960-9822(98)00019-0

Llavanera, M., Delgado-bermúdez, A., Olives, S., Mateo-otero, Y., Recuero, S., Bonet, S., et al. (2020). Glutathione S-transferases play a crucial role in mitochondrial function, plasma membrane stability and oxidative regulation of mammalian sperm. *Antioxidants* 9, 1–16. doi: 10.3390/antiox9020100

Llavanera, M., Delgado-Bermuìdez, A., Fernandez-Fuertes, B., Recuero, S., Mateo, Y., Bonet, S., et al. (2019a). GSTM3, but not IZUMO1, is a cryotolerance marker of boar sperm. *J. Anim. Sci. Biotechnol.* 10:61. doi: 10.1186/s40104-019-0370-5

Llavanera, M., Mateo-Otero, Y., Bonet, S., Barranco, I., Fernández-Fuertes, B., and Yeste, M. (2019b). The triple role of glutathione S-transferases in mammalian male fertility. *Cell. Mol. Life Sci.* 77:2331–2342. doi: 10.1007/s00018-019-03405-w

Luna, C., Mendoza, N., Casao, A., Pérez-Pé, R., Cebrián-Pérez, J. A., and Muiño-Blanco, T. (2017). c-Jun N-terminal kinase and p38 mitogen-activated protein kinase pathways link capacitation with apoptosis and seminal plasma proteins protect sperm by interfering with both routes. *Biol. Reprod.* 96, 800–815.doi: 10.1093/biolre/iox017

Mathew, N., Kalyanasundaram, M., and Balaraman, K. (2006). Glutathione S -transferase (GST) inhibitors. *Expert Opin. Ther. Pat.* 16, 431–444. doi: 10.1517/13543776.16.4.431

Mukhtar, H., Lee, I. P., and Bend, J. R. (1978). Glutathione S-transferase activities in rat and mouse sperm and human semen. *Biochem. Biophys. Res. Commun.* 83, 1093–1098. doi: 10.1016/0006-291X(78)91507-3

Nagy, S., Jansen, J., Topper, E. K., and Gadella, B. M. (2003). A triple-stain flow cytometric method to assess plasma- and acrosome-membrane integrity of cryopreserved bovine sperm immediately after thawing in presence of egg-yolk particles. *Biol. Reprod.* 68, 1828–1835. doi: 10.1095/biolreprod.102.011445

Okamura, T., Antoun, G., Keir, S. T., Friedman, H., Bigner, D. D., and Ali-Osman, F. (2015). Phosphorylation of glutathione s-transferase p1 (gstp1) by epidermal growth factor receptor (EGFR) promotes formation of the gstp1-c-jun n-terminal kinase (JNK) complex and suppresses JNK downstream signaling and apoptosis in brain tumor cells. *J. Biol. Chem.* 290, 30866–30878.doi: 10.1074/jbc.M115.656140

Ortega-Ferrusola, C., Sotillo-Galan, Y., Varela-Fernandez, E., Gallardo-Bolanos, J. M., Muriel, A., Gonzalez-Fernandez, L., et al. (2007). Detection of "apoptosis-like" changes during the cryopreservation process in equine sperm. *J. Androl.* 29, 213–221.doi: 10.2164/jandrol.107.003640

Parent, S., Lefièvre, L., Brindle, Y., and Sullivan, R. (1999). Bull subfertility is associated with low levels of a sperm membrane antigen. *Mol. Reprod. Dev.* 52, 57–65.doi: 10.1002/(SICI)1098-2795(199901)52:1<57::AID-MRD8<3.0.CO;2-U

Peddinti, D., Nanduri, B., Kaya, A., Feugang, J. M., Burgess, S. C., and Memili, E. (2008). Comprehensive proteomic analysis of bovine spermatozoa of varying fertility rates and identification of biomarkers associated with fertility. *BMC Syst. Biol.* 2:1–13. doi: 10.1186/1752-0509-2-19

Pérez-Patino, C., Parrilla, I., Li, J., Barranco, I., Martínez, E. A., Rodriguez-Martínez, H., et al. (2019). The proteome of pig spermatozoa is remodeled during ejaculation. *Mol. Cell. Proteomics* 18, 41–50.doi: 10.1074/mcp.RA118.000840

Rathi, R., Colenbrander, B., Bevers, M. M., and Gadella, B. M. (2001). Evaluation of in vitro capacitation of stallion spermatozoa. *Biol. Reprod.* 65, 462–470. doi: 10.1095/biolreprod65.2.462

Rodrigues-Silva, H. V., Rodriguez-Villamil, P., de Magalhães, F. F., Nunes, T. G. P., de Freitas, L. A., Ribeiro, L. R., et al. (2018). Seminal plasma and sperm proteome of ring-tailed coatis (Nasua nasua, Linnaeus, 1766). *Theriogenology* 111, 34–42.doi: 10.1016/j.theriogenology.2017.12.036

Safarinejad, M. R., Shafiei, N., and Safarinejad, S. (2010). The association of glutathione-S-transferase gene polymorphisms (GSTM1, GSTT1, GSTP1) with idiopathic male infertility. *J. Hum. Genet.* 55, 565–570.doi: 10.1038/jhg.2010.59

Song, X., Zhao, Y., Cai, Q., Zhang, Y., and Niu, Y. (2013). Association of the Glutathione S-transferases M1 and T1 polymorphism with male infertility: a meta-analysis. *J. Assist. Reprod. Genet.* 30, 131–141.doi: 10.1007/s10815-012-9907-7

Storey, B. T. (2008). Mammalian sperm metabolism: oxygen and sugar, friend and foe. *Int. J. Dev. Biol.* 52, 427–437.doi: 10.1387/ijdb.072522bs

Tang, M., Wang, S., Wang, W., Cao, Q., Qin, C., Liu, B., et al. (2012). The glutathione-S-transferase gene polymorphisms (GSTM1 and GSTT1) and idiopathic male infertility risk: a meta-analysis. *Gene* 511, 218–223.doi: 10.1016/j.gene.2012.09.054

Turella, P., Cerella, C., Filomeni, G., Bullo, A., De Maria, F., Ghibelli, L., et al. (2005). Proapoptotic activity of new glutathione S-transferase inhibitors. *Cancer Res.* 65, 3751–3761. doi: 10.1158/0008-5472.CAN-04-3903

Vani, G. T., Mukesh, N., Siva Prasad, B., Rama Devi, P., Hema Prasad, M., Rani, P. U., et al. (2010). Role of glutathione S-transferase Mu-1 (GSTM1) polymorphism in oligospermic infertile males. *Andrologia* 42, 213–217.doi: 10.1111/j.1439-0272.2009.00971.x

Vicens, A., Borziak, K., Karr, T. L., Roldan, E. R. S., and Dorus, S. (2017). Comparative sperm proteomics in mouse species with divergent mating systems. *Mol. Biol. Evol.* 34, 1403–1416.doi: 10.1093/molbev/msx084

Vívenes, C. Y., Peralta-Arias, R. D., Camejo, M. I., Guerrero, K., Fernández, V. H., Piñero, S., et al. (2009). Biochemical identification of dynein-ATPase activity in human sperm. *Z. Naturforsch. C J. Biosci.* 64, 747–753.doi: 10.1515/znc-2009-9-1022

Wang, G., Guo, Y., Zhou, T., Shi, X., Yu, J., Yang, Y., et al. (2013). In-depth proteomic analysis of the human sperm reveals complex protein compositions. *J. Proteomics* 79, 114–122.doi: 10.1016/j.jprot.2012.12.008

Wang, T., Arifoglu, P., Ronai, Z., and Tew, K. D. (2001). Glutathione S-transferase P1–1 (GSTP1–1) inhibits c-Jun N-terminal kinase (JNK1) signaling through interaction with the C terminus. *J. Biol. Chem.* 276, 20999–21003.doi: 10.1074/jbc.M101355200

Win, S., Than, T. A., and Kaplowitz, N. (2018). The regulation of JNK signaling pathways in cell death through the interplay with mitochondrial SAB and upstream post-translational effects. *Int. J. Mol. Sci.* 19:3657.doi: 10.3390/ijms19113657

Wu, J. H., and Batist, G. (2013). Glutathione and glutathione analogues; therapeutic potentials. *Biochim. Biophys. Acta* 1830, 3350–3353.doi: 10.1016/j.bbagen.2012.11.016

Zigo, M., Maòásková-Postlerová, P., Zuidema, D., Kerns, K., Jonáková, V., Tùmová, L., et al. (2020). Porcine model for the study of sperm capacitation, fertilization and male fertility. *Cell Tissue Res.* 380, 237–262.

Conflict of Interest: The authors declare that the research was conducted in the absence of any commercial or financial relationships that could be construed as a potential conflict of interest.

frontiers in Cell and Developmental Biology

ORIGINAL RESEARCH
published: 19 March 2021
doi: 10.3389/fcell.2021.627439

Unraveling Stage-Dependent Expression Patterns of Circular RNAs and Their Related ceRNA Modulation in Ovine Postnatal Testis Development

*Taotao Li[1], Ruirui Luo[1], Xia Wang[1], Huihui Wang[1], Xingxu Zhao[2], Yunxia Guo[3], Haitao Jiang[4] and Youji Ma[1]**

[1] College of Animal Science and Technology, Gansu Agricultural University, Lanzhou, China, [2] College of Veterinary Medicine, Gansu Agricultural University, Lanzhou, China, [3] College of Life Science, Hebei Agricultural University, Baoding, China, [4] Wenshang County Inspection and Testing Center, Jining, China

OPEN ACCESS

Edited by:
Andreina Cesari, Consejo Nacional de Investigaciones Científicas y Técnicas (CONICET), Argentina

Reviewed by:
Weihua Huang, New York Medical College, United States
Sebastian Giusti, Consejo Nacional de Investigaciones Científicas y Técnicas (CONICET), Argentina

***Correspondence:**
Youji Ma
yjma@gsau.edu.cn

Specialty section:
This article was submitted to Cell Growth and Division, a section of the journal Frontiers in Cell and Developmental Biology

Received: 17 November 2020
Accepted: 03 March 2021
Published: 19 March 2021

Citation:
Li T, Luo R, Wang X, Wang H, Zhao X, Guo Y, Jiang H and Ma Y (2021) Unraveling Stage-Dependent Expression Patterns of Circular RNAs and Their Related ceRNA Modulation in Ovine Postnatal Testis Development. Front. Cell Dev. Biol. 9:627439. doi: 10.3389/fcell.2021.627439

Circular RNAs (circRNAs) have been shown to function in the reproductive systems including testis. However, their expression, as well as function in testicular development of sheep remain undefined. Herein, we performed RNA sequencing to reveal circRNA temporal expression patterns in testes of Tibetan sheep from different stages of maturation (3M, 3-month-old; 1Y, 1-year-old; 3Y, 3-year-old). A total of 3,982, 414, and 4,060 differentially expressed (DE) circRNAs were uncovered from 3M vs 1Y, 1Y vs 3Y, and 3M vs 3Y, respectively. Functional enrichment assessment indicated that the source genes of DE circRNAs were primarily engaged in spermatogenesis and testicular immune privilege including blood–testis barrier (BTB). We subsequently constructed the core circRNA–miRNA–mRNA interaction network for genes related to testicular function, such as spermatogenesis, germ cell development, BTB, and cell cycle/meiosis. Furthermore, we validated the target associations between either circ_024949, circ_026259 or IGF1, and oar-miR-29b in this network, and revealed their similar expression signatures in developmental testes that they were extensively expressed in germ cells, Leydig cells, and Sertoli cells, thus suggesting their broad functions in the functional maintenance of Leydig cells and Sertoli cells, as well as the development and maturation of male germ cells. Meanwhile, circ_026259 was shown to promote IGF1 expression through inhibition of oar-miR-29b in sheep Sertoli cells. This work gives the first global view for the expression and regulation of circRNAs in sheep testis, which will be helpful for providing new insights into the molecular mechanism of ovine testis function.

Keywords: circRNAs, sheep, testis, spermatogenesis, ceRNA

INTRODUCTION

The testis is the only specific organ known to be capable of generating male gametes (spermatozoa), essential for male fertility. In mammals, spermatozoa present in the testis are generated by spermatogenesis, which is subdivided into three distinct phases: mitotic renewal, proliferation, and differentiation of spermatogonia, meiotic progression of spermatocytes, as well as differentiation

of haploid spermatids (Zhou R. et al., 2019). Spermatogenesis is a highly coordinated, precise, and dynamic cell differentiation process that is reflected in the complex testicular gene modulation and gene expression processes. The genome of testicular cells is actively transcribed into RNAs that besides protein-coding messenger RNAs (mRNAs), involves many non-coding RNAs consisting of circular RNAs (circRNAs), as well as microRNAs (miRNAs) to regulate and yield the phase-specific gene expression patterns (Kotaja, 2014; Hu et al., 2018).

Circular RNAs are a prominent class of newly discovered closed circular RNA molecules in eukaryotes generated by the alternative shearing of precursor mRNAs (Li et al., 2018). One of the major functions of circRNAs is to modulate miRNA activity by functioning as either a competitive endogenous RNA (ceRNA) or as an miRNA sponge, consequently modulating the gene expression (Zhong et al., 2018). Existing literature shows that circRNAs are participated in diverse biological processes in mammals such as growth (Zhang P. et al., 2019), development (Salzman, 2016; Zhang P. et al., 2019), reproduction (Zhou F. et al., 2019), and immunity (Yang et al., 2018). For instance, circRNA-9119 can function as a endogenous sponge or ceRNA to upregulate the expression of RIG-I and TLR3 in mouse testicular somatic cells (Sertoli cells and Leydig cells) through competitive binding with miR-26a/miR-136, thus contributing to the pro-inflammatory activities in orchitis (Qin et al., 2019). In sheep, mounting research evidence has also shown circRNAs are abundant in the transcriptome of ovine tissues as well like mammary gland (Hao et al., 2020), pituitary (Li et al., 2019), uterus (La et al., 2020), and muscle (Cao et al., 2018), but it is not known whether this exists and functions in ovine testis.

Tibetan sheep (*Ovis aries*), a well-known Chinese domestic sheep breed, is mainly distributed in Qinghai-Tibet Plateau (QTP) over 3,000 m above sea level, which provides food and livelihoods to the local farmers and herdsmen (Wang et al., 2019), and serves a pivotal role in the QTP ecosystem functions (Jing et al., 2020). Due to the long-term excessive dependence on grazing that lacks supplementary feeding, the main reproductive characteristics of Tibetan sheep are late sexual maturity and low reproductive rates. Hence, insight into the underlying mechanisms of testicular development of male Tibetan sheep is of great significance for the reproductive biology of sheep. Here, we assume that the expressions and functions of these genes are partially or entirely regulated by circRNAs. In order to validate this hypothesis, herein, we explored the dynamic circRNA expression profiling in developmental Tibetan sheep testes at distinct reproductive stages with the aid of high-throughput RNA sequencing (RNA-seq) technology.

MATERIALS AND METHODS

Animals

Overall, 24 healthy male Tibetan sheep (Ganjia, Xiahe, China; altitude >3,000 m) were used in study, divided in three age groups (n = 8 for each age group): 3-month-old (3 M; sexually immature), 1-year-old (1Y; sexually mature), and 3-year-old (3Y; adult). The right testes were harvested immediately after sacrifice of all animals, briefly washed with PBS, and deep-frozen quickly in liquid nitrogen for RNA and protein extraction or fixed in 4% paraformaldehyde for making paraffin sections.

RNA Isolation, Library Preparation, and circRNA Sequencing

The Trizol reagent (Invitrogen, United States) was employed to extract the total RNA and their concentration and quality were explored by NanoDrop Spectrophotometer (NanoDrop, United States), Agilent 2100 Bioanalyzer (Agilent Technologies, United States), as well as RNase free agarose gel electrophoresis. Of eight RNA samples for each age group, four were selected randomly for RNA-seq, and all samples were used for qPCR validations. For RNA-seq, ribosomal RNA (rRNA) was depleted with a Ribo-Zero Gold rRNA Removal Kit (Illumina, United States). The remaining RNAs were used to construct the strand specific sequencing library. Briefly, RNAs were fragmented (approximately 200 bp), then converted into 1st-strand cDNA via reverse transcription with random hexamer primers. Next, the 2nd-strand cDNA was processed with dNTPs, RNase H, DNA polymerase I, and buffer. QiaQuick PCR was used to purify the cDNA fragments, and then end repaired and base A introduced, and ligated into Illumina sequencing adapters. Then, the 2nd-strand cDNA was depleted by the UNG enzyme (Uracil-N-Glycosylase). The digested products were size-selected and PCR amplified to generate RNA-seq libraries, followed by sequencing on an Illumina HiSeq4000 system (150-bp paired-end reads; Illumina, United States) at Gene *Denovo* Co., Guangzhou, China.

Identification of circRNAs

The clean reads were acquired by discarding low-quality reads, including reads with adapters, reads bearing greater than 10% of unknown bases (N) and reads with greater than 50% of low-quality (Q-value $\leq$ 20) bases. We mapped the resulting high-quality reads to the sheep Oar_v4.0 reference genome using TopHat2 (Kim et al., 2013). The 20 bp sequences from the two ends for each unmapped read (Anchors reads) were re-aligned to the reference genome with bowtie2 aligner, and subsequently submitted to Find_Circ software (Memczak et al., 2013) with default parameters to identify circRNA.

Functional Annotation and Enrichment Analysis of circRNA Source Genes

The previous literature review showed that one of the functions of CircRNAs is realized through modulating the expression of its source gene (Qu et al., 2015; Shao et al., 2021). To interpret the potential biological roles of circRNAs, Gene Ontology (GO) annotation, as well as Kyoto Encyclopedia of Genes and Genomes (KEGG) pathway analysis of circRNA source genes were thus carried out using GO web resource (http://www.geneontology.org/) and KEGG web portal (http://www.genome.jp/kegg/pathway.html).

Quantification of circRNA Abundance and Differential Expression Evaluation

The expression abundance of the identified circRNAs was computed by RPM (reads per million mapping) method. EdgeR package in R[1] was employed to obtain the differentially expressed (DE) circRNAs between every two age groups. The circRNAs with a $|$ fold change$|$ $>$ 2.0 and p-value $<$0.05 were regarded as significant differentially expressed.

Integrated Analysis of circRNAs–miRNAs–mRNAs

Based on our previous Illumina HiSeq miRNA and mRNA sequencing data from the same samples (NCBI SRA accessions for mRNA sequencing data: SRR11397689-SRR11397700; NCBI SRA accessions for mRNA sequencing data: SRR11348536-SRR11348547), the associations between circRNAs/mRNAs and miRNAs were estimated by using Mireap,[2] TargetScan 7.0,[3] as well as Miranda.[4] CircRNA-miRNA-mRNA ceRNA regulatory network was built as per the following criteria: (1) Expression association between circRNA-miRNA or mRNA-miRNA was assessed by Spearman rank correlation coefficient (SCC); we selected the pairs with SCC $<$ -0.7 as negatively co-expressed circRNA–miRNA pairs or mRNA–miRNA pairs. (2) Expression association between circRNA-mRNA was determined via Pearson correlation coefficient (PCC); we selected the pairs with PCC $>$ 0.9 as co-expressed circRNA–mRNA pairs. (3) The p-value was computed based on a hypergeometric cumulative distribution function test to assess shared miRNA sponges between circRNA–mRNA; we chose the pairs with a p-value of $<$0.05 as final ceRNA pairs. For these mRNAs in network, GO and KEGG enrichment assessment were conducted to further elucidate the function of circRNAs. The ceRNA network related to testicular function was visualized by Cytoscape 3.8.

Dual Luciferase Reporter

The wild-type (WT) and mutant-type (MUT) circ_024949, circ_026259, and IGF1 3′-UTR containing the putative binding site of oar-miR-29b were purchased from GENEWIZ (Suzhou, China) and subsequently inserted into the pmirGLO luciferase reporter vector *Xho*I/*Sal*I sites (Promega, United States). Oar-miR-29b mimic and mimic negative control (NC) were bought by Jima (Shanghai, China), and their sequences are provided in **Supplementary Table 1**. The luciferase reporter plasmids (circ_024949 WT, circ_024949 MUT, circ_026259 WT, circ_026259 MUT, IGF1 3′-UTR WT, or IGF1 3′-UTR MUT) were transfected with oar-miR-29b mimic or mimic NC into 293T cells using Lipofectamine 2000 transfection vehicle (Invitrogen, Carlsbad, CA, United States) as per the instructions provided by vendors. The firefly, as well as renilla luciferase activities were examined at 48 h after transfection by the Dual-Luciferase Reporter Assay System (Promega, United States). The relative luciferase enzyme activity was shown as ratios of firefly luciferase to renilla luciferase. Three repeated experiments were set up in each group.

Isolation, Culturing, and Transfection of Sheep Sertoli Cells

Testes were collected from healthy Tibetan sheep aged three-month-old, sterilized with 75% alcohol and then transported to the laboratory within 30 min in PBS buffer containing penicillin and streptomycin on ice. Sertoli cells were isolated as described recently (Gao et al., 2020), with some alterations. Briefly, under aseptic conditions, testes were rinsed twice with PBS after removal of the tunica albuginea, and seminiferous tubules were minced into paste and digested with type IV collagenase (1 mg/mL) for 1 h at 37°C. After centrifugation, the supernatant was discarded and digested with 0.25% trypsin for 20 min at 37°C. The digestion was terminated with DMEM/F12 supplemented with 10% FBS (Gibco, United States), and the digested cells were filtered through 100-, 200-, and 300-mesh screen. After centrifugation, cells were washed with PBS, resuspended in high-glucose DMEM containing 10% FBS, seeded in culture flasks, and routinely cultured at 37°C in 5 % CO_2. After 6 h of culture, the medium was removed and changed with fresh medium to discard the suspending germ cells. After a continued culture time of 18 h, the supernatant was discarded and 0.05% trypsin was added to transiently digest cells before addition of fresh medium. When the cells reached ∼80% confluency, the above steps were repeated 3–4 times to remove residual germ cells and to obtain pure Sertoli cells. The isolated sheep Sertoli cells were identified by RT-PCR and immunofluorescence staining with antibodies against Vimentin and SOX9.

The linear sequence of circ_026259 derived from KLHL5 gene was synthesized and cloned into the *Eco*RI and *Bam*HI restriction sites of overexpression vector pCD25-ciR (pCD25-circ_026259; Geneseed, Guangzhou, China), which included a forward and backward circular frame to promote circularization. Small interfering RNAs (siRNAs) targeting circ_026259 (si1-circ_026259 and si2-circ_026259), oar-miR-29b inhibitor, or the corresponding negative controls (si-NC and inhibitor NC) were provided by Jima (Shanghai, China), and their sequences are listed in **Supplementary Table 1**. For transient transfections, Sertoli cells were seeded in culture plates in a proper density and 24 h later transfected with pCD25-circ_026259, control vector (pCD25-circ), si1-circ_026259, si2-circ_026259, si-NC, oar-miR-29b mimic/inhibitor, or mimic/inhibitor NC using Lipofectamine 2000 reagent (Invitrogen) per as recommended by the provider. Cells were harvested 48 h after transfection for assessment of the transfection efficiency and subsequent analysis.

PCR Analysis

The total RNA was isolated from cells and tissues with TRIzol reagent (TransGen, Beijing, China), and reverse transcribed to cDNA using an Evo M-MLV RT Kit with gDNA Clean for qPCR (Accurate, Hunan, China). The cytoplasmic and nuclear RNAs from Sertoli cells were prepared using PARIS^{TM} kit (Invitrogen) as per the instructions provided by vendors. For

[1] http://www.rproject.org/

[2] https://sourceforge.net/projects/mireap/

[3] http://www.targetscan.org

[4] http://miranda.org.uk/

RNase R treatment, 1 μg total RNA was incubated for 30 min at 37°C with 1μL RNase R (20 U; Epicentre, United States), and then deactivated RNase R at 80°C for 10 min. RT-PCR was carried out using 2× Pro Taq Master Mix kit (Accurate) as the per manufacturer's instructions. qPCR was done under the following conditions: 95°C for 30 s, then 40 two-step amplification cycles of 95°C for 5 s and 60°C for 30 s. Divergent primers used for amplification of circRNA-specific back splice junctions were designed. All primers used were synthesized by Tsingke (Xi'an, China). Details of the primers used are presented in **Supplementary Table 2**. β-actin or GAPDH was used as an internal reference gene for circRNA and mRNA, and U6, for miRNA. The expression levels relative to internal reference gene were computed by $2^{-\Delta\Delta Ct}$ approach. PCR products were confirmed via electrophoresis on 1.5% agarose gels was employed to confirm the PCR products and bands were extracted and subjected to Sanger sequencing.

In situ Hybridization and Immunofluorescence

Digoxigenin (DIG)-labeled RNA antisense probes for circ_024949 (5′-ATATTGATAGAGAGCTTT CCCTAAATGTGT-3′), circ_026259 (5′-TACTATTGGAAG TCCTGTGGTGCAAGAAG-3′), oar-miR-29b (5′-ACACTGA TTTCAAATGGTGCTA-3′), and IGF1 (5′-TGAA ATAAAAGCCCCTGTCTCCGCACACGAA-3′) were purchased from General Biosystems (Anhui, China) for *in situ* hybridization. After conventional dewaxing and rehydration, 5-μm paraffin sections or fixed Sertoli cells were digested in proteinase K solution and bloked with 3% H_2O_2/methanol. Pre-hybridization, hybridization and washing were conducted according to standard methods. After this step, probe signals were visualized with mouse anti-DIG antibody (HRP-conjugated) and direct FITC-TSA kit (Servicebio, Wuhan, China). The nuclei were counterstained by DAPI. Cells or the adjacent sections were hybridized with sense probes and without probes to produce negative controls. For immunofluorescence staining of testis tissue sections, sections were blocked with 5% BSA (Solarbio, Beijing, China) prior to incubation with rabbit anti-IGF1 polyclonal antibody (1:200; Bioss, Beijing, China) overnight at 4°C. Then, sections were added with goat anti-rabbit IgG labeled with CY3 (1:200; Servicebio, Wuhan, China) and counterstained with DAPI. The sections were seen in Nikon fluorescence microscope (Eclipse C1, Tokyo, Japan) and imaged with CaseViewer software. For immunofluorescence cell staining, Sertoli cells were fixed, permeabilized, and subsequently incubated with primary antibodies against Vimentin (1:200; Bioss, China) or SOX9 (1:200; Bioss, China) followed by incubation with FITC-conjugated secondary antibody. The remaining procedures were the same as above.

Western Blot

Proteins from testes and Sertoli cells were extracted with RIPA buffer and separated on 12% SDS-PAGE gel. After transfer, the PVDF blot membranes were blocked and then probed with rabbit polyclonal antibody against IGF1 (1: 500, Bioss, Beijing, China) at 4°C overnight. Anti-β-actin polyclonal antibody (1:1,500, Bioss, Beijing, China) was used as an internal reference. These blots were further conjugated with a goat anti-rabbit IgG secondary antibody labeled with HRP (1: 5,000, Bioss, Beijing, China) via incubation and revealed with ECL kit (NCM Biotech, Suzhou, China) and exposed to X-ray films. Quantification of the blot intensities was performed using the AlphaEaseFC software.

Statistics

Data among/between groups were analyzed using SPSS 21.0 software (SPSS, Inc., Chicago, IL, United States) with one-way ANOVA followed by LSD *post hoc* test, or the independent samples t test; the results are indicated as the mean ± SD. The differences between two groups were marked by $^{*}P < 0.05$ and $^{**}P < 0.01$.

RESULTS

Overview of circRNA Sequencing

After the raw reads were filtered, a total of 994,655,502 high-quality clean reads (85,301,018 from 3M group, 78,331,884 from 1Y group, and 85,030,974 from 3Y group) were obtained. There were 14.88, 17.46, and 18.67% of the high-quality reads that were not aligned to the sheep reference genome in 3M, 1Y, and 3Y groups, respectively, and 20 bp sequences (Anchors reads) on both ends of which were selected for re-alignment with the reference genome to identify circRNA. Specific information regarding the overall analysis of the sequencing data is presented in **Supplementary Table 3**. RNA-seq data has been deposited to the SRA database in NCBI (SRA accessions: SRR11348536-SRR11348547). In total, 31,148 circRNAs were identified in this study, which were named and numbered from circ_000001 to circ_031148. According to their position on the ovine genome, the vast majority of these circRNAs were showed to have originated from protein-coding exons of genes, while many others were originated from antisense or intronic sites (**Figure 1A**). Most of the circRNAs were between 200 and 700 nt long, with 400 nt being the most abundant length (**Figure 1B**). These circRNAs were distributed on all chromosomes including 26 autosomes and X chromosome, but were mainly existed in chromosomes 1, 2, and 3 (**Figure 1C**).

Differential Expression Analysis

Overall, 3982 (2,079 up-regulated; 1,903 down-regulated), 414 (201 up-regulated; 213 down-regulated), and 4,060 DE circRNAs (2,107 up-regulated; 1,953 down-regulated) were found in 3M vs 1Y, 1Y vs 3Y, and 3M vs 3Y groups, respectively (**Figures 2A,C**). Details about these circRNAs are available in **Supplementary Tables 4–6**. Among these, 44 circRNAs were co-expressed in testes from three age groups (**Figure 2B**). To characterize the dynamics of circRNA expression in developmental testes, we performed trend analysis of differentially expressed circRNAs in testes at three developmental stages. Here, we identified seven main circRNA profiles, where each represented a characteristic expression pattern (**Figure 2D**). Of these, three patterns, including profile 0 (continuously down-regulated), profile

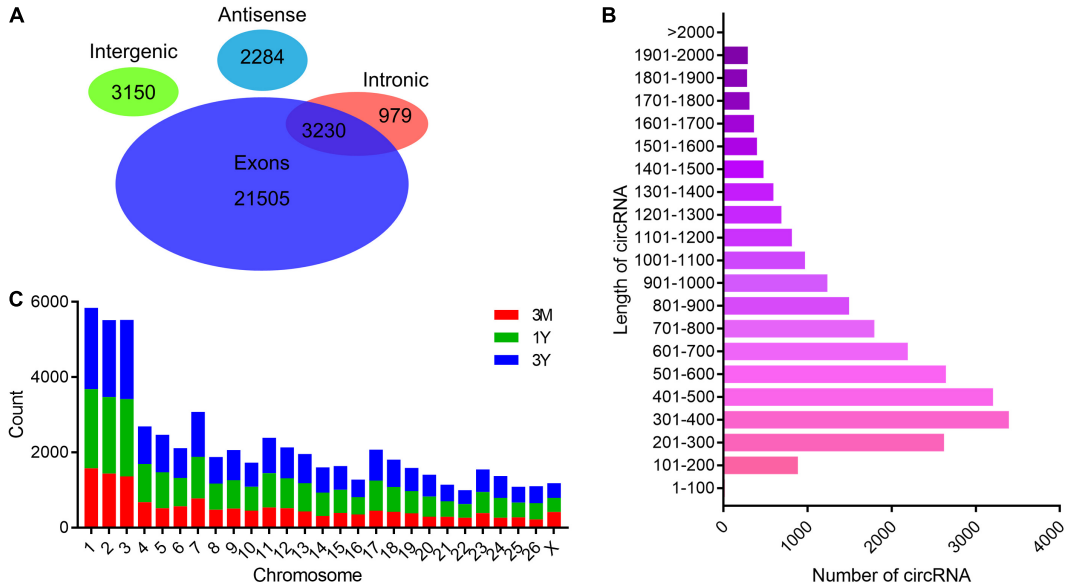

FIGURE 1 | General features of circRNAs. **(A)** Venn diagram indicating that circRNAs numbers originated from different genomic sites. **(B)** Length distributions for the identified circRNAs. **(C)** Chromosome distribution map of circRNAs. 3M, 1Y, and 3Y refer respectively to 3-month-old, 1-year-old, and 3-year-old.

1(firstly down-regulated followed by no change), and profile 6 (firstly up-regulated followed by no change) were significant.

Validation of CircRNA Expression by qPCR

The divergent primers for their junction sites from ten randomly selected DE circRNAs were used to determine the presence of these circRNAs (**Figure 3A**). The qPCR results suggested that expression profiles for these ten circRNAs were congruent with the RNA-sequencing results (**Figure 3B**). The 1.5% agarose gel electrophoresis shows the expected size of a single band for each selected circRNA (**Figure 3C**). The produced fragment was then sequenced by Sanger sequencing, and results showed the sequence information of circular junction for these circRNAs, obtained by Sanger sequencing, were exactly the same as circRNA sequencing (**Figure 3D**). These suggest that the sequencing data and expression of circRNAs identified in this study are reliable.

Enrichment and Functional Annotation Analysis for Source Genes of DE circRNAs

In 3M vs 1Y, 3,694 of the identified 3,982 DE circRNAs were derived from 2,079 source genes, and residual 288 circRNAs were derived from intergenic regions, having no source genes; in 1Y vs 3Y group, 370 of the identified 414 DE circRNAs were derived from 339 source genes, and residual 44 circRNAs were derived from intergenic regions, having no source genes; in 3M vs 3Y, 3,767 of the uncovered4060 DE circRNAs were derived from 2,119 source genes, and residual 293 circRNAs were originated from intergenic regions, having no source genes. To evaluate the biological roles of circRNAs, we mapped all the source genes for these DE circRNAs into GO terms in the GO resource and signaling pathways in the KEGG database. In total, 187, 73, and 182 GO terms for 3M vs 1Y, and 1Y vs 3Y, and 3M vs 3Y, respectively, was significantly enriched (**Supplementary Table 7**). These GO terms were mostly involved in biological processes such as reproduction, growth or development, immune system, and metabolism (**Figure 4A**). KEGG analysis indicated that the source genes for DE circRNAs, in 3M vs 1Y and 3M vs 3Y, were significantly enriched in cell cycle, oocyte meiosis, adherens junction, TGF-beta signaling, mTOR signaling, Hippo signaling, and other signaling pathways (**Figure 4B**); the source genes for DE circRNAs, in 1Y vs 3Y, were significantly enriched in tight junction, mTOR signaling, regulation of actin cytoskeleton, VEGF signaling, estrogen signaling pathway and other pathways (**Figure 4B**).

CircRNA–miRNA–mRNA Network Construction and Functional Enrichment of mRNAs in Network

To further gain insights into the biological roles of these DE circRNAs, the ceRNA regulatory networks through the integration of our previous miRNA and mRNA sequencing data were constructed for circRNA–miRNA–mRNA interactions based on the "ceRNA hypothesis." See **Supplementary Table 8** for the list of mRNAs in the network. GO analysis showed that mRNAs derived genes in ceRNA network, on the biological processes, were mainly involved in, cellular component organization or biogenesis, reproduction, cellular process, development, as well as biological adhesion (**Figure 4C**); on the cellular components, were mainly included organelle, membrane, and extracellular matrix (**Figure 4C**); on the molecular function, mainly clustered with signal transducer activity, binding, catalytic activity, as well as transcription factor activity (**Figure 4C**).

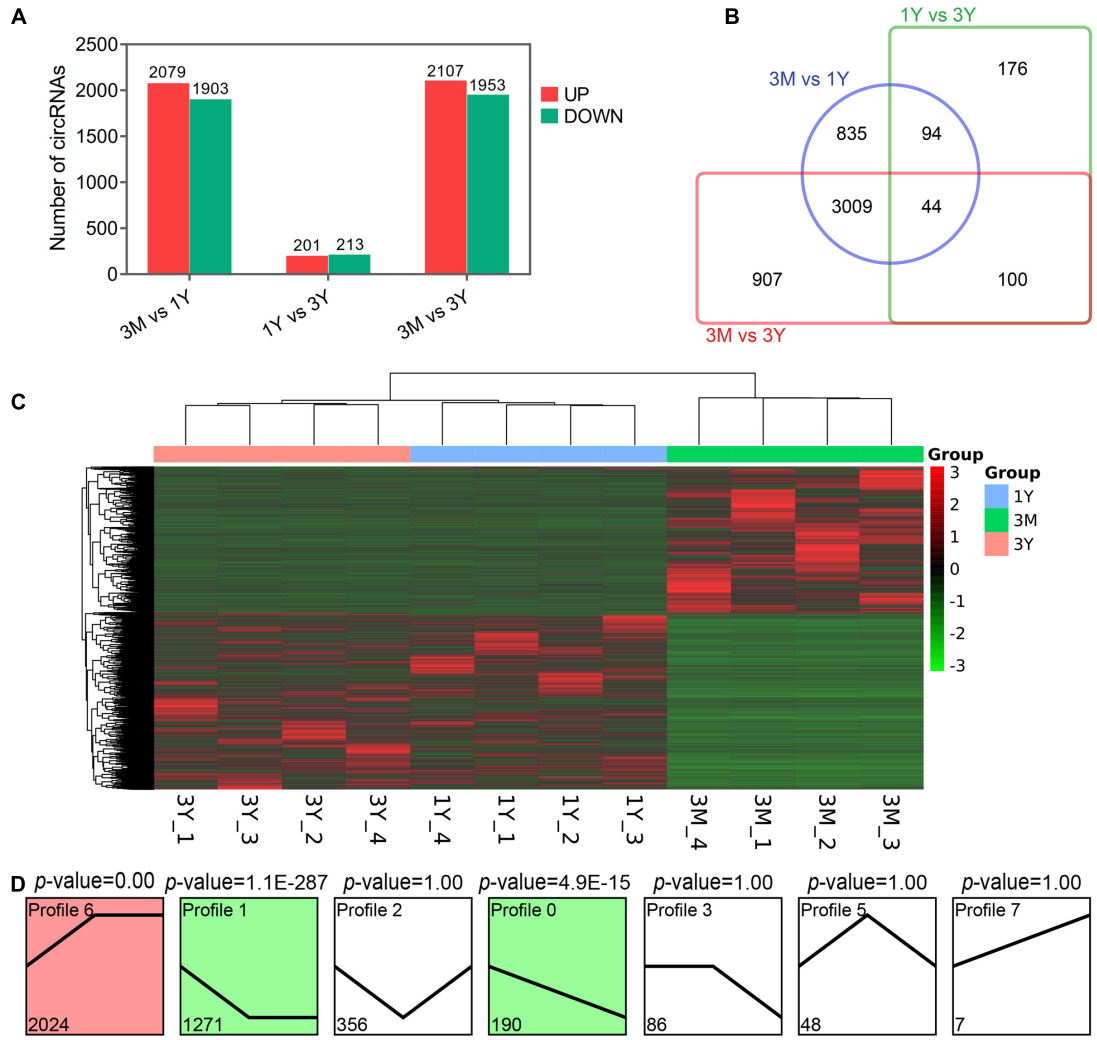

FIGURE 2 | Summary of differential expression analysis of the annotated circRNAs. **(A)** Statistics of differential circRNAs. **(B)** A Venn diagram indicating the shared and unique differential circRNAs. **(C)** Clustering heat map of differential circRNA expression. Red corresponds to upregulation; Green corresponds to downregulation. **(D)** Trend analysis of differential circRNAs. 3M, 1Y, and 3Y refer respectively to 3-month-old, 1-year-old, and 3-year-old.

KEGG assessment indicated that these mRNAs derived genes were engaged in adherens junction, focal adhesion, ECM–receptor interaction, TGF-beta signaling, modulation of actin cytoskeleton, signaling cascades modulating pluripotency of stem cells, MAPK signaling, Wnt signaling, and so on (**Figure 4D**). The heatmap revealed that there were 1,335 genes which are shared by DE circRNA source genes and DE mRNAs (**Figure 4E**). Further functional analysis using GO and KEGG databases revealed these shared genes were primarily implicated in the biological processes such as reproduction, cellular process, development, growth and immunity (**Supplementary Figure 1**), and were significantly enriched in cell cycle, ECM–receptor interaction, TGF-beta signaling, mTOR, and other signaling pathway (**Figure 4F** and **Supplementary Table 9**), which were similar to the functional enrichment analysis results above. In the circRNA–miRNA–mRNA regulatory network, 28 known spermatogenesis-related genes (e.g., IGF1, DMRTC2, etc.) were potentially regulated by 143 circRNA–miRNA pairs covering 107 DE circRNAs and 24 DE miRNAs (**Figure 5**); 6 genes related to germ cell development were potentially regulated by 34 circRNA–miRNA pairs covering 33 DE circRNAs and 10 DE miRNAs (**Figure 5**); 16 cell cycle- or meiosis-related genes were potentially regulated by 140 circRNA-miRNA pairs covering 96 DE circRNAs and 18 DE miRNAs (**Figure 5**); 7 genes associated with blood–testis barrier (BTB) were potentially regulated by 45 circRNA–miRNA pairs covering 39 DE circRNAs and 9 DE miRNAs (**Figure 5**).

Validation of Targeting Relationships Between circ_024949/circ_026259/IGF1 and oar-miR-29b and Their Tissue Expression Characteristics

Based on the same expression trends between circRNAs and mRNAs and the inverse expression trends between

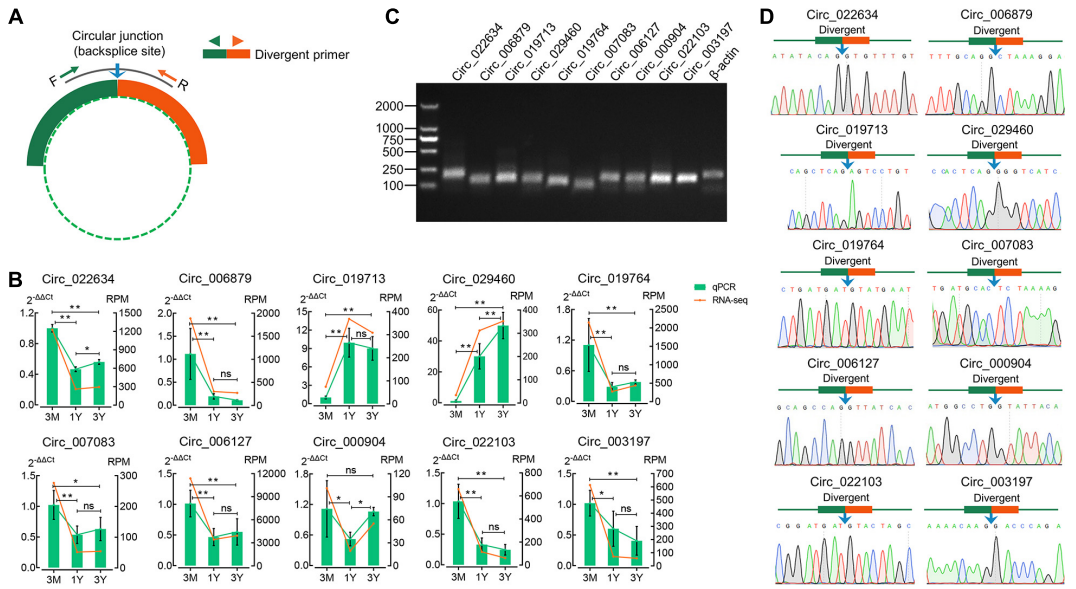

FIGURE 3 | Verification of eight randomly selected circRNAs from RNA-Seq. **(A)** Divergent primers were designed for circRNA validation. **(B)** Comparison between qPCR and RNA-seq results. **(C)** Visualization of the PCR products on a 1.5% agarose electrophoresis gel. **(D)** Circular junctions were confirmed by Sanger sequencing. 3M, 1Y, and 3Y refer respectively to 3-month-old, 1-year-old, and 3-year-old. Two asterisks (**), one asterisk (*), and ns (non-significant) denote $P < 0.01$, $P < 0.05$, and $P > 0.05$, respectively.

circRNAs/mRNAs and miRNAs in testes at three development stages, circRNA–miRNA–mRNA regulatory network involved in spermatogenesis were further screened, which consists of 20 differentially expressed circRNAs, 11 miRNAs, and 11 mRNAs (**Figure 6A**). IGF1, a known important regulator of spermatogenesis (Potter and DeFalco, 2017; Neirijnck et al., 2019), is found to be present in this regulatory network, and potentially regulated by circ_026259/circ_024949/circ_012373-oar-miR-29b axis where circ_026259 and circ_024949 exhibit a higher abundance (**Supplementary Tables 4–6**) and a more significant relationship (circ_026259/IGF1, $P = 0.0078$; circ_024949/IGF1, $P = 0.0169$) compared to circ_012373 ($P = 0.0303$). Based on these considerations, we selected circ_026259 and circ_024949 to verify their targeting relationships between circ_024949 and oar-miR-29b, circ_026259 and oar-miR-29b, and IGF1 and oar-miR-29b, and to assess their expression patterns.

The putative binding sites of circ_024949, circ_026259 and IGF1-3′UTR with oar-miR-29b are provided in **Figure 6B**. Dual-luciferase reporter assay indicated that oar-miR-29b significantly suppressed the luciferase activities for co-transfecting with wild types of circ_024949, circ_026259, or IGF1-3′UTR compared with oar-miR-29b negative control ($P < 0.01$), while no effect on the mutant types of circ_024949, circ_026259 or IGF1-3′UTR ($P < 0.05$) (**Figure 6C**). These results initially confirmed the direct interactions between circ_026259/circ_024949/IGF1 and oar-miR-29b. Subsequently, RT-PCR and qPCR results demonstrated that the relative RNA expression of circ_024949, circ_026259, and IGF1 gradually decreased (**Figures 6D,E**), while that of oar-miR-29b progressively increased with the advance of ages, showing excellent agreement with our results obtained by RNA-seq (**Figure 6E**). Sanger sequencing corroborated the back-splicing junction sites in the qPCR products of circ_024949 and circ_026259 amplified by divergent primers (**Figure 6F**). Pearson's correlation analysis indicated that there was a strong negative correlation between circ_024949 and oar-miR-29b, circ_026259 and oar-miR-29b, oar-miR-29b and IGF1 ($R = -0.878, -0.820, -0.899$, $P < 0.001$) (**Figure 6G**). *In situ* hybridization revealed that RNA distribution patterns for circ_024949, circ_026259, oar-miR-29b and IGF1 were very similar in developmental testes and extensively existed in various testicular cells (such as germ cells, Leydig cells, and Sertoli cells) (**Figure 6H**). Consistent with the mRNA level, IGF1 protein expression gradually decreased with age (**Figure 6I**), and localized ubiquitously to various germ cells as well as Leydig cells and Sertoli cells and, with intense expression in spermatozoa and the cytoplasm of Leydig cells from 1Y and 3Y, as well as the seminiferous epithelium from 3M (**Figure 6J**).

Circ_026259 Regulated IGF1 Expression by Targeting oar-miR-29b in Testicular Sertoli Cells

On the basis of our above experiment results and prior literature documenting a crucial role for IGF1 in Sertoli cells which modulates cell proliferation (Cannarella et al., 2018; Johnson et al., 2020), we thus chose to focus on Sertoli cells for more detailed investigation in ovine testicular cells. Here we isolated ovine primary Sertoli cells using two-step enzymatic digestion and the isolated primary cells strongly expressed the Sertoli cell-specific markers Vimentin and SOX9 (**Figures 7A,B**), suggesting successful isolation of Sertoli cells from sheep testis tissues.

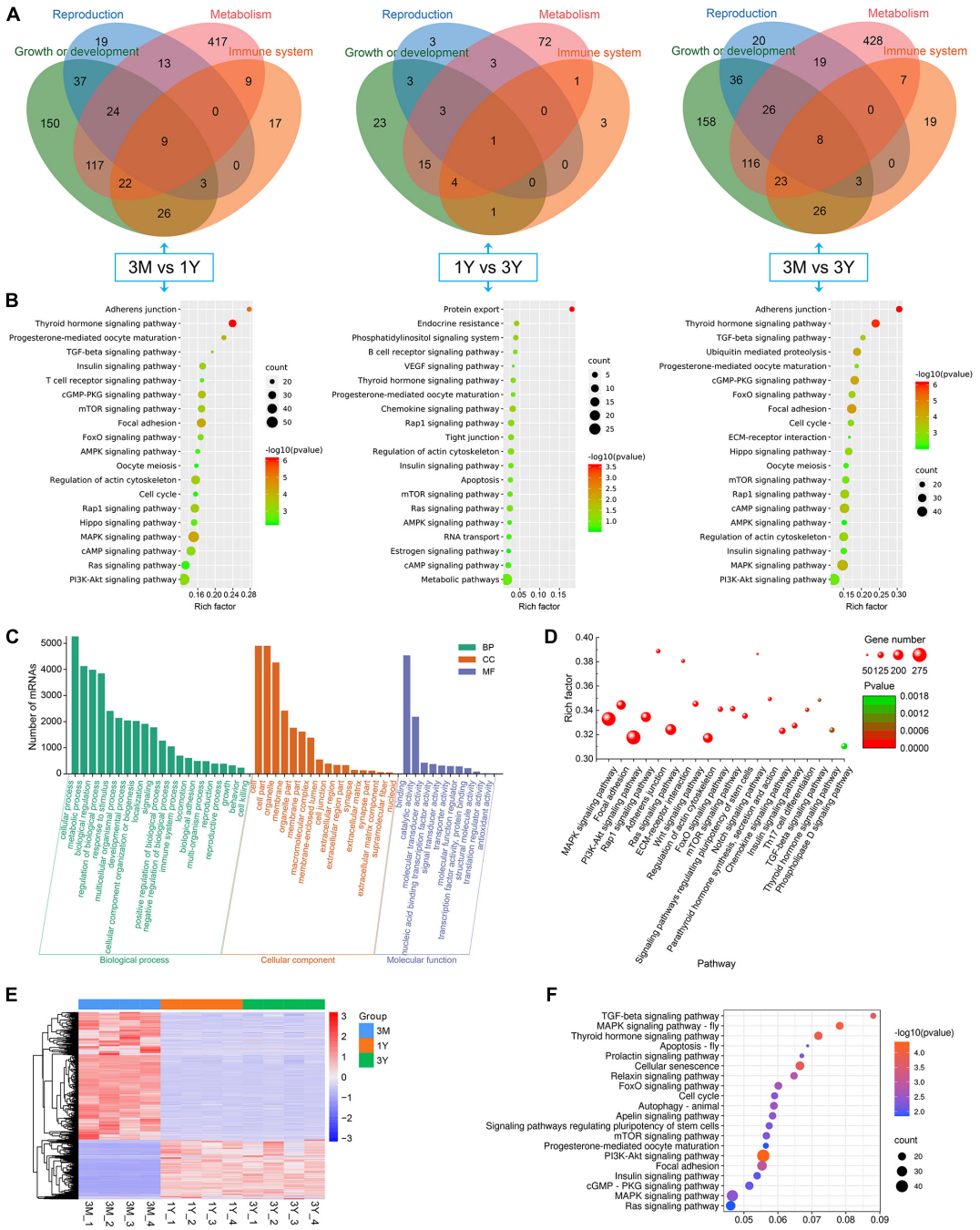

FIGURE 4 | Functional annotation and enrichment analysis. **(A)** Functional classifcation and **(B)** KEGG pathway assessment of the source genes of differential circRNAs. **(C)** GO annotation and **(D)** KEGG enrichment of mRNAs in circRNA–miRNA–mRNA regulatory network. **(E)** Expression heatmap and **(F)** significantly enriched KEGG pathways of genes shared between DE circRNA source genes and DE mRNAs. 3M, 1Y, and 3Y refer respectively to 3-month-old, 1-year-old, and 3-year-old.

Circ_026259 was therefore chosen for subsequent oar-miR-29b/IGF1 axis analysis in Sertoli cells since circ_026259 showed a higher RNA abundance compared to circ_024949, either as RNA-seq and qPCR data from testicular tissues or qPCR data from Sertoli cells (data not shown). Bioinformatics revealed that circ_026259, with 730 bp in length, is derived from the exon 2, exon 3, exon 4, and exon 5 of KLHL5 gene, and the end of exon 2 and exon 5 was back-spliced to form the circular structure (**Figure 7C**). We further confirmed its circular character using the RNase R digestion method, RT-PCR and Sanger sequencing (**Figure 7C**), corroborating the existence of circ_026259 in Sertoli cells. Circ_026259 was mainly located in the cytoplasm of Sertoli

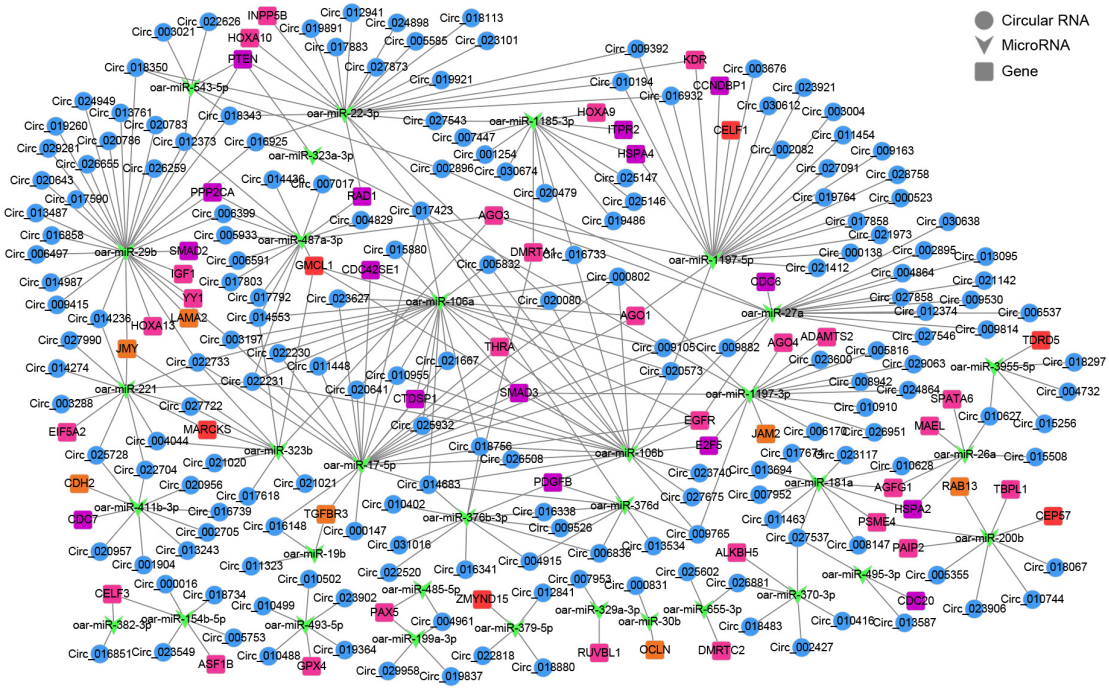

FIGURE 5 | The circRNA–miRNA–mRNA interaction network. Blue circles represent circRNAs, green V shape represents miRNAs, and squares with different colors represent genes belonging to different functional classification (pink, spermatogenesis; orange, blood-testis barrier; red, germ cell development; purple, cell cycle or meiosis).

cells but expression was also found in the nucleus (**Figures 7D,E**), based on nuclear and cytoplasmic fractionation and FISH, which suggest that circ_026259 may exert its action through ceRNA regulation pattern.

To explore whether circ_026259 regulates the expression of IGF1 in Sertoli cells, circ_026259 overexpression and knockdown experiments were carried out *in vitro*. The transfection of PCD25-circ_026259 plasmid significantly enhanced the expression of circ_026259 in Sertoli cells (**Figure 7F**). We used two siRNAs targeting the junction site of circ_026259 and showed that circ_026259 expression was effectively decreased by transfection with two siRNAs (si1-circ_026259, si2-circ_026259) in comparison with the control and si-NC groups (**Figure 7F**), where si1-circ_026259 exhibited more potent knockdown effects and was therefore selected for subsequent investigation. We next examined the expression of oar-miR-29b upon overexpression or knockdown of circ_026259 in Sertoli cells, and the results demonstrated that the expression of oar-miR-29b was significantly inhibited by overexpressing circ_026259, which was significantly enhanced through circ_026259 knockdown (**Figure 7G**). Overexpression of oar-miR-29b significantly suppressed the expression of IGF1, whereas its knockdown significantly increased IGF1 expression (**Figures 7H,I**). Additionally, circ_026259 overexpression can restore the repression of IGF1 expression at mRNA and protein levels by oar-miR-29b to certain extent (**Figure 7J**). Together, this series of experiments support that circ_026259 as a miR-29b sponge to indirectly modulate the expression of IGF1.

DISCUSSION

The testis is a strongly transcriptionally active organ whose main functions is to produce sperm through spermatogenesis (Witt et al., 2019). CircRNAs, as an abundant non-coding RNA in the eukaryotic transcriptome, are important modulators involved in modulating expression of genes at the transcriptional, post-transcriptional as well as translational levels and miRNA functions (Ebbesen et al., 2017). Herein, we first identified and characterized the expression patterns of circRNAs in developmental sheep testes via high-throughput sequencing, as well as bioinformatics analysis. Here, 3,982, 414, and 4,060 DE circRNAs were identified in 3M vs 1Y, 1Y vs 3Y, and 3M vs 3Y groups, respectively. These differential circRNAs were clustered into seven overall expression patterns of which three patterns involved 3,485 DE circRNAs showed significant clustering. Among these, with the increase of age during testicular development, 190, 1,271, and 2,024 circRNAs exhibited the expression trends of continuous decreasing, of first decreasing followed by no change, and of increasing followed by no change, respectively. The qPCR analysis and Sanger sequencing were done to validate circRNA sequencing data, and results support that circRNAs obtained in this study are of high quality and reliable.

To explore the roles of circRNAs in developmental sheep testis, functional analysis of the source genes of DE circRNAs was conducted. GO functional annotation indicated that circRNA source genes mainly participated in biological processes

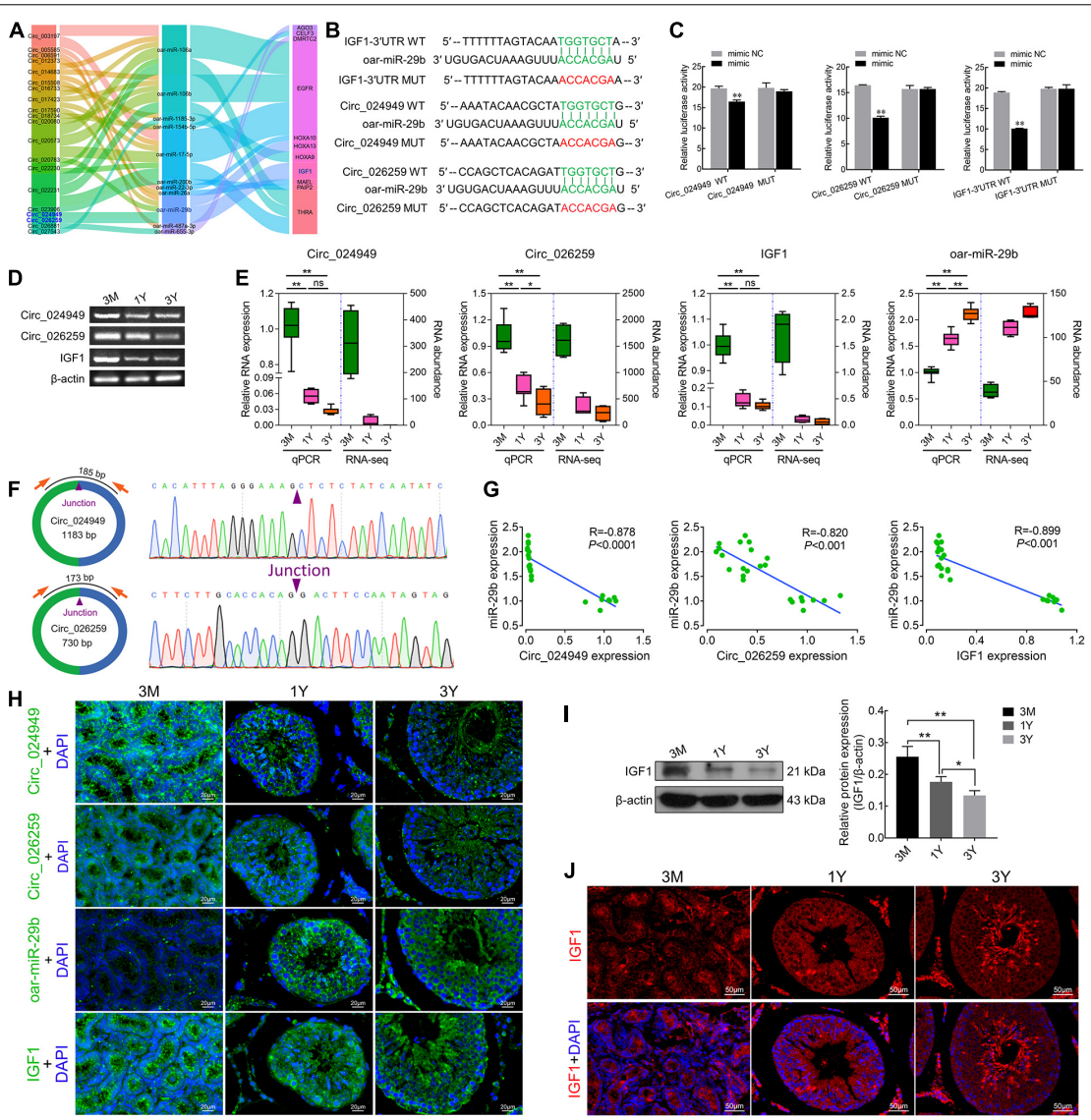

FIGURE 6 | The targeting relationships between circ_024949/circ_026259/IGF1 and miR-29b as well as their expression correlations. **(A)** Sankey plot of the circRNA-miRNA-mRNA network enriched for spermatogenesis-related genes. **(B)** Putative binding sites revealed by bioinformatics analysis. **(C)** Dual-luciferase assays were used to validate the binding sites between circ_024949/circ_026259/IGF1-3′UTR and oar-miR-29b. **(D)** RT-PCR and **(E)** qPCR analysis for the relative RNA expression. **(F)** Divergent primers **(left panels)** and Sanger sequencing **(right panels)** used for the amplification of circular junctions of circ_024949 and circ_026259. **(G)** Correlation analysis between oar-miR-29b and circ_024949/circ_026259/IGF1 expression. **(H)** RNA fluorescence *in situ* hybridization analysis. **(I)** IGF1 protein expression assessed by Western blot. **(J)** Immunofluorescence staining for IGF1 protein. 3M, 1Y, and 3Y refer respectively to 3-month-old, 1-year-old and 3-year-old. Two asterisks (**), one asterisk (*), and ns (non-significant) denote $P < 0.01$, $P < 0.05$, and $P > 0.05$, respectively.

including reproduction, growth and development. For instance, in 3M vs 1Y and 3M vs 3Y, 8 common DE circRNAs were generated from DAZL and BOLL that belong to deleted in azoospermia (DAZ) gene family associated with germ cell development and spermatogenesis (Fu et al., 2015); 29 DE circRNAs were derived from 15 genes coding for cell division cycle-related proteins (e.g., CDC14B, CDC20B, CDC6, GAK, CDK6, CDK12-13, CDK17, etc.). In 1Y vs 3Y, differential circRNA circ_025151 was generated from SMAD5, a gene has been demonstrated to promote cell proliferation and inhibit apoptosis of Sertoli cells in pigs (Luo et al., 2020); circ_012965 was derived from SPIN1 that is a gene associated with meiotic progression and meiotic cell cycle in mammals (Choi et al., 2019). It is suggestive of a function for these circRNAs in testicular cell cycle progression and cell development thereby participating in the regulation of spermatogenesis and testis development.

Notably, in this study, some of circRNA source genes were linked to the annotation correlated with the function of the immune system. Besides spermatogenesis and steroidogenesis, the testis has also been considered as an immunological privileged organ where immune responses are limited to protect

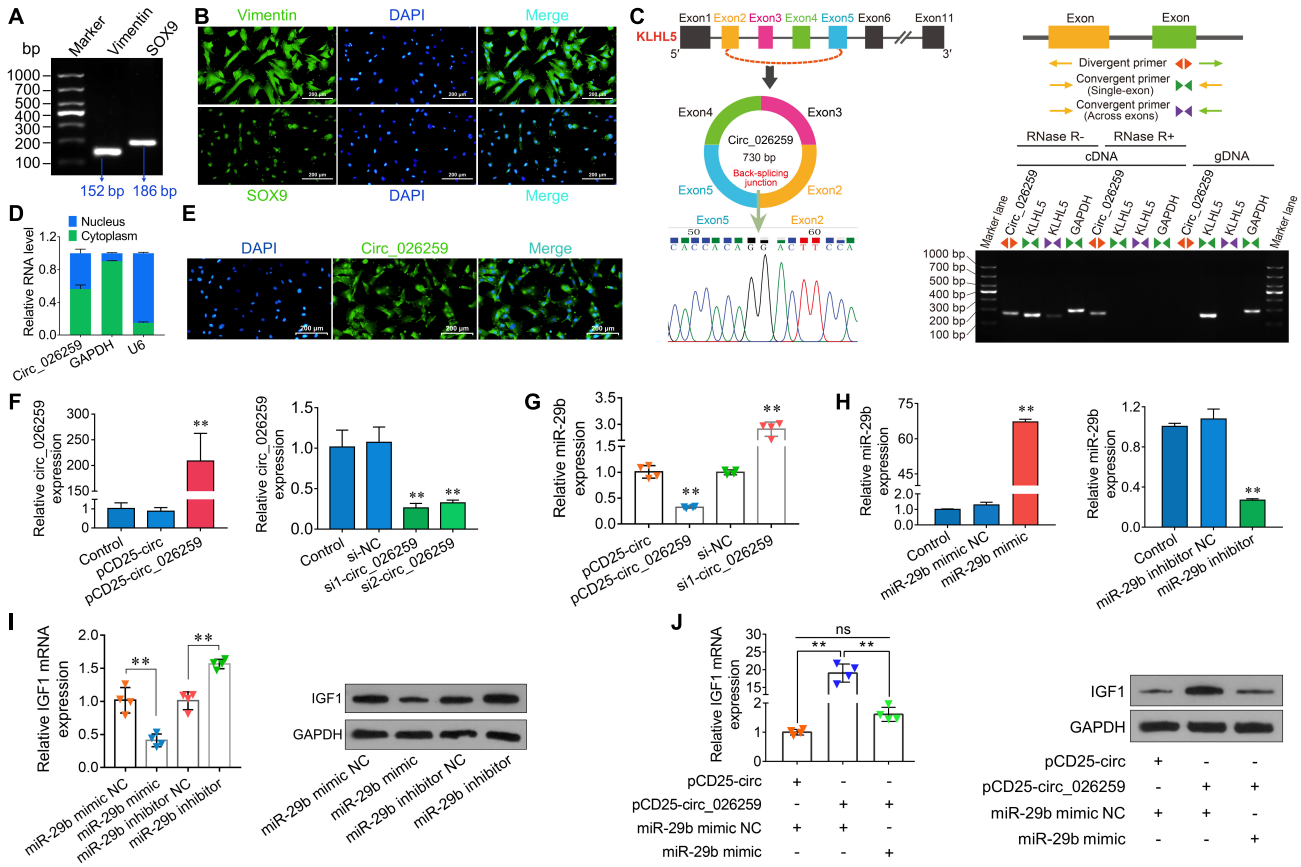

FIGURE 7 | Characterization and expression analysis of circ_026259 and effects of circ_026259 on oar-miR-29b and IGF1 expression in sheep Sertoli cells. **(A)** RT-PCR and **(B)** immunofluorescence assays of marker genes (Vimentin and SOX9) were performed to identify the primary Tibetan sheep Sertoli cells. **(C)** The structure characteristics of circ_026259. **(Left upper panel)** Schematic illustration showing circularization of circ_026259 originated from exon 2 to exon 5 of the ovine KLHL5 gene. **(Right panel)** Divergent primers amplified circ_026259 in cDNA in Sertoli cells with or without RNase R, but not genomic DNA (gDNA). **(Left lower panel)** Sanger sequencing confirmed the back-splicing junction of circ_026259. **(D)** qPCR detection and **(E)** FISH localization of circ_026259 in Sertoli cells. **(F)** Examination of circ_026259 overexpression **(left panel)** and knockdown **(right panel)** efficiency by qPCR. **(G)** Effects of overexpression and knockdown of circ_026259 on expression of oar-miR-29b. **(H)** Examination of oar-miR-29b overexpression **(left panel)** and knockdown **(right panel)** efficiency by qPCR. **(I)** Effects of overexpression and knockdown of oar-miR-29b on IGF1 mRNA and protein expression. **(Left panel)** IGF1 mRNA levels relative to GAPDH. **(Right panel)** the representative images showing IGF1 protein expression levels obtained using Western blot. **(J)** Circ_026259 overexpression can rescue the suppressive effects of oar-miR-29b on IGF1 mRNA and protein expression in Sertoli cells. **(Left panel)** the relative mRNA levels of IGF1. **(Right panel)** the representative Western blot images showing IGF1 protein expression. ** denotes $P < 0.01$.

immunogenic germ cells from an immune attack and to sustain the immune homeostasis required for normal spermatogenesis (Zhao et al., 2014). The blood-testis barrier has long been known to be a crucial part of the testicular immune privilege to sequester auto-antigenic germ cells and is one of the tightest tissue barrier present in mammals, which is primarily formed by the integrins (Yan et al., 2007) and junctional complex (Smith and Braun, 2012; Mruk and Cheng, 2015) between Sertoli cell-Sertoli cell, Sertoli cell-matrix and Sertoli cell-germ cell (e.g., tight junctions, adherens junctions) to sustain the barrier integrity and function. As expected, we found that 12 DE circRNAs shared by 3M vs 1Y and 3M vs 3Y groups were derived from eight genes (CTNNA1, NECTIN3, GJC1, TNS1, STRN, SMAD2, NUMBL, and TGFB2) associated with cell junctions, including cell-cell junction, cell-substrate junction and adherens junction. Twelve common DE circRNAs were derived from genes encoding integrin molecules, including ITGA4, ITGA9, ITGAL, ITGAV, ITGB1, ITGB8, ITGB3BP, and ITGBL1.

Moreover, the intratesticular interstitial space interspersed between the seminiferous tubules contains a variety of immune cell population of immune system engaged in the regulation of immune responses against microbial infections: macrophages, lymphocytes (mainly T cells), dendritic cells, as well as mast cells (Pérez et al., 2013). During testicular development, these immune cells contribute to sustaining immune homeostasis via the involvement of immune tolerance, local immunosuppression and decreased immune activation (Meinhardt and Hedger, 2011). In this study, in 3M vs 1Y and 3M vs 3Y, 77 shared source genes for DE circRNAs were linked with immune response based on GO annotation. For example, circ_001819 and circ_001824 derived from CBLB gene and circ_023878 and circ_023884 derived from GLI3 gene were

annotated to negative regulation of lymphocyte activation; six DE circRNAs (circ_025570, circ_021583, circ_004726, circ_028039, circ_028043 and circ_028044) generated from four genes: MEF2C, BCL2L11, STAT5B and HIF1A, were annotated as participating in lymphocyte/leukocyte homeostasis. Compared with 3M vs 1Y and 3M vs 3Y, however, there were only 10 source genes for DE circRNAs, in 1Y vs 3Y, were found to be implicaed in immune response based on GO annotation, which might be responsible for no significant changes in intratesticular immune microenvironment in post-pubertal (sexually mature and adult) sheep testis. One of the major functions of testicular immune privilege is to protect germ cells (especially meiotic germ cell including the spermatozoa) from systemic auto-immune attack (Meng et al., 2011). As we all know, prepubertal testis do not undergo spermatogenesis until pubertal onset when wave of spermatogenesis begins, including mitotic proliferation of spermatogonia and initiation of the meiotic program of spermatocytes, to allow testis to produce mature spermatozoa up to old age.

Likewise, a KEGG analysis domonstrated that the source genes for DE circRNAs, in 3M vs 1Y and 3M vs 3Y, were mostly enriched in the signaling pathways associated with reproduction [e.g., oocyte meiosis, insulin signaling, VEGF signaling (Kang et al., 2015), progesterone-mediated oocyte maturation, etc.], spermatogenesis [e.g., mTOR signaling (Jesus et al., 2017), Hippo signaling (Zhang G.M. et al., 2019), TGF-beta signaling (Fan et al., 2012), cell cycle, etc.], BTB [e.g., adherens junction (Mruk and Cheng, 2015; Stanton, 2016), modulation of actin cytoskeleton (Mruk and Cheng, 2015), focal adhesion (Mruk and Cheng, 2015), ECM-receptor interaction (Siu and Cheng, 2008), etc.], and immune responses [e.g., T cell receptor signaling, PI3K-Akt signaling, leukocyte transendothelial migration, etc.]; in 1Y vs 3Y, were mainly enriched in the signaling pathways associated with reproduction [e.g., estrogen signaling, progesterone-mediated oocyte maturation, VEGF signaling (Kang et al., 2015), etc.], BTB [e.g., tight junction (Mruk and Cheng, 2015; Stanton, 2016), modulation of actin cytoskeleton (Mruk and Cheng, 2015), etc.], and immune responses (e.g., chemokine signaling, B cell receptor signaling, etc.].

Multiple lines of evidence demonstrated that one of the primary functions of circRNAs is to act as miRNA sponges to indirectly regulate expression of downstream target gene for miRNAs (Zhong et al., 2018). Thus, we combined with previous miRNA-seq and mRNA-seq data and further analyzed circRNA–miRNA–mRNA interaction network based on ceRNAs to reveal the functions involved by these DE circRNAs. The results revealed by GO analysis indicated that these target genes were assigned to several main biological processes, including cellular process, development, biological adhesion, and reproduction. By analyzing the results of KEGG pathway enrichment, we also discovered that they significantly enriched in pathways linked with spermatogenesis or testicular immune privilege, such as Wnt signaling (Kang et al., 2015), TGF-beta signaling (Fan et al., 2012), signaling cascades modulating pluripotency of stem cells, modulation of actin cytoskeleton (Mruk and Cheng, 2015), adherens junction (Mruk and Cheng, 2015; Stanton, 2016), focal adhesion (Mruk and Cheng, 2015), ECM–receptor interaction (Siu and Cheng, 2008), and chemokine signaling. Additionally, similar functional enrichment results were found in GO analysis and KEGG analysis of the common genes between differentially expressed circRNAs' souce genes and differentially expressed mRNAs.

According to GO and KEGG analysis of mRNAs in ceRNA network, the target genes related to spermatogenesis, blood-testis barrier, germ cell development, cell cycle or meiosis were selected to build a circRNA–miRNA–mRNA network. As a result, there were 259 circRNA–miRNA pairs and 97 miRNA–mRNA pairs in the constructed network, involving 180 circRNAs, 33 miRNAs, and 57 genes. Among these, IGF1, a known testicular development gene (Cannarella et al., 2018; Neirijnck et al., 2019), was predicted to be modulated by circ_024949/circ_026259-oar-miR-29b signals, and the subsequent dual-luciferase assays confirmed that circ_024949/circ_026259/IGF1 shared the same oar-miR-29b target site. It has been reported that IGF1 is widely expressed in various cell types in the testis, containing germ cells, Leydig cells, and Sertoli cells to modulate their development and functions (Potter and DeFalco, 2017; Cannarella et al., 2018). Similarly, our results indicated that at the protein level, IGF1 protein was wildly existed in various germ cells, along with existence in Leydig cells and Sertoli cells, suggestive of its multiple roles in development and maturation of germ cells as well as functional maintenance of testicular somatic cells. miR-29b, a member of miR-29 family, has been documented to be closely related to male fertility (Menezes et al., 2020). This study showed that oar-miR-29b was remarkably up-regulated in post-pubescent sheep testis (1- and 3-year-old) relative to pre-pubescent (3-month-old), which is in agreement with previous reports in canine testis (Kasimanickam and Kasimanickam, 2015). Consistent with the results indicated in the RNA-seq data, however, RT-PCR and qPCR results revealed that the exepression of circ_024949, circ_026259 and IGF1 decreased gradually with development from 3-month-old to 3-year-old testes, suggesting that their expression negatively correlated with oar-miR-29b. The subsequent *in situ* hybridization analysis revealed that circ_024949, circ_026259, oar-miR-29b and IGF1 were all located in various germ cells, Leydig cells and Sertoli cells, which was largely consistent with a previous report on the subcellular localization patterns of testicular IGF1 mRNA (Yuan et al., 2018). This further implied the interactions between either circ_024949, circ_026259, or IGF1 and oar-miR-29b, as well as their potential modulation for the development of testicular germ and somatic cells.

Given the existing literature outlining the importance of IGF1 in Sertoli cell development (Cannarella et al., 2018; Johnson et al., 2020) and the above findings, we successfully isolated ovine primary Sertoli cells to further evaluate the regulatory effect of circ_026259 (having a higher expression compared to circ04949 in Sertoli cells) on IGF1 expression through oar-miR-29b in testicular cells. The results from the study by overexpression or knockdown of circ_026259 and oar-miR-29b demonstrated the positive effects of circ_026259 on IGF1 mRNA and protein expression via repressing oar-miR-29b in Sertoli cells.

Additionally, IGF1, as a growth factor secreted by testicular cells (especially Leydig cells), may possess immunosuppressive

property in mammalian testis (Pérez et al., 2013; Potter and DeFalco, 2017). A recent study documented that IGF1 functions in the intestinal immune homeostasis (Zheng et al., 2018). These reports together raise the possibility that IGF1 expression may also contribute to the maintenance of immunologic homeostasis during testis development, but whether IGF1 is functional in this and the mechanistic details of regulation by which IGF1 remain to be elucidated. Regardless, these data somewhat enrich our understanding of the functionality of IGF1 in sheep testis and how its expression is regulated.

In conclusion, this is the first documentation elucidating circRNA dynamic expression patterns across three reproductive stages in postnatal sheep testes and describing circRNA-associated miRNA-gene network implicated in testicular function; as well as the first to confirm that circ_024949 and circ_026259 were likely to jointly regulate IGF1 expression through direct targeting of oar-miR-29b, and therefore had multiple functions in development of germ cells and functional maintenance of Sertoli cells and Leydig cells during ram spermatogenesis. Further, circ_026259, a novel circular RNA derived from KLHL5 exons, was confirmed to negatively modulate IGF1 expression by inhibiting oar-miR-29b in sheep Sertoli cells. These findings provide novel vision and direction for the future exploration of the regulatory mechanisms of testicular development and function in sheep.

DATA AVAILABILITY STATEMENT

RNA-seq data has been deposited to the SRA database in NCBI (accession numbers: SRR11348536-SRR11348547).

ETHICS STATEMENT

The animal study was reviewed and approved by Laboratory Animal Welfare and Ethics Committee of Gansu Agricultural University. Written informed consent was obtained from the owners for the participation of their animals in this study.

AUTHOR CONTRIBUTIONS

TL and YM conceived and designed the study. XW, HW, and HJ collected the samples. TL, RL, XW, and HW performed the experiments and analyzed the data. TL wrote the manuscript. XZ, YG, and YM contributed to the revisions of the manuscript. All authors read and approved the manuscript.

FUNDING

This work was supported by the National Key R&D Program of China (2018YFD0502100), Fostering Foundation for the Excellent Ph.D. Dissertation of Gansu Agricultural University (YB2018001), and National Natural Science Foundation of China (31960662).

ACKNOWLEDGMENTS

We thank the Guangzhou Genedenovo Biotechnology Co., Ltd., for assisting in RNA sequencing.

SUPPLEMENTARY MATERIAL

The Supplementary Material for this article can be found online at: https://www.frontiersin.org/articles/10.3389/fcell.2021.627439/full#supplementary-material

Supplementary Figure 1 | GO annotation of the genes shared between DE circRNA source genes and DE mRNAs.

Supplementary Table 1 | RNA sequences used for transfection.

Supplementary Table 2 | A list of primers used in PCR analysis.

Supplementary Table 3 | Summary statistics of circular RNA sequencing data.

Supplementary Table 4 | List of differentially expressed circRNAs between 3M and 1Y.

Supplementary Table 5 | List of differentially expressed circRNAs between 3M and 3Y.

Supplementary Table 6 | List of differentially expressed circRNAs between 1Y and 3Y.

Supplementary Table 7 | GO annotation of source genes for differentially expressed circRNAs.

Supplementary Table 8 | The mRNA expression list in ceRNA network.

Supplementary Table 9 | KEGG analysis of the genes shared between DE circRNA source genes and DE mRNAs.

REFERENCES

Cannarella, R., Condorelli, R., La Vignera, S., and Calogero, A. (2018). Effects of the insulin-like growth factor system on testicular differentiation and function: a review of the literature. *Andrology* 6, 3–9. doi: 10.1111/andr.12444

Cao, Y., You, S., Yao, Y., Liu, Z. J., Hazi, W., Li, C. Y., et al. (2018). Expression profiles of circular RNAs in sheep skeletal muscle. *Asian Australas. J. Anim. Sci.* 31, 1550–1557. doi: 10.5713/ajas.17.0563

Choi, J., Zhou, W., Nie, Z., Niu, Y., Shin, K., and Cui, X. (2019). Spindlin1 alters the metaphase to anaphase transition in meiosis I through regulation of BUB3 expression in porcine oocytes. *J. Cell. Physiol.* 234, 8963–8974. doi: 10.1002/jcp.27566

Ebbesen, K. K., Hansen, T. B., and Kjems, J. (2017). Insights into circular RNA biology. *RNA Biol.* 14, 1035–1045. doi: 10.1080/15476286.2016.1271524

Fan, Y. S., Hu, Y. J., and Yang, W. X. (2012). TGF-β superfamily: how does it regulate testis development. *Mol. Biol. Rep.* 39, 4727–4741. doi: 10.1007/s11033-011-1265-5

Fu, X., Cheng, S., Wang, L., Yin, S., De Felici, M., and Shen, W. (2015). DAZ family proteins, key players for germ cell development. *Int. J. Biol. Sci.* 11, 1226–1235. doi: 10.7150/ijbs.11536

Gao, Y., Lu, W., Jian, L., Machaty, Z., and Luo, H. (2020). Vitamin E promotes ovine Sertoli cell proliferation by regulation of genes associated with cell division and the cell cycle. *Anim. Biotechnol.* doi: 10.1080/10495398.2020.1788044 [Epub ahead of print].

Hao, Z., Zhou, H., Hickford, J. G. H., Gong, H., Wang, J., Hu, J., et al. (2020). Identification and characterization of circular RNA in lactating mammary glands from two breeds of sheep with different milk production profiles using RNA-Seq. *Genomics* 112, 2186–2193. doi: 10.1016/j.ygeno.2019.12.014

Hu, J., Sun, F., and Handel, M. A. (2018). Nuclear localization of EIF4G3 suggests a role for the XY body in translational regulation during spermatogenesis in mice. *Biol. Reprod.* 98, 102–114. doi: 10.1093/biolre/iox150

Jesus, T. T., Oliveira, P. F., Sousa, M., Cheng, C. Y., and Alves, M. G. (2017). Mammalian target of rapamycin (mTOR): A central regulator of male fertility? *Crit. Rev. Biochem. Mol. Biol.* 52, 235–253. doi: 10.1080/10409238.2017.1279120

Jing, X., Wang, W., Degen, A., Guo, Y., Kang, J., Liu, P., et al. (2020). Tibetan sheep have a high capacity to absorb and to regulate metabolism of SCFA in the rumen epithelium to adapt to low energy intake. *Br. J. Nutr.* 123, 721–736. doi: 10.1017/s0007114519003222

Johnson, C., Kastelic, J., and Thundathil, J. (2020). Role of Akt and mammalian target of rapamycin signalling in insulin-like growth factor 1-mediated cell proliferation in porcine Sertoli cells. *Reprod. Fertil. Dev.* 32, 929–940. doi: 10.1071/rd19460

Kang, Y., Zheng, B., Shen, B., Chen, Y., Wang, L., Wang, J., et al. (2015). CRISPR/Cas9-mediated Dax1 knockout in the monkey recapitulates human AHC-HH. *Hum. Mol. Genet.* 24, 7255–7264. doi: 10.1093/hmg/ddv425

Kasimanickam, V. R., and Kasimanickam, R. K. (2015). Differential expression of microRNAs in sexually immature and mature canine testes. *Theriogenology* 83, 394–398.e1. doi: 10.1016/j.theriogenology.2014.10.003

Kim, D., Pertea, G., Trapnell, C., Pimentel, H., Kelley, R., and Salzberg, S. (2013). TopHat2: accurate alignment of transcriptomes in the presence of insertions, deletions and gene fusions. *Genome Biol.* 14:R36. doi: 10.1186/gb-2013-14-4-r36

Kotaja, N. (2014). MicroRNAs and Spermatogenesis. *Fertil. Steril.* 101, 1552–1562. doi: 10.1016/j.fertnstert.2014.04.025

La, Y., He, X., Zhang, L., Di, R., Wang, X., Gan, S., et al. (2020). Comprehensive analysis of differentially expressed profiles of mRNA, lncRNA, and circRNA in the uterus of seasonal reproduction sheep. *Genes* 11:301. doi: 10.3390/genes11030301

Li, X., Li, C., Wei, J., Ni, W., Xu, Y., Yao, R., et al. (2019). Comprehensive expression profiling analysis of pituitary indicates that circRNA participates in the regulation of sheep estrus. *Genes* 10:90. doi: 10.3390/genes10020090

Li, X., Yang, L., and Chen, L. L. (2018). The biogenesis, functions, and challenges of circular RNAs. *Mol. Cell* 71, 428–442. doi: 10.1016/j.molcel.2018.06.034

Luo, H., Chen, B., Weng, B., Tang, X., Chen, Y., Yang, A., et al. (2020). miR-130a promotes immature porcine Sertoli cell growth by activating SMAD5 through the TGF-β-PI3K/AKT signaling pathway. *FASEB J.* 34, 15164–15179. doi: 10.1096/fj.202001384R

Meinhardt, A., and Hedger, M. (2011). Immunological, paracrine and endocrine aspects of testicular immune privilege. *Mol. Cell. Endocrinol.* 335, 60–68. doi: 10.1016/j.mce.2010.03.022

Memczak, S., Jens, M., Elefsinioti, A., Torti, F., Krueger, J., Rybak, A., et al. (2013). Circular RNAs are a large class of animal RNAs with regulatory potency. *Nature* 495, 333–338. doi: 10.1038/nature11928

Menezes, E. S. B., Badial, P. R., El Debaky, H., Husna, A. U., Ugur, M. R., Kaya, A., et al. (2020). Sperm miR-15a and miR-29b are associated with bull fertility. *Andrologia* 52:e13412. doi: 10.1111/and.13412

Meng, J., Greenlee, A., Taub, C., and Braun, R. (2011). Sertoli cell-specific deletion of the androgen receptor compromises testicular immune privilege in mice. *Biol. Reprod.* 85, 254–260. doi: 10.1095/biolreprod.110.090621

Mruk, D., and Cheng, C. (2015). The mammalian blood-testis barrier: its biology and regulation. *Endocr. Rev.* 36, 564–591. doi: 10.1210/er.2014-1101

Neirijnck, Y., Papaioannou, M., and Nef, S. (2019). The insulin/IGF system in mammalian sexual development and reproduction. *Int. J. Mol. Sci.* 20:4440. doi: 10.3390/ijms20184440

Pérez, C., Theas, M., Jacobo, P., Jarazo-Dietrich, S., Guazzone, V., and Lustig, L. (2013). Dual role of immune cells in the testis: protective or pathogenic for germ cells? *Spermatogenesis* 3:e23870. doi: 10.4161/spmg.23870

Potter, S., and DeFalco, T. (2017). Role of the testis interstitial compartment in spermatogonial stem cell function. *Reproduction* 153, R151–R162. doi: 10.1530/rep-16-0588

Qin, L., Lin, J., and Xie, X. (2019). CircRNA-9119 suppresses poly I:C induced inflammation in Leydig and Sertoli cells via TLR3 and RIG-I signal pathways. *Mol. Med.* 25:28. doi: 10.1186/s10020-019-0094-1

Qu, S., Yang, X., Li, X., Wang, J., Gao, Y., Shang, R., et al. (2015). Circular RNA: a new star of noncoding RNAs. *Cancer Lett.* 365, 141–148. doi: 10.1016/j.canlet.2015.06.003

Salzman, J. (2016). Circular RNA expression: its potential regulation and function. *Trends Genet.* 32, 309–316. doi: 10.1016/j.tig.2016.03.002

Shao, T., Pan, Y., and Xiong, X. (2021). Circular RNA: an important player with multiple facets to regulate its parental gene expression. *Mol. Ther. Nucleic Acids* 23, 369–376. doi: 10.1016/j.omtn.2020.11.008

Siu, M. K. Y., and Cheng, C. Y. (2008). Extracellular matrix and its role in spermatogenesis. *Adv. Exp. Med. Biol.* 636, 74–91. doi: 10.1007/978-0-387-09597-4_5

Smith, B., and Braun, R. (2012). Germ cell migration across Sertoli cell tight junctions. *Science* 338, 798–802. doi: 10.1126/science.1219969

Stanton, P. (2016). Regulation of the blood-testis barrier. *Semin. Cell Dev. Biol.* 59, 166–173. doi: 10.1016/j.semcdb.2016.06.018

Wang, X., Li, T., Liu, N., Zhang, H., Zhao, X., and Ma, Y. (2019). Characterization of GLOD4 in Leydig cells of Tibetan sheep during different stages of maturity. *Genes* 10:796. doi: 10.3390/genes10100796

Witt, E., Benjamin, S., Svetec, N., and Zhao, L. (2019). DrosophilaTestis single-cell RNA-seq reveals the dynamics of de novo gene transcription and germline mutational bias in *Drosophila*. *eLife* 8:e47138. doi: 10.7554/eLife.47138

Yan, H., Mruk, D., Lee, W., and Cheng, C. (2007). Ectoplasmic specialization: a friend or a foe of spermatogenesis? *Bioessays* 29, 36–48. doi: 10.1002/bies.20513

Yang, L., Fu, J., and Zhou, Y. (2018). Circular RNAs and their emerging roles in immune regulation. *Front. Immunol.* 9:2977. doi: 10.3389/fimmu.2018.02977

Yuan, C., Chen, K., Zhu, Y., Yuan, Y., and Li, M. (2018). Medaka igf1 identifies somatic cells and meiotic germ cells of both sexes. *Gene* 642, 423–429. doi: 10.1016/j.gene.2017.11.037

Zhang, G. M., Zhang, T. T., An, S. Y., El-Samahy, M. A., Yang, H., Wan, Y. J., et al. (2019). Expression of Hippo signaling pathway components in Hu sheep male reproductive tract and spermatozoa. *Theriogenology* 126, 239–248. doi: 10.1016/j.theriogenology.2018.12.029

Zhang, P., Chao, Z., Zhang, R., Ding, R., Wang, Y., Wu, W., et al. (2019). Circular RNA regulation of myogenesis. *Cells* 8:885. doi: 10.3390/cells8080885

Zhao, S., Zhu, W., Xue, S., and Han, D. (2014). Testicular defense systems: immune privilege and innate immunity. *Cell. Mol. Immunol.* 11, 428–437. doi: 10.1038/cmi.2014.38

Zheng, Y., Song, Y., Han, Q., Liu, W., Xu, J., Yu, Z., et al. (2018). Intestinal epithelial cell-specific IGF1 promotes the expansion of intestinal stem cells during epithelial regeneration and functions on the intestinal immune homeostasis. *Am. J. Physiol. Endocrinol. Metab.* 315, E638–E649. doi: 10.1152/ajpendo.00022.2018

Zhong, Y., Du, Y., Yang, X., Mo, Y., Fan, C., Xiong, F., et al. (2018). Circular RNAs function as ceRNAs to regulate and control human cancer progression. *Mol. Cancer* 17:79. doi: 10.1186/s12943-018-0827-8

Zhou, F., Chen, W., Jiang, Y., and He, Z. (2019). Regulation of long non-coding RNAs and circular RNAs in spermatogonial stem cells. *Reproduction* 158, R15–R25. doi: 10.1530/REP-18-0517

Zhou, R., Wu, J., Liu, B., Jiang, Y., Chen, W., Li, J., et al. (2019). The roles and mechanisms of Leydig cells and myoid cells in regulating spermatogenesis. *Cell. Mol. Life Sci.* 76, 2681–2695. doi: 10.1007/s00018-019-03101-9

Conflict of Interest: The authors declare that the research was conducted in the absence of any commercial or financial relationships that could be construed as a potential conflict of interest.

frontiers in Cell and Developmental Biology

ORIGINAL RESEARCH
published: 09 April 2021
doi: 10.3389/fcell.2021.655866

Proteomic Changes Associated With Sperm Fertilizing Ability in Meat-Type Roosters

Anaïs Vitorino Carvalho[1†], Laura Soler[2†], Aurore Thélie[1], Isabelle Grasseau[1], Luiz Cordeiro[1], Daniel Tomas[1,2,3], Ana-Paula Teixeira-Gomes[3,4], Valérie Labas[1,2,3] and Elisabeth Blesblois[1]*

[1] CNRS, INRAE, Université de Tours, IFCE, Nouzilly, France, [2] INRAE, ENVT, INP-Purpan, UPS, UMR Toxalim, Toulouse, France, [3] INRAE, Université de Tours, CHU de Tours, Plate-forme PIXANIM (Phénotypage par Imagerie in/ex vivo de l'Animal à la Molécule), Nouzilly, France, [4] INRAE, ISP, Université de Tours, Nouzilly, France

OPEN ACCESS

Edited by:
Silvina Perez-Martinez, CONICET Centro de Estudios Farmacológicos y Botánicos (CEFYBO), Argentina

Reviewed by:
Inmaculada Parrilla, University of Murcia, Spain
Woo-Sung Kwon, Kyungpook National University, South Korea

***Correspondence:**
Anaïs Vitorino Carvalho
anais.carvalho@inrae.fr

[†] These authors have contributed equally to this work

Specialty section:
This article was submitted to Cell Growth and Division, a section of the journal Frontiers in Cell and Developmental Biology

Received: 19 January 2021
Accepted: 03 March 2021
Published: 09 April 2021

Citation:
Vitorino Carvalho A, Soler L, Thélie A, Grasseau I, Cordeiro L, Tomas D, Teixeira-Gomes A-P, Labas V and Blesblois E (2021) Proteomic Changes Associated With Sperm Fertilizing Ability in Meat-Type Roosters. Front. Cell Dev. Biol. 9:655866. doi: 10.3389/fcell.2021.655866

The molecular basis of male fertility remains unclear, especially in chickens, where decades of genetic selection increased male fertility variability as a side effect. As transcription and translation are highly limited in sperm, proteins are key molecules defining their functionality, making proteomic approaches one of the most adequate methods to investigate sperm capacity. In this context, it is interesting to combine complementary proteomic approaches to maximize the identification of proteins related to sperm-fertilizing ability. In the present study, we aimed at identifying proteins related to fertility in meat-type roosters, showing fertility variability. Fertile roosters (fertility rates higher than 70% after artificial insemination) differed from subfertile roosters (fertility rates lower than 40%) in their sperm mass motility. Fertile and subfertile sperm protein contents were compared using two complementary label-free quantitative proteomic methods: Intact Cell MALDI-TOF-Mass Spectrometry and GeLC-MS/MS. Combining the two strategies, 57 proteins were identified as differentially abundant. Most of them were described for the first time as differentially abundant according to fertility in this species. These proteins were involved in various molecular pathways including flagellum integrity and movement, mitochondrial functions, sperm maturation, and storage in female tract as well as oocyte–sperm interaction. Collectively, our data improved our understanding of chicken sperm biology by revealing new actors involved in the complexity of male fertility that depends on multiple cell functions to reach optimal rates. This explains the inability of reductionist *in vitro* fertility testing in predicting male fertility and suggests that the use of a combination of markers is a promising approach.

Keywords: sperm, chicken, proteomic, fertility, semen

INTRODUCTION

Male fertility depends on the optimal functioning of all processes needed for sperm to fertilize the oocyte. The fertilizing ability of sperm is therefore reliant on the correct development and maturation of sperm cells including the acquisition of motility, structural integrity, viability, and its capacities to penetrate into the oocyte. Each aspect of these sperm functions are classically

investigated by *in vitro* tests to diagnose fertility perturbations (WHO, 2010). However, these tests results are poorly correlated with *in vivo* male fertility in humans and in animals, suggesting the responsibility of more subtle dysfunctions of sperm biology (or putative combination of several suboptimal functions) in male subfertility, potentially revealed by molecular analysis (Soler et al., 2016a; Jodar et al., 2017).

Among the technical approaches available to investigate the molecular basis of male fertility, proteomics is particularly adequate (Kovac et al., 2013). Indeed, transcription and translation are very limited in mature sperm cells. Furthermore, proteins are considered as major effectors of cell functions (Jodar et al., 2017). Thus, sperm cell biology and activity are conditioned by the protein types, their abundance, and their posttranslational modifications at a given moment. Currently, mass spectrometry (MS)-based proteomics has been the most relevant approach to compare the sperm proteome from individuals with normal fertility and ones presenting difficulties to procreate in humans (Jodar et al., 2017; Bracke et al., 2018) and in animals (Park et al., 2013). Proteomic analysis of sperm cells provides two types of knowledge: on the one hand, global proteome analysis informs on the molecular pathways essential for sperm biology, and on the other hand, it helps identify potential male fertility biomarkers. These biomarkers are largely needed to predict the individual fertility capacity in human medicine (Jodar et al., 2017), animal reproduction (Druart et al., 2019), and genetic conservation programs of endangered breeds and species (Soler et al., 2020). Whereas each proteomic method provides a large amount of data and may propose potential biomarkers, due to the advantages and disadvantages of each methodology, a single approach cannot apprehend the complexities of male fertility. For instance, the Intact Cell MALDI-TOF Mass Spectrometry (ICM-MS) approach is a high-throughput methodology allowing the characterization of endogenous peptidoforms and proteoforms (<20 kDa) present in intact and whole cells without previous protein extraction or separation (Soler et al., 2020), at the difference of the bottom-up proteomic approach using a GeLC-MS/MS strategy allowing a larger overview of proteomes from extracted and digested protein samples.

Chicken is not only a popular laboratory model mainly for research on embryology, genetics, and behavior but also the first animal protein source for human consumption (FAO, 2020). Rooster fertility has decreased over the last decades in commercial breeds as a side effect of genetic selection especially for meat production (Rauw et al., 1998), but the molecular pathways involved in impaired sperm biology remain unclear. Previous investigations revealed that proteomic approaches applied to sperm cells are highly valuable to discriminate fertile and subfertile roosters (Labas et al., 2015; Soler et al., 2016a), but the molecular pathways involved in the sperm-fertilizing ability remains poorly described.

Here, to increase our understanding of subfertility causes in chickens, we first evaluated the semen quality from fertile and subfertile meat-type roosters in order to identify sperm defects relative to the fertility reduction observed in some animals. Furthermore, we used two complementary label-free quantitative proteomic approaches (ICM-MS and GeLC-MS/MS) at the individual level, in order to identify the proteins relative to sperm-fertilizing ability in chickens and potentially linked them to sperm quality defects and identify new cellular impairments not revealed by classical *in vitro* semen quality evaluation.

MATERIALS AND METHODS

Animals

All experiments were carried out in accordance with the European welfare and the French Direction of Veterinary Services regulations (agreement number C37–175-1) as previously described (Soler et al., 2016a). Animal rearing was performed in the PEAT INRAe Poultry Experimental Facility (2018)[1]. Briefly, 360 adult ISABROWN females (ISA, Ploufragan, France) and 36 meat-line males acquired from Hubbard and Novogen (Quintin, France) were housed under a 14L/10D photoperiod and fed with standard diet of 12.5 MJ/day, supplemented with calcium for the females. Whereas males were housed in individual battery cages, hens were reared in groups of 5 animals.

Semen Collection

Semen were collected twice a week by massage (Burrows and Quinn, 1937) for 5 weeks for *in vitro* analysis or *in vivo* fertility determination. After collection, sperm concentrations were immediately determined by light absorption (Accucell photometer, IMV Technologies, L'Aigle, France) at a wavelength of 530 nm (Brillard and McDaniel, 1985) and semen were diluted 1:1 in Beltsville Poultry Semen Extender (BPSE) (Sellier et al., 2006). Semen were used directly to analyze semen or inseminate females and aliquoted for proteomic investigation.

In vivo Fertility Determination

To estimate the individual *in vivo* fertility of each male, 10 females per male were intravaginal artificially inseminated (AI) with a dose of 10^8 sperm cells/female, two times at 1 week interval. Females were all fertile with almost one egg per day and randomly attributed to males. Fertility was determined by egg candling (from days 2 to 9 after the first AI and days 2–23 after the second AI). The fertility rate (FR) was defined as the percentage of fertile egg on the total number of analyzed egg (about 250 for each male). Males with FR >70% ($n = 14$) were considered fertile (F), whereas the subfertile (SF) population was associated with a FR <40% ($n = 11$) (Soler et al., 2016a). Nine animals per fertility status (F or SF) were randomly selected and included in this analysis. The difference of fertility between F and SF animals was explored by Mann–Whitney test, and significant difference was defined at 5% ($p \leq 0.05$; R studio, R software version 4.0.2) (Allaire, 2015; R Core Team, 2017).

In vitro Semen Analysis

As previously described (Labas et al., 2015; Soler et al., 2016a), semen quality was investigated with several *in vitro* parameters

[1]https://doi.org/10.15454/1.5572326250887292E12

on F and SF animals. 7–8 ejaculates per rooster, collected in a period of 20 days, were included in the evaluation. Sperm volume was defined by weighing (ml), and sperm concentration was determined by light absorption (10^9 sperm/ml), as previously described. Sperm viability (%) was determined with SYBR-14/propidium iodide fluorescent dyes, as previously described (Soler et al., 2016a), on at least 300 marked sperm per individual sample. Mass motility, defined as the movement of sperm group, was defined on a motility scale previously described (Blesbois et al., 2008): 0 as a total lack of movement and 9 as the presence of representing whirlwinds covering 30–60% of the observed area. Furthermore, objective measurements of motility were evaluated using the computer-assisted sperm analysis (CASA) system with an HTM-IVOS (Hamilton–Thorn Motility Analyzer, IVOS) (Blesbois et al., 2008). Thus, motility parameters such as straight-line velocity (VSL, μm/s), curvilinear velocity (VCL, μm/s), and average path velocity (VAP, μm/s) were individually determined as the mean of two semen samples. These parameters were also used to determine the percentages of motile, rapid, and progressive sperms as a motile sperm presented a VAP $>$ 5 μm/s, rapid sperms showed a VAP $>$ 50 μm/s, and a progressive cell was defined by a VAP $>$ 50 μm/s. All preparations and observation were performed by the same observer. Each parameter was subjected to the Mann–Whitney test on the animal subset included in this analysis (9 animals F and 9 roosters SF; R studio, R software version 4.0.2) (Allaire, 2015; R Core Team, 2017). The statistical significance was defined at 5% ($p \leq 0.05$).

Intact Cell MALDI-TOF–Mass Spectrometry

Whole and intact sperm cells from F and SF roosters ($n = 9$) were analyzed by ICM-MS. Three ejaculated semen samples were collected from each male on BPSE as previously described. Sperm cells were isolated by centrifugation (600 × *g*, 10 min at 4°C). Sperm cells were washed twice with 1 ml of Tris Sucrose Buffer (TSB, 20 mM Tris–HCl, pH 6.8, and 260 mM sucrose) and then resuspended at 10^6 sperm/μl. Using the dried droplet method, 1 μl of cell suspension was overlain with 2.5 μl of sinapinic acid matrix solution at 20 mg/ml dissolved in 50% acetonitrile/50% water in the presence of 2% trifluoroacetic acid. Twelve replicates were spotted for each sample onto an MTP Ground Steel 384 MALDI plate (Bruker Daltonics, Germany). The matrix/sample mix was allowed to evaporate at room temperature for 30 min. MS acquisitions were performed using a Bruker UltrafleXtreme MALDI-TOF instrument (Bruker Daltonics, Germany) equipped with a Smartbeam laser at a 2-kHz laser repetition rate following an automated method controlled by FlexControl 3.0 software (Bruker Daltonics, Germany). Spectra were obtained in positive linear ion mode in the m/z 1,000–20,000 range and collected from each spot as a sum of 1,000 laser shots in 5 shot steps (total of 5,000 spectra per spot). The parameters used for spectra acquisition were ion source 1, 25 kV; ion source 2, 23.55 kV; lens, 7 kV; pulsed ion extraction; and laser parameter set, large. Spectra were acquired three consecutive times per spot (36 technical replicates per sample). External calibration was applied using a mixture of known peptides and proteins as Glu1-fibrinopeptide B $[M + H]^+ = 1\ 571.59$ m/z, ACTH (fragments 18–39) $[M + H]^+ = 2\ 466.68$ m/z, insulin $[M + H]^+ = 5\ 734.52$ m/z and ubiquitin $[M + H]^+ = 8\ 565.76$ m/z, cytochrome C $[M + H]^+ = 12\ 360{,}97$ m/z, and myoglobin $[M + H]^+ = 16\ 952.31$ m/z. To increase mass accuracy (mass error $< 0.05\%$), internal calibration was subsequently applied to all spectra. The latter was achieved by performing a lock mass correction using flexAnalysis 4.0 software (Bruker) with the mass of the highest-intensity peak in the middle of the mass range, corresponding to the protein phosphoglycerate kinase (7,983.457 m/z). All spectra were converted in format mzXML using the CompassXport tool (Bruker Daltonics) and treated using the free and open-source analysis software R (version 3.6.1) along with specific package for Quantitative Analysis of Mass Spectrometry Data as MALDIquant (v1.19.3) (Gibb and Strimmer, 2012). The spectra were treated using the square root intensities, and the baseline estimation was based on the TopHat filter (van Herk, 1992; Gil and Werman, 1993). Spectra were smoothed using the Savitzky–Golay filter, realigned using prominent peaks, and normalized on intensity using the total ion current (TIC) method (Filzmoser and Walczak, 2014). Peaks were detected using the Median Absolute Deviation (MAD) method with a signal-to-noise ≥ 2. To retain only quality spectra for each sperm sample, the dataset ($n = 36$ technical spectra) was filtered by correlation analyses by comparing the spectra two by two. Then, we computed filter-based correlation coefficients with iterations from 40 to 90% for each technical spectrum vs. all other spectra of the same class. All retained spectra were merged to generate a total average spectrum for each sample. The *x*-axis of spectra represented the m/z values of biomolecules, and the *y*-axis represented the normalized peak intensities.

The intra-assay precisions of the ICM-MS acquisitions were determined by calculating the coefficient of variation (% CV) of the normalized peak-intensity values from the technical replicates for each ejaculate ($n = 27$). The CV% are ranged from 16.71 to 46.88% with a mean CV at 29.41%. The inter-assay precision was determined by calculating the % CV of the mean peak-normalized values for the three ejaculates of all animals. For F and SF populations, the mean% CV did not exceed 36.76 and 36.38%, respectively.

The MS data did not pass the normality and homogeneity QQ plot and Kolmogorov–Smirnov tests. Therefore, for comparative analyses, data were submitted to the non-parametric Mann–Whitney or Wilcoxon test to characterize changes between the two fertility conditions. M/z were considered significantly differential when a $p < 0.05$ and a fold-change ratio (FC) ≤ 0.66 or ≥ 1.5. Principal component analysis (PCA) and volcano plot were performed using the gplots (v3.0.3) and FactoMineR (v2.1) packages of the R software (R Core Team, 2017).

The peaks observed by ICM-MS were annotated using a home database generated from *Gallus gallus* sperm top-down proteomics, containing ∼800 biomolecules already identified in chicken spermatozoa (Soler et al., 2016a,b). The ICM-MS peaks were aligned to theoretical peptidoform and proteoform average masses $[M + H]^+$ considering their posttranslational

modifications, with a mass tolerance $\leq$ 0.05% ($\pm$ 500 ppm) (**Supplementary Data 1**).

Bottom-Up Proteomic by GeLC-MS/MS

Four animals from each fertility status (SF and F) were randomly selected to be analyzed by a bottom-up proteomic approach combining SDS-PAGE fractionation, in-gel protein digestion by trypsin, and nano-Liquid Chromatography coupled to high-resolution tandem mass spectrometry (GeLC-MS/MS). Briefly, proteins were extracted as previously described (Labas et al., 2015) and 50 μg of total protein was submitted to SDS-PAGE (4–20%, 8.3 × 6 cm × 1.5 mm). After Coomassie Blue staining, each gel lane was fractionated into 11 slices. Gel pieces were washed in water with acetonitrile (1:1), then cysteine reduction and alkylation were performed by successive incubations with 10 mM dithiothreitol in 50 mM NH_4HCO_3 (30 min, at 56°C) and 55 mM iodoacetamide in 50 mM NH_4HCO_3 (20 min, at room temperature, in the dark). Digestion was carried out overnight using 25 mM NH_4HCO_3 with bovine trypsin (sequencing grade, Roche Diagnostics, Paris, France) at 12.5 ng/μl. Peptides were extracted and dried using a SPD1010 speedvac system (ThermoSavant, Thermo Fisher Scientific). For each protein band, the resultant peptide mixture was reconstituted with 30 μl of 0.1% formic acid and 2% acetonitrile, sonicated for 10 min and analyzed by nanoLC-MS/MS in triplicate. Proteomic experiments were performed using an LTQ Orbitrap Velos mass spectrometer coupled to an Ultimate® 3000 RSLC Ultra High-Pressure Liquid Chromatographer (Thermo Fisher Scientific, Bremen, Germany) as previously described (Labas et al., 2015). A peptide mixture (5 μl) was loaded on a trap column for desalting and separated using a nano-column. The gradient consisted of 4–55% B for 90 min at a 300 nl/min flow rate. The mass spectrometer was operated in positive data-dependent mode using Xcalibur software (version 2.1; Thermo Fisher Scientific, San Jose, CA). In the scan range of m/z 300–1,800 with a targeted resolution at 60,000, the 20 most intense peptide ions with charge states $\geq$ 2 were fragmented using Collision Induced Dissociation (CID). A lock mass corresponding to polydimethylcyclosiloxane ions [m/z, 445.1200025 $(Si(CH_3)_2O)_6$] was enabled for accurate mass measurements.

Protein data identification was performed using Mascot search engine version 2.7.0.1 (Matrix Science, London, United Kingdom) combined to Proteome Discoverer 2.1.1.21 software (Thermo Fisher Scientific, Bremen, Germany), against the chordata section of the non-redundant NCBI database (download august 2020). The search parameters included trypsin as a protease with two allowed missed cleavages and carbamidomethylcysteine, methionine oxidation, and acetylation of N-term protein as variable modifications. The tolerance of the ions was set to 5 ppm for parent and 0.8 Da for fragment ion matches. Mascot results obtained from the target and decoy databases searches were subjected to Scaffold software (v 4.11.1, Proteome Software, Portland, United States) using the protein cluster analysis option (assemble proteins into clusters based on shared peptide evidence). Peptide and protein identifications were validated and accepted if they could be established at greater than 95.0% probability as specified by the Peptide Prophet algorithm (Keller et al., 2002) and by the Protein Prophet algorithm (Nesvizhskii et al., 2003), respectively. Protein identifications were accepted if they contained at least two identified peptides. The correspondent% decoy false discovery rate (FDR) done by Scaffold software was < 0.0% regarding the number of protein/clusters, and FDR was < 0.00% for the 141,914 spectra, which was in accordance with FDR values acceptable by Mass Spectrometry Data Interpretation Guidelines (<1%) (Deutsch et al., 2016). Quantifications were based on a label-free approach using two independent quantitative methods: the Spectral Counting (SC) using the "Weighed Spectra" method (Liu et al., 2004) and the Average Precursor Intensity (API) method (Cox et al., 2014). A *t*-test was performed to characterize changes between F and SF roosters. Differences were considered statistically significant for *t*-test with a $p < 0.05$. Limits of an average normalized weighted spectra (NWS) of $\geq$ 5 and fold change of $\leq$ 0.71 or $\geq$ 1.4 were included to increase the validity of comparison. MS data have been deposited to the ProteomeXchange Consortium via the PRIDE partner repository (Vizcaíno et al., 2014) with the dataset identifier PXD022322 and 10.6019/PXD022322.

For each significant cluster, one significant protein with an annotation (exclusion of LOC proteins without gene symbol and defined by their gene loci), a unique gene symbol, and a gene description has been randomly chosen to represent the cluster ($n = 39$, **Supplementary Data 2**). When the unique gene was defined as significant by SC and API methods, the SC analysis was kept. The mean signal of each differentially abundant protein (DAP) with unique gene symbol for each individual was calculated based on the three technical replicates by animal (**Supplementary Data 2**). Data exploration was performed with R (version 4.0.2) (R Core Team, 2017). Protein abundances obtained by GeLC-MS/MS, mass motility, and fertility contributions to the sample variability were explored by principal component analysis (PCA) with the package factoextra (version 1.0.7).

Western Blotting

Sperm cells were separated by centrifugation (600 × *g*, 10 min, 20°C) from the seminal plasma for 4 F and 4 SF males randomly selected. Sperm proteins were extracted by sonication in lysis buffer (150 mM NaCl, 10 mM Tris–HCl, 1 mM EGTA, 1 mM EDTA, 200 mM sodium fluoride, 4 mM sodium pyrophosphate, 2 mM sodium orthovanadate, 1% Triton X-100, and 0.5% NP40) with protease inhibitor EDTA-free (1 tablet/10 ml buffer, 04693159001, Roche Diagnostics, Mannheim, Germany). Twenty-five micrograms of protein was included in gradient 8–16% gradient SDS-PAGE, before being transferred onto nitrocellulose membranes (Amersham Protran 0.2 μm NC, 10-600001, GE Healthcare Life Science, Germany). Total protein staining on membranes was achieved using Revert™ 700 Total Protein Stain (cat. 926-11011, LI-COR Biosciences, United States) according to the manufacturer's instructions and scanned with the Odyssey CLx Imaging System (LI-COR Biosciences, Germany). Membranes were incubated with primary antibody overnight at 4°C, then incubated with the appropriate fluorescent-conjugated secondary antibody, IRDye 800CW goat

anti-rabbit (cat. 926-32211, LI-COR Biosciences, United States) or IRDye 800CW goat anti-mouse (cat. 926-32210, LI-COR Biosciences, United States), diluted 1:2,000 in Odyssey blocking buffer (cat. 927-50000, LI-COR Biosciences, United States) diluted 1:1 (v:v) in Tris-buffered saline buffer (TBS) (cat. N14581, Interchim Life Sciences, France). The optimized primary antibodies were used as follows: rabbit anti-lysozyme (1:500) and mouse anti-ovotransferrin [1:1,000, mouse (Gautron et al., 2001)] in 0.1% Tween 20 TBS (TBS, cat. N14581, Interchim Life Sciences, France; Tween-20, cat. P9516, Sigma, Germany) with 5% (w/v) non-fat dry milk, at room temperature. The antibodies raised against lysozyme and ovotransferrin were a kind gift from S. Réhault-Godbert and J. Gautron (INRAE, University of Tours, BOA, Nouzilly, France). It was produced by ProteoGenix (Schiltigheim, France) after immunization of rabbits with purified egg white lysozyme (Sigma-Aldrich, Saint-Quentin-Fallavier, France). A protein-specific band signal was normalized against total protein stain signal, and differences were evaluated using a Mann–Whitney test (R studio, R software version 4.0.2) (Allaire, 2015; R Core Team, 2017). The statistical significance was defined at 5% ($p < 0.05$).

RESULTS

Fertility and *in vitro* Characterization of Semen

The *in vitro* characterization of the semen from F and SF roosters included the investigation of volume, concentration, viability, and several motility parameters. The significant decrease of *in vivo* fertility observed in SF animals is associated with a reduction of mass motility (**Figure 1**). No significant impact was observed on the other *in vitro* parameters investigated, i.e., volume, concentration, viability, and other motility parameters, obtained with CASA analysis.

Comparison of Sperm ICM-MS Profiles From F and SF Roosters

We firstly applied the ICM-MS approach to sperm sampled from F and SF roosters (**Figure 2** and **Supplementary Data 1**). Sperm ICM-MS profiling from meat-line roosters revealed 211 detected peaks in total (**Figure 2A**). Descriptive analysis performed by PCA reported a clear segregation of F and SF samples based on PCA1 (55.33%) and PCA3 (8.97%) (**Figure 2B**). The differential analysis revealed 36 m/z peaks differentially abundant between F and SF animals ($p < 0.05$, **Figure 2C**). Among them, 7 presented a fold-change ratio (FC) ≤ 0.66 or ≥ 1.5 (**Figure 2C**). The annotation of these peaks was performed by computational confrontation against a homemade database of chicken sperm proteoforms and peptidoforms identified by Top-Down MS (Soler et al., 2016a). Three differential peaks with low m/z corresponding to peptidoforms (as results of protein degradation) were reported: cilia- and flagella-associated protein 100 (CFAP100, 1730.81 m/z, NPFTIPPDIDIFAIR), alpha enolase (ENO1, 1805.64 m/z, AAVPSGASTGIYEALELR) and tubulin beta-7 chain (TUBB7, 6789.49 m/z, SGPFGQIFRPDNFVFGQ SGAGNNWAKGHYTEGAELVDSVLDVVRKEAESCDCLQGF QLTHSLG). Manual annotation allowed to describe one

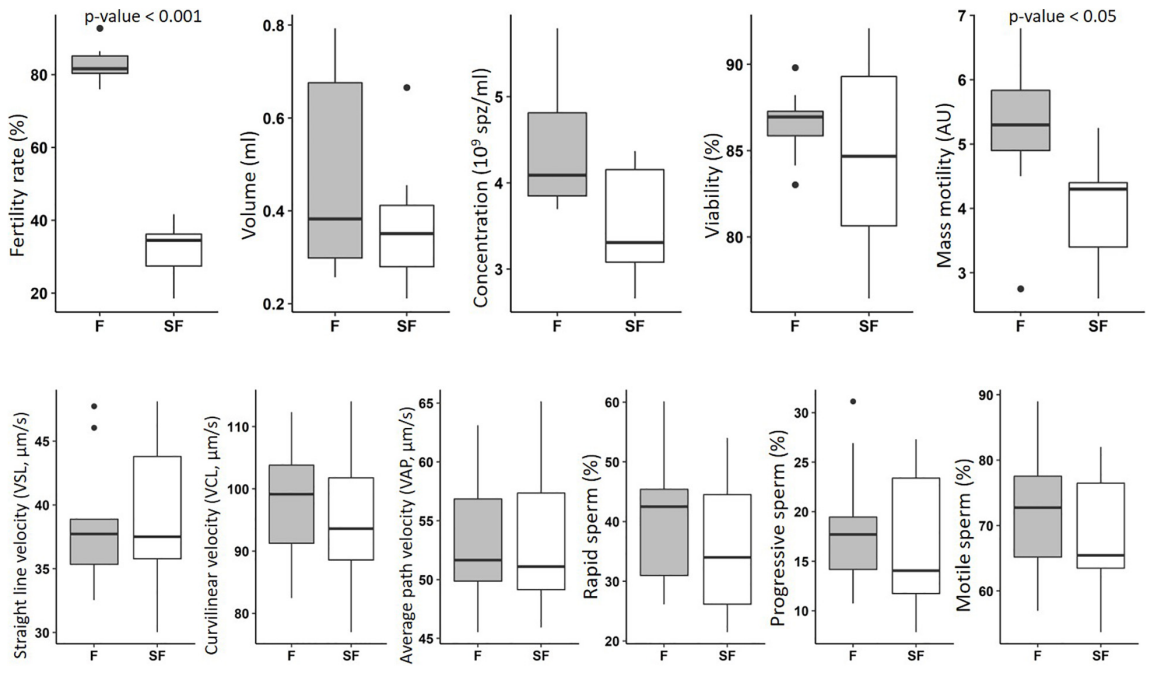

FIGURE 1 | *In vitro* characterization of semen from fertile (F) and subfertile (SF) meat-line chickens. Semen samples (9 roosters per fertility status) were subjected to *in vitro* evaluation including the determination of volume, concentration, viability, and several motility parameters. F animals in gray; SF animals in white. Data were analyzed with Mann–Whitney test and statistical difference was defined with $p \leq 0.05$.

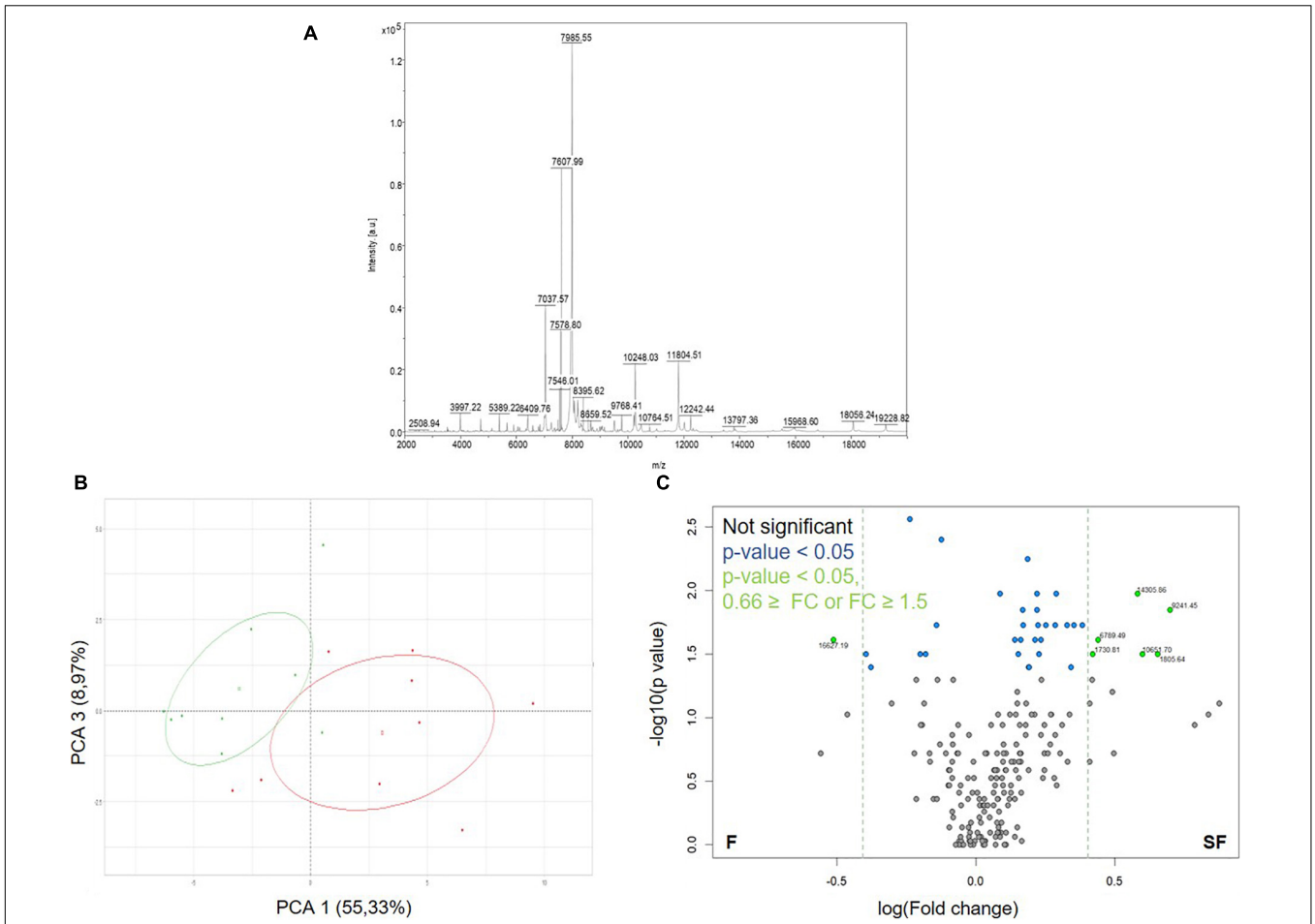

FIGURE 2 | Protein content exploration of sperm from fertile (F) and subfertile (SF) meat-line roosters by ICM-MS. **(A)** Representative sperm cell ICM-MS spectra from one F animal. **(B)** Principal component analysis (PCA) of ICM-MS signals obtained for F (in green) and SF (in red) roosters. **(C)** Volcano plot analysis between F and SF animals of detected m/z peaks ($n = 211$). Gray points indicate not significant peaks, blue ones, peaks with a significant abundance difference between F and SF animals ($p < 0.05$), and green ones, the significant peaks presenting a fold change (FC) ≤ 0.66 or ≥ 1.5.

whole protein: Lysozyme (LYZ, 14305.86 m/z). These three peptidoforms and one protein were more abundant in SF sperm cells than in F samples (**Figure 2C**).

Comparison of Sperm Proteome From F and SF Roosters by GeLC-MS/MS Analysis

To increase the number of identified DAP and obtain a global overview of semen proteome, we applied a bottom-up proteomic approach and compared F and SF sperm cell profiles. The GeLC-MS/MS investigation of sperm protein content of F and SF animals allowed the detection of 745 proteins included in 327 clusters. Among them, 27 and 50 DAP were identified by the SC and API quantitative methods, respectively, and 7 were comforted by both approaches. Consequently, a total of 84 DAP were identified with differential abundance between F and SF roosters by GeLC-MS/MS analysis (**Table 1**).

A list of unique genes was developed based on DAP with a gene description and a gene symbol corresponding to the described protein (i.e., DAP list obtained from GeLC-MS/MS without LOC proteins, $n = 39$) (**Supplementary Data 2**). This list was used for functional analysis. Combined with animal fertility status and semen mass motility, the PCA analysis (**Figure 3**) revealed that the first dimension (52.6% of the variability) represented animals clustering according to their fertility status and their sperm mass motility. According to this dimension, proteins with unique genes and annotation were speared by their expression fold change: with negative values, the more abundant proteins in SF roosters, and with positive value, the ones more abundant in F roosters. Dimension 2 only represented 14.4% of the variability (**Figure 3**) and preferentially represented interindividual variability within a fertility status.

Western Blotting

The differential abundance of ovotransferrin (TF) and lysozyme (LYZ) was validated by western blotting. Both proteins presented a significant differential abundance between F and SF sperm,

TABLE 1 | Differentially abundant proteins between fertile (F) and subfertile (SF) meat-line chickens identified by GeLC-MS/MS.

					Spectral counting		API	
#	**Gene description**	**Accession number**	**Molecular weight (kDa)**	**Gene symbol**	***p*-value**	**F/SF FC**	***p*-value**	**F/SF FC**
1.51	Tubulin beta-1 chain isoform X2 [*Electrophorus electricus*]	XP_026866564.1	49	TUBB1	0.240	0.80	**0.029**	**0.70**
1.53	Beta tubulin, partial [*Gillichthys mirabilis*]	AAL24510.1	17		0.087	0.70	**0.011**	**1.90**
2.35	Tubulin alpha-2 chain isoform X2 [*Numida meleagris*]	XP_021246036.1	43	LOC110395670	0.380	1.30	**0.039**	**0.60**
2.38	Tubulin alpha-8 chain-like [*Cebus capucinus imitator*]	XP_017390722.1	53	LOC108309094	0.210	0.80	**0.043**	**0.70**
2.53	Tubulin alpha-8 chain-like [*Sphaeramia orbicularis*]	XP_029994229.1	51	LOC115422205	0.030	0.50	**0.005**	**0.40**
6.4	Hexokinase-3 isoform X1 [*Coturnix japonica*]	XP_015731713.1	109	HK3	0.700	1.10	**0.002**	**1.90**
6.6	Hexokinase-3-like [*Tyto alba alba*]	XP_032839590.1	105	LOC104357108	0.091	6.80	**0.049**	**2.60**
7.25	Hypothetical protein A6R68_14483, partial [*Neotoma lepida*]	OBS74971.1	39		0.009	2.80	**0.016**	**3.30**
8.1	Fructose-bisphosphate aldolase A isoform X2 [*Equus caballus*]	XP_003362760.1	39	ALDOA	0.065	1.10	**0.010**	**1.60**
8.1	Fructose-bisphosphate aldolase C, partial [*Lepidosiren paradoxa*]	BAD17883.1	36		**0.019**	**2.80**	0.170	1.40
8.14	Fructose-bisphosphate aldolase A-like, partial [*Apteryx rowi*]	XP_025921567.1	29	LOC112966083	**0.019**	**1.80**	0.100	1.20
8.2	Fructose-bisphosphate aldolase A [*Corvus moneduloides*]	XP_031953954.1	39	ALDOA	0.027	1.30	**0.004**	**1.50**
8.3	Fructose-bisphosphate aldolase A-like [*Meleagris gallopavo*]	XP_019467335.1	8	LOC104917114	0.096	1.20	**0.003**	**1.70**
8.4	Fructose-bisphosphate aldolase A isoform X1 [*Desmodus rotundus*]	XP_024416190.1	45	ALDOA	0.200	1.10	**0.003**	**1.80**
8.5	Fructose-bisphosphate aldolase A-like [*Numida meleagris*]	XP_021239723.1	14	LOC110392092	0.140	1.10	**0.043**	**1.50**
8.6	Aldolase, fructose-bisphosphate A S homeolog [*Xenopus laevis*]	NP_001079649.1	39	ALDOA	0.340	1.10	**0.006**	**1.70**
8.7	Fructose-bisphosphate aldolase A [*Pogona vitticeps*]	XP_020654424.1	40	ALDOA	0.150	1.20	**0.042**	**1.50**
8.8	Fructose-bisphosphate aldolase A, partial [*Pygoscelis adeliae*]	KFW62523.1	17	LOC103925596	**0.046**	**1.40**	0.150	1.20
8.9	Fructose-bisphosphate aldolase C [*Coturnix japonica*]	XP_015736436.1	39	ALDOC	**0.024**	**1.50**	**0.017**	**1.50**
10.1	Creatine kinase B-type [*Gallus gallus*]	NP_990641.1	43	CKB	**0.011**	**1.50**	**0.046**	**1.50**
10.11	Creatine kinase B-type isoform X1 [*Nanorana parkeri*]	XP_018412106.1	43	CKB	0.420	1.30	**0.044**	**1.60**
10.13	Creatine kinase M-type [*Papio anubis*]	XP_003915756.1	43		0.094	2.00	**0.003**	**6.20**
10.2	Creatine kinase B-type isoform X1 [*Gallus gallus*]	XP_015142790.1	42	CKB	**0.043**	**1.40**	0.055	1.50
10.3	Creatine kinase B-type isoform X1 [*Apteryx mantelli mantelli*]	XP_013796252.1	43	CKB	**0.013**	**1.40**	0.160	1.30
10.5	Creatine kinase, brain, isoform CRA_a [*Homo sapiens*]	EAW81820.1	43	CKB	**0.020**	**1.40**	0.790	0.90
10.6	Creatine kinase B-type isoform X1 [*Chaetura pelagica*]	XP_010006458.1	43	CKB	**0.011**	**1.70**	0.150	1.50
10.9	Creatine kinase B-type [*Mesocricetus auratus*]	XP_005068378.1	43	CKB	**0.048**	**1.40**	0.330	0.70
13.3	Hypothetical protein CIB84_011751 [*Bambusicola thoracicus*]	POI24503.1	12		0.160	1.20	**0.010**	**1.70**
14.1	Ovotransferrin [*Gallus gallus*]	P02789.2	78	TF	**0.028**	**1.40**	0.260	1.40
14.2	Ovotransferrin BC type [*Gallus gallus*]	BAE16339.1	78	TF	**0.042**	**1.40**	0.390	1.30

(Continued)

TABLE 1 | Continued

#	Gene description	Accession number	Molecular weight (kDa)	Gene symbol	Spectral counting		API	
					p-value	F/SF FC	*p*-value	F/SF FC
18.1	ATP synthase subunit alpha, mitochondrial, partial [*Colius striatus*]	XP_010196224.1	58	ATP5F1A	**0.001**	**0.70**	0.760	1.00
18.5	ATP synthase subunit alpha, mitochondrial-like [*Arvicanthis niloticus*]	XP_034353318.1	60	LOC117705093	0.005	0.60	**0.008**	**1.60**
22.1	Keratin 1 [*Homo sapiens*]	AAG41947.1	66	KRT1	**0.019**	**1.60**	0.095	1.80
22.3	Keratin, type II cytoskeletal 1 isoform X2 [*Macaca mulatta*]	XP_001098182.2	65	KRT1	**0.034**	**2.10**	0.360	1.40
22.8	Keratin, type II cytoskeletal 6A isoform X2 [*Pongo abelii*]	XP_024113011.1	57	LOC100449906	**0.002**	**4.30**	**0.012**	**2.70**
24.1	Heat shock protein Hsp70 [*Gallus gallus*]	AAN18280.1	70	HSPA2	**0.045**	**1.60**	0.750	1.10
24.7	Heat shock 70 kDa protein [*Gallus gallus*]	BBO36590.1	70	HSPA2	**0.024**	**2.00**	0.910	1.00
27.2	Hypothetical protein N333_09691, partial [*Nestor notabilis*]	KFQ42654.1	45	GOT2	0.530	0.90	**0.005**	**1.70**
32.1	Hypothetical protein ASZ78_016751 [*Callipepla squamata*]	OXB67628.1	45		**0.003**	**1.80**	0.140	1.30
32.11	Phosphoglycerate kinase 1 [*Paralichthys olivaceus*]	XP_019941634.1	44	PGK1	0.110	1.80	**0.040**	**1.80**
32.2	Phosphoglycerate kinase 1 [*Ceratotherium simum simum*]	XP_004442122.1	45	LOC101387600	**0.001**	**1.60**	**0.010**	**1.80**
32.3	Phosphoglycerate kinase 1 [*Echeneis naucrates*]	XP_029374590.1	44	PGK1	0.020	1.60	**0.045**	**1.50**
32.8	Phosphoglycerate kinase 2-like [*Ictidomys tridecemlineatus*]	XP_005318639.1	45	LOC101964802	0.002	1.60	**0.014**	**1.70**
33.1	Keratin 10 [*Homo sapiens*]	AAH34697.1	59	KRT10	**0.010**	**1.50**	0.900	1.00
33.2	Keratin, type I cytoskeletal 9 [*Homo sapiens*]	NP_000217.2	62	KRT9	**0.022**	**2.30**	0.170	2.00
33.3	Keratin 14 [*Homo sapiens*]	AAH02690.1	52	KRT14	**0.000**	**4.20**	0.180	1.70
46	Unnamed protein product, partial [*Gallus gallus*]	CAA30161.1	54	LOC107051274	**0.000**	**0.30**	0.400	0.80
49.1	Mitochondria-eating protein isoform X1 [*Gallus gallus*]	XP_004936087.1	62	SPATA18	**0.001**	**1.60**	0.094	1.40
56.1	Citrate synthase, mitochondrial isoform X2 [*Gallus gallus*]	XP_015155774.1	56	CS	**0.020**	**1.40**	**0.003**	**1.90**
59	Hypothetical protein CIB84_000737 [*Bambusicola thoracicus*]	POI35507.1	30		**0.013**	**1.60**	0.420	1.20
60.1	Cytochrome c [*Gallus gallus*]	NP_001072946.1	12	CYCS	**0.037**	**0.60**	0.310	1.20
63.1	Spermatid-specific manchette-related protein 1 isoform X2 [*Gallus gallus*]	XP_004937159.1	30	CZH9orf24	**0.030**	**0.30**	0.180	0.60
65.1	Complex I assembly factor ACAD9, mitochondrial [*Gallus gallus*]	NP_001006136.1	68	ACAD9	**0.009**	**1.60**	0.980	1.00
65.2	Acyl-CoA dehydrogenase family member 9, mitochondrial [*Rhincodon typus*]	XP_020383709.1	70	ACAD9	0.015	3.00	**0.032**	**4.60**
68.4	Hypothetical protein parPi_0021429 [*Paroedura picta*]	GCF58429.1	47		0.580	0.90	**0.047**	**1.50**
69.3	Long-chain specific acyl-CoA dehydrogenase, mitochondrial [*Monopterus albus*]	XP_020470903.1	50	ACADL	0.430	1.20	**0.039**	**1.40**
82.3	Ornithine aminotransferase, mitochondrial [*Phaethon lepturus*]	XP_010295191.1	48	OAT	0.013	2.20	**0.038**	**1.70**
89.1	T-complex protein 1 subunit zeta [*Gallus gallus*]	NP_001006216.1	58	CCT6A	**0.014**	**1.50**	0.540	1.20

(Continued)

TABLE 1 | Continued

#	Gene description	Accession number	Molecular weight (kDa)	Gene symbol	Spectral counting		API	
					p-value	F/SF FC	*p*-value	F/SF FC
89.4	T-complex protein 1 subunit zeta [*Phascolarctos cinereus*]	XP_020862612.1	58	CCT6A	0.070	2.20	**0.004**	**3.60**
91.2	Superoxide dismutase [Mn], mitochondrial, partial [*Thamnophis sirtalis*]	XP_013926038.1	18	SOD2	0.072	0.80	**0.039**	**0.70**
92.1	T-complex protein 1 subunit alpha, partial [*Eudyptula novaehollandiae*]	KAF1505402.1	62		0.710	1.10	**0.044**	**1.60**
92.2	Thermosome subunit beta [*Turdus rufiventris*]	KAF4796296.1	48		0.220	1.40	**0.032**	**1.50**
92.3	PREDICTED: T-complex protein 1 subunit alpha [*Anolis carolinensis*]	XP_003215812.1	60	TCP1	0.560	1.20	**0.033**	**1.60**
93.1	Hypothetical protein RCJMB04_35g11 [*Gallus gallus*]	CAG32769.1	55	LOC107056139	0.130	2.00	**0.022**	**2.40**
98.1	Tektin-3 [*Gallus gallus*]	XP_004946137.1	56	TEKT3	0.067	0.00	**0.031**	**0.00**
103.1	Peroxisomal carnitine O-octanoyltransferase [*Gallus gallus*]	XP_003640711.1	70	CROT	0.400	1.30	**0.019**	**2.50**
135.1	T-complex protein 1 subunit delta [*Gallus gallus*]	NP_996761.1	58	CCT4	0.590	1.20	**0.035**	**4.00**
135.2	T-complex protein 1 subunit delta-like [*Trachypithecus francoisi*]	XP_033033221.1	58	LOC117063540	0.100	2.00	**0.002**	**3.10**
138.1	Tektin-4 [*Gallus gallus*]	XP_414831.1	53	TEKT4	0.051	0.20	**0.012**	**0.20**
139	Dynein light chain LC6, flagellar outer arm [*Gallus gallus*]	XP_001233550.2	10	DYL2	0.180	1.60	**0.008**	**3.50**
148.1	Lysozyme [*Gallus gallus*]	P00698.1	16	LYZ	**0.001**	**0.30**	**0.001**	**0.40**
153	Apolipoprotein A-I [*Gallus gallus*]	AAA48597.1	31	APOA1	**0.008**	**0.50**	0.510	0.90
178.1	cAMP and cAMP-inhibited cGMP 3',5'-cyclic phosphodiesterase 10A isoform X1 [*Gallus gallus*]	XP_004935608.1	116	PDE10A	0.260	1.60	**0.034**	**2.80**
187	Transthyretin isoform 2 [*Gallus gallus*]	NP_001268427.1	19	TTR	**0.013**	**0.60**	**0.025**	**0.70**
217.1	Plasminogen [*Gallus gallus*]	XP_419618.2	91	PLG	0.006	0.00	**0.015**	**0.00**
224.1	Hypothetical protein N338_03343, partial [*Podiceps cristatus*]	KFZ67843.1	43		0.007	2.90	**0.001**	**2.70**
253.1	Annexin A1 [*Gallus gallus*]	NP_996789.1	39	ANXA1	0.031	0.03	**0.030**	**0.00**
263	Hypothetical protein ASZ78_013233 [*Callipepla squamata*]	OXB59879.1	23		0.021	2.10	**0.007**	**2.10**
264	Immunoglobulin heavy chain variable region, partial [*Gallus gallus*]	BAA11105.1	11		0.002	0.40	**0.000**	**0.30**
275.1	Nucleoside diphosphate kinase homolog 5 [*Gallus gallus*]	NP_001244300.2	24	NME5	0.092	0.20	**0.048**	**0.20**
284.1	Acetyl-CoA acetyltransferase, cytosolic [*Gallus gallus*]	NP_001034376.2	41	ACAT2	0.058	4.20	**0.027**	**6.10**
293	Alpha-2-HS-glycoprotein [*Gallus gallus*]	XP_422764.1	37	AHSG	0.028	0.00	**0.014**	**0.00**
310.1	Disintegrin and metalloproteinase domain-containing protein 32-like [*Gallus gallus*]	XP_024998701.1	82	ADAM32	0.027	4.20	**0.026**	**3.50**
311.1	Hypothetical protein CIB84_002892 [*Bambusicola thoracicus*]	POI33356.1	51		0.019	0.00	**0.025**	**0.00**

Significant abundance differences were characterized between F and SF animals by applying t-test and retaining only accession numbers with p-values ≤ 0.05 associated with a fold-change ratio (FC) ≤ 0.71 or ≥ 1.4. Significant peptides are indicated with bold characters within columns corresponding to spectral counting and API (Average Precursor Intensity) quantitative methods. #: number of the considered cluster (before the point) and peptides (after the point).

and abundance changes were in the same direction as in the proteomic analysis (**Figure 4** and **Table 2**). A decrease of TF was revealed in SF samples by western blotting as well as by GeLC-MS/MS, and LYZ was more abundant in SF animals in western blotting as well as in ICM-MS, GeLC-MS/MS approaches (**Figure 4** and **Table 2**).

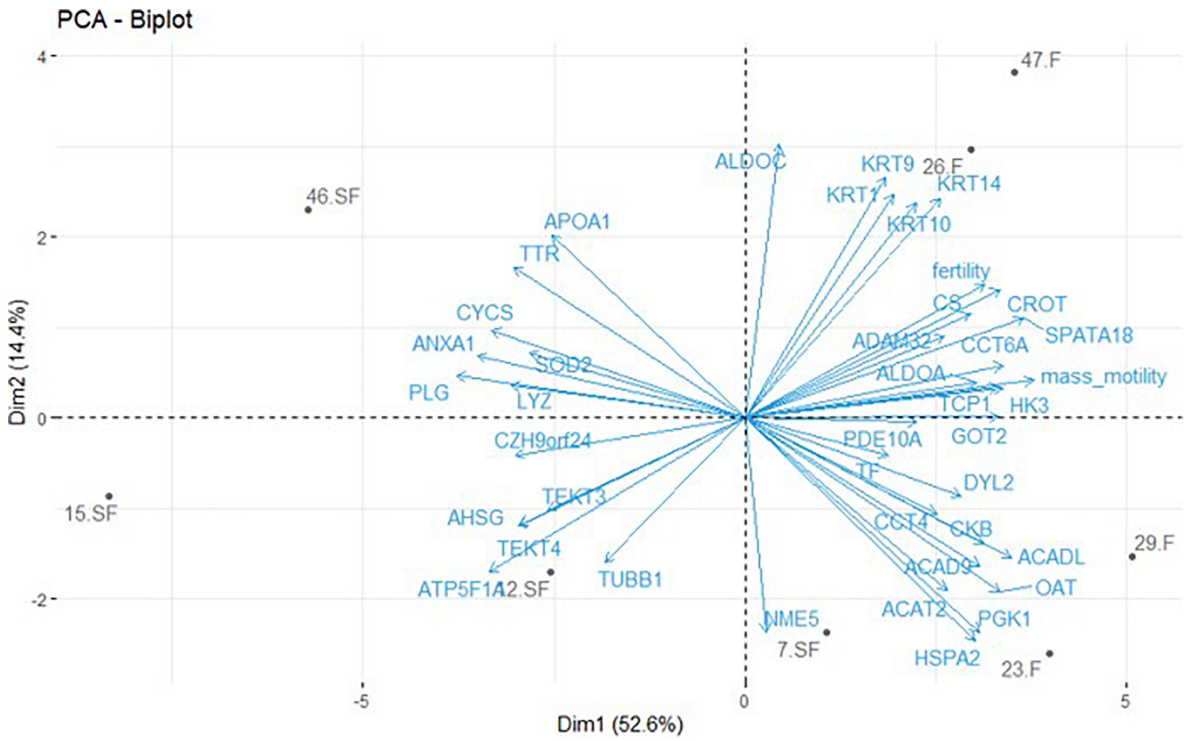

FIGURE 3 | Principal component analysis (PCA) of protein abundances obtained by GeLC-MS/MS with unique gene identification combined with fertility status and semen mass motility. Only DAP with a unique gene and an annotation (exclusion of LOC proteins) were included in this analysis. One significant DAP per cluster was retained and the mean signal calculated based on the three technical replicates obtained for each animal. Animals are revealed by their identification number and their fertility status (F = fertile; SF = subfertile). Animals are represented in gray and protein contribution as well as semen parameters in blue.

DISCUSSION

The molecular basis of male fertility remains unclear, especially in chickens, where decades of genetic selection induced an important increase in male fertility variability as a side effect (Soler et al., 2016a). To determine the crucial proteins involved in sperm-fertilizing abilities in order to decipher the impaired molecular pathways in subfertile animals and potentially link them to semen defects as causes of subfertility, *in vivo* rooster fertility was determined by AI in order to evaluate sperm-fertilizing ability and define animals according to their fertility status, i.e., fertile (FR > 70%) or subfertile (FR < 40%). Semen from F and SF roosters were then collected and *in vitro* characterized, and sperm protein content was analyzed by two complementary proteomic approaches, showing important candidates involved in the variations in sperm fertilizing ability.

In various species, sperm characteristic is evaluated by classical *in vitro* tests (WHO, 2010), evaluating semen volume, concentration, mass motility, and individual cell motility. Here, these tests revealed that the observed fertility reduction in some individuals of meat-type roosters was mainly associated with a decrease of mass motility, whereas the individual sperm motility analysis by CASA was not impacted (**Figure 1**). However, the small non-significant reduction of percentages of motile, rapid, and progressive sperm obtained by individual investigation may, at the scale of the whole ejaculate, result in the observed reduction of mass motility. Thus, small differences of sperm cell motility at the individual scale may result to a significant reduction of the whole sperm cell movement of the ejaculate, leading to a reduction of male fertility. In sheep, the association of mass motility reduction and impaired fertility has been reported (David et al., 2015). In addition to the individual movement of each sperm cell, the collective progress of sperm cells also appeared necessary to successfully reach the oocyte. So, our data revealed that, at least, one of the causes of subfertility in meat-type roosters was relative to sperm motility defects. However, we showed also that other sperm functions are affected.

To explore differences in sperm protein content between F and SF roosters, we used two complementary proteomic approaches: the ICM-MS and the GeLC-MS/MS. Indeed, whereas ICM-MS focused on the identification of small proteins and peptidoforms, as a result of protein degradation, without protein isolation, GeLC-MS/MS determines larger proteins previously extracted and digested. In contrast to GeLC-MS/MS (**Supplementary Data 3**), the ICM-MS approach succeeded in segregating F and SF animals on the basis of 211 detected peaks (**Figure 2**). Interestingly, PCA analysis revealed a more important variability within SF animals than within F animals, suggesting that causes of fertility reduction in SF roosters were multiple, corresponding to various proteomic profiles, as previously described (Labas et al., 2015). Furthermore, our data revealed that three of the differentially abundant peaks revealed by ICM-MS correspond to

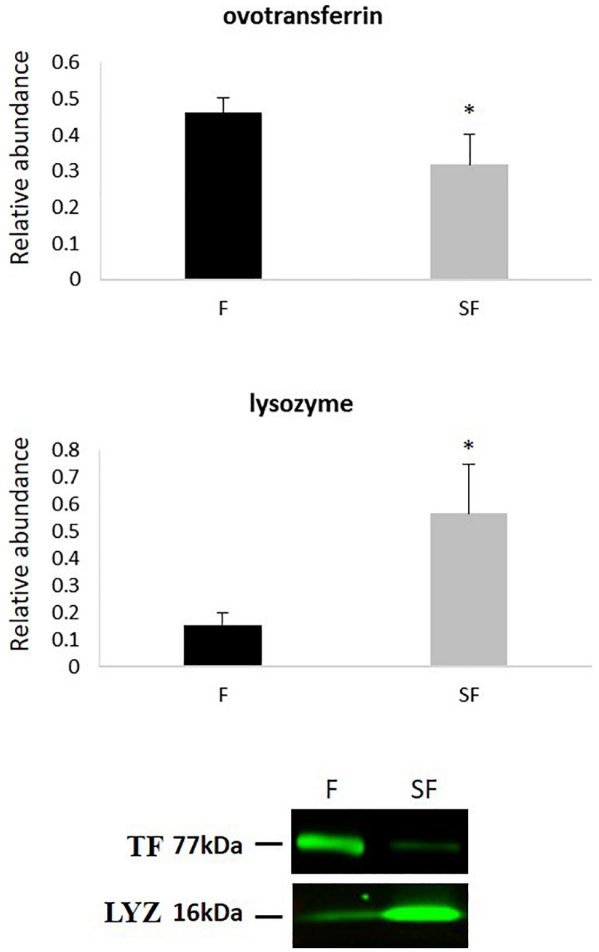

FIGURE 4 | Western-blot quantification and signals of ovotransferrin (TF) and lysozyme (LYZ) in sperm from fertile (F) and subfertile (SF) roosters. *$p < 0.05$.

peptidoforms of CFAP100, TUBB7, and ENO1 (whose functions are described later), all more abundant in SF animals than in F roosters (**Figure 2**). These products certainly result from proteolytic events which could only be identified by ICM-MS methodology, known for highlighting specific or unspecific protease activities generally unrevealed by classical proteomics (Labas et al., 2018). Consequently, an increase of proteolytic events could be assumed in SF sperm, leading to defects on various molecular pathways involved in sperm-fertilizing ability. Moreover, the origin of the peptidoforms identified by ICM-MS remains a challenge, because of the limitation of exhaustive top-down MS databases for exhaustive proteome, as shown in our study by the absence of annotation of other differentially abundant peaks (**Figure 2**). Thus, whereas ICM-MS appeared to be limited to develop an exhaustive list of proteins involved in sperm-fertilizing abilities, it remains an efficient and sensitive methodology for the identification of small proteins and larger protein degradation products, using small amounts of sperm cells ($\sim 10^5$–10^6 cells/spot) without prior sample preparation, making the ICM-MS approach a promising test to evaluate quality semen and diagnose male fertility, as previously described (Soler et al., 2016a, 2020).

In order to increase the list of DAP involved in chicken sperm-fertilizing abilities, we therefore used the GeLC-MS/MS method and identified 54 DAP between roosters of the two fertility status (**Figure 3** and **Table 1**), increasing the list of DAP involved in meat-line rooster sperm-fertilizing ability to 57 proteins. For most of them (at the exception of tubulins, tektins, and ovotransferrin), this data is the first report of their involvement in rooster fertility (Labas et al., 2015; Soler et al., 2016a). The difference of abundance of 2 DAP, one more abundant in F animals—ovotransferrin (TF)—and another more abundant in SF roosters—lysozyme (LYZ), was confirmed by immunoblot (**Figure 4** and **Table 2**). This finding underlines the complementariness of our combined approach associating ICM-MS and classical bottom-up proteomics (Labas et al., 2015) for characterization of markers. Of note, both label-free quantitative proteomic approaches revealed LYZ as significantly more abundant in SF animals when compared to F roosters (**Figures 2–4** and **Table 2**), and immunoblot confirmed the robustness of these quantifications. Altogether, these DAP reflect major dysregulations of flagellum integrity and functions, mitochondria activity, sperm maturation, and cellular interaction.

As a direct reflect of the observed reduction of mass motility, the axoneme integrity appeared impacted by the deregulation of TUBB (beta tubulins) and TEKT (tektins) abundances, crucial components of this cytoskeletal structure forming the flagellum core (Popodi et al., 2005; Raff et al., 2008). Whereas TEKT absence leads to a reduction of sperm motility in mice (Roy et al., 2007, 2009), the increase of TUBB and TEKT family members in SF sperm may increase the flagellum rigidity, also leading to a reduction of sperm motility. Interestingly, a perturbation of TEKT in SF animals was already reported in previous studies (Labas et al., 2015; Soler et al., 2016a), confirming the importance of these proteins in chicken sperm-fertilizing ability. However, total variation TUBB abundance may not be the only cause of TUBB influence on axoneme formation, since an increase of proteolytic regulation of TUBB7 has been revealed by ICM-MS experiments (**Figure 2**). Furthermore, multiple members of the TCP/CCT family were less abundant in SF sperm and these proteins are known to be involved in the cytoskeleton integrity by modeling of newly synthetized actin and tubulin monomers (Brackley and Grantham, 2011). Consistently with our data, reduction of their expression is associated with sperm

TABLE 2 | Comparison of the protein abundance fold change between fertile (F) and subfertile (SF) sperm obtained by ICM-MS, GeLC-MS/MS, and western blotting for ovotransferrin and lysozyme.

Protein name	Fold change (F/SF)		
	ICM-MS	GeLC-MS/MS (spectral counting)	Immunoblotting
Ovotransferrin	/	1.4	1.5
Lysozyme	0.5	0.3	0.3

motility decrease (Castaneda et al., 2020). Whereas not revealed in sperm cells, the presence of CFAP100 (cilia- and flagella-associated protein 100) is crucial for the ciliary movement of *Chlamydomonas reinhardtii*, as involved in the regulation of axoneme assembly (Yamamoto et al., 2013). A similar function could be suggested in chicken sperm, and the degradation of CFAP100 by proteolysis may impair the flagellum movement. In addition to the axoneme constitution, the fibrous sheath composition and activity also appeared impaired, especially with the dysregulation of proteins relative to local energy production like ALDOA (aldolase A), HK3 (hexokinase 3), and DYL2 (dynein light chain 2). ALDOA and HK3 would be involved in the flagellum glycolysis process needed for local ATP production (Krisfalusi et al., 2006; Nakamura et al., 2008), and DYL2 in the response of the CA^{2+} wave responsible for flagellum beating (Mizuno et al., 2012). Similarly, ENO1, present in the tail of sperm cells, is a glycolytic enzyme regulating enzyme activity to produce the energy in microtubules and to protect male gametes against oxidative stress (Park et al., 2013, 2019). ALDOA, HK3, and DYL2 were less abundant in SF animals, and ENO1 was more degraded in SF roosters, suggesting a reduction in local energy for flagellum movement and beating, and is consistent with the observed reduction of mass motility in SF individuals. PCA analysis suggests a positive correlation between mass motility and ALDOA, TCP1, DYL2, and HK3 (**Figure 3**). However, correlation analysis implies large sample size (Bujang and Baharum, 2016) and, thus, these putative correlations should be validated on a larger sample size, by immunoblot for instance.

Our data also revealed numerous DAP involved in mitochondria integrity and activity such as CS, SPATA18, ACAD9/L, OAT, ATP5A1, SOD2, and CYCS (**Figure 5**). Some of these actors, such as CYCS (cytochrome C) or SOD2 (superoxide dismutase 2), are known to be involved in the oxygen stress response of sperm cells (Wang et al., 2003; Yan et al., 2014). High abundance of OAT (ornithine aminotransferase) and ATP5F1A (ATP synthase F1 subunit alpha) has been reported in high-quality sperm in bovine and human (D'Amours et al., 2019; Panner Selvam et al., 2019). Obviously, impairment in mitochondria integrity and activity may impact the whole-cell physiology, including its motility. Several proteins involved in the energy transduction, such as CKB (creatine kinase B-type), was less abundant in SF roosters. The abundance of CKB is linked with sperm cell maturity in mammals (WHO, 2010), and its abundance is linked to sperm motility in mammals (Parte et al., 2012) and fish (Dietrich et al., 2016). This finding underlines the importance of energy transduction for chicken sperm functions, and not only the energy production.

Interestingly, proteomic approaches developed here also revealed dysregulations in molecular pathways linked to events occurring in the female tracts, and not accessed by classical *in vitro* semen quality evaluation, as performed here. For instance, our data revealed a higher level of ANXA1 (annexin A1) in SF animals. The presence of ANXA1 has been reported in seminal plasma in mammals (Candenas and Chianese, 2020), and in chickens (Labas et al., 2015; Li et al., 2020). Sperm surface annexins have been associated with the adhesion of sperm to oviductal cells in mammals in order to hold sperm in oviductal reservoir (Ignotz et al., 2007; Teijeiro et al., 2009). In chickens, sperm storage into the female tract occurs during weeks within sperm storage tubules (King et al., 2002). Thus, the reduction of ANXA1 in SF sperm may sign the reduction of sperm capacities to be stored into the female tract. Furthermore, our data reported a high amount of APOA1 in SF animals. APOA1 has been reported in chicken seminal plasma in higher quantity in SF animals (Labas et al., 2015), suggesting a differential impact of seminal plasma in sperm maturation. In mammals, APOA1 is present in the sperm head and known to induce cholesterol efflux in spermatozoa necessary for sperm capacitation (Kwon et al., 2014). The modification of the APOA1 amount in chicken sperm in relation with the fertility suggests a sperm maturation deregulation. Moreover, in humans, a decline of sperm motility was observed when sperm APOA1 was inhibited by the presence of antibodies (Chi et al., 2018), suggesting a decrease of sperm motility subsequently to the reduction of sperm maturation. Finally, multiple proteins are known to be involved in the oocyte–sperm interaction in mammals such as the chaperone HSPA2 (Redgrove et al., 2012), LYZ (Herrero et al., 2005; Sun et al., 2011), and ADAM32 (Vicens et al., 2014). Thus, recent studies described that LYZ is present in the

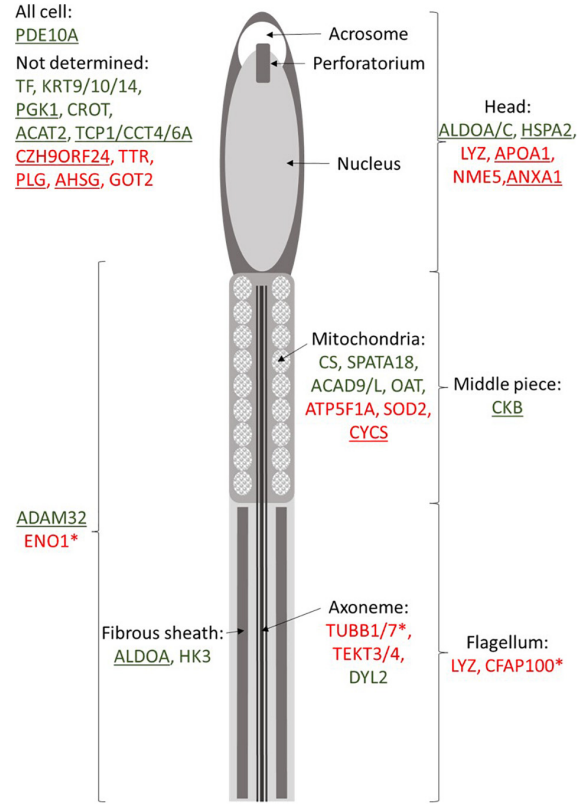

FIGURE 5 | Putative localization of proteins identified as relative to meat-line rooster fertility. Peptidoforms resulting from protein degradation revealed by ICM-MS are noted with asterisks. Green indicates proteins more abundant in fertile animals, and red represents proteins and peptidoforms more abundant in subfertile roosters. Underlined proteins are the one present in chicken seminal plasma (Labas et al., 2015).

sperm cell surface and that its neutralization in male rats induces male infertility, by impairing acrosome reaction (Sun et al., 2011; Narmadha and Yenugu, 2016). Actually, LYZ abundance observed by immunoblot was not statistically correlated with any of the sperm quality parameters tested *in vitro* (**Supplementary Data 4**), which were all indicators of motility abilities and not of the acrosome integrity. Testing the acrosome functionality *in vitro* is challenging in chicken sperm (Lemoine et al., 2008) and not classically performed to evaluate semen quality. In this context, it would be interesting to investigate if LYZ abundance could represent an indirect measure of acrosome performance. Additionally, whereas not directly involved in oocyte–sperm interaction, PDE10 is essential to acrosome reaction and thus to oocyte–sperm fusion in mammals (Maréchal et al., 2017). Similar functions could be expected in chicken sperm. Another example with the mammalian equivalent of TF, the lactoferrin (LT), has been reported to be expressed by the epididymis, capable of sperm binding (Jin et al., 1997), increasing the membrane functionality of cryopreserved sperm (Martins et al., 2018), and modulating the oocyte–sperm interaction (Zumoffen et al., 2015). Thus, similar functions could be assumed for avian equivalent, the TF, which may also be involved in the oocyte–sperm interaction, and its reduction in sperm from SF roosters may sign a putative dysregulation of oocyte recognition by sperm cells in SF animals. Further investigations will be necessary to explore the role of these proteins in oocyte–sperm interaction in chicken.

Collectively, our data revealed that the fertility reduction observed in some meat-type roosters may be partly related to the decrease of sperm mass motility. However, among the 50 proteins newly revealed by the developed proteomic strategies and linked for the first time to the chicken fertility status, not all appeared directly relative to motility defects. In fact, other molecular pathways seemed to be impaired, including mitochondria functions, sperm maturation, and events occurring into the female tract, including storage as well as oocyte–sperm interaction. Therefore, our data confirmed the complexity of sperm-fertilizing capacity, a phenomenon not classically revealed by *in vitro* semen quality evaluation. Thus, it is crucial to obtain a large overview of the sperm proteome at the individual level to decipher the maximum of the mechanisms involved in sperm-fertilizing capacity. Here, we showed that ICM-MS and GeLC-MS/MS approaches were complementary to discriminate animals according to their fertility status based on multiple markers (peptidoforms and proteoforms) and to identify impairments into sperm biological pathways, respectively. Among the proteins identified here, some, such as ENO1, are also known as fertility markers in bull sperm cells (Park et al., 2013, 2019). Thus, these data are thus highly valuable to better understand the molecular processes involved in chicken sperm-fertilizing abilities, but also in the identification of putative robust male fertility biomarkers shared by different animal species.

DATA AVAILABILITY STATEMENT

The datasets presented in this study can be found in online repositories. The names of the repository/repositories and accession number(s) can be found in the article/**Supplementary Material**.

ETHICS STATEMENT

All experiments were carried out in accordance with the European welfare and the French Direction of Veterinary Services regulations (agreement number C37–175-1) as previously described.

AUTHOR CONTRIBUTIONS

EB designed the research. LS, AT, IG, LC, A-PT-G, and VL performed the research. AVC, DT, EB, and VL analyzed the data. AVC, LS, VL, and EB wrote the manuscript. All authors contributed to the article and approved the submitted version.

FUNDING

This work was supported by the French National Infrastructure of Research CRB anim funded by the "Investissements d'avenir," ANR-11-INBS-0003 and from the French National Institute of Agronomic and Environmental Research (INRAe). The high-resolution mass spectrometer was financed (SMHART project) by the European Regional Development Fund (ERDF), the Conseil Régional du Centre, the French National Institute of Agronomic and Environmental Research (INRAe), and the French National Institute of Health and Medical Research (Inserm).

ACKNOWLEDGMENTS

We would like to thank the personnel of avian experimental unit (UE-PEAT, INRAe, Nouzilly).

SUPPLEMENTARY MATERIAL

The Supplementary Material for this article can be found online at: https://www.frontiersin.org/articles/10.3389/fcell.2021.655866/full#supplementary-material

Supplementary Data 1 | ICM-MS differential analysis. Each mass represents one peak and the difference between fertile (F) and subfertile (SF) animals ($n = 9$) was by non-parametric Mann-Whitney or Wilcoxon test to determine the p-value.

Supplementary Data 2 | DAP revealed by GeLC-MS/MS included in PCA analysis. Only DAP with a gene description and a gene symbol not corresponding to LOC were included.

Supplementary Data 3 | PCA analysis of GeLC-MS/MS. PCA analysis was conducted based on all the list of 84 DAP revealed by GeLC-MS/MS, with a preferential selection of SC differential.

Supplementary Data 4 | Correlation analysis of western-blot abundance quantifications of ovotransferrin (WB_TF) and lyzosyme (WB_LYZ), fertility rate and *in vitro* semen quality evaluation parameters. Square including dot presents significant correlation ($p < 0.05$). Dot color and intensity corresponds to correlation direction and strength, respectively.

REFERENCES

Allaire, J. J. (2015). *RStudio: Integrated development environment for R*. Boston: RStudio, Inc.

Blesbois, E., Grasseau, I., Seigneurin, F., Mignon-Grasteau, S., Saint Jalme, M., and Mialon-Richard, M. M. (2008). Predictors of success of semen cryopreservation in chickens. *Theriogenology* 69, 252–261. doi: 10.1016/j.theriogenology.2007.09.019

Bracke, A., Peeters, K., Punjabi, U., Hoogewijs, D., and Dewilde, S. (2018). A search for molecular mechanisms underlying male idiopathic infertility. *Reprod. Biomed. Online* 36, 327–339. doi: 10.1016/j.rbmo.2017.12.005

Brackley, K. I., and Grantham, J. (2011). Interactions between the actin filament capping and severing protein gelsolin and the molecular chaperone CCT: Evidence for nonclassical substrate interactions. *Cell Stress Chaperones* 16, 173–179. doi: 10.1007/s12192-010-0230-x

Brillard, J. P., and McDaniel, G. R. (1985). The reliability and efficiency of various methods for estimating spermatozoa concentration. *Poult. Sci.* 64, 155–158. doi: 10.3382/ps.0640155

Bujang, M. A., and Baharum, N. (2016). Sample Size Guideline for Correlation Analysis. *World J. Soc. Sci. Res.* 3:37. doi: 10.22158/wjssr.v3n1p37

Burrows, W. H., and Quinn, J. P. (1937). The Collection of Spermatozoa from the Domestic Fowl and Turkey. *Poult. Sci.* 16, 19–24. doi: 10.3382/ps.0160019

Candenas, L., and Chianese, R. (2020). Exosome composition and seminal plasma proteome: A promising source of biomarkers of male infertility. *Int. J. Mol. Sci.* 21:7022. doi: 10.3390/ijms21197022

Castaneda, J. M., Miyata, H., Archambeault, D. R., Satouh, Y., Yu, Z., Ikawa, M., et al. (2020). Mouse t-complex protein 11 is important for progressive motility in sperm. *Biol. Reprod.* 102, 852–862. doi: 10.1093/biolre/ioz226

Chi, X., Xiang, D., Liang, S., Hu, C., and Wang, C. (2018). Apolipoprotein A1 localization in sperms and its antibody's effect on human sperm function. *Chinese J. Lab. Med.* 41, 664–668.

Cox, J., Hein, M. Y., Luber, C. A., Paron, I., Nagaraj, N., and Mann, M. (2014). Accurate proteome-wide label-free quantification by delayed normalization and maximal peptide ratio extraction, termed MaxLFQ. *Mol. Cell. Proteomics* 13, 2513–2526. doi: 10.1074/mcp.M113.031591

D'Amours, O., Calvo, É, Bourassa, S., Vincent, P., Blondin, P., and Sullivan, R. (2019). Proteomic markers of low and high fertility bovine spermatozoa separated by Percoll gradient. *Mol. Reprod. Dev.* 86, 999–1012. doi: 10.1002/mrd.23174

David, I., Kohnke, P., Lagriffoul, G., Praud, O., Plouarboué, F., Degond, P., et al. (2015). Mass sperm motility is associated with fertility in sheep. *Anim. Reprod. Sci.* 161, 75–81. doi: 10.1016/j.anireprosci.2015.08.006

Deutsch, E. W., Overall, C. M., Van Eyk, J. E., Baker, M. S., Paik, Y. K., Weintraub, S. T., et al. (2016). Human Proteome Project Mass Spectrometry Data Interpretation Guidelines 2.1. *J. Proteome Res.* 15, 3961–3970. doi: 10.1021/acs.jproteome.6b00392

Dietrich, M. A., Dietrich, G. J., Mostek, A., and Ciereszko, A. (2016). Motility of carp spermatozoa is associated with profound changes in the sperm proteome. *J. Proteomics* 138, 124–135. doi: 10.1016/j.jprot.2016.02.029

Druart, X., Rickard, J. P., Tsikis, G., and de Graaf, S. P. (2019). Seminal plasma proteins as markers of sperm fertility. *Theriogenology* 137, 30–35. doi: 10.1016/j.theriogenology.2019.05.034

FAO (2020). *Overview of global meat market developments in 2019*. Rome: FAO.

Filzmoser, P., and Walczak, B. (2014). What can go wrong at the data normalization step for identification of biomarkers? *J. Chromatogr. A.* 1362, 194–205. doi: 10.1016/j.chroma.2014.08.050

Gautron, J., Hincke, M. T., Panheleux, M., Garcia-Ruiz, J. M., Boldicke, T., and Nys, Y. (2001). Ovotransferrin is a matrix protein of the hen eggshell membranes and basal calcified layer. *Connect. Tissue Res.* 42, 255–267. doi: 10.3109/03008200109016840

Gibb, S., and Strimmer, K. (2012). Maldiquant: A versatile R package for the analysis of mass spectrometry data. *Bioinformatics* 28, 2270–2271. doi: 10.1093/bioinformatics/bts447

Gil, J., and Werman, M. (1993). Computing 2-D Min, Median, and Max Filters. *IEEE Trans. Pattern Anal. Mach. Intell.* 15, 504–507. doi: 10.1109/34.211471

Herrero, M. B., Mandal, A., Digilio, L. C., Coonrod, S. A., Maier, B., and Herr, J. C. (2005). Mouse SLLP1, a sperm lysozyme-like protein involved in sperm-egg binding and fertilization. *Dev. Biol.* 284, 126–142. doi: 10.1016/j.ydbio.2005.05.008

Ignotz, G. G., Cho, M. Y., and Suarez, S. S. (2007). Annexins are candidate oviductal receptors for bovine sperm surface proteins and thus may serve to hold bovine sperm in the oviductal reservoir. *Biol. Reprod.* 77, 906–913. doi: 10.1095/biolreprod.107.062505

Jin, Y. Z., Bannai, S., Dacheux, F., Dacheux, J. L., and Okamura, N. (1997). Direct evidence for the secretion of lactoferrin and its binding to sperm in the porcine epididymis. *Mol. Reprod. Dev.* 47, 490–496. doi: 10.1002/(sici)1098-2795(199708)47:4

Jodar, M., Soler-Ventura, A., and Oliva, R. (2017). Semen proteomics and male infertility. *J. Proteomics* 162, 125–134. doi: 10.1016/j.jprot.2016.08.018

Keller, A., Nesvizhskii, A. I., Kolker, E., and Aebersold, R. (2002). Empirical statistical model to estimate the accuracy of peptide identifications made by MS/MS and database search. *Anal. Chem.* 74, 5383–5392. doi: 10.1021/ac025747h

King, L. M., Brillard, J. P., Garrett, W. M., Bakst, M. R., and Donoghue, A. M. (2002). Segregation of spermatozoa within sperm storage tubules of fowl and turkey hens. *Reproduction* 123, 79–86. doi: 10.1530/rep.0.1230079

Kovac, J. R., Pastuszak, A. W., and Lamb, D. J. (2013). The use of genomics, proteomics, and metabolomics in identifying biomarkers of male infertility. *Fertil. Steril.* 99, 998–1007. doi: 10.1016/j.fertnstert.2013.01.111

Krisfalusi, M., Miki, K., Magyar, P. L., and O'Brien, D. A. (2006). Multiple glycolytic enzymes are tightly bound to the fibrous sheath of mouse spermatozoa. *Biol. Reprod.* 75, 270–278. doi: 10.1095/biolreprod.105.049684

Kwon, W. S., Rahman, M. S., Lee, J. S., Kim, J., Yoon, S. J., Park, Y. J., et al. (2014). A comprehensive proteomic approach to identifying capacitation related proteins in boar spermatozoa. *BMC Genomics* 15:897. doi: 10.1186/1471-2164-15-897

Labas, V., Grasseau, I., Cahier, K., Gargaros, A., Harichaux, G., Teixeira-Gomes, A. P., et al. (2015). Qualitative and quantitative peptidomic and proteomic approaches to phenotyping chicken semen. *J. Proteomics* 112, 313–335. doi: 10.1016/j.jprot.2014.07.024

Labas, V., Teixeira-Gomes, A. P., Bouguereau, L., Gargaros, A., Spina, L., Marestaing, A., et al. (2018). Intact cell MALDI-TOF mass spectrometry on single bovine oocyte and follicular cells combined with top-down proteomics: A novel approach to characterise markers of oocyte maturation. *J. Proteomics* 175, 56–74. doi: 10.1016/j.jprot.2017.03.027

Lemoine, M., Grasseau, I., Brillard, J. P., and Blesbois, E. (2008). A reappraisal of the factors involved in in vitro initiation of the acrosome reaction in chicken spermatozoa. *Reproduction* 136, 391–399. doi: 10.1530/REP-08-0094

Li, Y., Sun, Y., Ni, A., Shi, L., Wang, P., Isa, A. M., et al. (2020). Seminal Plasma Proteome as an Indicator of Sperm Dysfunction and Low Sperm Motility. *Mol. Cell. Proteomics* 19, 1035–1046. doi: 10.1074/mcp.ra120.002017

Liu, H., Sadygov, R. G., and Yates, J. R. (2004). A model for random sampling and estimation of relative protein abundance in shotgun proteomics. *Anal. Chem.* 76, 4193–4201. doi: 10.1021/ac0498563

Maréchal, L., Guillemette, C., Goupil, S., Blondin, P., Leclerc, P., and Richard, F. J. (2017). Cyclic nucleotide phosphodiesterases in human spermatozoa and seminal fluid: Presence of an active PDE10A in human spermatozoa. *Biochim. Biophys. Acta Gen. Subj.* 1861, 147–156. doi: 10.1016/j.bbagen.2016.11.006

Martins, H. S., da Silva, G. C., Cortes, S. F., Paes, F. O., Martins Filho, O. A., Araujo, M. S. S., et al. (2018). Lactoferrin increases sperm membrane functionality of frozen equine semen. *Reprod. Domest. Anim.* 53, 617–623. doi: 10.1111/rda.13148

Mizuno, K., Shiba, K., Okai, M., Takahashi, Y., Shitaka, Y., Oiwa, K., et al. (2012). Calaxin drives sperm chemotaxis by Ca2+-mediated direct modulation of a dynein motor. *Proc. Natl. Acad. Sci. U S A.* 109, 20497–20502. doi: 10.1073/pnas.1217018109

Nakamura, N., Shibata, H., O'Brien, D. A., Mori, C., and Eddy, E. M. (2008). Spermatogenic cell-specific type 1 hexokinase is the predominant hexokinase in sperm. *Mol. Reprod. Dev.* 75, 632–640. doi: 10.1002/mrd.20791

Narmadha, G., and Yenugu, S. (2016). Immunization against lysozyme-like proteins affect sperm function and fertility in the rat. *J. Reprod. Immunol.* 118, 100–108. doi: 10.1016/j.jri.2016.11.001

Nesvizhskii, A. I., Keller, A., Kolker, E., and Aebersold, R. (2003). A statistical model for identifying proteins by tandem mass spectrometry. *Anal. Chem.* 75, 4646–4658. doi: 10.1021/ac0341261

Panner Selvam, M. K., Agarwal, A., and Pushparaj, P. N. (2019). A quantitative global proteomics approach to understanding the functional pathways dysregulated in the spermatozoa of asthenozoospermic testicular cancer patients. *Andrology* 7, 454–462. doi: 10.1111/andr.12620

Park, Y. J., Kim, J., You, Y. A., and Pang, M. G. (2013). Proteomic revolution to improve tools for evaluating male fertility in animals. *J. Proteome Res.* 12, 4738–4747. doi: 10.1021/pr400639x

Park, Y. J., Pang, W. K., Ryu, D. Y., Song, W. H., Rahman, M. S., and Pang, M. G. (2019). Optimized combination of multiple biomarkers to improve diagnostic accuracy in male fertility. *Theriogenology* 139, 106–112. doi: 10.1016/j.theriogenology.2019.07.029

Parte, P. P., Rao, P., Redij, S., Lobo, V., D'Souza, S. J., Gajbhiye, R., et al. (2012). Sperm phosphoproteome profiling by ultra performance liquid chromatography followed by data independent analysis (LC-MSE) reveals altered proteomic signatures in asthenozoospermia. *J. Proteomics* 75, 5861–5871. doi: 10.1016/j.jprot.2012.07.003

Popodi, E. M., Hoyle, H. D., Turner, F. R., and Raff, E. C. (2005). The proximal region of the β-tubulin C-terminal tail is sufficient for axoneme assembly. *Cell Motil. Cytoskeleton* 62, 48–64. doi: 10.1002/cm.20085

R Core Team (2017). *R: A language and environment for statistical computing*. Vienna: R Core Team.

Raff, E. C., Hoyle, H. D., Popodi, E. M., and Turner, F. R. (2008). Axoneme β-Tubulin Sequence Determines Attachment of Outer Dynein Arms. *Curr. Biol.* 18, 911–914. doi: 10.1016/j.cub.2008.05.031

Rauw, W. M., Kanis, E., Noordhuizen-Stassen, E. N., and Grommers, F. J. (1998). Undesirable side effects of selection for high production efficiency in farm animals: A review. *Livest. Prod. Sci.* 56, 15–33. doi: 10.1016/S0301-6226(98)00147-X

Redgrove, K. A., Nixon, B., Baker, M. A., Hetherington, L., Baker, G., Liu, D. Y., et al. (2012). The Molecular Chaperone HSPA2 Plays a Key Role in Regulating the Expression of Sperm Surface Receptors That Mediate Sperm-Egg Recognition. *PLoS One* 7:e50851. doi: 10.1371/journal.pone.0050851

Roy, A., Lin, Y. N., Agno, J. E., Demayo, F. J., and Matzuk, M. M. (2009). Tektin 3 is required for progressive sperm motility in mice. *Mol. Reprod. Dev.* 76, 453–459. doi: 10.1002/mrd.20957

Roy, A., Lin, Y.-N., Agno, J. E., DeMayo, F. J., and Matzuk, M. M. (2007). Absence of tektin 4 causes asthenozoospermia and subfertility in male mice. *FASEB J.* 21, 1013–1025. doi: 10.1096/fj.06-7035com

Sellier, N., Brillard, J. P., Dupuy, V., and Bakst, M. R. (2006). Comparative staging of embryo development in chicken, turkey, duck, goose, guinea fowl, and Japanese quail assessed from five hours after fertilization through seventy-two hours of incubation. *J. Appl. Poult. Res.* 15, 219–228. doi: 10.1093/japr/15.2.219

Soler, L., Labas, V., Thélie, A., Grasseau, I., Teixeira-Gomes, A. P., and Blesbois, E. (2016a). Intact cell MALDI-TOF MS on sperm: A molecular test for male fertility diagnosis. *Mol. Cell. Proteomics* 15, 1998–2010. doi: 10.1074/mcp.M116.058289

Soler, L., Labas, V., Thélie, A., Teixeira-Gomes, A. P., Grasseau, I., Bouguereau, L., et al. (2016b). Data on endogenous chicken sperm peptides and small proteins obtained through Top-Down High Resolution Mass Spectrometry. *Data Br.* 8, 1421–1425. doi: 10.1016/j.dib.2016.07.050

Soler, L., Uzbekova, S., Blesbois, E., Druart, X., and Labas, V. (2020). Intact cell MALDI-TOF mass spectrometry, a promising proteomic profiling method in farm animal clinical and reproduction research. *Theriogenology* 150, 113–121. doi: 10.1016/j.theriogenology.2020.02.037

Sun, R., Shen, R., Li, J., Xu, G., Chi, J., Li, L., et al. (2011). Lyzl4, a novel mouse sperm-related protein, is involved in fertilization. *Acta Biochim. Biophys. Sin.* 43, 346–353. doi: 10.1093/abbs/gmr017

Teijeiro, J. M., Ignotz, G. G., and Marini, P. E. (2009). Annexin A2 is involved in pig (Sus scrota) sperm-oviduct interaction. *Mol. Reprod. Dev.* 76, 334–341. doi: 10.1002/mrd.20958

van Herk, M. (1992). A fast algorithm for local minimum and maximum filters on rectangular and octagonal kernels. *Pattern Recognit. Lett.* 13, 517–521. doi: 10.1016/0167-8655(92)90069-C

Vicens, A., Lüke, L., and Roldan, E. R. S. (2014). Proteins involved in motility and sperm-egg interaction evolve more rapidly in mouse spermatozoa. *PLoS One* 9:e91302. doi: 10.1371/journal.pone.0091302

Vizcaíno, J. A., Deutsch, E. W., Wang, R., Csordas, A., Reisinger, F., Ríos, D., et al. (2014). ProteomeXchange provides globally coordinated proteomics data submission and dissemination. *Nat. Biotechnol.* 32, 223–226. doi: 10.1038/nbt.2839

Wang, X., Sharma, R. K., Sikka, S. C., Thomas, A. J., Falcone, T., and Agarwal, A. (2003). Oxidative stress is associated with increased apoptosis leading to spermatozoa DNA damage in patients with male factor infertility. *Fertil. Steril.* 80, 531–535. doi: 10.1016/S0015-0282(03)00756-8

WHO (2010). *Examination and processing of human semen*. Geneva: WHO, doi: 10.1038/aja.2008.57

Yamamoto, R., Song, K., Yanagisawa, H., Fox, L., Yagi, T., Wirschell, M., et al. (2013). The MIA complex is a conserved and novel dynein regulator essential for normal ciliary motility. *J. Cell Biol.* 201, 263–278. doi: 10.1083/jcb.201211048

Yan, L., Liu, J., Wu, S., Zhang, S., Ji, G., and Gu, A. (2014). Seminal superoxide dismutase activity and its relationship with semen quality and SOD gene polymorphism. *J. Assist. Reprod. Genet.* 31, 549–554. doi: 10.1007/s10815-014-0215-2

Zumoffen, C. M., Massa, E., Caille, A. M., Munuce, M. J., and Ghersevich, S. A. (2015). Effects of lactoferrin, a protein present in the female reproductive tract, on parameters of human sperm capacitation and gamete interaction. *Andrology* 3, 1068–1075. doi: 10.1111/andr.12093

Conflict of Interest: The authors declare that the research was conducted in the absence of any commercial or financial relationships that could be construed as a potential conflict of interest.

frontiers in Cell and Developmental Biology

ORIGINAL RESEARCH
published: 30 April 2021
doi: 10.3389/fcell.2021.669182

Species-Specific Differences in Sperm Chromatin Decondensation Between Eutherian Mammals Underlie Distinct Lysis Requirements

Jordi Ribas-Maynou[1,2], Estela Garcia-Bonavila[1,2], Carlos O. Hidalgo[3], Jaime Catalán[4], Jordi Miró[4] and Marc Yeste[1,2]*

[1] Biotechnology of Animal and Human Reproduction (TechnoSperm), Institute of Food and Agricultural Technology, University of Girona, Girona, Spain, [2] Unit of Cell Biology, Department of Biology, Faculty of Sciences, University of Girona, Girona, Spain, [3] Department of Animal Selection and Reproduction, Regional Agrifood Research and Development Service of Asturias (SERIDA), Gijón, Spain, [4] Equine Reproduction Service, Department of Animal Medicine and Surgery, Faculty of Veterinary Medicine, Autonomous University of Barcelona, Bellaterra, Spain

OPEN ACCESS

Edited by:
Silvina Perez-Martinez, CONICET Centro de Estudios Farmacológicos y Botánicos (CEFYBO), Argentina

Reviewed by:
Juan Carlos Calvo, CONICET Instituto de Biología y Medicina Experimental (IBYME), Argentina
Xin Zhiguo Li, University of Rochester, United States

***Correspondence:**
Jordi Ribas-Maynou
jordi.ribasmaynou@udg.edu
orcid.org/0000-0002-9101-2044

Specialty section:
This article was submitted to Cell Growth and Division, a section of the journal Frontiers in Cell and Developmental Biology

Received: *18 February 2021*
Accepted: *12 April 2021*
Published: *30 April 2021*

Citation:
Ribas-Maynou J, Garcia-Bonavila E, Hidalgo CO, Catalán J, Miró J and Yeste M (2021) Species-Specific Differences in Sperm Chromatin Decondensation Between Eutherian Mammals Underlie Distinct Lysis Requirements. Front. Cell Dev. Biol. 9:669182. doi: 10.3389/fcell.2021.669182

Sperm present a highly particular DNA condensation that is acquired during their differentiation. Protamines are key elements for DNA condensation. However, whereas the presence of protamine 1 (P1) is conserved across mammalian species, that of protamine 2 (P2) has evolved differentially, existing only few species that use both protamines for sperm DNA condensation. In addition, altered P1/P2 ratios and alterations in the expression of P1 have previously been associated to infertility and DNA damage disorders. On the other hand, different methods evaluating DNA integrity, such as Sperm Chromatin Dispersion (SCD) and Comet tests, need a previous complete DNA decondensation to properly assess DNA breaks. Related with this, the present study aims to analyze the resilience of sperm DNA to decodensation in different eutherian mammals. Sperm samples from humans, horses, cattle, pigs and donkeys were used. Samples were embedded in low melting point agarose and treated with lysis solutions to induce DNA decondensation and formation of sperm haloes. The treatment consisted of three steps: (1) incubation in SDS + DTT for 30 min; (2) incubation in DTT + NaCl for 30 min; and (3) incubation in DTT + NaCl with or without proteinase K for a variable time of 0, 30, or 180 min. How incubation with the third lysis solution (with or without proteinase K) for 0, 30, and 180 min affected DNA decondensation was tested through analyzing core and halo diameters in 50 sperm per sample. Halo/core length ratio was used as an indicator of complete chromatin decondensation. While incubation time with the third lysis solution had no impact on halo/core length ratios in species having P1 and P2 (human, equine and donkey), DNA decondensation of pig and cattle sperm, which only present P1, significantly ($P < 0.05$) increased following incubation with the third lysis solution for 180 min. In addition, the inclusion of proteinase K was found to accelerate DNA decondensation. In conclusion, longer incubations in lysis solution

including proteinase K lead to higher DNA decondensation in porcine and bovine sperm. This suggests that tests intended to analyze DNA damage, such as halo or Comet assays, require complete chromatin deprotamination to achieve high sensitivity in the detection of DNA breaks.

Keywords: sperm, DNA condensation, DNA damage, protamine, mammals

INTRODUCTION

Different proteins encoded in nuclear and mitochondrial DNA allow cells to accomplish multiple functions to survive and proliferate. Nuclear chromatin consists of a complex of DNA and histone octamers. Histone octamers are formed by histones 2A, 2B, 3, and 4 (H2A, H2B, H3, and H4) and are separated with linker DNA of about 20–60 base pairs; each octamer condenses around 146 base pairs of DNA. The DNA-histone complex is highly supercoiled, forms chromatin fibers of 100–400 Kb in length and is organized in loop domains (Luger et al., 1997; Rao et al., 2014; Gibson et al., 2019). According to the models of chromatin organization, in each of these loops can one find a matrix attachment region (MAR) whose function is attaching chromatin to the nuclear matrix, a protein scaffold that supports nuclear organization (Ward, 2010) and contributes to the regulation of DNA replication and transcription in somatic cells, providing epigenetic plasticity for gene expression (Getzenberg, 1994; Linnemann et al., 2009; Ji et al., 2013; Narwade et al., 2019).

Spermatozoa are highly differentiated cells whose main function is the transport of genetic material to the oocyte through the female reproductive tract. To achieve this, millions of years of evolution have conferred mammalian sperm with highly specialized characteristics, such as the presence of flagellum, organization of mid-piece, and a very particular chromatin condensation and organization, as DNA is mainly condensed in protamines rather than in histones (Ward and Coffey, 1991; Wykes and Krawetz, 2003; Oliva, 2006). Organization of sperm chromatin changes during spermatogenesis, as histones are replaced by protamines through a series of events that, in some species such as humans, mouse, rat or sheep, involve transition nuclear proteins (Fuentes-Mascorro et al., 2000; Kierszenbaum, 2001; Hao et al., 2019). Condensation of sperm DNA through protamines protects genetic information from damaging agents (Zini and Libman, 2006), facilitating the delivery of an intact genetic material to the future embryo. This is very relevant as sperm DNA damage has been proposed as an important affectation that may underlie fertilization failure, poor embryo development, miscarriage and the production of unhealthy offspring (Makker et al., 2009; Lewis and Simon, 2010). These effects, however, are subject to the DNA damage repair capacity provided by the oocyte and, in this regard, different works described the activation of embryo checkpoints upon fertilization with damaged sperm (Adiga et al., 2007; Toyoshima, 2009). Also, a recent study in humans showed that ICSI cycles performed with sperm containing DNA damage depict lower embryo quality, pregnancy and implantation rates and higher miscarriage rates in older than in younger women (<36 years old) (Setti et al., 2021).

Protamines are arginine-rich proteins sized about half of the size of a typical histone and with highly positive charge, features that result in a tight binding to the nuclear sperm DNA, neutralizing the phosphodiester backbone (Balhorn, 1982). Protamine-DNA complex is responsible for the higher level of DNA condensation of spermatozoa compared to somatic cells; nuclear sperm DNA is known to be about six times more condensed than mitotic chromosomes, resulting in a nucleus with about 44 times less volume than that of a mouse liver cell (Ward and Coffey, 1991). Due to this DNA condensation, sperm chromatin is transcriptionally silent and, after fertilization, the replacement of protamines by histones is one of the main processes happening in the male pronuclear stage (Ajduk et al., 2006; Ward, 2010). In mammals, two different types of protamines (protamine 1 and protamine 2 family) are encoded in the genome. While protamine 1 is present in sperm from all species, protamine 2 family, formed by P2, P3, and P4 components, is only found in species such as humans, mice and horses (Fuentes-Mascorro et al., 2000; Corzett et al., 2002; Oliva, 2006; Gosálvez et al., 2011). Whereas protamine 1 is synthesized as a mature protein, those belonging to protamine 2 family (mainly P2, P3, and P4 are present in a minor percentage) need post-translational proteolysis prior to conversion into the mature form (Oliva, 2006). As Protamine 2 family proteins have never been found to compact sperm DNA alone, they appear not to be capable of condensing sperm chromatin without protamine 1 (Corzett et al., 2002). Alterations in the expression of protamine 1 have been shown to be linked to sperm morphology anomalies and premature DNA condensation during sperm differentiation (Peschon et al., 1989; Lee et al., 1995); alterations in protamine 2 content lead to male infertility and DNA damage (Aoki et al., 2005; Nanassy et al., 2011), as confirmed by *Prm2*$^{\pm}$ knockouts (Oliva and Dixon, 1991; Cho et al., 2001).

The currently accepted model for chromatin organization in mammalian sperm purports that protamine-DNA complex forms toroidal structures, which condense about 48 kb of DNA, and are estimated to measure between 60 and 100 nm in diameter and 20 nm in thickness (Brewer et al., 1999, 2003; Miller et al., 2010). These toroidal structures are stabilized by disulfide covalent bonds between neighbor protamines, and are linked through uncoiled linker DNA in toroid linker regions (TLR). The function of TLR is to attach the chromatin to the nuclear matrix and is thus supposed to contain matrix attachment regions (MAR; Ward, 2010). Toroid linker regions are assumed to be condensed in histones containing complex epigenetic information that may play a crucial role in the very early zygote by influencing gene expression after fertilization and during early embryo development (Jung et al., 2017; Yoshida et al., 2018). In

the context of sperm chromatin, localization of histone regions in gene-rich or gene-poor DNA is a subject of much debate among scientists, as different methodologies have been shown to lead to opposite results (Yamaguchi et al., 2018). Moreover, it has been demonstrated that different species may have different percentages of histone-condensed DNA, ranging between 3 and 15% in humans, between 1 and 15% in mouse or even at higher rates (like 50%) in some marsupials (Fuentes-Mascorro et al., 2000; Hammoud et al., 2009; Miller et al., 2010; Samans et al., 2014). Despite the fact that the toroidal DNA and the linker DNA coupled to the nuclear matrix constitute the main unit of chromatin structure, evidences obtained through freeze-fracture, circular dichroism and atomic force microscopy support the presence of a higher superstructure of sperm chromatin, composed by parallel stacks of lamellar sheets oriented to the nuclear long axis in bulls, bucks and men (Koehler et al., 1983; Fuentes-Mascorro et al., 2000). Also, other evidences support a nodular chromatin sub-organization, sized between 100 and 300 nm, in mouse, human, cattle and rat sperm (Allen et al., 1993; Haaf and Ward, 1995). However, the presence of smaller nucleosome-like particles is not discarded, especially in the nuclear periphery (Allen et al., 1996). Regardless of chromatin superorganization, different studies also reported a chromosomal region-specific organization, since centromeres were found to be positioned in the most internal parts of the sperm nucleus, whereas telomeres that remain condensed in histones appeared to attach to the internal nuclear membrane, positioned in the external parts of the nucleus (Zalensky et al., 1997; Mudrak et al., 2005; Zalensky and Zalenskaya, 2007). Moreover, other authors showed that chromosomal territories exist in the sperm nucleus, leading to a precise organization of chromosomal DNA (Luetjens et al., 1999; Zalenskaya and Zalensky, 2004; Foster et al., 2005).

While the high degree of sperm DNA condensation requires protamines to be replaced by histones upon fertilization, it also represents a challenge for the *in vitro* study of sperm chromatin. In this sense, previous studies tested the *in vivo* sperm DNA decondensation of different animal species after microinjection of hamster oocytes; whereas nuclei of human, mouse, chinchilla and hamster sperm were properly decondensed, this was not the case of cattle or rat sperm (Perreault et al., 1988). The same study showed that, while DTT and SDS led to sperm DNA decondensation, incubation with these two agents needed to be 10 times longer in cattle than in human sperm to achieve similar levels of decondensation (Perreault et al., 1988). Nowadays, NaCl is known to be strictly necessary to remove protamines from DNA, a required step to achieve complete DNA decondensation and form sperm haloes of decondensed chromatin, leaving TLR attached to the nuclear matrix (Mohar et al., 2002; Sotolongo et al., 2003).

Different methods require complete sperm DNA decondensation to evaluate DNA breaks. DNA fragmentation assays, such as the SCD test, rely on the differential chromatin decondensation of spermatozoa containing DNA breaks compared to those with non-damaged DNA (Fernández et al., 2003; Cortés-Gutiérrez et al., 2009). Likewise, the Comet assay requires complete DNA decondensation for migration of fragments and the subsequent formation of the Comet tail, and some protocols include incubations with proteinase K overnight (Simon et al., 2014; Ribas-Maynou and Benet, 2019). Even the TUNEL assay has been proposed to display higher sensitivity following mild decondensation with DTT (Mitchell et al., 2011). Decondensation of sperm chromatin is therefore applied to multiple species, with several studies linking DNA breaks to fertility disorders (Pérez-Llano et al., 2010; Gosálvez et al., 2011; Esteves et al., 2020; Ribas-Maynou et al., 2020).

Against this background, this study aimed at comparing the decondensation capacity of sperm DNA between different species, some described to contain both protamine 1 and protamine 2, and others known to have protamine 1 only.

MATERIALS AND METHODS

Reagents

Unless stated, all reagents used for this study were purchased from Sigma-Aldrich (St. Louis, MO, United States).

Sperm Sample Obtaining and Cryopreservation

Human Sperm

Five human semen samples were obtained from healthy volunteers that were recruited by University of Girona, Spain. All donors signed an informed consent before providing their biological samples, and the study was approved by the Ethics Committee, Josep Trueta Hospital, Spain (Reference PTI-HUMA 10012018) thus complying with the Helsinki declaration for the research with human specimens. All men provided a semen sample through ejaculation in a sterile cup. This ejaculation was maintained at 37°C for 30 min and was subsequently cryopreserved.

Cryopreservation was performed using Test Yolk Buffer (TYB, 14% glycerol, 30% egg yolk, 1.98% glucose, 1.72% sodium citrate, and 2% glycine, pH 7.4). Briefly, each semen sample was gently mixed 1:1 (v:v) with TYB, poured into a 0.5-mL cryotube, and cooled down in an isopropyl alcohol bath placed within a −80°C freezer for 12 h. Afterward, cryotubes were transferred to liquid nitrogen. Samples were thawed by submerging cryotubes in a water bath at 37°C, and then diluted with PBS (1:3 dilution), added drop-by-drop in order to avoid osmotic shock.

Pig Sperm

Researchers did not manipulate animals, but semen samples were rather purchased from a local farm (Servicios Genéticos Porcinos, S.L.; Roda de Ter, Spain), which provided commercial, standard doses (90 mL) intended to artificial insemination (AI). A total of five semen samples were obtained from five sexually mature Piétrain boars of proven fertility. Ejaculates were collected using the gloved-hand method, and the sperm rich fraction was diluted to 3.3×10^7 spermatozoa/mL with a long-term commercial extender (Vitasem LD; Magapor SL, Zaragoza, Spain).

Cryopreservation was performed using the following protocol. First, 50-mL aliquots were centrifuged at 2,400 × g and 15°C for 3 min, and sperm suspensions were diluted in β-lactose-egg yolk (LEY) medium (80% v:v lactose, 20% egg yolk) to

a final concentration of 1.5×10^9 sperm/mL. Thereafter, all aliquots were cooled down to a final temperature of 5°C, at a rate of −0.1°C/min. Then, samples were diluted to a final concentration of 1×10^9 sperm/mL in LEYGO medium, which consisted of LEY medium supplemented with 6% v:v glycerol and 1.5% Orvus ES Paste (Equex STM; Nova Chemical Sales Inc., Scituate, MA, United States). Finally, samples were packed into 0.5-mL plastic straws (Minitüb, Tiefenbach, Germany), and a programmable controlled-rate freezer (Ice-Cube, Minitüb) was used to cryopreserve samples at the following cooling rates: 6°C/min from 5 to −5°C (100 s); −39.82°C/min from −5 to −80°C (113 s); holt at −80°C for 30 s; and cooled at −60°C/min from −80 to −150°C (70 s). Samples were finally plunged into liquid nitrogen.

Samples were thawed through submerging a 0.5-mL straw in a 38 °C water bath for 15 s, with shaking. The entire volume of the straw was diluted in three volumes (1:3, v:v) of pre-warmed Beltsville Thawing Solution (BTS).

Horse Sperm

Five cryopreserved straws from five separate animals were used. All stallions were donors of proven fertility, and were housed at the Equine Reproduction Service, Autonomous University of Barcelona (Spain), which is a European Union approved equine semen collection center (Authorization code: ES09RS01E). Semen samples were obtained using a Hannover-type artificial vagina (MiniTüb, Tiefenbach, Germany) that contains a nylon mesh filter to separate the ejaculate gel fraction. The obtained ejaculates were directly diluted (1:5, v:v) in previously warmed (37°C) Kenney buffer (49% glucose, w:v; 24% powdered milk, w:v).

Cryopreservation was performed according to the following protocol: first, samples were centrifuged at 600 × g and 20°C for 15 min. Then, pellets were resuspended in BotuCRYO commercial extender (Botupharma, Botucatu, Brazil) to reach a concentration of 2×10^6 viable sperm/mL. Samples were then packaged into 0.5-mL straws and frozen in a programmable freezer (Ice-Cube) as follows: (i) −0.25°C/min from 20 to 5°C (60 min); (ii) −4.75°C/min from 5 to −90°C (20 min); and (iii) −11.11°C/min from −90 to −120°C (2.7 min). Straws were finally plunged into liquid nitrogen for storage.

Thawing was performed by submerging straws in a water bath at 38°C for 20 s. The volume of each straw was diluted in three volumes of pre-warmed Kenney medium (1:3, v:v).

Donkey Sperm

Five semen samples coming from five different jackasses of proven fertility were used. Animals were located at the Equine Reproduction Service, Autonomous University of Barcelona (Bellaterra, Spain). Semen samples were obtained using a Hannover artificial vagina (Minitüb) with a nylon mesh filter to remove the gel fraction. Immediately after collection, semen was mixed with Kenney extender (1:5, v:v) at 37°C.

For cryopreservation, the following protocol was used: first, diluted semen was centrifuged at 600 × g and 20°C for 15 min, and pellets were resuspended in 2 mL of INRA-freeze freezing extender (INRA, Paris, France). Then, concentration and motility were evaluated, and samples were diluted again to reach a final concentration of 2×10^6 viable sperm/mL. Following this, sperm were packaged into 0.5-mL straws and frozen with a programmable freezer (Ice-Cube, Minitüb) with the following cooling rates: (i) from 20 to 5°C at a rate of −0.25°C/min; (ii) from 5 to −90°C at a rate of −4.75°C/min; and (iii) from −90 to −120°C at a rate of −11.11°C/min. Finally, straws were plunged into liquid nitrogen and stored.

For thawing, straws were submerged in a water bath at 38°C for 20 s, and the content was diluted with three volumes of in 1.5 mL of Kenney medium at 37°C per straw.

Cattle Sperm

Five separate samples from five healthy and sexually mature Holstein bulls were used. All animals were kept in an artificial insemination center (Cenero-Asturias, Gijón, Spain), and ejaculates were collected through an artificial vagina. Collected semen was diluted in Bioxcell extender reaching a concentration of 92×10^6 sperm/mL. Then, samples were cooled down to 4°C at a rate of −0.2°C/min, and after 3 h of equilibration, extended semen was packaged into 0.25-mL straws containing 23×10^6 sperm/straw.

Cryopreservation was performed in a programmable freezer (Digit-cool; IMV Technologies, L'Aigle, France) following the standard curve for bovine sperm: −5°C/min from 4 to −10°C, −40°C/min from −10 to −100°C, and −20°C/min from −100 to −140°C. Thawing was performed by submerging straws in a water bath at 38°C for 40 s, with shaking.

Halo Formation

Halo formation was induced following the same protocol for all species. First, samples were diluted in phosphate-buffered saline (PBS) to reach a final concentration of 1×10^6 sperm/mL. Meanwhile, an aliquot of low melting point agarose at 1% was melted at 70°C for 10 min and warmed to 37.5°C for further 10 min. Next, the sample and low melting point agarose were mixed at a 1:2 (v:v) ratio, obtaining a final agarose concentration of 0.66%. A drop of 6 μL of the mixture was then dispensed onto an agarose pre-treated slide, covered with a 8-mm circular coverslip, and allowed to jellify on a metal cold plate at 4°C for 5 min. Afterward, the coverslip was gently removed and the slide was incubated in a first lysis solution (0.8 M Tris-HCl, 0.8 M DTT, 1% SDS; pH = 7.5) at room temperature for 30 min. Following this, slides were incubated in a second lysis solution (0.4 M Tris-HCl, 0.4 M DTT, 50 mM EDTA, 2 M NaCl, 1% Tween20; pH = 7.5) at room temperature for 30 min. At this point, slides were differentially incubated with a third lysis solution that contained proteinase K (0.4 M Tris-HCl, 0.4 M DTT, 50 mM EDTA, 2 M NaCl, 1% Tween20, 100 μg/mL proteinase K; pH = 7.5). Incubation with this third lysis solution was also performed at room temperature for 0, 30, or 180 min. To assess the effect of incubating pig and cattle sperm with proteinase K, decondensation with a third lysis solution that did not contain proteinase K (0.4 M Tris-HCl, 0.4 M DTT, 50 mM EDTA, 2 M NaCl, 1% Tween20, 100 μg/mL proteinase K; pH = 7.5) was also performed for 0, 30, or 180 min. After all lysis steps, slides were washed with a neutral pH solution (0.4 M Tris-HCl, pH

7.5) for 5 min, and dehydrated in ethanol series (70, 90, and 100%; 2 min/step).

Assessment of DNA Decondensation

Halo and core diameters are used as DNA decondensation indicators. In order to obtain both measures, samples were labeled with Safeview DNA stain (NBS Biologicals, Huntingdon, United Kingdom) prior to evaluation under a Zeiss Imager Z1 epifluorescence microscope (Carl Zeiss AG, Oberkochen, Germany). Captures at 1,000× magnification of at least 50 cells per experimental condition were obtained using Axiovision 4.6 software (Carl Zeiss AG, Oberkochen, Germany). In these captures, exposure time was adapted to correctly differentiate haloes from core sperm heads. From these pictures, diameters of the core and the halo were measured as indicated in **Figure 1**, using the Image J measurement tool. These diameters were obtained in duplicate, and mean values were calculated for each sperm cell. In order to normalize data, a scale bar was used to obtain the correspondence of pixels to μm at the resolution used (1,388 × 1,040 pixels).

Staining of Nuclear DNA in Non-decondensed Sperm Cells

In order to measure the size of nuclear DNA, a sperm sample from each species was smeared onto a glass slide, permeabilized with PBS containing 0.25% Triton X-100 for 2 min, and stained with Safeview DNA stain. Measures of nuclear core were made following the same procedure depicted in **Figure 1**.

Statistics

Data were analyzed using the Statistics Package for the Social Sciences software (IBM SPSS ver. 25; IBM Corp., Armonk, NY, United States). Graphs were drawn using GraphPad Prism Software (GraphPad; San Diego, CA, United States). Once data were recorded and compiled, normal distribution and homogeneity of variances were checked through Shapiro-Wilk and Levene tests. Since, even after linear transformation [log(x), arcsine $\sqrt{x}$, $\sqrt{x}$], data did not fit with parametric assumptions, Scheirer-Ray-Hare and Mann-Whitney tests were run. A significance level of 95% for the confidence interval was established to consider statistically significant differences.

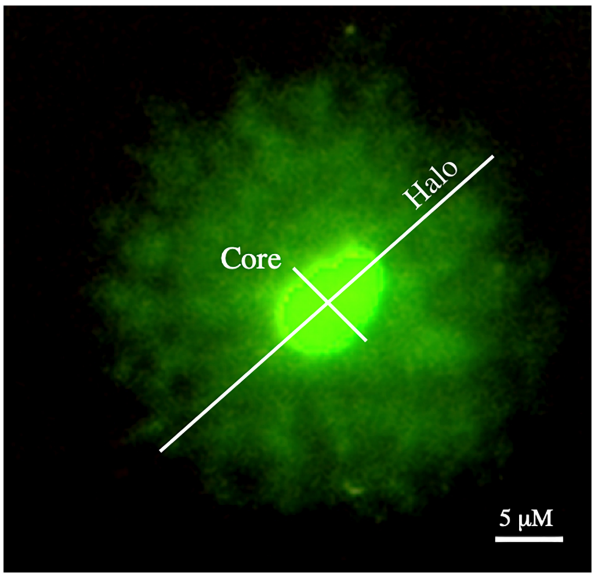

FIGURE 1 | Measurement of core and halo in sperm cells with decondensed chromatin.

RESULTS

Figure 2 shows the formation of sperm haloes in different species, following different incubation times with proteinase K (third lysis step). The application of the third lysis step containing proteinase K had a differential effect on the separate species studied. Whilst human, horse and donkey sperm did not present higher decondensation when incubated with proteinase K for a longer period (third lysis step), pig and cattle sperm showed higher DNA decondensation after incubation with proteinase K and exhibited larger sperm haloes.

Lysis Solutions Used for Halo Formation Induce Nuclear Core Decondensation

Following DNA staining of sperm spreads/smears, dimensions of nuclei were found to be: 4.14 μm ± 0.41 μm (mean ± standard deviation) for human sperm, 3.62 μm ± 0.55 μm for horse sperm, 3.89 μm ± 0.52 μm for donkey sperm, 4.43 μm ± 0.34 μm for pig sperm, and 4.80 μm ± 0.34 μm for cattle sperm. While treatment with lysis solutions that did not contain proteinase K led to chromatin decondensation of sperm core, the extent of that decondensation differed between species. In effect, while, after this step, the cores of human, horse and donkey sperm were 7.11 μm ± 0.96 μm, 5.67 μm ± 0.55 μm, and 5.83 ± 0.35, respectively, they were found to measure 4.98 μm ± 0.50 μm in pig sperm and 4.34 μm ± 0.79 μm in cattle sperm. In spite of this, this increase in the diameter of the core, which indicated DNA decondensation, was statistically significant in all cases (human, $P < 0.001$; horse, $P < 0.001$; donkey, $P < 0.001$; pig, $P < 0.001$; and cattle, $P = 0.004$).

Moreover, nuclear core also showed an increase in decondensation associated to the additional treatment of sperm cells with a lysis solution containing proteinase K (**Table 1**). This increase was statistically significant in horse, donkey, porcine and bovine sperm when comparing 180 min of incubation with 0 min of incubation ($P < 0.05$); and in human, porcine and bovine sperm when comparing 180 min of incubation with 30 min of incubation ($P < 0.05$).

Prolonged Lysis Incubation Contributes to Higher Efficiency in Protamine Removal

Table 1 shows the effect of incubation in the third lysis solution containing proteinase K on halo diameter. We observed that

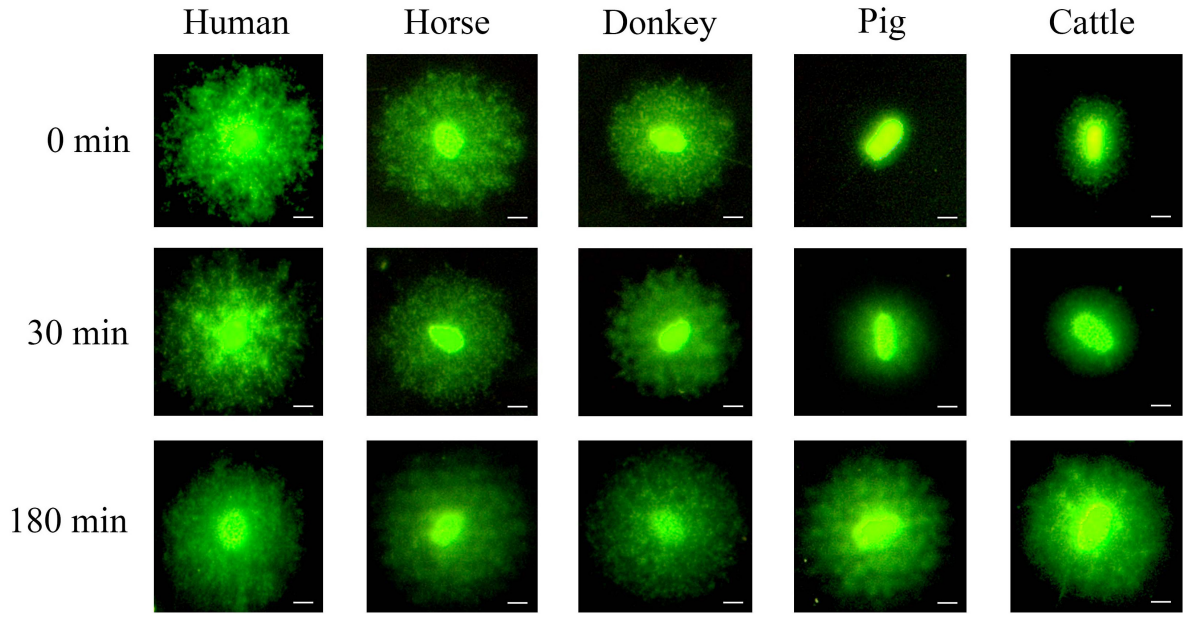

FIGURE 2 | Decondensation of sperm DNA through the formation of sperm haloes. It is worth noting that porcine and bovine sperm presented higher DNA decondensation with increasing incubation times over the third lysis step containing proteinase K. In contrast, no significant changes in human, horse and donkey sperm were observed. Scale bar: 5 μm.

TABLE 1 | Effect of the third lysis solution containing proteinase K on halo and core diameter in different species.

	Incubation time (min)	Human	Horse	Donkey	Pig	Cattle
Core with (μm)	0	7.11 ± 0.96	5.67 ± 0.55	5.83 ± 0.35	4.98 ± 0.50	4.34 ± 0.79
	30	6.62 ± 1.17	6.92 ± 0.58[a]	6.32 ± 0.64	5.28 ± 0.39	6.05 ± 0.58[a]
	180	8.19 ± 0.98[b]	6.96 ± 1.60[a]	7.15 ± 0.79[a]	6.37 ± 0.61[a,b]	7.16 ± 1.01[a,b]
Halo + core diameter (μm)	0	32.45 ± 0.86	22.91 ± 1.46	25.18 ± 3.67	8.62 ± 1.04	10.36 ± 3.71
	30	27.74 ± 2.54[a]	30.28 ± 1.39[a]	24.55 ± 2.78	15.87 ± 1.32[a]	20.15 ± 3.22[a]
	180	37.76 ± 1.46[a,b]	30.69 ± 2.41[a]	29.32 ± 2.82[b]	25.81 ± 1.53[a,b]	29.17 ± 2.50[a,b]
Halo/Core ratio	0	4.68 ± 0.51	4.15 ± 0.47	4.40 ± 0.64	1.77 ± 0.20	2.40 ± 0.40
	30	4.32 ± 0.51	4.57 ± 0.53	4.00 ± 0.37	3.05 ± 0.14[a]	3.36 ± 0.22[a]
	180	4.77 ± 0.64	4.68 ± 0.63	4.17 ± 0.19	4.13 ± 0.39[a,b]	4.19 ± 0.38[a,b]

[a] *Statistical differences with respect to incubation with proteinase K for 0 min (P<0.05).*
[b] *Statistical differences with respect to incubation with proteinase K for 30 min (P<0.05).*

exposure to proteinase K led to higher halo diameters in all species. In effect, there was a significant ($P < 0.05$) increase in halo diameters of human, horse, pig and cattle sperm, when 0 and 180 min of incubation were compared. Furthermore, 180-min incubations compared to their 30-min counterparts also showed a significant increase in halo diameters of human, donkey, pig and cattle sperm ($P < 0.05$). However, and in spite of these significant differences, the extent of the increase of halo diameter in porcine and bovine sperm was much higher (**Table 1**).

The Halo/Core Ratio Reflects the Decondensation Status of a Sperm DNA

Since both sperm haloes and cores showed an increased size associated to proteinase K lysis treatment, the relationship between halo size and core size appeared to be an indicator of sperm DNA decondensation. **Figure 3** and **Table 1** show the halo/core ratio for all species involved in this study. Interestingly, while human, horse and donkey sperm did not exhibit an increase in halo/core ratios associated to longer proteinase k treatments ($P > 0.05$), these ratios augmented in porcine and bovine sperm (0 min vs. 30 min; 30 min vs. 180 min; $P < 0.05$).

The Inclusion of Proteinase K in the Third Lysis Solution Accelerates DNA Decondensation

To determine the importance of including proteinase K in the third lysis solution, we tested DNA decondensation in pig and cattle sperm after incubation with the same lysis solution without proteinase K for 30 and 180 min. **Table 2** shows core diameter, halo diameter and halo/core ratio after such incubations. **Figure 4** depicts halo/core ratio as a measure of DNA decondensation. When proteinase K was included, halo diameter significantly increased both in pig and cattle sperm after 30 and 180 min of incubation ($P < 0.001$). Similarly, all tested conditions also augmented halo/core ratios in both species ($P < 0.001$).

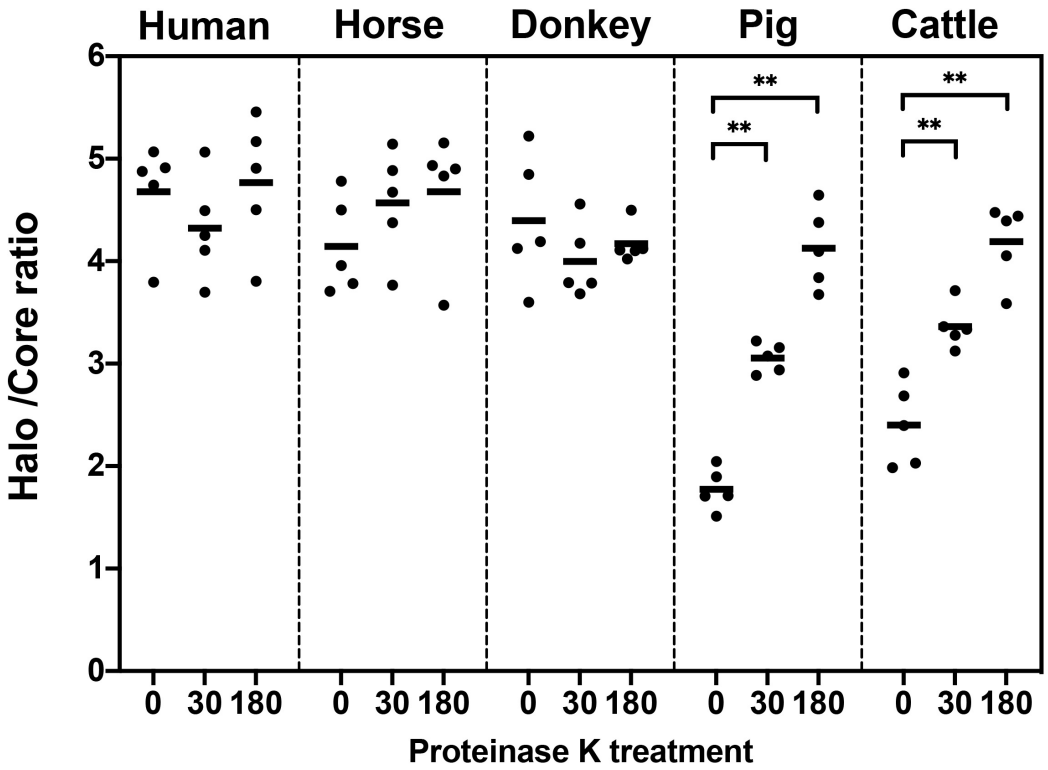

FIGURE 3 | Halo/core ratio in relation to proteinase K treatment (0, 30, or 180 min). **Statistically significant differences ($P < 0.05$).

TABLE 2 | DNA decondensation of pig and cattle sperm after incubation in the third lysis solution with or without proteinase K.

		Pig		Cattle	
	Incubation time (min)	**− Proteinase K**	**+ Proteinase K**	**− Proteinase K**	**+ Proteinase K**
Core with (μm)	0	4.85 ± 0.85		4.22 ± 0.95	
	30	5.30 ± 0.57	5.20 ± 0.81	6.01 ± 1.03	5.95 ± 0.91
	180	4.80 ± 0.53	6.24 ± 0.91**	6.63 ± 0.68	7.02 ± 1.38*
Halo + core diameter (μm)	0	8.37 ± 8.37		9.87 ± 9.87	
	30	10.99 ± 10.99	15.49 ± 15.49**	16.20 ± 16.20	19.54 ± 19.54**
	180	14.92 ± 14.92	25.63 ± 25.63**	21.40 ± 21.40	28.83 ± 28.83**
Halo/Core ratio	0	1.76 ± 0.35		2.38 ± 0.62	
	30	2.10 ± 0.37	3.04 ± 0.54**	2.75 ± 0.51	3.32 ± 0.50**
	180	3.13 ± 0.45	4.19 ± 0.72**	3.26 ± 0.45	4.23 ± 0.74**

**Statistical differences with respect to incubation without proteinase K (P<0.05).*
***Statistical differences with respect to incubation without proteinase K (P<0.001).*

DISCUSSION

In the present study, we observed complete decondensation of sperm DNA when samples were exposed to a lysis solution containing proteinase K for a long period (up to 180 min). We found inter-specific differences regarding sperm chromatin decondensation following that lysis treatment since, while human, horse and donkey sperm did not effectively augment their DNA decondensation, pig and cattle sperm achieved a 2.3- and 1.75-fold increase, respectively (based on halo/core ratios). Moreover, in an additional experiment, we could establish that proteinase K accelerates DNA decondensation in pig and cattle sperm.

A high DNA condensation up to almost crystalline state is a key feature that is only present in paternal germ cells and allows them to transport the male genome through the female tract to reach the oocyte. This highly condensed state helps in the protection of sperm cells from genotoxic damage to which they are exposed (Adiga et al., 2007; Marchetti et al., 2015). Due to their transcriptional silence and the loss of most of their cytoplasmic proteins, sperm cells are devoid of DNA repair systems; however, they are continuously exposed to exogenous and endogenous DNA damage, caused mainly through oxidative stress (Aitken and De Iuliis, 2007). Not only are reactive oxygen species produced by sperm mitochondria through oxidative phosphorylation, which is essential for ATP generation

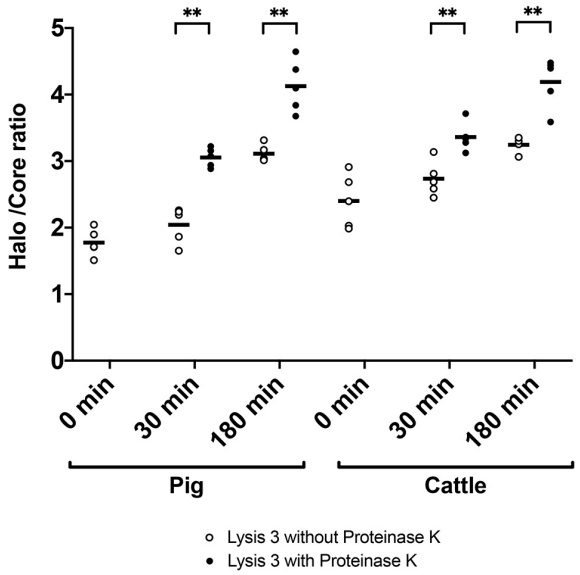

FIGURE 4 | Halo/core ratios for incubations (0, 30, or 180 min) of pig and cattle sperm in the third lysis solution without (empty dots) or with proteinase K (filled dots). **Statistically significant differences ($P < 0.001$).

(Camello-Almaraz et al., 2006), but can also result from the presence of immature sperm, leucocytes, and other exogenous effectors, such as pollutants, heat stress, infections, radiations, or other toxicants (Agarwal et al., 2008; Ribas-Maynou et al., 2020).

Different methods that indirectly evaluate DNA integrity are based on the differential decondensation of sperm cells that contain DNA breaks. In this context, *in vitro* DNA decondensation is required in order for external and internal chromatin to be accessible. As previous studies showed, methods evaluating sperm DNA integrity differ in their sensitivity to detect the actual DNA damage (Ribas-Maynou et al., 2013; Simon et al., 2014). In this regard, achieving complete *in vitro* DNA decondensation is critical to increase the sensitivity of methods evaluating its integrity, thus allowing researchers to obtain reliable values of DNA damage. In fact, some authors explained the low sensitivity of techniques assessing DNA integrity through the hypothesis of "the iceberg tip," which surmises that, while some sperm detected as "normal" actually have DNA breaks, they are out of the method threshold (Gosálvez et al., 2013; Cho et al., 2017).

In the present study, we found that pig and cattle sperm present higher grade of DNA condensation, which is related to an increased difficulty to achieve its complete decondensation *in vitro* and form a sperm halo in an agarose matrix (**Figure 2**). In pigs, previous studies using the SCD test considered that sperm with non-fragmented DNA lacked a halo, whereas those with fragmented DNA showed a large halo (Enciso et al., 2006; Alkmin et al., 2013; Batista et al., 2016). As shown for pig sperm after 0 min of incubation in the third lysis solution containing proteinase K (**Figure 2**), the lack of halo identified in other studies (Enciso et al., 2006) could be due to an incomplete DNA decondensation. Therefore, when complete DNA decondensation was achieved following incubation in the third lysis solution containing proteinase K for 180 min, sperm with non-fragmented DNA showed large halos, as occurs when the halo assay is used with human sperm (Fernández et al., 2005). Remarkably, our results showed that complete sperm DNA decondensation is more easily achieved in the human than in the pig. In effect, in order for similar levels of decondensed DNA to be obtained, pig sperm were observed to need a longer lysis treatment with proteinase K. In fact, proteinase K was found to act as a DNA decondensation accelerator, probably because it degrades protamines extracted by the lysis buffer (**Figure 4**). Previous studies using the SCD test in pig sperm lysed for 5 min, regardless of the composition of solutions (Enciso et al., 2006; Alkmin et al., 2013; Yeste et al., 2013a,b; Batista et al., 2016), are in agreement with our results. In a similar way, using the Comet assay in pig sperm without a long lysis containing proteinase K has also been suggested to lead to sensitivity-compromised results (Pérez-Llano et al., 2010; Enciso et al., 2011). Also matching with our data, a previous study aimed at elucidating alkaline labile sites in pig sperm showed the need of incubating these cells in a lysis solution containing SDS, DTT and proteinase K for 3.5 h at 37°C to observe the same amount of those sites in leukocytes from the same species (Cortés-Gutiérrez et al., 2009). Furthermore, other authors incubated pig sperm with lysis solutions containing proteinase K and found that Comet images depicted complete DNA decondensation (Fraser and Strzezek, 2005).

Regarding the analysis of sperm DNA integrity in cattle, previous studies showed that sperm with non-fragmented DNA depicted small halos, whereas those with fragmented DNA presented big halos, which was in agreement with what found in pigs (García-Macías et al., 2007; Dogan et al., 2015). Our results also indicated that bovine sperm exhibited a small halo when either not exposed or shortly exposed to proteinase K for 30 min. However, when the time of incubation with proteinase K increased, sperm chromatin of bovine sperm completely decondensed, in a similar fashion to what observed in other species (**Figure 3**). Thus, our results confirm that proteinase K acts as an accelerator of DNA decondensation, and suggest that previous studies evaluating DNA fragmentation in bovine sperm could not have decondensed DNA enough, since the lysis period was, regardless of the solutions used, short (10 min) (García-Macías et al., 2007; Dogan et al., 2015). The use of the Comet assay in cattle sperm also demonstrated that longer lysis treatments increased the degree of DNA decondensation (Villani et al., 2010). However, it remains unclear whether exposure to lysis solutions overnight in Fraser and Strzezek (2005) could have induced artifactual DNA breaks, thus misestimating the actual results.

It is widely known that sperm DNA in humans and horses is condensed around both protamine 1 and protamine 2, whereas only protamine 1 but not protamine 2 is present in the chromatin of pig and cattle sperm (Corzett et al., 2002). Moreover, morphometric studies indicated that pig and cattle sperm display a bigger disk-shaped nucleus, whereas human and horse sperm are smaller and more oval-shaped (Gu et al., 2019).

Our results on the resilience of sperm DNA to decondensation in the aforementioned species suggest that while sperm containing only protamine 1 display less efficiency in condensing their DNA, they have stronger protamine-protamine junctions. In fact, protamine 1 in pig sperm displays the highest number of cysteine residues (10 residues) compared to other species, such as donkey (8 residues), horse (7 residues) or human (6 residues), which would support the relevance of disulfide bonds between protamines in the pig (Gosálvez et al., 2011). Furthermore, bovine protamine 1 has less cysteine residues (7 residues) than its pig counterpart, which could explain the less degree of DNA decondensation observed at 0 min of incubation with the third lysis solution (Gosálvez et al., 2011). Alternatively, sperm from species containing both P1 and P2 appear to exhibit higher DNA condensation, with the contraindication of having less protamine-protamine unions, as different protamines from P2 family have less cysteine residues than P1 (Corzett et al., 2002; Oliva, 2006). Moreover, when the number cysteine residues of P1 is related to the P1/P2 ratio, the amount of cysteine residues in sperm chromatin (cysteine residues of P1 × %P1) in each species appears to be linked to the degree of DNA condensation (halo/core ratio) after 0 min of incubation with the third lysis solution (**Supplementary Table 1**). All the aforementioned could also explain why alterations in the relative amounts of protamine 2 lead to higher sperm DNA decondensation, and underlie DNA damage and infertility (Aoki et al., 2005; García-Peiró et al., 2011; Nanassy et al., 2011).

CONCLUSION

In conclusion, long lysis treatment of porcine and bovine sperm is required for complete sperm DNA decondensation in these species. This is not necessary for human, horse and donkey sperm, as lysis solutions used in previous studies led to complete DNA decondensation without any additional treatment. Moreover, we observed that the inclusion of proteinase K accelerates DNA decondensation. Thus, we hypothesize that the species-specific differences in the resilience of sperm DNA to decondensation rely upon whether sperm DNA is condensed around protamine 1 and protamine 2, or around protamine 1 only.

DATA AVAILABILITY STATEMENT

The original contributions presented in the study are included in the article/**Supplementary Material**, further inquiries can be directed to the corresponding author/s.

ETHICS STATEMENT

The studies involving human participants were reviewed and approved by the Josep Trueta Hospital Ethics Committee (Reference PTI-HUMA 10012018). The patients/participants provided their written informed consent to participate in this study.

AUTHOR CONTRIBUTIONS

JR-M conceived the study, performed the experiments, analyzed the data, run statistics, wrote the manuscript, and approved the final version. EG-B performed the experiments, critically revised the document, and approved the final version. CH, JC, and JM cryopreserved semen samples, critically revised the manuscript, and approved the final document. MY contributed to the experimental design, coordinated the work, discussed results, critically revised the manuscript, and approved the final document. All authors contributed to the article and approved the submitted version.

FUNDING

The authors acknowledge the support from the Ministry of Science and Innovation, Spain (Grant No. AGL2017-88329-R), the Regional Government of Catalonia, Spain (Grant No. 2017-SGR-1229), la Marató de TV3 (Grant No. 214/857-202039), and University of Girona (Postdoc UdG-2020, to JR-M).

SUPPLEMENTARY MATERIAL

The Supplementary Material for this article can be found online at: https://www.frontiersin.org/articles/10.3389/fcell.2021.669182/full#supplementary-material

REFERENCES

Adiga, S. K., Toyoshima, M., Shiraishi, K., Shimura, T., Takeda, J., Taga, M., et al. (2007). p21 provides stage specific DNA damage control to preimplantation embryos. *Oncogene* 26, 6141–6149. doi: 10.1038/sj.onc.1210444

Agarwal, A., Makker, K., and Sharma, R. (2008). Clinical relevance of oxidative stress in male factor infertility: an update. *Am. J. Reprod. Immunol.* 59, 2–11. doi: 10.1111/j.1600-0897.2007.00559.x

Aitken, R. J., and De Iuliis, G. N. (2007). Origins and consequences of DNA damage in male germ cells. *Reprod. Biomed. Online* 14, 727–733.

Ajduk, A., Yamauchi, Y., and Ward, M. A. (2006). Sperm chromatin remodeling after intracytoplasmic sperm injection differs from that of in vitro fertilization. *Biol. Reprod.* 75, 442–451. doi: 10.1095/biolreprod.106.053223

Alkmin, D. V., Martinez-Alborcia, M. J., Parrilla, I., Vazquez, J. M., Martinez, E. A., and Roca, J. (2013). The nuclear DNA longevity in cryopreserved boar spermatozoa assessed using the Sperm-Sus-Halomax. *Theriogenology* 79, 1294–1300. doi: 10.1016/j.theriogenology.2013.02.026

Allen, M. J., Bradbury, E. M., and Balhorn, R. (1996). The chromatin structure of well-spread demembranated sperm nuclei revealed by atomic force microscopy. *Scanning Microsc.* 10, 989–996.

Allen, M. J., Lee, C., Lee, J. D., Pogany, G. C., Balooch, M., Siekhaus, W. J., et al. (1993). Atomic force microscopy of mammalian sperm chromatin. *Chromosoma* 102, 623–630. doi: 10.1007/BF00352310

Aoki, V. W., Moskovtsev, S. I., Willis, J., Liu, L., Mullen, J. B. M., and Carrell, D. T. (2005). DNA integrity is compromised in protamine-deficient human sperm. *J. Androl.* 26, 741–748. doi: 10.2164/jandrol.05063

Balhorn, R. (1982). A model for the structure of chromatin in mammalian sperm. *J. Cell Biol.* 93, 298–305.

Batista, C., van Lier, E., and Petrocelli, H. (2016). Dynamics of sperm DNA fragmentation in raw boar semen and fertility. *Reprod. Domest. Anim.* 51, 774–780. doi: 10.1111/rda.12749

Brewer, L., Corzett, M., Lau, E. Y., and Balhorn, R. (2003). Dynamics of protamine 1 binding to single DNA molecules. *J. Biol. Chem.* 278, 42403–42408. doi: 10.1074/jbc.M303610200

Brewer, L. R., Corzett, M., and Balhorn, R. (1999). Protamine-induced condensation and decondensation of the same DNA molecule. *Science* 286, 120–123.

Camello-Almaraz, C., Gomez-Pinilla, P. J., Pozo, M. J., and Camello, P. J. (2006). Mitochondrial reactive oxygen species and Ca2+ signaling. *Am. J. Physiol. Cell Physiol.* 291, C1082–C1088. doi: 10.1152/ajpcell.00217.2006

Cho, C., Willis, W. D., Goulding, E. H., Jung-Ha, H., Choi, Y. C., Hecht, N. B., et al. (2001). Haploinsufficiency of protamine-1 or -2 causes infertility in mice. *Nat. Genet.* 28, 82–86. doi: 10.1038/ng0501-82

Cho, C.-L., Agarwal, A., Majzoub, A., and Esteves, S. C. (2017). The correct interpretation of sperm DNA fragmentation test. *Transl. Androl. Urol.* 6, S621–S623. doi: 10.21037/tau.2017.06.25

Cortés-Gutiérrez, E. I., Crespo, F., Serres-Dalmau, C., Gutiérrez de las Rozas, A. L., Dávila-Rodríguez, M. I., López-Fernández, C., et al. (2009). Assessment of sperm DNA fragmentation in stallion (*Equus caballus*) and donkey (*Equus asinus*) using the sperm chromatin dispersion test. *Reprod. Domest. Anim.* 44, 823–828. doi: 10.1111/j.1439-0531.2008.01091.x

Corzett, M., Mazrimas, J., and Balhorn, R. (2002). Protamine 1: protamine 2 stoichiometry in the sperm of eutherian mammals. *Mol. Reprod. Dev.* 61, 519–527. doi: 10.1002/mrd.10105

Dogan, S., Vargovic, P., Oliveira, R., Belser, L. E., Kaya, A., Moura, A., et al. (2015). Sperm protamine-status correlates to the fertility of breeding bulls. *Biol. Reprod.* 92:92. doi: 10.1095/biolreprod.114.124255

Enciso, M., Johnston, S. D., and Gosálvez, J. (2011). Differential resistance of mammalian sperm chromatin to oxidative stress as assessed by a two-tailed comet assay. *Reprod. Fertil. Dev.* 23, 633–637. doi: 10.1071/RD10269

Enciso, M., López-Fernández, C., Fernández, J. L., García, P., Gosálbez, A., and Gosálvez, J. (2006). A new method to analyze boar sperm DNA fragmentation under bright-field or fluorescence microscopy. *Theriogenology* 65, 308–316. doi: 10.1016/j.theriogenology.2005.05.044

Esteves, S. C., Zini, A., Coward, R. M., Evenson, D. P., Gosálvez, J., Lewis, S. E. M., et al. (2020). Sperm DNA fragmentation testing: summary evidence and clinical practice recommendations. *Andrologia* 53:e13874. doi: 10.1111/and.13874

Fernández, J. L., Muriel, L., Goyanes, V., Segrelles, E., Gosálvez, J., Enciso, M., et al. (2005). Simple determination of human sperm DNA fragmentation with an improved sperm chromatin dispersion test. *Fertil. Steril.* 84, 833–842. doi: 10.1016/j.fertnstert.2004.11.089

Fernández, J. L., Muriel, L., Rivero, M. T., Goyanes, V., Vazquez, R., and Alvarez, J. G. (2003). The sperm chromatin dispersion test: a simple method for the determination of sperm DNA fragmentation. *J. Androl.* 24, 59–66. doi: 10.1002/j.1939-4640.2003.tb02641.x

Foster, H. A., Abeydeera, L. R., Griffin, D. K., and Bridger, J. M. (2005). Non-random chromosome positioning in mammalian sperm nuclei, with migration of the sex chromosomes during late spermatogenesis. *J. Cell Sci.* 118, 1811–1820. doi: 10.1242/jcs.02301

Fraser, L., and Strzezek, J. (2005). Effects of freezing-thawing on DNA integrity of boar spermatozoa assessed by the neutral comet assay. *Reprod. Domest. Anim.* 40, 530–536. doi: 10.1111/j.1439-0531.2005.00626.x

Fuentes-Mascorro, G., Serrano, H., and Rosado, A. (2000). Sperm chromatin. *Arch. Androl.* 45, 215–225.

García-Macías, V., de Paz, P., Martinez-Pastor, F., Alvarez, M., Gomes-Alves, S., Bernardo, J., et al. (2007). DNA fragmentation assessment by flow cytometry and sperm-bos-halomax (bright-field microscopy and fluorescence microscopy) in bull sperm. *Int. J. Androl.* 30, 88–98. doi: 10.1111/j.1365-2605.2006.00723.x

García-Peiró, A., Martínez-Heredia, J., Oliver-Bonet, M., Abad, C., Amengual, M. J., Navarro, J., et al. (2011). Protamine 1 to protamine 2 ratio correlates with dynamic aspects of DNA fragmentation in human sperm. *Fertil. Steril.* 95, 105–109. doi: 10.1016/j.fertnstert.2010.06.053

Getzenberg, R. H. (1994). Nuclear matrix and the regulation of gene expression: tissue specificity. *J. Cell. Biochem.* 55, 22–31. doi: 10.1002/jcb.240550105

Gibson, B. A., Doolittle, L. K., Schneider, M. W. G., Jensen, L. E., Gamarra, N., Henry, L., et al. (2019). Organization of chromatin by intrinsic and regulated phase separation. *Cell* 179, 470–484. doi: 10.1016/j.cell.2019.08.037

Gosálvez, J., Caballero, P., López-Fernández, C., Ortega, L., Guijarro, J. A., Fernández, J. L., et al. (2013). Can DNA fragmentation of neat or swim-up spermatozoa be used to predict pregnancy following ICSI of fertile oocyte donors? *Asian J. Androl.* 15, 812–818. doi: 10.1038/aja.2013.74

Gosálvez, J., López-Fernández, C., Fernández, J. L., Gouraud, A., and Holt, W. V. (2011). Relationships between the dynamics of iatrogenic DNA damage and genomic design in mammalian spermatozoa from eleven species. *Mol. Reprod. Dev.* 78, 951–961. doi: 10.1002/mrd.21394

Gu, N.-H., Zhao, W.-L., Wang, G.-S., and Sun, F. (2019). Comparative analysis of mammalian sperm ultrastructure reveals relationships between sperm morphology, mitochondrial functions and motility. *Reprod. Biol. Endocrinol.* 17:66. doi: 10.1186/s12958-019-0510-y

Haaf, T., and Ward, D. (1995). Higher order nuclear structure in mammalian sperm revealed by in situ hybridization and extended chromatin fibers. *Exp. Cell Res.* 219, 604–611. doi: 10.1006/EXCR.1995.1270

Hammoud, S. S., Nix, D. A., Zhang, H., Purwar, J., Carrell, D. T., and Cairns, B. R. (2009). Distinctive chromatin in human sperm packages genes for embryo development. *Nature* 460, 473–478. doi: 10.1038/nature08162

Hao, S.-L., Ni, F.-D., and Yang, W.-X. (2019). The dynamics and regulation of chromatin remodeling during spermiogenesis. *Gene* 706, 201–210. doi: 10.1016/j.gene.2019.05.027

Ji, L., Xu, R., Lu, L., Zhang, J., Yang, G., Huang, J., et al. (2013). TM6, a novel nuclear matrix attachment region, enhances its flanking gene expression through influencing their chromatin structure. *Mol. Cells* 36, 127–137. doi: 10.1007/s10059-013-0092-z

Jung, Y. H., Sauria, M. E. G., Lyu, X., Cheema, M. S., Ausio, J., Taylor, J., et al. (2017). Chromatin states in mouse sperm correlate with embryonic and adult regulatory landscapes. *Cell Rep.* 18, 1366–1382. doi: 10.1016/j.celrep.2017.01.034

Kierszenbaum, A. L. (2001). Transition nuclear proteins during spermiogenesis: unrepaired DNA breaks not allowed. *Mol. Reprod. Dev.* 58, 357–358.

Koehler, J. K., Würschmidt, U., and Larsen, M. P. (1983). Nuclear and chromatin structure in rat spermatozoa. *Gamete Res.* 8, 357–370. doi: 10.1002/mrd.1120080406

Lee, K., Haugen, H. S., Clegg, C. H., and Braun, R. E. (1995). Premature translation of protamine 1 mRNA causes precocious nuclear condensation and arrests spermatid differentiation in mice. *Proc. Natl. Acad. Sci. U. S. A.* 92, 12451–12455. doi: 10.1073/pnas.92.26.12451

Lewis, S. E. M., and Simon, L. (2010). Clinical implications of sperm DNA damage. *Hum. Fertil.* 13, 201–207. doi: 10.3109/14647273.2010.528823

Linnemann, A. K., Platts, A. E., and Krawetz, S. A. (2009). Differential nuclear scaffold/matrix attachment marks expressed genes. *Hum. Mol. Genet.* 18, 645–654. doi: 10.1093/hmg/ddn394

Luetjens, C. M., Payne, C., and Schatten, G. (1999). Non-random chromosome positioning in human sperm and sex chromosome anomalies following intracytoplasmic sperm injection. *Lancet* 353:1240. doi: 10.1016/S0140-6736(99)80059-2

Luger, K., Mäder, A. W., Richmond, R. K., Sargent, D. F., and Richmond, T. J. (1997). Crystal structure of the nucleosome core particle at 2.8 A resolution. *Nature* 389, 251–260. doi: 10.1038/38444

Makker, K., Agarwal, A., and Sharma, R. (2009). Oxidative stress & male infertility. *Indian J. Med. Res.* 129, 357–367.

Marchetti, F., Bishop, J., Gingerich, J., and Wyrobek, A. J. (2015). Meiotic interstrand DNA damage escapes paternal repair and causes chromosomal aberrations in the zygote by maternal misrepair. *Sci. Rep.* 5:7689. doi: 10.1038/srep07689

Miller, D., Brinkworth, M., and Iles, D. (2010). Paternal DNA packaging in spermatozoa: more than the sum of its parts? DNA, histones, protamines and epigenetics. *Reproduction* 139, 287–301. doi: 10.1530/REP-09-0281

Mitchell, L. A., De Iuliis, G. N., and Aitken, R. J. (2011). The TUNEL assay consistently underestimates DNA damage in human spermatozoa and is influenced by DNA compaction and cell vitality: development of an improved methodology. *Int. J. Androl.* 34, 2–13. doi: 10.1111/j.1365-2605.2009.01042.x

Mohar, I., Szczygiel, M. A., Yanagimachi, R., and Ward, W. S. (2002). Sperm nuclear halos can transform into normal chromosomes after injection into oocytes. *Mol. Reprod. Dev.* 62, 416–420. doi: 10.1002/mrd.10147

Mudrak, O., Tomilin, N., and Zalensky, A. (2005). Chromosome architecture in the decondensing human sperm nucleus. *J. Cell Sci.* 118, 4541–4550. doi: 10.1242/jcs.02581

Nanassy, L., Liu, L., Griffin, J., and Carrell, D. T. (2011). The clinical utility of the protamine 1/protamine 2 ratio in sperm. *Protein Pept. Lett.* 18, 772–777.

Narwade, N., Patel, S., Alam, A., Chattopadhyay, S., Mittal, S., and Kulkarni, A. (2019). Mapping of scaffold/matrix attachment regions in human genome: a data mining exercise. *Nucleic Acids Res.* 47, 7247–7261. doi: 10.1093/nar/gkz562

Oliva, R. (2006). Protamines and male infertility. *Hum. Reprod. Update* 12, 417–435. doi: 10.1093/humupd/dml009

Oliva, R., and Dixon, G. H. (1991). Vertebrate protamine genes and the histone-to-protamine replacement reaction. *Prog. Nucleic Acid Res. Mol. Biol.* 40, 25–94. doi: 10.1016/s0079-6603(08)60839-9

Pérez-Llano, B., López-Fernández, C., García-Casado, P., Arroyo, F., Gosalbez, A., Sala, R., et al. (2010). Dynamics of sperm DNA fragmentation in the swine: ejaculate and temperature effects. *Anim. Reprod. Sci.* 119, 235–243. doi: 10.1016/j.anireprosci.2010.01.002

Perreault, S. D., Barbee, R. R., Elstein, K. H., Zucker, R. M., and Keefer, C. L. (1988). Interspecies differences in the stability of mammalian sperm nuclei assessed in vivo by sperm microinjection and in vitro by flow cytometry. *Biol. Reprod.* 39, 157–167. doi: 10.1095/biolreprod39.1.157

Peschon, J. J., Behringer, R. R., Palmiter, R. D., and Brinster, R. L. (1989). Expression of mouse protamine 1 genes in transgenic mice. *Ann. N. Y. Acad. Sci.* 564, 186–197. doi: 10.1111/j.1749-6632.1989.tb25897.x

Rao, S. S. P., Huntley, M. H., Durand, N. C., Stamenova, E. K., Bochkov, I. D., Robinson, J. T., et al. (2014). A 3D map of the human genome at kilobase resolution reveals principles of chromatin looping. *Cell* 159, 1665–1680. doi: 10.1016/J.CELL.2014.11.021

Ribas-Maynou, J., and Benet, J. (2019). Single and double strand sperm DNA damage: different reproductive effects on male fertility. *Genes* 10:105. doi: 10.3390/genes10020105

Ribas-Maynou, J., García-Peiró, A., Fernández-Encinas, A., Abad, C., Amengual, M. J. J., Prada, E., et al. (2013). Comprehensive analysis of sperm DNA fragmentation by five different assays: TUNEL assay, SCSA, SCD test and alkaline and neutral comet assay. *Andrology* 1, 715–722. doi: 10.1111/j.2047-2927.2013.00111.x

Ribas-Maynou, J., Yeste, M., and Salas-Huetos, A. (2020). The relationship between sperm oxidative stress alterations and IVF/ICSI outcomes: a systematic review from nonhuman mammals. *Biology* 9, 1–18. doi: 10.3390/biology9070178

Samans, B., Yang, Y., Krebs, S., Sarode, G. V., Blum, H., Reichenbach, M., et al. (2014). Uniformity of nucleosome preservation pattern in mammalian sperm and its connection to repetitive DNA elements. *Dev. Cell* 30, 23–35. doi: 10.1016/j.devcel.2014.05.023

Setti, A. S., Braga, D. P., de, A. F., Provenza, R. R., Iaconelli, A., and Borges, E. (2021). Oocyte ability to repair sperm DNA fragmentation: the impact of maternal age on intracytoplasmic sperm injection outcomes. *Fertil. Steril.* S0015-0282(20)32617-0. doi: 10.1016/j.fertnstert.2020.10.045 [Epub ahead of print].

Simon, L., Liu, L., Murphy, K., Ge, S., Hotaling, J., Aston, K. I., et al. (2014). Comparative analysis of three sperm DNA damage assays and sperm nuclear protein content in couples undergoing assisted reproduction treatment. *Hum. Reprod.* 29, 904–917. doi: 10.1093/humrep/deu040

Sotolongo, B., Lino, E., and Ward, W. S. (2003). Ability of hamster spermatozoa to digest their own DNA. *Biol. Reprod.* 69, 2029–2035. doi: 10.1095/biolreprod.103.020594

Toyoshima, M. (2009). Analysis of p53 dependent damage response in sperm-irradiated mouse embryos. *J. Radiat. Res.* 50, 11–17.

Villani, P., Eleuteri, P., Grollino, M. G., Rescia, M., Altavista, P., Spanò, M., et al. (2010). Sperm DNA fragmentation induced by DNAse I and hydrogen peroxide: an in vitro comparative study among different mammalian species. *Reproduction* 140, 445–452. doi: 10.1530/REP-10-0176

Ward, W. S. (2010). Function of sperm chromatin structural elements in fertilization and development. *Mol. Hum. Reprod.* 16, 30–36. doi: 10.1093/molehr/gap080

Ward, W. S., and Coffey, D. S. (1991). DNA packaging and organization in mammalian spermatozoa: comparison with somatic cells. *Biol. Reprod.* 44, 569–574.

Wykes, S. M., and Krawetz, S. A. (2003). The structural organization of sperm chromatin. *J. Biol. Chem.* 278, 29471–29477. doi: 10.1074/jbc.M304545200

Yamaguchi, K., Hada, M., Fukuda, Y., Inoue, E., Makino, Y., Katou, Y., et al. (2018). Re-evaluating the localization of sperm-retained histones revealed the modification-dependent accumulation in specific genome regions. *Cell Rep.* 23, 3920–3932. doi: 10.1016/j.celrep.2018.05.094

Yeste, M., Estrada, E., Casas, I., Bonet, S., and Rodríguez-Gil, J. E. (2013a). Good and bad freezability boar ejaculates differ in the integrity of nucleoprotein structure after freeze-thawing but not in ROS levels. *Theriogenology* 79, 929–939. doi: 10.1016/j.theriogenology.2013.01.008

Yeste, M., Flores, E., Estrada, E., Bonet, S., Rigau, T., and Rodríguez-Gil, J. E. (2013b). Reduced glutathione and procaine hydrochloride protect the nucleoprotein structure of boar spermatozoa during freeze-thawing by stabilising disulfide bonds. *Reprod. Fertil. Dev.* 25, 1036–1050. doi: 10.1071/RD12230

Yoshida, K., Muratani, M., Araki, H., Miura, F., Suzuki, T., Dohmae, N., et al. (2018). Mapping of histone-binding sites in histone replacement-completed spermatozoa. *Nat. Commun.* 9:3885. doi: 10.1038/s41467-018-06243-9

Zalenskaya, I. A., and Zalensky, A. O. (2004). Non-random positioning of chromosomes in human sperm nuclei. *Chromosome Res.* 12, 163–173.

Zalensky, A., and Zalenskaya, I. (2007). Organization of chromosomes in spermatozoa: an additional layer of epigenetic information? *Biochem. Soc. Trans.* 35, 609–611. doi: 10.1042/BST0350609

Zalensky, A. O., Tomilin, N. V., Zalenskaya, I. A., Teplitz, R. L., and Bradbury, E. M. (1997). Telomere-telomere interactions and candidate telomere binding protein(s) in mammalian sperm cells. *Exp. Cell Res.* 232, 29–41. doi: 10.1006/excr.1997.3482

Zini, A., and Libman, J. (2006). Sperm DNA damage: clinical significance in the era of assisted reproduction. *CMAJ* 175, 495–500. doi: 10.1503/cmaj.060218

Conflict of Interest: The authors declare that the research was conducted in the absence of any commercial or financial relationships that could be construed as a potential conflict of interest.

frontiers in Cell and Developmental Biology

ORIGINAL RESEARCH
published: 03 May 2021
doi: 10.3389/fcell.2021.670021

Oocyte Meiotic Competence in the Domestic Cat Model: Novel Roles for Nuclear Proteins BRD2 and NPM1

*Daniela R. Chavez, Pei-Chih Lee and Pierre Comizzoli**

Smithsonian Conservation Biology Institute, National Zoological Park, Washington, DC, United States

To participate in fertilization and embryo development, oocytes stored within the mammalian female ovary must resume meiosis as they are arrested in meiotic prophase I. This ability to resume meiosis, known as meiotic competence, requires the tight regulation of cellular metabolism and chromatin configuration. Previously, we identified nuclear proteins associated with the transition from the pre-antral to the antral follicular stage, the time at which oocytes gain meiotic competence. In this study, the objective was to specifically investigate three candidate nuclear factors: bromodomain containing protein 2 (BRD2), nucleophosmin 1 (NPM1), and asparaginase-like 1 (ASRGL1). Although these three factors have been implicated with folliculogenesis or reproductive pathologies, their requirement during oocyte maturation is unproven in any system. Experiments were conducted using different stages of oocytes isolated from adult cat ovaries. The presence of candidate factors in developing oocytes was confirmed by immunostaining. While BRD2 and ASRGL1 protein increased between pre-antral and the antral stages, changes in NPM1 protein levels between stages were not observed. Using protein inhibition experiments, we found that most BRD2 or NPM1-inhibited oocytes were incapable of participating in fertilization or embryo development. Further exploration revealed that inhibition of BRD2 and NPM-1 in cumulus-oocyte-complexes prevented oocytes from maturing to the metaphase II stage. Rather, they remained at the germinal vesicle stage or arrested shortly after meiotic resumption. We therefore have identified novel factors playing critical roles in domestic cat oocyte meiotic competence. The identification of these factors will contribute to improvement of domestic cat assisted reproduction and could serve as biomarkers of meiotically competent oocytes in other species.

Keywords: oocyte, meiotic competence, domestic cat, fertility, germinal vesicle

OPEN ACCESS

Edited by:
Andreina Cesari, Consejo Nacional de Investigaciones Científicas y Técnicas (CONICET), Argentina

Reviewed by:
Jason Herrick, Omaha's Henry Doorly Zoo and Aquarium, United States
Zsolt Gabor Venkei, Whitehead Institute for Biomedical Research, United States

***Correspondence:**
Pierre Comizzoli
Comizzolip@si.edu

Specialty section:
This article was submitted to Cell Growth and Division, a section of the journal Frontiers in Cell and Developmental Biology

Received: *19 February 2021*
Accepted: *12 April 2021*
Published: *03 May 2021*

Citation:
Chavez DR, Lee P-C and Comizzoli P (2021) Oocyte Meiotic Competence in the Domestic Cat Model: Novel Roles for Nuclear Proteins BRD2 and NPM1. Front. Cell Dev. Biol. 9:670021. doi: 10.3389/fcell.2021.670021

INTRODUCTION

Mammalian reproduction relies on oocytes that develop the exclusive capacity to participate in fertilization and support early embryo development. The pool of early stage oocytes within the female ovary suspend development at birth, and remain in meiotic prophase I, also called the germinal vesicle (GV) stage. At this stage, oocytes are incapable of fertilization until hormonal cyclicity begins, when GV oocytes can resume meiosis and mature before fertilization. The ability to exit meiotic prophase I and resume meiosis is known as meiotic competence, which is gained

when oocytes develop from the immature pre-antral stage to the antral stage. During this transition, oocytes grow in size, and store critical proteins and nutrients needed for meiotic resumption, all of which is critical to sexual reproduction (Coticchio et al., 2015).

Important cellular maturation events occur in the nucleus and cytoplasm of oocytes during meiotic maturation. These events include chromatin condensation during germinal vesicle breakdown (GVBD), chromatin modifications and remodeling, chromosome segregation mediated by the meiotic spindle, polar body extrusion, changes to the cytoplasmic metabolic environment and cell-cell signaling with adjacent somatic cells. Each of these events is critical to sustain such a large cell through fertilization and early embryo development (Coticchio et al., 2015; Clarke, 2018; Conti and Franciosi, 2018). Importantly, the GV oocyte accomplishes these processes almost exclusively without new transcription and relies on stored RNA to generate the proteins required for these processes. Thus, the GV oocyte is fully loaded with the cellular machinery and proteins required to perform these dramatic changes.

To increase our knowledge of oocyte development, our laboratory, as well as other research teams, have used the domestic cat as a model. The domestic cat is a critical biomedical model to complement and expand findings in rodent models as several aspects of feline reproduction more accurately represent human reproductive biology than do rodent models. For example, oocyte size, asymmetrical embryonic divisions, a shared environment with humans and a genome with extensive synteny to the human genome make the cat a cost-effective, non-invasive biomedical model that could improve artificial reproductive technology (ART) in humans (O'Brien et al., 2001). It also is an excellent model for rare and endangered felids (O'Brien et al., 2001; Herrick, 2019; Thongphakdee et al., 2020). Specifically, understanding oocyte maturation is essential to develop fertility treatments for both humans and endangered felids. Both can greatly benefit from improved *in vitro* maturation (IVM) of GV oocytes as they can be acquired without what is often harmful hormonal stimulation (Thongphakdee et al., 2020).

In the cat model, GVs acquire full meiotic competence during the transition from the pre-antral to the antral stage. This has been demonstrated using GV transfer experiments showing that antral, but not pre-antral GVs transferred to mature cytoplasts are capable of meiotic maturation (Comizzoli et al., 2011). In a recent proteomics study, the levels of 74 GV proteins were found to change during the transition from the pre-antral to antral stage (Lee et al., 2018). Our aim in the current study was to validate and further characterize candidate proteins that can serve as markers of competent oocytes. Identification of these markers could help expand our understanding of oocyte development and be applied to improve ART by using them to assess the efficacy of female fertility preservation methods, especially ones focusing on preservation of the GV alone (Graves-Herring et al., 2013; Elliott et al., 2015; Lee and Comizzoli, 2019).

Selection of proteins to investigate was based on the following criteria: (1) proteins with various functions known to be critical to oocyte development such as chromatin structure/regulation and cellular metabolism, (2) proteins previously associated with reproduction/oocytes, and (3) proteins not extensively studied in oocytes yet. Thus, we chose three proteins; bromodomain-containing 2 (BRD2), nucleophosmin 1 (NPM1), and asparaginase like-1 (ASRGL1). BRD2 (also known as female sterile homeotic related gene-1, Fsrg1) is a bromodomain extra terminal protein that is broadly expressed in many cell types including reproductive tissues such as the ovary, oocytes, uterus, and testis (Rhee et al., 1998; Trousdale and Wolgemuth, 2004; Smith and Zhou, 2016). BRD2 is known to regulate transcription, is important for DNA double-stranded break repair and is critical for embryonic development as null BRD2 mutant mice display embryonic lethality with neural tube defects (Gyuris et al., 2009; Hnilicová et al., 2013; Gursoy-Yuzugullu et al., 2017). While expression of BRD2 has been observed throughout mouse folliculogensis, it has not been tested for a role in the oocyte (Rhee et al., 1998; Trousdale and Wolgemuth, 2004; Smith and Zhou, 2016; Mathur et al., 2017; Lim et al., 2019). NPM1 is a histone chaperone important in ribosome biogenesis, regulation of apoptosis and chromatin remodeling (Box et al., 2016; Yu et al., 2021). Additionally, misregulation of NPM1 has been implicated in various cancers (Lim et al., 2019; Kuravi et al., 2021; Yu et al., 2021). However, a role for NPM1 during folliculogenesis has not been identified. Finally, we selected a protein important for cellular metabolism. ASRGL1 is a ubiquitously-expressed aspariginase enzyme present in the mammalian uterus and is highly expressed in the brain and testes (Bush et al., 2002; Dieterich et al., 2003). Recently, ASRGL1 has been explored as a biomarker for uterine carcinomas (Edqvist et al., 2015; Huvila et al., 2018). To date, a role of ASRGL1 in the oocyte has not been identified.

The objective of the study was to identify novel factors that contribute to oocyte meiotic competence using the domestic cat model. Specifically, our aim was to test the role of three candidate proteins that we previously identified to be associated with oocyte development during the transition from the less competent pre-antral to the meiotically competent antral stage. We hypothesized that changes in the protein levels in the nucleus observed previously by our group suggested these factors are potential contributors to overall fertility by regulating oocyte maturation and/or embryo development.

MATERIALS AND METHODS

Ovarian Follicle and Oocyte Collection

Ovaries from adult (>1 year) domestic cats were obtained after routine ovariohysterectomy from local veterinary clinics. The study did not require the approval of the Animal Care and Use Committee of the Smithsonian Conservation Biology Institute because cat ovaries were collected at local veterinary clinics as byproducts from owner-requested routine ovariohysterectomies. Reproductive tracts were immediately stored in PBS (1X Gibco Dulbecco's Phosphate-Buffered Saline, 0.5 mg/mL penicillin and streptomycin) at 4°C for transportation to the laboratory and used for experiments within 24 h of surgeries (Johnston et al., 1989; Wood et al., 1997; Otoi et al., 2001; Naoi et al., 2007). Pre-antral follicles (100–400 μm, and one layer of granulosa

cells) and grade 1 and grade 2 (>400 μm, follicles with a fluid-filled antrum and > 3 layers of cumulus cells) antral stage cumulus cell-oocyte complexes (COCs) from antral follicles were mechanically isolated from ovaries into HEPES (Sigma)-buffered minimal essential medium (MEM, Gibco) supplemented with 100 μg/mL streptomycin, 100 μg/mL penicillin, 4 mg/mL bovine serum albumen (BSA), 2 mM L-glutamine, and 1 mM pyruvate (Wood and Wildt, 1997; Lee et al., 2018).

Validation of Antibody Specificity for Candidate Proteins

To validate the specificity of the antibodies used, western blots were performed for each protein investigated using ovarian tissue lysate (**Supplementary Figure 1**). Half an ovary was snap frozen until used for western blots. Thawed tissue was repeatedly sliced on ice and cells lysed in RIPA buffer (R0278 [Sigma]) containing a mix of protease inhibitors [P8340 ([Sigma)] and 100 μM phenylmethylsulfonly fluoride. Tissue was sonicated on ice for 3 × 10 s at 60% amplitude. SDS sample buffer (Bio-Rad) was added and lysates were incubated for 95°C for 10 min and briefly maintained on ice prior to being resolved by SDS-PAGE [pre-made 4–15% Mini-Pro-TEAN TGX precast gels (Bio-Rad) or hand-made 10%] together with Precision Plus Protein Dual Color molecular weight standard (Bio-Rad). Proteins were transferred to activated polyvinylidene fluoride membranes (Millipore Sigma). Membranes were blocked for 1 h at room temperature in 4% BSA then incubated in primary antibodies overnight at 4°C. Following 3 × 10 min washes, membranes were incubated in secondary antibody [anti-mouse or rabbit IgG conjugated to horseradish peroxidase (Sigma)] and washed 3 × 10 min each. Chemiluminescence was detected with Clarity Western ECL Substrate (Bio-Rad, United States) and imaged with the PXi4 imaging system (Syngene).

Immunostaining of Proteins (Experiment 1)

Oocytes from pre-antral (n = 55) and antral follicles (n = 66) were pooled from different ovaries (in at least 2 replicates) and allocated to one of the three protein staining groups. To visualize proteins within the GV, granulosa cells were mechanically removed from pre-antral oocytes by dissecting with two needles and removed from antral oocytes using a stripper pipette. Antibodies against BRD2 (Abcam 139690), NPM-1 (Abcam 10530), and ASRGL1 (Proteintech 11400-1-AP) were used for identification of protein localization. Oocytes were fixed in 4% paraformaldehyde (PFA) in PBS (Thermo Fisher Scientific) for 30 min at room temperature or at 4°C overnight. Fixed oocytes were rinsed twice in wash solution [2% fetal bovine serum (FBS, Irvine Scientific, United States), 0.5% Triton X-100 in PBS] and blocked twice in saturation solution (20% FBS, 0.5% triton X-100 in PBS) for 15 min at 38.5°C. Oocytes were incubated with primary antibodies (1:500 dilution for each) in saturation solution at 4°C overnight. As a negative control, non-immune IgG from rabbit or mouse was used on a subset of oocytes (**Supplementary Figure 2**). Following three 10 min washes, cells were incubated with a fluorescein isothiocyanate (FITC)-conjugated secondary antibody [anti-mouse F0257 or anti-rabbit F0382 (Sigma)] in wash solution at 38.5°C for 1 h followed by three washes at 38.5°C and mounted on slides with mounting medium [Vectashield with DAPI (Vector Laboratories)] containing DAPI. Stained oocytes were imaged using an Olympus BX41 epifluorescence microscope and SPOT software version 5.0.27. The excitation and detection wavelengths were 488 and 492–544 nm for FITC, respectively, and 405 and 415–487 nm for DAPI. Relative nuclear and cytoplasmic fluorescence intensity was quantified using ImageJ software (National Institutes of Health, United States). For nuclear localized proteins (BRD2 and NPM1), fluorescence intensity of the nuclear FITC signal was normalized to a background signal measurement proportionally sized to the nuclear area that was taken from the cytoplasm and subtracted from total fluorescence intensity prior to calculating intensity in arbitrary units. Total fluorescence intensity then was normalized to either the GV (for nuclear fluorescence) or oocyte (for cytoplasmic fluorescence) size and DNA signal intensity. The DNA signal intensity was normalized to background DAPI signal as described above for FITC signal normalization (Lee et al., 2018).

Antibody Transfection Prior to *in vitro* Maturation (Experiments 2 and 3)

Protein inhibition for Experiments 2 and 3 (**Figure 1**) was performed by transfecting antibodies against candidate proteins into COCs as described by Li et al. (2015) using the Chariot peptide nanoparticle transfection reagent (Active motif, United States). This transfection method was previously verified by our group to reduce protein activity of PDE3A in cat oocytes (Li et al., 2015; Lee et al., 2018). PDE3A is a well-characterized phosphodiesterase required for cAMP degradation, which is necessary for meiotic resumption (Richard et al., 2001; Conti et al., 2002; Thomas et al., 2002). For the experiments in this study, we used PDE3A as a positive control for antibody transfection.

Antibody-Chariot complexes were assembled according to the manufacturer's instructions by mixing 2 μL of Chariot in 50 μL of H_2O with 1.5 μg of antibody in 50 μL of PBS for 30 min at room temperature. The assembled complexes were added to the COCs in equal amount of culture medium [MEM (Sigma-Aldrich, United States) supplemented with 1 mM pyruvate, 2 mM L-glutamine, 100 IU/mL penicillin, 100 μg/mL streptomycin and 4 mg/mL BSA]. COCs were incubated at 38.5°C with 5% CO_2 for 3 h before adding another 200 μL of culture medium and further incubating for a total of 24 h (**Figure 1**). To prevent meiotic resumption during the transfection, 250 nM of milrinone (Sigma-Aldrich, United States) was added to the medium (except for in the fresh control treatment group) during the course of transfection (Grupen et al., 2006; Lee et al., 2018).

Following Chariot transfection, COCs were rinsed three times in SAGE blastocyst media (SAGE, Denmark) to remove milrinone. For IVM, COCs were incubated in a 50 μL drop of SAGE media containing 1 μg/mL ovine FSH (National Hormone and Pituitary Program, United States) and 1 μg/mL ovine LH

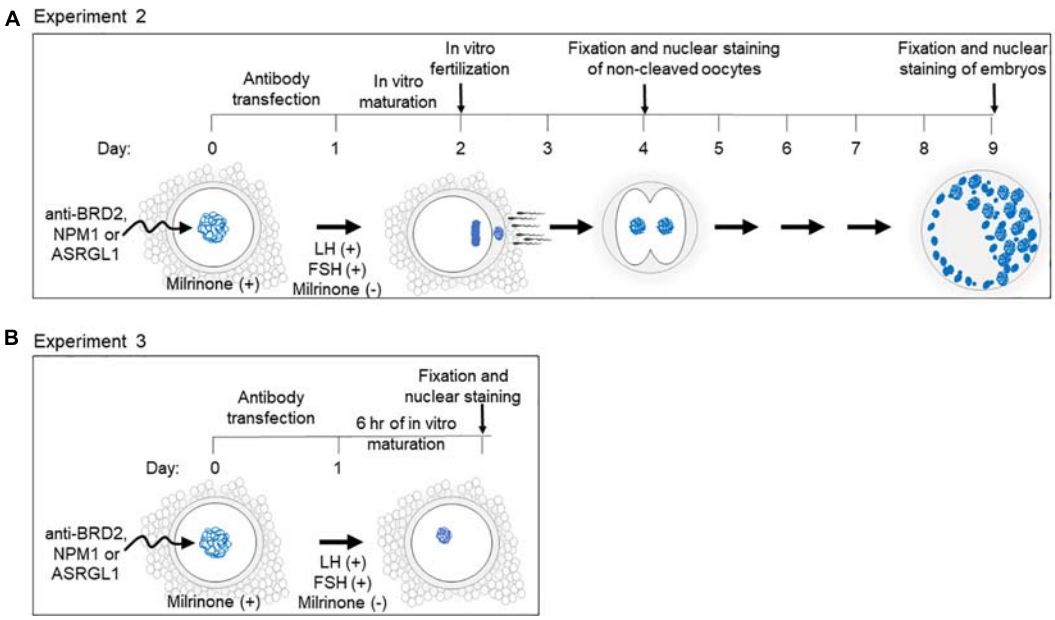

FIGURE 1 | Schematic of experimental design and timeline for **(A)** Experiment 2 and **(B)** Experiment 3.

(National Hormone and Pituitary Program, United States) for either 24 h (experiment 2) or 6 h (experiment 3).

Experiment 2: Effect of Protein Inhibition on *in vitro* Maturation, Fertilization, and Early Embryo Development

For each candidate protein, between 129 and 159 COCs in 2–4 replicates were divided amongst the following treatment groups: (1) mock transfection negative control (chariot transfection reagent alone), (2) PDE3A positive control (transfection with anti-PDE3A), (3) BRD2, NPM1 or ASRGL1 (candidate protein antibody transfection (**Figure 1**). Due to the inability to include fresh controls in every experimental repeat, the fresh control group could not be included in statistical analysis. However, it indicated the standard values in our regular experimental conditions.

Following antibody transfection described above and IVM, COCs were incubated for *in vitro* fertilization (IVF) with 2×10^6 motile cells/mL of fresh or frozen-thawed domestic cat epididymal spermatozoa for 24 h. Oocytes then were mechanically denuded and gently rinsed three times in SAGE blastocyst medium before *in vitro* culture in 50 μL SAGE blastocyst media (5–15 presumptive zygotes per drop). Non-cleaved oocytes were removed from culture the following day, fixed in 4% PFA, and stained with DAPI (**Figure 1**). Oocyte meiotic stages were evaluated according to our standards (Comizzoli et al., 2011). Non-cleaved oocytes with fragmented or abnormal nuclei were classified as degraded. Cleaved embryos were culture for a total of 7 days (after IVF), fixed in 4% PFA, and stained with DAPI (**Figure 1**). Embryonic stage was determined by counting the number of blastomeres. Morula was classified as having 16–63 blastomeres and blastocysts were classified as having at least 64 blastomeres with the presence of a blastocele (Comizzoli et al., 2011).

Experiment 3: Antibody Transfection Followed by Short *in vitro* Maturation

A total of 148 oocytes (in 3 replicates) were equally and randomly allocated to one of the treatment groups (BRD2 inhibition, mock transfection; NMP1 inhibition, mock transfection). Oocytes were transfected with antibodies and underwent IVM as described above. After 6 h of IVM (**Figure 1**), oocytes were fixed in 4% PFA and processed for microtubule immunostaining (anti-beta-tubulin; Thermo MA5-11732; 1:150) as well as DAPI counterstaining following the protocol mentioned above.

Statistical Analysis

Differences in fluorescence intensity in antibody staining of candidate proteins and 6 h IVM antibody transfection experiments were analyzed using a *T*-test. Antibody transfection experiments with multiple comparisons of oocytes and embryo stages were analyzed by ANOVA and Tukey's multiple comparisons test (Prism v6.05; GraphPad Software, United States). Proportions of embryos were compared using a Chi-square test.

RESULTS

Experiment 1: BRD2, NPM1, and ASRGL1 Protein Localization During Oocyte Development

We first sought to compare the localization of candidate proteins in oocytes of pre-antral vs. antral follicular stage oocytes using

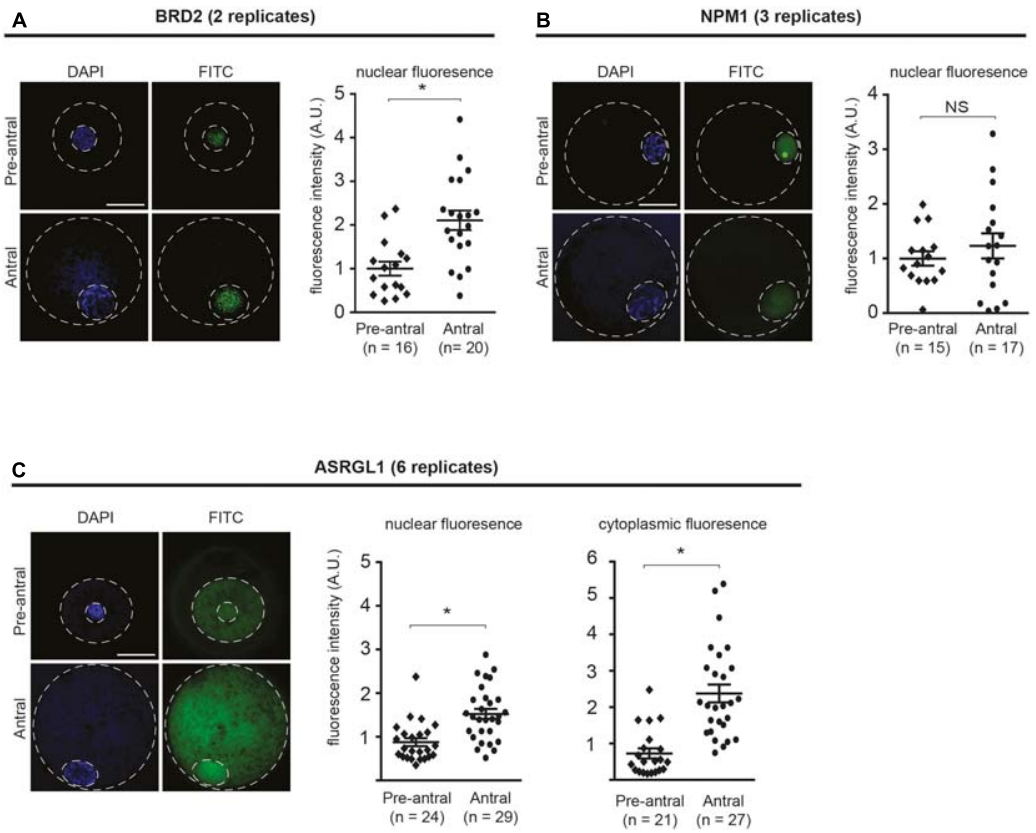

FIGURE 2 | Localization of BRD2, NPM1, and ASRGL1 in pre-antral and antral oocytes. **(A)** BRD2, **(B)** NPM1, **(C)** ASRGL1. In left panels, representative images of pre-antral and antral oocytes. Outer dashed line delineates oocyte boundary and inner dashed line delineates germinal vesicle. Scale bars = 50 μm. In right panel graphs, quantification of normalized nuclear or cytoplasmic fluorescence intensity for each antibody in pre-antral and antral oocytes. Each data point indicates one oocyte. Bars show means ± SEM. *$P < 0.05$.

immunofluorescent staining (**Figure 2**). Antibody specificity was confirmed by the presence of a protein band at the expected size using SDS-PAGE (**Supplementary Figure 1**). The two proteins involved in chromatin regulation, BRD2 and NPM1, were present in oocyte nuclei (**Figures 2A,B**). Specifically, BRD2 was detected in a punctate pattern throughout the nucleoplasm in both pre-antral and antral oocytes (**Figure 2A**). Quantification of fluorescence intensity revealed an increase of BRD2 protein ($P < 0.05$) in antral oocytes as compared to pre-antral counterparts (**Figure 2A**). NPM-1 was localized to the nucleus in both pre-antral and antral oocytes (**Figure 2B**). While there was no change in NPM-1 fluorescence intensity between the pre-antral and antral stages ($P > 0.05$), staining in pre-antral oocytes was concentrated in the nucleolus. Interestingly, in antral oocytes, NPM1 localization changed to a diffuse nucleoplasmic pattern (**Figure 2B**). The protein involved in cellular metabolism, ASRGL1 was present in a punctate pattern throughout the nucleoplasm and cytoplasm (**Figure 2C**). ASRGL1 fluorescence intensity increased ($P < 0.05$) in antral oocytes compared to pre-antral counterparts in both the nucleoplasm and the cytoplasm (**Figure 2C**). Changes observed in protein levels (BRD2 and ASRGL1) or subcellular localization (NPM1) suggested that these proteins might be involved in the critical transition period from an immature pre-antral to an antral oocyte (capable of meiotic maturation and competent for embryo development after fertilization).

Experiment 2: Influence of Inhibition of BRD2, NPM1, and ASRGL1 on Subsequent Meiotic Resumption and Fertilization

To better characterize the role of candidate oocyte competence proteins, we inhibited BRD2, NPM1, and ASRGL1 in antral stage COCs by transfecting antibodies into COCs followed by IVM and IVF. We then examined the influence on subsequent meiotic resumption and early embryo development (**Figure 1**). To confirm transfection in each experiment, we included anti-PDE3A as a positive control. When BRD2 or NPM1 antibodies were transfected into COCs, a lower proportion of oocytes matured *in vitro*, were fertilized, and formed advanced embryos compared to mock transfection controls ($P < 0.05$) (**Table 1**). Specifically, only 15.2% of BRD2-inhibited and 1.2% of NPM1-inhibited oocytes were fertilized and cleaved as compared to 47.0 and 52.8% in respective mock transfection controls (**Table 1**). Analysis of chromatin status in oocytes that did not cleave

TABLE 1 | Influence of the inhibition of BRD2, NPM1, and ASRGL1 in immature oocytes from antral follicles on the subsequent nuclear maturation and developmental competence.

Candidate protein (number of experimental replicates)	Treatment (total number of oocytes, total number of cleaved embryos across all replicates)	Percentages relative to the total number of oocytes					Proportions of embryo stages relative to the total number of cleaved embryos after 7 days of *in vitro* culture			
		Germinal vesicle oocytes*	Metaphase I oocytes*	Metaphase II oocytes*	Degraded*	Cleaved embryos	< 8-cells	8–16-cells	Morulae	Blastocysts
Fresh (4)	Fresh control (60, 38)	9.4 (± 4.7)	6.9 (± 5.5)	68.5 (± 6.0)	14.8 (± 5.0)	63.2 (± 2.8)	21.1	21.1	42.1	15.8
BRD2 (3)	Mock transfection (42, 22)	9.4^{b} (± 4.1)	2.5^{a} (± 2.5)	52.0^{a} (± 5.9)	36.2^{a} (± 5.1)	47.0^{a} (± 4.0)	41.0^{a}	41.0	18.1	0.0
	PDE3A control (39, 2)	68.5^{a} (± 8.1)	1.9^{a} (± 1.9)	7.6^{b} (± 2.7)	22.0^{a} (± 6.5)	5.0^{b} (± 3.1)	100.0^{a}	0.0	0.0	0.0
	BRD2 inhibition (50, 6)	46.9^{ab} (± 15.7)	7.9^{a} (± 5.1)	18.0^{b} (± 12.7)	27.3^{a} (± 9.3)	15.2^{b} (± 10.0)	100.0^{a}	0.0	0.0	0.0
NPM1 (2)	Mock transfection (22, 13)	13.9^{a} (± 13.9)	12.5^{a} (± 12.5)	65.3^{a} (± 9.7)	8.3^{a} (± 5.6)	52.8^{a} (± 2.8)	23.1^{a}	7.7^{a}	69.2	0.0
	PDE3A control (23, 8)	55.9^{ab} (± 19.1)	2.7^{a} (± 2.7)	30.9^{ab} (± 5.9)	10.5^{a} (± 7.0)	28.3^{b} (± 3.3)	87.5^{a}	12.5^{a}	0.0	0.0
	NPM-1 inhibition (53, 1)	72.2^{b} (± 2.2)	5.0^{a} (± 5.0)	1.2^{b} (± 1.2)	21.6^{a} (± 8.2)	1.2^{c} (± 1.2)	100.0^{a}	0.0	0.0	0.0
ASRGL1 (3)	Mock transfection (34, 15)	24.7^{b} (± 9.8)	14.1^{a} (± 10.0)	51.3^{ab} (± 9.2)	9.8^{a} (± 5.3)	44.2^{ab} (± 9.7)	40.0^{a}	0.0	46.7^{a}	13.3^{a}
	PDE3A control (32, 2)	72.7^{a} (± 2.7)	0.0^{a} (± 0.0)	13.7^{b} (± 8.3)	13.7^{a} (± 6.9)	9.5^{b} (± 9.5)	100.0^{a}	0.0	0.0	0.0
	ASRGL1 inhibition (76, 42)	13.9^{b} (± 6.1)	6.2^{a} (± 3.6)	68.9^{a} (± 9.6)	11.1^{a} (± 7.4)	51.0^{a} (± 4.5)	26.2^{a}	14.3	45.2^{a}	14.3^{a}

**Nuclear status from non-cleaved oocytes; Metaphase II values also include oocytes that were fertilized and cleaved.*
Values expressed as mean ± standard error of the mean (SEM), except for embryo stages (overall percentages).
Within the column of a given protein, percentages with different superscripts a–c differ ($P < 0.05$).
Fresh controls were performed on separate batches of oocytes and thus not included in the statistical analysis.

revealed that majority of BRD2 and/or NPM1-inhibited oocytes were still arrested at the GV stage (46.9% for BRD2 and 72.2% for NPM1) or degraded (27.3% for BRD2 and 21.6% for NPM1) (**Table 1**). Percentages of oocytes reaching the metaphase II stage were lower after BRD2 inhibition (18.0%) and after NPM1 inhibition (1.2%) compared to the mock transfections (**Table 1**). While the majority of BRD2-, and NPM1-inhibited COCs failed to mature and be fertilized, a small number cleaved and were capable of forming embryos with less than 8 blastomeres (**Table 1**). Embryo development resulting from those two treatment groups was less successful than in mock transfection controls (**Table 1**). We suspected that these oocytes were inefficiently transfected with antibodies as we similarly observed a low level of cleavage and embryo development in PDE3A controls. Interestingly, transfection of ASRGL1 did not hinder ($P > 0.05$) maturation, fertilization, or embryo development compared to mock transfection controls (**Table 1**).

Experiment 3: Influence of Inhibition of BRD2 and NPM1 on Early Meiotic Maturation Events

Experiments assessing embryo development showed that BRD2 and NPM1-inhibited COCs were incapable of fertilization and suggested this failure may be due to failed meiotic maturation. To precisely determine the stage at which BRD2 or NPM1 were critical to maturation, we analyzed inhibited COCs during the time at which they were just beginning to respond to the hormonal maturation signals LH and FSH (6 h of IVM).

Following 6 h of exposure to IVM conditions, we analyzed the nuclear stage by observing chromatin configuration and the meiotic spindle using anti-β-Tubulin (**Figure 3A**). We found that BRD2-inhibited oocytes remained at the GV stage ($P < 0.05$) whereas mock transfection controls entered meiosis in higher proportions ($P < 0.05$) (**Figures 3B,C**). Similarly, only a very small percentages of NPM1-inhibited oocytes could resume meiosis compared to controls ($P < 0.05$) (**Figures 3D,E**). In addition, NPM1 inhibition caused a phenotype—GV compaction—that was not observed with BRD2 inhibition (**Figure 4A**). As compared to mock controls, GV compaction occurred in 27% of NPM1-inhibited oocytes compared to only 9% of mock transfection control oocytes ($P < 0.05$) (**Figure 4B**). While it is unlikely meiosis could proceed through to the metaphase II stage in just 6 h, it is likely that a small proportion of control COCs escaped milrinone inhibition and entered meiosis during the 1 day transfection period. These experiments showed that BRD2 and NPM1 were important for early meiotic maturation events as inhibition of either of the two resulted in oocytes that fail to respond to exogenous LH and FSH meiotic maturation signals.

DISCUSSION

Our results identified two novel regulators of oocyte meiotic competence, the nuclear transcription factor BRD2 and the nucleolar protein NPM1. Using immunostaining, we observed changes in protein levels and/or localization for all three proteins, suggesting they are regulated during development, and may contribute to fertility. Using protein inhibition assays, we targeted candidate proteins by transfecting antibodies against candidate proteins into COCs. We found that inhibition of both nuclear proteins, BRD2 and NPM1, resulted in oocytes that could not mature, be fertilized nor form embryos. ASRGL1 inhibition did not hinder meiotic maturation or embryo development. Further analysis of early meiotic resumption stages by observation of the meiotic spindle and chromatin configuration demonstrated that inhibition of BRD2 and NPM1 renders oocytes unable to resume meiosis and thus unable to participate in fertilization and embryo development. Together, our data show that we have identified BRD2 and NPM1 as two novel regulators of oocyte meiotic competence.

By immunostaining pre-antral and antral oocytes, we observed BRD2 to be present in the nucleus during folliculogenesis. BRD2 is known to be involved in chromatin remodeling and transcriptional regulation (Trousdale and Wolgemuth, 2004; Peng et al., 2006; Hnilicová et al., 2013). As expected, we observed BRD2 in the nucleus, similar to the nuclear localization of BRD2 previously reported in various cell types including in developing mouse oocytes (Trousdale and Wolgemuth, 2004). Quantification of fluorescence intensity of BRD2 showed a slight upregulation of BRD2 protein from the pre-antral to the antral stage. While this result differs from that our previous proteomics study in which BRD2 was found to be downregulated in antral oocytes as compared to pre-antral, we suspect that differences between the studies could be attributed a low level of somatic cell contamination in the proteomics study (Lee et al., 2018).

Our experiments showed that BRD2 played a role during meiotic resumption as inhibition of BRD2 in antral stage COCs prevented meiotic maturation and oocytes remained at the GV stage despite the presence of exogenous LH and FSH meiotic maturation signals. In the only former study on BRD2 during folliculogenesis (Trousdale and Wolgemuth, 2004), demonstrated that BRD2 expression was highly regulated throughout mouse oocyte development and predicted that BRD2 could play a role in meiotic resumption as the yeast homolog has been shown to be critical during meiosis (Chua and Roeder, 1995; Kanatsu-Shinohara et al., 2000; Filippakopoulos et al., 2012). While it has never formally been tested, here we found that in the cat, BRD2 is indeed important for meiotic resumption. We hypothesize that disrupting BRD2 in antral oocytes, a stage during which transcription is largely quiescent, causes aberrant transcription that is detrimental to proper meiotic resumption. Indeed, BRD2 has been shown to regulate the transcription of critical cell cycle genes via binding to acetylated histone 4 (Owen et al., 2000; Sinha et al., 2005).

In our second set of experiments, where we analyzed very early stages of meiotic resumption, most BRD2-inhibited oocytes did not show any sign of resuming meiosis while control oocytes had begun to respond to LH and FSH signals. In fact, BRD2-inhibited oocytes appeared to be normal, healthy GV stage cells, indicating that the requirement for BRD2 is early, perhaps when cell cycle checkpoints for meiotic resumption are critical. Our analysis of BRD2, together with the existing

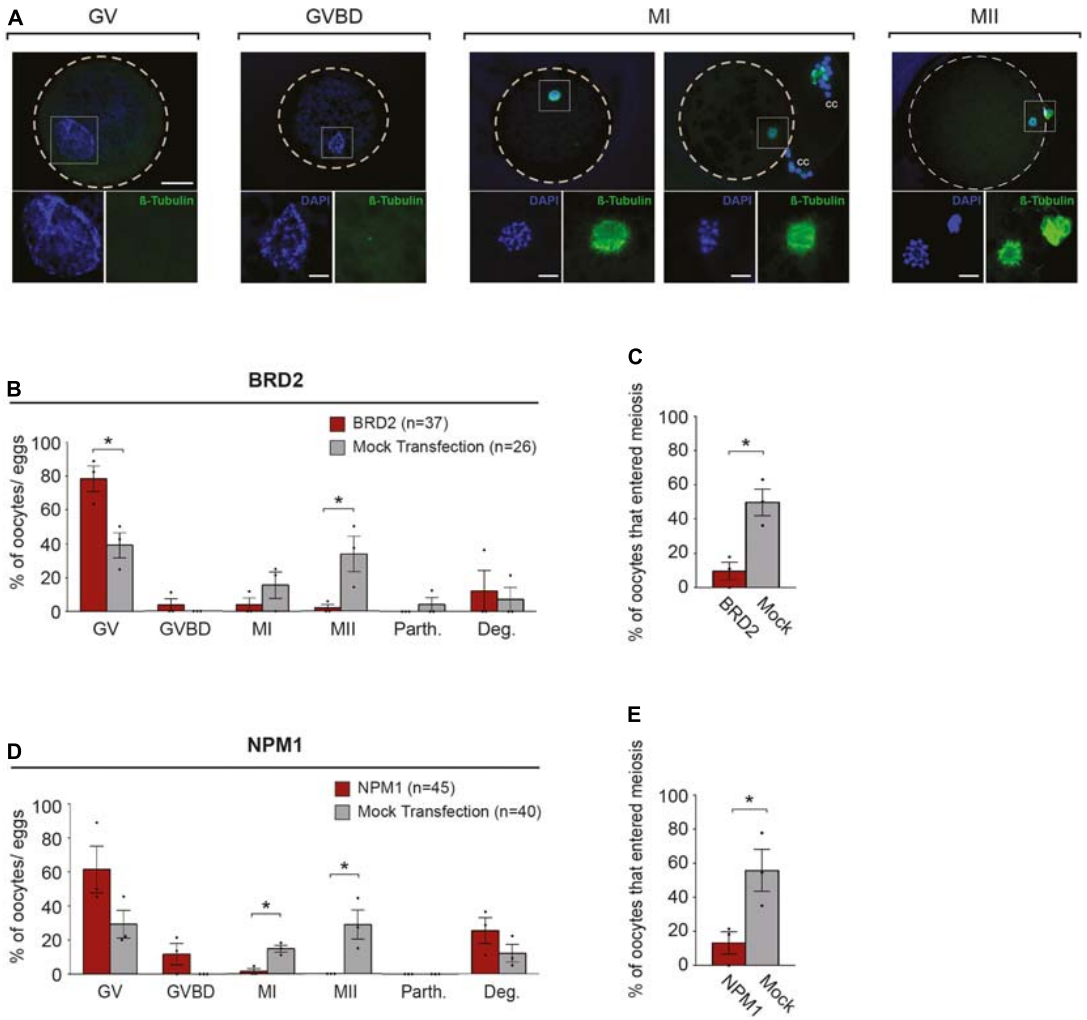

FIGURE 3 | Meiotic progression of BRD2 and NPM1-inhibited oocytes following 6 h of *in vitro* maturation (IVM). **(A)** Representative images of meiotic stages: GV- germinal vesicle, GVBD- germinal vesicle break-down, MI- metaphase I, and MII- metaphase II. Top images: merged FITC (anti-β-Tubulin) and DAPI images. Outer dashed line delineates oocyte boundary. Scale bar = 50 μm. Lower images in squares: magnified area of chromatin configuration (DAPI) and meiotic spindle (β-Tubulin). Scale bar = 10 μm. cc = cumulus cells. **(B,D)** Bar graphs showing the percentage of oocytes in each meiotic stage following protein inhibition and 6 h of IVM. GV, GVBD, MI, MII, Parth.- parthenotes, Deg.- degraded. **(C,E)** Bar graphs showing percentage of oocytes that entered meiosis following 6 h of IVM. Red bars = indicated protein inhibited, Gray bars = mock transfection control. Bars show mean ± SEM (3 replicates). $^*P < 0.05$.

studies of BRD2 molecular mechanisms during mitosis, meiosis and transcriptional regulation, leads us to predict that in our experiments, cell cycle regulation is disrupted thereby preventing early meiotic events from initiating. Although we cannot rule out the notion that BRD2 in cumulus cells contributes to the observed phenotype, former experiments in the mouse show that BRD2 localization is not disrupted in FSH or GDF9 mutants (Trousdale and Wolgemuth, 2004). This suggests that the effect is likely driven by BRD2 in the oocyte itself rather than in cumulus cells that signal oocytes to mature through their FSH and LH receptors (Buccione et al., 1990). While many studies have demonstrated BRD2 is critical during mitosis and even meiosis in sperm cells, our work shows for the first time its role during meiotic maturation in the oocyte in a large, non-rodent mammalian system (Philipps et al., 2008). In future experiments, it would be interesting to determine if BRD2 in cat oocytes is also regulating cell cycle by regulating acetylated histone 4 as has been shown in other systems (Gursoy-Yuzugullu et al., 2017).

NPM1 is a nuclear protein involved in chromatin regulation, RNA transport and ribosome biogenesis (Box et al., 2016). During cat folliculogenesis, we observed NPM1 protein localization change from nucleolar localization in pre-antral stage oocytes to diffuse throughout the nucleoplasm in antral oocytes. This nucleolar to nucleoplasmic localization pattern of NPM1 localization has also been reported in cell lines (Korgaonkar et al., 2005). That study found that a change from nucleolar to nucleoplasmic localization was induced by stressors and was followed by transcription of genes involved in cell-cycle arrest,

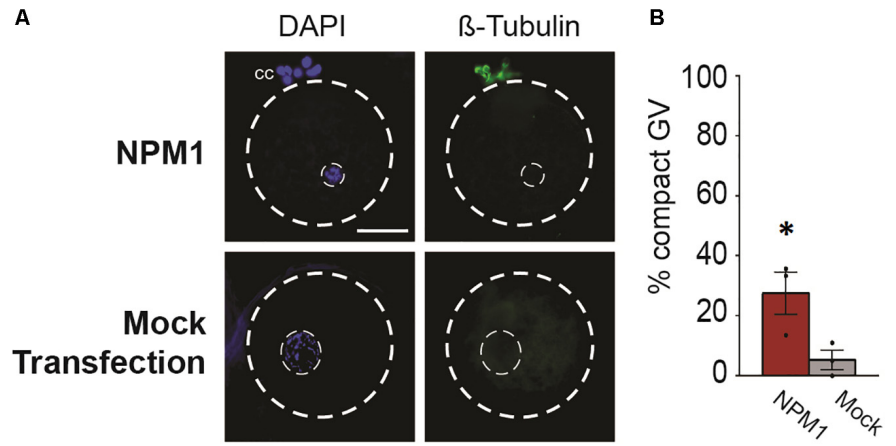

FIGURE 4 | Compact nuclear phenotype of NPM1-inhibited oocytes. **(A)** Representative images of NPM1-inhibited oocytes with compact germinal vesicle (GV) phenotype. Meiotic spindle immunostained with anti-β-Tubulin, DNA stained with DAPI. Outer dashed line delineates oocyte boundary, inner dashed line delineates germinal vesicle. Scale bar = 50 μm. **(B)** Bar graph shows% of oocytes with a compact GV phenotype following 6 h IVM. Bars show mean ± SEM (3 replicates). $^{*}P < 0.05$.

DNA repair and apoptosis. Intriguingly, the closely related NPM2 protein, which is in the same nucleophosmin family as NPM1, is known to be important for meiotic maturation. NPM2 null mutant female mice are infertile or subfertile due to aberrant nucleolar chromatin organization that leads to early embryonic lethality (Burns et al., 2003). In particular, NPM2 is required for the surrounded nucleolar (SN) chromatin configuration that is associated with the ability to resume meiosis in many systems including mice. While the cat differs in that it does not acquire the SN chromatin configuration as a part of normal folliculogenesis, NPM1 structure is very similar to NPM2, with the exception of also possessing a nucleolar localization signal that is not present in NPM2 (Burns et al., 2003; Fuente et al., 2004; Comizzoli et al., 2011; Box et al., 2016). We postulate that NPM1, like NPM2, is important for proper chromatin organization required for meiotic resumption. Furthermore, by examining early meiotic maturation in NPM1-inhibited oocytes, we found a significant proportion of GVs had become compacted, perhaps indicating that some chromatin remodeling events required for meiosis are beginning to occur or are misregulated and thus insufficient to proceed with normal chromosome segregation and produce fertilizable eggs. Future investigation of NPM1 in the cat should explore how NPM1 interacts with known nucleophosmin-interacting pathways and why misregulation can lead to the nuclear compaction phenotype we observed.

ASRGL1 was present in the nucleoplasm as well as the cytoplasm, a localization pattern similar to that of ASRGL1 in other somatic cell types and in testicular tissue (Bush et al., 2002; Dieterich et al., 2003; Huvila et al., 2018). While we did observe an increase in both nuclear and cytoplasmic ASRGL1 at the antral stage, inhibition of ASRGL1 did not interfere with meiotic maturation or embryo development. In fact, ASRGL1-inhibited COCs tended to have higher blastocyst rates as compared to mock transfection controls. Although the trend was not statistically significant, it was an intriguing observation. Although we did not observe any significant phenotypes following ASRGL1 inhibition, we cannot rule out the possibility that our ASRGL1 antibody inefficiently inhibits the protein in COCs or that a higher concentration, or longer inhibition may reveal a role for ASRGL1.

Together, the protein localization analysis adds to our previous proteomic study (Lee et al., 2018) by demonstrating that these proteins are present in developing cat oocytes and that their abundance and/or localization is regulated. Our investigation revealed that two of the three candidate proteins, BRD2 and NPM1, are required for meiotic competence. Although the mechanisms by which BRD2 and NPM1 contribute to competence remain unknown in this system, previous work in other animals provides several potential hypotheses to be tested in future studies. This could be studied by analyzing proteins computationally predicted to interact with BRD2 and NPM1 or shown in other model systems to interact with them. Furthermore, future analysis could examine more general markers of oocyte competence and health such as apoptotic markers or by analyzing reactive oxygen species that can be damaging to overall oocyte viability.

In summary, this study highlights the fact that the molecular underpinnings of gametes are often similar to those found in somatic cells and are adapted for the specialized cell divisions, regulation of genomic DNA configuration and cellular metabolism required by gametes during meiosis. While the proteins we investigated have been studied in other somatic cells, we show here for the first time that BRD2 and NPM1 are critical regulators of meiotic maturation in a large, non-inbred mammalian system. The discovery that these proteins are important during oocyte development in the domestic cat will assist in developing novel fertility preservation techniques focusing on oocyte preservation and IVM. Not only will these techniques contribute to endangered felid conservation but also hold promise for use in human reproductive medicine.

DATA AVAILABILITY STATEMENT

The raw data supporting the conclusions of this article will be made available by the authors, without undue reservation.

AUTHOR CONTRIBUTIONS

DC and P-CL designed the experiments. DC performed the experiments, analyzed the data, and wrote the manuscript. PC contributed to study design, data interpretation, and article revision. All authors contributed to the article and approved the submitted version.

FUNDING

Research reported in this publication was supported by the Office of the Director, National Institutes of Health under Award No. R01OD023139. The content was solely the responsibility of the authors and does not necessarily represent the official views of the National Institutes of Health.

ACKNOWLEDGMENTS

We are grateful to Drs. Brent Whitaker (Animal Rescue Inc.), Keiko Antoku, and Joy Lewis (Spay Now Animal Surgery Clinic) and their staff for providing domestic cat ovaries. We are also grateful to our interns Laura Thompkins for assistance with ASRGL1 antibody staining and imaging and Katie Skudlarek for assistance with the NPM1 western blot.

SUPPLEMENTARY MATERIAL

The Supplementary Material for this article can be found online at: https://www.frontiersin.org/articles/10.3389/fcell.2021.670021/full#supplementary-material

Supplementary Figure 1 | Western blots of candidate proteins with respective IgG negative control antibodies. **(A)** BRD2, **(B)** NPM1, **(C)** ASRGL1.

Supplementary Figure 2 | Representative images of rabbit or mouse non-immune IgG negative controls for BRD2, NPM1, and ASRGL1. Scale bars = 50 μ m.

REFERENCES

Box, J. K., Paquet, N., Adams, M. N., Boucher, D., Bolderson, E., O'Byrne, K. J., et al. (2016). Nucleophosmin: from structure and function to disease development. *BMC Mol. Biol.* 17:19. doi: 10.1186/s12867-016-0073-9

Buccione, R., Vanderhyden, B. C., Caron, P. J., and Eppig, J. J. (1990). FSH-induced expansion of the mouse cumulus oophorus in vitro is dependent upon a specific factor(s) secreted by the oocyte. *Dev. Biol.* 138, 16–25. doi: 10.1016/0012-1606(90)90172-f

Burns, K. H., Viveiros, M. M., Ren, Y., Wang, P., DeMayo, F. J., Frail, D. E., et al. (2003). Roles of NPM2 in chromatin and nucleolar organization in oocytes and embryos. *Science* 300, 633–636. doi: 10.1126/science.1081813

Bush, L. A., Herr, J. C., Wolkowicz, M., Sherman, N. E., Shore, A., and Flickinger, C. J. (2002). A novel asparaginase-like protein is a sperm autoantigen in rats. *Mol. Reprod. Dev.* 62, 233–247. doi: 10.1002/mrd.10092

Chua, P., and Roeder, G. S. (1995). Bdf1, a yeast chromosomal protein required for sporulation. *Mol. Cell Biol.* 15, 3685–3696. doi: 10.1128/mcb.15.7.3685

Clarke, H. J. (2018). Regulation of germ cell development by intercellular signaling in the mammalian ovarian follicle. *Wiley Interdiscip. Rev. Dev. Biol.* 7:e294. doi: 10.1002/wdev.294

Comizzoli, P., Pukazhenthi, B. S., and Wildt, D. E. (2011). The competence of germinal vesicle oocytes is unrelated to nuclear chromatin configuration and strictly depends on cytoplasmic quantity and quality in the cat model. *Hum. Reprod. Oxf. Engl.* 26, 2165–2177. doi: 10.1093/humrep/der176

Conti, M., Andersen, C. B., Richard, F., Mehats, C., Chun, S.-Y., Horner, K., et al. (2002). Role of cyclic nucleotide signaling in oocyte maturation. *Mol. Cell Endocrinol.* 187, 153–159. doi: 10.1016/s0303-7207(01)00686-4

Conti, M., and Franciosi, F. (2018). Acquisition of oocyte competence to develop as an embryo: integrated nuclear and cytoplasmic events. *Hum. Reprod. Update* 24, 245–266. doi: 10.1093/humupd/dmx040

Coticchio, G., Canto, M., Renzini, M., Guglielmo, M., Brambillasca, F., Turchi, D., et al. (2015). Oocyte maturation: gamete-somatic cells interactions, meiotic resumption, cytoskeletal dynamics and cytoplasmic reorganization. *Hum. Reprod. Update* 21, 427–454. doi: 10.1093/humupd/dmv011

Dieterich, D. C., Landwehr, M., Reissner, C., Smalla, K., Richter, K., Wolf, G., et al. (2003). Gliap- a novel untypical l-asparaginase localized to rat brain astrocytes. *J. Neurochem.* 85, 1117–1125. doi: 10.1046/j.1471-4159.2003.01766.x

Edqvist, P.-H. D., Huvila, J., Forsström, B., Talve, L., Carpén, O., Salvesen, H. B., et al. (2015). Loss of ASRGL1 expression is an independent biomarker for disease-specific survival in endometrioid endometrial carcinoma. *Gynecol. Oncol.* 137, 529–537. doi: 10.1016/j.ygyno.2015.03.055

Elliott, G., Lee, P., Paramore, E., Vorst, M., and Comizzoli, P. (2015). Resilience of oocyte germinal vesicles to microwave-assisted drying in the domestic cat model. *Biopreserv .Biobank.* 13, 164–171. doi: 10.1089/bio.2014.0078

Filippakopoulos, P., Picaud, S., Mangos, M., Keates, T., Lambert, J.-P., Barsyte-Lovejoy, D., et al. (2012). Histone recognition and large-scale structural analysis of the human bromodomain family. *Cell* 149, 214–231. doi: 10.1016/j.cell.2012.02.013

Fuente, R., Viveiros, M. M., Burns, K. H., Adashi, E. Y., Matzuk, M. M., and Eppig, J. J. (2004). Major chromatin remodeling in the germinal vesicle (GV) of mammalian oocytes is dispensable for global transcriptional silencing but required for centromeric heterochromatin function. *Science* 275, 447–458. doi: 10.1016/j.ydbio.2004.08.028

Graves-Herring, J. E., Wildt, D. E., and Comizzoli, P. (2013). Retention of structure and function of the cat germinal vesicle after air-drying and storage at suprazero temperature. *Biol. Reprod.* 88:139. doi: 10.1095/biolreprod.113.108472

Grupen, C. G., Fung, M., and Armstrong, D. T. (2006). Effects of milrinone and butyrolactone-I on porcine oocyte meiotic progression and developmental competence. *Reprod. Ferti. Dev.* 18, 309–317. doi: 10.1071/rd05125

Gursoy-Yuzugullu, O., Carman, C., and Price, B. D. (2017). Spatially restricted loading of BRD2 at DNA double-strand breaks protects H4 acetylation domains and promotes DNA repair. *Sci. Rep. U. K.* 7:12921. doi: 10.1038/s41598-017-13036-5

Gyuris, A., Donovan, D. J., Seymour, K. A., Lovasco, L. A., Smilowitz, N. R., Halperin, A. L. P., et al. (2009). The chromatin-targeting protein Brd2 is required for neural tube closure and embryogenesis. *Biochim. Biophys. Acta Bba Gene Regul. Mech.* 1789, 413–421. doi: 10.1016/j.bbagrm.2009.03.005

Herrick, J. R. (2019). Assisted reproductive technologies for endangered species conservation: developing sophisticated protocols with limited access to animals with unique reproductive mechanisms. *Biol. Reprod.* 100, 1158–1170. doi: 10.1093/biolre/ioz025

Hnilicová, J., Hozeifi, S., Stejskalová, E., Dušková, E., Poser, I., Humpolíčková, J., et al. (2013). The C-terminal domain of Brd2 is important for chromatin interaction and regulation of transcription and alternative splicing. *Mol. Biol. Cell* 24, 3557–3568. doi: 10.1091/mbc.e13-06-0303

Huvila, J., Laajala, T. D., Edqvist, P.-H., Mardinoglu, A., Talve, L., Pontén, F., et al. (2018). Combined ASRGL1 and p53 immunohistochemistry as an independent predictor of survival in endometrioid endometrial carcinoma. *Gynecol. Oncol.* 149, 173–180. doi: 10.1016/j.ygyno.2018.02.016

Johnston, L. A., O'Brien, S. J., and Wildt, D. E. (1989). In vitro maturation and fertilization of domestic cat follicular oocytes. *Gamete Res.* 24, 343–356. doi: 10.1002/mrd.1120240310

Kanatsu-Shinohara, M., Schultz, R. M., and Kopf, G. S. (2000). Acquisition of meiotic competence in mouse oocytes: absolute amounts of p34cdc2, Cyclin B1, cdc25C, and wee1 in meiotically incompetent and competent oocytes. *Biol. Reprod.* 63, 1610–1616. doi: 10.1095/biolreprod63.6.1610

Korgaonkar, C., Hagen, J., Tompkins, V., Frazier, A. A., Allamargot, C., Quelle, F. W., et al. (2005). Nucleophosmin (B23) Targets ARF to Nucleoli and Inhibits Its Function. *Mol. Cell Biol.* 25, 1258–1271. doi: 10.1128/mcb.25.4.1258-1271.2005

Kuravi, S., Cheng, J., Fangman, G., Polireddy, K., McCormick, S., Lin, T. L., et al. (2021). Preclinical evaluation of gilteritinib on NPM1-ALK driven anaplastic large cell lymphoma cells. *Mol. Cancer Res.* molcanres.0738.2020. doi: 10.1158/1541-7786.mcr-20-0738

Lee, P., and Comizzoli, P. (2019). Desiccation and supra-zero temperature storage of cat germinal vesicles lead to less structural damage and similar epigenetic alterations compared to cryopreservation. *Mol. Reprod. Dev.* 86, 1822–1831. doi: 10.1002/mrd.23276

Lee, P.-C., Wildt, D. E., and Comizzoli, P. (2018). Proteomic analysis of germinal vesicles in the domestic cat model reveals candidate nuclear proteins involved in oocyte competence acquisition. *Mol. Hum.Reprod.* 24, 14–26. doi: 10.1093/molehr/gax059

Li, R., Jin, Z., Gao, L., Liu, P., Yang, Z., and Zhang, D. (2015). Effective protein inhibition in intact mouse oocytes through peptide nanoparticle-mediated antibody transfection. *Peerj Prepr.* 3:e1566v1. doi: 10.7287/peerj.preprints.1566v1

Lim, R., Nguyen-Ngo, C., and Lappas, M. (2019). Targeting bromodomain-containing proteins to prevent spontaneous preterm birth. *Clin. Sci. Lond. Engl.* 133, 2379–2400. doi: 10.1042/cs20190919

Mathur, S., Deshmukh, P., Tripathi, S., Marimuthu, P., and Padmanabhan, B. (2017). Insights into the crystal structure of BRD2-BD2 – phenanthridinone complex and theoretical studies on phenanthridinone analogs. *J. Biomol. Struct. Dyn.* 36, 1–50. doi: 10.1080/07391102.2017.1353441

Naoi, H., Otoi, T., Shimamura, T., Karja, N. W., Agung, B., Shimizu, R., et al. (2007). Developmental competence of cat oocytes from ovaries stored at various temperature for 24 h. *J. Reprod. Dev.* 53, 271–277. doi: 10.1262/jrd.18115

O'Brien, S. J., Menotti-Raymond, M., Murphy, W. J., and Yuhki, N. (2001). The feline genome project. *Annu. Rev. Genet.* 36, 657–686. doi: 10.1146/annurev.genet.36.060602.145553

Otoi, T., Murakami, M., Ooka, A., Karja, N. W. K., and Suzuki, T. (2001). Effects of size and storage temperature on meiotic competence of domestic cat oocytes. *Vet. Record* 148, 116–118. doi: 10.1136/vr.148.4.116

Owen, D. J., Ornaghi, P., Yang, J., Lowe, N., Evans, P. R., Ballario, P., et al. (2000). The structural basis for the recognition of acetylated histone H4 by the bromodomain of histone acetyltransferase Gcn5p. *Embo J.* 19, 6141–6149. doi: 10.1093/emboj/19.22.6141

Peng, J., Dong, W., Chen, L., Zou, T., Qi, Y., and Liu, Y. (2006). Brd2 is a TBP-associated protein and recruits TBP into E2F-1 transcriptional complex in response to serum stimulation. *Mol. Cell Biochem,* 294, 45–54. doi: 10.1007/s11010-006-9223-6

Philipps, D. L., Wigglesworth, K., Hartford, S. A., Sun, F., Pattabiraman, S., Schimenti, K., et al. (2008). The dual bromodomain and WD repeat-containing mouse protein BRWD1 is required for normal spermiogenesis and the oocyte–embryo transition. *Dev. Biol.* 317, 72–82. doi: 10.1016/j.ydbio.2008.02.018

Rhee, K., Brunori, M., Besset, V., Trousdale, R., and Wolgemuth, D. J. (1998). Expression and potential role of Fsrg1, a murine bromodomain-containing homologue of the Drosophila gene female sterile homeotic. *J. Cell Sci.* 111(Pt 23), 3541–3550.

Richard, F. J., Tsafriri, A., and Conti, M. (2001). Role of phosphodiesterase Type 3A in rat oocyte maturation1. *Biol. Reprod.* 65, 1444–1451. doi: 10.1095/biolreprod65.5.1444

Sinha, A., Faller, D. V., and Denis, G. V. (2005). Bromodomain analysis of Brd2-dependent transcriptional activation of cyclin A1. *Biochem. J.* 387, 257–269. doi: 10.1042/bj20041793

Smith, S. G., and Zhou, M.-M. (2016). The bromodomain: a new target in emerging epigenetic medicine. *ACS Chem. Biol.* 11, 598–608. doi: 10.1021/acschembio.5b00831

Thomas, R. E., Armstrong, D. T., and Gilchrist, R. B. (2002). Differential effects of specific phosphodiesterase isoenzyme inhibitors on bovine oocyte meiotic maturation. *Dev. Biol.* 244, 215–225. doi: 10.1006/dbio.2002.0609

Thongphakdee, A., Sukparangsi, W., Comizzoli, P., and Chatdarong, K. (2020). Reproductive biology and biotechnologies in wild felids. *Theriogenology* 150, 360–373. doi: 10.1016/j.theriogenology.2020.02.004

Trousdale, R., and Wolgemuth, D. J. (2004). Bromodomain containing 2 (Brd2) is expressed in distinct patterns during ovarian folliculogenesis independent of FSH or GDF9 action. *Mol. Reprod. Dev.* 68, 261–268. doi: 10.1002/mrd.20059

Wood, T. C., Montali, R. J., and Wildt, D. E. (1997). Follicle-oocyte atresia and temporal taphonomy in cold-stored domestic cat ovaries. *Mol. Reprod. Dev.* 46, 190–200. doi: 10.1002/(sici)1098-2795(199702)46:2<190::aid-mrd9<3.0.co;2-l

Wood, T. C., and Wildt, D. E. (1997). Effect of the quality of the cumulus–oocyte complex in the domestic cat on the ability of oocytes to mature, fertilize and develop into blastocysts in vitro. *Reproduction* 110, 355–360. doi: 10.1530/jrf.0.1100355

Yu, A. C. Y., Chern, Y.-J., Zhang, P., Pasiliao, C. C., Rahman, M., Chang, G., et al. (2021). Inhibition of nucleophosmin 1 suppresses colorectal cancer tumor growth of patient -derived xenografts via activation of p53 and inhibition of AKT. *Cancer Biol. Ther.* 22, 112–123. doi: 10.1080/15384047.2020.1839278

Conflict of Interest: The authors declare that the research was conducted in the absence of any commercial or financial relationships that could be construed as a potential conflict of interest.

frontiers in Cell and Developmental Biology

ORIGINAL RESEARCH
published: 06 May 2021
doi: 10.3389/fcell.2021.657366

Compromised MPS1 Activity Induces Multipolar Spindle Formation in Oocytes From Aged Mares: Establishing the Horse as a Natural Animal Model to Study Age-Induced Oocyte Meiotic Spindle Instability

*Marilena Rizzo[1,2], Tom A. E. Stout[1], Santo Cristarella[2], Marco Quartuccio[2], Geert J. P. L. Kops[3] and Marta De Ruijter-Villani[1]**

[1] Department of Clinical Sciences, Faculty of Veterinary Medicine, Utrecht University, Utrecht, Netherlands, [2] Department of Veterinary Sciences, Messina University, Messina, Italy, [3] Oncode Institute, Hubrecht Institute–KNAW and University Medical Center Utrecht, Utrecht, Netherlands

OPEN ACCESS

Edited by:
Silvina Perez-Martinez, CONICET Centro de Estudios Farmacológicos y Botánicos (CEFYBO), Argentina

Reviewed by:
Marie-Hélène Verlhac, Centre National de la Recherche Scientifique (CNRS), France
Cheng-guang Liang, Inner Mongolia University, China

***Correspondence:**
Marta De Ruijter-Villani
m.villani@uu.nl

Specialty section:
This article was submitted to Cell Growth and Division, a section of the journal Frontiers in Cell and Developmental Biology

Received: *22 January 2021*
Accepted: *12 April 2021*
Published: *06 May 2021*

Citation:
Rizzo M, Stout TAE, Cristarella S, Quartuccio M, Kops GJPL and De Ruijter-Villani M (2021) Compromised MPS1 Activity Induces Multipolar Spindle Formation in Oocytes From Aged Mares: Establishing the Horse as a Natural Animal Model to Study Age-Induced Oocyte Meiotic Spindle Instability. Front. Cell Dev. Biol. 9:657366. doi: 10.3389/fcell.2021.657366

Aneuploidy originating during meiosis in oocytes is the major cause of reduced fertility, implantation failure and miscarriage in women beyond their mid-thirties. Loss of chromosome cohesion, and defective microtubule dynamics and spindle assembly are, in turn, the major contributors to the error-prone nature of chromosome segregation in the oocytes of older women. However, the underlying molecular defects are not well understood. Altered function of MPS1 and AURKC have been shown to induce multipolar spindle phenotypes in murine oocytes and cancer cells, however, their role in reproductive aging associated oocyte aneuploidy is not known. Although age-related gamete and embryonic aneuploidy has been studied in female rodents, the horse may be a more appropriate animal model. Similar to women, aged mares suffer from reduced fertility and an increased incidence of oocyte aneuploidy. Moreover, mares show a long interval (decades) to reproductive senescence and, unlike rodents but similar to women, horse oocytes assemble the meiotic spindle in a slow and unstable manner, independent of microtubule organizing centers. In this study we found that oocytes from aged mares have lower expression of mRNA for *Mps1, Spc25* and *AurkC* than oocytes from young mares while gene expression for other meiosis regulators did not differ. To assess the ability of horse oocytes to correctly form a bipolar spindle, *in vitro* matured MII oocytes were allowed to re-form their spindle after nocodazole-induced microtubule depolymerization. To investigate the importance of MPS1 and AURKC function in spindle (re)assembly, various concentrations of a MPS1 inhibitor (MPS1i, Compound 5) or an AURK inhibitor (AURKi, ZM447439) were included after nocodazole washout. MII oocytes from aged mares showed a higher incidence of spindle abnormalities after exposure to MPS1i. In contrast, Aurora kinase inhibition severely impaired microtubule organization and spindle formation in all oocytes, irrespective of mare age. In conclusion, gene expression for the kinases *Mps1, Spc25,* and *AurkC* is reduced in oocytes

from aged mares. Moreover, spindle (re)assembly in aged mares' oocytes is more unstable when Mps1 is inhibited. Overall, this suggests that compromised Mps1 activity predisposes to meiotic spindle instability in aged mare oocytes. This spindle instability could predispose to chromosome segregation errors.

Keywords: oocyte, aneuploidy, maternal aging, horse, spindle

INTRODUCTION

Aneuploidy originating during oocyte meiosis is the leading cause of pregnancy loss and infertility in women beyond their mid-thirties, with approximately 60% of their oocytes retaining the wrong number of chromosomes (Herbert et al., 2015; Gruhn et al., 2019, p. 1466–1469). Chromosomal analysis suggests that oocytes from older women fail to reliably protect centromeric cohesion and establish correct monopolar kinetochore–microtubule attachments (Herbert et al., 2015; Gruhn et al., 2019, p. 1466–1469; Zielinska et al., 2019, p. 3749–3765.e7). As women age, progressive weakening of sister chromatid cohesion in oocytes arrested in meiosis I prophase hinders the ability of sister kinetochores to form a single functional unit, and of sister chromatids to remain physically linked until the onset of anaphase of meiosis II (Shomper et al., 2014, p. 1171–1179; Herbert et al., 2015; Zielinska et al., 2015). Studies in mouse oocytes have demonstrated that cohesion loss is a major contributor to aneuploidy in aged females (Chiang et al., 2010, p. 1522–1528; Lister et al., 2010, p. 1511–1521; Burkhardt et al., 2016, p. 678–685). Moreover, loss of cohesins from centromeric regions induces broadening of the centromeric chromatin and fragmentation of the associated kinetochores (Zielinska et al., 2019, p. 3749–3765.e7); since fragmented kinetochores are more likely to interact with multiple microtubule bundles, they are prone to allowing attachment of microtubules emanating from opposite spindle poles (merotely) (Zielinska et al., 2019, p. 3749–3765.e7). Merotelically attached kinetochores/chromosomes are likely to lag behind at anaphase onset and give rise to chromosome segregation errors (Zielinska et al., 2019, p. 3749–3765.e7). Although cohesion loss is recognized as the major contributor to meiotic aneuploidy, other factors have been recognized to play an important role in the origin of meiotic segregation errors in human oocytes. Vulnerable crossover configurations, such as peri-centromeric, telomeric, or missing crossovers, appear to contribute to disruption of the "bivalent" structure (the association of two replicated homologous chromosomes) needed for accurate segregation during meiosis I (Shomper et al., 2014, p. 1171–1179; Herbert et al., 2015; Zielinska et al., 2015). Moreover, the intrinsic spindle instability typical of human oocytes, with up to the 80% of oocytes displaying transient multipolar spindles, has been proposed to predispose to chromosome segregation errors by promoting the establishment of incorrect merotelic mictotubule-kinetochore attachments (Holubcová et al., 2015, p. 572–573). A recent study on mice showed that oocyte spindle instability increases in aged individuals. However, altered microtubule dynamics were not attributable to age-related chromatin changes since transferring the nucleus of a young oocyte into the cytoplasm of an old one did not lead to a reduction of the incidence of multipolar spindle formation (Nakagawa and FitzHarris, 2017, p. 1040–1047). Although spindle instability is a well described phenomenon in human oocytes, the underlying molecular defects are not understood (Holubcová et al., 2015, p. 572–573; Nakagawa and FitzHarris, 2017, p. 1040–1047).

Mono Polar Spindle 1 (MPS1) kinase and Aurora kinase C (AURKC) are two of the master regulators of the meiotic divisions and known primarily for their roles in ensuring correct microtubule-kinetochore interaction and K-fiber assembly (Hached et al., 2011, p. 2261–2271); however they also localize to Microtubule Organizing Centers (MTOCs) and the spindle poles. MTOCs are the major microtubule nucleators during the process of murine oocyte spindle assembly and must cluster at the spindle poles to yield a stable bipolar spindle. A recent study in mice showed that the process of MTOC clustering at the oocyte spindle poles is very similar to centrosome clustering in cancer cells expressing supra-numerary centrosomes (Breuer et al., 2010, p. 1251–1260). Perturbation of MPS1 and AURK localization at the MTOCs and spindle poles has been shown to result in the inability to cluster MTOCs, resulting in multipolar spindle phenotypes in murine oocytes and cancer cells (Kwiatkowski et al., 2010, p. 359–368; Balboula and Schindler, 2014; Balboula et al., 2015, 2016, p. 3648–3660).

We therefore hypothesized that a reduction in MPS1 and AURKC kinase activity could play a role in reproductive aging-induced spindle instability and consequent aneuploidy in oocytes. The main obstacle to studying age-related compromise of oocyte spindle stability is the lack of an animal model in which spindle dynamics closely mimic those in human oocytes. Although rodents have been used in previous studies, their mechanism of meiotic spindle assembly and their chromosome conformation is different to that of human oocytes (Holubcová et al., 2015, p. 572–573; Mogessie et al., 2018). The similarities between women and mares with regard to the duration of oocyte prophase arrest (years to decades) and the time interval to reproductive senescence, suggest that the mare could represent a valuable "natural" model for studying the processes underlying reproductive aging. Both human and equine oocytes present meta- and submetacentric chromosomes, which are considered to present a greater structural challenge to the establishment of stable bipolar microtubule attachments than rodents' telocentric chromosomes (Raudsepp and Chowdhary, 1999, p. 103–114; Holubcová et al., 2015, p. 572–573). Unlike rodents, human and horse oocytes assemble the meiotic spindle in a slow and unstable manner, independent of microtubule organizing centers (MTOCs) (Tremoleda et al., 2001, p. 260–269; Li et al., 2006,

p. 661–667; Holubcová et al., 2015, p. 572–573). After nuclear envelope breakdown (NEBD), the microtubules start nucleating from the chromosomes, and γ-tubulin is only detectable on the minus ends of the microtubules as a diffuse staining at the spindle poles (Li et al., 2006, p. 661–667; Roeles and Tsiavaliaris, 2019). We recently showed that the age-related change in the incidence of aneuploidy in MII oocytes from mares (15% in young and 55% in old mares) is comparable to that reported for women (20% in women younger than 35 years; 60% in women older than 35 years) (Chiang et al., 2010, p. 1522–1528; Lister et al., 2010, p. 1511–1521; Fragouli et al., 2011, p. 286–295; Rizzo et al., 2020, p. 22220–22232). Moreover, the mechanics of mis-segregation appear to be analogous, since the majority of aneuploidies observed in aged mare oocytes were the result of premature separation of sister chromatids (Rizzo et al., 2020). The aim of the present study was to investigate the effects of advanced maternal age on MPS1 and AURKC gene expression, and examine whether function of these kinases plays an essential role in stabilizing spindle bipolarity in oocytes.

RESULTS

Six hundred and forty cumulus-oocytes-complexes (COCs) were collected from the ovaries of 118 mares (41 young and 77 old mares). Mare ages ranged between 2 and 14 years (mean ± SD: 8.9 ± 4.1 years) for the young group, and between 16 and 28 years (mean ± SD: 20.3 ± 3.7 years) for the old group.

For the gene expression study, 320 oocytes were divided into 8 groups on the basis of mare age (young vs. old), cumulus appearance before maturation (compact vs. expanded) and extrusion of the first polar body after maturation (MII and non-MII). For each of the 8 groups, 4 pools of 10 oocytes were used for mRNA extraction.

Three hundred and twenty oocytes that showed first polar body extrusion after *in vitro* maturation were randomly selected for examination of the effects of inhibitors and immunofluorescent analysis. Of the immune-stained oocytes, 68 (24 and 44 from young and old mares, respectively) had to be excluded due to inadequate immunofluorescent staining for tubulin or chromatin. A schematic representation of the study design, together with images of equine oocytes with or without a polar body, and an expanded or compact cumulus investment, are shown in **Figure 1**.

Gene Expression for *MPS1* and *AURKC* Is Reduced in Oocytes From Aged Mares

When we examined expression of a range of candidate regulators of chromosome segregation during meiosis, we found no effect of maturation stage (germinal vesicle vs. MII) or initial cumulus appearance (compact vs. expanded). However, we observed a significant reduction in gene expression for *MPS1*, *Spc25* and *AURKC* in oocytes from aged (≥16 years) compared to young (≤14 years) mares (**Figure 2**). By contrast, gene expression for *Mad2L2, Bub1, Bub3, Bub1B, Ndc80,* and *AURKB* was similar between the two age groups (**Supplementary Figure 1**).

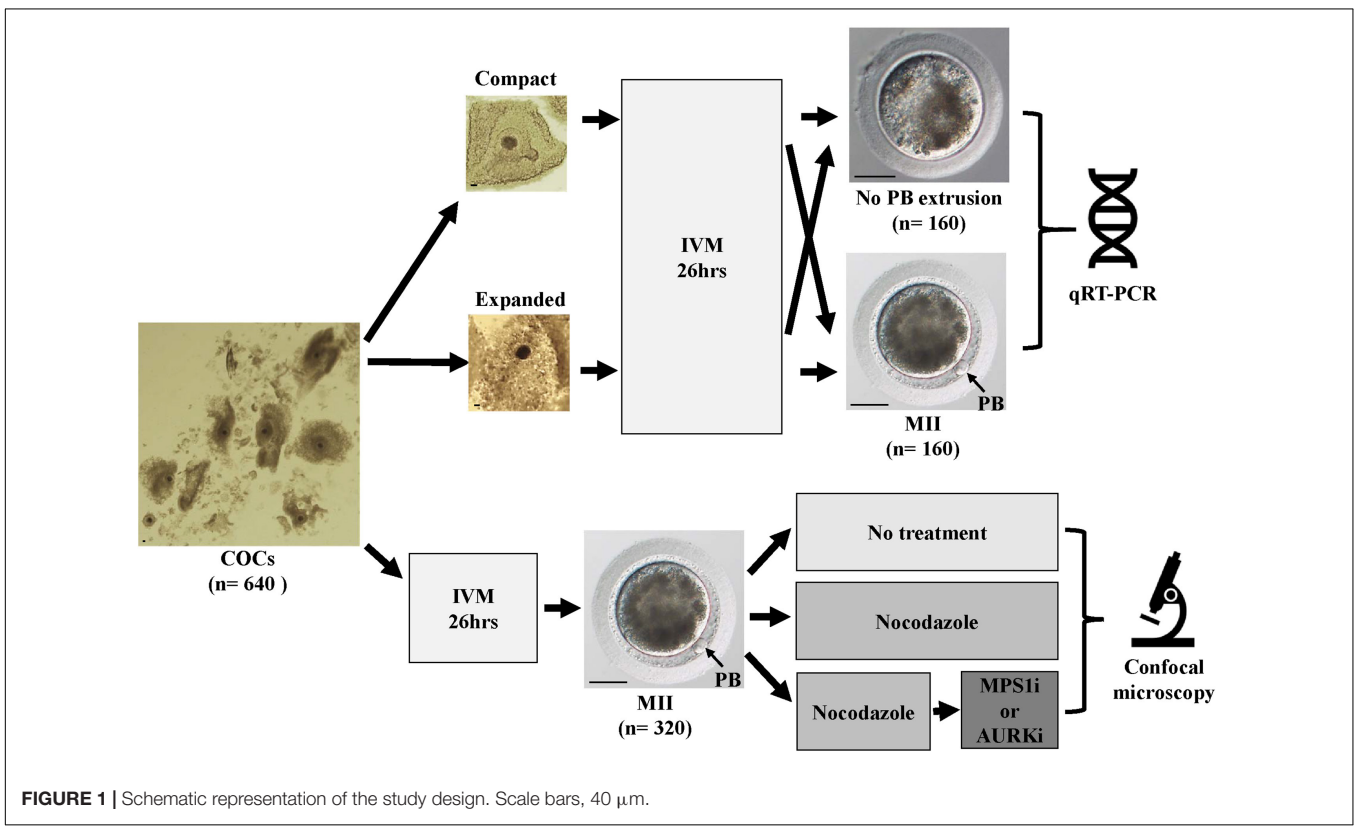

FIGURE 1 | Schematic representation of the study design. Scale bars, 40 μm.

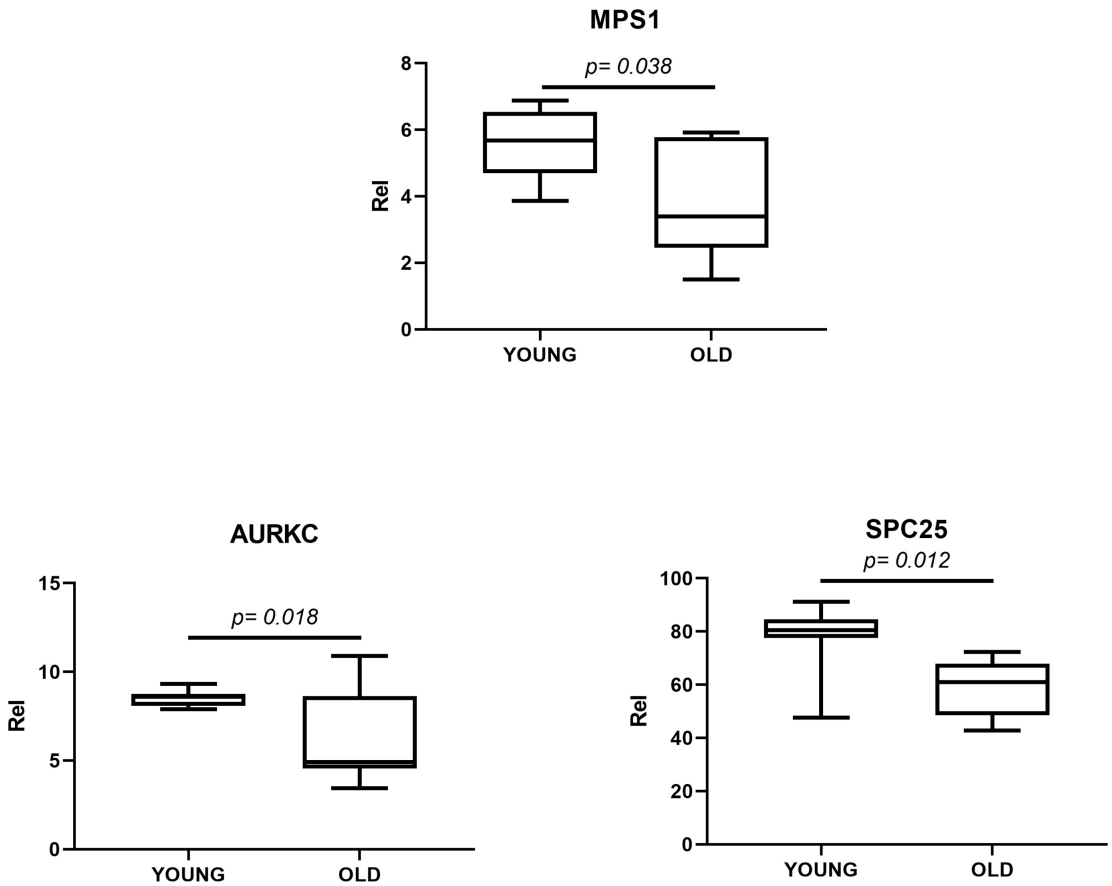

FIGURE 2 | mRNA expression for *Mps1*, *Spc25* and *AurkC* in oocytes from young (≤14 years) and old (≥16 years) mares. The box plot shows the interquartile range, with the median value indicated by the horizontal line; whiskers show the range.

To investigate the ability of oocytes to correctly form a bipolar spindle, *in vitro* matured MII oocytes were allowed to re-form a spindle after nocodazole-induced microtubule depolymerization. To further establish whether MPS1 and AURKC played important roles in spindle (re)assembly, increasing concentrations of a MPS1 inhibitor (MPS1i, Compound 5) or an AURK inhibitor (AURKi, ZM447439) were added to the post-nocodazole washout maturation medium. Morphology of MII spindles was classified as described by Baudoin and Cimini (2018, p. 215–227; **Table 1**).

Reduced Mps1 Function Induces Multipolar Spindle Formation in Oocytes From Aged Mares

Oocytes from aged mares showed multipolar spindle formation after treatment with both tested concentrations of MPS1i, whereas oocytes from young mares only showed spindle abnormalities when exposed to the higher dose of inhibitor (**Table 2**). No abnormal spindles were observed in young mare oocytes that were not treated, were exposed to Nocodazole washout only or treated with 200 nM MPS1i after Nocodazole washout (0/60; **Figure 3A**). Only after treatment with 500 nM MPS1i following Nocodazole washout was a significant increase in the incidence of abnormal spindle formation observed (9/40) (23 vs. 0%, P = 0.021; **Figure 3B**). Similarly, no difference in the incidence of spindle abnormalities was observed in oocytes

TABLE 1 | Diagrammatic representations and descriptions of all spindle abnormalities documented in the present study.

Spindle defects	Appearance	Description
Monopolar		Presence of only one spindle pole.
Multipolar	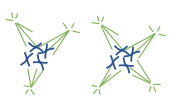	Presence of more than two spindle poles.
Bent		Spindle presenting a curved spindle axis instead of straight.
Absent		Failure of microtubules to organize in a spindle, absence of chromosome congression.

TABLE 2 | Number, type and frequency of spindle abnormalities in MII oocytes from young (≤14 years) and old (≥16 years) mares, treated with MPS1i (0, 200, or 500 nM) or AURKi (0, 5, or 10 μM) after Nocodazole washout.

Maternal age (years)		≤14					≥16				
N. of abnormal spindles (%)		Monopolar	Multipolar	Bent	Absent	Total	Monopolar	Multipolar	Bent	Absent	Total
Treatment	Control	0	0	0	0	0/22 (0%)[a]	0	0	1	0	1/19 (5%)[a]
	0nM MPS1i/0μM AURKi	0	0	0	0	0/20 (0%)[a]	0	3	0	0	3/19 (15%)[ab]
	200nM MPS1i	0	0	0	0	0/18 (0%)[a]	0	6	1	0	7/21 (33%)[b]
	500nM MPS1i	0	7	2	0	9/40 (23%)[b]	0	8	0	0	8/22 (36%)[b]
	5μM AURKi	0	2	0	1	4/15 (27%)[b]	3	0	1	0	3/12 (25%)[ab]
	10μM AURKi	3	0	0	5	8/21 (38%)[b]	7	0	0	5	12/23 (52%)[b]

Oocytes in the control groups were not treated with nocodazole nor inhibitors. Totals that share the same supe rscript do not differ significantly; $P < 0.05$.

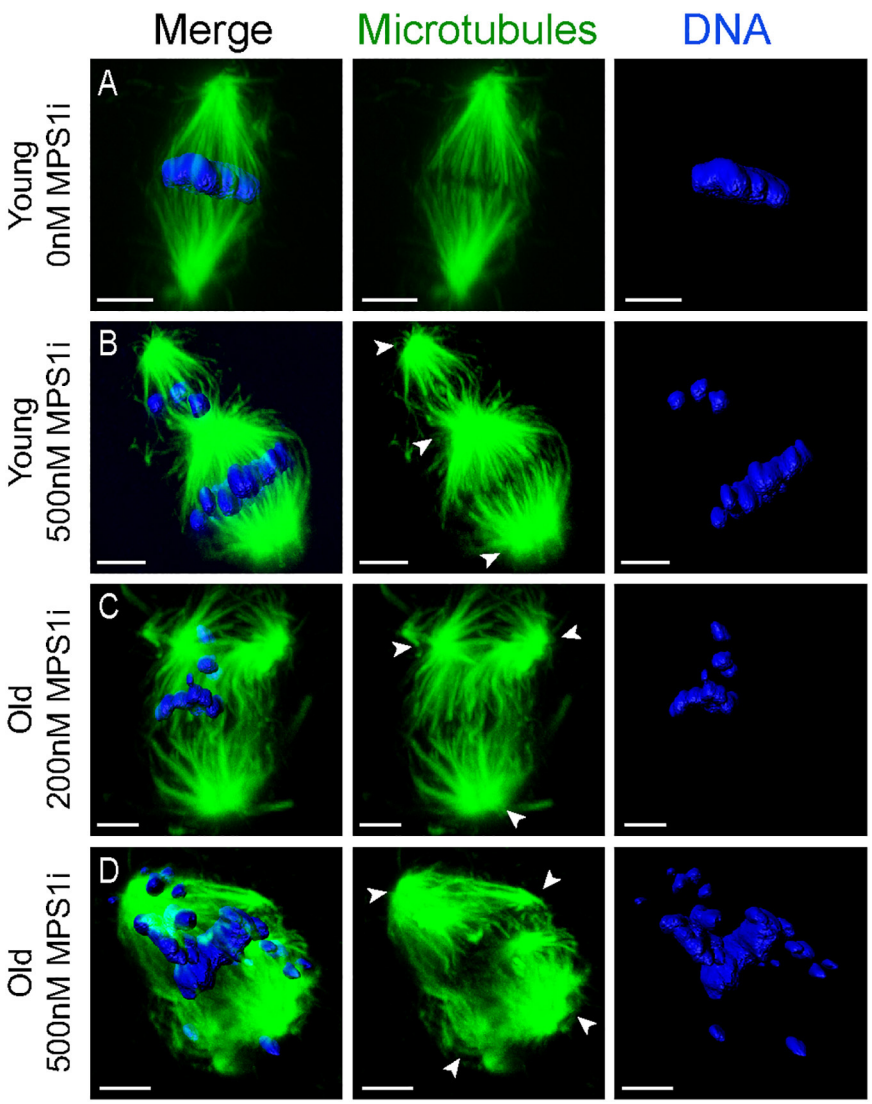

FIGURE 3 | Representative images of spindles of horse MII oocytes treated with MPS1i after Nocodazole washout. Maximum intensity projections of confocal sections. Microtubules (alpha-tubulin, green); chromatin (Hoechst, blue). Scale bars, 5 μm. **(A)** Bipolar spindle from a young mare's oocyte treated with 0 nM of MPS1i; **(B)** tripolar spindle from a young mare's oocyte treated with 500 nM of MPS1i; **(C)** tripolar spindle from an old mare's oocyte treated with 200 nM of MPS1i; **(D)** tetrapolar spindle from an old mare's oocyte treated with 500 nM of MPS1i. Arrowheads indicate the spindle poles.

from aged mares not exposed to any treatment (5%, 1/19), or exposed to Nocodazole washout only (16%, 3/19). However, aged mares' oocytes were susceptible to both concentrations of MPS1i, showing an increased incidence of tri- and tetrapolar spindles compared to the control group (7/21 [33%; $P = 0.046$] and 8/22 [36%; $P = 0.024$] for 200 and 500 nM MPS1i, respectively) (**Figures 3C,D**). The incidence of multipolar spindles was also significantly higher in aged compared to young mares' oocytes treated with 200 nM of MPS1i (33% aged vs. 0% young; $P = 0.01$).

Of the oocytes with bipolar spindles, oocytes from aged mares showed a higher incidence of chromosome misalignment than those from young mares (**Supplementary Table 1**). This age-related difference was significant in every treatment group except the 200 nM MPS1i. Specifically, aged mare oocytes showed a total incidence of chromosome misalignment of 44% (8/18), 56% (9/16), 29% (4/14), and 71% (10/14) in the non-treated Control, Nocodazole, 200 and 500 nM MPS1i groups, respectively, compared to 5% (1/22; $P = 0.006$), 10% (2/20; $P = 0.004$), 22% (4/18; $P = 0.7$), and 23% (7/31; $P = 0.002$) for young mare oocytes (**Supplementary Figure 2**). No significant difference in the incidence of chromosome misalignment was observed between the different treatments within either age group.

The Aurora Kinase Inhibitor AURKi Severely Impairs Microtubule Organization and Spindle Formation in Mare Oocytes

Treatment with AURKi after Nocodazole washout increased the incidence of spindle abnormalities in oocytes from both young [27% (4/15; $P = 0.021$) and 38% (8/21; $P = 0.001$) for the 5 and 10 μM AURKi groups, respectively] and aged mares [52% (12/23) for the 10 μM AURKi group; $P = 0.005$], but not aged mare oocytes treated with 5 μM AURKi (25%, 3/12; $P = 0.27$) (**Table 2**). The most common abnormalities observed in oocytes treated with 5 μM AURKi were multipolar (in young mares oocytes; **Figure 4A**) or monopolar spindles (in aged mares oocytes; **Figure 4B**), while the most prominent abnormalities after treatment with 10 μM AURKi were monopolar spindles and the complete absence of spindle assembly and chromosome congression (**Figure 4C**). Oocytes treated with AURKi which did re-form a bipolar spindle, did not show an increased incidence of mis-aligned chromosomes compared to the control or Nocodazole treatment groups (**Supplementary Table 1**).

DISCUSSION

The results of the present study show that *in vitro* matured MII oocytes from aged mares have reduced mRNA expression for three meiotic regulators: *Mps1*, *AurkC,* and *Spc25*. We hypothesized that the reduced mRNA expression of *Mps1* and *AurkC* could result in a similar reduction in abundance of their respective proteins, leading to an impairment of their activity during the meiotic divisions. Although we attempted to assess Mps1, Spc25 and AurkC protein abundance in oocytes via immunofluorescence, the absence of adequately specific antibodies prevented us from being able to quantify their expression. Instead, to test the hypothesis that compromised Mps1 or AurkC activity may contribute to spindle instability in oocytes from aged mares, we evaluated the ability of oocytes from both young and old mares to re-assemble a metaphase II spindle after nocodazole-induced microtubule de-polymerization in the presence of different concentrations of an inhibitor for either Mps1 (MPS1i) or AURKC (AURKi); we were not able to obtain a validated inhibitor for Spc25. Whereas treatment with 500 nM MPS1i resulted in an increase in the incidence of tri- and tetrapolar spindles in oocytes from both young and old mares, treatment with 200 nM MPS1i induced multipolar spindles only in oocytes from old mares. The incidence of chromosome misalignment after MPS1i inhibition did not differ statistically when compared to the Nocodazole groups. Therefore, it seems that the inhibition of MPS1 in horse oocytes mainly affects bipolar spindle formation rather than chromosome alignment *per se*. The observation that oocytes from aged mares showed a higher frequency of misaligned chromosomes than oocytes from young mares, in all groups other than the 200 nM MPS1i treatment, is in accordance with previous observations in equine

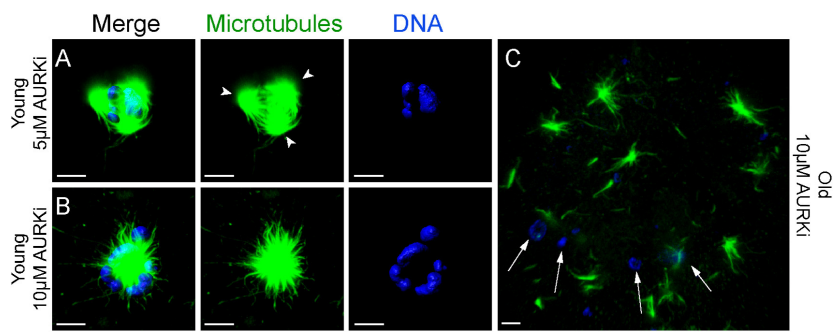

FIGURE 4 | Representative images of spindles of horse MII oocytes treated with Aurki after Nocodazole washout. Maximum intensity projections of confocal sections. Microtubules (alpha-tubulin, green); chromatin (Hoechst, blue). Scale bars, 5 μm. **(A)** Tripolar spindle from a young mare's oocyte treated with 5 μM of AURKi; arrowheads indicate the spindle poles; **(B)** monopolar spindle from a young mare's oocyte treated with 10 μM of AURKi; **(C)** complete absence of spindle assembly and failure of chromosome congression from an old mare's oocyte treated with 10 μM AURKi; white arrows indicate condensed chromatin dispersed within the cytosol.

TABLE 3 | Details of the primer pairs for target and housekeeping genes used in the present study.

Gene	Sequence	T_a (°C)	Amplicon size (bp)	GenBank Accession no.
MAD2L1	F: 5′-GCAGTTTGATATTGAGTGTGAC-3′R: 5′-TCCTGATTCCTCCCATTTCTC-3′	58°	213	XM_001503199.3
BUB1	F: 5′-GACTCAAATACGGAACAAAGG-3′R: 5′-TCTGTCTTCATTTACCCACTG-3′	60°	209	XM_005599825.1
BUB3	F: 5′-GAAGTACGCCTTCAAGTGTC-3′R: 5′-TTTACGAATCCATCAGAACCAC-3′	62°	125	XM_005602172.1
BUB1B	F: 5′-GCAGATATGATATTTCAGGAAGGG-3′R: 5′-CTGGTTTGAAGCCTTGAGAG-3′	58°	251	XM_005603154.1
MPS	F: 5′-GGTTCAAGTAAGGTATTTCAGG-3′R: 5′-ATTTCCACACTCCATTACCA-3′	58°	215	XM_001499324.3
NDC80	F: 5′-AGTTGAATATAAGCAGACCCAC-3′R: 5′-GCTTGTAGGGACTTCATGGA-3′	62°	231	XM_001492535.3
SPC25	F: 5′-GCAGACTTGTATAAAGATCGAC-3′R: 5′-CTATCTGACACTTCATAGTCCC-3′	60°	157	XM_005601567.1
AURKB	F: 5′-GAAGAAGAGCCATTTCATCGT-3′R: 5′-ACTCCAGAATCAAGTAGATCCT-3′	62°	178	XM_001504814.3
AURKC	F: 5′-GCATCTACAACACCCAAATATCC-3′R: 5′-GTTCTCGGGCTTAATATCCCT-3′	60°	225	XM_005596580.1
PGK1	F: 5′-CTGTGGGTGTATTTGAATGG-3′R: 5′-GACTTTATCCTCCGTGTTCC-3′	54°	151	XM_005614287.1
SRP14	F: 5′-CTGAAGAAGTATGACGGTCG-3′R: 5′-CCATCAGTAGCTCTCAACAG-3′	55°	101	XM_001503583.3

and human oocytes (Battaglia et al., 1996, p. 2217–2222; Rizzo et al., 2019, p. 252–257).

Mps1 has several functions during meiosis. Localization of Mps1 to the kinetochores is required for correct timing of prometaphase, correct AURKC localization and chromosome alignment, and to prevent precocious anaphase activation (Hached et al., 2011, p. 2261–2271). Mps1-depleted murine oocytes fail to correctly localize AURKC, suggesting that Mps1 is an important regulator of the chromosomal passenger complex (CPC; composed of AURKC, INCENP, survivin and borealin) in oocytes (Hached et al., 2011, p. 2261–2271; Nguyen et al., 2018, p. 3458–3468.e5). Moreover, Mps1 has been shown to localize at the spindle poles and Mps1-depleted oocytes show abnormal spindle formation; nevertheless, the exact function of Mps1 in microtubule clustering and spindle assembly in oocytes is still unknown (Hached et al., 2011, p. 2261–2271; Marquardt et al., 2016, p. 7828–7833). It has recently been shown that the CPC regulates both centrosome clustering in cancer cells with supernumerary centrosomes, and MTOC clustering in mouse oocytes (Leber et al., 2010; Balboula et al., 2016, p. 3648–3660). Mps1 disruption in cancer cells inhibits this clustering, leading to the formation of multipolar spindles (Kwiatkowski et al., 2010, p. 359–368). It is possible that, similar to cancer cells with supernumerary centrosomes, the clustering of the multiple acentrosomal spindle poles in oocytes lacking MTOCs is also regulated by Mps1 and CPC. It therefore seems reasonable to speculate that, as females age, impaired Mps1 function in their oocytes increases the risk of multipolar spindle formation.

In the present study, treatment with AURKi induced spindle abnormalities with a similar frequency in oocytes from both young and aged mares. The most frequent abnormalities observed were the formation of monopolar spindles and the complete absence of spindle assembly and chromosome congression. These findings are similar to what has previously been observed in Xenopus egg extracts and mouse oocytes treated with the same aurora kinase inhibitor (Wang et al., 2008, p. 1104–1111; Lane et al., 2010, p. 521–530). In Xenopus egg extracts, AurkB stabilizes spindle microtubules by inhibiting the activity of the catastrophe kinesin MCAK (Shao et al., 2012, p. 2672–2680; Ems-Mcclung et al., 2013, p. 2491–2499). Similarly, inhibition of AurkB/C in murine oocytes, by treatment with 5–10 μM AURKi, decreased MCAK phosphorylation and induced the formation of multipolar, monopolar and apolar spindles (Shuda et al., 2009, p. 1094–1105; Vogt et al., 2010, p. 665–684). We therefore propose that the spindle abnormalities observed in horse oocytes after Aurki treatment are a consequence of MCAK-dependent instability of the spindle microtubules. However since young and aged oocytes were similarly affected by this inhibition, this mechanism doesn't seems to play an important role in reproductive aging associated oocyte aneuploidy.

CONCLUSION

Oocytes from mares of advanced age show a reduced expression of genes encoding for three regulators of meiosis, *Mps1*, *AurkC,* and *Spc25*. Moreover, oocytes from aged mares show an increased sensitivity to Mps1 inhibition, but not to AURK inhibition, when compared to oocytes from young mares. We therefore propose that compromised Mps1 activity in oocytes from aged mares contributes to reproductive-aging induced spindle instability, which in turn might predispose to aneuploidy.

MATERIALS AND METHODS

Oocyte Collection and *in vitro* Maturation

Ovaries were collected from slaughtered mares within 15 min of death, divided into two groups depending on the age of the mare (young, ≤14 years; old, ≥16 years) and transported to the laboratory within 4 h at 21–25°C as described previously (Rizzo et al., 2019, p. 252–257). Cumulus-Oocyte Complexes (COCs) were recovered from the ovaries by scraping the follicle wall and flushing out the dislodged COCs using embryo flushing medium (Euroflush, IMV Technologies, Leeuwarden, the Netherland) as previously described (Rizzo et al., 2019, p. 252–257). A dissecting microscope with 10–60× magnification was used for evaluating the recovered COCs. Only oocytes with at least one layer of intact cumulus cells were used for these studies; denuded oocytes were discarded. For the PCR experiment, COCs were further subdivided depending on cumulus morphology at recovery (Compact or Expanded).

The oocytes were then washed in Hepes-buffered synthetic oviduct fluid (H-SOF; Avantea, Cremona, Italy) and subsequently matured *in vitro* for 26 h at 38.5°C in 5% CO_2-in-air in a 50:50 mixture of Dulbecco's minimal essential medium (DMEM) and Ham's F12 (GIBCO BRL Life Technologies, Bleiswijk, The Netherlands) supplemented with 10% fetal calf serum (Sigma-Aldrich Chemical Co., St. Louis, Missouri, United States), 0.125 μg/mL epidermal growth factor (Peprotech Inc., Rocky Hill, New Jersey, United States), 0.1 IU/mL follicle-stimulating hormone, 0.6 mmol/L cysteine and 0.1 mmol/L cysteamine (Sigma-Aldrich Chemical Co.), 0.1% insulin, 0.1% transferrin and 0.1% sodium selenite (VWR International BV, Amsterdam, The Netherlands). After maturation, oocytes were denuded from the surrounding cumulus cells by gentle pipetting through a fine bore pipette, after a brief exposure to a 1 μg/mL solution of hyaluronidase (Sigma-Aldrich Chemical Co., St. Louis, Missouri, United States) in H-SOF. For the PCR experiments, oocytes were further divided into two groups depending on the presence or absence of the first polar body. For the inhibition experiments, only oocytes showing polar body extrusion were used.

RNA Extraction, cDNA Synthesis and Quantitative Real Time-PCR (qRT-PCR)

Oocytes used for qRT-PCR were divided into 8 groups depending on the mare's age (young or old), cumulus appearance before *in vitro* maturation (compact or expanded) and the presence or absence of a polar body after *in vitro* maturation (MII or non-MII). Oocytes were briefly washed in PBS (B. Braun, Hessen, Germany), and then transferred with a minimum amount of medium into pre-labeled cryovials, snap frozen in liquid nitrogen and stored at -80°C. Total RNA was extracted from pools of 10 oocytes (n = 4 per group) using the Invisorb® Spin Cell RNA Mini Kit (Invitek, Berlin, Germany) according to the manufacturer's instructions. Each pool of oocytes was lysed in 600 ml lysis buffer, and total RNA was eluted with 20 μl RNase-free water, after which RNA concentration and integrity were measured as described previously (de Ruijter-Villani et al., 2013, p. 979–989). The RNA was then treated with DNAse I (30 min at 37°C followed by 10 min at 65°C; 1 IU/mg of RNA; RNAse-Free DNase set, Qiagen Valencia, California, United States) and reverse transcribed into cDNA in a total volume of 20 μl containing 10 μl of sample using Superscript III (Invitrogen Corporation, Carlsbad, California, United States) as described previously (de Ruijter-Villani et al., 2013, p. 979–989). Minus RT blanks were prepared from 5 μl of sample under the same conditions, but in the absence of reverse transcriptase. Primer pairs (**Table 3**) for target genes (*Mad2, Bub1, Bub3, Bub1b, Mps1, Ndc80, Spc25, AurkB, AurkC*) and housekeeping genes (*Pgk1* and *Srp14*) were designed using PerlPrimer (Marshall, 2004, p. 2471–2472) and produced at Eurogentec (Seraing, Belgium). Primer specificity was tested by DNA sequencing (ABI PRISM 310 Genetic analyzer; Applied Bio-system, Foster City, California, United States). Real-time PCR was performed as described previously (de Ruijter-Villani et al., 2013, p. 979–989) in 15 μl of reaction mix that included 7.5 μl of IQ SYBR® Green Supermix (BioRad, Veenendaal, Netherlands), 0.5 mM of primer, and 1 μl of cDNA, on an IQ5 Real-Time PCR detection System (BioRad). The cycle conditions were composed of an initial denaturation at 95°C for 3 min, followed by 40 amplification cycles consisting of 95°C for 3 min, the primer-specific annealing temperature (**Table 3**) for 30 s and 72°C for 45 s. A melting curve and standard curve were performed for each gene to verify product specificity and enable expression quantification. The stability of the housekeeping genes was determined using GeNorm (Vandesompele et al., 2002) and the geometric mean of the expression of SRP14 and PGK1 was used for normalizing the starting quantities of the target genes.

Nocodazole, MPS1i and AURKi Treatment of Oocytes

The function of the two kinases Mps1 and AurkC was investigated using two inhibitory drugs, namely Mps1i or compound 5 (kindly supplied by Prof. Geert Kops Hubrecht Institute, Utrecht, the Netherlands) (Kwiatkowski et al., 2010, p. 359–368) and AURKi or ZM447439 (CAS 331771, Sigma-Aldrich Chemical Co., St. Louis, Missouri, United States). In order to evaluate the function of Mps1 and AurkC on spindle assembly, mature oocytes displaying a polar body were first incubated for 10 min at 38°C with 5% CO_2 in IVM medium containing 20 μM Nocodazole (M1404, Sigma-Aldrich Chemical Co., St. Louis, Missouri, United States) to depolymerize the MII-spindle. Following Nocodazole washout, the oocytes were left to re-form their spindle for 120 min in IVM medium with different concentrations of either MPS1i (0, 200, or 500 nM) or AURKi (0, 5, or 10 μM). The oocytes in the control group were not treated with nocodazole or inhibitors.

Oocyte Fixation

Before fixing, all oocytes were exposed to cold shock on ice for 9 min to depolymerize unstable microtubules. The oocytes were then treated with a glycerol-based microtubule-stabilizing solution (Medium M) for 1 h at 37°C (Simerly and Schatten, 1993), (25% (v/v) glycerol, 50 mM KCl, 0.5 mM $MgCl_2$, 0.1 mM EDTA, 0.1 mM EGTA, 1 mM 2-mercaptoethanol, 50 mM imidazole, 4% Triton-X-100, and 25 mM phenylmethylsulphonylfuoride; pH 6.7: all from Sigma-Aldrich Chemical Co.), and subsequently fixed with a 2% solution of paraformaldehyde (Electron Microscopy Sciences, Hatfield, Pennsylvania, United States) in PBS.

Immunostaining, Confocal Imaging and 3-Dimensional Image Analysis

Fixed oocytes were immunostained for α-tubulin and chromatin as described previously (Rizzo et al., 2019, p. 252–257). Shortly, oocytes were washed in PBS with 3 mg/ml PVP (Sigma-Aldrich Chemical Co.) (PBS-PVP) three times for 5 min before being incubated over-night in PBS containing 1:250 mouse monoclonal anti-α-tubulin antibody (T5168, Sigma-Aldrich Chemical Co.) at 4°C. Oocytes where then washed twice for 5 min in a 0.1% solution of BSA (Sigma-Aldrich Chemical Co.) in PBS and incubated for 1 h at Room Temperature (RT) in blocking solution containing 0.1 M glycine, 1% goat serum, 0.01% Triton

X-100, 0.5% BSA, and 0.02% sodium azide (all from Sigma-Aldrich Chemical Co.), followed by incubation in the dark at 37°C in PBS containing 0.5% Triton X-100, 0.5% BSA and a 1:100 Goat Anti-Mouse Alexa Fluor® 488 antibody (A11029, Invitrogen Corporation, Carlsbad, California, United States). After two washing steps of 5 min in PBS containing 0.1% BSA and 0.1% Triton X-100, and two washing steps of 5 min in PBS alone, the oocytes were incubated in the dark for 30 min at RT in PBS-PVP containing 5 μg/ml of Hoechst (Hoechst 33342, Sigma-Aldrich Chemical Co.). After a brief wash in PBS-PVP, the oocytes were mounted on glass slides (SuperfrostPlus; Menzel, Braunschweig, Germany) with Vectashield (Vector Laboratories, Burlingame, California, United States) to avoid photobleaching. Image acquisition was performed using a confocal laser scanning microscope (Leica TCS-SPE-II; Leica Microsystems, Wetzlar, Germany) equipped with a 63× objective. Hoechst 33342 was stimulated with a 405 nm laser and the emission was detected between 414 and 466 nm (blue channel), Alexa Fluor 488 was separately stimulated with a 488 nm laser and emission was detected in the 511–577 nm range (green channel). Metaphase II spindles were identified, and sequential sections were taken throughout the whole spindle at 0.42-μm intervals (z-step size). Image-acquisition and analysis of spindle morphology and chromosome alignment were performed using 3D analysis software (Imaris 8.1; Bitplane AG, Zurich, Switzerland) as described previously by Rizzo et al. (2019, p. 252–257). Gross morphology of MII spindles were classified as described by Baudoin and Cimini (2018, p. 215–227; **Table 1**). Chromosome misalignment was classified as absent when all chromosomes were on the metaphase plate, mild if up to 5 chromosomes were displaced from the spindle equator and severe if more than 5 chromosomes were displaced from the spindle equator, as described previously (Rizzo et al., 2019, p. 252–257).

Statistical Analysis

QRT-PCR data were analyzed using SPSS 16.0 for Windows (SPSS Inc., Chicago, IL). To obtain continuous normally distributed data sets, the relative starting quantities were subjected to natural logarithmic transformation. Data were analyzed using a two-way between-groups ANOVA, followed by a *post hoc* Tukey test. When a significant effect of the interaction was found, the analysis of simple effects was conducted by running separate one-way ANOVAs.

The incidence of spindle abnormalities and chromosome misalignment between age and treatment groups were compared by Fisher's exact and Cochran-Mantel-Haenszel tests, using a Chi-squared analysis performed using IBM SPSS Statistics for Windows (Version 24.0, Armonk, New Your, United States). Results were considered statistically significant when $P \leq 0.05$.

DATA AVAILABILITY STATEMENT

The raw data supporting the conclusions of this article will be made available by the authors, without undue reservation.

AUTHOR CONTRIBUTIONS

MD and MR-V conceived the project, further designed and conducted the experiments and wrote the original draft of the manuscript. MD performed the formal analysis. TS and GK contributed to conception of the work and edited the manuscript. SC and MQ edited the manuscript. All authors contributed to the interpretation of the data and read and approved the final manuscript.

ACKNOWLEDGMENTS

Confocal microscopy and 3D-analysis were performed at the Center for Cellular Imaging (CCI) at the Faculty of Veterinary Medicine, Utrecht. The authors would like to thank Richard Wubbolts and Esther van 't Veld for their assistance during confocal imaging and Heiko Henning for his help with statistical analysis.

SUPPLEMENTARY MATERIAL

The Supplementary Material for this article can be found online at: https://www.frontiersin.org/articles/10.3389/fcell.2021.657366/full#supplementary-material

Supplementary Figure 1 | mRNA expression for *Mad2L2, Bub1, Bub3, Bub1B, Ndc80,* and *AURKB* in oocytes from young (≤14 years) and old (≥16 years) mares. The box plot shows the interquartile range, with the median value indicated by the horizontal line; whiskers show the range.

Supplementary Figure 2 | Representative images of spindles of MII oocytes showing chromosome misalignment. Maximum intensity projections of confocal sections. Microtubules (alpha-tubulin, green); chromatin (Hoechst, blue). Scale bars, 5 μm. **(A)** bipolar spindle with all chromosomes on the metaphase plate from a young mare's oocyte treated with 0 μM of MPS1i; **(B)** bipolar spindle with mild chromosome misalignment from an old mare's oocyte treated with 0 μM of MPS1i; **(C)** bipolar spindle with mild chromosome misalignment from an old mare's oocyte treated with 0 μM of MPS1i; **(D)** bipolar spindle with severe chromosome misalignment from an old mare's oocyte treated with 500 μM of MPS1i.

Supplementary Table 1 | Number, type and frequency of mild and severe chromosome misalignment in bipolar spindles of MII oocytes from young (≤14 years) and old (≥16 years) mares, treated with MPS1i (0, 200, or 500 nM) or AURKi (0, 5, or 10 μM) after Nocodazole washout. Oocytes in the control groups were not treated with nocodazole or an inhibitor. Totals that share the same superscript do not differ significantly; $P < 0.05$.

REFERENCES

Balboula, A. Z., and Schindler, K. (2014). Selective disruption of aurora C kinase reveals distinct functions from aurora B kinase during meiosis in mouse oocytes. *PLoS Genet.* 10:e1004194. doi: 10.1371/journal.pgen.1004194

Balboula, A. Z., Nguyen, A. L., Gentilello, A. S., Quartuccio, S. M., Drutovic, D., Solc, P., et al. (2016). Haspin kinase regulates microtubule-organizing center clustering and stability through Aurora kinase C in mouse oocytes. *J. Cell Sci.* 129, 3648–3660. doi: 10.1242/jcs.189340

Balboula, A. Z., Stein, P., Schultz, R. M., and Schindler, K. (2015). RBBP4 regulates histone deacetylation and bipolar spindle assembly during oocyte maturation in the mouse. *Biol. Reprod.* 92:105.

Battaglia, D. E., Goodwin, P., Klein, N. A., and Soules, M. R. (1996). Influence of maternal age on meiotic spindle assembly in oocytes from naturally cycling

women. *Hum. Reprod.* 11, 2217–2222. doi: 10.1093/oxfordjournals.humrep.a019080

Baudoin, N. C., and Cimini, D. (2018). A guide to classifying mitotic stages and mitotic defects in fixed cells. *Chromosoma* 127, 215–227. doi: 10.1007/s00412-018-0660-2

Breuer, M., Kolano, A., Kwon, M., Li, C., Tsai, T., Pellman, D., et al. (2010). HURP permits MTOC sorting for robust meiotic spindle bipolarity, similar to extra centrosome clustering in cancer cells. *J. Cell Biol.* 191, 1251–1260. doi: 10.1083/jcb.201005065

Burkhardt, S., Borsos, M., Szydlowska, A., Godwin, J., Williams, S. A., Cohen, P. E., et al. (2016). Chromosome cohesion established by Rec8-Cohesin in fetal oocytes is maintained without detectable turnover in oocytes arrested for months in mice. *Curr. Biol.* 26, 678–685. doi: 10.1016/j.cub.2015.12.073

Chiang, T., Duncan, F. E., Schindler, K., Schultz, R. M., and Lampson, M. A. (2010). Evidence that weakened centromere cohesion is a leading cause of age-related aneuploidy in oocytes. *Curr. Biol.* 20, 1522–1528. doi: 10.1016/j.cub.2010.06.069

de Ruijter-Villani, M., van Boxtel, P. R. M., and Stout, T. A. E. (2013). Fibroblast growth factor-2 expression in the preimplantation equine conceptus and endometrium of pregnant and cyclic mares. *Theriogenology* 80, 979–989. doi: 10.1016/j.theriogenology.2013.07.024

Ems-Mcclung, S. C., Hainline, S. G., Devare, J., Zong, H., Cai, S., Carnes, S. K., et al. (2013). Aurora B inhibits MCAK activity through a phosphoconformational switch that reduces microtubule association. *Curr. Biol.* 23, 2491–2499. doi: 10.1016/j.cub.2013.10.054

Fragouli, E., Alfarawati, S., Goodall, N., Sánchez-García, J. F., Colls, P., and Wells, D. (2011). The cytogenetics of polar bodies: insights into female meiosis and the diagnosis of aneuploidy. *Mol. Hum. Reprod.* 17, 286–295. doi: 10.1093/molehr/gar024

Gruhn, J. R., Zielinska, A. P., Shukla, V., Blanshard, R., Capalbo, A., Cimadomo, D., et al. (2019). Chromosome errors in human eggs shape natural fertility over reproductive life span. *Science* 365, 1466–1469. doi: 10.1126/science.aav7321

Hached, K., Xie, S. Z., Buffin, E., Cladière, D., Rachez, C., Sacras, M., et al. (2011). Mps1 at kinetochores is essential for female mouse meiosis I. *Development* 138, 2261–2271. doi: 10.1242/dev.061317

Herbert, M., Kalleas, D., Cooney, D., Lamb, M., and Lister, L. (2015). Meiosis and maternal aging: insights from aneuploid oocytes and trisomy births. *Cold Spring Harb. Perspect. Biol.* 7:a017970. doi: 10.1101/cshperspect.a017970

Holubcová, Z., Blayney, M., Elder, K., and Schuh, M. (2015). Error-prone chromosome-mediated spindle assembly favors chromosome segregation defects in human oocytes. *Obstet. Gynecol. Surv.* 70, 572–573. doi: 10.1097/ogx.0000000000000240

Kwiatkowski, N., Jelluma, N., Filippakopoulos, P., Soundararajan, M., Manak, M. S., Kwon, M., et al. (2010). Small-molecule kinase inhibitors provide insight into Mps1 cell cycle function. *Nat. Chem. Biol.* 6, 359–368. doi: 10.1038/nchembio.345

Lane, S. I. R., Chang, H., Jennings, P. C., and Jones, K. T. (2010). The Aurora kinase inhibitor ZM447439 accelerates first meiosis in mouse oocytes by overriding the spindle assembly checkpoint. *Reproduction* 140, 521–530. doi: 10.1530/rep-10-0223

Leber, B., Maier, B., Fuchs, F., Chi, J., Riffel, P., Anderhub, S., et al. (2010). Proteins required for centrosome clustering in cancer cells. *Sci. Transl. Med.* 2:33ra38. doi: 10.1126/scitranslmed.3000915

Li, X., Qin, Y., Wilsher, S., and Allen, W. R. (2006). Centrosome changes during meiosis in horse oocytes and first embryonic cell cycle organization following parthenogenesis, fertilization and nuclear transfer. *Reproduction* 131, 661–667. doi: 10.1530/rep.1.00795

Lister, L. M., Kouznetsova, A., Hyslop, L. A., Kalleas, D., Pace, S. L., Barel, J. C., et al. (2010). Age-related meiotic segregation errors in mammalian oocytes are preceded by depletion of cohesin and Sgo2. *Curr. Biol.* 20, 1511–1521. doi: 10.1016/j.cub.2010.08.023

Marquardt, J. R., Perkins, J. L., Beuoy, K. J., and Fisk, H. A. (2016). Modular elements of the TPR domain in the Mps1 N terminus differentially target Mps1 to the centrosome and kinetochore. *Proc. Natl. Acad. Sci. U. S. A.* 113, 7828–7833. doi: 10.1073/pnas.1607421113

Marshall, O. J. (2004). PerlPrimer: cross-platform, graphical primer design for standard, bisulphite and real-time PCR. *Bioinformatics* 20, 2471–2472. doi: 10.1093/bioinformatics/bth254

Mogessie, B., Scheffler, K., and Schuh, M. (2018). Assembly and positioning of the oocyte meiotic spindle. *Annu. Rev. Cell Dev. Biol.* 34, 381–403. doi: 10.1146/annurev-cellbio-100616-060553

Nakagawa, S., and FitzHarris, G. (2017). Intrinsically defective microtubule dynamics contribute to age-related chromosome segregation errors in mouse oocyte meiosis-I. *Curr.Biol.* 27, 1040–1047. doi: 10.1016/j.cub.2017.02.025

Nguyen, A. L., Drutovic, D., Vazquez, B. N., El Yakoubi, W., Gentilello, A. S., Malumbres, M., et al. (2018). Genetic interactions between the aurora kinases reveal new requirements for AURKB and AURKC during oocyte meiosis. *Curr. Biol.* 28, 3458–3468.e5.

Raudsepp, T., and Chowdhary, B. P. (1999). Construction of chromosome-specific paints for meta- and submetacentric autosomes and the sex chromosomes in the horse and their use to detect homologous chromosomal segments in the donkey. *Chromosome Res.* 7, 103–114.

Rizzo, M., Ducheyne, K. D., Deelen, C., Beitsma, M., Cristarella, S., Quartuccio, M., et al. (2019). Advanced mare age impairs the ability of in vitro-matured oocytes to correctly align chromosomes on the metaphase plate. *Equine Vet. J.* 51, 252–257. doi: 10.1111/evj.12995

Rizzo, M., Preez, N. D., Ducheyne, K. D., Deelen, C., Beitsma, M. M., Stout, T. A. E., et al. (2020). The horse as a natural model to study reproductive aging-induced aneuploidy and weakened centromeric cohesion in oocytes. *Aging* 12, 22220–22232. doi: 10.18632/aging.104159

Roeles, J., and Tsiavaliaris, G. (2019). Actin-microtubule interplay coordinates spindle assembly in human oocytes. *Nat. Commun.* 10:4651.

Shao, H., Ma, C., Zhang, X., Li, R., Miller, A. L., Bement, W. M., et al. (2012). Aurora B regulates spindle bipolarity in meiosis in vertebrate oocytes. *Cell Cycle* 11, 2672–2680. doi: 10.4161/cc.21016

Shomper, M., Lappa, C., and FitzHarris, G. (2014). Kinetochore microtubule establishment is defective in oocytes from aged mice. *Cell Cycle* 13, 1171–1179. doi: 10.4161/cc.28046

Shuda, K., Schindler, K., Ma, J., Schultz, R. M., and Donovan, P. J. (2009). Aurora kinase B modulates chromosome alignment in mouse oocytes. *Mol. Reprod. Dev.* 76, 1094–1105. doi: 10.1002/mrd.21075

Simerly, C., and Schatten, G. (1993). Techniques for localization of specific molecules in oocytes and embryos. *Methods Enzymol.* 225, 516–553. doi: 10.1016/0076-6879(93)25035-z

Tremoleda, J. L., Schoevers, E. J., Stout, T. A. E., Colenbrander, B., and Bevers, M. M. (2001). Organisation of the cytoskeleton during in vitro maturation of horse oocytes. *Mol. Reprod. Dev.* 60, 260–269. doi: 10.1002/mrd.1086

Vandesompele, J., De Preter, K., Pattyn, F., Poppe, B., Van Roy, N., De Paepe, A., et al. (2002). Accurate normalization of real-time quantitative RT-PCR data by geometric averaging of multiple internal control genes. *Genome Biol.* 3:research0034.1.

Vogt, E., Sanhaji, M., Klein, W., Seidel, T., Wordeman, L., and Eichenlaub-Ritter, U. (2010). MCAK is present at centromeres, midspindle and chiasmata and involved in silencing of the spindle assembly checkpoint in mammalian oocytes. *Mol. Hum. Reprod.* 16, 665–684. doi: 10.1093/molehr/gaq025

Wang, L., Yan, M., Xu, D., Cao, J., Zhu, X., Zeng, Y., et al. (2008). Requirement of aurora-A kinase in astral microtubule polymerization and spindle microtubule flux. *Cell Cycle* 7, 1104–1111. doi: 10.4161/cc.7.8.5738

Zielinska, A. P., Bellou, E., Sharma, N., Frombach, A., Seres, K. B., Gruhn, J. R., et al. (2019). Meiotic kinetochores fragment into multiple lobes upon cohesin loss in aging eggs. *Curr. Biol.* 29, 3749–3765.e7.

Zielinska, A. P., Holubcova, Z., Blayney, M., Elder, K., and Schuh, M. (2015). Sister kinetochore splitting and precocious disintegration of bivalents could explain the maternal age effect. *eLife* 4:e11389.

Conflict of Interest: The authors declare that the research was conducted in the absence of any commercial or financial relationships that could be construed as a potential conflict of interest.

frontiers in Cell and Developmental Biology

ORIGINAL RESEARCH
published: 07 May 2021
doi: 10.3389/fcell.2021.655794

NADPH Oxidase 5 and Melatonin: Involvement in Ram Sperm Capacitation

*Sara Miguel-Jiménez, Blanca Pina-Beltrán, Silvia Gimeno-Martos, Melissa Carvajal-Serna, Adriana Casao and Rosaura Pérez-Pe**

Grupo BIOFITER-Departamento de Bioquímica y Biología Molecular y Celular – Instituto Universitario de Investigación en Ciencias Ambientales de Aragón (IUCA), Facultad de Veterinaria, Universidad de Zaragoza, Zaragoza, Spain

Reactive oxygen species (ROS) play an essential role in mammalian sperm capacitation. NADPH oxidase 5 (NOX5) has been described as the main source of ROS production in some mammalian spermatozoa, such as human and equine. On the other hand, melatonin can decrease cellular ROS levels and regulates NOX activity in somatic cells. Therefore, the objectives of this work were (1) to identify NOX5 in ram spermatozoa and analyze its possible changes during *in vitro* capacitation and (2) to investigate the effect of melatonin on NOX5 expression and localization and on superoxide levels in capacitated ram spermatozoa. Protein bands associated with NOX5 were detected by Western blot analysis. Likewise, indirect immunofluorescence (IIF) revealed six different immunotypes for NOX5, which varied throughout *in vitro* capacitation. Superoxide ($O_2^{\cdot -}$), evaluated by DHE/Yo-Pro-1, rose after *in vitro* capacitation and in the presence of the calcium ionophore A23187 but decreased in the presence of the NOX inhibitor GKT136901. GKT also reduced the percentage of capacitated and acrosome-reacted spermatozoa that had increased during incubation in capacitating conditions. The presence of melatonin at micromolar concentrations avoided the increment in $O_2^{\cdot -}$ and the changes in NOX5 immunotypes provoked by capacitation. In conclusion, NOX5 is present in ram spermatozoa and the changes in its distribution, associated with sperm capacitation, can be prevented by melatonin. To this extent, it could imply that melatonin exerts its antioxidant role, at least in part, by modulating NOX5 activity during ram sperm capacitation.

Keywords: ram spermatozoa, capacitation, NADPH oxidase, NOX5, melatonin, reactive oxygen species

OPEN ACCESS

Edited by:
Ana Josefa Soler, University of Castilla-La Mancha, Spain

Reviewed by:
David Martin Hidalgo, University of Porto, Portugal
Satoshi Kishigami, University of Yamanashi, Japan

****Correspondence:***
Rosaura Pérez-Pe
rosperez@unizar.es

Specialty section:
This article was submitted to Cell Growth and Division, a section of the journal Frontiers in Cell and Developmental Biology

Received: *19 January 2021*
Accepted: *24 March 2021*
Published: *07 May 2021*

Citation:
Miguel-Jiménez S, Pina-Beltrán B, Gimeno-Martos S, Carvajal-Serna M, Casao A and Pérez-Pe R (2021) NADPH Oxidase 5 and Melatonin: Involvement in Ram Sperm Capacitation. Front. Cell Dev. Biol. 9:655794. doi: 10.3389/fcell.2021.655794

INTRODUCTION

Reactive oxygen species (ROS), such as superoxide anion ($O_2^{\cdot -}$), are involved in sperm functionality under physiological conditions. ROS are essential for processes like capacitation, hyperactivation, acrosome reaction, and sperm-oocyte fusion (Griveau and Le Lannou, 1994; de Lamirande and Gagnon, 1995; O'Flaherty, 2015), but an excess can be detrimental to the sperm function (reviewed by Dutta et al., 2019).

It is well known that sperm cells by themselves can generate the superoxide anion (Aitken and Clarkson, 1987; Alvarez et al., 1987) which spontaneously or enzymatically dismutates to hydrogen

peroxide (H_2O_2) (Halliwell and Gutteridge, 1989). The enzymes responsible for this superoxide production are the NADPH oxidases (NOX) (Bedard and Krause, 2007; Maghzal et al., 2012) and, more specifically, the NOX5 in mammal spermatozoa (Ghanbari et al., 2018). This isoform has some characteristics that differentiate it from other NOX family members (reviewed by Touyz et al., 2019). NOX5 does not need the NADPH oxidase subunit for its activation, but it is entirely calcium-dependent, thanks to the calcium-binding sites on its N-terminal. There is a high-level expression of NOX5 mRNA in the human testis (Banfi et al., 2001), and the presence of the enzyme has also been described in human (Musset et al., 2012), canine (Setyawan et al., 2016), and equine (Sabeur and Ball, 2007) spermatozoa. The fact that the addition of a calcium ionophore (A23187) to spermatozoa induces ROS generation (Aitken et al., 1992; de Lamirande et al., 1998) suggests that NOX5 is the primary source of ROS in these cells (Banfi et al., 2001). However, there is no NOX5 gene or protein in murine spermatozoa, which indicates that, at least in this species, another source must be involved in the superoxide generation (Vernet et al., 2001), such as mitochondria (Koppers et al., 2008) or inflammatory leukocytes (Whittington et al., 1999).

An increase in the production of ROS [superoxide anion (O_2^{--}), hydrogen peroxide (H_2O_2), nitric oxide (NO·), and peroxynitrite ($ONOO^-$)] is one of the essential events that occur during sperm capacitation (de Lamirande and Gagnon, 1995; Herrero et al., 2003; O'Flaherty et al., 2004b). According to Ghanbari et al. (2018), the NOX5 enzyme must be involved in this process, due to its capacity to produce O_2^{--}. Other authors also assumed that the superoxide produced by NOX5, and the peroxides derived from it, activate the adenylyl cyclase, and thus the cAMP-PKA pathway (Zhang and Zheng, 1996; O'Flaherty, 2015; Moreno-Irusta et al., 2020), which finally leads to the phosphorylation of the tyrosine residues associated with sperm capacitation, as described in human and rat (Lewis and Aitken, 2001; O'Flaherty et al., 2004a). This process may also occur in ram spermatozoa. However, to the best of our knowledge, the NOX5 isoform has not been identified in ram spermatozoa.

Ovine reproduction has a marked seasonality, controlled by the secretion of melatonin from the pineal gland. This hormone directly affects the synthesis and secretion of the gonadotropic hormones via the hypothalamic–pituitary axis (Bittman et al., 1983). It is also synthesized by the reproductive tract (Gonzalez-Arto et al., 2016), and it is present in reproductive fluids, such as seminal plasma (Casao et al., 2010a) or follicular fluid (Brzezinski et al., 1987). Thus, as we have demonstrated over recent years, melatonin directly affects ram sperm functionality and modulates capacitation, decreasing apoptosis markers and oxidative stress (Casao et al., 2010b; Gimeno-Martos et al., 2019; Miguel-Jimenez et al., 2020). The well-known antioxidant capacity of melatonin may be the reason for its anti-apoptotic action since elevated ROS levels lead to early cell death (Rao and Gangadharan, 2008; Casao et al., 2010b; du Plessis et al., 2010; Jang et al., 2010; Espino et al., 2011; Gimeno-Martos et al., 2019; Miguel-Jimenez et al., 2020). Furthermore, a recent study in somatic cells (Patino et al., 2016) found an antioxidant melatonin effect throughout NOX regulation.

Considering NOX5 as the principal source of ROS in mammalian spermatozoa, the involvement of ROS in sperm capacitation and the effects of melatonin on regulating this process in ram, we set out to determine whether the effect of this hormone on ram sperm capacitation is mediated by the reduction of superoxide levels through NOX5 activity modulation. For this purpose, the objectives of this work were to detect the NOX5 isoform in ram spermatozoa (1), to determine superoxide and NOX5 involvement in ram sperm capacitation (2), and finally, to investigate how melatonin affects the expression and localization of NOX5 and superoxide levels in capacitated ram spermatozoa (3).

MATERIALS AND METHODS

Unless otherwise stated, all reagents were purchased from Merck KGaA (Darmstadt, Germany).

Semen Collection and Processing

Semen was collected from nine *Rasa Aragonesa* rams (2–4 years old) with the aid of an artificial vagina. All the rams belonged to the Rasa Aragonesa National Breeding Association (Asociación Nacional de Criadores de Ganado Ovino Selecto de Raza Rasa Aragonesa, ANGRA) and were kept at the Experimental Farm of the University of Zaragoza Veterinary School under the same nutritional conditions. All experimental procedures were performed under the project license PI39/17 approved by the University of Zaragoza Ethics Committee for Animal Experiments, following the Spanish Policy for Animal Protection RD53/2013, which meets the European Union Directive 2010/63 on the protection of animals used for experimental and other scientific purposes.

After 2 days of abstinence, two successive ejaculates were collected, and second ejaculates were pooled and processed together to avoid individual differences (Ollero et al., 1996). The ejaculates were kept at 37°C until analysis.

In order to obtain a plasma-free sperm population, a dextran/swim-up procedure (García-López et al., 1996) was performed in a medium with the following composition: 200 mM sucrose, 50 mM NaCl, 2.7 mM $CaCl_2$, 18.6 mM sodium lactate, 21 mM HEPES, 10 mM KCl, 2.8 mM glucose, 0.4 mM $MgSO_4$, 0.3 mM sodium pyruvate, 0.3 mM K_2HPO_4, 5 mg/mL bovine serum albumin (BSA), 30 mg/mL dextran, 1.5 IU/mL penicillin, and 1.5 mg/mL streptomycin, pH 6.5.

Sperm concentration was calculated in duplicate using a Neubauer chamber (Marienfeld, Lauda-Königshofen, Germany).

In vitro Capacitation

Swim-up-selected spermatozoa, in aliquots of 1.6×10^8 cells/mL, were incubated for 3 h at 39°C in a humidified incubator with 5% CO_2 in the air. Incubations were performed in a complete TALP medium (Parrish et al., 1988) containing 100 mM NaCl, 3.1 mM KCl, 25 mM $NaHCO_3$, 0.3 mM NaH_2PO_4, 21.6 mM Na lactate, 3 mM $CaCl_2$, 0.4 mM $MgCl_2$, 10 mM HEPES, 1 mM Na pyruvate, 5 mM glucose, and 5 mg/mL bovine serum albumin (BSA), with a pH of 7.3 (TALP samples). Several cAMP-elevating

agents, already proven for capacitating ram spermatozoa (Grasa et al., 2006; Colas et al., 2008) and composed of 1 mM dibutyryl (db)-cAMP, 1 mM caffeine, 1 mM theophylline, 0.2 mM okadaic acid, and 2.5 mM methyl-b-cyclodextrin, were added to the TALP medium to induce *in vitro* capacitation (capacitated-control samples, Cap-C).

To further investigate the role of NOX5 during *in vitro* capacitation, the NOX inhibitor 2-(2-chlorophenyl)-4-methyl-5-(pyridin-2-ylmethyl)-1*H*-pyrazolo[4,3-*c*]pyridine-3,6(2H,5H)-dione (GKT136901, GKT) was added to the capacitation medium at final concentrations of 1 μM (Musset et al., 2012; Altenhofer et al., 2015). Taking into account that the activation of NOX5 is calcium-dependent (Banfi et al., 2001), 1 μM calcium ionophore A23187 was added to the sperm samples to evaluate the effect of NOX5 activation on changes related to capacitation.

Melatonin was solubilized in dimethyl sulfoxide (DMSO) and phosphate-buffered saline (PBS: 137 mM NaCl, 2.7 mM KCl, 8.1 mM Na_2HPO_4, and 1.76 KH_2PO_4, pH 7.4) and added to the capacitation medium at a final concentration of 1 μM. The final concentration of DMSO in all the melatonin samples was 0.1%. To account for the potential adverse effect of DMSO, the same concentration was included in capacitated-control samples to which no melatonin had been added.

Thus, the experimental groups in the present study were swim-up (spermatozoa selected by the dextran/swim-up method before inducing *in vitro* capacitation), TALP samples (spermatozoa incubated under capacitating conditions without cAMP-elevating agents), and capacitated-control (Cap-C, spermatozoa incubated under capacitating conditions in TALP medium with cAMP-elevating agents). Each compound (GKT136901, calcium ionophore A23187, melatonin or a combination of them) was added at 1 μM concentration to samples incubated in TALP and high-cAMP medium samples.

Sperm Motility Evaluation

Total and progressive motility was evaluated using the motility module of OpenCASA, a free open-source software that we recently developed (Alquezar-Baeta et al., 2019). Two drops of 2 μL of each sample, diluted to a final concentration of 3×10^7 cells/mL, were placed in a pre-warmed Makler counting chamber (Sefi Medical Instruments, Haifa, Israel) and maintained at 37°C during all the analyses by a heated slide holder. Spermatozoa were recorded with a video camera (Basler acA1920; Basler Vision Components, Ahrensburg, Germany) mounted on a microscope (Nikon Eclipse 50i, Nikon Instruments Int, Tokyo, Japan) equipped with a 10 × negative-phase contrast lens.

Recorded videos were evaluated with the following settings: 60 frames per second, 120 frames, 800 × 600 pixel image resolution, 10 μm^2 minimum cell size, 100 μm^2 maximum cell size, STR (straightness coefficient) > 80% and VAP (mean velocity) > 90%, 10 μm/s minimum VCL (curvilinear velocity), 100 μm/s VCL lower threshold, 200 m/s VCL upper threshold, 30 frames minimum track length, and 20 μm maximum displacement between frames.

Flow Cytometry Analysis

All the measurements were performed on a Beckman Coulter FC 500 flow cytometer (Beckman Coulter Inc., Brea, CA, United States) equipped with two excitation lasers (air-cooled Argon ion laser 488 nm and Red Solid state laser 633 nm); five absorbance filters (FL1-525, FL2-575, FL3-610, FL4-675, and FL5-755; ± 5 nm each band pass filter); and CXP software. A minimum of 20,000 events were evaluated in all the experiments. The sperm population was identified for further analysis on the basis of its specific forward (FS) and side-scatter (SS) properties; thus, other events were excluded. A flow rate stabilized at 200–300 cells/s was used.

Sperm Membrane Integrity

Sperm viability, considered as the integrity of the cell plasma membrane, was assessed by adding 3 μL of 1 mM carboxyfluorescein diacetate (CFDA), 1.5 mM propidium iodide (PI), and 5 μL of formaldehyde (0.5% (v/v) in water) to a final concentration of 5×10^6 cells/mL in a 300 μL volume, based on a modification of the procedure described by Harrison and Vickers (1990). Samples were incubated at 37°C in darkness for 15 min. For the sperm viability analysis, the Argon laser and filters FL1-525 and FL4-675 nm were used to avoid overlapping. The monitored parameters were FS log, SS log, FL1 log (CFDA), and FL4 log (PI). The percentage of viable spermatozoa (PI-/CFDA+) was evaluated.

Superoxide Levels

To detect intracellular superoxide ($O_2^{\cdot -}$) levels in viable spermatozoa, cells (500 μL at 5×10^6 cells/mL) were loaded with 4 μM DHE and 40 nM Yo-Pro-1 (Thermo Fisher Scientific, Waltham, MA, United States) fluorochromes (Guthrie and Welch, 2006) and incubated at 37°C for 40 min in darkness. Hydroethidine is permeable to cells, and it is oxidized by $O_2^{\cdot -}$ to the red fluorescent compound ethidium (E), which was detected with the FL4-675-nm filter in the flow cytometer. Yo-Pro-1 labels cells with destabilized membrane (non-viable) with green fluorescence, detectable with the FL1-525-nm filter. Viable cells with intact membrane do not show fluorescence. Dot plots showed four different populations: viable cells with high $O_2^{\cdot -}$ production (Yo-Pro-1-/E+), viable cells with low $O_2^{\cdot -}$ production (Yo-Pro-1-/E-), non-viable cells with low $O_2^{\cdot -}$ production (Yo-Pro-1+/E-), and non-viable cells with high $O_2^{\cdot -}$ production (Yo-Pro-1+/E+). The percentage of viable spermatozoa with high superoxide levels (Yo-Pro-1-/E+) was evaluated.

Intracellular Calcium

To assess intracellular calcium levels, aliquots of 500 μL (5×10^6 cells/mL) were incubated with 2 μM Fluo-4-AM and 0.02% pluronic acid for 15 min at 37°C in darkness (both from Thermo Fisher Scientific, Waltham, MA, United States) and 1.5 mM PI. After this, a flow cytometer was used to evaluate the stained samples, as described previously, using the Argon laser and filters FL1-525 and FL4-675 nm. The monitored parameters were FS log, SS log, FL1 log (Fluo-4-AM), and FL4 log (PI).

The percentage of viable spermatozoa with high calcium levels (Fluo-4-AM+/PI-) was evaluated.

Determination of Capacitation Status

The sperm capacitation state was evaluated using the chlortetracycline (CTC) assay (Ward and Storey, 1984) that we previously validated for the evaluation of capacitation and acrosome reaction-like changes in ram spermatozoa (Grasa et al., 2006). A CTC solution (750 μM; Sigma-Aldrich Corp., St. Louis, MO, United States) was prepared daily in a buffer containing 20 mM Tris, 130 mM NaCl, and 5 μM cysteine, pH 7.8, and passed through a 0.22-μm filter. After that, 20 μL of CTC solution was added to 18 μL of each sperm sample, fixed with 5 μL of 1.25% (w/v) paraformaldehyde in 0.5 M Tris–HCl (pH 7.8) and incubated at 4°C in the dark for 30 min. Six microliters of the stained sample was placed onto a glass slide and mixed with 2 μL of 0.22 M 1,4-diazabicyclo[2.2.2]octane (DABCO) in glycerol:PBS (9:1 v/v). The samples were covered with 24 × 60 mm coverslips, sealed with transparent enamel, and stored in the dark at −20°C until evaluation. The samples were examined using a Nikon Eclipse E-400 microscope (Nikon Corporation, Kanagawa, Japan) under epifluorescence illumination with a V-2A filter, and at least 200 spermatozoa were scored per sample. Three sperm patterns were identified (Gillan et al., 1997): non-capacitated (even distribution of fluorescence on the head, with or without a bright equatorial band), capacitated (with fluorescence in the acrosome), and acrosome-reacted cells (showing no fluorescence on the head, with or without a bright equatorial band).

Indirect Immunofluorescence

NOX5 localization was revealed by indirect immunofluorescence analyses (IIF). Sperm samples were diluted (2×10^6 cells/mL) in PBS and fixed in 0.5% (v/v) formaldehyde at room temperature for 20 min. Then, cells were centrifugated at 900 × *g*, and the pellet was resuspended in 500 μL PBS. Forty microliters of cell suspension was placed onto Superfrost slides (Superfrost Plus; Thermo Fisher Scientific, Waltham, MA, United States) and permeabilized with 0.5% (v/v) Triton X-100 in PBS for 15 min. Afterward, the cells were fixed again with paraformaldehyde 1.25% (w/v) in Tris–HCl 0.5 M for 5 min and washed three times with PBS. Non-specific binding sites were blocked with 5% (w/v) BSA in PBS for 5 h in a wet chamber. Slides were rewashed in PBS and incubated at 4°C overnight in a wet chamber with the primary antibody anti-NOX5 (Abcam, Cambridge, UK Cat# ab191010) 1/25 in PBS with 1% (v/v) BSA. The next morning, the samples were washed three times with PBS and incubated with the secondary antibody (Alexa Fluor 488 chicken anti-rabbit; Thermo Fisher Scientific; Cat#A-21441, RRID:AB_2535859), diluted 1/600 (v/v) in PBS with 1% (v/v) BSA for 90 min at room temperature in a wet chamber. Slides were then washed three times with PBS before the addition of 6 μL of 0.22 M 1,4-diazabicyclo[2.2.2]octane (DABCO) in glycerol:PBS (9:1 v/v) to enhance and preserve cell fluorescence. The slides were covered with a coverslip and sealed with transparent enamel. Cells were visualized with a Nikon Eclipse E400 microscope (Nikon, Tokyo, Japan) under epifluorescence illumination using a B-2A filter (×1,000). All samples were processed in duplicate, and at least 150 spermatozoa were scored per slide.

The specificity of the anti-NOX5 antibody was tested by the peptide blocking method. The antibody was neutralized with the immunizing blocking peptide (ProteoGenix, Schiltigheim, France) at a final concentration of 2.5 μg/mL in PBS with 1% BSA for 2 h at room temperature. The neutralized antibody was then used side by side with the antibody alone in two identical slides, and the results were comparatively analyzed. No signal was detected when using the neutralized antibody, which means that the antibody has high affinity for the NOX5 protein.

Western Blotting

For NOX5 detection, sperm proteins were extracted from spermatozoa, as previously described by Colas et al. (2008). Aliquots of 3.2×10^7 cells were centrifuged at 900 × g for 5 min. The supernatant was discarded, and the pellet was resuspended in 200 μL of extraction sample buffer [ESB; 68.6mM Tris–HCl (pH 6.8), 2% SDS (w/v)] with a 10% protease inhibitor cocktail. After incubation at 100°C in a sand bath for 5 min, the samples were centrifuged again at 7,500 × g for 5 min at 4°C. The supernatant was recovered, and β-mercaptoethanol, glycerol, and bromophenol blue (in 10% glycerol) were added to final concentrations of 5, 1, and 0.002% (v/v), respectively. Lysates were stored at -20°C.

Sperm extracted proteins (50 μL, 1–2 mg/mL) were separated in one dimension by 10% sodium dodecyl sulfate polyacrylamide gel electrophoresis (SDS-PAGE) (Laemmli, 1970) and transferred onto a PVDF membrane using a transfer unit (Trans-Blot Turbo Transfer System, Bio-Rad, Hercules, CA, United States). Non-specific sites on the PVDF membrane were blocked with 5% BSA (w/v) in PBS for 4 h. The proteins were immunodetected by incubating overnight at 4°C with a rabbit primary anti-NOX5 (Abcam, Cambridge, UK Cat# ab191010) diluted 1/400 in 0.1% (v/v) Tween-20 in PBS containing 1% (w/v) BSA. A mouse anti-tubulin antibody (Santa Cruz Biotechnology Cat# sc-8035, RRID:AB_628408) was used as a loading control (dilution 1/1,000). We used the commercial HeLa cell lysate (Abcam, Cambridge, United Kingdom), recommended explicitly by the antibody manufacturer, as a positive control. After extensive washing with 0.1% (v/v) Tween-20 PBS, membranes were incubated for 75 min at room temperature with the secondary antibodies donkey anti-rabbit (IRDye 680RD Donkey anti-Rabbit IgG antibody, LI-COR Biosciences Cat# 926-68073, RRID:AB_10954442) and donkey anti-mouse (RDye 800CW Donkey anti-Mouse IgG antibody, LI-COR Biosciences Cat# 926-32212, RRID:AB_621847) diluted 1/15,000 in 0.1% (v/v) Tween-20 PBS containing 1% (v/v) BSA. After extensive washing, the membranes were scanned using the Odyssey CLx Imaging System (LI-COR Biosciences, Lincoln, NE, United States).

The specificity of the anti-NOX5 antibody was tested by the peptide blocking method, as in the IIF assay. The neutralized antibody was used side by side with the antibody alone in two identical western blot membranes, and the results were comparatively analyzed. No signal was detected when using the neutralized antibody, which means that the antibody has high affinity for the NOX5 protein.

Western blot images were quantified using Odyssey Clx Infrared Imaging System software (Li-COR Biosciences, Lincoln, NE, United States) to determine the NOX5 protein bands' relative intensity, normalized to the tubulin control.

Statistical Analysis

Differences between the groups in motility, superoxide levels, viability, CTC staining, and NOX5 immunotypes were analyzed by means of the chi-square test. Differences in NOX5 expression profiles evaluated by western blot were analyzed by ANOVA followed by the Bonferroni *post hoc* test after evaluation of the data distribution by the Kolmogorov–Smirnov test. All statistical analyses were performed using GraphPad Prism 5 (v. 5.03; GraphPad Software, La Jolla, CA, United States).

RESULTS

All data obtained from the sperm samples capacitated without cAMP-elevating agents (TALP samples) are shown in the **Supplementary Material**, as this treatment had scarce effects on spermatozoa. The most evident changes were obtained after capacitating with cAMP-elevating agents, so that we focused on them.

NOX5 Immunodetection and Immunolocalization in Ram Spermatozoa

Western blot analysis identified protein bands with a molecular weight compatible with NOX5 (∼85 kDa) in swim-up, TALP samples, and capacitated control (Cap-C) samples (**Figure 1**). The molecular weights of these bands matched those found in the positive control. Besides, bands at 45 kDa and 30 kDa were detected.

Immunofluorescence analysis revealed the presence of the NOX5 enzyme in ram spermatozoa, and six different immunotypes were distinguished (**Figure 2**): immunotype 1, with labeling only at the midpiece; immunotype 2, with labeled acrosomal region; immunotype 3, labeling the apical edge; immunotype 4, labeling the apical edge and postacrosomal region; immunotype 5, labeling acrosomal and postacrosomal regions; and immunotype 6, with postacrosomal labeling. Also, all the immunotypes presented fluorescence at the midpiece.

Influence of NOX5 in Ram Sperm Capacitation

After demonstrating the presence of NOX5 in ram spermatozoa, we wanted to evaluate how the inhibition (by addition of GKT136901) or activation of NOX5 (by the increase in intracellular calcium provoked by the addition of calcium ionophore A23187) influenced some events related with sperm capacitation, such as changes in motility, CTC staining patterns, and superoxide levels. However, first, we verified that the addition of the ionophore was indeed capable of causing the calcium to enter inside the cell (**Supplementary Figure 1**).

Influence of NOX5 on Superoxide Intracellular Levels During Incubation in Capacitating Conditions

Superoxide intracellular levels ($O_2^{\cdot -}$), were assessed by flow cytometry, and the results are shown in **Figure 3**. *In vitro* capacitation with cAMP-elevating agents provoked an increase in the percentage of live spermatozoa with high $O_2^{\cdot -}$ levels (Yo-Pro-1-/E+), and the incubation with the NOX5 inhibitor partially limited this increase ($p < 0.05$). Meanwhile, the activation of NOX5 by the calcium ionophore trebled the Yo-Pro-1-/E + population ($p < 0.0001$). When the calcium ionophore was added in the presence of the GKT, there was still an increase of $O_2^{\cdot -}$ ($p < 0.0001$), but to a much lesser extent (24.53% ± 3.35%) than when the ionophore alone was added (45.83% ± 5.83%) (**Figure 3**).

Influence of NOX5 on Capacitation Status During Incubation in Capacitating Conditions

According to the chlortetracycline analysis (CTC), the percentage of capacitated spermatozoa significantly increased after a 3 h incubation under capacitating conditions (Cap-C, 57.71% ± 3.22%) compared to the swim-up samples (22.66% ± 1.5%, $p < 0.05$), as shown in **Figure 4**. The NOX5 inhibitor partially prevented sperm capacitation (52.85% ± 3.68%, $p < 0.05$). On the other hand, the addition of the calcium ionophore caused a significant percentage of acrosome-reacted spermatozoa ($p < 0.0001$). When GKT was added together with the calcium ionophore, there was a significant reduction in the percentage of acrosome-reacted spermatozoa compared with the same samples in the presence of the ionophore alone (10.50% ± 2.50% vs. 31.50% ± 3.80%, $p < 0.0001$).

Influence of NOX5 on Sperm Motility During Incubation in Capacitating Conditions

Total and progressive motility significantly decreased after *in vitro* capacitation with cAMP-elevating agents (**Figure 5**). No significant effects on total motility were found in the presence of GKT, but the NOX5 inhibitor was able to increase progressive motility (15.63% ± 4.45% vs. 22.18% ± 3.77%, $p < 0.001$). However, the addition of the calcium ionophore dramatically compromised total motility ($p < 0.0001$) and the spermatozoa were not able to move progressively at all. The presence of GKT was not able to revert this effect. Viability evaluation revealed that sperm membrane integrity was not compromised in any of the experimental conditions (**Supplementary Figure 2**).

Influence of Melatonin on the NOX5 Action on ram Spermatozoa

Once the existence and localization of the NADPH oxidase 5 in ram spermatozoa and its effects on sperm capacitation and functionality were confirmed, we continued further to elucidate whether the action of melatonin on ram sperm capacitation is mediated by its interaction with NOX5. Previously, we checked the effectiveness of the incubation in capacitating conditions and the already described decapacitating action of melatonin at 1 μM concentration on ram spermatozoa (Casao et al., 2010b) by CTC analysis. Melatonin was able to reduce the percentage

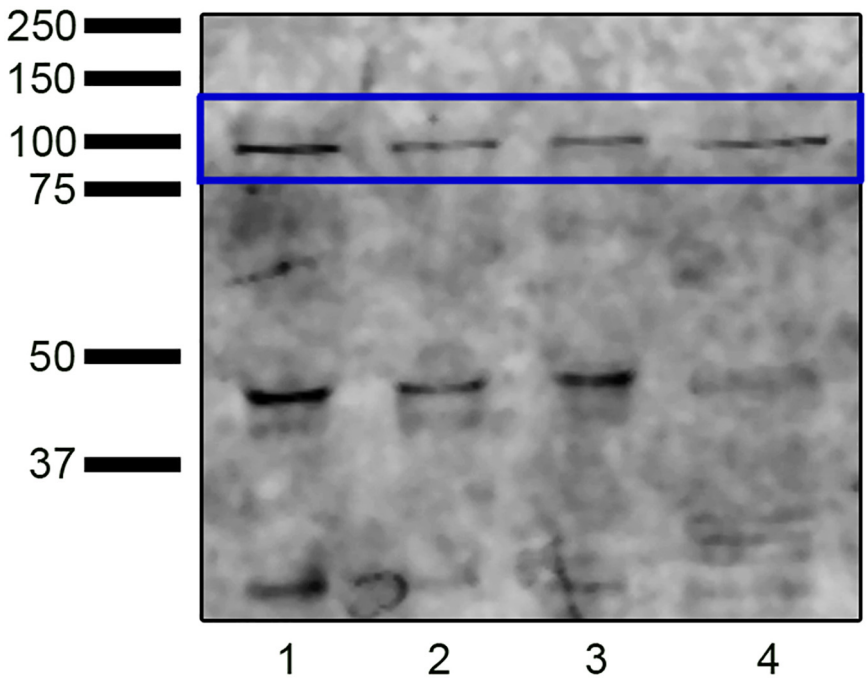

FIGURE 1 | Western blot analysis revealing the presence of NADPH oxidase 5 in ram sperm protein extracts from swim-up selected samples (lane 1) and samples incubated in capacitating conditions without (TALP, lane 2) or with cAMP elevating agents (Cap-C, lane 3). Positive control (lane 4): HeLa cell lysate.

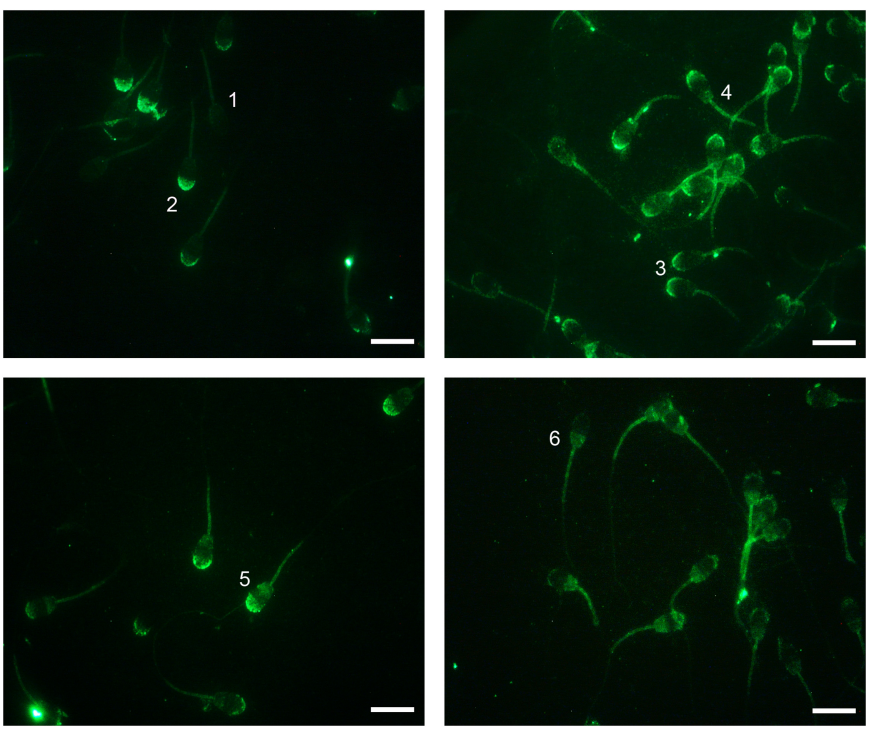

FIGURE 2 | Indirect immunofluorescence (IIF) localization of NOX5 evaluated by fluorescence microscopy in ram spermatozoa. Six immunotypes can be seen: labeling in midpiece (1); in the acrosomal region (2); in the apical edge (3); in the apical edge + postacrosomal region (4); in the acrosomal and postacrosomal regions (5); and in the postacrosomal region (6). All of them present midpiece labeling. Original magnification ×1,000. Scale bars = 10 μm.

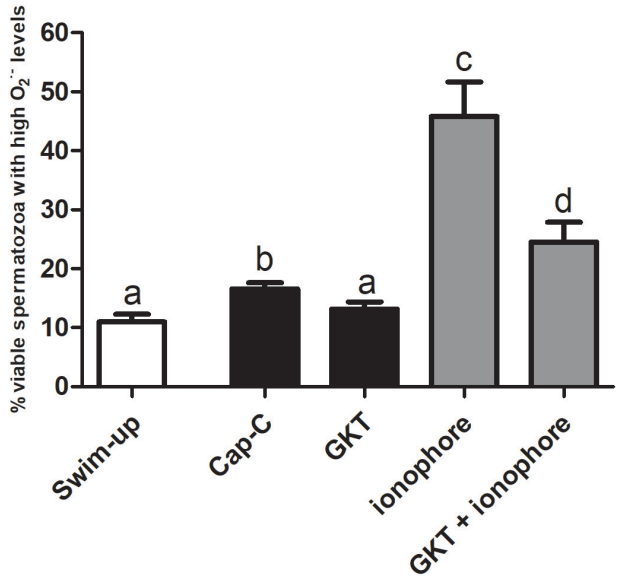

FIGURE 3 | Percentage of live spermatozoa with high superoxide levels (Yo-Pro-1–/E+) assessed by flow cytometry before (swim-up, white bars) and after *in vitro* capacitation with cAMP-elevating agents (Cap-C, black bars) and with GKT136901 (GKT, 1 μM) or/and calcium ionophore A23187 (ionophore, 1 μM, gray bars). Data are shown as mean ± S.E.M. ($n = 6$). Different letters indicate significant differences ($p < 0.05$).

of capacitated spermatozoa in Cap-C samples (44.87% ± 4.58% vs. 59.13% ± 4.16%, $p < 0.001$, **Figure 6**) in a similar extent to the NOX5 inhibitor (GKT, 50% ± 2.74%). Moreover, the incubation with melatonin ameliorated the ionophore effects, presenting a lower percentage of capacitated and acrosome-reacted spermatozoa, and more non-capacitated ($p < 0.01$) than in the ionophore samples.

Effect of Melatonin on Superoxide Levels

Regarding the production of the superoxides, melatonin prevented the superoxide production in live spermatozoa to a significant degree when compared to Cap-C samples ($p < 0.01$, **Figure 7**), even maintaining the same levels as before the capacitation induction (swim-up samples). The addition of calcium ionophore to the melatonin-preincubated sample did not reach the same superoxide levels as when added alone. Thus, melatonin prevented the superoxide production at the same level as the NOX5 inhibitor GKT136901 did.

Effect of Melatonin on NOX5 Levels and Immunolocation in Capacitated Samples

In order to better understand the results, and since the postacrosomal labeling was sometimes diffuse, we grouped those immunotypes that labeled the acrosomal region (immunotypes 2 and 5) and the apical edge (immunotypes 3 and 4) regardless of the postacrosomal staining (**Figure 8**). Before capacitation, in the swim-up selected samples, the primary localization for NOX5 was in the acrosomal region (40.85% ± 6.549417% inmunotypes 2 + 5) and the apical edge (47.9% 4 ± 4.47% immunotypes 3 + 4). The induction of *in vitro* capacitation with cAMP-elevating agents (Cap-C samples) produced a different redistribution of NOX5 ($p < 0.05$), with a lesser proportion of acrosomal immunotypes (2 + 5) and a higher percentage of immunotype 6 (postacrosomal region).

The addition of 1 μM melatonin resulted in the spermatozoa showing different labeling patterns. Thus, melatonin partially prevented the rise in the percentage of immunotype 6 that *in vitro* capacitation caused ($p < 0.05$) and led to an inversion in the proportion of acrosomal (47.41% ± 5.68%) and apical (37.74% ± 3.97%) immunotypes, compared to the Cap-C samples (32.140% ± 5.80% and 49.48% ± 4.63% respectively).

The incubation with GKT during sperm capacitation or the final addition of calcium ionophore to the samples did not provoke significant changes in the percentage of acrosomal and apical immunotypes comparing to the Cap-C samples. However, there was a higher proportion of midpiece labeling in all the samples incubated with ionophore ($p < 0.05$), and the combination of melatonin and GKT with calcium ionophore did not show significant differences compared to the ionophore samples.

Western blot assays were performed to investigate whether the melatonin effects on ram sperm-capacitated samples were mediated by changes in the NOX5 levels (**Figure 9**). The quantification of NOX5 bands by densitometry, after their normalization with the α-tubulin loading control (∼50 kDa), revealed no significant differences between the samples.

DISCUSSION

The discovery of NADPH oxidases clarified the source of ROS production in several cell types (Panday et al., 2015). In spermatozoa, the superoxide production was attributed, until several years ago, solely to leukocytes present in semen samples and related to pathological processes (Plante et al., 1994; Whittington et al., 1999). Nowadays, it is commonly assumed that the generation of ROS in spermatozoa would be mediated by autonomous NADPH oxidase activity and that certain levels of ROS would be necessary for some physiological events (reviewed in Bedard and Krause, 2007). NOX5 was discovered in 2001 in human testis, uterus, spleen, and lymph node (Banfi et al., 2001; Cheng et al., 2001). Some years later, it was found in equine (Sabeur and Ball, 2007), human (Musset et al., 2012; Ghani et al., 2013) and canine spermatozoa (Setyawan et al., 2016).

In the present study, we have demonstrated, for the first time, the presence of the NOX5 isoform in ram spermatozoa by Western blot and by indirect immunofluorescence. The 85-kDa protein band detected on the immunoblot matched with the protein detected in equine spermatozoa (Sabeur and Ball, 2007) and similarly with the 75 kDa protein in human spermatozoa (Musset et al., 2012). Likewise, the lower molecular weight protein bands also detected in ram sperm had previously been observed in equine spermatozoa, and the authors noted that they could correspond to proteolytic processes (Sabeur and Ball, 2007).

According to NOX5 localization in ram spermatozoa, we have described six different immunotypes, in contrast with

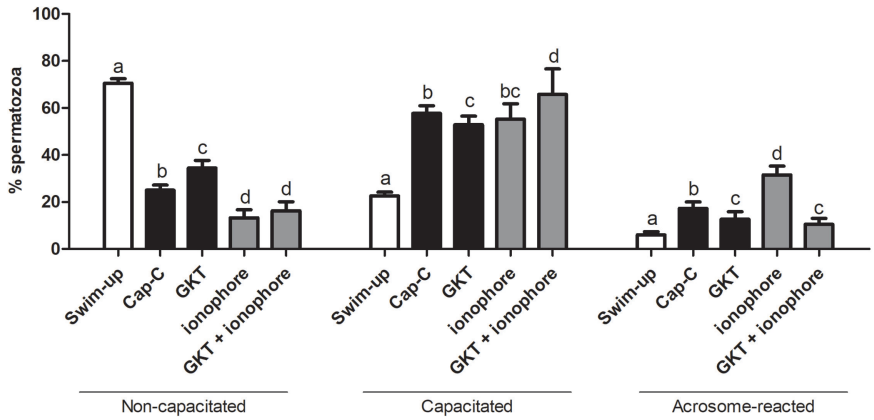

FIGURE 4 | Assessment of capacitation status, evaluated by chlortetracycline (CTC), in ram spermatozoa before (swim-up, white bars) and after *in vitro* capacitation with cAMP-elevating agents (Cap-C, black bars) and with GKT136901 (GKT, 1 μM) or/and calcium ionophore A23187 (ionophore, 1 μM, gray bars). Data of non-capacitated, capacitated, and acrosome-reacted spermatozoa are mean percentages ± SEM ($n = 6$). Different letters within the same group indicate significant differences ($p < 0.05$).

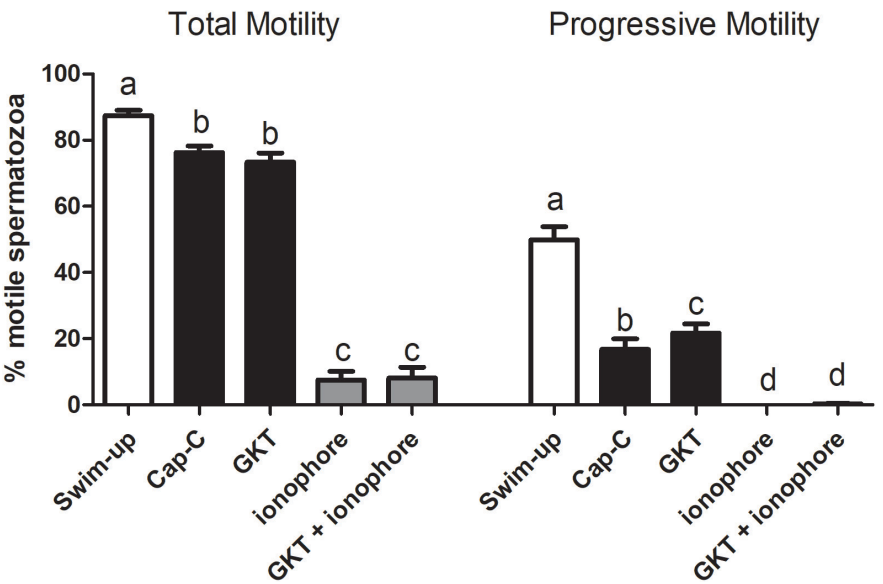

FIGURE 5 | Percentage of total motile (left) and progressive (right) spermatozoa before (swim-up, white bars) and after *in vitro* capacitation with cAMP-elevating agents (Cap-C, black bars) and with GKT136901 (GKT, 1 μM) or/and calcium ionophore A23187 (ionophore, 1 μM, gray bars). Data are shown as mean ± SEM ($n = 6$). Different letters indicate significant differences ($p < 0.05$).

the one or two immunotypes found in human (Musset et al., 2012) and equine (Sabeur and Ball, 2007) spermatozoa, respectively. Thus, NOX5 localization in spermatozoa seems to vary depending on the species. A significant finding of the present work is the evidence, for the first time, that incubation in capacitating conditions triggered a redistribution of NOX5 in ram spermatozoa. These findings suggest that the NOX5 could be involved in ram sperm capacitation, probably by regulating ROS production.

NOX5 product (superoxide anion) increased its levels in samples incubated under capacitating conditions, as reported in human, equine, and boar spermatozoa (de Lamirande and Gagnon, 1995; O'Flaherty et al., 2005; Burnaugh et al., 2007). Activation of NOX5, by the addition of ionophore A23187, dramatically increased superoxide levels in ram spermatozoa, as previously reported in human and equine (Griveau and Le Lannou, 1994; Aitken et al., 1997; Ball et al., 2001; Burnaugh et al., 2007). Inhibition of NOX5 by the addition of the NOX inhibitor (GKT136901) reduced the superoxide generation in samples incubated in capacitating conditions in the presence of cAMP-elevating agents.

We have also demonstrated that NOX5 is involved in ram sperm capacitation, since its inhibition by GKT136901 reduced the percentage of capacitated and acrosome-reacted spermatozoa

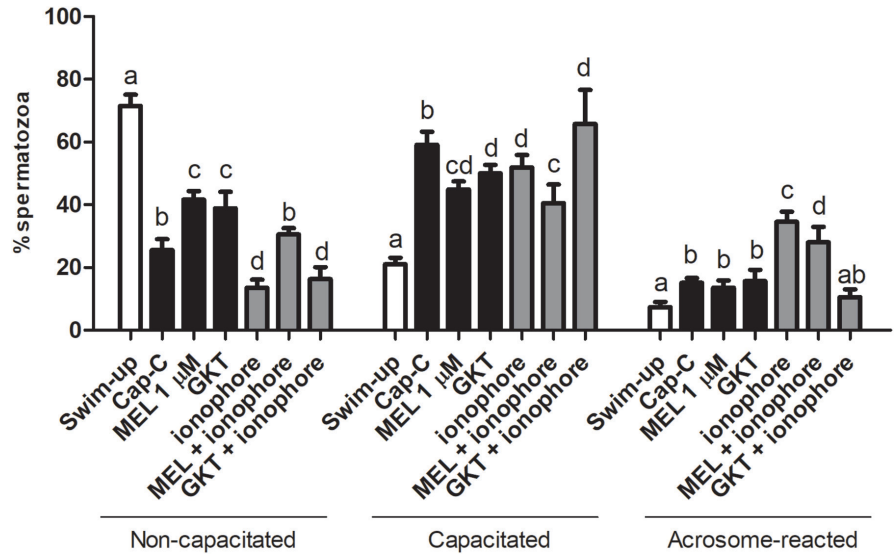

FIGURE 6 | Assessment of capacitation status, evaluated by CTC, in ram spermatozoa before (swim-up, white bars) and after *in vitro* capacitation with cAMP-elevating agents (Cap-C, black bars) and with melatonin (MEL, 1 μM), GKT163901 (GKT, 1 μM), calcium ionophore A23187 (ionophore, 1 μM, gray bars), and a combination of MEL or GKT with ionophore. Data of non-capacitated, capacitated, and acrosome-reacted spermatozoa are mean percentages ± SEM ($n = 6$). Different letters within the same group indicate significant differences ($p < 0.05$).

that had increased during incubation in capacitating conditions. NOX5 activation by ionophore led to a high increment in acrosome-reacted sperm that could be prevented in part by the addition of GKT136901. It is well known that A23187 induces the acrosome reaction in the sperm of many species (Yanagimachi, 1975) and can also immobilize them (Hong et al., 1985; Visconti et al., 1999). In the present study, we observed the same ionophore side effect on motility; however, it did not affect viability, in concordance with the findings of other authors (Suarez et al., 1987). In contrast with different results showing a reduction of sperm motility and viability as a consequence of the inhibition of the NOX5 activity (Ghanbari et al., 2018), we observed an increase in the progressive motility in high cAMP-capacitated samples.

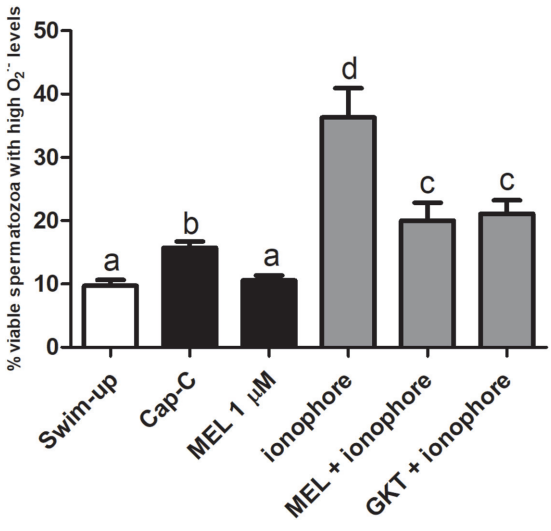

FIGURE 7 | Percentage of live sperm with high superoxide levels (Yo-Pro-1–/E+) assessed by flow cytometry before (swim-up, white bars) and after *in vitro* capacitation with cAMP-elevating agents (Cap-C, black bars) and with melatonin (MEL) 1 μM or/and calcium ionophore A23187 (ionophore, gray bars), plus a GKT136901 with ionophore sample (GKT + ionophore). Data are shown as mean ± SEM ($n = 6$). Different letters indicate significant differences ($p < 0.05$).

Although other NOX isoforms have been described in spermatozoa from other species (Sabeur and Ball, 2007; Musset et al., 2012; Ghani et al., 2013; Setyawan et al., 2016), on the basis of the results derived from the use of the NOX inhibitor (GKT136901) and the calcium induction, we could postulate that NOX5 is an important source of ROS in ram spermatozoa. This isoform is the only one that has calcium-binding sites, and calcium is crucial for NOX5 activation (reviewed by Touyz et al., 2019). Consequently, the superoxide levels reached after calcium-ionophore addition supported the view that NOX5 is a ROS source in ram spermatozoa. Other authors concluded the same for spermatozoa from other species and affirmed that NOX5 regulates numerous redox-dependent processes in spermatozoa under physiological conditions (Musset et al., 2012; Ghanbari et al., 2018).

Melatonin plays an important role in sperm functionality (Jang et al., 2010; Ortiz et al., 2011), and its antioxidant capacity has been reported in spermatozoa from different species (Succu et al., 2011; Karimfar et al., 2015; Pang et al., 2016; Appiah et al., 2019). It has been demonstrated that, in ram spermatozoa, melatonin is involved in the capacitation process and prevents apoptosis and oxidative stress (Casao et al., 2010b; Gonzalez-Arto et al., 2016; Gimeno-Martos et al., 2019; Pool et al., 2021).

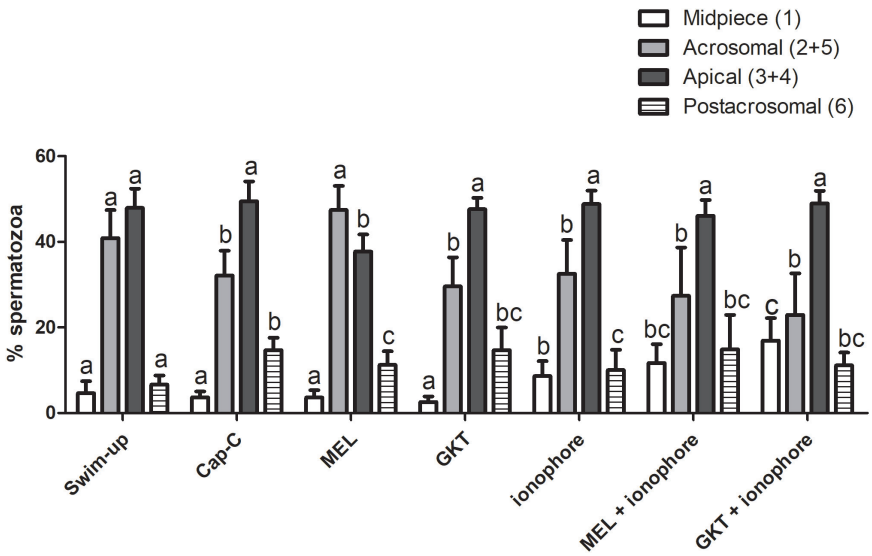

FIGURE 8 | Percentages of the immunotypes for NOX5 in swim-up selected and *in vitro* capacitated ram spermatozoa with cAMP-elevating agents (Cap-C), and with melatonin (MEL) 1 μM, GKT163901 (GKT, 1 μM), calcium ionophore A23187 (ionophore, 1 μM), and a combination of MEL or GKT with ionophore. Immunotypes are represented as follows: (1) plain white bars (2 + 5) plain gray bars (3 + 4) plain black bars, and (6) horizontal striped bars. Results are shown as mean ± SEM (n = 6 for swim-up, Cap-C and Mel; *n* = 3 for GKT, ionophore, MEL + ionophore, GKT + ionophore). Different letters indicate statistical differences between treatments ($p < 0.05$).

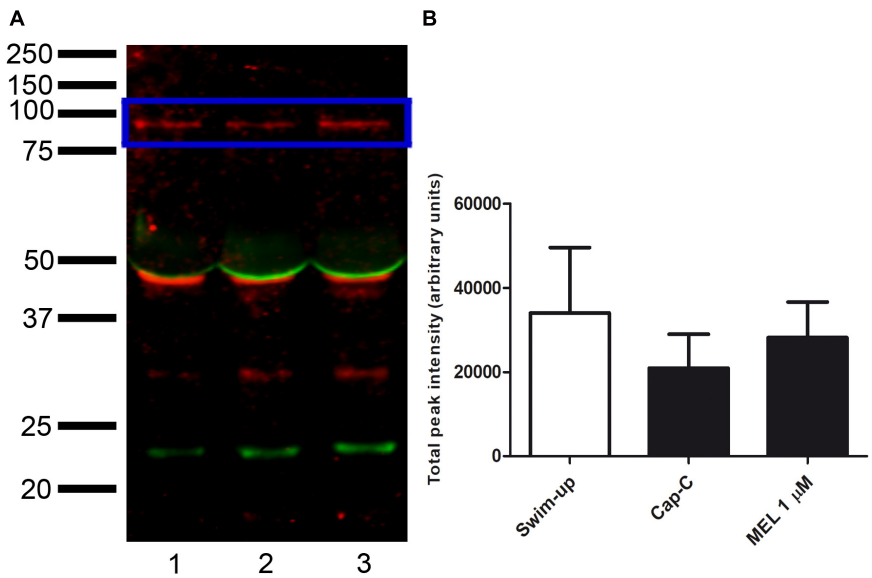

FIGURE 9 | (A) Western blot analysis of the presence of NADPH oxidase 5 (blue box) in swim-up selected (lane 1) and incubated 3 h in capacitating conditions with cAMP-elevating agents (Cap-C, lane 2) ram spermatozoa protein extracts. Effect of melatonin 1 μM (MEL 1 μM) in capacitated samples with high cAMP (lane 3). **(B)** Densitometry quantification of NOX5 normalized to α-tubulin (loading control, orange box) (*n* = 6).

In previous works, we showed the capacity of melatonin to prevent ram sperm capacitation at micromolar concentrations (Casao et al., 2010b), in concordance with the present results. This effect appears to be due, at least in part, to its antioxidant capacity, since a melatonin-mediated decrease in general ROS levels in ram (Gimeno-Martos et al., 2019), rabbit (Zhu et al., 2019), bull (Ashrafi et al., 2013), or mouse (Chen et al., 2016) has been described. In contrast, du Plessis et al. (2010) reported no melatonin effect on ROS levels in human spermatozoa, neither did Pool et al. (2021) in frozen-thawed ram spermatozoa, but interestingly, they concluded that melatonin is specifically able to reduce mitochondrial superoxide production. In this work, we have shown that the addition of 1 μM melatonin to the ram sperm samples specifically prevented the increase

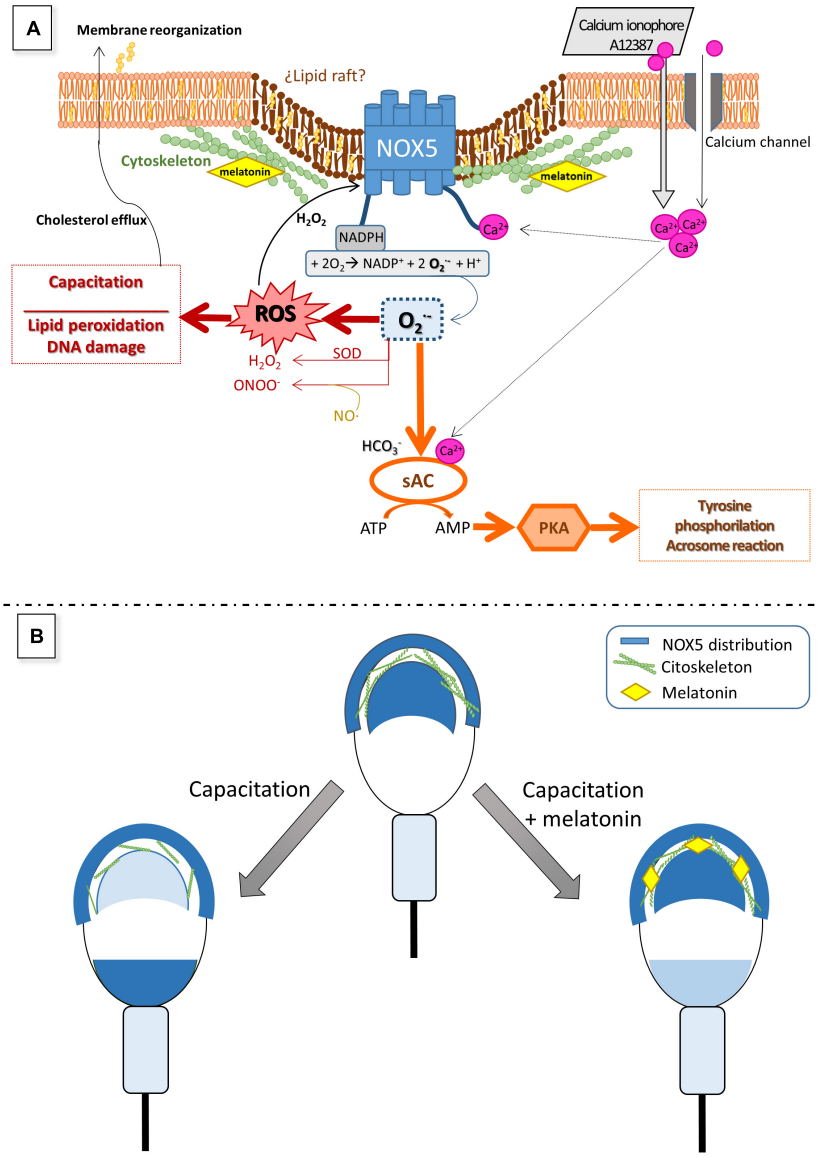

FIGURE 10 | Hypothetical model to explain the role of NOX5 in ram spermatozoa **(A)** and changes in its localization during sperm capacitation **(B)**, as well as the putative effect of melatonin on NOX5 **(A,B)**. Calcium entry from the extracellular media through multiple calcium channels in sperm membrane directly activates NOX5 throughout the N-terminal calcium-binding domains. NOX5 activation generates superoxide which quickly dismutates in H_2O_2 and other ROS that take part in numerous signaling pathways, including capacitation processes and NOX5 reactivation. Lewis and Aitken (2001) also proposed that superoxides, together with bicarbonate and calcium, can activate a soluble adenyl cyclase (sAC) which produces cAMP leading to the activation of protein kinase A (PKA). PKA provokes an increase in tyrosine phosphorylation, a crucial event for the ongoing of the capacitation process. The findings of the present work showing that the NOX inhibitor, GKT136901, is able to reduce the rate of ram-capacitated spermatozoa, will support this postulated mechanism. Regarding NOX5 localization, mainly in the acrosome region and the apical edge, we have demonstrated that it changes during ram sperm capacitation. To explain this redistribution we could hypothesize that NOX5 could be embedded in lipid rafts, as it has been demonstrated in somatic cells (Anagnostopoulou et al., 2020). During the capacitation process, the cholesterol efflux from the sperm membrane allows the reorganization of the lipid rafts (van Gestel et al., 2005), giving new protein distributions, and modulating their activity (Kawano et al., 2011). This lipid raft redistribution was demonstrated to be the mechanism by which NOX5 could modulate its activity, in certain somatic cells (Anagnostopoulou et al., 2020). The cytoskeleton plays a fundamental part in the rearrangement of the membrane during sperm capacitation (Brener et al., 2003). Our previous results showed that melatonin modulates ram sperm capacitation and stabilizes the sperm cytoskeleton at micromolar concentrations. Considering these evidences, we postulate that melatonin is able to avoid NOX5 changes in localization associated with sperm capacitation by means of cytoskeleton stabilization, resulting in a lower superoxide production. Panel **(A)** of the figure is based on a model proposed by Aitken and Baker (2020).

in superoxide levels provoked by *in vitro* capacitation. This evidence points to a possible action of melatonin through the NOX5 enzyme, an important source of superoxide in spermatozoa. Furthermore, the incubation with melatonin prior to the addition of calcium ionophore limited the superoxide production that the ionophore triggered alone, as did the NOX

inhibitor (GKT136901). Moreover, we have shown here that melatonin was able to modify the NOX5 distribution in ram spermatozoa, preventing the changes in localization provoked by *in vitro* capacitation. It is worth mentioning that we have recently reported the effect of melatonin on cytoskeletal remodeling during *in vitro* ram sperm capacitation, concluding that 1 μM melatonin prevents such changes, according to the actin and α-tubulin distribution (Carvajal-Serna et al., 2020). The melatonin action on the cytoskeleton has been also reported in somatic cells (Benítez-King, 2006). Thus, we could postulate that melatonin could affect NOX5 distribution and modulate its capacity to produce superoxides through this stabilizing action on the cytoskeleton, as we proposed in the hypothetical model shown in **Figure 10**. On the contrary, the incubation with the NOX inhibitor or the calcium ionophore addition did not alter the NOX5 distribution during sperm capacitation, probably because these compounds have a direct modulating action on the enzyme and they could not modify its distribution by themselves. The addition of ionophore after incubation with melatonin avoided its stabilizing effect on cytoskeleton, probably as a consequence of the high increment in intracellular calcium. The fact that NOX5 levels, analyzed by Western blot and quantified by densitometry, did not significantly change after incubation in capacitating conditions, with or without melatonin, may support the previous hypothesis that NOX5 could regulate its action depending on its cell location.

The results from this work have evidenced, for the first time, the presence of NADPH oxidase 5 in ram spermatozoa and the existence of six different immunotypes depending on its location. NOX5 is active and involved in ram sperm capacitation. Finally, melatonin modified the NOX5 location and prevented the oxidative stress deriving from the capacitation process. The findings of this study can be understood as a new insight into the action of melatonin on ram sperm capacitation through NOX5 modulation.

DATA AVAILABILITY STATEMENT

The datasets generated for this study can be found in the figshare repository doi: 10.6084/m9.figshare.13603226, **Supplementary Material** can be found in the figshare repository doi: 10.6084/m9.figshare.13606394.

ETHICS STATEMENT

The animal study was reviewed and approved by PI39/17 approved by the University of Zaragoza Ethics Committee for Animal Experiments.

AUTHOR CONTRIBUTIONS

RP-P and AC: conceptualization, supervision, and writing—review and editing. SM-J, BP-B, SG-M, and MC-S: methodology. SM-J, BP-B, SG-M, and AC: formal analysis. SM-J, MC-S, BP-B, RP-P, and AC: investigation. SM-J, BP-B, RP-P, and AC: data curation. SM-J: writing—original draft preparation. RP-P: project administration, funding acquisition. All authors have read and agreed to the published version of the manuscript.

FUNDING

This research was funded by CICYT AGL-2017-83799-R and DGA A07 17R. SM-J was a predoctoral contract from the Diputación General de Aragón (DGA).

ACKNOWLEDGMENTS

We would like to acknowledge the use of the Servicio General de Apoyo a la Investigación-SAI (Universidad de Zaragoza), ANGRA, for supplying the sires and S. Morales for the collection of semen samples.

SUPPLEMENTARY MATERIAL

The Supplementary Material for this article can be found online at: https://www.frontiersin.org/articles/10.3389/fcell.2021.655794/full#supplementary-material

REFERENCES

Aitken, R. J., and Baker, M. A. (2020). The Role of genetics and oxidative stress in the etiology of male infertility—a unifying hypothesis? *Front. Endocrinol.* 11:581838. doi: 10.3389/fendo.2020.581838

Aitken, R. J., and Clarkson, J. S. (1987). Cellular basis of defective sperm function and its association with the genesis of reactive oxygen species by human spermatozoa. *J. Reprod. Fertil.* 81, 459–469. doi: 10.1530/jrf.0.0810459

Aitken, R. J., Buckingham, D. W., and West, K. M. (1992). Reactive oxygen species and human spermatozoa: analysis of the cellular mechanisms involved in luminol- and lucigenin-dependent chemiluminescence. *J. Cell Physiol.* 151, 466–477. doi: 10.1002/jcp.1041510305

Aitken, R. J., Fisher, H. M., Fulton, N., Gomez, E., Knox, W., Lewis, B., et al. (1997). Reactive oxygen species generation by human spermatozoa is induced by exogenous NADPH and inhibited by the flavoprotein inhibitors diphenylene iodonium and quinacrine. *Mol. Reprod. Dev.* 47, 468–482. doi: 10.1002/(sici)1098-2795(199708)47:4<468::aid-mrd14>3.0.co;2-s

Alquezar-Baeta, C., Gimeno-Martos, S., Miguel-Jimenez, S., Santolaria, P., Yaniz, J., Palacin, I., et al. (2019). OpenCASA: a new open-source and scalable tool for sperm quality analysis. *PLoS Comput. Biol.* 15:e1006691. doi: 10.1371/journal.pcbi.1006691

Altenhofer, S., Radermacher, K. A., Kleikers, P. W., Wingler, K., and Schmidt, H. H. (2015). Evolution of NADPH oxidase inhibitors: selectivity and mechanisms for target engagement. *Antioxid. Redox Signal.* 23, 406–427. doi: 10.1089/ars.2013.5814

Alvarez, J. G., Touchstone, J. C., Blasco, L., and Storey, B. T. (1987). Spontaneous lipid peroxidation and production of hydrogen peroxide and superoxide in human spermatozoa. superoxide dismutase as major enzyme protectant against oxygen toxicity. *J. Androl.* 8, 338–348. doi: 10.1002/j.1939-4640.1987.tb00973.x

Anagnostopoulou, A., Camargo, L. L., Rodrigues, D., Montezano, A. C., and Touyz, R. M. (2020). Importance of cholesterol-rich microdomains in the regulation of

Nox isoforms and redox signaling in human vascular smooth muscle cells. *Sci. Rep.* 10:17818.

Appiah, M. O., He, B., Lu, W., and Wang, J. (2019). Antioxidative effect of melatonin on cryopreserved chicken semen. *Cryobiology* 89, 90–95. doi: 10.1016/j.cryobiol.2019.05.001

Ashrafi, I., Kohram, H., and Ardabili, F. F. (2013). Antioxidative effects of melatonin on kinetics, microscopic and oxidative parameters of cryopreserved bull spermatozoa. *Anim. Reprod. Sci.* 139, 25–30. doi: 10.1016/j.anireprosci.2013.03.016

Ball, B. A., Vo, A. T., and Baumber, J. (2001). Generation of reactive oxygen species by equine spermatozoa. *Am. J. Vet. Res.* 62, 508–515. doi: 10.2460/ajvr.2001.62.508

Banfi, B., Molnar, G., Maturana, A., Steger, K., Hegedus, B., Demaurex, N., et al. (2001). A Ca(2+)-activated NADPH oxidase in testis, spleen, and lymph nodes. *J. Biol. Chem.* 276, 37594–37601. doi: 10.1074/jbc.m103034200

Bedard, K., and Krause, K. H. (2007). The NOX family of ROS-generating NADPH oxidases: physiology and pathophysiology. *Physiol. Rev.* 87, 245–313. doi: 10.1152/physrev.00044.2005

Benítez-King, G. (2006). Melatonin as a cytoskeletal modulator: implications for cell physiology and disease. *J. Pineal Res.* 40, 1–9. doi: 10.1111/j.1600-079x.2005.00282.x

Bittman, E. L., Dempsey, R. J., and Karsch, F. J. (1983). Pineal melatonin secretion drives the reproductive response to daylength in the ewe. *Endocrinology* 113, 2276–2283. doi: 10.1210/endo-113-6-2276

Brener, E., Rubinstein, S., Cohen, G., Shternall, K., Rivlin, J., and Breitbart, H. (2003). Remodeling of the actin cytoskeleton during mammalian sperm capacitation and acrosome reaction1. *Biol. Reprod.* 68, 837–845. doi: 10.1095/biolreprod.102.009233

Brzezinski, A., Seibel, M. M., Lynch, H. J., Deng, M. H., and Wurtman, R. J. (1987). Melatonin in human preovulatory follicular fluid. *J. Clin. Endocrinol. Metab.* 64, 865–867. doi: 10.1210/jcem-64-4-865

Burnaugh, L., Sabeur, K., and Ball, B. A. (2007). Generation of superoxide anion by equine spermatozoa as detected by dihydroethidium. *Theriogenology* 67, 580–589. doi: 10.1016/j.theriogenology.2006.07.021

Carvajal-Serna, M., Paesa, M., Barale, J., Gimeno-Martos, S., Peña-Delgado, V., Miguel-Jiménez, S., et al. (2020). Effect of melatonin on actin and α-tubulin distribution related to in vitro capacitation in ram sperm. *Anim. Reprod. Sci.* 220:106363. doi: 10.1016/j.anireprosci.2020.106363

Casao, A., Cebrian, I., Asumpcao, M. E., Perez-Pe, R., Abecia, J. A., Forcada, F., et al. (2010a). Seasonal variations of melatonin in ram seminal plasma are correlated to those of testosterone and antioxidant enzymes. *Reprod. Biol. Endocrinol.* 8:59. doi: 10.1186/1477-7827-8-59

Casao, A., Mendoza, N., Perez-Pe, R., Grasa, P., Abecia, J. A., Forcada, F., et al. (2010b). Melatonin prevents capacitation and apoptotic-like changes of ram spermatozoa and increases fertility rate. *J. Pineal Res.* 48, 39–46. doi: 10.1111/j.1600-079x.2009.00722.x

Chen, X. J., Zhang, Y., Jia, G. X., Meng, Q. G., Bunch, T. D., Liu, G. S., et al. (2016). Effect of melatonin supplementation on cryopreserved sperm quality in mouse. *Cryo Lett.* 37, 115–122.

Cheng, G., Cao, Z., Xu, X., Van Meir, E. G., and Lambeth, J. D. (2001). Homologs of gp91phox: cloning and tissue expression of Nox3, Nox4, and Nox5. *Gene* 269, 131–140. doi: 10.1016/s0378-1119(01)00449-8

Colas, C., James, P., Howes, L., Jones, R., Cebrian-Perez, J. A., and Muino-Blanco, T. (2008). Cyclic-AMP initiates protein tyrosine phosphorylation independent of cholesterol efflux during ram sperm capacitation. *Reprod. Fertil. Dev.* 20, 649–658. doi: 10.1071/rd08023

de Lamirande, E., and Gagnon, C. (1995). Impact of reactive oxygen species on spermatozoa: a balancing act between beneficial and detrimental effects. *Hum. Reprod.* 10(Suppl. 1), 15–21. doi: 10.1093/humrep/10.suppl_1.15

de Lamirande, E., Harakat, A., and Gagnon, C. (1998). Human sperm capacitation induced by biological fluids and progesterone, but not by NADH or NADPH, is associated with the production of superoxide anion. *J. Androl.* 19, 215–225. doi: 10.1016/s0008-6363(99)00183-2

du Plessis, S. S., Hagenaar, K., and Lampiao, F. (2010). The in vitro effects of melatonin on human sperm function and its scavenging activities on NO and ROS. *Andrologia* 42, 112–116. doi: 10.1111/j.1439-0272.2009.00964.x

Dutta, S., Majzoub, A., and Agarwal, A. (2019). Oxidative stress and sperm function: a systematic review on evaluation and management. *Arab J. Urol.* 17, 87–97. doi: 10.1080/2090598x.2019.1599624

Espino, J., Ortiz, A., Bejarano, I., Lozano, G. M., Monllor, F., Garcia, J. F., et al. (2011). Melatonin protects human spermatozoa from apoptosis via melatonin receptor- and extracellular signal-regulated kinase-mediated pathways. *Fertil. Steril.* 95, 2290–2296. doi: 10.1016/j.fertnstert.2011.03.063

García-López, N., Ollero, M., Muiño-Blanco, T., and Cebrián-Pérez, J. A. (1996). A dextran swim-up procedure for separation of highly motile and viable ram spermatozoa from seminal plasma. *Theriogenology* 46, 141–151. doi: 10.1016/0093-691x(96)00149-5

Ghanbari, H., Keshtgar, S., and Kazeroni, M. (2018). Inhibition of the CatSper channel and NOX5 enzyme activity affects the functions of the progesterone-stimulated human sperm. *Iran J. Med. Sci.* 43, 18–25.

Ghani, E., Keshtgar, S., Habibagahi, M., Ghannadi, A., and Kazeroni, M. (2013). Expression of NOX5 in human teratozoospermia compared to normozoospermia. *Andrologia* 45, 351–356. doi: 10.1111/and.12023

Gillan, L., Evans, G., and Maxwell, W. M. (1997). Capacitation status and fertility of fresh and frozen-thawed ram spermatozoa. *Reprod. Fertil. Dev.* 9, 481–487. doi: 10.1071/r96046

Gimeno-Martos, S., Casao, A., Yeste, M., Cebrian-Perez, J. A., Muino-Blanco, T., and Perez-Pe, R. (2019). Melatonin reduces cAMP-stimulated capacitation of ram spermatozoa. *Reprod. Fertil. Dev.* 31, 420–431. doi: 10.1071/rd18087

Gonzalez-Arto, M., Hamilton, T. R., Gallego, M., Gaspar-Torrubia, E., Aguilar, D., Serrano-Blesa, E., et al. (2016). Evidence of melatonin synthesis in the ram reproductive tract. *Andrology* 4, 163–171. doi: 10.1111/andr.12117

Grasa, P., Cebrian-Perez, J. A., and Muino-Blanco, T. (2006). Signal transduction mechanisms involved in in vitro ram sperm capacitation. *Reproduction* 132, 721–732. doi: 10.1530/rep.1.00770

Griveau, J. F., and Le Lannou, D. (1994). Effects of antioxidants on human sperm preparation techniques. *Int. J. Androl.* 17, 225–231.

Guthrie, H. D., and Welch, G. R. (2006). Determination of intracellular reactive oxygen species and high mitochondrial membrane potential in Percoll-treated viable boar sperm using fluorescence-activated flow cytometry. *J. Anim. Sci.* 84, 2089–2100. doi: 10.2527/jas.2005-766

Halliwell, B., and Gutteridge, J. (1989). *Free Radicals in Biology and Medicine*. Oxford: Clarendon Press.

Harrison, R. A., and Vickers, S. E. (1990). Use of fluorescent probes to assess membrane integrity in mammalian spermatozoa. *J. Reprod. Fertil.* 88, 343–352. doi: 10.1530/jrf.0.0880343

Herrero, M. B., De Lamirande, E., and Gagnon, C. (2003). Nitric oxide is a signaling molecule in spermatozoa. *Curr. Pharm. Des.* 9, 419–425. doi: 10.2174/1381612033391720

Hong, C. Y., Chiang, B. N., Ku, J., Wei, Y. H., and Fong, J. C. (1985). Calcium antagonists stimulate sperm motility in ejaculated human semen. *Br. J. Clin. Pharmacol.* 19, 45–49. doi: 10.1111/j.1365-2125.1985.tb02611.x

Jang, H. Y., Kim, Y. H., Kim, B. W., Park, I. C., Cheong, H. T., Kim, J. T., et al. (2010). Ameliorative effects of melatonin against hydrogen peroxide-induced oxidative stress on boar sperm characteristics and subsequent in vitro embryo development. *Reprod. Domest. Anim.* 45, 943–950. doi: 10.1111/j.1439-0531.2009.01466.x

Karimfar, M. H., Niazvand, F., Haghani, K., Ghafourian, S., Shirazi, R., and Bakhtiyari, S. (2015). The protective effects of melatonin against cryopreservation-induced oxidative stress in human sperm. *Int. J. Immunopathol. Pharmacol.* 28, 69–76. doi: 10.1177/0394632015572080

Kawano, N., Yoshida, K., Miyado, K., and Yoshida, M. (2011). Lipid Rafts: keys to sperm maturation, fertilization, and early embryogenesis. *J. Lipids* 2011:264706.

Koppers, A. J., De Iuliis, G. N., Finnie, J. M., Mclaughlin, E. A., and Aitken, R. J. (2008). Significance of mitochondrial reactive oxygen species in the generation of oxidative stress in spermatozoa. *J. Clin. Endocrinol. Metab.* 93, 3199–3207. doi: 10.1210/jc.2007-2616

Laemmli, U. K. (1970). Cleavage of structural proteins during the assembly of the head of bacteriophage T4. *Nature* 227, 680–685. doi: 10.1038/227680a0

Lewis, B., and Aitken, R. J. (2001). A redox-regulated tyrosine phosphorylation cascade in rat spermatozoa. *J. Androl.* 22, 611–622.

Maghzal, G. J., Krause, K. H., Stocker, R., and Jaquet, V. (2012). Detection of reactive oxygen species derived from the family of NOX NADPH oxidases. *Free Radic. Biol. Med.* 53, 1903–1918. doi: 10.1016/j.freeradbiomed.2012.09.002

Miguel-Jimenez, S., Carvajal-Serna, M., Calvo, S., Casao, A., Cebrian-Perez, J. A., Muino-Blanco, T., et al. (2020). Does melatonin exert its effect on ram sperm capacitation through nitric oxide synthase regulation? *Int. J. Mol. Sci.* 21:2093. doi: 10.3390/ijms21062093

Moreno-Irusta, A., Dominguez, E. M., Marin-Briggiler, C. I., Matamoros-Volante, A., Lucchesi, O., Tomes, C. N., et al. (2020). Reactive oxygen species are involved in the signaling of equine sperm chemotaxis. *Reproduction* 159, 423–436. doi: 10.1530/rep-19-0480

Musset, B., Clark, R. A., Decoursey, T. E., Petheo, G. L., Geiszt, M., Chen, Y., et al. (2012). NOX5 in human spermatozoa: expression, function, and regulation. *J. Biol. Chem.* 287, 9376–9388.

O'Flaherty, C. (2015). Redox regulation of mammalian sperm capacitation. *Asian J. Androl.* 17, 583–590. doi: 10.4103/1008-682x.153303

O'Flaherty, C., De Lamirande, E., and Gagnon, C. (2004a). Phosphorylation of the Arginine-X-X-(Serine/Threonine) motif in human sperm proteins during capacitation: modulation and protein kinase A dependency. *Mol. Hum. Reprod.* 10, 355–363. doi: 10.1093/molehr/gah046

O'Flaherty, C., De Lamirande, E., and Gagnon, C. (2005). Reactive oxygen species and protein kinases modulate the level of phospho-MEK-like proteins during human sperm capacitation. *Biol. Reprod.* 73, 94–105. doi: 10.1095/biolreprod.104.038794

O'Flaherty, C., Rodriguez, P., and Srivastava, S. (2004b). L-arginine promotes capacitation and acrosome reaction in cryopreserved bovine spermatozoa. *Biochim. Biophys. Acta* 1674, 215–221. doi: 10.1016/j.bbagen.2004.06.020

Ollero, M., Muino-Blanco, T., Lopez-Perez, M. J., and Cebrian-Perez, J. A. (1996). Viability of ram spermatozoa in relation to the abstinence period and successive ejaculations. *Int. J. Androl.* 19, 287–292. doi: 10.1111/j.1365-2605.1996.tb00477.x

Ortiz, A., Espino, J., Bejarano, I., Lozano, G. M., Monllor, F., Garcia, J. F., et al. (2011). High endogenous melatonin concentrations enhance sperm quality and short-term in vitro exposure to melatonin improves aspects of sperm motility. *J. Pineal Res.* 50, 132–139.

Panday, A., Sahoo, M. K., Osorio, D., and Batra, S. (2015). NADPH oxidases: an overview from structure to innate immunity-associated pathologies. *Cell Mol. Immunol.* 12, 5–23. doi: 10.1038/cmi.2014.89

Pang, Y. W., Sun, Y. Q., Jiang, X. L., Huang, Z. Q., Zhao, S. J., Du, W. H., et al. (2016). Protective effects of melatonin on bovine sperm characteristics and subsequent in vitro embryo development. *Mol. Reprod. Dev.* 83, 993–1002. doi: 10.1002/mrd.22742

Parrish, J. J., Susko-Parrish, J., Winer, M. A., and First, N. L. (1988). Capacitation of bovine sperm by heparin. *Biol. Reprod.* 38, 1171–1180.

Patino, P., Parada, E., Farre-Alins, V., Molz, S., Cacabelos, R., Marco-Contelles, J., et al. (2016). Melatonin protects against oxygen and glucose deprivation by decreasing extracellular glutamate and Nox-derived ROS in rat hippocampal slices. *Neurotoxicology* 57, 61–68. doi: 10.1016/j.neuro.2016.09.002

Plante, M., De Lamirande, E., and Gagnon, C. (1994). Reactive oxygen species released by activated neutrophils, but not by deficient spermatozoa, are sufficient to affect normal sperm motility. *Fertil. Steril.* 62, 387–393. doi: 10.1016/s0015-0282(16)56895-2

Pool, K. R., Rickard, J. P., and De Graaf, S. P. (2021). Melatonin improves the motility and DNA integrity of frozen-thawed ram spermatozoa likely via suppression of mitochondrial superoxide production. *Domest. Anim. Endocrinol.* 74:106516. doi: 10.1016/j.domaniend.2020.106516

Rao, M. V., and Gangadharan, B. (2008). Antioxidative potential of melatonin against mercury induced intoxication in spermatozoa in vitro. *Toxicol. In Vitro* 22, 935–942. doi: 10.1016/j.tiv.2008.01.014

Sabeur, K., and Ball, B. A. (2007). Characterization of NADPH oxidase 5 in equine testis and spermatozoa. *Reproduction* 134, 263–270. doi: 10.1530/rep-06-0120

Setyawan, E. M. N., Kim, M. J., Oh, H. J., Kim, G. A., Jo, Y. K., Lee, S. H., et al. (2016). Spermine reduces reactive oxygen species levels and decreases cryocapacitation in canine sperm cryopreservation. *Biochem. Biophys. Res. Commun.* 479, 927–932. doi: 10.1016/j.bbrc.2016.08.091

Suarez, S. S., Vincenti, L., and Ceglia, M. W. (1987). Hyperactivated motility induced in mouse sperm by calcium ionophore A23187 is reversible. *J. Exp. Zool.* 244, 331–336. doi: 10.1002/jez.1402440218

Succu, S., Berlinguer, F., Pasciu, V., Satta, V., Leoni, G. G., and Naitana, S. (2011). Melatonin protects ram spermatozoa from cryopreservation injuries in a dose-dependent manner. *J. Pineal Res.* 50, 310–318. doi: 10.1111/j.1600-079x.2010.00843.x

Touyz, R. M., Anagnostopoulou, A., Rios, F., Montezano, A. C., and Camargo, L. L. (2019). NOX5: molecular biology and pathophysiology. *Exp. Physiol.* 104, 605–616. doi: 10.1113/ep086204

van Gestel, R. A., Brewis, I. A., Ashton, P. R., Helms, J. B., Brouwers, J. F., and Gadella, B. M. (2005). Capacitation-dependent concentration of lipid rafts in the apical ridge head area of porcine sperm cells. *Mol. Hum. Reprod.* 11, 583–590. doi: 10.1093/molehr/gah200

Vernet, P., Fulton, N., Wallace, C., and Aitken, R. J. (2001). Analysis of reactive oxygen species generating systems in rat epididymal spermatozoa. *Biol. Reprod.* 65, 1102–1113. doi: 10.1095/biolreprod65.4.1102

Visconti, P. E., Stewart-Savage, J., Blasco, A., Battaglia, L., Miranda, P., Kopf, G. S., et al. (1999). Roles of bicarbonate, cAMP, and protein tyrosine phosphorylation on capacitation and the spontaneous acrosome reaction of hamster sperm. *Biol. Reprod.* 61, 76–84. doi: 10.1095/biolreprod61.1.76

Ward, C. R., and Storey, B. T. (1984). Determination of the time course of capacitation in mouse spermatozoa using a chlortetracycline fluorescence assay. *Dev. Biol.* 104, 287–296. doi: 10.1016/0012-1606(84)90084-8

Whittington, K., Harrison, S. C., Williams, K. M., Day, J. L., Mclaughlin, E. A., Hull, M. G., et al. (1999). Reactive oxygen species (ROS) production and the outcome of diagnostic tests of sperm function. *Int. J. Androl.* 22, 236–242. doi: 10.1046/j.1365-2605.1999.00174.x

Yanagimachi, R. (1975). Acceleration of the acrosome reaction and activation of guinea pig spermatozoa by detergents and other reagents. *Biol. Reprod.* 13, 519–526. doi: 10.1095/biolreprod13.5.519

Zhang, H., and Zheng, R. L. (1996). Promotion of human sperm capacitation by superoxide anion. *Free Radic. Res.* 24, 261–268. doi: 10.3109/10715769609088023

Zhu, Z., Li, R., Lv, Y., and Zeng, W. (2019). Melatonin protects rabbit spermatozoa from cryo-damage via decreasing oxidative stress. *Cryobiology* 88, 1–8. doi: 10.1016/j.cryobiol.2019.04.009

Conflict of Interest: The authors declare that the research was conducted in the absence of any commercial or financial relationships that could be construed as a potential conflict of interest.

frontiers in Cell and Developmental Biology

ORIGINAL RESEARCH
published: 28 May 2021
doi: 10.3389/fcell.2021.669974

Metabolite Profiling of Pig Seminal Plasma Identifies Potential Biomarkers for Sperm Resilience to Liquid Preservation

Yentel Mateo-Otero[1,2], Pol Fernández-López[3], Jordi Ribas-Maynou[1,2], Jordi Roca[4], Jordi Miró[5], Marc Yeste[1,2†] and Isabel Barranco[1,2,6*†]*

[1] Biotechnology of Animal and Human Reproduction (TechnoSperm), Institute of Food and Agricultural Technology, University of Girona, Girona, Spain, [2] Unit of Cell Biology, Department of Biology, Faculty of Sciences, University of Girona, Girona, Spain, [3] Centre d'Estudis Avançats de Blanes (CEAB), Spanish Research Council (CSIC), Girona, Spain, [4] Department of Animal Medicine and Surgery, Faculty of Veterinary Medicine, University of Murcia, Murcia, Spain, [5] Equine Reproduction Service, Department of Animal Medicine and Surgery, Faculty of Veterinary Medicine, Autonomous University of Barcelona, Barcelona, Spain, [6] Department of Veterinary Medical Sciences, Via Tolara di Sopra, Bologna, Italy

OPEN ACCESS

Edited by:
Ana Josefa Soler, University of Castilla-La Mancha, Spain

Reviewed by:
Felipe Martínez-Pastor, Universidad de León, Spain
Hideko Sone, Yokohama College of Pharmacy, Japan

***Correspondence:**
Marc Yeste
marc.yeste@udg.edu
Isabel Barranco
isabel.barranco@udg.edu

† These authors have contributed equally to this work and share senior authorship

Specialty section:
This article was submitted to Cell Growth and Division, a section of the journal Frontiers in Cell and Developmental Biology

Received: *19 February 2021*
Accepted: *28 April 2021*
Published: *28 May 2021*

Citation:
Mateo-Otero Y, Fernández-López P, Ribas-Maynou J, Roca J, Miró J, Yeste M and Barranco I (2021) Metabolite Profiling of Pig Seminal Plasma Identifies Potential Biomarkers for Sperm Resilience to Liquid Preservation. Front. Cell Dev. Biol. 9:669974. doi: 10.3389/fcell.2021.669974

Metabolomic approaches allow the study of downstream gene expression events since metabolites are considered as the products of cell signaling pathways. For this reason, many studies in humans have already been conducted to determine the influence of the metabolites present in seminal plasma (SP) on sperm physiology, and to identify putative biomarkers. However, in livestock species, these relationships are yet to be uncovered. Thus, the present study aimed to explore: (i) if concentrations of metabolites in pig SP are related to sperm quality and functionality, and (ii) if they could predict the sperm resilience to liquid storage at 17°C. To this end, 28 ejaculates were individually collected and split into three aliquots: one was used for SP analysis through nuclear magnetic resonance (NMR) spectroscopy; another served for the evaluation of sperm concentration and morphology; and the last one was utilized to determine sperm functionality parameters using computer-assisted sperm analysis (CASA) and flow cytometry after 0 h and 72 h of liquid-storage at 17°C. NMR analysis allowed the identification and quantification of 23 metabolites present in pig SP which, except for fumarate, were not observed to follow a breed-dependent behavior. Moreover, specific relationships between metabolites and sperm variables were identified: (i) glutamate, methanol, trimethylamine N-oxide, carnitine, and isoleucine were seen to be related to some sperm quality and functionality parameters evaluated immediately after semen collection; (ii) leucine, hypotaurine, carnitine and isoleucine were found to be associated to the sperm ability to withstand liquid storage; and (iii) Bayesian multiple regression models allowed the identification of metabolite patterns for specific sperm parameters at both 0 h and 72 h. The identification of these relationships opens up the possibility of further investigating these metabolites as potential sperm functional biomarkers.

Keywords: metabolite, metabolomic, seminal plasma, liquid storage, sperm quality, biomarkers, pig

INTRODUCTION

Artificial insemination (AI) remains the most valuable and efficient reproductive biotechnology used for pig breeding, gathering more than 90% of cases in countries with intensive pork production (Roca et al., 2016; Yeste, 2017; Waberski et al., 2019). In spite of the advances performed in cryopreservation procedures, liquid storage at 17 °C continues to be the most useful and preferable biotechnology for preserving pig seminal AI-doses until insemination is carried out (Kumaresan et al., 2009; Waberski et al., 2019). During liquid-storage of seminal AI-doses, sperm undergo injuries, leading to a decline in sperm quality, functionality and fertilizing ability within the first 72 h of storage (Waberski et al., 2011; Yeste, 2017). One of the main concerns is related to differences in the sperm ability to withstand liquid-storage between pig seminal AI-doses (Parrilla et al., 2012; Zakošek Pipan et al., 2014; Roca et al., 2015). This situation evidences that current sperm assessments used for ejaculate selection (which include sperm quantity, motility, and morphology) are not accurate enough to predict sperm fertilizing capacity after liquid preservation (Roca et al., 2016; Waberski et al., 2019). This limitation undermines the ability to face new challenges in swine industry, as implementing new AI-procedures (such as a reduction in sperm numbers/AI-dose) may lead to a decrease on *in vivo* fertility outcomes (Roca et al., 2016). In the last years, many efforts have been aimed at identifying biomarkers of sperm resilience to liquid preservation in seminal plasma (SP) (Barranco et al., 2015a,b, 2016, 2019, 2020; Recuero et al., 2019; Zakošek Pipan et al., 2014). The heterogeneous and complex composition of SP, together with the fact that this fluid is able to interact with sperm, make it a valuable source of potential biomarkers (Rodríguez-Martínez et al., 2011).

Over the last decade, -omics technologies (including proteomics, transcriptomics, metabolomics. . .) have emerged as powerful tools to uncover the molecular factors and regulatory networks involved in reproductive events, thus providing a worthwhile and broad strategy for the study of these multifactorial processes (Egea et al., 2014). Metabolomics employs spectral and analytical approaches to provide a large-scale identification of metabolites, which are the end-products of downstream events of gene expression (Goodacre et al., 2004). Hence, this technique leads to a more realistic approach of cellular physiological activities compared with other -omics, such as transcriptomics or proteomics (Singh and Sinclair, 2007). In the last few years, the study of metabolites as markers of patho- and physiological reproductive processes, in both males and females, has gained much relevance (Egea et al., 2014; Uyar and Seli, 2014; Minai-Tehrani et al., 2016; Nobakht and Gh, 2018; Darbandi et al., 2019; Asampille et al., 2020). Focusing on SP, several studies performed in humans reported that certain SP-metabolites are involved on sperm physiology and fertility disorders (Bonechi et al., 2015; Engel et al., 2019; Wang et al., 2019; Mumcu et al., 2020; Xu et al., 2020). In livestock species, only few reports conducted in cattle pointed out specific SP-metabolites as *in vivo* fertility biomarkers (Kumar et al., 2015; Cazaux Velho et al., 2018).

In a previous study, we described, for the first time, the pig SP metabolomic profile and we suggested that certain SP-metabolites could play a key role in reproductive processes (Mateo-Otero et al., 2020). As far as we know, there are no data about the relationship between SP-metabolites and the sperm ability to withstand liquid preservation in any species. Therefore, an exploratory approach was carried out to evaluate the putative relationship between sperm quality/functionality parameters of liquid-stored semen samples and SP-metabolites identified using nuclear magnetic resonance (NMR) spectroscopy. Specifically, the present study aimed to explore: (i) whether the concentration/presence of SP-metabolites in ejaculates collected from AI-boars is related with sperm quality/functionality parameters, and (ii) if such SP-metabolites could predict the resilience of seminal AI-doses to liquid preservation at 17°C. In this regard, these SP-metabolites may be of practical relevance for a better assessment of pig semen quality, contributing to the successful improvement of AI-efficiency.

MATERIALS AND METHODS

Reagents

Except as otherwise indicated, reagents were purchased from Merck KGaA (Darmstadt, Germany) and fluorochromes for sperm analysis from Thermo Fisher Scientific (Waltham, MA, USA). The commercial extender used to dilute semen samples was Biosem + (Magapor, Zaragoza, Spain).

Experimental Design

Twenty-eight entire ejaculates were individually collected from 28 healthy and fertile AI-boars (one ejaculate per boar) from different breeds (Pietrain, Duroc, Landrace and Tempo). The entire ejaculates were split into three aliquots. The first one was used for SP-harvesting, on which the metabolomic analysis was performed. The second one was utilized for sperm concentration and morphology assessments. The third aliquot was extended alike an AI-dose (30×10^6 sperm/mL in Biosem +) and stored up to 72 h at 17°C (FOC 120E Cooled Incubator; VELP Scientifica, Usmate, Italy). Sperm quality and functionality parameters were assessed in this latter aliquot at different time-points (0 and 72 h), in terms of sperm motility, viability, acrosome damage, intracellular hydrogen peroxide (H_2O_2) generation by viable sperm, and membrane lipid disorder in viable sperm.

Boars and Ejaculates

Ejaculates used in the present study were supplied by a Spanish AI-Centre (AIM Ibérica, Topigs Norsvin Spain; Calasparra, Murcia, Spain). This AI-Centre complies with Spanish (ES300130640127, August 2006) and European (ES13RS04P, July 2012) guidelines for animal health and welfare, and pig ejaculate collection and commercialization of AI-doses. As semen samples were provided by that AI-Centre and authors did not manipulate any animal, no ethical permission was needed.

All entire ejaculates were collected through a semi-automatic collection system (Collectist®, IMV Technologies, L'Aigle,

France) from sexually mature (1 to 3 years old), fertile boars that were subjected to routine collection (twice per week) for elaborating commercial AI-doses. These AI-boars were housed in individual pens with controlled environment temperature (15–25°C) and exposed to a total of 16 h of light (natural plus artificial). They were fed with commercial feedstuff consistent with the nutritional necessities of AI-boars, and were provided with water *ad libitum*. All ejaculates collected for this study fulfilled the sperm quality thresholds for commercial AI-doses (namely a minimum sperm concentration of 200 × 10^6 sperm/mL and more than 70% of motile sperm and 75% of sperm with normal morphology).

Seminal Plasma Processing and Storage

For SP-harvesting, ejaculates were subjected to double-centrifugation right after collection (1,500 × *g* for 10 min at room temperature Rotofix 32A, Hettich Centrifuge United Kingdom, Newport Pagnell, Buckinghamshire, England, United Kingdom). Subsequently, SP samples (second supernatants) were microscopically analyzed (Eclipse E400; Nikon, Tokyo, Japan) to warrant sperm absence. Finally, SP-samples were stored in cryotubes at −80°C (Ultra Low Freezer; Haier Inc., Qingdao, China) until metabolomic analysis was carried out, when they were thawed on ice.

Assessment of Sperm Quality and Functionality Parameters

Eight sperm quantity and functionality parameters were assessed in each semen sample, specifically: (i) sperm concentration, (ii) total sperm count, (iii) sperm morphology, (iv) sperm motility, (v) sperm plasma membrane integrity (viability), (vi) acrosome damage in viable sperm, (vii) intracellular H_2O_2 generation by viable sperm, and (viii) plasma membrane lipid disorder of viable sperm.

Sperm concentration was assessed by a high-precision automated cell counter (NucleoCounter® NC-100™, ChemoMetec, Allerod, Denmark). Then, the total sperm number of each ejaculate was calculated by multiplying sperm concentration per ejaculate volume (assessed in a graduated tube).

For sperm morphology assessment, semen samples were fixed with 0.12% formaldehyde saline solution (Panreac, Barcelona, Spain) and examined under a phase-contrast microscope at 1,000 × magnification (Nikon Labophot, Nikon, Tokio, Japan). A total of 200 sperm per sample were counted and classified as: (i) morphologically normal, (ii) with abnormal head, (iii) with acrosome defects, (iv) with proximal cytoplasmic droplets, (v) with distal cytoplasmic droplets, (vi) with folded tails, and (vii) with coiled tails.

Sperm motility was evaluated using a computer-assisted sperm analyzer (CASA, ISASV1®, Proiser R + D S.L., Paterna, Spain). With this purpose, 5 μL of each semen sample (30 × 10^6 sperm/mL in Biosem +) were pipetted onto a Makler chamber (Sefi Medical Instruments, Haifa, Israel), previously warmed to 38°C. In each semen sample, a total of ten different fields, gathering more than 600 sperm, were acquired and examined under an Olympus BX41 microscope (Olympus, Tokyo, Japan) with a negative phase-contrast field (Olympus 10 × 0.30 PLAN objective; Olympus). Percentages of sperm that showed an average path velocity ≥ 20 μm/s (total motile sperm) and that exhibited a rapid and progressive movement with a straight-line velocity ≥ 40 μm/s (progressive motile sperm) were recorded.

Sperm viability, acrosome damage, intracellular H_2O_2 production and membrane lipid disorder were assessed with a flow cytometer (BD FACS Canto II; Becton Dickinson & Company, Franklin Lakes, NJ, USA). The optical configuration of this device included three detector arrays: one octagon, which detects light from 488 nm laser (blue), and two trigons, which detect light from 633 nm (red) and 405 nm (violet) lasers. Data were collected and compensated using BD FACSDiva Software (Becton Dickinson & Company). Events were triggered by forward scatter (FSC) and side scatter (SSC), and non-sperm particles were gated out based on Hoechst 33342 (H-42) fluorescence, which was detected using 450/50 nm band-pass (BD) filter. For each semen sample and sperm parameter, three technical replicates (with 10,000 [H-42]-positive events each one) were evaluated. All fluorescence parameters were log-transformed, whereas FSC and SSC signals were linearly processed. Unstained and single-stained samples were used for setting electronic volume (EV) gain and compensations. For all samples, laser voltage and flow rate were constant.

Sperm viability and acrosome damage were assessed by triple-staining with H-42, propidium iodide (PI) and fluorescein-conjugated peanut agglutinin (PNA-FITC). Fluorescence of PI and PNA-FITC was detected using 670 nm long-pass (LP) filter and 530/30 nm BP filter, respectively. With this purpose, 100 μL of each semen sample (30 × 10^6 sperm/mL in Biosem +) were incubated with 3 μL H-42 (0.05 mg/mL in phosphate-buffered saline, PBS), 2 μL PI (0.5 mg/mL in PBS) and 2 μL PNA-FITC (100 μg/mL in PBS) for 10 min at 37°C (Sanyo MIR-153 incubator, Gemini BV, Apeldoorn, Netherlands). After this period, 400 μL PBS were added to each sample. Percentages of viable spermatozoa (H-42 + /PI-) with an intact (PNA-FITC-) and non-intact (PNA-FITC +) acrosome membrane were recorded.

To assess the intracellular H_2O_2 production by viable sperm, a triple-staining with H-42, PI, and 5- and 6-chloromethyl-2′,7′-dichlorodihydrofluorescein diacetate acetyl ester (CM-H_2DCFDA) was performed. Fluorescence of CM-H_2DCFDA was detected using 530/30 nm BP filter following excitation at 488 nm. Briefly, 50 μL of each semen sample (30 × 10^6 sperm/mL in Biosem +) were incubated with 1.5 μL H-42 (0.05 mg/mL in PBS), 1 μL PI (0.5 mg/mL in PBS), and 1 μL CM-H_2DCFDA (1 mM in dymetilsulfoxide, DMSO) in 950 μL of PBS at 37°C for 30 min. A semen sample incubated with all fluorochromes plus 1 μL of tert-butyl hydroperoxide solution (70% in distilled water) was used as a control. The percentage of viable sperm (H-42 + /PI-) that exhibited high intracellular H_2O_2 generation (2′,7′-dichlorofluorescein, DCF +) was recorded.

To evaluate membrane lipid disorder of viable sperm, a triple-staining with H-42, Yo-Pro-1, and Merocyanine 540 (M-540) was carried out. Fluorescence of M-540 and Yo-Pro-1 was detected using 585/42 nm and 530/30 nm BP filters, respectively. Fifty μL

of each semen sample (30×10^6 sperm/mL in Biosem +) were incubated with 2.5 μL H-42 and 10 μL Yo-Pro-1 (2.5 μM in DMSO) in 950 μL of PBS at 37°C for 8 min. After this period, 26 μL of M540 (0.1 mM in DMSO) were added to each sample and incubated at 37°C for further 2 min. The percentage of viable spermatozoa (H-42 + /Yo-Pro-1-) that exhibited high plasma membrane disorder (M-540 +) was recorded.

Ejaculate Resilience to Liquid Preservation

The ability of each sample to withstand liquid preservation was evaluated as the loss of sperm quality after 72 h. With this purpose, the following formula was used: $[(q1-q0)/q0] \times 100$, where q1 is the value of each sperm parameter after 72 h of liquid storage at 17°C, and q0 is the value of each sperm parameter evaluated immediately after ejaculate collection (0 h). This formula was applied to the following sperm parameters: (i) percentages of viable sperm, (ii) percentages of viable sperm with a non-intact acrosome, (iii) percentages of viable sperm with high intracellular H_2O_2 levels, (iv) percentages of viable sperm with high plasma membrane disorder, and (v) percentages of total motile sperm. Regarding progressive motility, proportions of progressively motile sperm at 0 h or 72 h were calculated relative to total motility as follows: (progressive motility)/(total motility) × 100.

^{1}H RMN Analysis

A 500-μL aliquot of thawed SP-samples was vortexed, and centrifuged at 14,000 g and 4 °C for 90 min (Rotofix 32A, Hettich Centrifuge UK; Newport Pagnell Buckinghamshire, United Kingdom) using 0.5 mL-Amicon®Ultra Centrifugal Filters to remove proteins and remaining cell debris. These filters were previously washed with PBS and prepared by centrifuging three times at 14,000 g and 4 °C for 20 min. Then, the eluted fraction was mixed with 100 μL PBS containing 10% D_2O with 0.33% of DSS (Merck KgaA, Darmstadt, Germany; pH 7.4), and transferred into a 5-mm Wilmad®NMR tube (Merck KgaA) to generate ^{1}H NMR spectra.

NMR spectra were obtained using a Bruker 600-MHz AVANCE III NMR spectrometer (Bruker Biospin, Rheinstetten, Germany) operating at a ^{1}H frequency of 600.13 MHz and a temperature of 300 °K with an equilibration period of 10 min. The ^{1}D-^{1}H-nuclear Overhauser effect spectroscopy (^{1}D-NOESY) pulse sequence from the Bruker library was used (noesygppr1d). Relevant parameters were: mixing time: 100 ms (d8), recovery delay: 2 s (d1), 90° pulse: 10.39 μs (p1), spectral width: 7211.539 Hz, spectral size: 32 k, number of scans: 128, and acquisition time: 2.27 s.

Data Processing and Analysis

Spectra were processed and analyzed with Chenomx 8.0 profiler. The software provides tools for automatic phase, baseline correction and reference calibration as well as metabolites libraries for profiling. Determination of concentration for each metabolite was calculated in relation to DSS concentration (0.216 mM).

Statistical Analysis

All analysis were performed using R software (version 4.0.2)[1]. For all analysis, the level of significance was set at $P \leq 0.05$. Statistical analysis of NMR data was performed in three steps. First, the breed effect on SP-metabolite concentration/presence was assessed performing a Wilcoxon rank sum test, which avoids the assumptions of normality and homoscedasticity as not all SP-metabolites fulfilled these requisites. The same test was also used to check whether age distribution between Duroc and Pietrain breeds differed.

Second, principal component analysis (PCA) was carried out to evaluate whether data could be categorized to few variables/components, as this avoided using all sperm parameters and made classifying ejaculates into two groups of high and low quality easier. As this could not be achieved, Pearson correlations were employed to quantify the relationship between single SP-metabolites and sperm parameters.

Third, multiple linear regression analyses were performed using a Bayesian framework with the functionality of the R package 'rstanarm' (R package version 2.21.1; Goodrich et al., 2020). All models were performed with a prior non-informative distribution, with the highest sensitivity and 4,000 iterations of sampling. The remaining sperm parameters were left by default. The Bayesian approach was chosen over the classical frequentist framework due to the nature of the dataset. Because linear regression models tend to be overfitted in datasets where the number of columns (variables or predictors) is similar to the number of rows (samples), Bayesian models allow quantifying the uncertainty of such models. In other words, it is possible to have a good sense of how much sensitive or precise these models are. This was performed for the two time-points (i.e., 0 h and 72 h) with the particularity that, for sperm resilience to liquid storage, logistic regression was used for modeling percentages of viable sperm with high intracellular H_2O_2 production and high plasma membrane destabilization. For these latter analyses, medians were used to discriminate the two quality groups: equal or below the median was considered as 0, and above the median was considered as 1. Finally, Pearson correlations were also calculated to determine inter-metabolite relationships.

RESULTS

Metabolite Profile of Pig SP and Differences Between Breeds

A total of 23 metabolites were identified and quantified in all SP-samples analyzed, observing that SP-metabolite concentrations varied between ejaculates (**Table 1**). The ^{1}H-NMR (noesygppr1d) profile of pig SP measured at 600 MHz is shown in **Figure 1**. The identified metabolites were categorized in the following chemical classes: (i) amino acids (n = 7; alanine, glutamate, isoleucine, leucine, phenylalanine, tyrosine, and valine); (ii) saccharides (n = 1; glucose); (iii) salts (n = 6; acetate, citrate, formate, fumarate, lactate, and malonate); (iv) alcohols (n = 2; ethanol and methanol); and (v) other organic compounds

[1] https://www.r-project.org/

(n = 5; carnitine, creatine, creatine-phosphate, hypotaurine, myo-inositol, sn-glycero-3-phosphocholine and trimethylamine N-oxide).

After identifying SP-metabolites, the breed effect on their concentration was evaluated (**Supplementary Table 1**) for Duroc (n = 11) and Pietrain (n = 14) breeds. Samples from Tempo and Landrace boars could not be included in the analysis because of the insufficient number of ejaculate samples (for Tempo, n = 2, and for Landrace, n = 1). Only the concentration of fumarate exhibited significant differences between breeds, the concentration of this metabolite being higher in Pietrain than in Duroc breeds (0.0034 mM vs. 0.0018 mM, $P < 0.01$; **Figure 2**). These differences in the concentration of fumarate could be assumed to be related to the boar breed due to the fact that all animals were housed in the same building. In fact, in order to evaluate a possible age effect, the Wilcoxon rank sum test was run and evidenced no differences in age distribution between Pietrain and Duroc breeds ($P > 0.05$). Therefore, considering that fumarate could be influenced by the boar breed, this metabolite was excluded from further analyses in order to specifically evaluate the effect of SP-metabolites on sperm physiology.

Relationship of SP-Metabolites With Sperm Quality and Functionality Parameters Assessed Immediately After Semen Collection

Sperm quality and functionality was first evaluated immediately after semen collection (**Supplementary Table 2**). PCA analysis was used to assess if one or few principal components (PC) explained enough variability, so as they could be used to categorize the sample by high and low sperm quality (**Figures 3A,B**). The results revealed that no PC exceeded the percentage of the variance explained (**Figure 3A**). Moreover, eight PC were required to achieve a good proportion of the variance explained (>90%; **Figure 3B**). Because no PC was representative enough for semen quality classification, all sperm parameters were individually analyzed.

Therefore, correlations between the concentration of SP-metabolites and specific sperm quality and functionality parameters were assessed (**Figure 3C**). Most of the correlations were observed to be from weak ($0.00 < R < 0.39$) to moderate ($0.40 < R < 0.69$) (Schober et al., 2018). The statistically significant correlations ($P < 0.050$) with the highest R scores were as follows: i) the percentage of viable sperm was positively correlated with glutamate concentration in SP ($R = 0.46$, $P = 0.014$); ii) the percentage of viable sperm with high intracellular H_2O_2 levels was positively correlated with methanol concentration in SP ($R = 0.42$, $P = 0.027$); iii) the percentage of viable sperm with high membrane destabilization was negatively correlated with trimethylamine N-oxide concentration in SP ($R = -0.38$, $P = 0.045$); and iv) the percentage of progressive motile sperm was negatively correlated with both carnitine ($R = -0.39$, $P = 0.043$) and isoleucine ($R = -0.39$, $P = 0.041$) concentrations in SP.

After the evaluation of individual correlations between SP-metabolites and sperm quality and functionality parameters, Bayesian multiple linear regression analysis was carried out. This multivariate analysis allows both the development of a potentially predictive model for each parameter and the quantification of the relative contribution of SP-metabolites to the model. Additionally, the use of a Bayesian framework allows the quantification of the uncertainty associated to each coefficient, which provides the whole distribution of the coefficients and not a single point estimate (i.e., the mean). A model was generated for every sperm quality and functionality parameter (**Supplementary Figure 1A-M**). In general, due to high uncertainties associated to coefficients, relationships between metabolites and sperm quality and functionality indicators could not be reported, except for three variables: i) percentages of viable sperm with high intracellular H_2O_2, which were positively influenced by tyrosine and carnitine, and negatively by valine and hypotaurine; ii) percentages of sperm with proximal droplets, which were positively influenced by creatine, formate, myo-inositol and tyrosine, and negatively by valine; and iii) percentages of sperm with folded tails, which were positively influenced by carnitine and methanol, and negatively by creatine and hypotaurine (**Figure 3D**).

TABLE 1 | Concentration of metabolites (mM) in pig seminal plasma (n = 28).

Metabolite	Median	Quartile 25	Quartile 75
Acetate	0.1312	0.1142	0.1431
Alanine	0.1257	0.0999	0.1778
Carnitine	0.7736	0.5943	1.1612
Citrate	6.6307	4.6555	8.5421
Creatine	0.3750	0.2487	0.4934
Creatine phosphate	0.0538	0.0433	0.0792
Ethanol	0.2020	0.1701	0.2203
Formate	0.1939	0.1790	0.2192
Fumarate	0.0022	0.0017	0.0032
Glucose	0.1480	0.0824	0.2476
Glutamate	0.4745	0.3590	0.6526
Hypotaurine	1.9639	1.5797	2.5621
Isoleucine	2.7658	2.1357	3.6582
Lactate	0.0477	0.0312	0.0616
Leucine	1.8198	1.3941	2.2803
Malonate	0.0633	0.0439	0.0730
Methanol	0.1106	0.0824	0.1635
Myo-Inositol	0.0557	0.0211	0.1208
Phenylalanine	4.2850	2.8488	5.3341
sn-Glycero-3-phosphocholine	24.3080	19.1166	30.3360
Trimethylamine N-oxide	0.2868	0.1614	0.4411
Tyrosine	0.0237	0.0176	0.0302
Valine	0.1039	0.0795	0.1376

Relationship Between SP-Metabolites and Sperm Resilience to Liquid Storage at 17°C for 72 h

Sperm quality and functionality were also assessed after 72 h of liquid storage (**Supplementary Table 3**). In order to evaluate whether any of the identified SP-metabolites could contribute

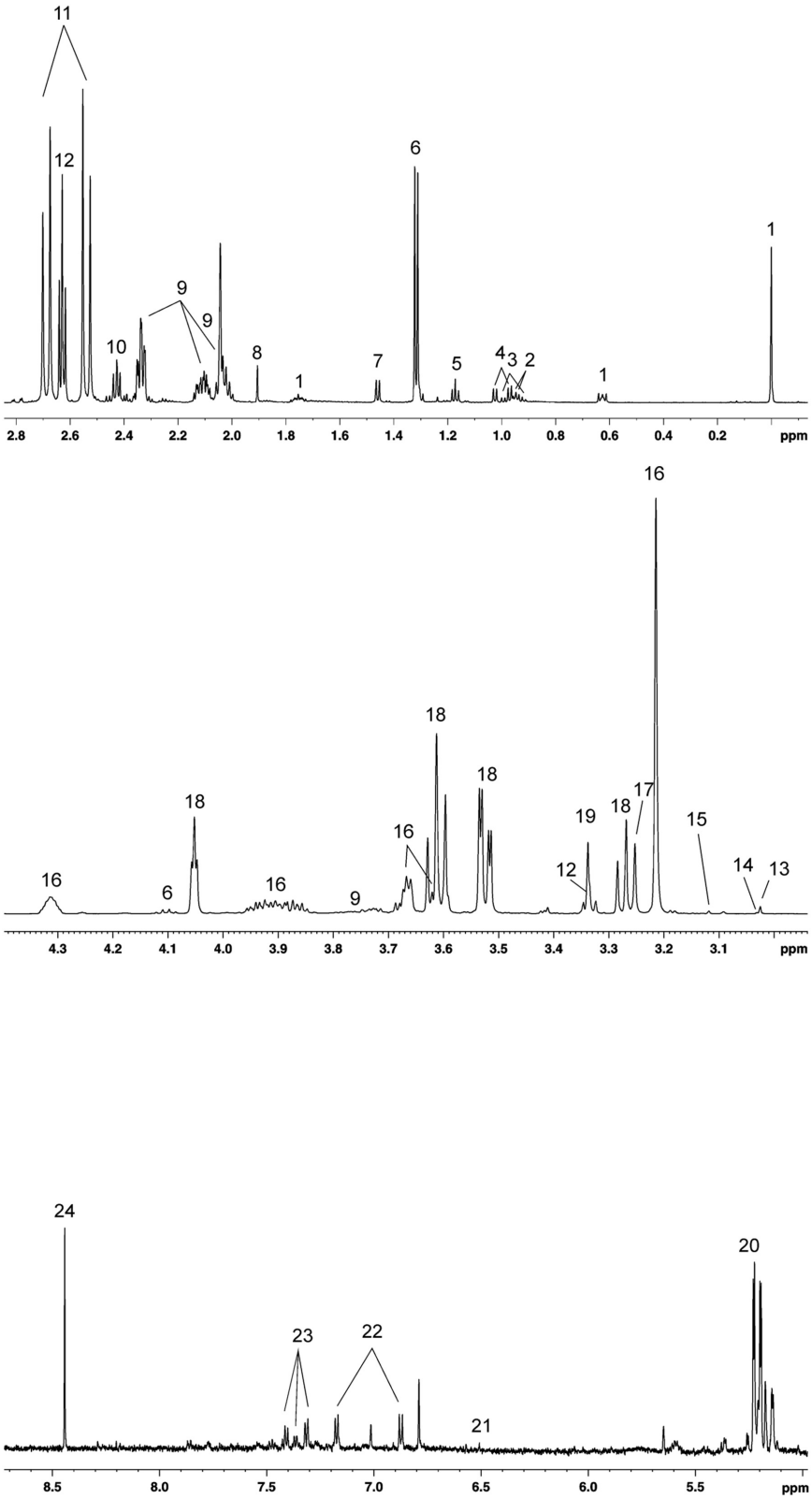

FIGURE 1 | 1H-NMR (noesygppr1d) profile (600MHz) from 0 to 8 ppm of pig seminal plasma. (1) DSS, (2) leucine, (3) isoleucine, (4) valine, (5) ethanol, (6) lactate, (7) alanine, (8) acetate, (9) glutamate, (10) carnitine, (11) citrate, (12) hypotaurine, (13) creatine, (14) creatine phosphate, (15) malonate, (16) sn-glycero-3-phosphocholine, (17) TMAO, (18) myo-inositol, (19) methanol, (20) glucose, (21) fumarate, (22) tyrosine, (23) phenylalanine, and (24) formate.

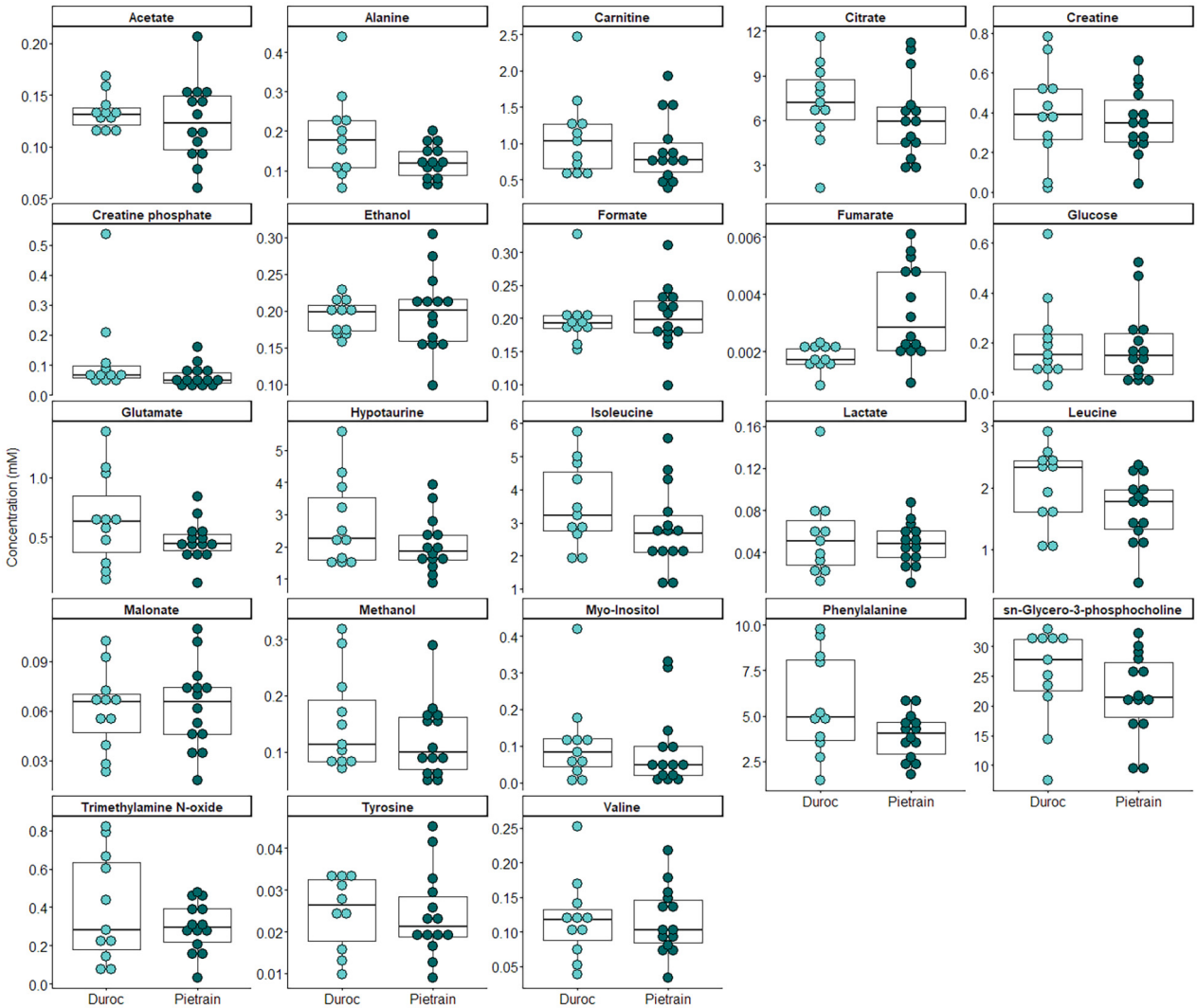

FIGURE 2 | Concentration of metabolites in seminal plasma from ejaculates (one per boar) of different pig breeds (Pietrain, $n = 14$ and Duroc, $n = 11$). Boxes enclose the 25th and 75th percentiles, the whiskers extend to the 5th and 95th percentiles, and the line indicates the median. Each dot represents the metabolite concentration from each ejaculate. Differences between breeds ($P < 0.05$) are represented as *.

to explain the sperm ability to withstand liquid storage at 17°C, correlations between concentrations of SP-metabolites and sperm quality and functionality parameters assessed after 72 h at 17°C were calculated (**Figure 4A**). As observed before, most correlations were found to be weak or moderate. The most relevant and significant ($P < 0.050$) correlations found in terms of higher R scores were: i) the percentage of viable sperm with non-intact acrosome, which was positively correlated with leucine (R = 0.40, $P = 0.038$); ii) the percentage of total motile sperm, which was negatively correlated with leucine (R = −0.40, $P = 0.039$); and iii) the percentage of progressive motile sperm, which was negatively correlated with carnitine (R = −0.41, $P = 0.031$), hypotaurine (R = −0.45, $P = 0.018$), isoleucine (R = −0.47, $P = 0.014$) and leucine (R = −0.43, $P = 0.024$).

Once the correlations between individual sperm parameters and SP-metabolites were analyzed, a Bayesian multiple linear regression analysis was run. Similar to previous findings, most of the models did not show significant contributions of SP-metabolites to sperm quality and functionality parameters after liquid storage at 17°C for 72 h (**Supplementary Figures 2A-G**). Nevertheless, two parameters, the percentage of viable sperm with high intracellular H_2O_2 and the percentage of viable sperm with high plasma membrane destabilization, exhibited two groups with different sperm resilience to liquid storage (**Figure 4B**). For this reason, logistic regression models were used for these two sperm parameters (**Figure 4C**). Concentrations of glucose and acetate in SP showed an opposite influence depending on the sperm parameter assessed. Thus, whereas acetate and glucose showed a positive and negative effect on viable sperm with high intracellular H_2O_2, respectively, the opposite pattern was observed in viable sperm with high membrane destabilization (i.e.,

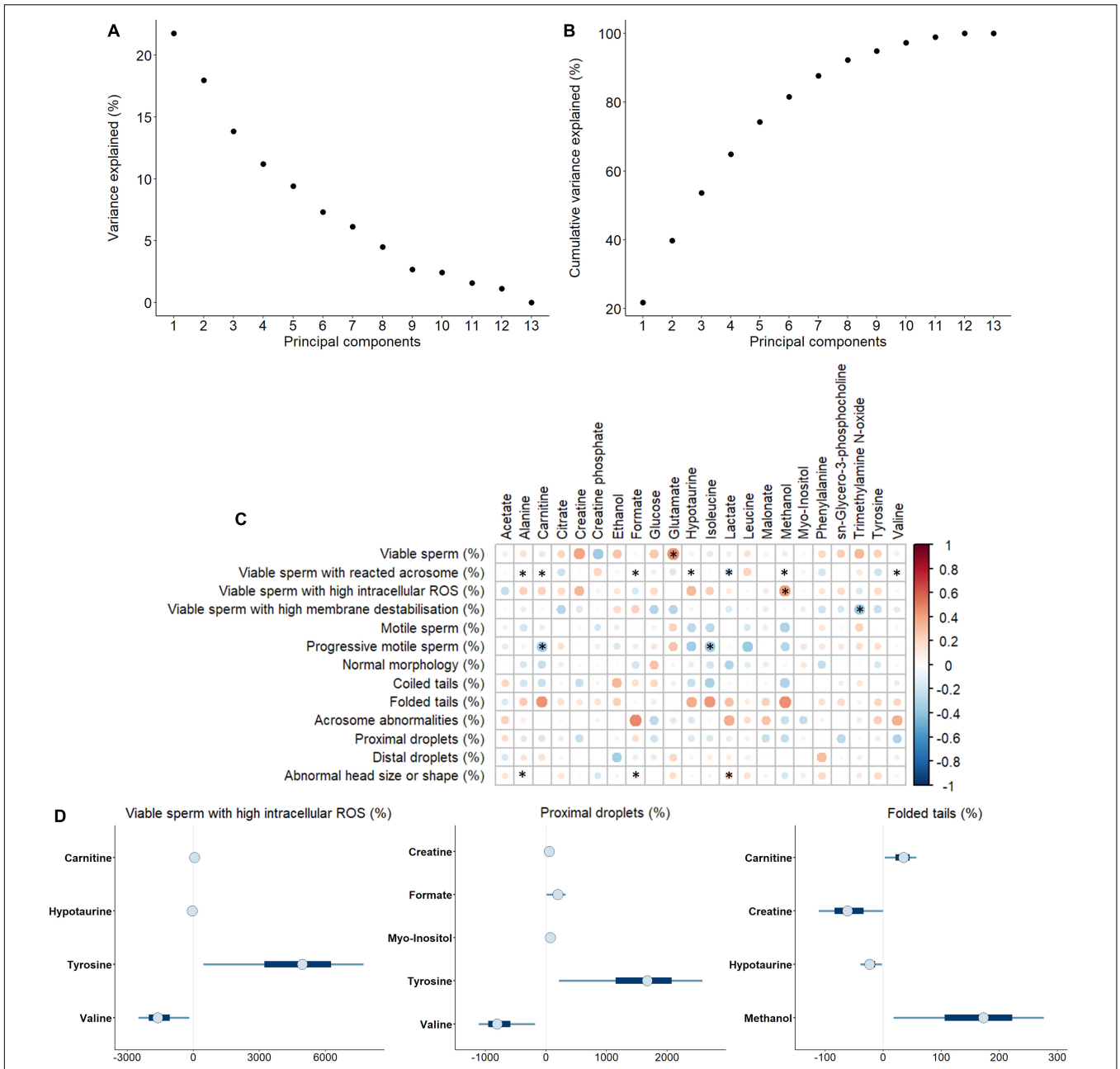

FIGURE 3 | (A) Variance explained by each principal component. **(B)** Cumulative variance explained by principal components. **(C)** Correlations between metabolites identified in pig seminal plasma and different sperm functionality parameters analyzed immediately after semen collection. The color saturation of red to blue represents the correlation coefficients (R) between metabolites, from 1 to -1, respectively. Significant correlations ($P < 0.05$) are marked with *. **(D)** Bayesian multiple linear regression models for percentage of viable sperm with high intracellular reactive oxygen species, ROS (H_2O_2), percentages of sperm with proximal droplets and percentages of sperm with folded tails. Thin lines represent the 90% credible intervals, and the blue box represents the 50% credible intervals. Dots represent the median estimated for each metabolite in the model.

glucose and acetate exhibiting a positive and a negative effect, respectively).

Correlations Between SP-Metabolites

Correlations between SP-metabolites were also analyzed and observed to vary with different magnitude (**Figure 5**). Interestingly, all significant correlations between SP-metabolites were found to be positive except for that observed between creatine and creatine phosphate (R = −0.38, $P < 0.01$). The most relevant positive correlations (R > 0.8 and $P < 0.01$; Schober et al., 2018) were: alanine vs. malonate (R = 0.80), carnitine vs. hypotaurine (R = 0.90), carnitine vs. isoleucine (R = 0.89), citrate vs. sn-glycero-3-phosphocholine (R = 0.88), citrate vs. tyrosine (R = 0.82), glutamate vs. trimethylamine

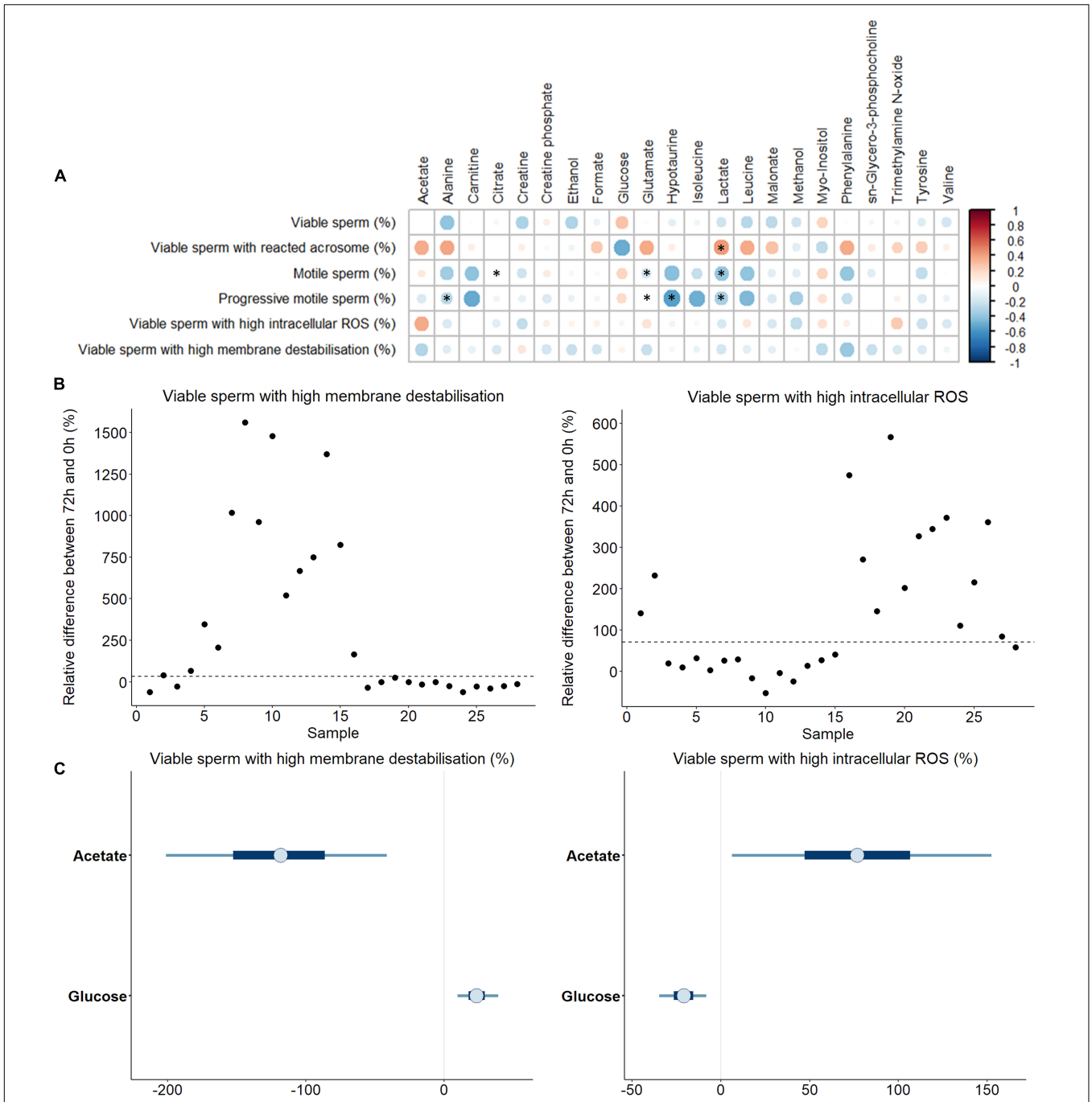

FIGURE 4 | (A) Correlations between metabolites identified in pig seminal plasma and different sperm quality and functionality parameters evaluating the quality loss after 72 h of liquid storage at 17 °C. The color saturation of red to blue represents the correlation coefficients (R) between metabolites, from 1 to −1, respectively. Significant correlations ($P < 0.05$) are marked with *. **(B)** Plot showing the relative differences of viable sperm with high membrane destabilization and with high intracellular reactive oxygen species, ROS (H_2O_2) for each SP sample. Two different sperm resilience to liquid storage patterns can be observed (marked with a discontinuous line). **(C)** Bayesian logistic regression models for the percentage viable sperm with high membrane destabilization and with high intracellular H_2O_2. Thin lines represent the 90% credible intervals, and the blue box represents the 50% credible intervals. Dots represent the median estimated for each metabolite in the model.

N-oxide (R = 0.83), hypotaurine vs. isoleucine (R = 0.92), hypotaurine vs. methanol (R = 0.83), isoleucine vs. methanol (R = 0.80), lactate vs. malonate (R = 0.92), lactate vs. tyrosine (R = 0.86), lactate vs. valine (R = 0.84), sn-glycero-3-phosphocholine vs. tyrosine (R = 0.80), and tyrosine vs. valine (R = 0.91).

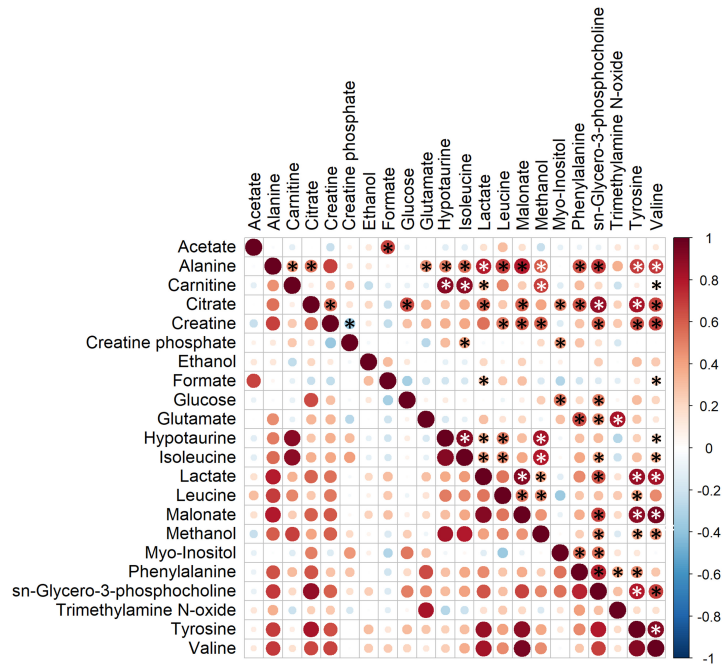

FIGURE 5 | Correlation plot of the twenty-three metabolites identified in boar seminal plasma. The color saturation from red to blue represents the Pearson correlation coefficients (R) between metabolites, from 1 to –1, respectively. Significant correlations ($P < 0.05$) are marked with *.

DISCUSSION

As far as we know, this is the first report that performed an in-depth metabolomic profile of pig SP quantifying the identified metabolites. Moreover, this is the first study conducted in a livestock species that explored the putative influence of SP-metabolites on sperm physiology and on the sperm resilience to liquid storage at 17 °C. Specifically, this exploratory study reported that: i) a total of 23 SP-metabolites were present at measurable concentrations in pig SP; ii) except for fumarate, no differences in SP-metabolites concentration were identified between pig breeds (Duroc and Pietrain); iii) glutamate, methanol, trimethylamine N-oxide, carnitine and isoleucine concentrations in SP were related to specific sperm quality and functionality parameters evaluated right after semen collection; iv) leucine, hypotaurine, carnitine and isoleucine concentrations in SP were found to be related with the sperm ability to withstand liquid storage; and v) Bayesian multiple regression models allowed the identification of putative metabolite patterns for specific sperm parameters. In addition, very strong relationships between SP-metabolites were also observed.

Metabolomic approaches allow the study of cellular metabolic products; these low-molecular-weight molecules can ultimately unveil the phenotype of the studied system (Deepinder et al., 2007). For this reason, studying the metabolome has been widely proposed as a promising tool for spermatology and male infertility diagnosis (Aitken, 2010; Kovac et al., 2013; Minai-Tehrani et al., 2016; Bracewell-Milnes et al., 2017; Moura et al., 2018). The NMR spectroscopy is one of the most used technologies in this field, because it provides a non-biased uniform detection of equal sensibility for all proton-containing molecules in samples, and requires little or no processing (Goodacre et al., 2004; Emwas et al., 2019). This analytical method has been widely used for SP-metabolite profiling of several mammalian species, including humans (Hamamah et al., 1993; Segalen et al., 1995; Gupta et al., 2011; Jayaraman et al., 2014; Bonechi et al., 2015; Mumcu et al., 2020), cattle (Kumar et al., 2015) and pigs (Kalic et al., 1997; Mateo-Otero et al., 2020). The present work identified and quantified a total of 23 metabolites in pig SP, including amino acids, saccharides, salts, alcohols, and other compounds. Compared to our previous work (Mateo-Otero et al., 2020), the present study quantified SP-metabolites, as well as identified new molecules (i.e., formate, fumarate, hypotaurine, isoleucine, malonate, myo-inositol, and trimethylamine N-oxide). These new findings may result from improvements in sample handling and purification, and the higher frequency and resolution of the NMR spectrometer. Additionally, while SP in pigs showed a metabolite profile similar to that reported in humans (Hamamah et al., 1993; Segalen et al., 1995; Gupta et al., 2011; Jayaraman et al., 2014; Bonechi et al., 2015; Mumcu et al., 2020), it differed from that found in cattle (Kumar et al., 2015). This was already reported in our previous work (Mateo-Otero et al., 2020) and was confirmed in the present study.

Regarding the new SP-metabolites identified in the present work, both isoleucine and malonate were also identified in the human SP (Gupta et al., 2011; Bonechi et al., 2015; Mumcu et al., 2020). Moreover, only some of the NMR studies carried out in humans quantified the identified metabolites (Gupta et al., 2011, 2013; Bonechi et al., 2015), generally reporting higher

SP-metabolite concentrations than those found herein for pigs (Hamamah et al., 1993; Segalen et al., 1995; Gupta et al., 2011; Jayaraman et al., 2014; Bonechi et al., 2015; Mumcu et al., 2020). Variations in SP metabolite profile or in their concentrations could contribute to reveal physiological differences between species in terms of sperm functionality and fertility. Nevertheless, sample handling and processing could also serve to explain these qualitative and quantitative discrepancies.

As aforementioned, one of the most relevant results of the present study was that concentrations of 23 metabolites present in pig SP were uncovered. In addition, we observed that concentrations of SP-metabolites varied between ejaculates. Since all boars had similar age, were housed under the same conditions, and were fed with the same commercial diet, we hypothesize that such variability could be related to pig breeds. However, when samples were divided considering breeds, no effect on SP-metabolites concentration was observed, except for fumarate, which exhibited higher levels in Pietrain than in Duroc boars. This agrees with most of the studies evaluating SP components in samples from different pig breeds, in which no breed effect was reported (Barranco et al., 2015b, 2016, 2020; Llavanera et al., 2020). However, since the sample size for each breed was limited in the present study, further research should verify this assumption. Nevertheless, considering our findings, one could assume that differences in the concentration of SP-metabolites found between boars could contribute to explain the disparity observed in their sperm quality parameters assessed immediately after semen collection or in their sperm resilience to liquid storage.

Many efforts have been focused on exploring pig SP composition with the aim to uncover SP biomarkers able to predict semen quality after ejaculate collection (López Rodríguez et al., 2012; Barranco et al., 2016, 2017, 2020; Llavanera et al., 2020). In the last years, the advances in metabolomic analytical methods have allowed the identification of SP-metabolites as potential sperm quality biomarkers in mammalian species, such as humans (Bonechi et al., 2015; Engel et al., 2019; Wang et al., 2019; Mumcu et al., 2020; Xu et al., 2020) and cattle (Moura et al., 2018). Our results suggest that metabolomic analysis of pig SP could offer a new source of sperm functionality biomarkers. Therefore, by using an exploratory approach, the present study evaluated the potential relationship of the concentration of SP-metabolites with sperm quality and functionality parameters assessed immediately after semen collection. While a strongly significant (P = 0.014) positive correlation between the concentration of glutamate in SP and sperm viability was observed, this does not fully agree with previous findings in which the addition of monosodium glutamate to fresh pig semen had no effect on the percentage of viable sperm during *in vitro* capacitation (Spinaci et al., 2017). On the other hand, a positive relationship (P = 0.027) between methanol concentration in SP and viable sperm with high H_2O_2 was found. These results do not come as a surprise when one considers the well-known oxidative stress-inducer role of this metabolite (Parthasarathy et al., 2006). In addition, a negative relationship (P = 0.045) between trimethylamine N-oxide concentration in SP and viable sperm with high membrane destabilization was detected. These results would be in agreement with the study by Darbandi et al. (2019) in men, who found that higher levels of this metabolite in human SP were related with high intracellular ROS levels in sperm and could ultimately cause membrane lipid peroxidation and, thus, membrane destabilization. Finally, our data indicated that concentrations of both carnitine (P = 0.043) and isoleucine (P = 0.041) in SP were negatively correlated to progressively motile sperm. Regarding carnitine, our results are in agreement with previous studies in humans using liquid chromatography-mass spectrometry (LC-MS) (Wang et al., 2019; Xu et al., 2020). This metabolite was found to be a potential SP-biomarker of poor semen quality (Wang et al., 2019), and to be positively related with sperm deformity rate (Xu et al., 2020). By contrast, our findings do not agree with the previous literature, since several studies reported the beneficial effect of supplementing diet with L-carnitine on sperm progressive motility in patients with different types of infertility (Lenzi et al., 2004; Garolla et al., 2005; Micic et al., 2019). On the other hand, a negative effect of isoleucine on sperm has been observed in buffalos, since poor semen quality is associated to low levels of isoleucine (Binsila et al., 2020). Our data indicated that each relationship has a different P value; while glutamate and sperm viability were found to have a very robust correlation coefficient (P = 0.014), the others ranged between P = 0.020 and P = 0.045. In this latter case, and despite the fact that these correlations had a high degree of confidence (> 95%), one could not exclude that some happened by chance (given that type I error increases with the number of correlations tested). For this reason, except for glutamate, the other relationships should be considered as a preliminary approximation to elucidate the effect of these SP-metabolites on sperm physiology. Thus, further experiments to validate the correlations observed in the present study are warranted. What is more, considering the aforementioned discrepancies between species, the actual effect of these metabolites on pig sperm needs to be addressed in future studies because species-specific regulation of SP-metabolites could be observed. Another possibility to explain such discrepancies could be that only moderate correlations were found between pig SP-metabolites and sperm quality parameters. Hence, specificity and sensibility of SP-metabolites should be tested and validated before their use as biomarkers.

This study was also able to explore whether concentrations of metabolites in SP were able to explain variations in sperm quality/functionality parameters using Bayesian multiple linear regression models. Only metabolites whose 90% credible intervals did not cross 0 in a Pareto distribution were considered as valid and, thus, as promising biomarkers. We did not find clear patterns for most of the quality parameters evaluated immediately after semen collection. However, models based on viable sperm with high intracellular ROS, sperm with proximal droplets and sperm with folded tails showed a positive or negative effect of specific SP-metabolites. Most relationships between metabolites have not yet been described in the literature; thus, further studies focused on determining whether these relationships have a biological significance are required.

Sperm quality of pig seminal AI-doses gradually declines during their storage at 17°C (Waberski et al., 2011; Yeste, 2017), showing differences in their sperm resilience to liquid preservation (Parrilla et al., 2012; Zakošek Pipan et al., 2014; Roca et al., 2015). While several studies have demonstrated that some SP-proteins are able to predict pig sperm resilience to liquid storage (Zakošek Pipan et al., 2014; Barranco et al., 2016, 2019; Parrilla et al., 2019; Llavanera et al., 2020), no study has, to the best of our knowledge, evaluated the potential relationship between SP-metabolite composition and the sperm ability to sustain 72 h of liquid storage. Our approach suggested that some SP-metabolites were positively and negatively related with the sperm functionality decline during liquid preservation. Leucine concentration in SP was found to be positively correlated with the percentage of viable sperm with a non-intact acrosome (P = 0.038) and negatively associated with the loss of total (P = 0.039) and progressive (P = 0.024) motility after 72 h of liquid storage. Despite the fact that no information regarding leucine effect on sperm performance is available in mammals, the addition of this metabolite is known to have a positive effect on the motility of zebrafish sperm (Zhang et al., 2017). Similarly, our findings revealed that hypotaurine concentration in SP was negatively related with higher loss of progressive motility (P = 0.018) after liquid storage at 17 °C. In this context, it is worth mentioning that hypotaurine supplementation has been reported to exert a positive impact upon sperm motility in mammalian species, such as hamsters (Boatman et al., 1990) or humans (Holmes et al., 1992; Brugnon et al., 2013). Finally, both carnitine (P = 0.031) and isoleucine (P = 0.014) were found to be negatively related with the loss of progressive motility after liquid storage. While information regarding the effect of isoleucine on sperm motility is yet to be reported, a study on L-carnitine supplementation during liquid storage of pig semen demonstrated that this metabolite could maintain sperm motility (Yang et al., 2020). Whilst all these data suggest that these metabolites may be promising biomarkers for motility prediction of seminal AI-doses after liquid storage, the different P values may, as pointed out before, imply different robustness in the relationships observed. In this regard, while correlations of isoleucine and hypotaurine with loss of progressive motility over liquid storage were high, those with P values oscillating between 0.020 and 0.040 would need further validation. For this reason, although our study can be considered as a first steppingstone in establishing biomarkers for the sperm resilience to liquid storage, further experiments are needed to confirm the exact role of SP-metabolites during that process.

In a similar fashion to the case of sperm quality evaluated immediately after semen collection, Bayesian multiple linear regression models did not identify clear metabolite concentration patterns explaining sperm quality loss. However, the percentage of viable sperm with high intracellular H_2O_2 and the percentage of viable sperm with high plasma membrane destabilization showed two distinct groups of low- and high-quality loss. For this reason, logistic regression models were considered to be appropriate to further study such relationships. Interestingly, concentrations of acetate and glucose in SP were observed to have opposite effects on both parameters. These findings are in agreement with the literature, as acetate production from glucose through pyruvate has been previously reported to occur in mammalian mitochondria (Liu et al., 2018). Our models showed that low levels of glucose and high levels of acetate have an impact on the percentage of viable sperm with high levels of ROS, which could be explained by the link between acetate production and ROS generation (Liu et al., 2018). On the other hand, glucose could also be involved in fatty acids and cholesterol synthesis (Wolfe, 1998). As we found that high levels of glucose and low levels of acetate influenced the percentage of viable sperm with high membrane destabilization, further studies should explore the exact mechanism that would underlie such observation.

In conclusion, the use of NMR spectroscopy analysis allowed the identification and quantification of 23 metabolites in pig SP. Our exploratory approach was able to suggest that the concentration of selected SP-metabolites was related to sperm quality and functionality parameters of liquid-stored semen samples and to the sperm ability to withstand liquid storage, which led to uncover potential biomarkers. Specifically, the concentration of glutamate in SP appeared to be related to sperm viability when evaluated immediately after ejaculate collection. Moreover, while concentrations of hypotaurine and isoleucine in SP could be involved in the sperm resilience to liquid storage, the pattern observed for glucose and acetate suggests that they could also play a role. Yet, these relationships can only be considered as a first steppingstone for metabolite biomarker identification, as they are pending to be validated in future studies. Nevertheless, this could have a very relevant impact on AI industry because the identification of such metabolites could contribute to improve: i) quality assessment of seminal AI-doses prior to AI; and ii) AI extenders through supplementation with specific metabolites to improve the sperm resilience to liquid storage. Moreover, further research including more semen samples should be conducted to determine whether these SP-metabolites could also be used as *in vivo* fertility biomarkers.

DATA AVAILABILITY STATEMENT

The raw data supporting the conclusions of this article will be made available by the authors, without undue reservation.

ETHICS STATEMENT

Ethical review and approval for animal participants was not required as samples were provided by the AI-Centre and authors did not manipulate any animals.

AUTHOR CONTRIBUTIONS

YM-O, MY, and IB: conceptualization. YM-O, PF-L, and IB: methodology. YM-O, PF-L, JR-M, MY, and IB: formal analysis and investigation. YM-O: writing – original draft preparation. JR-M, JM, JR, MY, and IB: writing – review and editing. JM, JR, and MY: funding acquisition.

IB and MY: supervision. All authors have read and agreed to the published version of the manuscript.

FUNDING

The present study was funded by the Ministry of Science and Innovation, Spain (Grants: RYC-2014-15581, AGL2017-88329-R, and FJCI-2017-31689), the Seneca Foundation Murcia, Spain (19892/GERM-15), and the Regional Government of Catalonia (Grants: 2017-SGR-1229 and 2020-FI-B-00412).

ACKNOWLEDGMENTS

The authors would like to thank Pau Nolis, from the Nuclear Magnetic Resonance Service, Autonomous University of Barcelona, for the metabolomic analysis and technical support. Moreover, the authors would also wish to thank AIM Iberica (Topigs Norsvin Iberica) for supplying the boar ejaculates.

SUPPLEMENTARY MATERIAL

The Supplementary Material for this article can be found online at: https://www.frontiersin.org/articles/10.3389/fcell.2021.669974/full#supplementary-material

Supplementary Figure 1 | (A-M). Complete Bayesian multiple linear regression models for all the parameters evaluated immediately after semen collection.

Supplementary Figure 2 | (A-F) Complete Bayesian multiple linear regression models for all the parameters evaluated immediately after semen collection. **(G,H)** Complete Bayesian logistic regression models for percentages of viable sperm with high membrane destabilization, and with high intracellular Ros.

Supplementary Table 1 | Metabolite concentrations (mM) in seminal plasma of Pietrain and Duroc breeds. Significant correlations ($P < 0.05$) are marked with *.

Supplementary Table 2 | Sperm quality and functionality parameters of pig semen samples ($n = 28$) assessed immediately after semen collection. Sd: Standard Deviation.

Supplementary Table 3 | Sperm quality loss of pig semen samples ($n = 28$) after 72 h of liquid storage at 17°C. Sd: Standard Deviation.

REFERENCES

Aitken, R. J. (2010). Whither must spermatozoa wander? The future of laboratory seminology. *Asian J. Androl.* 12, 99–103. doi: 10.1038/aja.2008.42

Asampille, G., Cheredath, A., Joseph, D., Adiga, S. K., and Atreya, H. S. (2020). The utility of nuclear magnetic resonance spectroscopy in assisted reproduction. *Open Biol.* 10:200092. doi: 10.1098/rsob.200092

Barranco, I., Fernandez-Fuertes, B., Padilla, L., Delgado-Bermúdez, A., Tvarijonaviciute, A., and Yeste, M. (2020). Seminal plasma anti-müllerian hormone: a potential Ai-boar fertility biomarker? *Biology* 9, 1–13. doi: 10.3390/biology9040078

Barranco, I., Padilla, L., Tvarijonaviciute, A., Parrilla, I., Martínez, E. A., Rodriguez-Martinez, H., et al. (2019). Levels of activity of superoxide dismutase in seminal plasma do not predict fertility of pig AI-semen doses. *Theriogenology* 140, 18–24. doi: 10.1016/j.theriogenology.2019.08.010

Barranco, I., Perez-Patiño, C., Tvarijonaviciute, A., Parrilla, I., Vicente-Carrillo, A., Alvarez-Rodriguez, M., et al. (2017). Active paraoxonase 1 is synthesised throughout the internal boar genital organs. *Reproduction* 154, 237–243. doi: 10.1530/REP-17-0300

Barranco, I., Tvarijonaviciute, A., Perez-Patino, C., Alkmin, D. V., Ceron, J. J., Martinez, E. A., et al. (2015a). The activity of paraoxonase type 1 (PON-1) in boar seminal plasma and its relationship with sperm quality, functionality, and in vivo fertility. *Andrology* 3, 315–320. doi: 10.1111/andr.309

Barranco, I., Tvarijonaviciute, A., Perez-Patinō, C., Parrilla, I., Ceron, J. J., Martinez, E. A., et al. (2015b). High total antioxidant capacity of the porcine seminal plasma (SP-TAC) relates to sperm survival and fertility. *Sci. Rep.* 5, 1–9. doi: 10.1038/srep18538

Barranco, S., Tvarijonaviciute, A., Perez-Patiho, C., Vicente-Carrillo, A., Parrilla, N., Ceron, J. J., et al. (2016). Glutathione peroxidase 5 is expressed by the entire pig male genital tract and once in the seminal plasma contributes to sperm survival and in vivo fertility. *PLoS One* 11:e0162958. doi: 10.1371/journal.pone.0162958

Binsila, B. K., Archana, S. S., Ramya, L., Swathi, D., Selvaraju, S., Gowda, N. S., et al. (2020). Elucidating the processes and pathways enriched in buffalo sperm proteome in regulating semen quality. *Cell Tissue Res.* 383, 881–903. doi: 10.1007/s00441-020-03303-9

Boatman, D. E., Bavister, B. D., and Cruz, E. (1990). Addition of hypotaurine can reactivate immotile golden hamster spermatozoa. *J. Androl.* 11, 66–72. doi: 10.1002/j.1939-4640.1990.tb01581.x

Bonechi, C., Collodel, G., Donati, A., Martini, S., Moretti, E., and Rossi, C. (2015). Discrimination of human semen specimens by NMR data, sperm parameters, and statistical analysis. *Syst. Biol. Reprod. Med.* 61, 353–359. doi: 10.3109/19396368.2015.1054003

Bracewell-Milnes, T., Saso, S., Abdalla, H., Nikolau, D., Norman-Taylor, J., Johnson, M., et al. (2017). Metabolomics as a tool to identify biomarkers to predict and improve outcomes in reproductive medicine: a systematic review. *Hum. Reprod. Update* 23, 723–736. doi: 10.1093/humupd/dmx023

Brugnon, F., Ouchchane, L., Pons-Rejraji, H., Artonne, C., Farigoule, M., and Janny, L. (2013). Density gradient centrifugation prior to cryopreservation and hypotaurine supplementation improve post-thaw quality of sperm from infertile men with oligoasthenoteratozoospermia. *Hum. Reprod.* 28, 2045–2057. doi: 10.1093/humrep/det253

Cazaux Velho, A. L., Menezes, E., Dinh, T., Kaya, A., Topper, E., Moura, A. A., et al. (2018). Metabolomic markers of fertility in bull seminal plasma. *PLoS One* 13:e0195279. doi: 10.1371/journal.pone.0195279

Darbandi, M., Darbandi, S., Agarwal, A., Baskaran, S., Dutta, S., Sengupta, P., et al. (2019). Reactive oxygen species-induced alterations in H19-Igf2 methylation patterns, seminal plasma metabolites, and semen quality. *J. Assist. Reprod. Genet.* 36, 241–253. doi: 10.1007/s10815-018-1350-y

Deepinder, F., Chowdary, H. T., and Agarwal, A. (2007). Role of metabolomic analysis of biomarkers in the management of male infertility. *Expert Rev. Mol. Diagn.* 7, 351–358. doi: 10.1586/14737159.7.4.351

Egea, R. R., Puchalt, N. G., Escrivá, M. M., and Varghese, A. C. (2014). OMICS: CURRENT and future perspectives in reproductive medicine and technology. *J. Hum. Reprod. Sci.* 7, 73–92. doi: 10.4103/0974-1208.138857

Emwas, A. H., Roy, R., McKay, R. T., Tenori, L., Saccenti, E., Nagana Gowda, G. A., et al. (2019). NMR spectroscopy for metabolomics research. *Metabolites* 9:123. doi: 10.3390/metabo9070123

Engel, K. M., Baumann, S., Rolle-Kampczyk, U., Schiller, J., von Bergen, M., and Grunewald, S. (2019). Metabolomic profiling reveals correlations between spermiogram parameters and the metabolites present in human spermatozoa and seminal plasma. *PLoS One* 14:e0211679. doi: 10.1371/journal.pone.0211679

Garolla, A., Maiorino, M., Roverato, A., Roveri, A., Ursini, F., and Foresta, C. (2005). Oral carnitine supplementation increases sperm motility in asthenozoospermic men with normal sperm phospholipid hydroperoxide glutathione peroxidase levels. *Fertil. Steril.* 83, 355–361. doi: 10.1016/j.fertnstert.2004.10.010

Goodacre, R., Vaidyanathan, S., Dunn, W. B., Harrigan, G. G., and Kell, D. B. (2004). Metabolomics by numbers: acquiring and understanding global metabolite data. *Trends Biotechnol.* 22, 245–252. doi: 10.1016/j.tibtech.2004.03.007

Goodrich, B., Gabry, J., Ali, I., and Brilleman, S. (2020). *rstanarm: Bayesian Applied Regression Modeling via Stan*. Available online at: https://mc-stan.org/rstanarm/ (accessed November 2, 2020).

Gupta, A., Mahdi, A. A., Ahmad, M. K., Shukla, K. K., Jaiswer, S. P., and Shankhwar, S. N. (2011). 1H NMR spectroscopic studies on human seminal plasma: a probative discriminant function analysis classification model. *J. Pharm. Biomed. Anal.* 54, 106–113. doi: 10.1016/j.jpba.2010.07.021

Gupta, A., Mahdi, A. A., Shukla, K. K., Ahmad, M. K., Bansal, N., Sankhwar, P., et al. (2013). Efficacy of *Withania somnifera* on seminal plasma metabolites of infertile males: a proton NMR study at 800 MHz. *J. Ethnopharmacol.* 149, 208–214. doi: 10.1016/j.jep.2013.06.024

Hamamah, S., Seguin, F., Barthelemy, C., Akoka, S., Le Pape, A., Lansac, J., et al. (1993). 1H nuclear magnetic resonance studies of seminal plasma from fertile and infertile men. *J. Reprod. Fertil.* 97, 51–55. doi: 10.1530/jrf.0.0970051

Holmes, R. P., Goodman, H. O., Shihabi, Z. K., and Jarow, J. P. (1992). The taurine and hypotaurine content of human semen. *J. Androl.* 13, 289–292. doi: 10.1002/j.1939-4640.1992.tb00317.x

Jayaraman, V., Ghosh, S., Sengupta, A., Srivastava, S., Sonawat, H. M., and Narayan, P. K. (2014). Identification of biochemical differences between different forms of male infertility by nuclear magnetic resonance (NMR) spectroscopy. *J. Assist. Reprod. Genet.* 31, 1195–1204. doi: 10.1007/s10815-014-0282-4

Kalic, M., Kamp, G., and Lauterwein, J. (1997). Nuclear magnetic resonance studies of boar seminal plasma. Problems encountered in the identification of small molecules: hypotaurine and carnitine. *NMR Biomed.* 10, 341–347. doi: 10.1002/(SICI)1099-1492(199710)10:7<341::AID-NBM464<3.0.CO;2-M

Kovac, J. R., Pastuszak, A. W., and Lamb, D. J. (2013). The use of genomics, proteomics, and metabolomics in identifying biomarkers of male infertility. *Fertil. Steril.* 99, 998–1007. doi: 10.1016/j.fertnstert.2013.01.111

Kumar, A., Kroetsch, T., Blondin, P., and Anzar, M. (2015). Fertility-associated metabolites in bull seminal plasma and blood serum: 1H nuclear magnetic resonance analysis. *Mol. Reprod. Dev.* 82, 123–131. doi: 10.1002/mrd.22450

Kumaresan, A., Kadirvel, G., Bujarbaruah, K. M., Bardoloi, R. K., Das, A., Kumar, S., et al. (2009). Preservation of boar semen at 18 degrees C induces lipid peroxidation and apoptosis like changes in spermatozoa. *Anim. Reprod. Sci.* 110, 162–171. doi: 10.1016/j.anireprosci.2008.01.006

Lenzi, A., Sgrò, P., Salacone, P., Paoli, D., Gilio, B., Lombardo, F., et al. (2004). A placebo-controlled double-blind randomized trial of the use of combined L-carnitine and L-acetyl-carnitine treatment in men with asthenozoospermia. *Fertil. Steril.* 81, 1578–1584. doi: 10.1016/j.fertnstert.2003.10.034

Liu, X., Cooper, D. E., Cluntun, A. A., Warmoes, M. O., Zhao, S., Reid, M. A., et al. (2018). Acetate production from glucose and coupling to mitochondrial metabolism in mammals. *Cell* 175, 502.e13–513.e13. doi: 10.1016/j.cell.2018.08.040

Llavanera, M., Delgado-Bermúdez, A., Mateo-Otero, Y., Padilla, L., Romeu, X., Roca, J., et al. (2020). Exploring seminal plasma GSTM3 as a quality and in vivo fertility biomarker in pigs—relationship with sperm morphology. *Antioxidants* 9, 1–14. doi: 10.3390/antiox9080741

López Rodríguez, A., Rijsselaere, T., Beek, J., Vyt, P., Soom, A., Van, et al. (2012). Boar seminal plasma components and their relation with semen quality. *Syst. Biol. Reprod. Med.* 59, 5–12. doi: 10.3109/19396368.2012.725120

Mateo-Otero, Y., Fernández-López, P., Gil-Caballero, S., Fernandez-Fuertes, B., Bonet, S., Barranco, I., et al. (2020). 1H nuclear magnetic resonance of pig seminal plasma reveals intra-ejaculate variation in metabolites. *Biomolecules* 10, 1–16. doi: 10.3390/biom10060906

Micic, S., Lalic, N., Djordjevic, D., Bojanic, N., Bogavac-Stanojevic, N., Busetto, G. M., et al. (2019). Double-blind, randomised, placebo-controlled trial on the effect of L-carnitine and L-acetylcarnitine on sperm parameters in men with idiopathic oligoasthenozoospermia. *Andrologia* 51:e13267. doi: 10.1111/and.13267

Minai-Tehrani, A., Jafarzadeh, N., and Gilany, K. (2016). Metabolomics: a state-of-the-art technology for better understanding of male infertility. *Andrologia* 48, 609–616. doi: 10.1111/and.12496

Moura, A. A., Memili, E., Portela, A. M. R., Viana, A. G., Velho, A. L. C., Bezerra, M. J. B., et al. (2018). Seminal plasma proteins and metabolites: effects on sperm function and potential as fertility markers. *Anim. Reprod.* 15, 691–702. doi: 10.21451/1984-3143-AR2018-0029

Mumcu, A., Karaer, A., Dogan, B., and Tuncay, G. (2020). Metabolomics analysis of seminal plasma in patients with idiopathic Oligoasthenoteratozoospermia using high-resolution NMR spectroscopy. *Andrology* 8, 450–456. doi: 10.1111/andr.12707

Nobakht, M., and Gh, B. F. (2018). Application of metabolomics to preeclampsia diagnosis. *Syst. Biol. Reprod. Med.* 64, 324–339. doi: 10.1080/19396368.2018.1482968

Parrilla, I., del Olmo, D., Sijses, L., Martinez-Alborcia, M. J., Cuello, C., Vazquez, J. M., et al. (2012). Differences in the ability of spermatozoa from individual boar ejaculates to withstand different semen-processing techniques. *Anim. Reprod. Sci.* 132, 66–73. doi: 10.1016/j.anireprosci.2012.04.003

Parrilla, I., Perez-Patiño, C., Li, J., Barranco, I., Padilla, L., Rodriguez-Martinez, H., et al. (2019). Boar semen proteomics and sperm preservation. *Theriogenology* 137, 23–29. doi: 10.1016/j.theriogenology.2019.05.033

Parthasarathy, N. J., Kumar, R. S., Manikandan, S., Narayanan, G. S., Kumar, R. V., and Devi, R. S. (2006). Effect of methanol-induced oxidative stress on the neuroimmune system of experimental rats. *Chem. Biol. Interact.* 161, 14–25. doi: 10.1016/j.cbi.2006.02.005

Recuero, S., Fernandez-Fuertes, B., Bonet, S., Barranco, I., and Yeste, M. (2019). Potential of seminal plasma to improve the fertility of frozen-thawed boar spermatozoa. *Theriogenology* 137, 36–42. doi: 10.1016/j.theriogenology.2019.05.035

Roca, J., Broekhuijse, M. L. W. J., Parrilla, I., Rodriguez-Martinez, H., Martinez, E. A., and Bolarin, A. (2015). Boar differences in artificial insemination outcomes: can they be minimized? *Reprod. Domest. Anim.* 50, 48–55. doi: 10.1111/rda.12530

Roca, J., Parrilla, I., Bolarin, A., Martinez, E. A., and Rodriguez-Martinez, H. (2016). Will AI in pigs become more efficient? *Theriogenology* 86, 187–193. doi: 10.1016/j.theriogenology.2015.11.026

Rodríguez-Martínez, H., Kvist, U., Ernerudh, J., Sanz, L., and Calvete, J. J. (2011). Seminal plasma proteins: what role do they play? *Am. J. Reprod. Immunol.* 66, 11–22. doi: 10.1111/j.1600-0897.2011.01033.x

Schober, P., Boer, C., and Schwarte, L. A. (2018). Correlation coefficients: appropriate use and interpretation. *Anesth. Analg.* 126, 1763–1768. doi: 10.1213/ANE.0000000000002864

Segalen, J., de Certaines, J. D., Le Calvé, M., Colleu, D., Bansard, J. Y., and Rio, M. (1995). Fertilization attempts: use of automatic spectrum analysis. *J. Reprod. Fertil.* 103, 181–187.

Singh, R., and Sinclair, K. D. (2007). Metabolomics: approaches to assessing oocyte and embryo quality. *Theriogenology* 68(Suppl. 1), S56–S62. doi: 10.1016/j.theriogenology.2007.04.007

Spinaci, M., Bucci, D., Gadani, B., Porcu, E., Tamanini, C., and Galeati, G. (2017). Pig sperm preincubation and gamete coincubation with glutamate enhance sperm-oocyte binding and in vitro fertilization. *Theriogenology* 95, 149–153. doi: 10.1016/j.theriogenology.2017.03.017

Uyar, A., and Seli, E. (2014). Metabolomic assessment of embryo viability. *Semin. Reprod. Med.* 32, 141–152. doi: 10.1055/s-0033-1363556

Waberski, D., Henning, H., and Petrunkina, A. M. (2011). Assessment of storage effects in liquid preserved boar semen. *Reprod. Domest. Anim.* 46, 45–48. doi: 10.1111/j.1439-0531.2011.01836.x

Waberski, D., Riesenbeck, A., Schulze, M., Weitze, K. F., and Johnson, L. (2019). Application of preserved boar semen for artificial insemination: past, present and future challenges. *Theriogenology* 137, 2–7. doi: 10.1016/j.theriogenology.2019.05.030

Wang, Y. X., Wu, Y., Chen, H. G., Duan, P., Wang, L., Shen, H. Q., et al. (2019). Seminal plasma metabolome in relation to semen quality and urinary phthalate metabolites among Chinese adult men. *Environ. Int.* 129, 354–363. doi: 10.1016/j.envint.2019.05.043

Wolfe, R. R. (1998). Metabolic interactions between glucose and fatty acids in humans. *Am. J. Clin. Nutr.* 67, 519S–526S. doi: 10.1093/ajcn/67.3.519S

Xu, Y., Lu, H., Wang, Y., Zhang, Z., and Wu, Q. (2020). Comprehensive metabolic profiles of seminal plasma with different forms of male infertility and their correlation with sperm parameters. *J. Pharm. Biomed. Anal.* 177:112888. doi: 10.1016/j.jpba.2019.112888

Yang, K., Wang, N., Guo, H. T., Wang, J. R., Sun, H. H., Sun, L. Z., et al. (2020). Effect of L-carnitine on sperm quality during liquid storage of boar semen. *Asian Austral. J. Anim. Sci.* 33, 1763–1769. doi: 10.5713/ajas.19.0455

Yeste, M. (2017). State-of-the-art of boar sperm preservation in liquid and frozen state. *Anim. Reprod.* 14, 69–81. doi: 10.21451/1984-3143-AR895

Zakošek Pipan, M., Mrkun, J., Kosec, M., Nemec Svete, A., and Zrimšek, P. (2014). Superoxide dismutase: a predicting factor for boar semen characteristics for short-term preservation. *Biomed Res. Int.* 2014:105280. doi: 10.1155/2014/105280

Zhang, J., Zhang, X., Liu, Y., Su, Z., Ullah Dawar, F., Dan, H., et al. (2017). Leucine mediates autophagosome-lysosome fusion and improves sperm motility by activating the PI3K/Akt pathway. *Oncotarget* 8, 111807–111818. doi: 10.18632/oncotarget.22910

Conflict of Interest: The authors declare that the research was conducted in the absence of any commercial or financial relationships that could be construed as a potential conflict of interest.

frontiers in Cell and Developmental Biology

ORIGINAL RESEARCH
published: 08 June 2021
doi: 10.3389/fcell.2021.683199

Aldose Reductase B1 in Pig Seminal Plasma: Identification, Localization in Reproductive Tissues, and Relationship With Quality and Sperm Preservation

Yentel Mateo-Otero[1,2†], Estel Viñolas-Vergés[1,2†], Marc Llavanera[1,2], Jordi Ribas-Maynou[1,2], Jordi Roca[3], Marc Yeste[1,2‡] and Isabel Barranco[4*‡]*

[1] Biotechnology of Animal and Human Reproduction (TechnoSperm), Institute of Food and Agricultural Technology, University of Girona, Girona, Spain, [2] Unit of Cell Biology, Department of Biology, Faculty of Sciences, University of Girona, Girona, Spain, [3] Department of Medicine and Animal Surgery, Faculty of Veterinary Medicine, University of Murcia, Murcia, Spain, [4] Department of Veterinary Medical Sciences, University of Bologna, Bologna, Italy

Aldose reductase B1 (AKR1B1), a NADPH-dependent enzyme that belongs to the aldo-keto reductase protein superfamily, has been reported to be involved in both male and female reproductive physiology. The objectives of this study were: (1) to evaluate the concentration of SP-AKR1B1 in pig ejaculate fractions; (2) to describe the immunohistochemical localization of AKR1B1 alongside the boar genital tract; (3) to evaluate the relationship between SP-AKR1B1 and sperm quality/functionality parameters. Ejaculates from seven boars (one ejaculate per boar) were collected in separate portions [the first 10 mL of the sperm rich fraction (SRF-P1), the rest of the SRF (SRF-P2), and the post-SRF (PSRF)], and the concentration of SP-AKR1B1 was assessed using an enzyme-linked immunosorbent assay (ELISA). Immunohistochemistry and immunoblotting targeting was conducted in the reproductive tissues of these boars. Additionally, the entire ejaculates of 14 boars (one ejaculate per boar) were collected and split into three separate aliquots for: (i) SP-AKR1B1 quantification; (ii) assessment of sperm concentration and morphology; and (iii) evaluation of sperm quality and functionality parameters upon ejaculate collection (0 h) and after 72 h of liquid storage at 17°C. Concentration of AKR1B1 in the SP of SRF-P1 (458.2 ± 116.33 ng/mL) was lower ($P < 0.05$) than that of SRF-P2 (1105.0 ± 229.80 ng/mL) and PSRF (1342.4 ± 260.18 ng/mL). Monomeric and dimeric AKR1B1 forms were expressed alongside the reproductive tissues, except in the bulbourethral glands. No relationship between SP-AKR1B1 and sperm quality/functionality parameters was observed either at 0 h or after 72 h of storage at 17°C. In conclusion, AKR1B1 is expressed in the reproductive organs of boars (except bulbourethral glands) and a higher concentration is found in the PSRF suggesting that seminal vesicles would be the main secretory source. However, this enzyme does not appear to be related to sperm quality/functionality or to the sperm ability to withstand liquid storage at 17°C.

Keywords: aldose reductase B1, AKR1B1, seminal plasma, ejaculate fractions, sperm physiology, pig

OPEN ACCESS

Edited by:
Silvina Perez-Martinez, CONICET Centro de Estudios Farmacológicos y Botánicos (CEFYBO), Argentina

Reviewed by:
Elizabeth Breininger, Consejo Nacional de Investigaciones Científicas y Técnicas (CONICET), Argentina
Tzongshi Lu, Brigham and Women's Hospital and Harvard Medical School, United States

***Correspondence:**
Marc Yeste
marc.yeste@udg.edu
Isabel Barranco
isabel.barranco@unibo.it

†These authors have contributed equally to this work and share first authorship

‡These authors have contributed equally to this work and share senior authorship

Specialty section:
This article was submitted to Cell Growth and Division, a section of the journal Frontiers in Cell and Developmental Biology

Received: *20 March 2021*
Accepted: *18 May 2021*
Published: *08 June 2021*

Citation:
Mateo-Otero Y, Viñolas-Vergés E, Llavanera M, Ribas-Maynou J, Roca J, Yeste M and Barranco I (2021) Aldose Reductase B1 in Pig Seminal Plasma: Identification, Localization in Reproductive Tissues, and Relationship With Quality and Sperm Preservation. Front. Cell Dev. Biol. 9:683199. doi: 10.3389/fcell.2021.683199

INTRODUCTION

Aldose reductase B1 (AKR1B1 or ALR2), a NADPH-dependent enzyme that belongs to the aldo-keto reductase protein superfamily (Bohren et al., 1989; Hyndman et al., 2003), has been reported to play an essential role in both male and female reproductive systems in humans (Bresson et al., 2011), cattle (Frenette et al., 2004; Girouard et al., 2009), rats (Kobayashi et al., 2002), sheep (Yang et al., 2019), and pigs (Steinhauser et al., 2016; Pérez-Patiño et al., 2018). This enzyme is known to be involved in the polyol pathway for fructose production, specifically in the conversion of glucose into sorbitol (Kobayashi et al., 2002). Interestingly, this pathway has been observed to occur during both epididymal sperm maturation in humans, cattle, and mice (Frenette et al., 2004, 2006; Jagoe et al., 2013) and conceptus peri-implantation period in pigs (Steinhauser et al., 2016). On the other hand, aldo-keto reductase enzymes have also been found to be implicated in catalyzing the reductive detoxification of carbonyl compounds within the genital tract of rat males (Kobayashi et al., 2002; Iuchi et al., 2004) and in prostaglandin 2 α synthesis (PGF2α) in pigs and humans (Bresson et al., 2011; Seo et al., 2014). As previous studies reported that AKR1B1 is expressed in the endometrium of humans (Bresson et al., 2011) and pigs (Seo et al., 2014) and is involved in PGF2α synthesis, it has been suggested that it could ultimately modulate conceptus implantation through regulation of endometrial gene expression in mammals (Kennedy et al., 2007; Seo et al., 2014). Finally, and reinforcing the belief that this protein plays a major role in reproduction, an in-depth proteomic analysis of pig seminal plasma (SP) revealed that AKR1B1 is positively related to *in vivo* fertility outcomes (Pérez-Patiño et al., 2018).

Seminal plasma, a complex fluid composed of secretions from the testis, epididymis, and male accessory sex glands, mixes with sperm upon ejaculation (Garner and Hafez, 2000). Although the classical roles attributed to SP are acting as a vehicle and serving as a nourishment media for sperm (Garner and Hafez, 2000), mounting evidence indicates that it plays a vital role for sperm function and modulates their fertilizing ability (Rodríguez-Martínez et al., 2011; Locatello et al., 2013). Moreover, SP also interacts with the female reproductive tract modulating the immune environment, a critical point required for successful pregnancy (O'Leary et al., 2004; Robertson, 2007; Schjenken and Robertson, 2014). For this reason, much research has focused on exploring the composition of SP, pointing to some SP-components as potential biomarkers of (in) fertility in several mammalian species (Novak et al., 2010; Milardi et al., 2013; Muhammad Aslam et al., 2014; Cazaux Velho et al., 2018; Pérez-Patiño et al., 2018; Leahy et al., 2019). In this regard, AKR1B1 in SP would be a clear candidate for a fertility biomarker due to its proven relationship with *in vivo* fertility (Pérez-Patiño et al., 2018). However, the mechanism through which SP-AKR1B1 could positively affect fertility in mammals remains unclear.

While the presence of AKR1B1 alongside the female reproductive system of several mammalian species has been extensively reported (Bresson et al., 2011; Seo et al., 2014; Steinhauser et al., 2016), the information about its role in the male genital tract and sperm physiology is scarce. Moreover, although AKR1B1 has been related to epididymal maturation in cattle (Frenette et al., 2004, 2006; Girouard et al., 2009) and mouse (Jagoe et al., 2013), the exact protein synthesis site in the male reproductive system is yet to be reported. In this sense, fractional emission of pig ejaculate offers a valuable opportunity to explore the contributions of specific male sex accessory glands to SP composition (Rodríguez-Martínez et al., 2009). Three fractions/portions can be objectively collected with clear differences in the SP source: (a) the first 10 mL of the so-called sperm rich fraction (SRF-P1), rich in sperm and with SP mainly originating from the epididymis; (b) the rest of SRF (SRF-P2), also rich in sperm and with SP mainly coming from the prostate (Rodríguez-Martínez et al., 2005, 2009), and, (c) the post-SRF (PSRF), poor in sperm and with SP mainly arising from the seminal vesicles (Einarsson, 1971; Rodríguez-Martínez et al., 2005, 2009; Saravia et al., 2009; Rodríguez-Martínez et al., 2011). Interestingly, the SP from these ejaculate portions has also been found to vary in terms of proteomic, metabolomic, and antioxidant capacity (Saravia et al., 2009; Rodríguez-Martínez et al., 2011; Barranco et al., 2015, 2016, 2017; Perez-Patiño et al., 2016; Mateo-Otero et al., 2020).

Considering the well-described relationship of SP-AKR1B1 with *in vivo* fertility outcomes in pigs (Pérez-Patiño et al., 2018) and the multiple key roles of AKR1B1 in reproductive physiology, the overall aim of the present study was to characterize the synthesis of SP-AKR1B1 alongside the male genital tract and to evaluate its involvement in sperm function. To this end, the specific objectives were: (1) to evaluate the concentration of SP-AKR1B1 in different pig ejaculate fractions; (2) to describe the immunohistochemical localization of AKR1B1 alongside the boar reproductive system; and (3) to evaluate the relationship between SP-AKR1B1 and sperm quality/functionality parameters in semen samples (sperm morphology, motility, viability, intracellular H_2O_2 production, acrosome integrity, and lipid disorder of plasma membrane). These sperm variables were assessed upon ejaculate collection and after 72 h of storage at 17°C, as liquid storage for that period of time is the most common method for preserving pig semen prior to conducting AI (Kumaresan et al., 2009; Waberski et al., 2019).

MATERIALS AND METHODS

Animals and Samples

All samples were supplied by an Artificial Insemination (AI) Center of AIM Ibérica located in Calasparra (Murcia, Spain), which fulfills the Spanish (ES300130640127; August 2006) and European (ES13RS04P; July 2012) legislation on commercialization of pig semen and animal health and welfare. Samples (ejaculates and reproductive tissues) were obtained from healthy and sexually mature boars (aged 18–36 months) from different breeds and crossbreeds (Pietrain and Duroc). Boars were housed individually in a building with controlled conditions of air temperature (15–25°C) and light (16 h per day), were fed with a commercial diet according to the nutritional requirements of adult boars (Chiba, 2009), and had *ad libitum* access to water.

Sperm quality of each ejaculate used in the experiment was assessed immediately after ejaculation following the standard procedures used in the AI center. All samples fulfilled the standards of sperm number and quality thresholds for the preparation of semen doses used for AI, specifically, (i) more than 200×10^6 spermatozoa/mL, (ii) more than 70% of motile sperm, and (iii) more than 75% of morphologically normal sperm.

Boars were slaughtered in a commercial slaughterhouse (La Mata de los Olmos, Teruel, Spain) for genetic replacement reasons while they were still healthy and suitable as semen donors. Once slaughtered, tissue samples (1 cm × 1 cm and 1 mm thick) from testis, epididymis, and accessory sex glands were collected. Fresh (for immunoblotting analysis) or fixed (4% phosphate-buffered formalin for immunohistochemical analysis) tissue samples were immediately frozen in liquid nitrogen.

Experimental Design

Experiment 1: SP-AKR1B1 Concentration in Ejaculate Portions

For the study of SP-AKR1B1 concentration in ejaculate fractions, the three fractions/portions (SRF-P1, SRF-P2, and PSRF) of seven ejaculates were collected separately, using the gloved hand method. The concentration of AKR1B1 in the SP of each portion was assessed using a porcine-specific enzyme-linked immunosorbent assay (ELISA), as described below.

Experiment 2: Expression of AKR1B1 in Male Reproductive Organs

Immunohistochemical and targeted immunoblotting analyses were conducted to find out which organs of the male reproductive system secreted AKR1B1. The samples, from three boars, came from medial testis; caput, corpus, and cauda segments of epididymis; and mid-areas of the prostate, seminal vesicles and bulbourethral glands.

Experiment 3: Relationship Between SP-AKR1B1 and Sperm Quality/Functionality Parameters

Entire ejaculates from 14 boars (one ejaculate per boar) were collected using a semi-automatic collection method (Collectis®, IMV Technologies, L'Aigle, France) and split into three aliquots. The first aliquot was used for sperm concentration and morphology assessment. The second one was extended alike AI-dose (30×10^6 sperm/mL in Biosem+ extender, Magapor, Zaragoza, Spain) and used to evaluate sperm quality and functionality parameters (sperm motility and viability, intracellular H_2O_2 production by viable sperm, and acrosome damage and plasma membrane lipid disorder of viable sperm) after ejaculate collection (0 h) and after 72 h of liquid storage at 17°C. Finally, the third aliquot was centrifuged to obtain SP. Next, SP samples were stored at −80°C until the concentration of AKR1B1 was analyzed with an ELISA assay.

Seminal Plasma Processing and Storage

Immediately after ejaculate collection, semen samples were centrifuged twice at 1,500 *g* and room temperature for 10 min (Rotofix 32A, Hettich Centrifuges UK, Newport Pagnell, Buckinghamshire, United Kingdom), following a previously described protocol (Perez-Patiño et al., 2016; Li et al., 2018; Barranco et al., 2019; Padilla et al., 2020). After the second centrifugation cycle, the supernatant was examined under a microscope (Eclipse E400, Nikon, Melville, NY, United States) to verify that it was sperm-free. Then, SP samples were split into cryotubes and stored at −80°C (Ultra Low Freezer, Haier Inc., Qingdao, China) until analysis. Samples were thawed on ice prior to evaluation.

Immunoblotting

In order to lysate tissue samples, 50 mg of each tissue was resuspended in 800 μL of lysis buffer (xTractor® Buffer; Takara Bio, Mountain View, CA, United States) supplemented with 50 U DNase I (Takara Bio), 1% protease inhibitor cocktail, and 700 mM sodium orthovanadate. After incubation at 4°C for 10 min, samples were disrupted mechanically four times using a TissueLyzer II (Qiagen, Hilden, Germany) set at 30 strokes/s for 5 min at 4°C. Subsequently, centrifugation at 12,000 *g* and 4°C for 30 min was carried out in order to obtain the supernatants, which were finally collected and stored at −80°C. Finally, total protein was quantified in triplicate by a detergent compatible (DC) method (BioRad).

For each tissue sample, 10 μg of total protein was diluted in 10 μL of miliQ water. Then, 10 μL of Laemmli reducing buffer 2× supplemented with 5% (v/v) β-mercaptoethanol (BioRad) was added to samples and boiled at 95°C for 5 min. Following this, a total volume of 20 μL per sample was loaded onto a polyacrylamide gradient (8–16%) gel (Mini-PROTEAN® TGX Stain-FreeTM Precast Gels, Bio-Rad); electrophoresis ran at 120–150 V for approximately 1 h. After electrophoresis, total protein content was visualized by UV exposition and acquisition using a G:BOX Chemi XL system (SynGene, Frederick, MD, United States). Afterward, proteins from the resulting gels were transferred onto polyvinylidene difluoride (PVDF) membranes using Trans-Blot® Turbo™ (BioRad). Next, membranes were blocked in blocking buffer (10 mmol/L Tris, 150 mmol/L NaCl, 0.05% Tween-20, and 5% bovine serum albumin; pH = 7.3) (Roche Diagnostics, S.L., Basel, Switzerland) at room temperature for 1 h under agitation. One of the blocked membranes was incubated with the anti-AKR1B1 primary antibody (ref. HPA026425, Prestige Antibodies; Merck, Germany) diluted in blocking solution (1:2,000; v:v), and the other membrane with the same primary antibody (1:2000, v:v) and its blocking peptide (ref. APREST77862, Prestige Antibodies; Merck) 20 times more concentrated than the antibody. Both membranes were incubated at 4°C overnight. Next, membranes were washed three times with TBS-Tween 20 1× (10 mmol/L Tris, 150 mmol/L NaCl, and 0.05% Tween-20; pH = 7.3) for 5 min before incubation with an anti-rabbit, secondary antibody conjugated with HRP (ref. P0448; Sigma Aldrich) diluted in blocking solution (1:3,000; v:v). Membranes were washed 10 times and finally revealed using a chemiluminescent substrate (Immobilion™ Western Detection Reagents, Millipore); images were scanned with G:BOX Chemi XL 1.4.

Immunohistochemistry

The sections of paraffin-embedded tissue samples (male reproductive organs and liver as a positive control) were immunohistochemically stained using an avidin-biotin complex protocol (Vector Laboratories, Burlingame, CA, United States). Briefly, sections were first deparaffinized two times using Histo-Clear II (Electron Microscopy Sciences, Hatfield, England) and progressively rehydrated through a decreasing ethanol series from 100 to 70% and distilled water. Next, and in order to allow antigen retrieval, sections were microwaved four times in 10 mM Tris-1 mM EDTA buffer (pH = 9.0) for 5 min, with intermediate refiling with Tris-EDTA. Then, sections were washed with tap water and placed in racks. Samples were incubated with a blocking and permeabilizing solution composed of 3% bovine serum albumin (BSA) in 0.1% PBS-Tween at room temperature for 30 min. Afterward, sections were incubated overnight at 4°C with the rabbit anti-AKR1B1 primary antibody diluted 1:100 (v:v) in PBS with 1% Triton X-100 containing 3% BSA. As a negative control, the primary antibody was omitted. On the other hand, in order to prove antibody specificity, samples were incubated with the AKR1B1 primary antibody and its blocking peptide, which was 50 times in excess. The next day, sections were washed and subsequently incubated with a polyclonal goat anti-rabbit secondary antibody conjugated with biotin (EDM Millipore Corporation, Temecula, CA, United States) diluted 1:200 (v:v) in PBS containing 1% Triton X-100 and 3% BSA at room temperature for 30 min. Sections were then washed and incubated with 3% H_2O_2 in BSA-PBS for 20 min to block endogenous peroxidase activity. Next, all sections were incubated with the VECTASTAIN ABC reagent (Vector Laboratories, Burlingame, CA, United States) for 1 h, and with DAB peroxidase substrate working solution (Vector Laboratories, Burlingame, CA, United States) for 10 min. Slides were counterstained with Harris hematoxylin (Thermo Fisher Scientific, Waltham, MA, United States), dehydrated with an increasing ethanol series, and mounted with Eukitt® mounting medium (PanReac, Barcelona, Spain). Finally, slides were microscopically evaluated and photographed using Nikon Eclipse EP2000-S (Nikon).

Enzyme-Linked Immunosorbent Assay

Concentration of AKR1B1 in SP was quantified using a porcine-specific quantitative sandwich ELISA kit (MBS9316209; MyBioSource, San Diego, CA, United States) following the manufacturer's manual. Briefly, to obtain the standard curve, 50 μL of AKR1B1 standards (0.625, 1.25, 2.5, 5, 10, and 20 ng/mL) was added to the plate in duplicate. On the other hand, SP samples were thawed, diluted in PBS 1× (1:75; v:v) and added to the plate in duplicate. The content of all wells, except the blank ones, was mixed with 100 μL of HRP-Conjugate Reagent, and the plate was subsequently incubated at 37°C for 60 min. After washing all wells four times, 50 μL of Chromogen A and 50 μL of Chromogen B were added. After mixing gently, the plate, protected from light, was incubated at 37°C for 15 min. Next, 50 μL of the Stop solution was added to all wells and, after 5 min, the plate was read at 450 nm using a microplate spectrophotometer (BioTek Epoch; BioTek, Winooski, Vermont, United States). The average of the duplicate reading for each standard was calculated and the average optical density from the blank was subtracted. Based on AKR1B1 standards, a linear regression curve interpolating AKR1B1 concentration from absorbance reading was calculated; the equation resulted to be: [AKR1B1] = Abs+0.038/0.0522, $R^2 = 0.9772$.

This ELISA kit was highly specific for porcine AKR1B1, showing a sensitivity of 0.1 ng/mL and a detection range of 0.625–20 ng/mL.

Sperm Quality and Functionality Parameters' Assessments

For evaluation of sperm quantity and functionality, seven parameters were assessed: (i) concentration, (ii) morphology, (iii) motility, (iv) viability, (v) intracellular H_2O_2 production by viable sperm, (vi) acrosome damage in viable sperm, and (vii) plasma membrane lipid disorder in viable sperm. Except for sperm concentration, which was only evaluated immediately after ejaculate collection (0 h), the other quality/functionality variables were determined at two time-points: after ejaculate collection (0 h) and after 72 h of liquid storage at 17°C (72 h).

For sperm concentration assessment, a high-precision automated cell counter (NucleoCounter®NC-100™, ChemoMetec, Allerod, Denmark) was used following manufacturer's recommendations. Sperm morphology was examined under a phase-contrast microscope at 1,000× magnification (Nikon Labophot, Nikon, Tokio, Japan) in semen samples diluted (1:1; v:v) with 0.12% formaldehyde saline solution (Panreac). A total of 200 sperm cells were counted and classified as morphologically normal if they did not exhibit abnormal head, acrosome defects, proximal cytoplasmic droplets, distal cytoplasmic droplets, folded tails, or coiled tails. Sperm motility was assessed using a computer-assisted sperm analyzer (CASA, ISASV1®, Proiser R+D S.L., Paterna, Spain). For this analysis, 5 μL of each semen sample (30×10^6 sperm/mL in Biosem+) was pipetted onto a pre-warmed (38°C) Makler chamber (Sefi Medical Instruments, Haifa, Israel). A total of 10 different fields per sample accumulating ≥600 sperm were acquired and examined. For further analysis, percentages of total motile sperm (sperm showing an average path velocity ≥20 μm/s) and progressively motile sperm (exhibiting rapid and progressive movement with a straight-line velocity ≥40 μm/s) were recorded.

Sperm viability, acrosome damage, intracellular H_2O_2 production, and membrane lipid disorder were assessed by flow cytometry (BD FACS Canto II; Becton Dickinson & Company, Franklin Lakes, NJ, United States). For each semen sample and sperm parameter, three technical replicates with 10,000 Hoechst 33342 (H-42; Merck)-positive events were evaluated.

Sperm viability and acrosome damage were assessed using a triple-staining with Hoechst 33342 (H-42), propidium iodide (PI; Merck), and fluorescein-conjugated peanut agglutinin

(PNA-FITC; Merck). Briefly, 100 μL of each semen sample (30 × 10^6 sperm/mL in Biosem+) was incubated with 3 μL H-42 (0.05 mg/mL in PBS), 2 μL PI (0.5 mg/mL in PBS), and 2 μL PNA-FITC (100 μg/mL in PBS) at 37°C (Sanyo MIR-153 incubator, Gemini BV, Apeldoorn, Netherlands) for 10 min. Next, 400 μL PBS was added to each sample. Percentages of viable spermatozoa (H-42+/PI-) with an intact (PNA-FITC-) and non-intact (PNA-FITC+) acrosome membrane were recorded.

To assess intracellular H_2O_2 production by viable sperm, a triple-staining with H-42, PI, and 5- and 6-chloromethyl-2′,7′-dichlorodihydrofluorescein diacetate acetyl ester (CM-H_2DCFDA; Merck) was prepared. Briefly, 50 μL of each semen sample (30 × 10^6 sperm/mL in Biosem+) was incubated with 1.5 μL H-42 (0.05 mg/mL in PBS 1×), 1 μL PI (0.5 mg/mL in PBS), and 1 μL CM-H_2DCFDA (1 mM in dymetilsulfoxide [DMSO]) in 950 μL PBS at 37°C for 30 min. An aliquot of each semen sample was incubated with all fluorochromes plus 1 μL of tert-butyl hydroperoxide solution (70% in distilled water) and was used as a positive control. The percentage of viable sperm (H-42+/PI−) that exhibited high intracellular H_2O_2 generation (2′,7′-di-chlorofluorescein [DCF]+) was recorded.

Finally, to evaluate the lipid disorder of plasma membrane in viable sperm, a triple-staining with H-42, Yo-Pro-1 (Merck), and Merocyanine 540 (M-540; Merck) was carried out. Briefly, 50 μL of each semen sample (30 × 10^6 sperm/mL in Biosem+) was incubated with 2.5 μL H-42 and 10 μL Yo-Pro-1 (2.5 μM in DMSO) in 950 μL PBS at 37°C for 8 min. After this period, 26 μL of M540 (0.1 mM in DMSO) was added to each sample and incubated at 37°C for 2 min. The percentage of viable spermatozoa (H-42+/Yo-Pro-1-) exhibiting lipid membrane disorder (M-540+) was recorded.

Statistical Analysis

Data were analyzed using the statistical package IBM SPSS 25.0 for Windows (IBM corp., Armonk, NY, United States). First, normal distribution was tested with Shapiro-Wilk test and homogeneity of variances was checked with Levene test. Concentrations of AKR1B1 between the three SP portions (i.e., SRF-P1, SRF-P2, and PSRF) were compared through one-way analysis of variance (ANOVA) followed by *post hoc* Sidak test. Ejaculates were classified based on their AKR1B1 concentration into groups through a two-step cluster analysis using the log-likelihood distance and the Schwarz's Bayesian criterion. Following this, sperm quality and functionality variables (sperm motility and viability, intracellular H_2O_2 production by viable sperm, acrosome damage in viable sperm, and plasma membrane lipid disorder in viable sperm) were compared between the two groups of ejaculates (high SP-AKR1B1 and low AKR1B1) with a linear mixed model followed by *post hoc* Sidak test. In this model, between-subjects factor was the ejaculate group and within-subjects factor was the time of semen storage at 17°C. When needed, data were linearly transformed with arcsine $\sqrt{x}$. The level of statistical significance was set at $P \leq 0.05$.

RESULTS

Experiment 1: SP-AKR1B1 Concentration in Ejaculate Portions

Concentrations of AKR1B1 in SP fractions/portions are shown in **Figure 1**. The SP from SRF-P1 from SRF-P1 exhibited the lowest ($P < 0.05$) AKR1B1 concentration (458.2 ± 116.33 ng/mL) compared to SRF-P2 (1105.0 ± 229.80 ng/mL) or PSRF (1342.4 ± 260.18 ng/mL). Moreover, no differences ($P > 0.05$) in AKR1B1 concentrations were found between SRF-P2 and PSRF. Finally, no breed effect was observed in SP-AKR1B1 concentration, as Pietrain and Duroc boars showed similar concentrations (522.2 ± 66.85 ng/mL vs. 691.7 ± 81.00 ng/mL; $P > 0.05$).

Experiment 2: Expression of AKR1B1 in Male Reproductive Organs

The immunoblotting assay revealed the presence of AKR1B1 along the entire male reproductive tissues except for bulbourethral glands (**Figure 2**). Specifically, two specific bands were detected: (i) a 36 kDa band was found in testis, epididymal caput and corpus, and seminal vesicles; and (ii) a ∼80 kDa band was also identified in testis, cauda, caput and corpus of epididymis, seminal vesicles, and prostate. Both bands also appeared in the positive control (liver). The two bands were not seen when membranes were incubated with AKR1B1 blocking peptide, revealing that they were specific for AKR1B1. Therefore, bands of ∼40 and ∼70 kDa should be considered as unspecific for this antibody.

The AKR1B1 protein was immunohistochemically detected in the reproductive tissues analyzed (**Figure 3**). Two controls

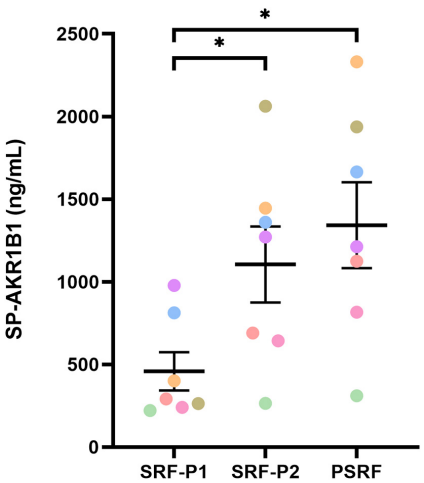

FIGURE 1 | Seminal plasma-AKR1B1 concentration (ng/mL) in the different pig ejaculate fractions: the first 10 mL of the sperm rich fraction (SRF-P1), the rest of the sperm rich fraction (SRF-P2), and post sperm rich fraction (PSRF). Data are represented as mean ± standard error of the mean. Different dot colors represent each individual ($n = 7$). Differences between fractions are indicated as * ($P \leq 0.05$).

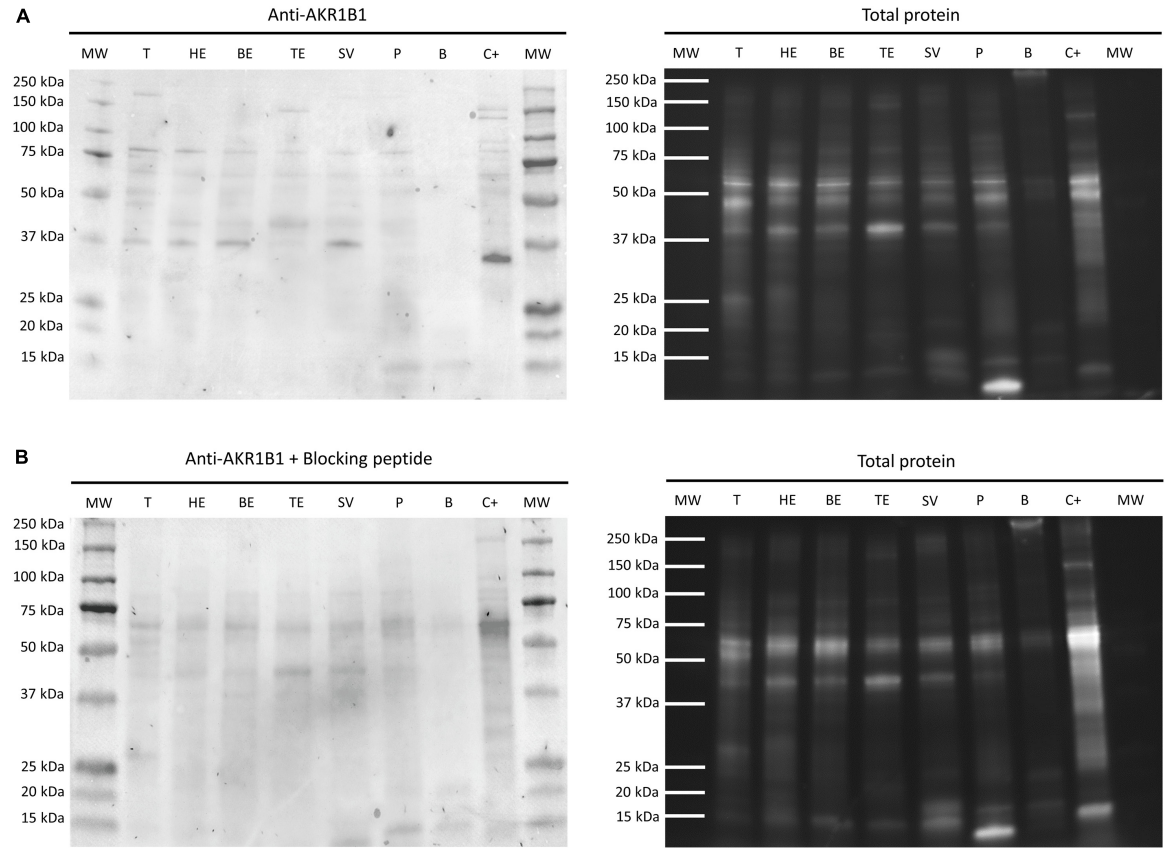

FIGURE 2 | Representative Western blot of **(A)** anti-AKR1B1 and **(B)** its corresponding blocking peptide, and their total protein controls in boar reproductive tissues. MW, molecular weight; T, testis; HE, caput epididymis; BE, corpus epididymis; TE, cauda epididymis; SV, seminal vesicles; P, prostate; B, bulbourethral glands; C+, liver.

were used: (i) the specificity of the primary antibody was confirmed in all tissues through incubation with the AKR1B1 primary antibody with blocking peptide and (ii) the specificity of the secondary antibody was proven with the omission of the primary antibody in all tissue samples. The presence of AKR1B1 was confirmed in all reproductive tissues except for bulbourethral glands, in which no staining was observed. In testis, AKR1B1 was observed in the interstitial tissue, specifically in the cytosol of Leydig cells, whereas no presence of the protein was detected in seminiferous tubules. Regarding epididymis, AKR1B1 was localized in basal and principal cells of the epithelia of all regions (caput, corpus, and cauda). In addition, both prostate and seminal vesicles showed cytoplasm immunostaining in glandular epithelial cells. Finally, AKR1B1 was undetectable in bulbourethral glands.

Experiment 3: Relationship Between SP-AKR1B1 and Sperm Quality and Functionality Parameters

In order to evaluate the relationship between SP-AKR1B1 and sperm quality and functionality parameters, 14 ejaculates were classified (hierarchical clustering; $P < 0.001$) into two groups: with low SP-AKR1B1 (ranging from 376.4 to 756.3 ng/mL, $n = 7$) and high SP-AKR1B1 levels (ranging from 842.2 to 1211.25 ng/mL, $n = 7$; **Figure 4**). No differences ($P > 0.05$) in any of the different sperm quality and functionality parameters assessed (sperm concentration, normal sperm morphology, total and progressive motility, viable sperm, viable sperm with high intracellular H_2O_2, viable sperm with a damaged acrosome, and viable sperm with high membrane destabilization) were observed between high and low SP-AKR1B1 groups at any evaluation time-point (0 and 72 h of storage at 17°C).

DISCUSSION

To the best of our knowledge, this is the first study characterizing the expression of AKR1B1 along the male reproductive system in livestock. Likewise, this report is also the first relating the concentration of AKR1B1 in SP with sperm quality and functionality parameters of liquid-stored semen samples. Specifically, the results showed that: (i) monomeric and dimeric AKR1B1 forms were expressed in all male reproductive tissues, except bulbourethral glands; (ii) AKR1B1 was expressed in Sertoli cells, basal and principal

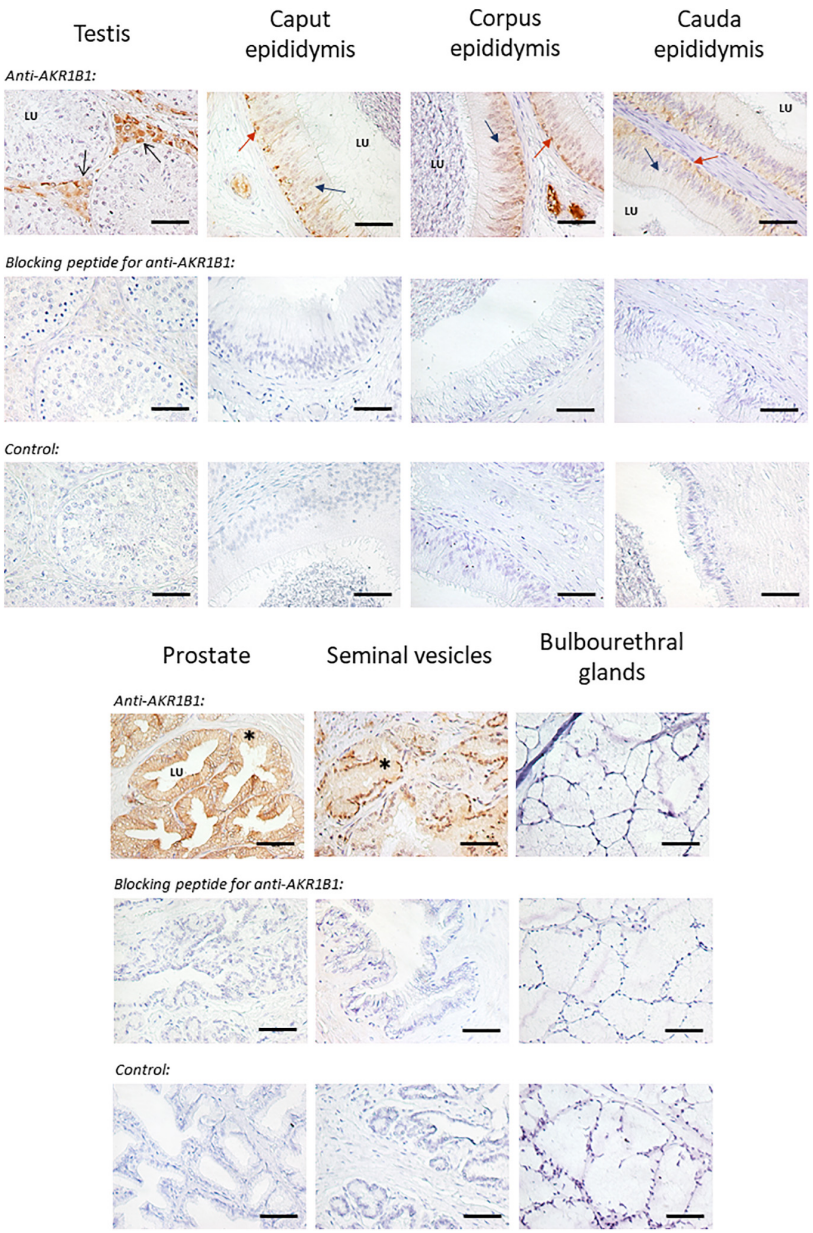

FIGURE 3 | Immunohistochemistry of AKR1B1 in boar genital organs (testis, caput, corpus, and cauda from the epididymis, prostate, seminal vesicles, and bulbourethral glands). The first row shows anti-AKR1B1 staining in each tissue. Specifically, Sertoli cells from testis (black arrow), principal (blue arrow), and basal cells (orange arrow) in the epididymis and glandular cells from prostate and seminal vesicles (indicated as *) appeared stained. Specificity of the primary antibody in all tissues/organs was confirmed by the absence of signal in blocking peptide assays (second row). Finally, negative control (third row) proved the specificity of the secondary antibody. LU, lumen. Scale bar = 50 μm.

epididymal cells, and glandular cells from the prostate and seminal vesicles; (iii) seminal vesicles were likely to contribute the most to the final SP-AKR1B1 concentration of the pig ejaculate; and (iv) SP-AKR1B1 levels were not related to sperm quality and functionality parameters, nor was this enzyme involved in the sperm resilience to preservation at 17°C for 72 h.

Characterization of SP components, including proteins or even metabolites, has been a source of sperm quality, functionality, and fertility biomarkers in several mammalian species (Milardi et al., 2013; Cazaux Velho et al., 2018; Moura et al., 2018; Pérez-Patiño et al., 2018). In this sense, as mentioned before, AKR1B1 has been reported to have multiple roles in the reproductive physiology of humans (Bresson et al., 2011), cattle (Frenette et al., 2004; Girouard et al., 2009), rodents (Kobayashi et al., 2002), and pigs (Steinhauser et al., 2016; Pérez-Patiño et al., 2018). However, no information regarding its synthesis along the male reproductive tract exists in any mammalian species.

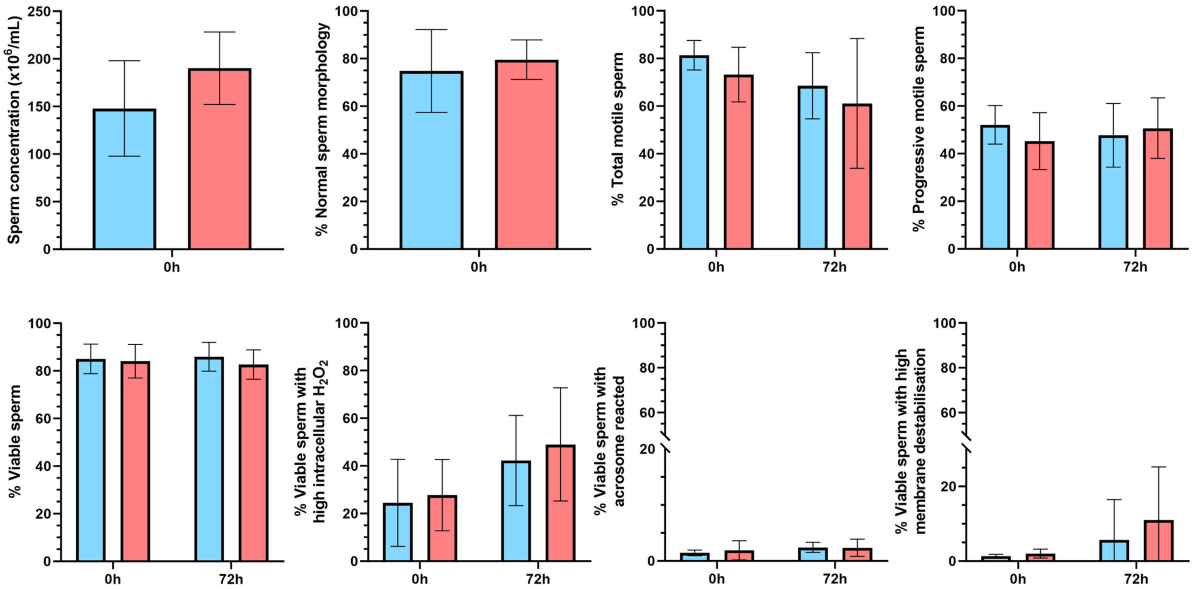

FIGURE 4 | Sperm quality and functionality parameters upon semen collection (0 h) and after 72 h of liquid storage at 17°C in two groups ejaculates clustered on the basis of AKR1B1 concentration in seminal plasma (SP) samples. Fourteen ejaculates were classified into two groups: with low SP-AKR1B1 levels (ranging from 376.4 to 756.3 ng/mL, $n = 7$; blue bars) and with high SP-AKR1B1 levels (ranging from 842.2 to 1211.25 ng/mL, $n = 7$; red bars). Data are represented as mean ± standard error of the mean.

The immunoblotting and immunohistochemistry results showed that AKR1B1 was expressed in testis, epididymis, and all accessory sex glands, except the bulbourethral ones. These results are in agreement with observations in male rats, in which the activity of aldose reductase was observed along all the male reproductive tract, except in bulbourethral glands that were not analyzed (Kobayashi et al., 2002; Iuchi et al., 2004). Moreover, other studies conducted in cattle and pigs demonstrated the presence of AKR1B1 in seminal vesicles (Samuels et al., 1962; Westfalewicz et al., 2017). This protein has been reported to interact with epididymal sperm during maturation (Frenette et al., 2003, 2006; Katoh et al., 2014), which would advise a role of AKR1B1 in sperm physiology. In this context, the presence of AKR1B1 has been proposed to contribute to the acquisition of sperm motility and fertilizing ability in pigs (Katoh et al., 2014), as well as to support bovine sperm survival during epididymal transit and storage (Frenette et al., 2003). In addition, our immunoblotting assay showed the presence of one or two specific bands (36 and ∼80 kDa) in most male reproductive tissues. While dimerization of AKR1B1 has been previously reported in ovine thymus (Yang et al., 2019) and bovine peripheral blood mononuclear cells (Yang et al., 2016), there are no previous studies of such a dimerization in SP samples from any mammalian species. Indeed, as monomeric and dimeric protein forms are known to have different cellular functions, further studies should address whether these forms could explain the different roles of SP-AKR1B1 in reproductive physiology.

Besides the presence of AKR1B1 along the male reproductive tract, our study found that this protein was only present in specific cell types, rather than in the lumen of the different organs. Specifically, in testis, only Leydig cells were stained with the anti-AKR1B1 antibody. Since these cells are implicated in hormonal secretion and spermatogenesis regulation (Zhou et al., 2019), one could hypothesize that AKR1B1 is involved in these processes. On the other hand, AKR1B1 was also found in both basal and principal cells along the entire epididymis and glandular cells from the prostate and seminal vesicles. Considering that all of these cell types are involved in protein secretion (Leung et al., 2004; Breton et al., 2019), the presence of AKR1B1 in SP can be assumed to be originated from the collective synthesis and secretion of the aforementioned organs. These findings are in agreement with a previous study conducted in bovine, in which aldose reductase was also reported to be present in the same epididymal and testicular cells lines (Frenette et al., 2003). However, this is the first report in a mammalian species describing that vesicle glands are the main synthesis site. Nevertheless, to the best of our knowledge, neither the exact contribution of the different male accessory glands to AKR1B1 levels in SP, nor its potential role on ejaculated sperm has been uncovered.

ELISA assay of the different ejaculate portions confirmed immunohistochemical and immunoblotting results, indicating that whereas AKR1B1 was present in the SP from all ejaculate portions, a higher concentration of this protein was found in the SP from PSRF. As aforementioned, SP from each ejaculate portion has a different origin: SP from SRF-P1 is mainly secreted by the epididymis, SP from SRF-P2 originates from the epididymis and prostate, and SP from PSRF is mainly produced by seminal vesicles (Einarsson, 1971; Rodríguez-Martínez et al., 2009; Saravia et al., 2009; Rodríguez-Martínez et al., 2011). Considering these results, one could hypothesize that seminal vesicles are the principal contributor for SP-AKR1B1 secretion to

the entire ejaculate. Similar results have been reported in bovine, where this enzyme is one of the most abundant proteins of the seminal vesicle fluid (Westfalewicz et al., 2017).

The present study also evaluated the relationship between SP-AKR1B1 concentration and sperm quality and functionality after both 0 and 72 h of liquid storage at 17°C. No relationship between SP-AKR1B1 concentration and any of the evaluated parameters, which included sperm concentration, normal sperm morphology, total and progressive motility, sperm viability, and percentages of viable sperm with high intracellular ROS, viable sperm with a damaged acrosome, and viable sperm with high membrane destabilization, was observed. To the best of our knowledge, there is scarce information regarding the role of AKR1B1 in sperm physiology. While AKR1B1 has been reported to be overexpressed in men with high seminal lipid peroxidation levels (Intasqui et al., 2015) and to be involved in porcine sperm capacitation (Katoh et al., 2014), none of these parameters were evaluated in the present study. Thus, taking into account the lack of influence of SP-AKR1B1 on sperm quality and functionality found in our study, together with the fact that the highest SP-AKR1B1 concentration was not found in the SRF (which contains most of the ejaculated sperm; Einarsson, 1971; Rodríguez-Martínez et al., 2009; Saravia et al., 2009; Rodríguez-Martínez et al., 2011), it is reasonable to surmise that SP-AKR1B1 does not play a major role on the sperm quality and functionality parameters assessed. However, this protein could play a crucial role on sperm lipid peroxidation or during capacitation. Further studies are required to evaluate this potential relationship.

Besides its relevance during epididymal maturation (Frenette et al., 2003; Katoh et al., 2014), SP-AKR1B1 could have a potential influence on the female reproductive tract, as it is expressed in the endometrium in humans (Chapdelaine et al., 2006; Bresson et al., 2011) and pigs (Seo et al., 2014; Steinhauser et al., 2016). In the uterus, the luminal AKR1B1 has been found to be involved in the polyol pathway during the conceptus peri-implantation period and, in porcine, its expression is downregulated as conceptus attaches to the endometrium (Steinhauser et al., 2016). On the other hand, uterine AKR1B1 is involved in progesterone synthesis in humans (Bresson et al., 2011) and pigs (Seo et al., 2014), thus contributing to prepare the endometrium for conceptus implantation as well as modulating the maternal immune system (Czyzyk et al., 2017). Our results, together with the fact that SP-AKR1B1 is linked with high *in vivo* pregnancy outcomes (Pérez-Patiño et al., 2018), suggest that SP-AKR1B1 could act jointly with the endometrial AKR1B1 to prepare the uterine environment for conceptus implantation. Another possibility could be that this protein has a direct impact on conceptus. In this sense, SP has been reported to exert a positive effect on pregnancy outcomes, specifically improving implantation and pregnancy rates in humans (Crawford et al., 2015; Saccone et al., 2019) and even modifying embryo gene expression in pigs (Martinez et al., 2020). Thus, it cannot be discarded the influence of SP-AKR1B1 on the improvement of embryo survival and even implantation, through the modulation of the uterine environment. In this regard, all these functions could be driven by both the soluble form of the protein in SP or by that contained in extracellular vesicles (EVs). SP EVs regulate sperm function through its integration to sperm membrane (Leahy et al., 2020) and their action on the female immune system (Zhang et al., 2020). Interestingly, bovine AKR1B1 has been reported to be associated to epididymal EVs (Frenette et al., 2006) and, in humans, seminal EVs have been found to contain aldose reductase (Zhang et al., 2020). In pigs, however, whether this protein is also in the cargo of SP EVs and participates in fertilization or embryo development remains to be explored.

AKR1B1 has been extensively demonstrated to play a role in female and male reproductive physiology. In pigs, SP-AKR1B1 has been reported to exert a positive impact on *in vivo* fertility outcomes. This study demonstrated that all male genital organs (except bulbourethral glands) are able to express AKR1B1. We also found that the concentration of AKR1B1 was higher in the post-SRF, suggesting that seminal vesicles could be the main contributor of this SP protein to the final ejaculate. Our results also indicated that SP-AKR1B1 is not associated to the quality and functionality parameters of sperm. These findings, together with the fact that this protein has been shown to be positively related to *in vivo* fertility (Pérez-Patiño et al., 2018), suggest that it could play an active role in the female reproductive tract, promoting sperm fecundity or even embryo development. Thus, further studies to determine the exact mechanism through which SP-AKR1B1 has a positive influence on *in vivo* fertility outcomes should be conducted.

DATA AVAILABILITY STATEMENT

The raw data supporting the conclusions of this article will be made available by the authors, without undue reservation.

AUTHOR CONTRIBUTIONS

YM-O, MY, and IB: conceptualization. YM-O, EV-V, and ML: methodology. YM-O, JR-M, MY, and IB: formal analysis and investigation. YM-O and EV-V: writing—original draft preparation. JR-M, JR, MY, and IB: writing—review and editing. JR and MY: funding acquisition. IB and MY: supervision. All authors read and agreed to the published version of the manuscript.

FUNDING

This study was funded by the Ministry of Science and Innovation, Spain (Grants: RYC-2014-15581 and AGL2017-88329-R), European Union's Horizon 2020 Research and innovation Scheme (H2020-MSCA-IF-2019-891382), the Seneca Foundation Murcia, Spain (19892/GERM-15), and the Regional Government of Catalonia (Grants: 2017-SGR-1229 and 2020-FI-B-00412).

ACKNOWLEDGMENTS

The authors would like to thank AIM Iberica (Topigs Norsvin Iberica, Spain) for boar ejaculates.

REFERENCES

Barranco, I., Padilla, L., Tvarijonaviciute, A., Parrilla, I., Martínez, E. A., Rodriguez-Martinez, H., et al. (2019). Levels of activity of superoxide dismutase in seminal plasma do not predict fertility of pig AI-semen doses. *Theriogenology* 140, 18–24. doi: 10.1016/j.theriogenology.2019.08.010

Barranco, I., Perez-Patiño, C., Tvarijonaviciute, A., Parrilla, I., Vicente-Carrillo, A., Alvarez-Rodriguez, M., et al. (2017). Active paraoxonase 1 is synthesised throughout the internal boar genital organs. *Reproduction* 154, 237–243. doi: 10.1530/REP-17-0300

Barranco, I., Tvarijonaviciute, A., Perez-Patinõ, C., Parrilla, I., Ceron, J. J., Martinez, E. A., et al. (2015). High total antioxidant capacity of the porcine seminal plasma (SP-TAC) relates to sperm survival and fertility. *Sci. Rep.* 5:18538. doi: 10.1038/srep18538

Barranco, S., Tvarijonaviciute, A., Perez-Patiho, C., Vicente-Carrillo, A., Parrilla, N., Ceron, J. J., et al. (2016). Glutathione peroxidase 5 is expressed by the entire pig male genital tract and once in the seminal plasma contributes to sperm survival and in vivo fertility. *PLoS One* 11:e0162958. doi: 10.1371/journal.pone.0162958

Bohren, K. M., Bullock, B., Wermuth, B., and Gabbay, K. H. (1989). The aldo-keto reductase superfamily. cDNAs and deduced amino acid sequences of human aldehyde and aldose reductases. *J. Biol. Chem.* 264, 9547–9551. doi: 10.1016/B978-0-12-801238-3.64092-8

Bresson, E., Boucher-Kovalik, S., Chapdelaine, P., Madore, E., Harvey, N., Laberge, P. Y., et al. (2011). The human aldose reductase AKR1B1 qualifies as the primary prostaglandin F synthase in the endometrium. *J. Clin. Endocrinol. Metab.* 96, 210–219. doi: 10.1210/jc.2010-1589

Breton, S., Nair, A. V., and Battistone, M. A. (2019). Epithelial dynamics in the epididymis: role in the maturation, protection, and storage of spermatozoa. *Andrology* 7, 631–643. doi: 10.1111/andr.12632

Cazaux Velho, A. L., Menezes, E., Dinh, T., Kaya, A., Topper, E., Moura, A. A., et al. (2018). Metabolomic markers of fertility in bull seminal plasma. *PLoS One* 13:e0195279. doi: 10.1371/journal.pone.0195279

Chapdelaine, P., Kang, J., Boucher-Kovalik, S., Caron, N., Tremblay, J. P., and Fortier, M. A. (2006). Decidualization and maintenance of a functional prostaglandin system in human endometrial cell lines following transformation with SV40 large T antigen. *Mol. Hum. Reprod.* 12, 309–319. doi: 10.1093/molehr/gal034

Chiba, L. (2009). "Pig nutrition and feeding," in *Animal Nutrition Handbook*, ed. L. Chiba (Auburn: Auburn University), 285–315.

Crawford, G., Ray, A., Gudi, A., Shah, A., and Homburg, R. (2015). The role of seminal plasma for improved outcomes during in vitro fertilization treatment: review of the literature and meta-analysis. *Hum. Reprod. Update* 21, 275–284. doi: 10.1093/humupd/dmu052

Czyzyk, A., Podfigurna, A., Genazzani, A. R., and Meczekalski, B. (2017). The role of progesterone therapy in early pregnancy: from physiological role to therapeutic utility. *Gynecol. Endocrinol.* 33, 421–424. doi: 10.1080/09513590.2017.1291615

Einarsson, S. (1971). Studies on the composition of epididymal content and semen in the boar. *Acta Vet. Scand. Suppl.* 36, 1–80.

Frenette, G., Girouard, J., and Sullivan, R. (2006). Comparison between epididymosomes collected in the intraluminal compartment of the bovine caput and cauda epididymidis. *Biol. Reprod.* 75, 885–890. doi: 10.1095/biolreprod.106.054692

Frenette, G., Lessard, C., Madore, E., Fortier, M. A., and Sullivan, R. (2003). Aldose reductase and macrophage migration inhibitory factor are associated with epididymosomes and spermatozoa in the bovine epididymis. *Biol. Reprod.* 69, 1586–1592. doi: 10.1095/biolreprod.103.019216

Frenette, G., Lessard, C., and Sullivan, R. (2004). Polyol pathway along the bovine epididymis. *Mol. Reprod. Dev.* 69, 448–456. doi: 10.1002/mrd.20170

Garner, D. L., and Hafez, E. S. E. (2000). "Spermatozoa and seminal plasma," in *Reproduction in Farm Animals*, eds B. Hafez and E. S. E. Hafez (Philadelphia, PA: Lippincott Williams & Wilkins), 96–109. doi: 10.1002/9781119265306.ch7

Girouard, J., Frenette, G., and Sullivan, R. (2009). Compartmentalization of proteins in epididymosomes coordinates the association of epididymal proteins with the different functional structures of bovine spermatozoa. *Biol. Reprod.* 80, 965–972. doi: 10.1095/biolreprod.108.073551

Hyndman, D., Bauman, D. R., Heredia, V. V., and Penning, T. M. (2003). The aldo-keto reductase superfamily homepage. *Chem. Biol. Interact.* 14, 621–631. doi: 10.1016/S0009-2797(02)00193-X

Intasqui, P., Antoniassi, M. P., Camargo, M., Nichi, M., Carvalho, V. M., Cardozo, K. H. M., et al. (2015). Differences in the seminal plasma proteome are associated with oxidative stress levels in men with normal semen parameters. *Fertil. Steril.* 104, 292–301. doi: 10.1016/j.fertnstert.2015.04.037

Iuchi, Y., Kaneko, T., Matsuki, S., Ishii, T., Ikeda, Y., Uchida, K., et al. (2004). Carbonyl stress and detoxification ability in the male genital tract and testis of rats. *Histochem. Cell Biol.* 121, 123–130. doi: 10.1007/s00418-003-0607-3

Jagoe, W. N., Howe, K., O'Brien, S. C., and Carroll, J. (2013). Identification of a role for a mouse sperm surface aldo-keto reductase (AKR1B7) and its human analogue in the detoxification of the reactive aldehyde, acrolein. *Andrologia* 45, 326–331. doi: 10.1111/and.12018

Katoh, Y., Takebayashi, K., Kikuchi, A., Iki, A., Kikuchi, K., Tamba, M., et al. (2014). Porcine sperm capacitation involves tyrosine phosphorylation and activation of aldose reductase. *Reproduction* 148, 389–401. doi: 10.1530/REP-14-0199

Kennedy, T. G., Gillio-Meina, C., and Phang, S. H. (2007). Prostaglandins and the initiation of blastocyst implantation and decidualization. *Reproduction* 134, 635–643. doi: 10.1530/REP-07-0328

Kobayashi, T., Kaneko, T., Iuchi, Y., Matsuki, S., Takahashi, M., Sasagawa, I., et al. (2002). Localization and physiological implication of aldose reductase and sorbitol dehydrogenase in reproductive tracts and spermatozoa of male rats. *J. Androl.* 23, 674–684. doi: 10.1002/j.1939-4640.2002.tb02310.x

Kumaresan, A., Kadirvel, G., Bujarbaruah, K. M., Bardoloi, R. K., Das, A., Kumar, S., et al. (2009). Preservation of boar semen at 18 degrees C induces lipid peroxidation and apoptosis like changes in spermatozoa. *Anim. Reprod. Sci.* 110, 162–171. doi: 10.1016/j.anireprosci.2008.01.006

Leahy, T., Rickard, J. P., Bernecic, N. C., Druart, X., and De Graaf, S. P. (2019). Ram seminal plasma and its functional proteomic assessment. *Reproduction* 157, R243–R256. doi: 10.1530/REP-18-0627

Leahy, T., Rickard, J. P., Pini, T., Gadella, B. M., and Graaf, S. P. (2020). Quantitative proteomic analysis of seminal plasma, sperm membrane proteins, and seminal extracellular vesicles suggests vesicular mechanisms aid in the removal and addition of proteins to the ram sperm membrane. *Proteomics* 20:1900289. doi: 10.1002/pmic.201900289

Leung, G. P. H., Cheung, K. H., Leung, C. T., Tsang, M. W., and Wong, P. Y. D. (2004). Regulation of epididymal principal cell functions by basal cells: role of transient receptor potential (Trp) proteins and cyclooxygenase-1 (COX-1). *Mol. Cell. Endocrinol.* 216, 5–13. doi: 10.1016/j.mce.2003.10.077

Li, J., Barranco, I., Tvarijonaviciute, A., Molina, M. F., Martinez, E. A., Rodriguez-Martinez, H., et al. (2018). Seminal plasma antioxidants are directly involved in boar sperm cryotolerance. *Theriogenology* 107, 27–35. doi: 10.1016/j.theriogenology.2017.10.035

Locatello, L., Poli, F., and Rasotto, M. B. (2013). Tactic-specific differences in seminal fluid influence sperm performance. *Proc. R. Soc. B Biol. Sci.* 280:20122891. doi: 10.1098/rspb.2012.2891

Martinez, C. A., Cambra, J. M., Gil, M. A., Parrilla, I., Alvarez-Rodriguez, M., Rodriguez-Martinez, H., et al. (2020). Seminal plasma induces overexpression of genes associated with embryo development and implantation in day-6 porcine blastocysts. *Int. J. Mol. Sci.* 21, 1–14. doi: 10.3390/ijms21103662

Mateo-Otero, Y., Fernández-López, P., Gil-Caballero, S., Fernandez-Fuertes, B., Bonet, S., Barranco, I., et al. (2020). 1H nuclear magnetic resonance of pig seminal plasma reveals intra-ejaculate variation in metabolites. *Biomolecules* 10, 1–16. doi: 10.3390/biom10060906

Milardi, D., Grande, G., Vincenzoni, F., Castagnola, M., and Marana, R. (2013). Proteomics of human seminal plasma: identification of biomarker candidates for fertility and infertility and the evolution of technology. *Mol. Reprod. Dev.* 80, 350–357. doi: 10.1002/mrd.22178

Moura, A. A., Memili, E., Portela, A. M. R., Viana, A. G., Velho, A. L. C., Bezerra, M. J. B., et al. (2018). Seminal plasma proteins and metabolites: effects on sperm function and potential as fertility markers. *Anim. Reprod.* 15, 691–702. doi: 10.21451/1984-3143-AR2018-0029

Muhammad Aslam, M. K., Kumaresan, A., Sharma, V. K., Tajmul, M., Chhillar, S., Chakravarty, A. K., et al. (2014). Identification of putative fertility markers in seminal plasma of crossbred bulls through differential proteomics. *Theriogenology* 82, 1254–1262.e1. doi: 10.1016/j.theriogenology.2014.08.007

Novak, S., Smith, T. A., Paradis, F., Burwash, L., Dyck, M. K., Foxcroft, G. R., et al. (2010). Biomarkers of in vivo fertility in sperm and seminal plasma of fertile stallions. *Theriogenology* 74, 956–967. doi: 10.1016/j.theriogenology.2010.04.025

O'Leary, S., Jasper, M. J., Warnes, G. M., Armstrong, D. T., and Robertson, S. A. (2004). Seminal plasma regulates endometrial cytokine expression, leukocyte recruitment and embryo development in the pig. *Reproduction* 128, 237–247. doi: 10.1530/rep.1.00160

Padilla, L., Barranco, I., Parrilla, I., Lucas, X., Rodriguez-Martinez, H., and Roca, J. (2020). Measurable cytokine concentrations in pig seminal plasma are modified by semen handling and storage. *Biology (Basel)* 9:276. doi: 10.3390/biology9090276

Perez-Patiño, C., Barranco, I., Parrilla, I., Valero, M. L., Martinez, E. A., Rodriguez-Martinez, H., et al. (2016). Characterization of the porcine seminal plasma proteome comparing ejaculate portions. *J. Proteomics* 142, 15–23. doi: 10.1016/j.jprot.2016.04.026

Pérez-Patiño, C., Parrilla, I., Barranco, I., Vergara-Barberán, M., Simó-Alfonso, E. F., Herrero-Martínez, J. M., et al. (2018). New in-depth analytical approach of the porcine seminal plasma proteome reveals potential fertility biomarkers. *J. Proteome Res.* 17, 1065–1076. doi: 10.1021/acs.jproteome.7b00728

Robertson, S. A. (2007). Seminal fluid signaling in the female reproductive tract: lessons from rodents and pigs. *J. Anim. Sci.* 85, 36–44. doi: 10.2527/jas.2006-578

Rodríguez-Martínez, H., Kvist, U., Ernerudh, J., Sanz, L., and Calvete, J. J. (2011). Seminal plasma proteins: what role do they play? *Am. J. Reprod. Immunol.* 66, 11–22. doi: 10.1111/j.1600-0897.2011.01033.x

Rodríguez-Martínez, H., Kvist, U., Saravia, F., Wallgren, M., Johannisson, A., Sanz, L., et al. (2009). The physiological roles of the boar ejaculate. *Soc. Reprod. Fertil. Suppl.* 66, 1–21.

Rodríguez-Martínez, H., Saravia, F., Wallgren, M., Tienthai, P., Johannisson, A., Vázquez, J. M., et al. (2005). Boar spermatozoa in the oviduct. *Theriogenology* 63, 514–535. doi: 10.1016/j.theriogenology.2004.09.028

Saccone, G., Di Spiezio Sardo, A., Ciardulli, A., Caissutti, C., Spinelli, M., Surbek, D., et al. (2019). Effectiveness of seminal plasma in in vitro fertilisation treatment: a systematic review and meta-analysis. *BJOG* 126, 220–225. doi: 10.1111/1471-0528.15004

Samuels, L. T., Harding, B. W., and Mann, T. (1962). Aldose reductase and ketose reductase in male accessory organs of reproduction. Distribution and relation to seminal fructose. *Biochem. J.* 84, 39–45. doi: 10.1042/bj0840039

Saravia, F., Wallgren, M., Johannisson, A., Calvete, J. J., Sanz, L., Peña, F. J., et al. (2009). Exposure to the seminal plasma of different portions of the boar ejaculate modulates the survival of spermatozoa cryopreserved in MiniFlatPacks. *Theriogenology* 71, 662–675. doi: 10.1016/j.theriogenology.2008.09.037

Schjenken, J. E., and Robertson, S. A. (2014). Seminal fluid and immune adaptation for pregnancy – comparative biology in mammalian species. *Reprod. Domest. Anim.* 49, 27–36. doi: 10.1111/rda.12383

Seo, H., Choi, Y., Shim, J., Yoo, I., and Ka, H. (2014). Comprehensive analysis of prostaglandin metabolic enzyme expression during pregnancy and the characterization of AKR1B1 as a prostaglandin F synthase at the maternal-conceptus interface in pigs. *Biol. Reprod.* 90, 1–13. doi: 10.1095/biolreprod.113.114926

Steinhauser, C. B., Landers, M., Myatt, L., Burghardt, R. C., Vallet, J. L., Bazer, F. W., et al. (2016). Fructose synthesis and transport at the uterine-placental interface of pigs: cell-specific localization of SLC2A5, SLC2A8, and components of the polyol pathway. *Biol. Reprod.* 95:108. doi: 10.1095/biolreprod.116.142174

Waberski, D., Riesenbeck, A., Schulze, M., Weitze, K. F., and Johnson, L. (2019). Application of preserved boar semen for artificial insemination: past, present and future challenges. *Theriogenology* 137, 2–7. doi: 10.1016/j.theriogenology.2019.05.030

Westfalewicz, B., Dietrich, M. A., Mostek, A., Partyka, A., Bielas, W., Nińańska, W., et al. (2017). Analysis of bull (*Bos taurus*) seminal vesicle fluid proteome in relation to seminal plasma proteome. *J. Dairy Sci.* 100, 2282–2298. doi: 10.3168/jds.2016-11866

Yang, L., Lv, W., Liu, Y., Chen, K., Xue, J., Wang, Q., et al. (2019). Effect of early pregnancy on the expression of prostaglandin synthases in the ovine thymus. *Theriogenology* 136, 166–171. doi: 10.1016/j.theriogenology.2019.06.040

Yang, L., Yao, X., Li, S., Chen, K., Wang, Y., Chen, L., et al. (2016). Expression of genes associated with luteolysis in peripheral blood mononuclear cells during early pregnancy in cattle. *Mol. Reprod. Dev.* 83, 509–515. doi: 10.1002/mrd.22647

Zhang, X., Vos, H. R., Tao, W., and Stoorvogel, W. (2020). Proteomic profiling of two distinct populations of extracellular vesicles isolated from human seminal plasma. *Int. J. Mol. Sci.* 21, 1–19. doi: 10.3390/ijms21217957

Zhou, R., Wu, J., Liu, B., Jiang, Y., Chen, W., Li, J., et al. (2019). The roles and mechanisms of Leydig cells and myoid cells in regulating spermatogenesis. *Cell. Mol. Life Sci.* 76, 2681–2695. doi: 10.1007/s00018-019-03101-9

Conflict of Interest: The authors declare that the research was conducted in the absence of any commercial or financial relationships that could be construed as a potential conflict of interest.

frontiers in Cell and Developmental Biology

ORIGINAL RESEARCH
published: 24 June 2021
doi: 10.3389/fcell.2021.660165

Desmosterol Incorporation Into Ram Sperm Membrane Before Cryopreservation Improves *in vitro* and *in vivo* Fertility

María de las Mercedes Carro[1†], Rafael R. A. Ramírez-Vasquez[1], Daniel A. Peñalva[2,3], Jorgelina Buschiazzo[1‡] and Federico A. Hozbor[1‡]*

[1] Instituto de Innovación para la Producción Agropecuaria y el Desarrollo Sostenible (IPADS Balcarce), Instituto Nacional de Tecnología Agropecuaria (INTA)—Consejo Nacional de Investigaciones Científicas y Técnicas (CONICET), Balcarce, Argentina, [2] Instituto de Investigaciones Bioquímicas de Bahía Blanca (INIBIBB), Consejo Nacional de Investigaciones Científicas y Técnicas (CONICET), Universidad Nacional del Sur (UNS), Bahía Blanca, Argentina, [3] Departamento de Biología, Bioquímica y Farmacia, Universidad Nacional del Sur (UNS), Bahía Blanca, Argentina

Pregnancy rates in ewes are markedly low after cervical insemination with frozen-thawed sperm. Sensitivity of ram sperm to freeze-thawing is related to the lipid composition of the membrane, particularly to its low sterol content. Recently, we proved that sterol content of ram sperm can be increased by treatment with methyl-β-cyclodextrin-sterol complexes and we provided mechanistic based evidence on the differential behavior of cholesterol and desmosterol in the ram sperm membrane. In the present study, we evaluated the role of increasing cholesterol and desmosterol content of ram sperm before cryopreservation, on the extent and distribution of sterols, cryocapacitation status, acrosome integrity, DNA damage associated with apoptosis and fertility competence *in vitro* and *in vivo* of post-thawed sperm. After freeze-thawing, similar levels of sterol content were evidenced in control sperm cells and in those pre-incubated with either cholesterol or desmosterol. Still, moderately higher levels of sterols were registered in treated sperm compared to the control, indicating no physiological excess of sterols after thawing or sterol losses that exceed the control. Live cell imaging of fluorescent cholesterol evidenced the presence of sperm sub-populations differentially affected by freeze-thawing. Similar unimodal frequency profiles were observed between sterol-enriched groups, while the control exhibited a sub-population of sperm compatible with low sterol content. Tyrosine phosphorylation was significantly lower when ram sperm incorporated cholesterol compared to the control. No difference in this capacitation parameter was found between the latter and desmosterol-enriched sperm. The percentage of sperm with damaged acrosomes post-thawing, assessed by a fluorescent lectin, was reduced in sperm that incorporated sterols before freezing, irrespective of the sterol class. These results suggest that sterols exert a stabilizing effect on the acrosome. No differences were found in levels of apoptotic DNA fragmentation among experimental groups. As to fertility trials, desmosterol-enriched sperm gave rise to higher rates of *in vitro* activated

OPEN ACCESS

Edited by:
Silvina Perez-Martinez, CONICET Centro de Estudios Farmacológicos y Botánicos (CEFYBO), Argentina

Reviewed by:
Fabrice Saez, Université Clermont Auvergne, France
Marc Yeste, University of Girona, Spain

***Correspondence:**
Jorgelina Buschiazzo
jbusch@criba.edu.ar

†Present address:
María de las Mercedes Carro
Center for Reproductive Genomics, Department of Biomedical Sciences, Cornell University, Ithaca, NY, United States

‡*These authors have contributed equally to this work*

Specialty section:
This article was submitted to Cell Growth and Division, a section of the journal Frontiers in Cell and Developmental Biology

Received: *28 January 2021*
Accepted: *03 June 2021*
Published: *24 June 2021*

Citation:
Carro M, Ramírez-Vasquez RRA, Peñalva DA, Buschiazzo J and Hozbor FA (2021) Desmosterol Incorporation Into Ram Sperm Membrane Before Cryopreservation Improves in vitro and in vivo Fertility. Front. Cell Dev. Biol. 9:660165. doi: 10.3389/fcell.2021.660165

oocytes by heterologous fertilization and to significantly lower pregnancy loss *in vivo*. Our research provides new insights on sterol incorporation into ram sperm prior to cryopreservation, in particular on the additional benefit of incorporating desmosterol as a strategy to improve fertility outcome.

Keywords: cryopreservation, ovine sperm, cholesterol, desmosterol, artificial insemination

INTRODUCTION

Artificial Insemination (AI) is an essential tool for animal production industry, enabling the introduction of valuable reproductive and productive genetic backgrounds into breeding programs. Long-term cryopreservation of the male gamete was a major contribution to the development of AI for many species. However, pregnancy rates in sheep inseminated *via* cervical with frozen-thawed sperm are markedly low, and therefore not feasible for commercial breeding programs (Alvarez et al., 2019). In this species, the complex anatomical structure of the cervix prevents intrauterine deposition of semen by routine methods, having to resort to laparoscopic intrauterine insemination. Cervical insemination is less invasive and has a lower ethical and practical cost than laparoscopic procedures. However, fertilization rates obtained with this method rarely exceed 40%, limiting the commercial use of cryopreserved ram sperm (Alvarez et al., 2019). The high sensitivity of ram sperm to cryopreservation reduces their survival and transport in the female reproductive tract (Gillan and Maxwell, 1999; Robinson et al., 2011) highlighting the need for improved semen freezing methods in this species.

Post-thaw sperm quality is quite different among animal species as a result of their different sensitivity to freezing and thawing (Holt, 2000). The low survival rate of cryopreserved sperm is associated with structural and functional alterations such as plasma membrane functionality loss (Sieme et al., 2015), cytoskeleton protein damage (McClean et al., 2007), acrosomal detachment or rupture (Cross and Hanks, 1991; Okabe, 2016), DNA damage (Valcarce et al., 2013), and mitochondrial impairment (Treulen et al., 2018). The low sterol/phospholipid ratio of ram sperm membranes has been identified as one of the most significant factors determining their low tolerance to cold temperatures (Mocé et al., 2010a). Sterols in mammalian sperm membranes are mainly represented by cholesterol and to a lesser extent by its immediate precursor, desmosterol, a cholesterol isomer with an extra double bond that diminishes its ordering potential in lipid bilayers (Vainio et al., 2006; Keber et al., 2013). Along with the reduced sterol content, ovine sperm have a lower content of desmosterol than sperm from other species, which is converted to cholesterol during sperm epididymal transit and maturation (Parks and Hammerstedt, 1985). While the efflux of sterols has a physiological role on sperm capacitation (Cross, 2003), sterol loss occurred during cryopreservation has a significant impact on sperm viability by inducing a premature capacitation-like state that shortens the life span of the spermatozoa (Mocé et al., 2010a).

Temperature decrease induces lateral lipid segregation, altering the lipid-lipid and lipid-protein interactions in the plasma membrane, compromising its functionality and integrity (Leahy and Gadella, 2011). It has been proposed that decreasing these lipid phase transitions during cooling is a strategy to reduce the sensitivity of sperm membranes to cryopreservation (Sieme et al., 2015). Sterols are known to modulate phase behavior of lipid membranes by increasing the order of acyl chains while maintaining lipid translational fluidity. High sterol content in sperm membranes during cooling keeps the phospholipid bilayer in a lamellar arrangement for a wider temperature range, reducing membrane phase transitions. Moreover, increasing sterol content of sperm before cryopreservation through incubation with sterols complexed with methyl-β-cyclodextrin (MβCD), a cyclic oligosaccharide used as a sterol donor, has been shown to reduce cryodamage in several species (Purdy and Graham, 2004; Moore et al., 2005; Müller et al., 2008), including the ram (Mocé et al., 2010b; Purdy et al., 2010; Motamedi-Mojdehi et al., 2014; Salmon et al., 2017). However, when AI was performed after MβCD-cholesterol treatment, no increase in pregnancy rates was reported (Purdy et al., 2010; Salmon et al., 2017). It is important to point out that many of these studies were performed in the presence of lipids from cryopreservation semen extenders containing egg yolk or skim milk.

Recently, we quantified the extent of cholesterol and desmosterol incorporation into ram sperm by incubation with MβCD-sterol complexes prior to cryopreservation in combination with a sterol-free extender (Carro et al., 2020). Through a biophysical approach, we demonstrated that both sterols similarly increased membrane lipid order according to total sterol increase, which was different depending on the MβCD-sterol concentration used. Treatment with 10 mM MβCD complexed either with cholesterol or desmosterol did not disturb lateral organization of the plasma membrane, improving its tolerance to osmotic stress and sperm total motility after refrigeration. Interestingly, when classical sperm quality parameters were evaluated after freeze-thawing, sterols showed a differential protective effect compared to non-treated sperm. While treatment with 10 mM MβCD-cholesterol increased sperm motility, membrane integrity and tolerance to osmotic stress, incorporation of desmosterol revealed an increased ability of ram sperm to withstand osmotic stress.

Based on these promising results and considering fertility outcomes of cryopreserved ram sperm as a primarily goal of our studies, we aimed at deepen our understanding of the role of cholesterol and desmosterol in ram sperm functionality and fertility. In the present study, we compared the extent and distribution of sterols, cryocapacitation status, acrosome integrity, DNA damage associated with apoptosis and *in vitro* and *in vivo* fertility competence of frozen-thawed ram sperm treated with cholesterol or desmosterol before cryopreservation.

MATERIALS AND METHODS

Chemicals and Reagents

Cholesterol, MβCD and FITC-Concanavalin A (ConA) were purchased from Sigma Chemical Company (St. Louis, MO, United States). Desmosterol and BODIPY-Cholesterol (BPY-Chol) were purchased from Avanti Polar Lipids (Alabaster, AL, United States). All solvents used in this study were HPLC grade (JT Baker, United States; UVE, Argentina).

Preparation of Methyl-β-Cyclodextrin-Sterol Complexes

MβCD-sterol complexes were prepared as reported previously (Carro et al., 2020). Briefly, a volume of cholesterol or desmosterol from a stock solution (10 μg/μL) in chloroform:methanol 1:1 (v/v) was added to a glass tube and the solvent was evaporated under a gentle stream of nitrogen for 1 h. A volume of 0.5 M stock solution of MβCD in Tris-citric acid buffer (300 mM Tris, pH 7.4, 95 mM citric acid) was subsequently added to the dried material (MβCD:sterol, 4:1 molar ratio) to reach the concentration of 40 mM MβCD:sterol. The mixture was clarified by vigorous mixing, subjected to bath sonication for 5 min and incubated in a rotating water bath at 37°C overnight. Before using the solution, it was centrifuged at 2000 × g for 10 min to remove excess of sterol crystals.

Semen Collection and Processing

Animals used in this study were handled in strict accordance with Good Animal Welfare Practices approved by the Institutional Committee for the Care and Use of Experimental Animals (CICUAE-Resolution 046/2016). Twenty mature Texel rams were kept on a ray grass, fescue and white clover pasture (37° 450 S, 58° 180 W), with water *ad libitum*. Semen was obtained using an artificial vagina during the breeding season in the southern hemisphere (March-June) following a routine collection of twice a week with at least 2 days of sexual abstinence. Only semen samples with mass motility ≥4 were processed. In order to avoid individual effects, semen from four randomly selected rams were pooled in each collection date. Pooled semen was divided into aliquots to conform each experimental group. The number of repetitions (number of pools) for each evaluation is indicated in the figure legend. Ejaculates were placed in a water bath at 32°C until processing. Sperm concentration was assessed in a Neubauer hemocytometer under light microscopy. Subsequently, semen was pooled with each male contributing the same number of spermatozoa and concentration was adjusted to 3,000 × 10^6 sperm/mL in pre-warmed (32°C) Tris-citric acid buffer. The pool was divided into three aliquots to conform each experimental group: Control (non-treated), Chol (pre-treated with 10 mM MβCD-cholesterol) and Des (pre-treated with 10 mM MβCD-desmosterol) and incubated for 15 min with 0 (control) or 10 mM MβCD-sterol. In order to remove MβCD molecules after incubation, spermatozoa were washed by centrifugation (1000 × g, 5 min) with pre-warmed extender or Tris-citric acid buffer followed by sperm cryopreservation.

Semen Cryopreservation

Semen pre-incubated with Tris-citric acid buffer (control) or MβCD-sterol (treatment) was diluted in three steps with a soy lecithin-based commercial extender (Andromed© Minitüb, Germany) to a final concentration of 400 × 10^6 sperm/mL and packaged into 0.25 mL straws (Minitüb, Germany). Temperature was progressively decreased from 32 to 5°C with a 0.1°C/min rate in a water bath and equilibrated for 2 h at 5°C. Straws were frozen in liquid nitrogen vapors (4 cm above the liquid level) for 10 min and finally stored in liquid nitrogen tanks. Thawing was performed by immersion of the straws in a water bath at 37°C for 30 s.

Quantification of Sperm Sterols

Spermatozoa were washed by centrifugation in citrate-EDTA buffer (35.5 mM sodium citrate, pH 7.4, 2.5 mM EDTA) at 2,500 × g for 10 min. Lipids were extracted with chloroform:methanol (1:2, v/v) according to Bligh and Dyer (1959). Total sterols were quantified by an analytical method using a commercially available enzymatic assay (Colestat Wiener Lab, Rosario, Argentina). An aliquot from the lipid extract, equivalent to 140 × 10^6 spermatozoa, was placed into a glass tube and dried under a nitrogen stream. The dried extract was resuspended in isopropyl alcohol and vigorously mixed for 1 min. In this procedure, 1 mL of Working Reagent was combined with 100 μL of isopropyl alcohol extract and incubated at room temperature (25°C) for 30 min. The absorbance was measured in a spectrophotometer at 505 nm and compared to a standard curve.

Cholesterol and desmosterol were quantified in cryopreserved ram sperm by reverse high-pressure liquid chromatography (HPLC). Lipid extracts from spermatozoa were spotted on thin-layer chromatography (TLC) plates (500 μM, silica gel G) along with commercial standards. The sterol fraction was resolved using hexane:ether:ammonia (45:65:1, v/v). Lipid bands were located under ultraviolet light after spraying the TLC plates with 2,7-dichlorofluorescein in methanol and exposing them to ammonia vapor. The sterol fraction was eluted with chloroform:methanol:water (5:5:1, v/v) and partitioned by the addition of 0.8 volumes of water. Reverse phase HPLC was performed at 40°C with a C18 HPLC column (Agilent Technologies, United States; 100 cm × 4.6 mm, 3.5 μM) equilibrated with methanol (100%) at a flow rate of 1 mL/min. A standard curve was done by monitoring absorbance of increasing concentrations of commercial standards at 205 nm. Peaks of each sterol were identified and plotted against the corresponding concentration to create the calibration curve.

Imaging of BODIPY-Cholesterol in Living Sperm

A stock solution (1 mM) of BPY-Chol was prepared in ethanol and stored in a dark glass tube at −20°C protected from light. A sperm suspension was diluted to a final concentration of 100 × 10^6 spermatozoa/mL in IVF-SOF medium supplemented with 1 μM of BPY-Chol and 0.5 μM propidium iodide and

incubated at 38.5°C under 5% CO_2 in humidified air for 1 h in the dark. After incubation, 20 μL of the sperm suspension was placed for 10 min on a slide previously coated with poly-L-lysine. Adhered cells were washed with IVF-SOF medium and observed using an epifluorescence inverted microscope (Nikon TE-300; Nikon, Tokyo, Japan). The fluorescent dye BPY-Chol was excited at 450–490 nm and digital photographs were taken with a DSfi1 camera (Nikon, Tokyo, Japan) connected to the microscope. Fluorescence intensity of sperm from randomly selected microscope fields was measured using the software Fiji (Schindelin et al., 2012) in background corrected images. A mask was created to locate each sperm-associated fluorescence and measure the mean gray value (MGV) from randomly selected fields at 40× magnification. At least 200 spermatozoa were counted in each image. To study differences in fluorescence intensity among spermatozoa within a population of cells, relative frequency histograms were performed by grouping MGV in 5-arbitrary fluorescence units (AFU) ranges.

Determination of Tyrosine Phosphorylation Levels by Western Blot

Sperm proteins were isolated following the protocol from Romarowski et al. (2015). Briefly, 10×10^6 spermatozoa from each group were washed by centrifugation in citrate-EDTA buffer at 800 × g for 3 min. The supernatant was removed and the pellet was resuspended in 100 μL of 62.5 mM Tris-HCl pH 6.8, 2% sodium dodecylsulfate (SDS) with 10% glycerol and boiled for 4 min. After centrifugation at 16000 × g for 5 min, supernatant was recovered, supplemented with 5% β-mercaptoethanol and boiled for 5 min once again. Bromophenol blue was added to reach a final concentration of 0.0005% and protein extracts were stored at −80°C until analysis by Western blot.

Protein extracts corresponding to 5×10^6 spermatozoa were separated by SDS-polyacrylamide gel electrophoresis (PAGE) (12.5% acrylamide) (Laemmli, 1970) and transferred to PVDF membranes (Immobilon-P, Millipore, Bedford, MA). Membranes were blocked overnight in TBS-T (20 mM Tris-HCl, pH 7.5, 150 mM NaCl, 0.05% Tween-20) supplemented with 0.5% BSA and 1% non-fat dry milk at 4°C followed by incubation with a mouse anti-phosphotyrosine antibody (pTyr) conjugated to HRP (ab16389, Abcam United Kingdom) diluted 1:2500 in TBS-T supplemented with 0.5% BSA for 4 h at room temperature. After pTyr detection, membranes were stripped with gentle shaking in stripping buffer (62.5 mM Tris-HCl, pH 6.8, 2% SDS, 100 mM β-mercaptoethanol) for 15 min at 55°C. Membranes were then blocked and incubated with a monoclonal mouse anti α-Tubulin antibody (α-Tub, T9026, Millipore Sigma, United States) diluted (1:5000) in 1% non-fat dry milk in TBS-T for 1 h at room temperature followed by secondary antibody incubation (Abcam, United Kingdom) diluted 1:10000 in TBS-T supplemented with 1% non-fat milk for 1 h at room temperature. Immunoreactive bands were revealed by chemiluminescence using the Bio-lumina kit (*Productos Biológicos*, Argentina) and autoradiographic films (General Electrics, United States). Films were scanned and quantified by densitometry with Fiji software (Schindelin et al., 2012).

Acrosome Status

Acrosome status integrity of frozen-thawed ram sperm was assessed by incubation with a fluorescent (FITC) Concanavalin A (ConA) (Ozaki et al., 2002). Sperm suspensions (10×10^6 cells) were washed by centrifugation at 800 × g for 3 min in PBS and fixed overnight at 4°C in 4% formaldehyde in PBS (pH 7.4). Cells were pelleted again, resuspended in 20 μL of PBS and smeared onto a slide previously coated with poly-L-lysine for 20 min. Slides were then washed with PBS and stained with ConA 100 μg/mL in PBS solution in the dark for 20 min at room temperature. After incubation, slides were washed again with PBS and covered with a coverslip. Spermatozoa were observed using an epifluorescence inverted microscope (Nikon TE-300; Nikon, Tokyo, Japan). The fluorescent lectin ConA was excited at 450–490 nm and digital photographs were taken with a DSfi1 camera (Nikon, Tokyo, Japan) connected to the microscope. Sperm with non-intact acrosome showed bright fluorescence in the acrosomal region (ConA+), while intact acrosome did not show fluorescence (ConA−). At least 200 spermatozoa were examined and the percentage of spermatozoa ConA+ was calculated for each group. The number of ConA+ sperm was normalized by the number of live sperm on each condition evaluated by the eosin-nigrosin exclusion test (Björndahl et al., 2003).

Detection of Apoptotic DNA Fragmentation

Apoptotic DNA fragmentation induced by cryopreservation was analyzed using the *in situ* Cell Death Detection Kit with fluorescein (Roche Diagnostics GmbH, Mannheim, Germany) that detects DNA breaks associated with apoptosis. This kit is based in the terminal deoxynucleotidyl transferase-mediated fluorescein dUTP nick-end labeling reaction (TUNEL) of free 3′-OH *termini* by terminal deoxynucleotidyl transferase (TdT). Thawed sperm were washed twice by centrifugation in 6 mL PBS supplemented with BSA (1 mg/mL) for 5 min at 200 × g. A drop of re-suspended spermatozoa was smeared on a glass slide, air dried and fixed with 4% formaldehyde in PBS for 60 min at room temperature and stored at 4°C until use. Slides were washed in PBS and cells were permeabilized with freshly prepared 0.1% Triton X-100 in 0.1% sodium citrate for 5 min on ice. Slides were rinsed twice with PBS, and cells were incubated with the TUNEL reaction mixture in the dark for 60 min at 37°C in a humidified chamber. After this period, slides were washed three times with PBS and analyzed by fluorescence microscopy using an excitation wavelength of 488 nm (Nikon TE-300; Nikon, Tokyo, Japan). Negative (omitting TdT from the reaction mixture) and positive (using DNase I, RQ1 Promega for 10 min at room temperature) controls were included in each trial. At least 200 sperm in each experimental group were evaluated to determine the percentage of TUNEL-positive sperm (green fluorescence in the head).

Heterologous *in vitro* Fertilization

Heterologous *in vitro* fertilization (IVF) using bovine oocytes was employed to assess the fertility of thawed ram sperm

samples according to García-Alvarez et al. (2009) with some modifications.

Oocyte Collection and *in vitro* Maturation

Bovine ovaries from cycling beef heifers (*Bos taurus taurus*) were collected from local slaughterhouses and transported within 60–90 min in a thermic container to the laboratory. *Cumulus*-oocyte complexes (COCs) were aspirated from follicles ranging from 2 to 8 mm in diameter by a vacuum system. COCs with homogeneous ooplasm and more than four complete layers of *cumulus* cells, corresponding to grades 1 and 2 according to de Loos et al. (1989) were selected under a stereomicroscope and washed 3 times in M199 supplemented with 0.5% Hepes (w/v). Selected COCs were incubated in four-well culture plates (NUNC, Thermo Fisher Scientific, Loughborough, Leicestershire, United Kingdom) in groups of 60 per well, with 400 μL of M199 medium (Sigma-Aldrich, United States), supplemented with 0.1 mg/ml L-glutamine, 2.2 mg/ml sodium bicarbonate and 0.1 IU/mL rhFSH (Gonal F-75, Serono, United Kingdom) for 22 h at 38.5°C under 5% CO_2 in humidified air.

In vitro Fertilization

Cumulus cells were partially removed from matured bovine oocytes by gently pipetting in M199-Hepes and oocytes were placed in four-well culture plates containing 400 μL of fertilization medium (SOF supplemented with 10% of estrous sheep serum and 40 μg/mL gentamycin). Thawed ram sperm were selected on a Percoll® (Sigma-Aldrich, United States) discontinuous density gradient (45/90%) and incubated for 10 min in the fertilization medium. Thawed sperm from each experimental group were co-incubated with the oocytes at a final concentration of 2.5×10^6 sperm/mL per well at 38.5°C in 5% CO_2 in humidified air for 48 h.

To assess IVF rates, oocytes were fixed in 2% glutaraldehyde in M199-Hepes for 10 min and stained with 5 μM bisBenzimide Hoechst 33342 for 20 min at room temperature. Oocytes were mounted on a slide with glycerol, covered with a coverslip and observed under an epifluorescence microscope (Nikon TE-300; Nikon, Tokyo, Japan) using excitation wavelength of 380 nm. Heterologous IVF rates were determined as the percentage of activated oocytes (presence of *pronuclei* or cell cleavage). Experimental groups were defined as matured oocytes co-incubated with frozen-thawed sperm non-treated (Control), pre-treated with 10 mM MβCD-Cholesterol (Chol) and pre-treated with 10 mM MβCD-Desmosterol (Des). Five heterologous IVF experiments were performed in total and the number of oocytes for each experimental condition was indicated in the figure legend.

In vivo fertility

To assess the effect of increasing sperm cholesterol or desmosterol content before freezing and thawing on *in vivo* fertility, we performed a cervical AI at fixed-time during the breeding season. For this purpose, 120 Texel ewes were randomly inseminated with frozen-thawed sperm from the three experimental groups (Control, Chol, Des) and pregnancy rate and lambing were recorded.

Estrous Synchronization

Synchronization of estrous was conducted by intravaginal sponges impregnated with medroxyprogesterone release (Progespon®, Syntex SA, Argentina, 60 mg per dose) and treated with oxytetracycline (Terramicina 100®, Zoetis, Argentina) for a period of 7 days. At sponge removal time, ewes were treated with equine chorionic gonadotropic (Novormon 5000®, Syntex, Argentina, 300 IU, im), and Cloprostenol (Ciclase®DL, 75 mg, im).

Artificial Insemination and Fertility Rates

Artificial Insemination was performed at fixed time, 48–50 h after withdrawal of intravaginal device. A dose of 100×10^6 frozen-thawed sperm (0.2 mL volume) was placed between the first and second cervical rings. Early pregnancy was determined by transrectal ultrasound (Aloka SSD 500, Hitachi, Japan) 30 days after AI and lambing was registered for each ewe between days 140 and 160 after AI procedure.

Statistical Analysis

Statistical analysis was carried out using InfoStat software (Di Rienzo et al., 2014). Sterol content and BPY-Chol fluorescence intensity were analyzed through analysis of variance (ANOVA), followed by *post hoc* test analysis of multiple comparisons by Fisher's Least Significant Difference (LSD Fisher). Shapiro-Wilk and Levene tests were carried out to verify normal distribution and homogeneity of variances, respectively. Tyrosine phosphorylation (densitometry) was analyzed by non-parametric Kruskall-Wallis test. Percentages of acrosome status, sterol composition, TUNEL-positive sperm and *in vitro* fertility were compared using Generalized Linear Mixed Models (GLMM) with Binomial family, *logit* link function and LSD Fisher contrast. *In vivo* fertility rates were compared using the Chi-square test for homogeneity. Differences were considered significant at $p < 0.05$.

RESULTS

Quantification and Distribution of Sterols in Cryopreserved Ram Sperm

To study the effect of increasing ram sperm sterol content on sperm functionality and fertility after cryopreservation, sperm were treated with 10 mM MβCD complexed either with cholesterol or desmosterol and subsequently frozen following a stepwise temperature decrease. After thawing, total sterol content was quantified from sperm lipid extracts with an enzymatic assay (**Figure 1A**) and the fraction corresponding to free sterols was resolved by reverse HPLC to assess the percentage distribution of free sterol classes in each group (**Figure 1B**). Sperm that incorporated cholesterol before freezing (Chol group) showed increased total sterol content compared to the control (**Figure 1A**). Nevertheless, the relative cholesterol and desmosterol percentage distribution within this group did not differ from the control, cholesterol being the main sterol (>93% of total sterols) in both experimental conditions (**Figure 1C**). On the contrary, sperm that incorporated desmosterol before cryopreservation (Des group) did not show a significant

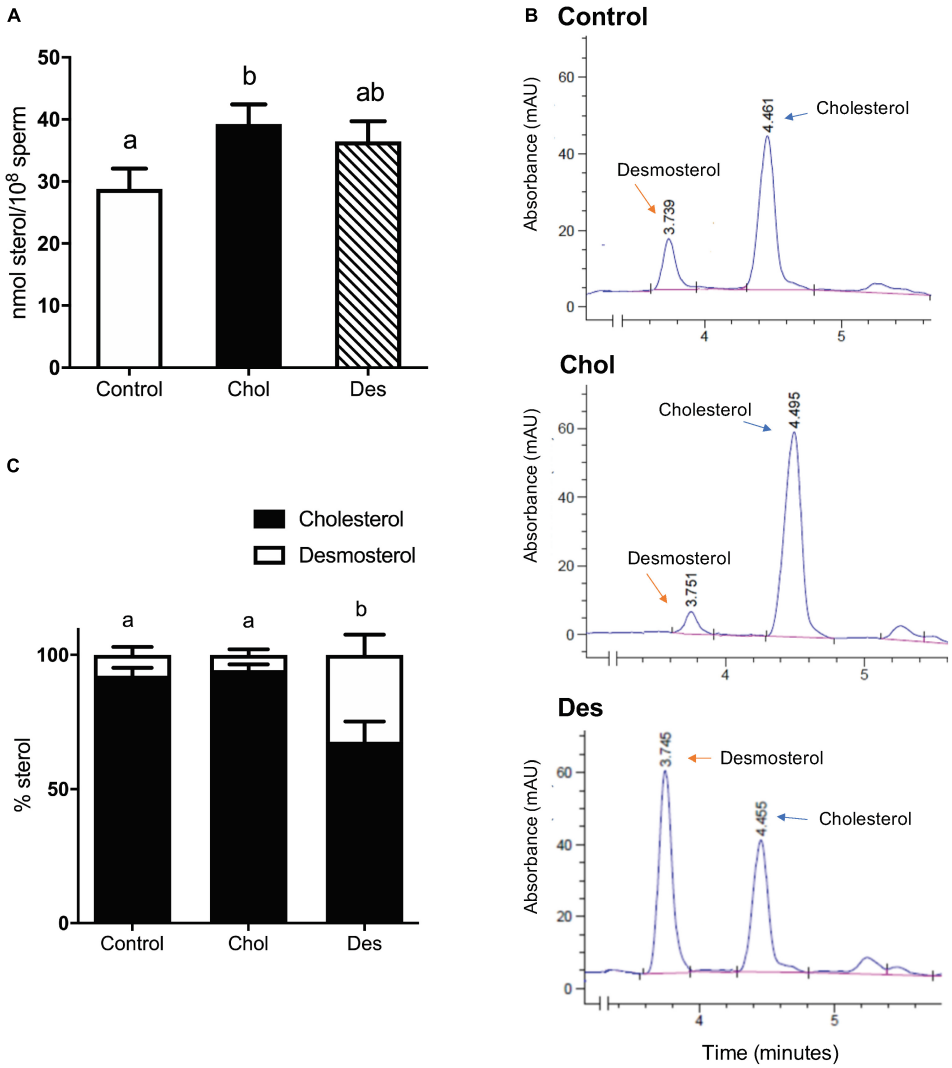

FIGURE 1 | Quantification of cholesterol and desmosterol in cryopreserved ram sperm pretreated with 10 mM MβCD-Chol (Chol) -Des (Des). **(A)** Effect of 10 mM MβCD-Chol or -Des pretreatment on total sterol content of frozen-thawed ram sperm. Results are expressed as nmol of sterols per 100 million sperm and represent mean values ± SEM of 7 (control y MβCD-Des) and 10 (MβCD-Chol) independent experiments. **(B)** Identification of cholesterol and desmosterol by HPLC in the ovine sperm sterol fraction of Control, Chol and Des groups. The peaks correspond to each sterol with the indicated retention times. **(C)** Quantification of cholesterol and desmosterol by HPLC in each experimental group. The results are expressed as percentage of sterols and represent the mean values ± SD of three independent measurements. Sterol content (%) among the experimental groups was compared by Generalized Linear Mixed Models (GLMM) with binomial distribution. The different letters (a, b) indicate significant differences ($p < 0.05$). Data were analyzed by ANOVA and mean values were compared using the *post hoc* test LSD of Fisher. Different letters (a, b) indicate significant differences ($p < 0.05$).

difference in total sterol content compared to the control or Chol group after thawing (**Figure 1A**). However, desmosterol content in this group was about five times higher (∼35% of total sterols) than the control or Chol group (**Figure 1C**).

Comparing Sterol Behavior in Cryopreserved Sperm by *in situ* Imaging of BODIPY-Cholesterol

To further investigate the sterol distribution and content of cholesterol and desmosterol in treated and non-treated sperm after cryopreservation, we incubated sperm with BPY-Chol (**Figure 2A**). Sperm that incorporated desmosterol before cryopreservation showed higher BPY-Chol fluorescence intensity levels with respect to the other experimental groups (**Figure 2B**). No statistical difference was found in BPY-Chol fluorescence intensity in sperm that incorporated cholesterol before freezing with respect to the control and Des group. As expected, living sperm incubated with BPY-Chol displayed differences in fluorescence intensities among cells, evidenced in fluorescence frequency histograms (**Figure 2C**). The presence of different mean fluorescence intensities per cell is compatible with the existence of different sterol content among cells within the same

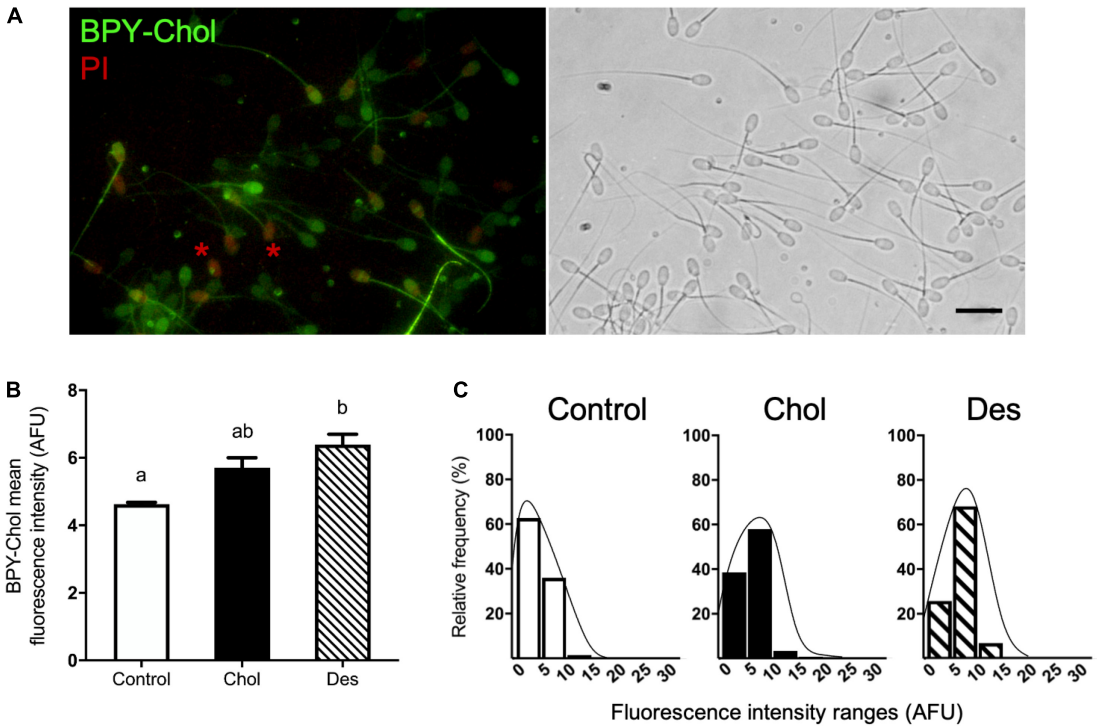

FIGURE 2 | Sterol distribution and content in cryopreserved ram spermatozoa estimated by BPY-Chol labeling of living cells. **(A)** Representative fluorescence image of BPY-Chol and PI in ram sperm with bright field on the right, scale bar represents 20 μm. Asterisks indicate representative PI-positive stained sperm. **(B)** Sterol content of cryopreserved ovine spermatozoa after cholesterol (Chol) or desmosterol (Des) incorporation through treatment with 10 mM MβCD-sterol complexes. Results are expressed as arbitrary fluorescence units (AFU) and represent mean values ± SEM ($N = 5$). Fluorescence measurements were automatized using masks in Fiji software. A total of 692, 451, and 864 cells were quantified for the control, Chol and Des groups, respectively. Data were analyzed by ANOVA and mean values were compared using the *post hoc* Bonferroni test. Different letters (a, b) indicate significant differences ($p < 0.05$). **(C)** Histograms of the relative frequencies of BPY-Chol mean fluorescence intensity measured per spermatozoa and grouped in ranges of 5 AFU for each experimental group. Lines estimate unimodal histogram distribution.

sperm population. All experimental groups showed a unimodal frequency distribution. While the majority of the cells in the control group displayed fluorescence intensities of 0–5 AFU, the most frequent values for pretreated sperm with MβCD-sterol ranged from 5 to 10 AFU, regardless of the type of sterol incorporated before freezing.

Effects of Sterol Incorporation on Tyrosine Phosphorylation Levels and Acrosome Integrity After Freeze-Thawing

To study the effect of cholesterol or desmosterol incorporation into ram sperm prior to freezing on the cryocapacitation status after thawing, premature activation of capacitation-like signaling induced by cryopreservation was evaluated through the analysis of tyrosine phosphorylation (**Figure 3A**). When ram sperm incorporated cholesterol prior to freezing, tyrosine phosphorylation levels of frozen-thawed sperm were significantly lower compared to the control (**Figure 3B**). On the other hand, sperm that previously incorporated desmosterol did not show a significant difference in this capacitation parameter compared to the control.

In order to evaluate the effect of the incorporation of sterols prior to freezing on the acrosome integrity, spermatozoa were incubated with the fluorescent lectin ConA. **Figure 4A** shows the binding of ConA to acrosomal glycoproteins as a consequence of the exposure of the internal acrosome membrane during acrosome reaction, or due to acrosome integrity loss (**Figures 4A,B**). Treatment with MβCD-Chol or -Des prior to freezing significantly decreased (∼20%) the percentage of ConA positive sperm after thawing compared to the control, indicating a higher percentage of intact acrosomes in sperm that incorporated either cholesterol or desmosterol (**Figure 4C**). No significant difference was observed between treatments with the different sterols.

Assessing DNA Damage Associated to Apoptosis in Cryopreserved Sperm

To evaluate differences in DNA fragmentation induced by freezing and thawing of ram sperm, we performed TUNEL analysis. After labeling of DNA strand breaks by TdT (**Figure 5**), we observed a low level of DNA fragmentation (0.8–1.5% TUNEL-positive cells) with no significant differences among experimental groups (**Table 1**).

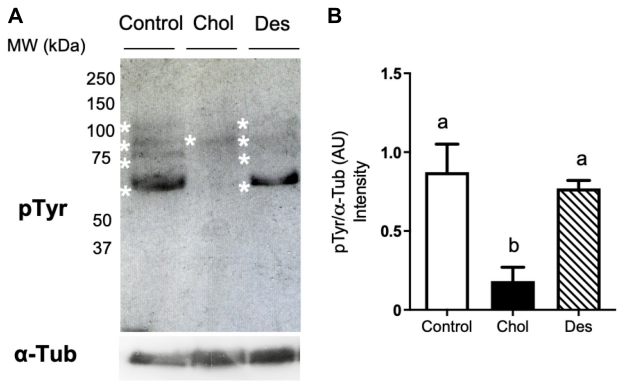

FIGURE 3 | Identification of tyrosine phosphorylated proteins in cryopreserved ram sperm pre-treated with 10 mM MβCD-Chol (Chol) or -Des (Des). Proteins were resolved by SDS-PAGE (12.5%), blotted using an anti-phosphotyrosine (pTyr) antibody and immunoreactive bands were revealed by chemiluminescence. **(A)** Representative set of the experimental groups showing pTyr detection. Asterisks indicate position of the different phospho-proteins. Each lane corresponds to 5×10^6 spermatozoa. Constitutive α-Tubulin (α-Tub) was used as loading control (lower panel). **(B)** Quantification of total intensity of immunoreactive bands per lane measured by densitometry (Fiji software) and expressed as arbitrary units (AU). Bars represent mean values ± SEM ($N = 4$). Data were analyzed by Kruskal-Wallis test. Different letters (a, b) indicate significant differences ($p < 0.05$).

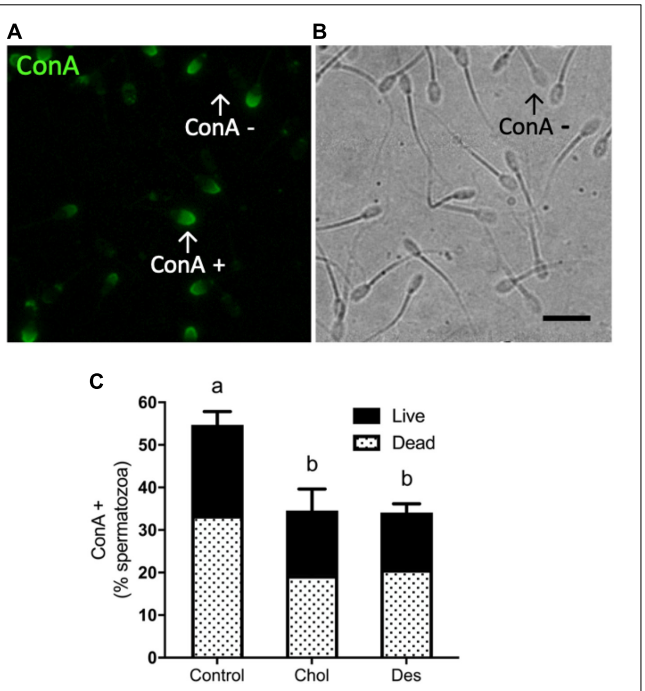

FIGURE 4 | Effect of sterol incorporation on acrosome integrity after cryopreservation **(A)** Representative fluorescence image of cryopreserved ram spermatozoa incubated with FITC-Concanavalin A (ConA) showing stained cells (ConA+). **(B)** Bright field image. Scale bar represents 20 μm. Arrows indicate ConA + and ConA− spermatic cells in counterpart images. **(C)** Percentage of ConA + ram spermatozoa after thawing showing the normalized percentages of live/dead spermatozoa. Stacked bars represent the mean values ± SEM ($N = 5$). Data were analyzed using Generalized Linear Mixed Models (GLMM) with Binomial family. The different letters (a, b) indicate significant differences ($p < 0.05$).

In vitro Fertilizing Competence of Cryopreserved Sperm

The fertilizing competence and ability of MβCD-sterol treated sperm to undergo capacitation and acrosome reaction physiologically after thawing was evaluated in heterologous IVF assays. After 48 h of *in vitro* culture, we evaluated the presence of *pronuclei* or oocyte cleavage as a consequence of oocyte activation by sperm (**Figure 6**). Developmental progress of oocytes that activated the cell division machinery resulted in asynchronous divisions and different stages of hybrid embryos (**Figures 6Ac–e**). Heterologous IVF with frozen-thawed ram sperm that incorporated desmosterol prior to freezing generated a higher percentage (>30%) of activated oocytes compared to the control and spermatozoa that incorporated cholesterol (**Figure 6B**). No statistical difference was observed between sperm treated with MβCD-Chol compared to the control.

In vivo Fertility Outcomes

To evaluate if incorporation of cholesterol or desmosterol prior to cryopreservation increases fertility competence of frozen-thawed ram sperm *in vivo*, we performed a fertility trial by cervical AI of ewes during the breeding season. No differences were found in pregnancy rates of ewes inseminated with cryopreserved ram sperm from the different experimental groups (**Table 2**). However, ewes inseminated with sperm that incorporated desmosterol prior to cryopreservation resulted in significantly higher rates of live born lambs related to pregnant ewes when compared to the control and Chol group, indicative of reduced pregnancy loss or embryonic mortality in this experimental group.

DISCUSSION

Recently, we provided mechanistic insight into the differential role of cholesterol and desmosterol in ram sperm membrane and we proposed a cryopreservation procedure compatible with a standard protocol employing a sterol-free semen extender (Carro et al., 2020). The present study is focused on determining how treatment of ram sperm with MβCD-sterols prior to freezing influences sperm functionality and fertilizing competence *in vitro* and *in vivo*. Under these experimental conditions, sperm that incorporated cholesterol prior to freezing exhibited moderately higher levels of total sterols after thawing compared to the control. On the other hand, sperm that incorporated desmosterol showed intermediate levels of total sterols, not differing from the control or the cholesterol group. Conversely, direct fluorescence of BPY-Chol to estimate relative levels of sterols showed intermediate fluorescence intensity in MβCD-cholesterol treated sperm and moderately higher BPY-Chol associated fluorescence in MβCD-desmosterol treated sperm with respect to the control. These differences are not relevant in magnitude and reflect that total sterol content after freeze-thawing in sperm that have incorporated cholesterol or desmosterol before freezing is marginally higher with respect to the control. Prior to freezing,

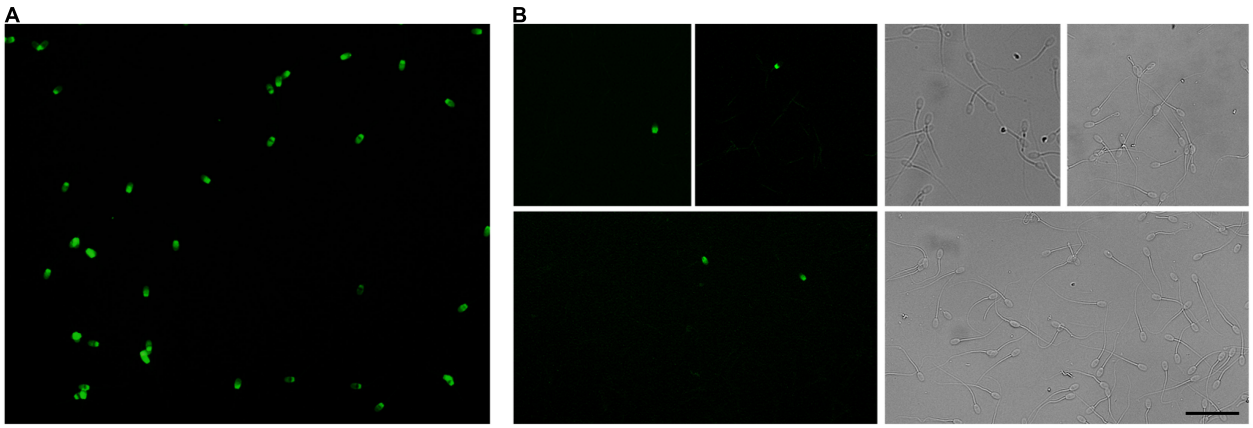

FIGURE 5 | Apoptosis associated DNA fragmentation in cryopreserved ram sperm. DNA breaks in thawed spermatozoa were labeled using the terminal deoxynucleotidyl transferase-mediated dUTP nick-end labeling reaction (TUNEL). TUNEL-positive ram spermatozoa show green fluorescence in the head. **(A)** Positive control achieved by DNase I treatment with all spermatozoa showing green fluorescence. **(B)** Representative TUNEL-positive sperm from experimental groups on the left panels and respective bright fields on the right. Scale bar represents 40 μm.

TABLE 1 | Percentages of TUNEL-positive ram sperm after thawing.

Experimental groups	Total sperm (N)	TUNEL-positive (% ± SEM)
Control	762	1.48 ± 0.89[a]
Chol	728	0.96 ± 0.21[a]
Des	756	0.77 ± 0.72[a]

DNA fragmentation was detected by the terminal deoxynucleotidyl transferase-mediated fluorescein dUTP nick-end labeling reaction (TUNEL) of free 3′-OH termini by terminal deoxynucleotidyl transferase (TdT). Data represent the mean values ± SEM (N = 3) and were analyzed using Generalized Linear Mixed Models (GLMM) with Binomial family. No differences were found among experimental groups ($p > 0.05$). [a] Means with the same letter are not significantly different.

sperm almost double the original sterol level after MβCD-sterol treatment, irrespective of the sterol used in the complex (Chol or Des) (Carro et al., 2020). Considering the relative proportions of sterols prior to freezing, it can be inferred that desmosterol decreased from ∼50% (prior to freezing) to 35% (after thawing). Sperm preloaded with desmosterol showed a significantly different sterol composition (still different after thawing) compared to the control or cholesterol group. It can be also assumed that loss of sterols induced by cryopreservation was higher in treated groups compared to the control and even more interestingly, desmosterol content of Des group seems to have been selectively reduced over cholesterol. Higher loss of sterols after freezing and thawing was also observed by others in ram sperm, when adding cholesterol (Mocé et al., 2010b). Altogether, these results indicate that the mechanism underlaying sterol loss induced by freeze-thawing likely involves actual loss of sperm membrane, also evidenced in the decrease of major components of membrane bilayers after cryopreservation such as phospholipids (Chakrabarty et al., 2007).

BPY-Chol fluorescence also revealed the presence of different co-existing cell sub-populations, compatible with different sterol contents (Hölttä-Vuori et al., 2016; Bernecic et al., 2019; Carro et al., 2020). Previously, fresh sperm from control and 10 mM MβCD-sterol treated groups evidenced 4–6 different sperm sub-populations (Carro et al., 2020). Here we show that all experimental groups displayed no more than 3 sperm sub-populations after freeze-thawing, suggesting that there is a selective reduction in sub-population quantity caused by freezing. Notably, sperm categories with low fluorescence intensity (low sterol content) were increased after cryopreservation, which was reflected in a modal value different from that reported in fresh sperm, particularly in sperm treated with MβCD-sterol. In these experimental groups, a single sub-population comprised ∼60% of the sperm cells after freeze-thawing. The control also evidenced a sub-population which comprised 60% of the sperm cells but these cells showed low fluorescence, compatible with a low sterol content. Sperm sub-populations were previously described regarding sperm morphology (Thurston et al., 1999), osmotic tolerance (Druart et al., 2009), *in vitro* capacitation ability (Gadella and Harrison, 2000), and *in vivo* acrosome reaction competence (La Spina et al., 2016). Interestingly, in rams with proven *in vivo* fertility, distribution of motility-based sub-populations varied between high and low fertility rams (Ledesma et al., 2017). Moreover, it was reported that cryopreservation reduces the number of motility-based sub-populations in fish sperm (Gallego et al., 2017). Findings from our study draw on evidence of the close relation between sterol content and sensitivity of sperm to cryopreservation and also highlight the different sensitivity of sperm sub-populations based on the sterol content.

Cryopreservation causes severe damage to ram sperm structure and functionality, compromising its ability to reach and fertilize the oocyte. The role of cholesterol in mammalian sperm capacitation is well-known. High cholesterol level in the sperm membrane prevents premature capacitation and acrosome exocytosis, while sterol efflux triggers capacitation and associated post-testicular sperm maturation in the female tract (Gadella and Leahy, 2015; Cohen et al., 2016). Cholesterol loss from sperm membranes caused by freeze-thawing induces a premature

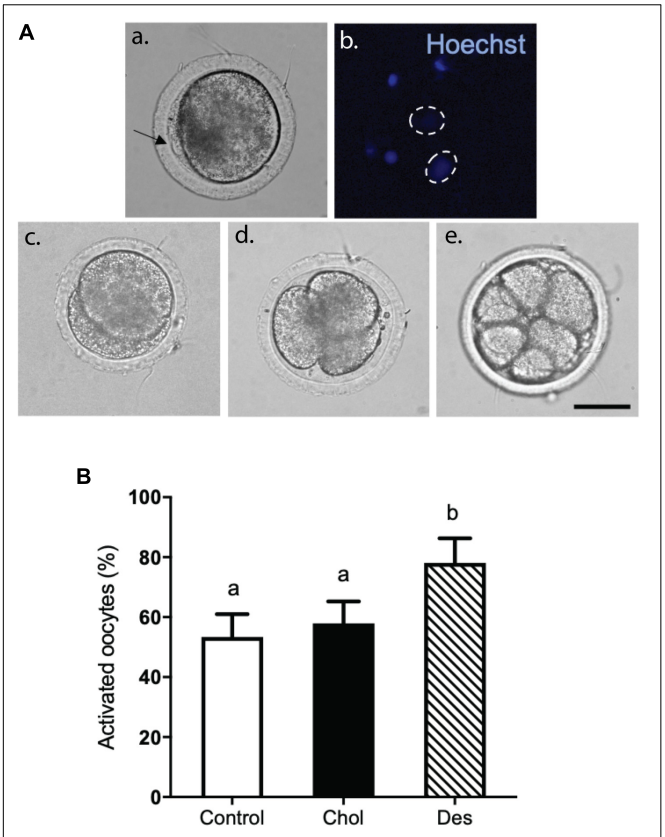

FIGURE 6 | Effect of sterol incorporation on the ability of cryopreserved ram sperm to activate bovine oocytes *in vitro*. **(A)** Different hybrid cleavage stages of activated bovine oocytes after heterologous IVF with cryopreserved ram sperm pretreated with 10 mM MβCD-Chol (Chol) or -Des (Des). After co-incubation with sperm, oocytes were fixed and stained with Hoechst 33342. **(a)** Bright field of inseminated oocyte. The arrow shows polar bodies and adhered sperm to *zona pellucida*. **(b)** Oocyte *pronuclei* stained with Hoechst 33342 denoted by dashed circles and hybrid embryos with two **(c)** three **(d)** and eight cells **(e)**. Scale bar: 50μm. **(B)** Activation rate after heterologous IVF. Results are shown as percentages of activated oocytes and represent mean values ± SEM of 5 independent experiments from a total of 205 control oocytes, 199 MβCD-Chol treated oocytes and 189 MβCD-Des treated oocytes. Data were analyzed using Generalized Linear Mixed Models (GLMM) with Binomial family. The different letters (a, b) indicate significant differences ($p < 0.05$).

capacitation-like state in the sperm (Cormier et al., 1997; Mocé et al., 2010a). Moreover, it has been reported that freezing and thawing triggers tyrosine phosphorylation in boar and stallion sperm (Green and Watson, 2001; Pommer et al., 2003). In our study, sperm that incorporated cholesterol maintained lower tyrosine phosphorylation levels after cryopreservation compared to control sperm and those that incorporated desmosterol. On the other hand, it has been reported that both cholesterol and desmosterol have the ability to prevent induction of human sperm capacitation *in vitro*, given by the planar structure of these sterols (Nimmo and Cross, 2003). Inhibition of sperm capacitation signaling by cholesterol could depend on the original level of this lipid at the plasma membrane (Darin-Bennett and White, 1977; Davis, 1981) and, therefore, may function differently in sperm with higher cholesterol to phospholipid ratios such as human sperm. In addition, non-effect of desmosterol on sperm tyrosine phosphorylation levels after cryopreservation highlights the differences between physiological capacitation and capacitation-like changes induced by freezing and thawing. Interestingly, it was recently shown that markers related to capacitation appear only in specific sub-populations of frozen-thawed stallion spermatozoa (Ortega-Ferrusola et al., 2017). Even when desmosterol-treated sperm exhibited more cryocapacitation compared to cholesterol-treated sperm, it is possible that non-capacitated sperm with good fertilizing potential still remains in the desmosterol group after freeze-thawing. Although cholesterol and desmosterol exerted differential effects on premature capacitation-like events induced by cryopreservation, they similarly decreased the percentage of acrosome-reacted sperm after freezing and thawing. Both sterols exerted a stabilizing effect on the acrosome, a Golgi-derived vesicle depleted of sterols at the membrane. Altogether, these results evidence that loss of acrosomal integrity after cryopreservation is more related to a mechanical stress, instead of a physiological triggering of acrosomal exocytosis (Nagy et al., 2003).

In vitro fertility after cholesterol incorporation has been previously evaluated in bull (Purdy and Graham, 2004), camel (Crichton et al., 2016), horse (Spizziri et al., 2010) boar (Blanch et al., 2012), and ram sperm (Mocé et al., 2010b). In accordance with our results, these reports showed that cholesterol incorporation does not increase the percentage of activated oocytes after IVF. However, evaluation of fertility outcome of cryopreserved sperm after desmosterol incorporation has not been explored. Moraes et al. (2010) reported that desmosterol incorporation into bull sperm does not improve binding to zona pellucida in fixed oocytes. Interestingly, we show novel results regarding significant activation of oocytes by desmosterol-enriched sperm after heterologous IVF. Frozen-thawed spermatozoa that incorporated desmosterol before cryopreservation contain approximately five times more desmosterol than the sperm that incorporated cholesterol. Sterols are also major components of membrane rafts, small domains that compartmentalize cellular processes and actively participate in sperm capacitation and fertilization (Gadella et al., 2008; Watanabe and Kondoh, 2011). However, cholesterol and desmosterol differ in their affinity to partition into these ordered domains (Vainio et al., 2006). Previously, we showed a reduced tendency of desmosterol compared to cholesterol for segregating into ordered domains (Carro et al., 2020). Therefore, it is likely to expect that a significant level of desmosterol over cholesterol could impact on membrane-dependent processes such as gamete interaction and fusion. Further research is needed to address how increased levels of desmosterol could affect membrane lateral organization, membrane topology, fusogenicity, and/or fertilization signaling.

As to *in vivo* fertility study, the insemination pilot trial carried out under these experimental conditions produced similar pregnancy rates in all experimental groups. Increased seminal quality of desmosterol-enriched sperm to withstand osmotic tolerance after cryopreservation (Carro et al., 2020),

TABLE 2 | *In vivo* fertility of frozen-thawed ram sperm pretreated with 10 mM MβCD-Chol (Chol) or 10 mM MβCD-Des (Des) after cervical AI.

Experimental groups	Inseminated ewes N	Pregnancy rate N (%)	Live born/Inseminated N (%)	Live born/Pregnant N (%)	Pregnancy loss N (%)
Control	49	24 (48.9)	17 (34.7)	17 (70.8)	7 (29.2)
Chol	52	22 (42.0)	13 (25.0)	13 (59.1)	9 (40.9)
Des	59	24 (40.7)	23 (39.0)	23 (95.8) **	1 (4.2)

*Pregnancy and birth rates were registered after cervical AI of 160 Texel ewes with frozen-thawed ram sperm. Pregnancy was detected at day 30 after insemination by ultrasonography. Data was analyzed by Chi- Square test for homogeneity. No differences were found in pregnancy rates (p = 0.68) or birth rates (p = 0.28) among the experimental groups. Statistically significant differences were found when live births relative to pregnancy were compared (p = 0.01). In particular, significant differences were found for the following comparisons: Control vs. Des (**p = 0.02) and Chol vs. Des (**p = 0.002). No differences were found for Control vs. Chol (p = 0. 40). Pregnancy loss is the counterpart of Live born/Pregnant.*

or increased ability to activate oocytes *in vitro* was not reflected into higher pregnancy rates. It is important to note that IVF assays bypass the physical barriers encountered by sperm in the female reproductive tract including physiological sperm selection, and therefore do not necessarily correlate with *in vivo* trials. Selection of sperm sub-populations are also blurred *in vitro*. However, when the lambing rates related to pregnancy were analyzed, ewes inseminated with spermatozoa that had incorporated desmosterol prior to freezing showed a significant increase in maintaining pregnancy to term, without registering almost any pregnancy loss or embryo mortality. It is widely accepted that progesterone is required for maintaining pregnancy (Spencer et al., 2004). Interestingly, it has been shown that progesterone inhibits the enzyme that converts desmosterol to cholesterol (DHCR24) in tissues and cells that accumulate desmosterol (Jansen et al., 2013). Upcoming fertility trials in extensive breeding programs coped with molecular analysis will contribute to a more comprehensive discussion.

On the other hand, membrane desmosterol could have contributed to better preserve male gamete genomic integrity. Even when we did not found differences in apoptotic DNA fragmentation assessed by TUNEL-reaction, other alterations produced in the chromatin structure could have been prevented by membrane desmosterol. Moderately low levels of DNA fragmentation were previously found by acridine orange (∼4%) and TUNEL (6%) in frozen-thawed ram sperm (Nur et al., 2010). Recently, ∼2.5% of DNA fragmentation index based on acridine orange was reported for ram sperm after cryopreservation (Peris-Frau et al., 2021). This study revealed that DNA methylation and apoptosis only increased after certain incubation times under capacitation conditions in cryopreserved spermatozoa, probably as a result of an early response to oxidative stress. It has been shown that sperm DNA damage is related to detrimental embryonic and/or fetal development in several species such as the bull (De Castro et al., 2016), fish (Pérez-Cerezales et al., 2010) and humans (Simon et al., 2014; Sedó et al., 2017). Moreover, epigenetic defects of the sperm could induce decreased developmental capacity of the generated embryos, providing a possible explanation for early pregnancy loss (Stuppia et al., 2015). Considering the growing evidence on male contribution to embryo development and involvement of gene regulators such as histone modifications and small non-coding RNAs (Baxter and Drake, 2019; Le Blévec et al., 2020), this emerging field of study deserves further research in domestic species, particularly in relation to biotechnologies applied for increasing reproductive efficiency.

Taken together, findings from our study reveal differential effects of cholesterol and desmosterol incorporation into ram sperm on functional parameters and fertility competence after cryopreservation. First, a different sterol composition characterized pre-treated sperm after freeze-thawing. Interestingly, sterol-based sperm sub-populations were differentially affected by freeze-thawing. Cholesterol incorporation reduced tyrosine phosphorylation levels mitigating the effects of cryopreservation on the induction of capacitation-like events. However, both sterols decreased damage caused by freeze-thawing to acrosome membranes. In this regard, treatment did not reduce the ability of sperm to undergo capacitation and acrosome reaction after cryopreservation, as shown here by IVF assay. Finally, we show that desmosterol-enriched sperm give rise to higher rates of *in vitro* activated oocytes by heterologous fertilization and to significantly lower pregnancy loss *in vivo*. These results are particularly important considering that increase of sperm desmosterol content has not been studied as a cryoprotective strategy. Our research provides new insights into desmosterol positive influence in ram sperm fertility. Moreover, our work opens a novel and challenging research subject aimed at elucidating biochemical and cellular processes involved in this protective mechanism. Deciphering epigenetic contribution of desmosterol-protective effect should be the focus of future studies.

DATA AVAILABILITY STATEMENT

The original contributions presented in the study are included in the article, further inquiries can be directed to the corresponding author/s.

ETHICS STATEMENT

The animal study was reviewed and approved by the Institutional Committee for the Care and Use of Experimental Animals (CICUAE-Resolution 046/2016).

AUTHOR CONTRIBUTIONS

MC: conceptualization, methodology, software, formal analysis, investigation, and writing—original draft. RR-V and DP: conceptualization, methodology, formal analysis, and investigation. JB: conceptualization, methodology, formal analysis, resources, writing-original draft, writing—review and editing, supervision, and funding acquisition. FH: conceptualization, investigation, resources, writing—review and editing, project administration, and funding acquisition. All authors contributed to the article and approved the submitted version.

FUNDING

This work was supported by funds granted by *Consejo Nacional de Investigaciones Científicas y Técnicas* (CONICET) (grant no. PIP-0273) to JB, *Agencia Nacional de Promoción Científica y Tecnológica* (ANPCyT) (grant no. PICT 2012-2983) to FH and (grant no. PICT 2017-4565) to JB, and *Instituto Nacional de Tecnología Agropecuaria* (INTA) (grant nos. PNSA 1115053, 5054: 20235, and 2019-PD-E5-I107-001-A017) to FH.

ACKNOWLEDGMENTS

We thank Dr. Robert J. Yamulla (Cornell SC Johnson School of Management, Ithaca, NY, United States) for English language improvements in the manuscript, Dr. Ignacio Gual for providing the sheep flock for the AI trial and Javier Mayorano, Dr. Alba Ledesma, and Dr. María Florencia Suqueli García for technical support. We also thank the Center for Vertebrate Genomics (CVG) from Cornell University, for the CVG leadership award granted to MC that helped cover publication costs.

REFERENCES

Alvarez, M., Anel-Lopez, L., Boixo, J. C., Chamorro, C., Neila-Montero, M., Montes-Garrido, R., et al. (2019). Current challenges in sheep artificial insemination: a particular insight. *Reprod. Domest. Anim.* 4, 32–40. doi: 10.1111/rda.13523

Baxter, F. A., and Drake, A. J. (2019). Non-genetic inheritance via the male germline in mammals. *Philos. Trans. R. Soc. B Biol. Sci.* 374:20180118. doi: 10.1098/rstb.2018.0118

Bernecic, N. C., Zhang, M., Gadella, B. M., Brouwers, J. F. H. M., Jansen, J. W. A., Arkesteijn, G. J. A., et al. (2019). BODIPY-cholesterol can be reliably used to monitor cholesterol efflux from capacitating mammalian spermatozoa. *Sci. Rep.* 9, 1–12. doi: 10.1038/s41598-019-45831-7

Björndahl, L., Söderlund, I., and Kvist, U. (2003). Evaluation of the one-step eosin-nigrosin staining technique for human sperm vitality assessment. *Hum. Reprod.* 18, 813–816. doi: 10.1093/humrep/deg199

Blanch, E., Tomás, C., Graham, J., and Mocé, E. (2012). Response of Boar Sperm to the Treatment with Cholesterol-Loaded Cyclodextrins Added Prior to Cryopreservation. *Reprod. Domest. Anim.* 47, 959–964. doi: 10.1111/j.1439-0531.2012.01999.x

Bligh, E. G., and Dyer, W. J. (1959). A rapid method of total lipid extraction and purification. *Can. J. Biochem. Physiol.* 37, 911–917. doi: 10.1139/o59-099

Carro, M. D. L. M., Peñalva, D. A., Antollini, S. S., Hozbor, F. A., and Buschiazzo, J. (2020). Cholesterol and desmosterol incorporation into ram sperm membrane before cryopreservation: effects on membrane biophysical properties and sperm quality. *Biochim. Biophys. Acta Biomembr.* 1862:183357. doi: 10.1016/j.bbamem.2020.183357

Chakrabarty, J., Banerjee, D., Pal, D., De, J., Ghosh, A., and Majumder, G. C. (2007). Shedding off specific lipid constituents from sperm cell membrane during cryopreservation. *Cryobiology* 54, 27–35. doi: 10.1016/j.cryobiol.2006.10.191

Cohen, R., Mukai, C., and Travis, A. J. (2016). Lipid regulation of acrosome exocytosis. *Adv. Anat. Embryol. Cell Biol.* 220, 107–127. doi: 10.1007/978-3-319-30567-7_6

Cormier, N., Sirard, M.-A., and Bailey, J. L. (1997). Premature capacitatin of bovine spermatozoa is initiated by cryopreservation. *J. Androl.* 18, 461–468. doi: 10.1002/j.1939-4640.1997.tb01953.x

Crichton, E. G., Malo, C., Pukazhenthi, B. S., Nagy, P., and Skidmore, J. A. (2016). Evaluation of cholesterol- treated dromedary camel sperm function by heterologous IVF and AI. *Anim. Reprod. Sci.* 174, 20–28. doi: 10.1016/j.anireprosci.2016.08.013

Cross, N. L. (2003). Decrease in Order of Human Sperm Lipids During Capacitation. *Biol. Reprod.* 69, 529–534. doi: 10.1095/biolreprod.102.013052

Cross, N. L., and Hanks, S. E. (1991). Effects of cryopreservation on human sperm acrosomes. *Hum. Reprod.* 6, 1279–1283. doi: 10.1093/oxfordjournals.humrep.a137526

Darin-Bennett, A., and White, I. G. (1977). Influence of the cholesterol content of mammalian spermatozoa on susceptibility to cold-shock. *Cryobiology* 14, 466–470. doi: 10.1016/0011-2240(77)90008-6

Davis, B. K. (1981). Timing of fertilization in mammals: sperm cholesterol/phospholipid ratio as a determinant of the capacitation interval (interspecies correlations/sperm cholesterol efflux/acrosome reaction). *Cell Biol.* 78, 7560–7564. doi: 10.1073/pnas.78.12.7560

De Castro, L. S., De Assis, P. M., Siqueira, A. F. P., Hamilton, T. R. S., Mendes, C. M., Losano, J. D. A., et al. (2016). Sperm oxidative stress is detrimental to embryo development: a dose-dependent study model and a new and more sensitive oxidative status evaluation. *Oxid. Med. Cell. Longev.* 2016:8213071. doi: 10.1155/2016/8213071

de Loos, F., van Vliet, C., van Maurik, P., and Kruip, T. A. M. (1989). Morphology of immature bovine oocytes. *Gamete Res.* 2, 197–204. doi: 10.1002/mrd.1120240207

Di Rienzo, J. A., Casanoves, F., Balzarini, M. G., Gonzalez, L., Tablada, M., and Robledo, C. W. (2014). *InfoStat. Grup. Infoestat, FCA*. Argentina: Univ. Nac. Córdoba.

Druart, X., Gatti, J. L., Huet, S., Dacheux, J. L., and Humblot, P. (2009). Hypotonic resistance of boar spermatozoa: sperm subpopulations and relationship with epididymal maturation and fertility. *Reproduction*. 137, 205–213. doi: 10.1530/REP-08-0225

Gadella, B., and Leahy, T. (2015). New insights into the regulation of cholesterol efflux from the sperm membrane. *Asian J. Androl.* 17, 561–7. doi: 10.4103/1008-682X.153309

Gadella, B. M., and Harrison, R. A. P. (2000). The capacitating agent bicarbonate induces protein kinase A-dependent changes in phospholipid transbilayer behavior in the sperm plasma membrane. *Development* 11, 2407–2420. doi: 10.1242/dev.127.11.2407

Gadella, B. M., Tsai, P. S., Boerke, A., and Brewis, I. A. (2008). Sperm head membrane reorganisation during capacitation. *Int. J. Dev. Biol.* 52, 473–480. doi: 10.1387/ijdb.082583bg

Gallego, V., Cavalcante, S. S., Fujimoto, R. Y., Carneiro, P. C. F., Azevedo, H. C., and Maria, A. N. (2017). Fish sperm subpopulations: changes after cryopreservation process and relationship with fertilization success in tambaqui (*Colossoma macropomum*). *Theriogenology* 1, 16–24. doi: 10.1016/j.theriogenology.2016.08.001

García-Alvarez, O., Maroto-Morales, A., Martínez-Pastor, F., Fernández-Santos, M., Esteso, M., Pérez-Guzmán, M., et al. (2009). Heterologous in vitro fertilization is a good procedure to assess the fertility of thawed ram

spermatozoa. *Theriogenology* 71, 643–650. doi: 10.1016/j.theriogenology.2008.09.036

Gillan, L., and Maxwell, W. M. C. (1999). The functional integrity and fate of cryopreserved ram spermatozoa in the female tract. *J. Reprod. Fertil.* 54, 271–283. doi: 10.1071/rd99074

Green, C. E., and Watson, P. F. (2001). Comparison of the capacitation-like state of cooled boar spermatozoa with true capacitation. *Reproduction* 122, 889–898. doi: 10.1530/rep.0.1220889

Holt, W. V. (2000). Fundamental aspects of sperm cryobiology: the importance of species and individual differences. *Theriogenology* 53, 47–58. doi: 10.1016/S0093-691X(99)00239-3

Hölttä-Vuori, M., Sezgin, E., Eggeling, C., and Ikonen, E. (2016). Use of BODIPY-Cholesterol (TF-Chol) for Visualizing Lysosomal Cholesterol Accumulation. *Traffic* 17, 1054–1057. doi: 10.1111/tra.12414

Jansen, M., Wang, W., Greco, D., Bellenchi, G. C., Di Porzio, U., Brown, A. J., et al. (2013). What dictates the accumulation of desmosterol in the developing brain? *FASEB J.* 27, 865–870. doi: 10.1096/fj.12-211235

Keber, R., Rozman, D., and Horvat, S. (2013). Sterols in spermatogenesis and sperm maturation. *J. Lipid Res.* 54, 20–33. doi: 10.1194/jlr.R032326

La Spina, F. A., Puga Molina, L. C., Romarowski, A., Vitale, A. M., Falzone, T. L., Krapf, D., et al. (2016). Mouse sperm begin to undergo acrosomal exocytosis in the upper isthmus of the oviduct. *Dev. Biol.* 41, 172–182. doi: 10.1016/j.ydbio.2016.02.006

Laemmli, U. K. (1970). Cleavage of structural proteins during the assembly of the head of bacteriophage T4. *Nature* 227, 680–685. doi: 10.1038/227680a0

Le Blévec, E., Muroňová, J., Ray, P. F., and Arnoult, C. (2020). Paternal epigenetics: mammalian sperm provide much more than DNA at fertilization. *Mol. Cell. Endocrinol.* 518:110964. doi: 10.1016/j.mce.2020.110964

Leahy, T., and Gadella, B. M. (2011). Sperm surface changes and physiological consequences induced by sperm handling and storage. *Reproduction* 142, 759–778. doi: 10.1530/REP-11-0310

Ledesma, A., Zalazar, L., Fernández-Alegre, E., Hozbor, F., Cesari, A., and Martínez-Pastor, F. (2017). Seminal plasma proteins modify the distribution of sperm subpopulations in cryopreserved semen of rams with lesser fertility. *Anim. Reprod. Sci.* 184, 44–50. doi: 10.1016/j.anireprosci.2017.06.015

McClean, R. V., Holt, W. V., and Johnston, S. D. (2007). Ultrastructural observations of cryoinjury in kangaroo spermatozoa. *Cryobiology* 54, 271–280. doi: 10.1016/j.cryobiol.2007.03.004

Mocé, E., Blanch, E., Tomás, C., and Graham, J. K. (2010a). Use of cholesterol in sperm cryopreservation: present moment and perspectives to future. *Reprod. Domest. Anim.* 45, 57–66. doi: 10.1111/j.1439-0531.2010.01635.x

Mocé, E., Purdy, P. H., and Graham, J. K. (2010b). Treating ram sperm with cholesterol-loaded cyclodextrins improves cryosurvival. *Anim. Reprod. Sci.* 118, 236–247. doi: 10.1016/j.anireprosci.2009.06.013

Moore, A. I., Squires, E. L., and Graham, J. K. (2005). Adding cholesterol to the stallion sperm plasma membrane improves cryosurvival. *Cryobiology* 51, 241–249. doi: 10.1016/j.cryobiol.2005.07.004

Moraes, E. A., Graham, J. K., Torres, C. A. A., Meyers, M., and Spizziri, B. (2010). Delivering cholesterol or cholestanol to bull sperm membranes improves cryosurvival. *Anim. Reprod. Sci.* 118, 148–154. doi: 10.1016/j.anireprosci.2009.08.002

Motamedi-Mojdehi, R., Roostaei-Ali Mehr, M., and Rajabi-Toustani, R. (2014). Effect of different levels of glycerol and cholesterol-loaded cyclodextrin on cryosurvival of ram spermatozoa. *Reprod. Domest. Anim.* 49, 65–70. doi: 10.1111/rda.12225

Müller, K., Müller, P., Pincemy, G., Kurz, A., and Labbe, C. (2008). Characterization of Sperm Plasma Membrane Properties after Cholesterol Modification: consequences for Cryopreservation of Rainbow Trout Spermatozoa1. *Biol. Reprod.* 78, 390–399. doi: 10.1095/biolreprod.107.064253

Nagy, S., Jansen, J., Topper, E. K., and Gadella, B. M. (2003). A Triple-Stain Flow Cytometric Method to Assess Plasma- and Acrosome-Membrane Integrity of Cryopreserved Bovine Sperm Immediately after Thawing in Presence of Egg-Yolk Particles1. *Biol. Reprod.* 68, 1828–1835. doi: 10.1095/biolreprod.102.011445

Nimmo, M. R., and Cross, N. L. (2003). Structural Features of Sterols Required to Inhibit Human Sperm Capacitation. *Biol. Reprod.* 68, 1308–1317. doi: 10.1095/biolreprod.102.008607

Nur, Z., Zik, B., Ustuner, B., Sagirkaya, H., and Ozguden, C. G. (2010). Effects of different cryoprotective agents on ram sperm morphology and DNAintegrity. *Theriogenology* 73, 1267–1275. doi: 10.1016/j.theriogenology.2009.12.007

Okabe, M. (2016). The Acrosome Reaction: a Historical Perspective. *Adv. Anat. Embryol. cell Biol.* 220, 1–13. doi: 10.1007/978-3-319-30567-7_1

Ortega-Ferrusola, C., Anel-López, L., Martín-Muñoz, P., Ortíz-Rodríguez, J. M., Gil, M. C., Alvarez, M., et al. (2017). Computational flow cytometry reveals that cryopreservation induces spermptosis but subpopulations of spermatozoa may experience capacitation-like changes. *Reproduction* 153, 293–304. doi: 10.1530/REP-16-0539

Ozaki, T., Takahashi, K., Kanasaki, H., and Miyazaki, K. (2002). Evaluation of acrosome reaction and viability of human sperm with two fluorescent dyes. *Arch. Gynecol. Obstet.* 266, 114–117. doi: 10.1007/s004040000112

Parks, J. E., and Hammerstedt, R. H. (1985). Development changes occurring in the lipids of ram epididymal spermatozoa plasma membrane. *Biol. Reprod.* 32, 653–668. doi: 10.1095/biolreprod32.3.653

Pérez-Cerezales, S., Martínez-Páramo, S., Beirão, J., and Herráez, M. P. (2010). Fertilization capacity with rainbow trout DNA-damaged sperm and embryo developmental success. *Reproduction* 139, 989–997. doi: 10.1530/REP-10-0037

Peris-Frau, P., Álvarez-Rodríguez, M., Martín-Maestro, A., Iniesta-Cuerda, M., Sánchez-Ajofrín, I., Medina-Chávez, D. A., et al. (2021). Unravelling how *in vitro* capacitation alters ram sperm chromatin before and after cryopreservation. *Andrology* 9, 414–425. doi: 10.1111/andr.12900

Pommer, A. C., Rutllant, J., and Meyers, S. A. (2003). Phosphorylation of Protein Tyrosine Residues in Fresh and Cryopreserved Stallion Spermatozoa under Capacitating Conditions1. *Biol. Reprod.* 68, 1208–1214. doi: 10.1095/biolreprod.102.011106

Purdy, P., and Graham, J. (2004). Effect of Adding Cholesterol to Bull Sperm Membranes on Sperm Capacitation, the Acrosome Reaction, and Fertility1. *Biol. Reprod.* 71, 522–527. doi: 10.1095/biolreprod.103.025577

Purdy, P. H., Mocé, E., Stobart, R., Murdoch, W. J., Moss, G. E., Larson, B., et al. (2010). The fertility of ram sperm held for 24 h at 5°C prior to cryopreservation. *Anim. Reprod. Sci.* 118, 231–235. doi: 10.1016/j.anireprosci.2009.06.014

Robinson, J. J., McKelvey, W. A. C., King, M. E., Mitchell, S. E., Mylne, M. J. A., McEvoy, T. G., et al. (2011). Traversing the ovine cervix - A challenge for cryopreserved semen and creative science. *Animal* 5, 1791–1804. doi: 10.1017/S1751731111000978

Romarowski, A., Battistone, M. A., La Spina, F. A., Puga Molina, L., del, C., Luque, G. M., et al. (2015). PKA-dependent phosphorylation of LIMK1 and Cofilin is essential for mouse sperm acrosomal exocytosis. *Dev. Biol.* 405, 237–249. doi: 10.1016/j.ydbio.2015.07.008

Salmon, V. M., Castonguay, F., Demers-Caron, V., Leclerc, P., and Bailey, J. L. (2017). Cholesterol-loaded cyclodextrin improves ram sperm cryoresistance in skim milk-extender. *Anim. Reprod. Sci.* 177, 1–11. doi: 10.1016/j.anireprosci.2016.11.011

Schindelin, J., Arganda-carreras, I., Frise, E., Kaynig, V., Longair, M., Pietzsch, T., et al. (2012). Fiji?: an open-source platform for biological-image analysis. *Nat. Methods* 9, 676–682. doi: 10.1038/nmeth.2019

Sedó, C. A., Bilinski, M., Lorenzi, D., Uriondo, H., Noblía, F., Longobucco, V., et al. (2017). Effect of sperm DNA fragmentation on embryo development: clinical and biological aspects. *J. Bras. Reprod. Assist.* 21, 343–350. doi: 10.5935/1518-0557.20170061

Sieme, H., Oldenhof, H., and Wolkers, W. F. (2015). Sperm Membrane Behaviour during Cooling and Cryopreservation. *Reprod. Domest. Anim.* 3, 20–26. doi: 10.1111/rda.12594

Simon, L., Murphy, K., Shamsi, M. B., Liu, L., Emery, B., Aston, K. I., et al. (2014). Paternal influence of sperm DNA integrity on early embryonic development. *Hum. Reprod.* 29, 2402–2412. doi: 10.1093/humrep/deu228

Spencer, T. E., Johnson, G. A., Burghardt, R. C., and Bazer, F. W. (2004). Progesterone and placental hormone actions on the uterus: insights from domestic animals. *Biol. Reprod.* 71, 2–10. doi: 10.1095/biolreprod.103.024133

Spizziri, B. E., Fox, M. H., Bruemmer, J. E., Squires, E. L., and Graham, J. K. (2010). Cholesterol-loaded-cyclodextrins and fertility potential of stallions spermatozoa. *Anim. Reprod. Sci.* 118, 255–264. doi: 10.1016/j.anireprosci.2009.08.001

Stuppia, L., Franzago, M., Ballerini, P., Gatta, V., and Antonucci, I. (2015). Epigenetics and male reproduction: the consequences of paternal lifestyle on fertility, embryo development, and children lifetime health. *Clin. Epigenetics* 71, 2–10. doi: 10.1186/s13148-015-0155-4

Thurston, L. M., Watson, P. F., and Holt, W. V. (1999). Sources of variation in the morphological characteristics of sperm subpopulations assessed objectively by a novel automated sperm morphology analysis system. *J. Reprod. Fertil.* 117, 271–280. doi: 10.1530/jrf.0.1170271

Treulen, F., Arias, M. E., Aguila, L., Uribe, P., and Felmer, R. (2018). Cryopreservation induces mitochondrial permeability transition in a bovine sperm model. *Cryobiology* 83, 65–74. doi: 10.1016/j.cryobiol.2018.06.001

Vainio, S., Jansen, M., Koivusalo, M., Róg, T., Karttunen, M., Vattulainen, I., et al. (2006). Significance of sterol structural specificity: desmosterol cannot replace cholesterol in lipid rafts. *J. Biol. Chem.* 281, 348–355. doi: 10.1074/jbc.M509530200

Valcarce, D. G., Cartón-García, F., Riesco, M. F., Herráez, M. P., and Robles, V. (2013). Analysis of DNA damage after human sperm cryopreservation in genes crucial for fertilization and early embryo development. *Andrology* 1, 723–730. doi: 10.1111/j.2047-2927.2013.00116.x

Watanabe, H., and Kondoh, G. (2011). Mouse sperm undergo GPI-anchored protein release associated with lipid raft reorganization and acrosome reaction to acquire fertility. *J. Cell Sci.* 124, 2573–2581. doi: 10.1242/jcs.086967

Conflict of Interest: The authors declare that the research was conducted in the absence of any commercial or financial relationships that could be construed as a potential conflict of interest.

frontiers in Cell and Developmental Biology

ORIGINAL RESEARCH
published: 16 July 2021
doi: 10.3389/fcell.2021.673961

Protein Identification of Spermatozoa and Seminal Plasma in Bottlenose Dolphin (*Tursiops truncatus*)

*Mari-Carmen Fuentes-Albero[1,2], Leopoldo González-Brusi[3], Paula Cots[3], Chiara Luongo[2], Silvia Abril-Sánchez[2], José Luis Ros-Santaella[4], Eliana Pintus[4], Sara Ruiz-Díaz[5], Carlos Barros-García[1], María-Jesús Sánchez-Calabuig[5,6], Daniel García-Párraga[1,7], Manuel Avilés[3], Mª José Izquierdo Rico[3] and Francisco Alberto García-Vázquez[2]**

[1] Department of Biology, Avanqua-Oceanogràfic S.L, Valencia, Spain, [2] Department of Physiology, Faculty of Veterinary Science, University of Murcia, Murcia, Spain, [3] Department of Cell Biology and Histology, Faculty of Medicine, University of Murcia, Murcia, Spain, [4] Department of Veterinary Sciences, Faculty of Agrobiology, Food and Natural Resources, Czech University of Life Sciences Prague, Prague, Czechia, [5] Department of Animal Reproduction, National Agricultural and Food Research and Technology Institute (INIA), Madrid, Spain, [6] Department of Medicine and Surgery, Faculty of Veterinary Science, Madrid, Spain, [7] Research Department, Fundación Oceanogràfic, Valencia, Spain

Proteins play an important role in many reproductive functions such as sperm maturation, sperm transit in the female genital tract or sperm-oocyte interaction. However, in general, little information concerning reproductive features is available in the case of aquatic animals. The present study aims to characterize the proteome of both spermatozoa and seminal plasma of bottlenose dolphins (*Tursiops truncatus*) as a model organism for cetaceans. Ejaculate samples were obtained from two trained dolphins housed in an aquarium. Spermatozoa and seminal plasma were analyzed by means of proteomic analyses using an LC-MS/MS, and a list with the gene symbols corresponding to each protein was submitted to the DAVID database. Of the 419 proteins identified in spermatozoa and 303 in seminal plasma, 111 proteins were shared by both. Furthermore, 70 proteins were identified as involved in reproductive processes, 39 in spermatozoa, and 31 in seminal plasma. The five most abundant proteins were also identified in these samples: AKAP3, ODF2, TUBB, GSTM3, ROPN1 for spermatozoa and CST11, LTF, ALB, HSP90B1, PIGR for seminal plasma. In conclusion, this study provides the first characterization of the proteome in cetacean sperm and seminal plasma, opening the way to future research into new biomarkers, the analysis of conservation capacity or possible additional applications in the field of assisted reproductive technologies.

Keywords: cetacean, proteomic analyses, semen, sperm cells, seminal plasma

OPEN ACCESS

Edited by:
Ana Josefa Soler, University of Castilla-La Mancha, Spain

Reviewed by:
Micaela Cerletti, National University of Mar del Plata, Argentina
Lucia Zalazar, Instituto de Investigaciones Biológicas, Consejo Nacional de Investigaciones Científicas y Técnicas, Argentina

****Correspondence:***
Francisco Alberto García-Vázquez
fagarcia@um.es

Specialty section:
This article was submitted to Cell Growth and Division, a section of the journal Frontiers in Cell and Developmental Biology

Received: *28 February 2021*
Accepted: *28 May 2021*
Published: *16 July 2021*

Citation:
Fuentes-Albero M-C, González-Brusi L, Cots P, Luongo C, Abril-Sánchez S, Ros-Santaella JL, Pintus E, Ruiz-Díaz S, Barros-García C, Sánchez-Calabuig M-J, García-Párraga D, Avilés M, Izquierdo Rico MJ and García-Vázquez FA (2021) Protein Identification of Spermatozoa and Seminal Plasma in Bottlenose Dolphin (Tursiops truncatus). Front. Cell Dev. Biol. 9:673961. doi: 10.3389/fcell.2021.673961

INTRODUCTION

Cetaceans, aquatic mammals from the Cetacea infraorder, are considered essential for marine ecosystems (Bowen, 1997; Uhen, 2007). Their populations are under enormous anthropogenic pressure, especially as a result of commercial overfishing, incidental captures in fisheries, and habitat degradation (Reeves et al., 2003; Parsons et al., 2014; Dolman and Brakes, 2018).

Indeed, many cetacean species are threatened or in danger of extinction (Davidson et al., 2012). This is why cetaceans are protected under many national, regional and international legislations including Appendix II of the Convention on International Trade in Endangered Species of Wild Fauna and Flora (CITES), which limits the movement of animals or their products between countries. However, study of their populations in the wild involves many limitations (Bowen, 1997; O'Brien and Robeck, 2010) and, in most cases, it is not possible to keep individuals in captivity due to their size, their gregarious population structure or other peculiarities of their ethology that make their *ex situ* maintenance highly difficult or almost impossible. Only some species, such as *Tursiops truncatus*, the common bottlenose dolphin, have a docile character and the ability to adapt well to captivity, which makes them ideal model organisms (Barratclough et al., 2019). Moreover, important information can be obtained from *ex situ* populations in order to deepen our knowledge of their features for conservation programs, but also to extrapolate the obtained knowledge to address problems related with other cetacean species (Barratclough et al., 2019).

During recent decades, aquariums and animal conservation centers have actively contributed to the conservation and reproduction of bottlenose dolphins through joint breeding programs (Katsumata, 2010). Initially, the movement and exchange of animals for reproductive purposes between centers was necessary, but this activity entailed certain risks that could affect the integrity of the animals (O'Brien and Robeck, 2010). Subsequently, the progress made in assisted reproductive technologies (ARTs) allowed the collection and management of gametes, thus ensuring their quality to maximize fertilization (Beirão et al., 2019). In order to minimize any impact on animal welfare, voluntary semen collection techniques through animal training have been routinely established in dolphin populations under human care (Robeck and O'Brien, 2004; Robeck et al., 2005). The collection of semen facilitates research activity and the exchange of reproductive cells between geographically distant centers for further use in artificial insemination programs (Robeck et al., 2005). For that purpose, methods based on refrigeration (Takenaka et al., 2013; Ruiz-Díaz et al., 2020) and freezing (Robeck and O'Brien, 2004; Robeck et al., 2013; Sánchez-Calabuig et al., 2015b, 2017) have been developed for dolphins, including techniques for preservation of seminal samples that have allowed the creation of a gene bank of high biological value for use in the future (Holt and Pickard, 1999).

A knowledge of the semen characteristics of a species of interest is essential to gain new insights, either to widen fundamental basic studies or for further application in ARTs. Semen is composed of the cellular part, the spermatozoa, and the liquid part, the seminal plasma. Bottlenose dolphin spermatozoa are known to have a long tail, a short but hydrodynamic head shape and a bulky midpiece (van der Horst et al., 2018), these high quality features being kept after collection (van der Horst et al., 2018; Ruiz-Díaz et al., 2020). Seminal plasma is a fluid coming mostly from the prostate, the only sexual accessory gland described in cetaceans (Harrison et al., 1969; Rommel et al., 2007; Suárez-Santana et al., 2020). The complex composition of seminal plasma plays a key role in both the male and female reproductive features of mammals. In the case of males, seminal plasma is involved in sperm maturation, motility, transport, capacitation or acrosome reaction (reviewed by Juyena and Stelletta, 2012). When the seminal plasma is deposited in the female genital tract, it affects the inflammatory and immune responses (reviewed by Bromfield, 2018), protecting sperm (Kawano et al., 2014; Luongo et al., 2019), and even having an impact on the offspring (Bromfield et al., 2014). Furthermore, it has been demonstrated that the proteins of reproductive fluids (including oviductal and uterine fluids, and seminal plasma) are involved in the interaction with the sperm proteome (Luongo et al., 2020; Rickard and de Graaf, 2020).

Proteomic analysis has been used to describe the sperm and seminal plasma proteome either in non-mammal species, such as fish (Ciereszko et al., 2017; Dietrich et al., 2017), and in mammals, such as murine (Baker et al., 2008; Vicens et al., 2017), porcine (Perez-Patiño et al., 2016; Recuero et al., 2019; Luongo et al., 2020), equine (Swegen et al., 2015; Guasti et al., 2020), ovine (Cardozo et al., 2006; Pini et al., 2016), caprine (Pinto et al., 2019; Zhu et al., 2020; Martínez-Fresneda et al., 2021), bovine (Peddinti et al., 2008; Byrne et al., 2012), non-human primates (Skerget et al., 2013), and human (Martínez-Heredia et al., 2006), but not yet in any cetacean species. Furthermore, such studies have permitted the identification of proteins that can act as biomarkers of fertility (Dacheux et al., 2012; Li et al., 2016; Rahman et al., 2017; Druart and de Graaf, 2018; Pérez-Patiño et al., 2018; Druart et al., 2019), their relevance for sperm preservation (Soleilhavoup et al., 2014; Parrilla et al., 2019; Peris-Frau et al., 2019; Ryu et al., 2019; Bajuk et al., 2020; De Lazari et al., 2020) or involvement in sperm functional traits (Intasqui et al., 2016; Bezerra et al., 2019; De Lazari et al., 2019). Moreover, seminal plasma proteins are influenced by the social and competitive environment (Ramm, 2014; Mead, 2018; Hopkins et al., 2019). Therefore, knowing the protein profile of semen dolphins may be especially relevant to better understand the biology of the species in light of the complex multi-male mating strategy of bottlenose dolphins.

Finally, knowing the proteome of ejaculated spermatozoa and seminal plasma may contribute to obtaining comprehensive information and to understanding functional implications for reproductive processes not only for dolphin species but for cetaceans in general. For this reason, this study aims to identify, describe, and classify for the first time, the sperm and seminal plasma proteins of dolphins and to compare them with the protein profiles in other species (bovine, canine, and human) previously described in the literature.

MATERIALS AND METHODS

Ethics of Experimentation

The samples were obtained from two trained dolphin males housed at the Oceanogràfic de Valencia following the Animal Care Protocol and policies of the aquarium. The animals were conditioned through positive reinforcement to participate in many different medical behaviors, including semen collection to provide basic husbandry care. Semen samples were obtained

through training following the same approach as previously published (Sánchez-Calabuig et al., 2017). Furthermore, the regulations and policies of EU legislation, Directive 2010/63/EU[1], were observed.

Animals

Semen samples were obtained from two adult males, who have lived in the same dolphin group since 2003. The estimated ages of both animals were 32 years (Male 1) and 27 years (Male 2) at the moment of the study. Both males live together with a stable social group in an outdoor pool that contains salty water at a temperature of 18–26°C. Both males successfully had previously sired several offspring. Their diet is based on frozen-thawed whole fish (herring-*Clupea harengus*, capelin-*Mallotus villosus*, blue whiting-*Micromesistius poutassou*, mackerel-*Scomber scombrus*, smelt-*Osmeridae*, squid-*Loligo* sp. and European sprat-*Sprattus sprattus*).

Semen Collection

Two ejaculates from each male were obtained by favoring extraction in the ventrum in an above water level position. The animals always collaborated with the trainers, who, through acoustic and tactile signals, favored extraction of the penis. The stimulation, which lasted a few seconds, ended in ejaculation. Sample was collected in a sterile LLDPE (linear low-density polyethylene) plastic bag (Sánchez-Calabuig et al., 2017). After collection, the following parameters were evaluated for each semen sample (as previously described by Ruiz-Díaz et al., 2020): pH, concentration (number of sperm/ml), total (%) and progressive motility (%) (evaluated by CASA system; 25 frames per second, and at least five random fields per sample), and viability (%) (200 spermatozoa per sample) (**Table 1**). All the samples were collected within 1 month (the days between sample extractions were 6 and 30 for Male 1 and Male 2, respectively).

Protein Extraction

The proteomic analysis was performed in the proteomics facility of SCSIE, University of Valencia which forms part of ProteoRed, PRB2-ISCIII, supported by grant PT13/0001. Semen samples were centrifugated at 800 × *g* for 5 min at 4°C to split the sample into two fractions (spermatozoa and seminal plasma). The fraction containing spermatozoa was washed twice (800 × *g* for 5 min, 4°C) in phosphate-buffered saline (PBS, Sigma-Aldrich®, Madrid, Spain) and the pellet was re-suspended in lysis buffer (50 mM Tris–HCl pH 8, 10 mM DTT and 2% SDS). The mixture was sonicated for 5 min, centrifuged 5 min at 15,870 × *g* and the resulting supernatant was transferred to a fresh microfuge tube (**Figure 1**). The seminal plasma was centrifuged twice (800 × *g* for 5 min, 4°C) to remove any remaining spermatozoa (microscopically verified).

The protein concentration obtained from both, spermatozoa and seminal plasma samples, was determined by Protein Quantification Assay Kit (Macherey-Nagel, Düren, Germany) according to the manufacturer's instructions. Twenty micrograms of protein were adjusted to a 40 μl final volume with Laemmli Sample buffer (Bio-Rad, Hercules, CA, United States) with 2–5% β-mercaptoethanol.

1D PAGE

The sample was denatured at 95°C for 5 min and then loaded into a 1D PAGE. Electrophoresis was performed using a 12% precast gel (Bio-Rad, Hercules, CA, United States) at 200 V for 5 min. Then, the gel was fixed with 40% ethanol/10% acetic acid for 1 h, stained with colloidal Coomassie (Bio-Rad, Hercules, CA, United States) for 1 h and scanned by Image Scanner (GE Healthcare).

In Gel Protein Digestion

The gel slide was digested with sequencing grade trypsin (Promega, Madison, WI, United States) as described elsewhere (Shevchenko et al., 1996). Briefly, isolated proteins were digested with trypsin (500 ng) at 37°C overnight. The digestion was quenched with 10% trifluoroacetic acid (TFA) at final concentration of 1%. And, after double extraction with neat acetonitrile (ACN), the peptide mixtures were dried in a rotary evaporator and resuspended with 20 μl of 2% ACN, 0.1% TFA.

Mass Spectrometry Analysis and Protein Identification

For liquid chromatography and tandem mass spectrometry (LC–MS/MS), 3 μl of a peptide mixture sample was loaded onto a trap column (3 μm C18-CL, 350 μm × 0.5 mm; Eksigent, CA, United States) and desalted with 0.1% TFA at 5 μl/min for 5 min. The peptides were then loaded onto an analytical column (3 μm C18-CL 120 Å, 0.075 × 150 mm; Eksigent, CA, United States) equilibrated with 5% ACN and 0.1% formic acid (FA). Elution was carried out with a linear gradient of 5–40% B in A for 45 min (A: 0.1% FA; B: ACN, 0.1% FA) at a flow rate of 300 nl/min. Peptides were analyzed in a nanoESIqQTOF mass spectrometer (6600plus TripleTOF, ABSciex, MA, United States).

Samples were ionized in a Source Type: Optiflow < 1 μl Nanoapplying 3.0 kV to the spray emitter at 200°C. Analysis was carried out in data-dependent mode. Survey MS1 scans were acquired from 350 to 1,400 m/z for 250 ms. The quadrupole resolution was set to "LOW" for MS2 experiments, which were acquired at 100–1,500 m/z for 25 ms in "high sensitivity" mode. The following switch criteria were used: charge 2+ to 4+; minimum intensity, 250 counts per second (cps). Up to 100 ions were selected for fragmentation after each survey scan. Dynamic exclusion was set to 15 s. The system sensitivity was controlled by analyzing 0.5 μg of K562 trypsin digestion (Sciex). Two thousand, eight hundred and seventy proteins were identified (FDR < 1%) in these conditions in a 45 min gradient.

Data were processed with ProteinPilot v. 5.0 (AB Sciex, Framingham, MA, United States), using the default parameters to generate a peak list directly from 6600 plus TripleTofwiff files. The Paragon algorithm (Shilov et al., 2007) of ProteinPilot v. 5.0 was used to search the Uniprot *Delphinidae* database (v 02.2020; 3513001 proteins in database) with the following parameters: Trypsin enzyme specificity, taxonomy non-restricted, and the search effort was set to rapid.

[1]https://eur-lex.europa.eu/legal-content/EN/TXT/?uri=CELEX:32010L0063

TABLE 1 | Seminal parameters of bottlenose dolphin males (*Tursiops truncatus*) used for proteomic analysis.

Parameters	Male 1			Male 2			Mean[2]
	S1	S2	Mean[1]	S1	S2	Mean[1]	
Concentration ($\times 10^6$ sperm/ml)	570.0	780.0	675.0 ± 148.5	200.0	770.0	485.0 ± 403.1	580.0 ± 289.2
pH	8.0	7.0	7.5 ± 0.7	7.5	7.0	7.2 ± 0.4	7.4 ± 0.5
Viability (%)	95.0	92.0	93.5 ± 1.1	88.0	90.0	89.0 ± 0.7	91.2 ± 1.5
Total motility (%)	69.0	77.0	73.0 ± 2.8	88.0	98.0	93.0 ± 3.5	83.0 ± 6.3
Progressive motility (%)	36.0	35.0	35.5 ± 0.4	24.0	29.0	26.5 ± 1.8	31.0 ± 2.8

S1 and S2 indicate sample 1 and sample 2, respectively.
[1]Represents the mean of S1 and S2 for each male.
[2]Represents the mean including the samples (S1 and S2) from both males. Mean data for concentration and pH are expressed as mean ± SD (standard deviation). Mean data for viability, total motility and progressive motility are expressed as mean ± SEM (standard error of the mean).

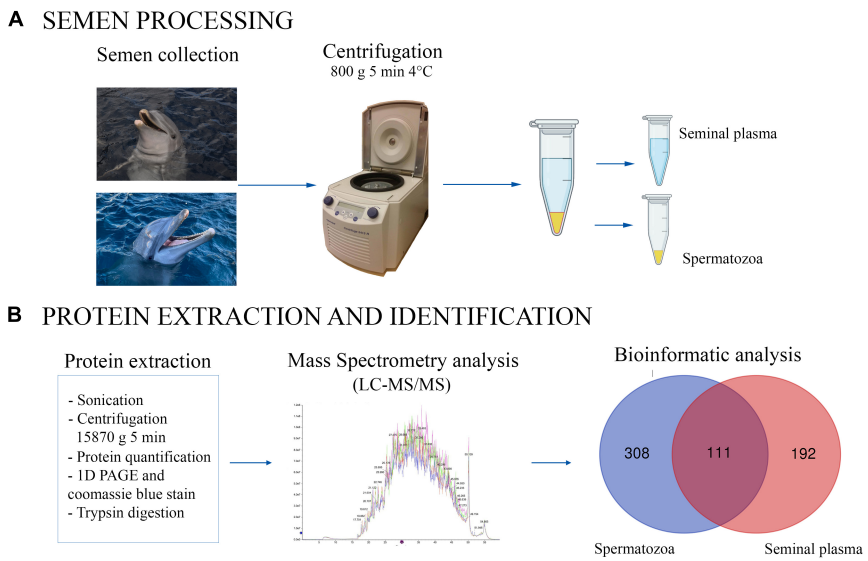

FIGURE 1 | Graphical representation of experimental process for bottlenose dolphin semen processing **(A)** and protein extraction and identification **(B)**. The Venn diagram shows the proteins found to be common (or not) to seminal plasma and spermatozoa.

Protein Identification

Protein Orthologs Identification

Uncharacterized proteins with no properly assigned gene symbol accounted for 15–25% of the proteins within each sample. To identify a direct ortholog for each uncharacterized protein, the proteins were filtered with a custom script written in Python (**Supplementary File 1**) making use of libraries Bio.Blast (Cock et al., 2009) SeqIO, StrinGIO and pandas. In essence, the algorythm performed parallel queries with the uncharacterized proteins against a database made with "makeblastdb" from a UniProt fasta database made by merging the Swissprot curated database with the *T. truncatus* TrEMBL dataset (release 2020_02). Candidate orthologs were then ranked from maximum to minimum sequence identity and those with a sequence identity within 5% of the maximum were selected. The results were then manually curated, reducing the uncharacterized proteins to 0.2–1% of the proteins within each sample. In some cases, it was not possible to distinguish the direct ortholog within the candidates (the case with several keratins) and thus the proteins where omitted from the biological annotation.

Biological Annotation

For the biological annotation, only the proteins identified in all the samples (seminal plasma or spermatozoa) were analyzed. A list with the gene symbols corresponding to each protein was submitted to DAVID [v6.8 (Huang et al., 2009)]. Because of the performance querying *versus* the *T. truncatus* database was very poor, the queries were made with the *Homo sapiens* database, as it is the best annotated organism. Unmapped IDs were checked for synonyms in GeneCard in order to avoid losing information by selecting those identifiers present in DAVID (which were not always the HGNC ones). All the Gene Ontology terms with a FDR < 0.01 were selected and classified into the three categories "biological process," "cellular component," and "molecular process."

The mass spectrometry proteomics data have been deposited to the ProteomeXchange Consortium via the PRIDE

(Perez-Riverol et al., 2019) partner repository with the dataset identifier PXD024588.

RESULTS

A total of 722 different proteins in seminal plasma and spermatozoa were identified in each of the four samples analyzed): 419 proteins in spermatozoa, and 303 in seminal plasma, of which 111 proteins were common to both, spermatozoa and seminal plasma (**Figure 1**). The total list of identified proteins for each analyzed sample (two per male) is shown in **Supplementary File 2** (sperm proteins) and **Supplementary File 3** (seminal plasma proteins). Moreover, the **Supplementary File 4** shows the list of the common proteins between spermatozoa and seminal plasma.

Since bovids and cetaceans are evolutionarily related (Vislobokova, 2013), belonging to the order Cetartiodactyla, a bovine dataset (Ramesha et al., 2020) was compared with dolphin. In addition, human as a biological model (Batruch et al., 2011; Baker et al., 2013; Amaral et al., 2014) and dogs (canids) (Aquino-Cortez et al., 2017; Araujo et al., 2020), because their only accessory sex gland is the prostate, as in dolphins, were also included in the comparison. The four species were therefore retrieved to evaluate the proteome profile of bottlenose dolphin spermatozoa and seminal plasma, resulting in the Venn diagram of **Figure 2**. The analysis revealed that 42 were identified in the spermatozoa of all four species, and 30 in the seminal plasma of the same. The number of co-present sperm proteins between animals were the following: (i) bull and dolphin, 362; (ii) man and dolphin, 375; and (iii) dog and dolphin, 58. The number of co-present seminal proteins were: (i) bull and dolphin, 218; (ii) man and dolphin, 213; and (iii) dog and dolphin, 51. These proteins are listed in **Supplementary File 5** (sperm) and **Supplementary File 6** (seminal plasma).

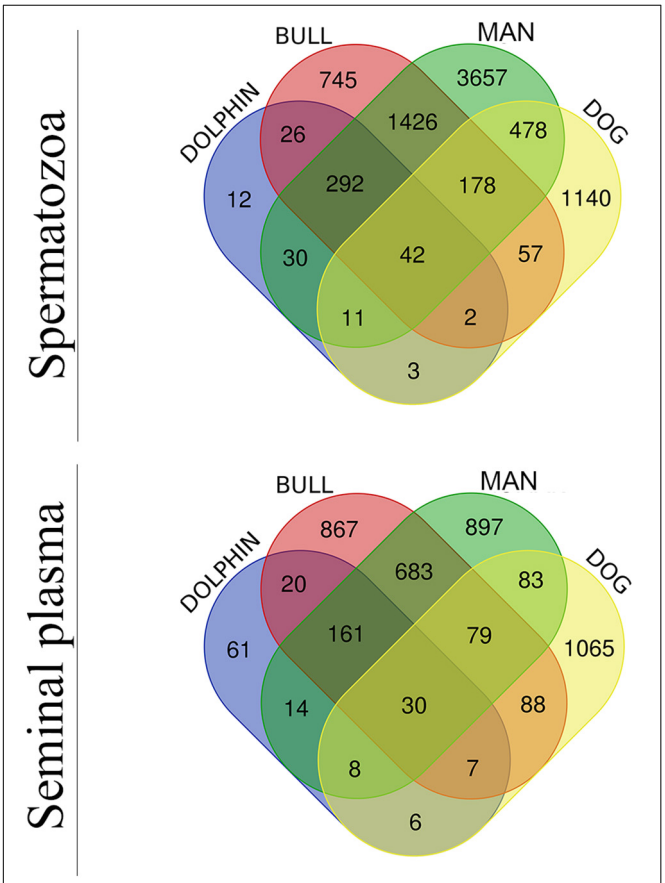

FIGURE 2 | Venn diagram of sperm (upper diagram) and seminal plasma (lower diagram) proteomes of man, bull, dog and dolphin.

Protein Profile of Bottlenose Dolphin Spermatozoa

As already mentioned, a total of 419 proteins were present in the spermatozoa of the four samples analyzed (two from each male). A complete protein list (ordered by the number of peptides) for the spermatozoa accompanied by the protein name, String ID dolphin, peptides, mean protein score (±SD), preferred name and annotation (*H. sapiens*) is presented in **Supplementary File 7**. A detailed search was carried out in the STRING database v 11.0[2] to obtain a description of the functions related with each of the proteins. The following cases were observed: (i) Proteins described for *T. truncatus* (269 proteins, 63.9%); (ii) Proteins described for *H. sapiens* (416 proteins, 99.3%); and (iii) Proteins not described in either of the above (3 proteins, 0.7%). Of the proteins belonging to the third case, one is described for *Mus musculus* (ADAM5), one in *Pan paniscus* (LRRC37A5P) and the other one has no description for any species (ATP6V1FNB).

A functional annotation of the proteins from *H. sapiens* sperm was peformed using DAVID software and divided into different categories: "Biological processes" (BP), "Cellular components" (CC), and "Molecular functions" (MF) (**Figure 3** and **Supplementary File 8**). Although there are different categories for each of the divisions made, the most abundant were those involved in oxidation-reduction processes (8.4%), spermatogenesis (6%), and protein folding (6%) in the case of BP (**Figure 3A**); extracellular exosome (41.6%), nucleus (36.3%), and mitochondrion (35.3%) in the case of CC (**Figure 3B**); and ATPbinding proteins (14.2%), ATPase activity (5.5%), and unfolded protein binding (5.3%) for MF (**Figure 3C**).

Of the total of 419 proteins identified in the spermatozoa, 39 are linked to sperm function categories (**Table 2**) such as cilia/flagela (17 proteins, 43.6%), sperm motility (10 proteins, 25.6%), capacitation and acrosome reaction (4 proteins, 10.3%), sperm-egg fusion (4 proteins, 10.3%), spermatogenesis and fertilization (2 proteins, 5.1%), and other functions (2 proteins, 5.1%). Not all 39 proteins involved in sperm functions are identified and/or described in the STRING program for dolphins, so we divided them into three different categories: (1) Proteins described for *T. truncatus* (27 proteins, 69.2%); (2) Proteins described for *H. sapiens* (35 proteins, 89.7%); and (3) Proteins described for *M. musculus* (1 protein, 2.6%). Twenty-four proteins were common to both categories (1 and 2).

[2]https://string-db.org/

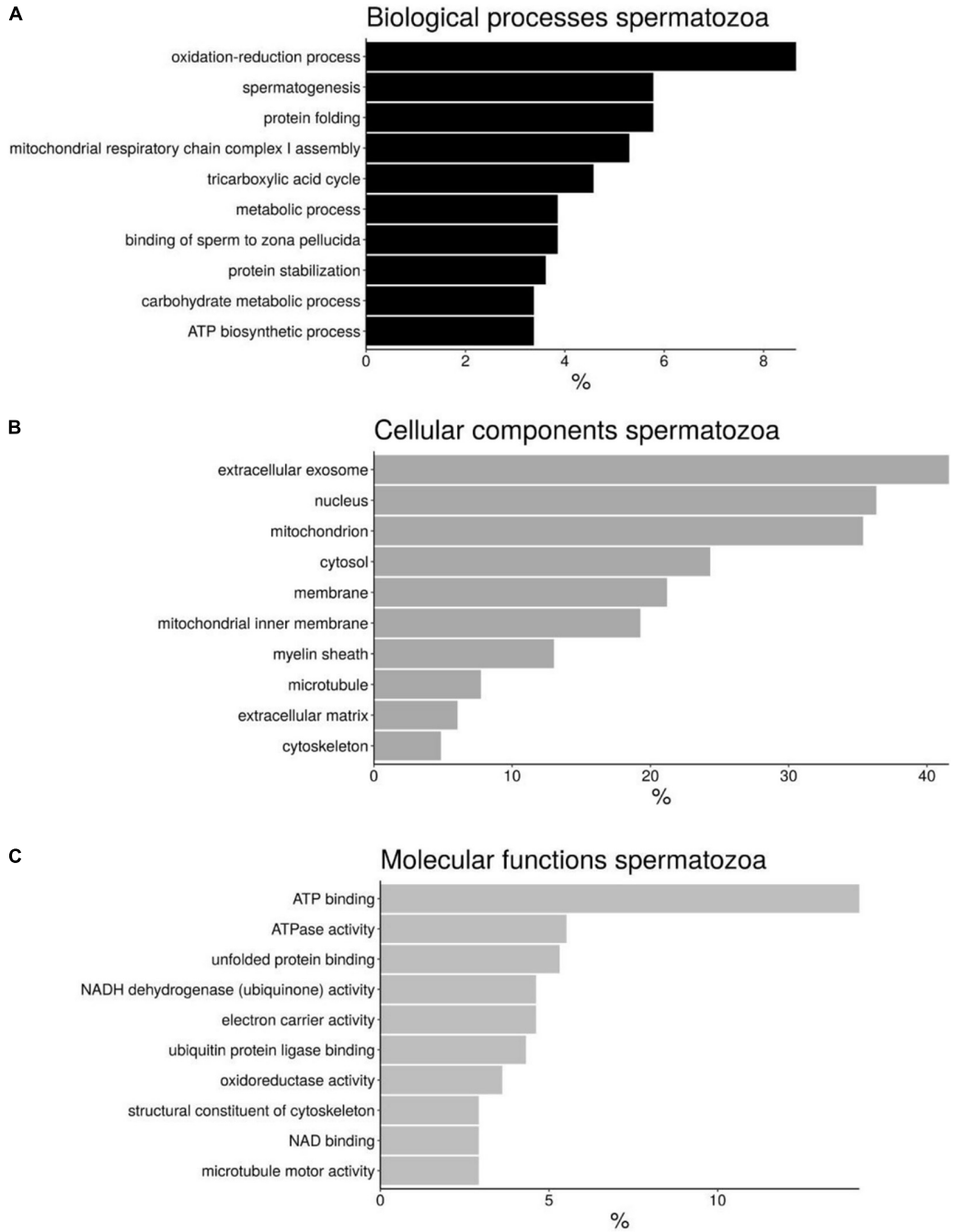

FIGURE 3 | Bar chart representing the gene ontology annotations of protein identified in bottlenose dolphin spermatozoa according to biological processes **(A)**, cellular components **(B)**, and molecular functions **(C)**.

Protein Profile of Bottlenose Dolphin Seminal Plasma

A total of 303 proteins were identified in the seminal plasma of the four samples obtained, two from each male. A complete protein list (ordered by the number of peptides) for the seminal plasma with protein name, String ID dolphin, peptides, mean protein score (±SD), preferred name and annotation (*H. sapiens*) is presented in **Supplementary File 9**. A detailed search was carried out in the STRING database v 11.0 (see text foot note 2) to obtain a description of the functions related to each of the proteins, finding the following: (i) Proteins described for *T. truncatus* (201 proteins, 66.1%); (ii) Proteins described for *H. sapiens* (298 proteins, 98.0%); (iii) Proteins not described in any of above (4 proteins, 1.3%). Of the proteins belonging to the

TABLE 2 | Proteins identified in dolphin spermatozoa linked to sperm function categories.

Function	Gene name	Protein
Spermatogenesis and fertilization	NME5 (1,2)	NME/NM23 family member 5 (NME5)
	SEPT12 (1,2)	Septin 12 (SEPT12)
Sperm–egg fusion	CD46 (2)	CD46 molecule (CD46)
	PKD2L2 (2)	Polycystin 2 like 2, transient receptor potential cation channel (PKD2L2)
	SPACA1 (1,2)	Sperm acrosome-associated 1 (SPACA1)
	ADAM5 (3)	ADAM metallo peptidase domain 5 (ADAM5)
Capacitation and acrosome reaction	ACRBP (1,2)	Acrosin binding protein (ACRBP)
	AKAP3 (1,2)	A-kinase anchoring protein 3 (AKAP3)
	CABYR (1,2)	Calcium binding tyrosine phosphorylation regulated (CABYR)
	DLD (1,2)	Dihydrolipoamide dehydrogenase (DLD)
Sperm motility	DNAH1 (1,2)	Dyneinaxonemal heavy chain 1 (DNAH1)
	DNAH10 (1,2)	Dyneinaxonemal heavy chain 10 (DNAH10)
	DNAH12 (1,2)	Dyneinaxonemal heavy chain 12 (DNAH12)
	DNAH17 (1,2)	Dyneinaxonemal heavy chain 17 (DNAH17)
	DNAH2 (1,2)	Dyneinaxonemal heavy chain 2 (DNAH2)
	DNAH3 (1,2)	Dyneinaxonemal heavy chain 3 (DNAH3)
	DNAH8 (1,2)	Dyneinaxonemal heavy chain 8 (DNAH8)
	EFHB (1,2)	EF-hand domain family member B (EFHB)
	ROPN1L (1,2)	Rhophilin-associated tail protein 1 like (ROPN1L)
	SLC25A31 (1,2)	Solute carrier family 25 member 31 (SLC25A31)
Cilia and flagela	CALM1 (1,2)	Calmodulin 1 (CALM1)
	CFAP20 (2)	Cilia- and flagella-associated protein 20 (CFAP20)
	CFAP43 (2)	Cilia- and flagella-associated protein 43 (CFAP43)
	CFAP52 (2)	Cilia- and flagella-associated protein 52 (CFAP52)
	CFAP58 (2)	Cilia- and flagella-associated protein 58 (CFAP58)
	CFAP61 (2)	Cilia- and flagella-associated protein 61 (CFAP61)
	DNALI1 (1,2)	Dyneinaxonemal light intermediate chain 1 (DNALI1)
	EFHC1 (1,2)	EF-hand domain containing 1 (EFHC1)
	ODF1 (1)	Outer dense fiber of sperm tails 1 (ODF1)
	ODF2 (1)	Outer dense fiber of sperm tails 2 (ODF2)
	ODF3 (1)	Outer dense fiber of sperm tails 3 (ODF3)
	PRKACB (2)	Protein kinase cAMP-activated catalytic subunit beta (PRKACB)
	RSPH9 (1,2)	Radial spoke head 9 homolog (RSPH9)
	SAXO1 (2)	Stabilizer of axonemal microtubules 1 (SAXO1)
	TBC1D21 (1,2)	TBC1 domain family member 21 (TBC1D21)
	TUBB (2)	Tubulin beta class I (TUBB)
	TUBB4B (2)	Tubulin beta 4B class IVb (TUBB4B)
Gonadal development	BANF1 (1,2)	Barrier to autointegration factor 1 (BANF1)
Testis	TCTE1 (1,2)	T-complex-associated-testis-expressed 1; Dynein regulatory complex (TCTE1)

The numbers in the "gene name" column refer to the source organism in which the proteins are described according to the STRING database: (1) described in Tursiops truncatus; (2) described in Homo sapiens; and (3) described in Mus musculus.

third case, all are described for *M. musculus* (ADAM1, ADAM5, DNAJB3 y MUC19), an animal with poliandric reproduction and sperm competition.

The proteins present in seminal plasma described in *H. sapiens* were distributed into 3 categories according DAVID software: "Biological process" (BP), "Cellular components" (CC), and "Molecular Function" (MF) (**Figure 4** and **Supplementary File 8**). Although there are different categories for each of the divisions made the most abundant are those involved in protein folding (10.6%), proteolysis (8%), and cell–cell adhesion (7.6%) for BP (**Figure 4A**); extracellular exosome (71.1%), cytosol (36.9%), and extracellular space (29.9%) for CC (**Figure 4B**); and protein binding (61.5%), unfolded protein binding (8.3%) and cadherin binding involved in cell-cell adhesion (7.6%) for MF (**Figure 4C**).

Of the 303 proteins identified in seminal plasma, 31 are involved in reproductive processes (**Table 3**) such as adhesion with zona pellucida (8 proteins, 25.8%), spermatogenesis (6 proteins, 19.3%), sperm motility process (4 proteins, 12.9%), the formation of microtubules involved in flagellar development (4 proteins, 12.9%), sperm maturation/capacitation (4 proteins, 12.9%), epididymal proteins (2 proteins, 6.5%), muellerian inhibitor (1 protein, 3.2%), oocyte maturation (1 protein, 3.2%), and testis protein (1 protein, 3.2%). Not all the 31 reproductive proteins are identified and/or described in the STRING program for dolphins, so we divided them into three different categories: (1) Those described in *T. truncatus* (29 proteins, 93.5%); (2) Those described in *H. sapiens* (17 proteins, 54.8%); and (3) Those described in *M. musculus* (2 proteins, 6.7%). All the proteins described in *H. sapiens* are also present in *T. truncatus.*

Protein–Protein Interaction Networks

All proteins were searched using STRING software. A total of 266 nodes and 1,452 edges were identified in *T. truncatus* spermatozoa (**Figure 5**), as well as 201 nodes and 804 edges in seminal plasma (**Figure 6**) for the protein–protein interaction (PPI) networks. Network nodes represent proteins and the line color indicates the type of interaction evident, light blue color for known interactions from curated databases, and pink color for interactions experimentally determined. The Predicted Interactions are represented by different colors: green for gene neighborhood, red for gene fusions and dark blue for gene co-occurrence. Other relations between proteins are identified

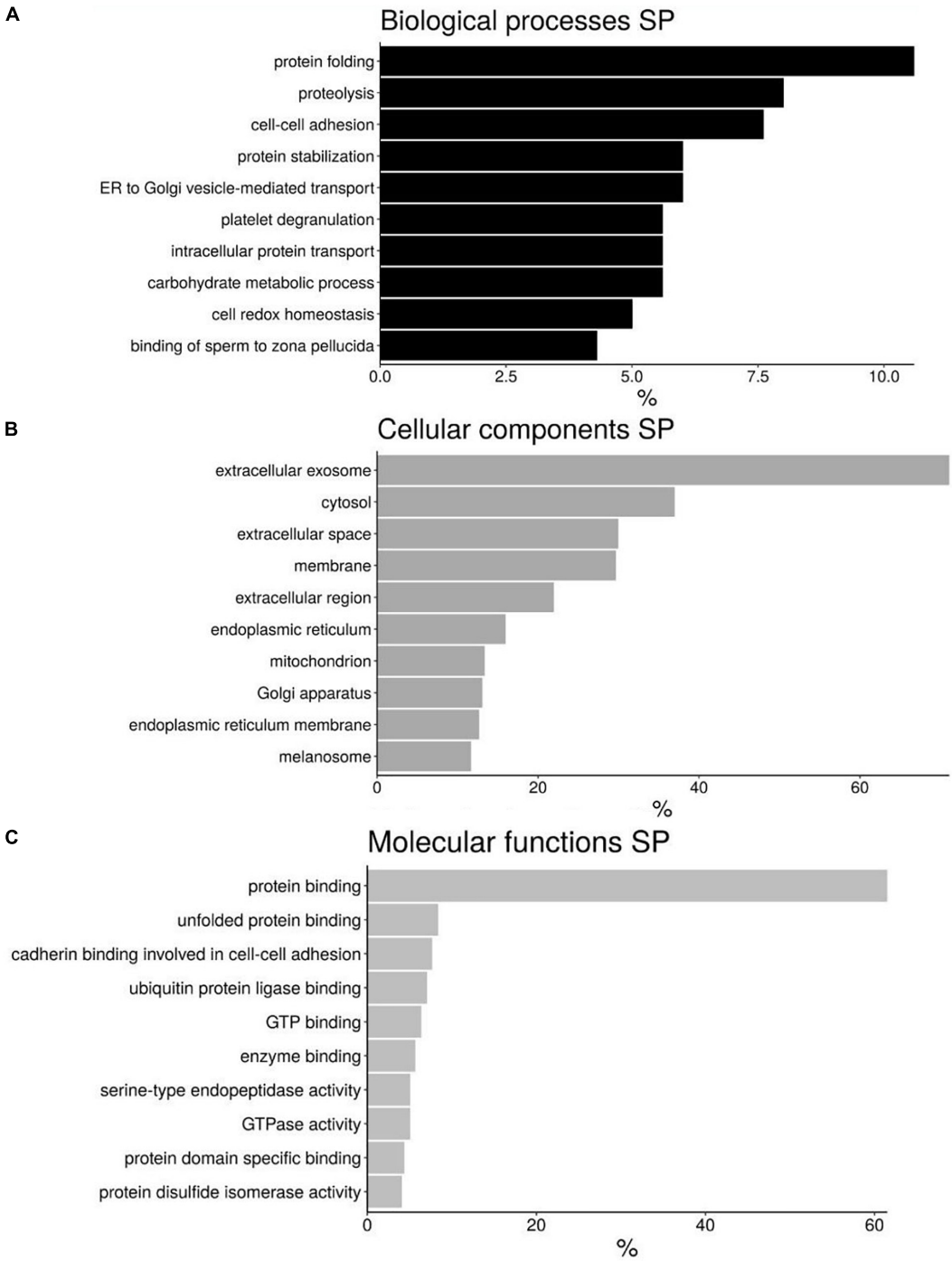

FIGURE 4 | Bar chart representing the gene ontology annotations of protein identified in bottlenose dolphin seminal plasma (SP) according to biological processes **(A)**, cellular components **(B)**, and molecular functions **(C)**.

with light green for text mining, black for co-expression and blue for protein homology. Query proteins are represented as colored nodes and the second shell of interactors are represented as white nodes. Empty nodes represent proteins of unknown 3D structure and filled nodes represent predicted or known structures.

DISCUSSION

Dolphins are one of the most studied marine mammals, mainly due to their easy maintenance in *ex situ* conditions compared to other cetaceans. Although dolphins can reproduce in captivity, the main problem is the inbreeding that occurs in small groups

TABLE 3 | Proteins identified in dolphin seminal plasma linked to sperm function categories.

Function	Gene name	Protein
Sperm motility (energy)		
	AK1 (1)	Adenylate kinase 1 (AK1)
	APOA1 (1,2)	Apolipoprotein A1 (APOA1)
	CKMT1 (1)	Creatine kinase mitochondrial 1A (CKMT1A)
	ROPN1 (1)	Rhophilin-associated tail protein 1 (ROPN1)
Sperm maturation/capacitation		
	ADAM1 (3)	ADAM metallo peptidase domain 1 (ADAM1)
	CST11 (1,2)	Cystatin-11 (CST11)
	AKAP3 (1,2)	A-kinase anchoring protein 3 (AKAP3)
	ROPN1L (1,2)	Rhophilin-associated tail protein 1 like (ROPN1L)
Sperm adhesion zona pellucida		
	ADAM2 (1)	ADAM metallo peptidase domain 2 (ADAM2)
	ADAM5 (3)	ADAM metallo peptidase domain 5 (ADAM5)
	CD9 (1,2)	CD9 molecule (CD9)
	CLGN (1,2)	Calmegin (CLGN)
	FETUB (1)	Fetuin B (FETUB)
	MFGE8 (1)	Milk fat globule-EGF factor 8 protein (MFGE8)
	PRSS37 (1,2)	Protease, serine 37 (PRSS37)
	TEX101 (1,2)	Testis expressed 101 (TEX101)
Epididymal		
	LCN6 (1,2)	Lipocalin 6 (LCN6)
	NPC2 (1)	NPC intracellular cholesterol transporter 2 (NPC2)
Muellerian inhibitor		
	AMH (1,2)	Anti-Muellerian hormone (AMH)
Oocyte maturation		
	CALR (1,2)	Calreticulin (CALR)
Spermatogenesis		
	BSG (1,2)	Basigin (Ok bloodgroup) (BSG)
	NAP1L4 (1,2)	Nucleosome assembly protein 1 like 4 (NAP1L4)
	PRKACB (1)	Protein kinase cAMP-activated catalytic subunit beta (PRKACB)
	RNASE10 (1)	Ribonuclease A (RNASE10)
	SHCBP1L (1,2)	SHC binding and spindle-associated 1 like (SHCBP1L)
	SPAG4 (1,2)	Sperm-associated antigen 4 (SPAG4)
Testis		
	PDILT (1,2)	Protein disulfide isomerase like, Testis expressed (PDILT)
Microtubules: cilia and flagella		
	CFAP36 (1)	Cilia- and flagella-associated protein 36 (CFAP36)
	PCMT1 (1,2)	Protein-l-isoaspartate (d-aspartate) *O*-methyl transferase (PCMT1)
	TUBB (1)	Tubulin beta class I (TUBB)
	TUBB4B (1)	Tubulin beta 4B class IVb (TUBB4B)

The numbers in the "gene name" column refer to the source organism where the proteins are described according to the STRING database: (1) described in Tursiops truncatus; (2) described in Homo sapiens; and (3) described in Mus musculus.

of animals. For this reason, their reproductive characteristics and subsequent improvements in ARTs are essential in these animals to ensure genetic spread and conservation. In this respect, studies of the semen protein composition has determined the possibility of using sperm freezing in different species (Soleilhavoup et al., 2014; Kasimanickam et al., 2019; Gaitskell-Phillips et al., 2021; Martínez-Fresneda et al., 2021), the identification of presumptive fertility biomarkers (Dacheux et al., 2012; Li et al., 2016; Rahman et al., 2017; Druart and de Graaf, 2018; Pérez-Patiño et al., 2018; Druart et al., 2019) or sperm traits (Intasqui et al., 2016; Bezerra et al., 2019; De Lazari et al., 2019). The present study describes the proteins in spermatozoa and seminal plasma of bottlenose dolphin. To the best of our knowledge, this study represents the first description of the semen proteome in any cetacean. A total of 722 proteins (common to the 4 samples analyzed) were described for sperm (419) and seminal plasma (303).

Proteins Identified in the Spermatozoa of Bottlenose Dolphin

The five most abundant proteins found in dolphin spermatozoa (based on the number of peptides identified) were the following: AKAP3, ODF2, TUBB, GSTM3, and ROPN1. Four of these proteins (AKAP3, ODF2, TUBB, and GSTM3) are also in the top five of highly abundant proteins in the spermatozoa of buffalo (Fu et al., 2019). AKAP3 protein was the most abundant sperm protein according to our data. This protein is not only essential for the formation of the subcellular structure of the sperm flagellum, sperm motility and male fertility in mice, but also for sperm capacitation. As is known, sperm capacitation is a series of biochemical and physiological changes that mammalian sperm must undergo to become fertile (Gervasi and Visconti, 2016). AKAP3 null mice sperm has low sperm motility, leading to sperm morphology abnormalities, the displacement of PKA subunits and misregulated PKA activity, a key factor during sperm capacitation, and in male sterility (Xu et al., 2020). Moreover, other proteins identified in our study, such as CABYR and ROPN1, interact with AKAP3 (Carr et al., 2001; Li et al., 2011). CABYR protein is a fibrous sheath calcium-binding tyrosine phosphorylation-regulated protein (Li et al., 2007), which associates with AKAP3 in human spermatozoa (Li et al., 2011). CABYR is located in the principal piece of the sperm flagellum (Li et al., 2007; Zhang et al., 2016) and it is involved in calcium-binding when phosphorylated during capacitation (Naaby-Hansen et al., 2002). Moreover, this protein is expressed in the oviduct of several species (Hanlon Newell et al., 2008; Martinez et al., 2020), where its expression increases in response to sperm entry. ODF2 is the second most abundant protein found in the spermatozoa of bottlenose dolphin. In mammalian sperm, the flagellum presents complex accessory structures surrounding the central axoneme, the outer dense fibers (ODFs) being part of these structures (Zhao et al., 2018). Dolphin sperm is not an exception, and ODFs are almost of similar form and size as in most other mammals (van der Horst et al., 2018). ODFs play a role in the protection of the sperm tail against shear forces during epididymal transport and ejaculation (Baltz et al., 1990). More than 14 polypeptides from mammalian

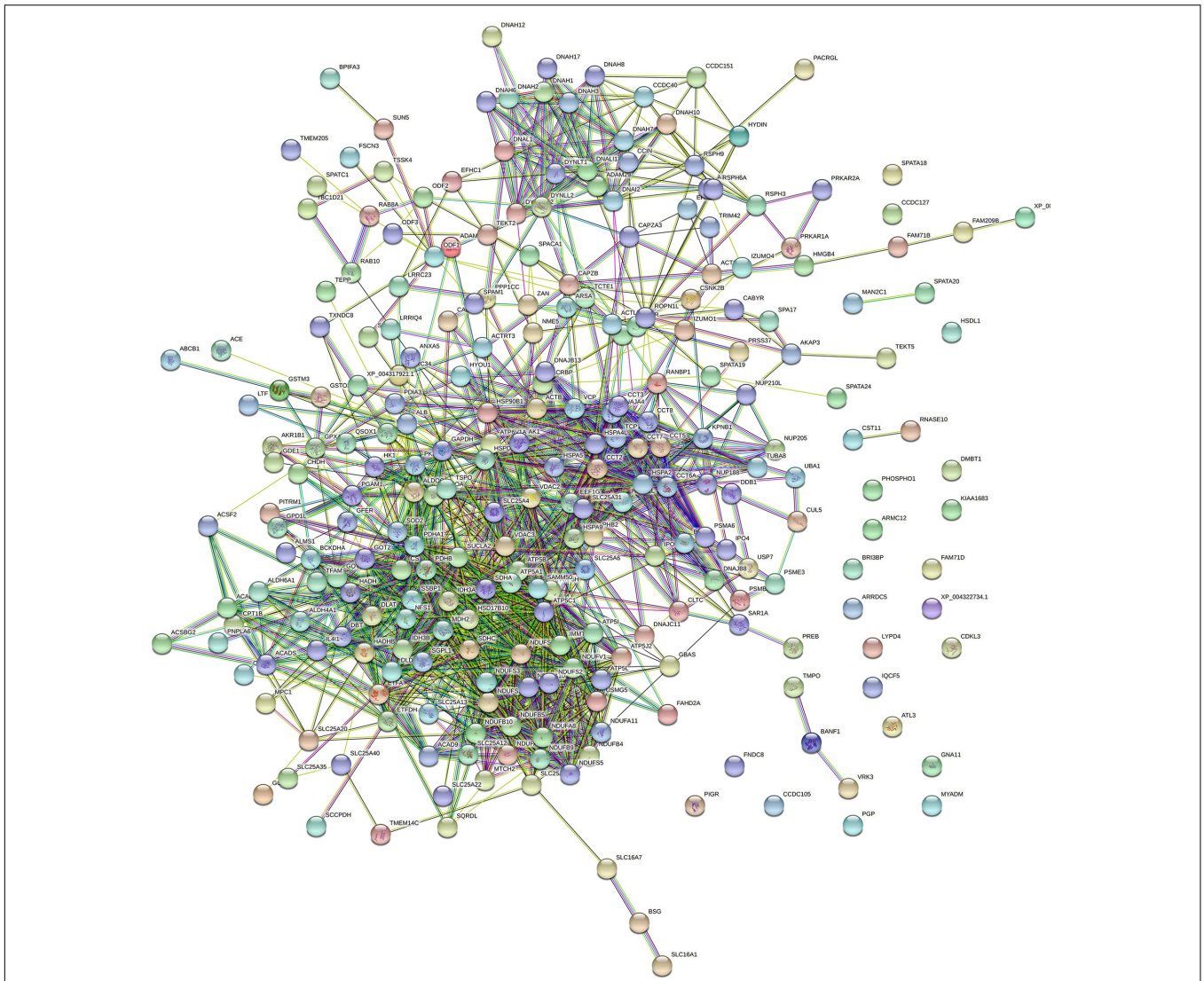

FIGURE 5 | STRING protein–protein interaction network showing the interactions of the spermatozoa proteins identified in bottlenose dolphin.

ODFs have been identified, including four major proteins (ODF1, ODF2, ODF3, and ODF4) (reviewed by Zhao et al., 2018). Our analysis identified ODF1, ODF2, and ODF3 in dolphin sperm, the most abundant being ODF2 protein. The disruption of ODF2 expression in mice reduced sperm motility, and is compatible with asthenozoospermia characteristics (Zhao et al., 2018). Moreover, ODF2 is indispensable for the neck midpiece connection, which is composed of a centrosome-derived component and a flagellar component (Ito et al., 2019). Tubulins are a family of proteins in which α- and β-tubulin are the major components of microtubules in spermatozoa (Kierszenbaum, 2002). TUBB and TUBB4B proteins are two of the tubulin proteins previously be found in the sperm of our analyzed dolphin samples. These proteins are important in the development of cilia and flagellum, but there is nothing in the bibliography which explains in detail the relation between this fact and the presence/absence of this group as fertility biomarkers, although TUBB protein exhibits clear differences in expression according to porcine litter size (Kwon et al., 2015b). GSTM3 is another protein situated among the five most abundant sperm proteins identified in our study. GSTM3 is a detoxification protein, which has been reported to play a key role in oocyte binding (Gopalakrishnan et al., 1998; Petit et al., 2013) and their interaction with the zona pellucida (Petit et al., 2013). Moreover, sperm GSTM3 has been proposed as a quality (Llavanera et al., 2020b), fertility (Kwon et al., 2015a) and cryotolerance (Llavanera et al., 2019) biomarker for pig sperm. Our data also report the presence of this protein in the seminal plasma of dolphins. Recently, it has been demonstrated that low concentration of GSTM3 in pig seminal plasma is related to an increased percentage of sperm abnormalities (Llavanera et al., 2020a). ROPN1 protein is found in sperm flagellum as part of the fibrous sheath, specifically located in the principal piece and end piece of the flagellum (Fujita et al., 2000; Chen et al., 2011). The expression level of ROPN1 was found to be significantly lower in asthenozoospermic men than in normozoospermic

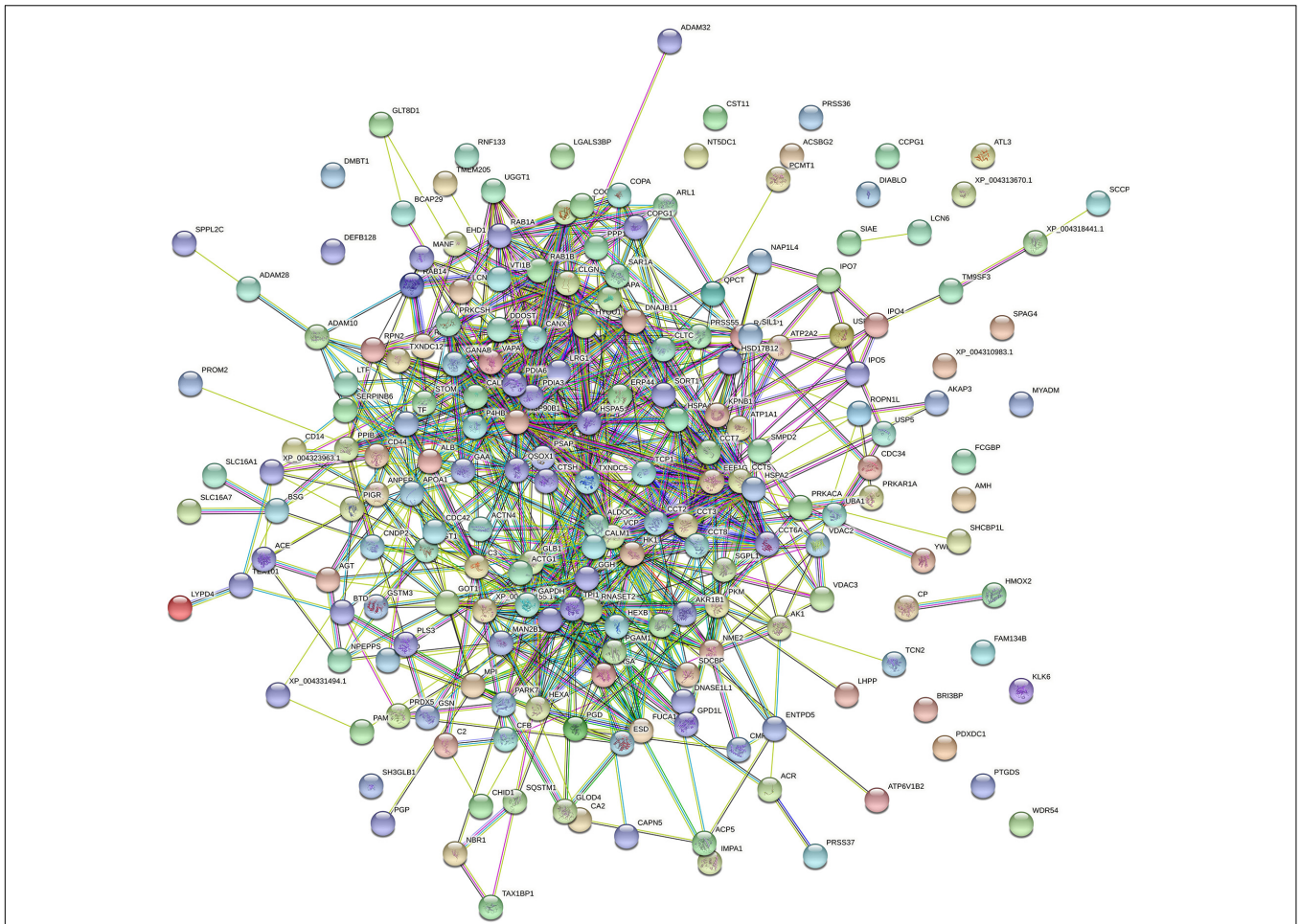

FIGURE 6 | STRING protein–protein interaction network showing the interactions of the seminal plasma proteins identified in bottlenose dolphin.

suggesting its involvement in sperm motility (Chen et al., 2011). When mice lacking ROPN1 were analyzed, the sperm exhibited altered motility, the same males being subfertile, and producting fewer and smaller litters (Fiedler et al., 2012). Indeed, a positive correlation between motility (progressive and total motile sperm number) and ROPN1/CABYR gene expression has been observed (Pelloni et al., 2018).

One interesting sperm protein identified in our data was IZUMO1. Sperm-egg fusion is accomplished through the interaction of a specific membrane proteins in sperm, IZUMO1 (Inoue et al., 2005), and oocyte, JUNO (Bianchi et al., 2014). During acrosome reaction, IZUMO1 relocates from the anterior head of the sperm to the site where fusion takes place and which was the first site to be shown as critical for gamete fusion (Inoue et al., 2005, 2011). Thus, our data suggest that gamete fusion is probably mediated by the same mechanism as that described in mouse.

Proteins Identified in the Seminal Plasma of Bottlenose Dolphin

As mentioned above, the seminal plasma of dolphins comes from the testis, epididymis and the prostate, the only accessory sex gland in this species (Harrison et al., 1969; Rommel et al., 2007; Suárez-Santana et al., 2020). Seminal plasma is not simply a transport fluid for sperm but also modulates the female genital tract environment (Bromfield, 2014). It also protects sperm during their journey toward the oocyte (Kawano et al., 2014; Luongo et al., 2019) and interacts with other reproductive fluids modifying the sperm proteome (Luongo et al., 2020). The five most abundant proteins (based on the number of peptides identified) represented in seminal plasma of dolphin were CST11, LTF, ALB, HSP90B1, and PIGR. Of these CST11 (Cystatin11) was seen to be the most abundant protein in the seminal plama of dolphin (and was also detected in the sperm). CST11 belongs to the cystatin type 2 family of cysteine protease inhibitor and exhibits antimicrobial activity *in vitro* (Magister and Kos, 2013), suggesting that cystatins defend the male reproductive tract against invading pathogens (Hamil et al., 2002; Fan et al., 2014). This protein has been detected throughout the epididymis (particularly in the initial segment) and in ejaculated human sperm (Hamil et al., 2002). LTF is a glycoprotein with antioxidant and antibacterial activities that is synthesized in the epididymis in mammals (Pearl and Roser, 2008) and has been detected in the prostate and seminal vesicles

in humans (Wichmann et al., 1989). It has been reported that the treatment of asthenoteratozoospermic males with LTF, combined with other natural antioxidants, significantly improves the motility of sperm cells (Piomboni et al., 2008). Moreover, a positive correlation between seminal plasma LFT concentration and sperm density was established in dogs (Kikuchi et al., 2003a) and horses (Kikuchi et al., 2003b). The addition of LTF to freezing sperm extender protected stallion sperm, increasing the percentage of sperm with functional membranes and decreased lipid oxidizing agents (Martins et al., 2018). ALB protein is positively related with sperm concentration, total sperm count and the percentage of morphologically normal spermatozoa, but negatively related with semen volume in humans (Elzanaty et al., 2007). In a study developed in Holstein bulls, high concentrations of this protein correlated with animals whose semen was classified as highly fertile (Kasimanickam et al., 2019), so this protein could be used as a biomarker of fertility. HSP90B1 is a molecular chaperone member of the heat shock protein 90 (HSP90) family. This protein is involved in the immune response (Graustein et al., 2018) in the suppression of cell apoptosis and autophagy (Sun et al., 2015). This function suggests a putative role for HSP90B1 once it is in the female genital tract after insemination, since it is known that seminal plasma modulates maternal immunity (Bromfield, 2018). PIGR is involved in the tissue homeostasis pathway (Panner Selvam et al., 2019) and its expression is regulated by cytokines, which show high levels in the seminal plasma of varicocele patients due to an inflammatory response (Zeinali et al., 2017). The presence of PIGR was previously reported in the semen of bulls (Rego et al., 2014) and cats (Mogielnicka-Brzozowska et al., 2020). In humans, PIGR expression was observed in the prostate (Sirigu et al., 1995) which agrees with our results as the prostate is the only accessory sex gland in dolphins.

NPC2 is one of the proteins found in abundance in the seminal plasma of bottlenose dolphin (the sixth most abundant protein). NPC2 has also been described to be among the most abundant secreted proteins in the epididymis in bovine (Belleannée et al., 2011). In the epididymal fluid, NPC2 participates in cholesterol efflux from the spermatozoa during epididymal sperm maturation (Légaré et al., 2006). Furthermore, capacitated NPC2$^{(-/-)}$ mice spermatozoa exhibited defective tyrosine phosphorylation patterns and a reduced ability to fertilize cumulus-oocyte complexes compared with wild-type spermatozoa, supporting the relevance of epididymal NPC2 in male mouse fertility (Busso et al., 2014). Recently, relative levels of two isoforms of NPC2 were found to be higher in the porcine seminal plasma of poor freezability ejaculates than in that with good freezability, suggesting that the NPC2 content may be useful for predict ejaculate freezability (Valencia et al., 2020).

Proteome Profile of Dolphin Spermatozoa and Seminal Plasma Compared to Other Species (Human, Bovine, and Canine)

Comparative analyses and a Venn diagram were made relating dolphin to other three species: bovine, canine and human. Bovine and porcine species are even-toed ungulates (artiodactyls), and closest living relatives of dolphin (Thewissen et al., 2007; Spaulding et al., 2009). Actually, both species (bovine and delphinus) share 362 of the 419 sperm proteins detected in the analysis (86.4%) and 218 of the 304 detected in seminal plasma protein (71.7%), appointing to the high number of conserved proteins between these animals. Likewise, dolphin sperm are able to attach and penetrate bovine ZP, even triggering the blockage of polyspermy (Sánchez-Calabuig et al., 2015a, 2017). The dog was also compared to dolphin because they both share the fact that of having only one accessory sex gland, the prostate. Dog and dolphin share 51 seminal plasma proteins, only 6 of which are exclusive to these animals (NBR1, BCAP29, KLK6, SQSTM1, SLC16A7, and MUC19). This suggests that, although prostate is the only accessory sex gland common to dogs and dolphins, the protein composition is not well conserved between species, and less than 25% of the seminal plasma proteins are shared. Moreover, as an outgroup, we also included human in the comparative analysis because of the availability proteomic data. The results indicated that 42 sperm proteins and 30 seminal plasma proteins are common to the four species.

FSIP2 is one of the sperm proteins identified as common to all four compared species (**Supplementary File 5**) (sixth position in the sperm protein list based on the number of identified peptides; **Supplementary File 7**). FISP2 is one of the main genes involved in the multiple morphological abnormalities of sperm flagella syndrome (Martinez et al., 2018). Moreover, mutations in FSIP2 lead to the absence of A-kinase anchoring protein 4 (AKAP4), a protein also detected in dolphin sperm. DNAH8 has also been found also to be common to the four species analyzed (**Supplementary File 5**) (tenth position in sperm protein list based on the number of identified peptides; **Supplementary File 7**). Loss-of-function mutation in DNAH8 is suggested to cause male infertility because of the multiple morphological abnormalities of sperm flagella syndrome, DNAH8 being essential for sperm flagellum formation (Yang et al., 2020). There are 12 sperm proteins that have only been identified in dolphin: LRRC37A5P, CFAP61, HOGA1, CCDC127, UBB, C6orf58, CST11, DEFB130, HEL-S-80P, ADAM10, ATP6V1FNB, and GCAT.

In the case of seminal plasma, LTF and ALB are present in all the compared species. ENO1, which has been recognized as a candidate for fertility marker in bulls (Park et al., 2019) is another protein conserved in the four species and a good freezability predictor in human (Jiang et al., 2015). It would be interesting to analyze ENO1 in dolphins with different degrees of fertility and as a possible component of an extender during preservation. A total of 61 proteins were exclusively detected in the sperm of dolphin but not in dogs, humans or bulls.

To evaluate whether the most abundant protein found in dolphin are also in the semen of other species (human and bovine) the most abundant protein situated in the first decile of the lists for sperm and seminal plasma of these species were analyzed. In the case of sperm proteins, 16 of them were shared across the three species (DNAH8, ODF2, NDUFS1, HSPA2, TUBB4B, HK1, TEKT5, DLAT, AKAP3, TEKT2, EFHC1, LTF, GSTM3, SDHA, TEKT3, and UQCRC2). Four of them are included in the top ten of the most abundant proteins detected in dolphin sperm (DNAH8, ODF2, AKAP3, and GSTM3). In the

case of seminal plasma, 13 proteins were shared between the three species (ACE, QSOX1, PDIA3, P4HB, HYOU1, HSPA5, ALB, GLB1, PIGR, LTF, HSP90B1, HSPA8, and HSP90AA1). Seven of them are included in the top ten of the most abundant proteins detected in the seminal plasma of dolphin (ACE, PDIA3, ALB, PIGR, LTF, HSP90B1, HSPA8, and HSP90AA1).

Protein differences between the species could be a result of different requirements for spermatozoa to interact with the female tract (Druart and de Graaf, 2018). The species here compared (human, bovine, canine, and dolphin) have vaginal semen deposition which can explain a similar protein profile between species for helping with cervical migration. Moreover, cross-species comparison of mammalian seminal plasma proteomes performed in seven species (bovine, sheep, goat, pig, horse, camel, and alpaca) revealed that the phylogenetic proximity between species could be related to the similarity of seminal plasma proteome (Druart et al., 2013).

CONCLUSION

In conclusion, this study provides an inventory of 722 proteins present in bottlenose dolphin semen. As demonstrated in most mammalian species, bottlenose dolphin semen proteome includes proteins that are essential to the sperm structure and function. Comparison of this proteome with other physio-pathologies enable the identification of semen markers for reproduction purposes. Moreover, this work opens the door to future research aimed at investigating a new molecular basis of sperm, proteins that are involved in sperm conservation, or those that can be used as biomarkers of sperm quality and fertility.

DATA AVAILABILITY STATEMENT

The mass spectrometry proteomics data have been deposited to the ProteomeXchange Consortium via the PRIDE partner repository with the dataset identifier PXD024588.

ETHICS STATEMENT

The samples were obtained from two trained dolphin males housed at the Oceanogràfic de Valencia following the Animal Care Protocol and policies of the aquarium. The animals were conditioned through positive reinforcement to participate in many different medical behaviors, including semen collection to provide basic husbandry care. Semen samples were obtained through training following the same approach as previously published (Sánchez-Calabuig et al., 2017). Furthermore, the regulations and policies of EU 143 legislation, Directive 2010/63/EU (https://eur-lex.europa.eu/legal144content/EN/TXT/?uri=CELEX:32010L0063), were observed.

AUTHOR CONTRIBUTIONS

MI and FG-V: conceptualization. M-CF-A, LG-B, PC, CL, SA-S, JR-S, EP, SR-D, CB-G, and DG-P: methodology. FG-V: validation and supervision. LG-B: formal analysis and data curation. M-CF-A, LG-B, CL, SA-S, JR-S, EP, SR-D, CB-G, M-JS-C, DG-P, MA, MI, and FG-V: investigation. M-CF-A, CB-G, and DG-P: resources. M-CF-A and FG-V: writing – original draft preparation. M-CF-A, LG-B, PC, CL, SA-S, JR-S, EP, SR-D, CB-G, M-JS-C, DG-P, MA, MI, and FG-V: review and editing. DG-P, MA, and FG-V: funding acquisition. All authors have read and agreed to the published version of the manuscript.

FUNDING

This research was supported by the Spanish Ministry of Science and Innovation (PID2019-106380RB-I00/AEI/10.1303/501100011033) and PGC2018-094781-B-I00 (MCINN/AEI/FEDER, UE), and Oceanogràfic Foundation.

ACKNOWLEDGMENTS

We are grateful to the aquarium Oceanogràfic Valencia staff, dolphin trainers and veterinarians for their assistance and commitment with animal care and for facilitating semen sample collections. We also thank M. Luz Valero of the Proteomic Service of the University of Valencia for her useful help and advice.

SUPPLEMENTARY MATERIAL

The Supplementary Material for this article can be found online at: https://www.frontiersin.org/articles/10.3389/fcell.2021.673961/full#supplementary-material

Supplementary File 1 | Python code used to identify the most similar orthologs for dolphin proteins without an official name. The code performs blast queries against a database composed of curated entries from Swissprot plus the Uniprot entries associated with *T. truncatus* (release 2020_02). Candidates for each query are selected within the top 5 matches with an official name, e-value of 0.001 and sequence identity of 60%. If the top match has over 99% identity its name is assigned to the problem protein of dolphin. Otherwise, all candidates within a margin of 5% identity are selected and their names compared. If there is no consensus for the name, the program writes their names and sequence identity and the alignment results are manually checked. If the program does not find any proteins matching the requisites a message is returned: "Check this protein, there are no near orthologs."

Supplementary File 2 | Individual lists of proteins identified in each of the sperm samples analyzed in bottlenose dolphin (*Tursiops truncatus*).

Supplementary File 3 | Individual lists of proteins identified in each of the seminal plasma samples analyzed in bottlenose dolphin (*Tursiops truncatus*).

Supplementary File 4 | List of common proteins to spermatozoa and seminal plasma in bottlenose dolphin (*Tursiops truncatus*).

Supplementary File 5 | List of sperm proteins common (or not) to bull, man, dog, and bottlenose dolphin.

Supplementary File 6 | List seminal plasma proteins common (or not) to bull, man, dog, and bottlenose dolphin.

Supplementary File 7 | Proteins identified in the sperm (common to all of the analyzed samples) of bottlenose dolphin (*Tursiops truncatus*).

Supplementary File 8 | Functional distribution of bottlenose dolphin (*Tursiops truncatus*) spermatozoa and seminal plasma from DAVID Bioinformatics Resources.

Supplementary File 9 | Proteins identified in the seminal plasma (common to all of the analyzed samples) of bottlenose dolphin (*Tursiops truncatus*).

REFERENCES

Amaral, A., Castillo, J., Ramalho-Santos, J., and Oliva, R. (2014). The combined human sperm proteome: cellular pathways and implications for basic and clinical science. *Hum. Reprod. Update* 20, 40–62. doi: 10.1093/humupd/dmt046

Aquino-Cortez, A., Pinheiro, B. Q., Lima, D. B. C., Silva, H. V. R., Mota-Filho, A. C., Martins, J. A. M., et al. (2017). Proteomic characterization of canine seminal plasma. *Theriogenology* 95, 178–186. doi: 10.1016/j.theriogenology.2017.03.016

Araujo, M. S., de Oliveira Henriques, Paulo, O. L., Paranzini, C. S., Scott, C., Codognoto, V. M., et al. (2020). Proteomic data of seminal plasma and spermatozoa of four purebred dogs. *Data Br.* 30:105498. doi: 10.1016/j.dib.2020.105498

Bajuk, B. P., Zrimšek, P., Pipan, M. Z., Tilocca, B., Soggiu, A., Bonizzi, L., et al. (2020). Proteomic analysis of fresh and liquid-stored boar spermatozoa. *Animals* 10:553. doi: 10.3390/ani10040553

Baker, M. A., Hetherington, L., Reeves, G. M., and Aitken, R. J. (2008). The mouse sperm proteome characterized via IPG strip prefractionation and LC-MS/MS identification. *Proteomics* 8, 1720–1730. doi: 10.1002/pmic.200701020

Baker, M. A., Naumovski, N., Hetherington, L., Weinberg, A., Velkov, T., and Aitken, R. J. (2013). Head and flagella subcompartmental proteomic analysis of human spermatozoa. *Proteomics* 13, 61–74. doi: 10.1002/pmic.201200350

Baltz, J. M., Williams, P. O., and Cone, R. A. (1990). Dense fibers protect mammalian sperm against damage. *Biol. Reprod.* 43, 485–491. doi: 10.1095/biolreprod43.3.485

Barratclough, A., Wells, R. S., Schwacke, L. H., Rowles, T. K., Gomez, F. M., Fauquier, D. A., et al. (2019). Health assessments of common bottlenose dolphins (*Tursiops truncatus*): past, present, and potential conservation applications. *Front. Vet. Sci.* 6:444. doi: 10.3389/fvets.2019.00444

Batruch, I., Lecker, I., Kagedan, D., Smith, C. R., Mullen, B. J., Grober, E., et al. (2011). Proteomic analysis of seminal plasma from normal volunteers and post-vasectomy patients identifies over 2000 proteins and candidate biomarkers of the urogenital system. *J. Proteome Res.* 10, 941–953. doi: 10.1021/pr100745u

Beirão, J., Boulais, M., Gallego, V., O'Brien, J. K., Peixoto, S., Robeck, T. R., et al. (2019). Sperm handling in aquatic animals for artificial reproduction. *Theriogenology* 133, 161–178. doi: 10.1016/j.theriogenology.2019.05.004

Belleannée, C., Labas, V., Teixeira-Gomes, A. P., Gatti, J. L., Dacheux, J. L., and Dacheux, F. (2011). Identification of luminal and secreted proteins in bull epididymis. *J. Proteomics* 74, 59–78. doi: 10.1016/j.jprot.2010.07.013

Bezerra, M. J. B., Arruda-Alencar, J. M., Martins, J. A. M., Viana, A. G. A., Viana Neto, A. M., Rêgo, J. P. A., et al. (2019). Major seminal plasma proteome of rabbits and associations with sperm quality. *Theriogenology* 128, 156–166. doi: 10.1016/j.theriogenology.2019.01.013

Bianchi, E., Doe, B., Goulding, D., and Wright, G. J. (2014). Juno is the egg Izumo receptor and is essential for mammalian fertilization. *Nature* 508, 483–487. doi: 10.1038/nature13203

Bowen, W. D. (1997). Role of marine mammals in aquatic ecosystems. *Mar. Ecol. Prog. Ser.* 158, 267–274. doi: 10.3354/meps158267

Bromfield, J. J. (2014). Seminal fluid and reproduction: much more than previously thought. *J. Assist. Reprod. Genet.* 31, 627–636. doi: 10.1007/s10815-014-0243-y

Bromfield, J. J. (2018). Review: the potential of seminal fluid mediated paternal-maternal communication to optimise pregnancy success. *Animal* 12, s104–s109. doi: 10.1017/S1751731118000083

Bromfield, J. J., Schjenken, J. E., Chin, P. Y., Care, A. S., Jasper, M. J., and Robertson, S. A. (2014). Maternal tract factors contribute to paternal seminal fluid impact on metabolic phenotype in offspring. *Proc. Natl. Acad. Sci. U S A.* 111, 2200–2205. doi: 10.1073/pnas.1305609111

Busso, D., Oñate-Alvarado, M. J., Balboa, E., Castro, J., Lizama, C., Morales, G., et al. (2014). Spermatozoa from mice deficient in Niemann-Pick disease type C2 (NPC2) protein have defective cholesterol content and reduced in vitro fertilising ability. *Reprod. Fertil. Dev.* 26, 609–621. doi: 10.1071/RD12059

Byrne, K., Leahy, T., Mcculloch, R., Colgrave, M. L., and Holland, M. K. (2012). Comprehensive mapping of the bull sperm surface proteome. *Proteomics* 12, 3559–3579. doi: 10.1002/pmic.201200133

Cardozo, J. A., Fernández-Juan, M., Forcada, F., Abecia, A., Muiño-Blanco, T., and Cebrián-Pérez, J. A. (2006). Monthly variations in ovine seminal plasma proteins analyzed by two-dimensional polyacrylamide gel electrophoresis. *Theriogenology* 66, 841–850. doi: 10.1016/j.theriogenology.2006.01.058

Carr, D. W., Fujita, A., Stentz, C. L., Liberty, G. A., Olson, G. E., and Narumiya, S. (2001). Identification of sperm-specific proteins that interact with a-kinase anchoring proteins in a manner similar to the Type II regulatory subunit of PKA. *J. Biol. Chem.* 276, 17332–17338. doi: 10.1074/jbc.M011252200

Chen, J., Wang, Y., Wei, B., Lai, Y., Yan, Q., Gui, Y., et al. (2011). Functional expression of ropporin in human testis and ejaculated spermatozoa. *J. Androl.* 32, 26–32. doi: 10.2164/jandrol.109.009662

Ciereszko, A., Dietrich, M. A., and Nynca, J. (2017). Fish semen proteomics — new opportunities in fish reproductive research. *Aquaculture* 472, 81–92. doi: 10.1016/j.aquaculture.2016.03.005

Cock, P. J. A., Antao, T., Chang, J. T., Chapman, B. A., Cox, C. J., Dalke, A., et al. (2009). Biopython: freely available python tools for computational molecular biology and bioinformatics. *Bioinformatics* 25, 1422–1423. doi: 10.1093/bioinformatics/btp163

Dacheux, J. L., Belleannée, C., Guyonnet, B., Labas, V., Teixeira-Gomes, A. P., Ecroyd, H., et al. (2012). The contribution of proteomics to understanding epididymal maturation of mammalian spermatozoa. *Syst. Biol. Reprod. Med.* 58, 197–210. doi: 10.3109/19396368.2012.663233

Davidson, A. D., Boyer, A. G., Kim, H., Pompa-Mansilla, S., Hamilton, M. J., Costa, D. P., et al. (2012). Drivers and hotspots of extinction risk in marine mammals. *Proc. Natl. Acad. Sci. U S A.* 109, 3395–3400. doi: 10.1073/pnas.1121469109

De Lazari, F. L., Sontag, E. R., Schneider, A., Araripe Moura, A. A., Vasconcelos, F. R., Nagano, C. S., et al. (2020). Proteomic identification of boar seminal plasma proteins related to sperm resistance to cooling at 17 °C. *Theriogenology* 147, 135–145. doi: 10.1016/j.theriogenology.2019.11.023

De Lazari, F. L., Sontag, E. R., Schneider, A., Moura, A. A. A., Vasconcelos, F. R., Nagano, C. S., et al. (2019). Seminal plasma proteins and their relationship with sperm motility and morphology in boars. *Andrologia* 51:e13222. doi: 10.1111/and.13222

Dietrich, M. A., Irnazarow, I., and Ciereszko, A. (2017). Proteomic identification of seminal plasma proteins related to the freezability of carp semen. *J. Proteomics* 162, 52–61. doi: 10.1016/j.jprot.2017.04.015

Dolman, S. J., and Brakes, P. (2018). Sustainable fisheries management and the welfare of bycaught and entangled cetaceans. *Front. Vet. Sci.* 5:287. doi: 10.3389/fvets.2018.00287

Druart, X., and de Graaf, S. (2018). Seminal plasma proteomes and sperm fertility. *Anim. Reprod. Sci.* 194, 33–40. doi: 10.1016/j.anireprosci.2018.04.061

Druart, X., Rickard, J. P., Mactier, S., Kohnke, P. L., Kershaw-Young, C. M., Bathgate, R., et al. (2013). Proteomic characterization and cross species comparison of mammalian seminal plasma. *J. Proteomics.* 91, 13–22. doi: 10.1016/j.jprot.2013.05.029

Druart, X., Rickard, J. P., Tsikis, G., and de Graaf, S. P. (2019). Seminal plasma proteins as markers of sperm fertility. *Theriogenology* 137, 30–35. doi: 10.1016/j.theriogenology.2019.05.034

Elzanaty, S., Erenpreiss, J., and Becker, C. (2007). Seminal plasma albumin: origin and relation to the male reproductive parameters. *Andrologia* 39, 60–65. doi: 10.1111/j.1439-0272.2007.00764.x

Fan, K., Jiang, J., Wang, Z., Fan, R., Yin, W., Sun, Y., et al. (2014). Expression and purification of soluble porcine cystatin 11 in pichia pastoris. *Appl. Biochem. Biotechnol.* 174, 1959–1968. doi: 10.1007/s12010-014-1148-z

Fiedler, S. E., Sisson, J. H., Wyatt, T. A., Pavlik, J. A., Gambling, T. M., Carson, J. L., et al. (2012). Loss of ASP but not ROPN1 reduces mammalian ciliary motility. *Cytoskeleton* 69, 22–32. doi: 10.1002/cm.20539

Fu, Q., Pan, L., Huang, D., Wang, Z., Hou, Z., and Zhang, M. (2019). Proteomic profiles of buffalo spermatozoa and seminal plasma. *Theriogenology* 134, 74–82. doi: 10.1016/j.theriogenology.2019.05.013

Fujita, A., Nakamura, K. I., Kato, T., Watanabe, N., Ishizaki, T., Kimura, K., et al. (2000). Ropporin, a sperm-specific binding protein of rhophilin, that is localized in the fibrous sheath of sperm flagella. *J. Cell Sci.* 113, 103–112. doi: 10.1242/jcs.113.1.103

Gaitskell-Phillips, G., Martín-Cano, F. E., Ortiz-Rodríguez, J. M., Silva-Rodríguez, A., Gil, M. C., Ortega-Ferrusola, C., et al. (2021). Differences in the proteome of stallion spermatozoa explain stallion-to-stallion variability in sperm quality post thaw†. *Biol. Reprod.* 104, 1097–1113. doi: 10.1093/biolre/ioab003

Gervasi, M. G., and Visconti, P. E. (2016). Chang's meaning of capacitation: a molecular perspective. *Mol. Reprod. Dev.* 83, 860–874. doi: 10.1002/mrd.22663

Gopalakrishnan, B., Aravinda, S., Pawshe, C. H., Totey, S. M., Nagpal, S., Salunke, D. M., et al. (1998). Studies on glutathione S-transferases important for sperm

function: evidence of catalytic activity-independent functions. *Biochem. J.* 329, 231–241. doi: 10.1042/bj3290231

Graustein, A. D., Misch, E. A., Musvosvi, M., Shey, M., Shah, J. A., Seshadri, C., et al. (2018). Toll-like receptor chaperone HSP90B1 and the immune response to mycobacteria. *PLoS One* 13:e0208940. doi: 10.1371/journal.pone.0208940

Guasti, P. N., Souza, F. F., Scott, C., Papa, P. M., Camargo, L. S., Schmith, R. A., et al. (2020). Equine seminal plasma and sperm membrane: functional proteomic assessment. *Theriogenology* 156, 70–81. doi: 10.1016/j.theriogenology.2020.06.014

Hamil, K. G., Liu, Q., Sivashanmugam, P., Yenugu, S., Soundararajan, R., Grossman, G., et al. (2002). Cystatin 11: a new member of the cystatin type 2 family. *Endocrinology* 143, 2787–2796. doi: 10.1210/endo.143.7.8925

Hanlon Newell, A. E., Fiedler, S. E., Ruan, J. M., Pan, J., Wang, P. J., Deininger, J., et al. (2008). Protein kinase A RII-like (R2D2) proteins exhibit differential localization and AKAP interaction. *Cell Motil. Cytoskeleton* 65, 539–552. doi: 10.1002/cm.20279

Harrison, R. J., Boice, R. C., and Brownell, R. L. (1969). Reproduction in wild and captive dolphins. *Nature* 222, 1143–1147. doi: 10.1038/2221143b0

Holt, W. V., and Pickard, A. R. (1999). Role of reproductive technologies and genetic resource banks in animal conservation. *Rev. Reprod.* 4, 143–150. doi: 10.1530/ror.0.0040143

Hopkins, B. R., Sepil, I., Thézénas, M. L., Craig, J. F., Miller, T., Charles, P. D., et al. (2019). Divergent allocation of sperm and the seminal proteome along a competition gradient in *Drosophila melanogaster*. *Proc. Natl. Acad. Sci. U S A.* 116, 17925–17933. doi: 10.1073/pnas.1906149116

Huang, D. W., Sherman, B. T., and Lempicki, R. A. (2009). Bioinformatics enrichment tools: paths toward the comprehensive functional analysis of large gene lists. *Nucleic Acids Res.* 37, 1–13. doi: 10.1093/nar/gkn923

Inoue, N., Ikawa, M., Isotani, A., and Okabe, M. (2005). The immunoglobulin superfamily protein Izumo is required for sperm to fuse with eggs. *Nature* 434, 234–238. doi: 10.1038/nature03362

Inoue, N., Ikawa, M., and Okabe, M. (2011). The mechanism of sperm-egg interaction and the involvement of IZUMO1 in fusion. *Asian J. Androl.* 13, 81–87. doi: 10.1038/aja.2010.70

Intasqui, P., Camargo, M., Antoniassi, M. P., Cedenho, A. P., Carvalho, V. M., Cardozo, K. H. M., et al. (2016). Association between the seminal plasma proteome and sperm functional traits. *Fertil. Steril.* 105, 617–628. doi: 10.1016/j.fertnstert.2015.11.005

Ito, C., Akutsu, H., Yao, R., Yoshida, K., Yamatoya, K., Mutoh, T., et al. (2019). Odf2 haploinsufficiency causes a new type of decapitated and decaudated spermatozoa. Odf2-DDS, in mice. *Sci. Rep.* 9:14249. doi: 10.1038/s41598-019-50516-50512

Jiang, X. P., Wang, S. Q., Wang, W., Xu, Y., Xu, Z., Tang, J. Y., et al. (2015). Enolase1 (ENO1) and glucose-6-phosphate isomerase (GPI) are good markers to predict human sperm freezability. *Cryobiology* 71, 141–145. doi: 10.1016/j.cryobiol.2015.04.006

Juyena, N. S., and Stelletta, C. (2012). Seminal plasma: an essential attribute to spermatozoa. *J. Androl.* 33, 536–551. doi: 10.2164/jandrol.110.012583

Kasimanickam, R. K., Kasimanickam, V. R., Arangasamy, A., and Kastelic, J. P. (2019). Sperm and seminal plasma proteomics of high- versus low-fertility holstein bulls. *Theriogenology* 126, 41–48. doi: 10.1016/j.theriogenology.2018.11.032

Katsumata, E. (2010). Study on reproduction of captive marine mammals. *J. Reprod. Dev.* 56, 1–8. doi: 10.1262/jrd.09-212E

Kawano, N., Araki, N., Yoshida, K., Hibino, T., Ohnami, N., Makino, M., et al. (2014). Seminal vesicle protein SVS2 is required for sperm survival in the uterus. *Proc. Natl. Acad. Sci. U S A.* 111, 4145–4150. doi: 10.1073/pnas.1320715111

Kierszenbaum, A. L. (2002). Sperm axoneme: a tale of tubulin posttranslation diversity. *Mol. Reprod. Dev.* 62, 1–3. doi: 10.1002/mrd.10139

Kikuchi, M., Mizoroki, S., Kubo, T., Ohiwa, Y., Kubota, M., Yamada, N., et al. (2003a). Seminal plasma lactoferrin but not transferrin reflects gonadal function in dogs. *J. Vet. Med. Sci.* 65, 679–684. doi: 10.1292/jvms.65.679

Kikuchi, M., Takao, Y., Tokuda, N., Ohnami, Y., Orino, K., and Watanabe, K. (2003b). Relationship between seminal plasma lactoferrin and gonadal function in horses. *J. Vet. Med. Sci.* 65, 1273–1274. doi: 10.1292/jvms.65.1273

Kwon, W. S., Oh, S. A., Kim, Y. J., Rahman, M. S., Park, Y. J., and Pang, M. G. (2015a). Proteomic approaches for profiling negative fertility markers in inferior boar spermatozoa. *Sci. Rep.* 5:13821. doi: 10.1038/srep13821

Kwon, W. S., Rahman, M. S., Ryu, D. Y., Park, Y. J., and Pang, M. G. (2015b). Increased male fertility using fertility-related biomarkers. *Sci. Rep.* 5:15654. doi: 10.1038/srep15654

Légaré, C., Thabet, M., Gatti, J. L., and Sullivan, R. (2006). HE1/NPC2 status in human reproductive tract and ejaculated spermatozoa: consequence of vasectomy. *Mol. Hum. Reprod.* 12, 461–468. doi: 10.1093/molehr/gal050

Li, C. J., Wang, D., and Zhou, X. (2016). Sperm proteome and reproductive technologies in mammals. *Anim. Reprod. Sci.* 173, 1–7. doi: 10.1016/j.anireprosci.2016.08.008

Li, Y. F., He, W., Jha, K. N., Klotz, K., Kim, Y. H., Mandal, A., et al. (2007). FSCB, a novel protein kinase A-phosphorylated calcium-binding protein, is a CABYR-binding partner involved in late steps of fibrous sheath biogenesis. *J. Biol. Chem.* 282, 34104–34119. doi: 10.1074/jbc.M702238200

Li, Y. F., He, W., Mandal, A., Kim, Y. H., Digilio, L., Klotz, K., et al. (2011). CABYR binds to AKAP3 and ropporin in the human sperm fibrous sheath. *Asian J. Androl.* 13, 266–274. doi: 10.1038/aja.2010.149

Llavanera, M., Delgado-Bermúdez, A., Fernandez-Fuertes, B., Recuero, S., Mateo, Y., Bonet, S., et al. (2019). GSTM3, but not IZUMO1, is a cryotolerance marker of boar sperm. *J. Anim. Sci. Biotechnol.* 10:61. doi: 10.1186/s40104-019-0370-375

Llavanera, M., Delgado-Bermúdez, A., Mateo-Otero, Y., Padilla, L., Romeu, X., Roca, J., et al. (2020a). Exploring seminal plasma GSTM3 as a quality and in vivo fertility biomarker in pigs—relationship with sperm morphology. *Antioxidants* 9:741. doi: 10.3390/antiox9080741

Llavanera, M., Delgado-bermúdez, A., Olives, S., Mateo-otero, Y., Recuero, S., Bonet, S., et al. (2020b). Glutathione S-transferases play a crucial role in mitochondrial function, plasma membrane stability and oxidative regulation of mammalian sperm. *Antioxidants* 9:100. doi: 10.3390/antiox9020100

Luongo, C., Abril-Sánchez, S., Hernández, J. G., and García-Vázquez, F. A. (2019). Seminal plasma mitigates the adverse effect of uterine fluid on boar spermatozoa. *Theriogenology* 136, 28–35. doi: 10.1016/j.theriogenology.2019.06.018

Luongo, C., González-Brusi, L., Cots-Rodríguez, P., Izquierdo-Rico, M. J., Avilés, M., and García-Vázquez, F. A. (2020). Sperm proteome after interaction with reproductive fluids in porcine: from the ejaculation to the fertilization site. *Int. J. Mol. Sci.* 21, 1–27. doi: 10.3390/ijms21176060

Magister, Š, and Kos, J. (2013). Cystatins in immune system. *J. Cancer* 4, 45–56. doi: 10.7150/jca.5044

Martinez, C. A., Alvarez-Rodriguez, M., Wright, D., and Rodriguez-Martinez, H. (2020). Does the pre-ovulatory pig oviduct rule sperm capacitation in vivo mediating transcriptomics of catsper channels? *Int. J. Mol. Sci.* 21:1840. doi: 10.3390/ijms21051840

Martinez, G., Kherraf, Z. E., Zouari, R., Mustapha, S. F., Ben, Saut, A., et al. (2018). Whole-exome sequencing identifies mutations in FSIP2 as a recurrent cause of multiple morphological abnormalities of the sperm flagella. *Hum. Reprod.* 33, 1973–1984. doi: 10.1093/humrep/dey264

Martínez-Fresneda, L., Sylvester, M., Shakeri, F., Bunes, A., Del Pozo, J. C., García-Vázquez, F. A., et al. (2021). Differential proteome between ejaculate and epididymal sperm represents a key factor for sperm freezability in wild small ruminants. *Cryobiology* 99, 64–77. doi: 10.1016/j.cryobiol.2021.01.012

Martínez-Heredia, J., Estanyol, J. M., Ballescà, J. L., and Oliva, R. (2006). Proteomic identification of human sperm proteins. *Proteomics* 6, 4356–4369. doi: 10.1002/pmic.200600094

Martins, H. S., da Silva, G. C., Cortes, S. F., Paes, F. O., Martins Filho, O. A., Araujo, M. S. S., et al. (2018). Lactoferrin increases sperm membrane functionality of frozen equine semen. *Reprod. Domest. Anim.* 53, 617–623. doi: 10.1111/rda.13148

Mead, J. G. (2018). Shepherd's beaked whale. *Encyclopedia Mar. Mamm.* 2018, 853–854. doi: 10.1016/B978-0-12-804327-1.00227-222

Mogielnicka-Brzozowska, M., Prochowska, S., Nižański, W., Bromke, M. A., Wiśniewski, J., Olejnik, B., et al. (2020). Proteome of cat semen obtained after urethral catheterization. *Theriogenology* 141, 68–81. doi: 10.1016/j.theriogenology.2019.09.003

Naaby-Hansen, S., Mandal, A., Wolkowicz, M. J., Sen, B., Westbrook, V. A., Shetty, J., et al. (2002). CABYR, a novel calcium-binding tyrosine phosphorylation-regulated fibrous sheath protein involved in capacitation. *Dev. Biol.* 242, 236–254. doi: 10.1006/dbio.2001.0527

O'Brien, J., and Robeck, T. (2010). The value of Ex situ cetacean populations in understanding reproductive physiology and developing assisted reproductive technology for Ex Situ and in Situ species management and conservation efforts. *Int. J. Comp. Psychol.* 23, 227–248. doi: 10.1017/cbo9781139051927.012

Panner Selvam, M., Agarwal, A., and Baskaran, S. (2019). Proteomic analysis of seminal plasma from bilateral varicocele patients indicates an oxidative state and increased inflammatory response. *Asian J. Androl.* 21, 544–550. doi: 10.4103/aja.aja_121_18

Park, Y. J., Pang, W. K., Ryu, D. Y., Song, W. H., Rahman, M. S., and Pang, M. G. (2019). Optimized combination of multiple biomarkers to improve diagnostic accuracy in male fertility. *Theriogenology* 139, 106–112. doi: 10.1016/j.theriogenology.2019.07.029

Parrilla, I., Perez-Patiño, C., Li, J., Barranco, I., Padilla, L., Rodriguez-Martinez, H., et al. (2019). Boar semen proteomics and sperm preservation. *Theriogenology* 137, 23–29. doi: 10.1016/j.theriogenology.2019.05.033

Parsons, E. C. M., Favaro, B., Aguirre, A. A., Bauer, A. L., Blight, L. K., Cigliano, J. A., et al. (2014). Seventy-one important questions for the conservation of marine biodiversity. *Conserv. Biol.* 28, 1206–1214. doi: 10.1111/cobi.12303

Pearl, C. A., and Roser, J. F. (2008). Expression of lactoferrin in the boar epididymis: effects of reduced estrogen. *Domest. Anim. Endocrinol.* 34, 153–159. doi: 10.1016/j.domaniend.2007.01.001

Peddinti, D., Nanduri, B., Kaya, A., Feugang, J. M., Burgess, S. C., and Memili, E. (2008). Comprehensive proteomic analysis of bovine spermatozoa of varying fertility rates and identification of biomarkers associated with fertility. *BMC Syst. Biol.* 2:19. doi: 10.1186/1752-0509-2-19

Pelloni, M., Paoli, D., Majoli, M., Pallotti, F., Carlini, T., Lenzi, A., et al. (2018). Molecular study of human sperm RNA: ropporin and CABYR in asthenozoospermia. *J. Endocrinol. Invest.* 41, 781–787. doi: 10.1007/s40618-017-0804-x

Perez-Patiño, C., Barranco, I., Parrilla, I., Martinez, E. A., Rodriguez-Martinez, H., and Roca, J. (2016). Extensive dataset of boar seminal plasma proteome displaying putative reproductive functions of identified proteins. *Data Br.* 8, 1370–1373. doi: 10.1016/j.dib.2016.07.037

Pérez-Patiño, C., Parrilla, I., Barranco, I., Vergara-Barberán, M., Simó-Alfonso, E. F., Herrero-Martínez, J. M., et al. (2018). New in-depth analytical approach of the porcine seminal plasma proteome reveals potential fertility biomarkers. *J. Proteome Res.* 17, 1065–1076. doi: 10.1021/acs.jproteome.7b00728

Perez-Riverol, Y., Csordas, A., Bai, J., Bernal-Llinares, M., Hewapathirana, S., Kundu, D. J., et al. (2019). The PRIDE database and related tools and resources in 2019: improving support for quantification data. *Nucleic Acids Res.* 47, D442–D450. doi: 10.1093/nar/gky1106

Peris-Frau, P., Martín-Maestro, A., Iniesta-Cuerda, M., Sánchez-Ajofrín, I., Mateos-Hernández, L., Garde, J. J., et al. (2019). Freezing-thawing procedures remodel the proteome of ram sperm before and after in vitro capacitation. *Int. J. Mol. Sci.* 20:4596. doi: 10.3390/ijms20184596

Petit, F. M., Serres, C., Bourgeon, F., Pineau, C., and Auer, J. (2013). Identification of sperm head proteins involved in zona pellucida binding. *Hum. Reprod.* 28, 852–865. doi: 10.1093/humrep/des452

Pini, T., Leahy, T., Soleilhavoup, C., Tsikis, G., Labas, V., Combes-Soia, L., et al. (2016). Proteomic investigation of ram spermatozoa and the proteins conferred by seminal plasma. *J. Proteome Res.* 15, 3700–3711. doi: 10.1021/acs.jproteome.6b00530

Pinto, T. M. F., Moreira, R. F., Matos, M. N. C., Soares, V. V. M., de Almeida Aguiar, M. V., de Aragão, P., et al. (2019). Evaluation of the proteomic profiles of ejaculated spermatozoa from Saanen bucks (*Capra hircus*). *Anim. Reprod.* 16, 902–913. doi: 10.21451/1984-3143-AR2019-0001

Piomboni, P., Gambera, L., Serafini, F., Campanella, G., Morgante, G., and De Leo, V. (2008). Sperm quality improvement after natural anti-oxidant treatment of asthenoteratospermic men with leukocytospermia. *Asian J. Androl.* 10, 201–206. doi: 10.1111/j.1745-7262.2008.00356.x

Rahman, M. S., Kwon, W. S., and Pang, M. G. (2017). Prediction of male fertility using capacitation-associated proteins in spermatozoa. *Mol. Reprod. Dev.* 84, 749–759. doi: 10.1002/mrd.22810

Ramesha, K. P., Mol, P., Kannegundla, U., Thota, L. N., Gopalakrishnan, L., Rana, E., et al. (2020). Deep proteome profiling of semen of indian indigenous malnad gidda (*Bos indicus*) cattle. *J. Proteome Res.* 19, 3364–3376. doi: 10.1021/acs.jproteome.0c00237

Ramm, S. A. (2014). Sperm competition and the evolution of reproductive systems. *Mol. Hum. Reprod.* 20, 1159–1160. doi: 10.1093/molehr/gau076

Recuero, S., Fernandez-Fuertes, B., Bonet, S., Barranco, I., and Yeste, M. (2019). Potential of seminal plasma to improve the fertility of frozen-thawed boar spermatozoa. *Theriogenology* 137, 36–42. doi: 10.1016/j.theriogenology.2019.05.035

Reeves, R. R., Smith, B. D., Crespo, E. A., Notarbartolo, and di Sciara, G. (2003). *Dolphins, Whales and Porpoises: 2002–2010. Conservation Action Plan for the World's Cetaceans. IUCN/SSC Cetacean Specialist Group*. Gland: IUCN.

Rego, J. P. A., Crisp, J. M., Moura, A. A., Nouwens, A. S., Li, Y., Venus, B., et al. (2014). Seminal plasma proteome of electroejaculated Bos indicus bulls. *Anim. Reprod. Sci.* 148, 1–17. doi: 10.1016/j.anireprosci.2014.04.016

Rickard, J. P., and de Graaf, S. P. (2020). Sperm surface changes and their consequences for sperm transit through the female reproductive tract. *Theriogenology* 150, 96–105. doi: 10.1016/j.theriogenology.2020.02.018

Robeck, T. R., Montano, G. A., Steinman, K. J., Smolensky, P., Sweeney, J., Osborn, S., et al. (2013). Development and evaluation of deep intra-uterine artificial insemination using cryopreserved sexed spermatozoa in bottlenose dolphins (*Tursiops truncatus*). *Anim. Reprod. Sci.* 139, 168–181. doi: 10.1016/j.anireprosci.2013.04.004

Robeck, T. R., and O'Brien, J. K. (2004). Effect of cryopreservation methods and precryopreservation storage on bottlenose dolphin (*Tursiops truncatus*) spermatozoa. *Biol. Reprod.* 70, 1340–1348. doi: 10.1095/biolreprod.103.025304

Robeck, T. R., Steinman, K. J., Yoshioka, M., Jensen, E., O'Brien, J. K., Katsumata, E., et al. (2005). Estrous cycle characterisation and artificial insemination using frozen-thawed spermatozoa in the bottlenose dolphin (*Tursiops truncatus*). *Reproduction* 129, 659–674. doi: 10.1530/rep.1.00516

Rommel, S., Pabst, D., and McLellan, W. (2007). "Functional anatomy of the cetacean reproductive system, with comparisons to the domestic dog," in *Reproductive Biology and Phylogeny of Cetacea*, eds B. G. M. Jamieson, and D. Miller (Boca Raton, FL: CRC Press), doi: 10.1201/b11001-5

Ruiz-Díaz, S., Luongo, C., Fuentes-Albero, M. C., Abril-Sánchez, S., Sánchez-Calabuig, M. J., Barros-García, C., et al. (2020). Effect of temperature and cell concentration on dolphin (*Tursiops truncatus*) spermatozoa quality evaluated at different days of refrigeration. *Anim. Reprod. Sci.* 212:106248. doi: 10.1016/j.anireprosci.2019.106248

Ryu, D. Y., Song, W. H., Pang, W. K., Yoon, S. J., Rahman, M. S., and Pang, M. G. (2019). Freezability biomarkers in bull epididymal spermatozoa. *Sci. Rep.* 9:12797. doi: 10.1038/s41598-019-49378-49375

Sánchez-Calabuig, M. J., de la Fuente, J., Laguna-Barraza, R., Beltrán-Breña, P., Martínez-Nevado, E., Johnston, S. D., et al. (2015a). Heterologous murine and bovine IVF using bottlenose dolphin (*Tursiops truncatus*) spermatozoa. *Theriogenology* 84, 983–994. doi: 10.1016/j.theriogenology.2015.06.001

Sánchez-Calabuig, M. J., López-Fernández, C., Johnston, S. D., Blyde, D., Cooper, J., Harrison, K., et al. (2015b). Effect of cryopreservation on the sperm DNA fragmentation dynamics of the bottlenose dolphin (*Tursiops truncatus*). *Reprod. Domest. Anim.* 50, 227–235. doi: 10.1111/rda.12474

Sánchez-Calabuig, M. J., García-Vázquez, F. A., Laguna-Barraza, R., Barros-García, C., García-Parraga, D., Rizos, D., et al. (2017). Bottlenose dolphin (*Tursiops truncatus*) spermatozoa: collection, cryopreservation, and heterologous in vitro fertilization. *J. Vis. Exp.* 2017:55237. doi: 10.3791/55237

Shevchenko, A., Jensen, O. N., Podtelejnikov, A. V., Sagliocco, F., Wilm, M., Vorm, O., et al. (1996). Linking genome and proteome by mass spectrometry: large-scale identification of yeast proteins from two dimensional gels. *Proc. Natl. Acad. Sci. U S A.* 93, 14440–14445. doi: 10.1073/pnas.93.25.14440

Shilov, I. V., Seymourt, S. L., Patel, A. A., Loboda, A., Tang, W. H., Keating, S. P., et al. (2007). The paragon algorithm, a next generation search engine that uses sequence temperature values sequence temperature values and feature probabilities to identify peptides from tandem mass spectra. *Mol. Cell. Proteomics* 6, 1638–1655. doi: 10.1074/mcp.T600050-MCP200

Sirigu, P., Perra, M. T., and Turno, F. (1995). Immunohistochemical study of secretory IGA in the human male reproductive tract. *Andrologia* 27, 335–339. doi: 10.1111/j.1439-0272.1995.tb01368.x

Skerget, S., Rosenow, M., Polpitiya, A., Petritis, K., Dorus, S., and Karr, T. L. (2013). The rhesus macaque (*macaca mulatta*) sperm proteome. *Mol. Cell. Proteomics* 12, 3052–3067. doi: 10.1074/mcp.M112.026476

Soleilhavoup, C., Tsikis, G., Labas, V., Harichaux, G., Kohnke, P. L., Dacheux, J. L., et al. (2014). Ram seminal plasma proteome and its impact on liquid

preservation of spermatozoa. *J. Proteomics* 109, 245–260. doi: 10.1016/j.jprot.2014.07.007

Spaulding, M., O'Leary, M. A., and Gatesy, J. (2009). Relationships of cetacea (Artiodactyla) among mammals: increased taxon sampling alters interpretations of key fossils and character evolution. *PLoS One* 4:e7062. doi: 10.1371/journal.pone.0007062

Suárez-Santana, C. M., Fernández, A., Sierra, E., Arbelo, M., Bernaldo, de Quirós, Y., et al. (2020). Comparative morphology, histology, and cytology of odontocete cetaceans prostates. *Anat. Rec.* 303, 2036–2053. doi: 10.1002/ar.24285

Sun, Y., Xiao, S., Chen, J., Wang, M., Zheng, Z., Song, S., et al. (2015). Heat shock protein 90 mediates the apoptosis and autophage in nicotinic-mycoepoxydienetreated HeLa cells. *Acta Biochim. Biophys. Sin. (Shanghai).* 47, 451–458. doi: 10.1093/abbs/gmv034

Swegen, A., Curry, B. J., Gibb, Z., Lambourne, S. R., Smith, N. D., and Aitken, R. J. (2015). Investigation of the stallion sperm proteome by mass spectrometry. *Reproduction* 149, 235–244. doi: 10.1530/REP-14-0500

Takenaka, A., Kashiwagi, N., Maezono, Y., Nakao, T., Wano, Y., Kakizoe, Y., et al. (2013). Study on the ejaculate characteristics and liquid storage of semen in the common bottlenose dolphin (*Tursiops truncatus*). *Japanese J. Zoo Wildl. Med.* 18, 107–114. doi: 10.5686/jjzwm.18.107

Thewissen, J. G. M., Cooper, L. N., Clementz, M. T., Bajpai, S., and Tiwari, B. N. (2007). Whales originated from aquatic artiodactyls in the Eocene epoch of India. *Nature* 450, 1190–1194. doi: 10.1038/nature06343

Uhen, M. D. (2007). Evolution of marine mammals: back to the sea after 300 million years. *Anat. Rec.* 290, 514–522. doi: 10.1002/ar.20545

Valencia, J., Yeste, M., Quintero-Moreno, A., Niño-Cardenas, C., del, P., and Henao, F. J. (2020). Relative content of Niemann-Pick C2 protein (NPC2) in seminal plasma, but not that of spermadhesin AQN-1, is related to boar sperm cryotolerance. *Theriogenology* 14, 181–189. doi: 10.1016/j.theriogenology.2019.10.023

van der Horst, G., Medger, K., Steckler, D., Luther, I., and Bartels, P. (2018). Bottlenose dolphin (*Tursiops truncatus*) sperm revisited: motility, morphology and ultrastructure of fresh sperm of consecutive ejaculates. *Anim. Reprod. Sci.* 195, 309–320. doi: 10.1016/j.anireprosci.2018.06.009

Vicens, A., Borziak, K., Karr, T. L., Roldan, E. R. S., and Dorus, S. (2017). Comparative sperm proteomics in mouse species with divergent mating systems. *Mol. Biol. Evol.* 34, 1403–1416. doi: 10.1093/molbev/msx084

Vislobokova, I. A. (2013). On the origin of cetartiodactyla: comparison of data on evolutionary morphology and molecular biology. *Paleontol. J.* 47, 321–334. doi: 10.1134/S003103011303012X

Wichmann, L., Vaalasti, A., Vaalasti, T., and Tuohimaa, P. (1989). Localization of lactoferrin in the male reproductive tract. *Int. J. Androl.* 12, 179–186. doi: 10.1111/j.1365-2605.1989.tb01302.x

Xu, K., Yang, L., Zhang, L., and Qi, H. (2020). Lack of AKAP3 disrupts integrity of the subcellular structure and proteome of mouse sperm and causes male sterility. *Development* 147:dev181057. doi: 10.1242/dev.181057

Yang, Y., Jiang, C., Zhang, X., Liu, X., Li, J., Qiao, X., et al. (2020). Loss-of-function mutation in DNAH8 induces asthenoteratospermia associated with multiple morphological abnormalities of the sperm flagella. *Clin. Genet.* 98, 396–401. doi: 10.1111/cge.13815

Zeinali, M., Hadian Amree, A., Khorramdelazad, H., Karami, H., and Abedinzadeh, M. (2017). Inflammatory and anti-inflammatory cytokines in the seminal plasma of infertile men suffering from varicocele. *Andrologia* 49, e12685. doi: 10.1111/and.12685

Zhang, X., Chen, M., Yu, R., Liu, B., Tian, Z., and Liu, S. (2016). FSCB phosphorylation regulates mouse spermatozoa capacitation through suppressing SUMOylation of ROPN1/ROPN1L. *Am. J. Transl. Res.* 8, 2776–2782.

Zhao, W., Li, Z., Ping, P., Wang, G., Yuan, X., and Sun, F. (2018). Outer dense fibers stabilize the axoneme to maintain sperm motility. *J. Cell. Mol. Med.* 22, 1755–1768. doi: 10.1111/jcmm.13457

Zhu, W., Cheng, X., Ren, C., Chen, J., Zhang, Y., Chen, Y., et al. (2020). Proteomic characterization and comparison of ram (*Ovis aries*) and buck (*Capra hircus*) spermatozoa proteome using a data independent acquisition mass spectometry (DIA-MS) approach. *PLoS One* 15:e0228656. doi: 10.1371/journal.pone.0228656

Conflict of Interest: The authors declare that the research was conducted in the absence of any commercial or financial relationships that could be construed as a potential conflict of interest.

frontiers in Cell and Developmental Biology

ORIGINAL RESEARCH
published: 01 September 2021
doi: 10.3389/fcell.2021.656438

Aquaporins Are Essential to Maintain Motility and Membrane Lipid Architecture During Mammalian Sperm Capacitation

*Ariadna Delgado-Bermúdez[1,2], Sandra Recuero[1,2], Marc Llavanera[1,2], Yentel Mateo-Otero[1,2], Andra Sandu[1,2], Isabel Barranco[1,2], Jordi Ribas-Maynou[1,2] and Marc Yeste[1,2]**

[1] Biotechnology of Animal and Human Reproduction (TechnoSperm), Institute of Food and Agricultural Technology, University of Girona, Girona, Spain, [2] Unit of Cell Biology, Department of Biology, Faculty of Sciences, University of Girona, Girona, Spain

OPEN ACCESS

Edited by:
Ana Josefa Soler, University of Castilla-La Mancha, Spain

Reviewed by:
María Gracia Gervasi, University of Massachusetts Amherst, United States
Felipe A. Navarrete, University of Massachusetts Amherst, United States

***Correspondence:**
Marc Yeste
marc.yeste@udg.edu

Specialty section:
This article was submitted to Cell Growth and Division, a section of the journal Frontiers in Cell and Developmental Biology

Received: *20 January 2021*
Accepted: *13 August 2021*
Published: *01 September 2021*

Citation:
Delgado-Bermúdez A, Recuero S, Llavanera M, Mateo-Otero Y, Sandu A, Barranco I, Ribas-Maynou J and Yeste M (2021) Aquaporins Are Essential to Maintain Motility and Membrane Lipid Architecture During Mammalian Sperm Capacitation. Front. Cell Dev. Biol. 9:656438. doi: 10.3389/fcell.2021.656438

Aquaporins are a family of ubiquitous transmembrane proteins that allow the transport of water and small molecules across the cell plasma membrane. The different members of this family present a characteristic distribution across different cell types, which is species-specific. In mammalian sperm, different AQPs, including AQP3, AQP7, and AQP11, have been identified; their main roles are related to osmoadaptation and sperm motility activation after ejaculation. Capacitation, which is a post-ejaculatory process that sperm must undergo to achieve fertilizing ability, is triggered by pH changes and different extracellular ions that are present in the female reproductive tract. Considering the function of AQPs and their influence on pH through the regulation of water flow, this study aimed to elucidate the potential role of different AQPs during *in vitro* sperm capacitation using three different transition metal compounds as AQP inhibitors. Cooper sulfate, a specific inhibitor of AQP3, caused a drastic increase in peroxide intracellular levels compared to the control. Mercury chloride, an unspecific inhibitor of all AQPs except AQP7 produced an increase in membrane lipid disorder and led to a decrease in sperm motility and kinetics parameters. Finally, the addition of silver sulfadiazine, an unspecific inhibitor of all AQPs, generated the same effects than mercury chloride, decreased the intracellular pH and altered tyrosine phosphorylation levels after the induction of the acrosome reaction. In the light of the aforementioned, (a) the permeability of AQP3 to peroxides does not seem to be crucial for sperm capacitation and acrosome reaction; (b) AQPs have a key role in preserving sperm motility during that process; and (c) AQPs as a whole seem to contribute to the maintenance of lipid membrane architecture during capacitation and may be related to the intracellular signaling pathways involved in the acrosome reaction. Hence, further research aimed to elucidate the mechanisms underlying the involvement of AQPs in mammalian sperm capacitation and acrosome reaction is warranted.

Keywords: aquaporins, spermatozoa, silver sulfadiazine, cooper sulfate, capacitation, mercury chloride

INTRODUCTION

Cell homeostasis relies on both the integrity and permeability of plasma membrane to water and electrolytes. Because of its amphipathic nature, additional mechanisms to simple diffusion are required in order for water and solutes to pass through the cell membrane (Watson, 2015). Aquaporins (AQPs) are ubiquitous transmembrane water proteins that allow the transport of water and small solutes across cell membranes (reviewed by Yeste et al., 2017). In mammalian cells, this family of channel proteins includes different members that are classified according to sequence similarity and solute permeability into: orthodox AQPs, aquaglyceroporins (GLPs) and superAQPs. The group of orthodox AQPs includes AQP0, AQP1, AQP2, AQP4, AQP5, AQP6, and AQP8, which are exclusively permeable to water. Aquaglyceroporins, which are permeable to water, glycerol, urea and other small electrolytes, include AQP3, AQP7, AQP9, and AQP10. Finally, the group of superAQPs comprises AQP11 and AQP12, which are localized in the membranes of intracellular organelles, present sequence variations to the other groups of AQPs and are involved in both water and glycerol transport.

Despite being ubiquitous, the distribution of AQPs across cell types and species is uneven and characteristic. Regarding mammalian sperm, AQP3, AQP7, and AQP11 have been identified in mouse (Yeung et al., 2009; Yeung and Cooper, 2010; Chen et al., 2011), human (Yeung et al., 2010; Laforenza et al., 2017), pig (Prieto-Martínez et al., 2014, 2015), cattle (Prieto-Martinez et al., 2016; Morató et al., 2018) and horse (Bonilla-Correal et al., 2017); AQP8 has been found in mouse (Yeung et al., 2009) and human spermatozoa (Yeung et al., 2010; Laforenza et al., 2017); and AQP9 has been reported to be present in pig sperm (Vicente-Carrillo et al., 2016). The main functions of AQPs in mammalian spermatozoa are volume regulation and osmoadaptation. In effect, AQP3 has a vital role in osmoregulation (Chen and Duan, 2011), which is of crucial importance in post-ejaculatory events, when sperm cells interact with the female tract. In addition, Prieto-Martínez et al. (2017) observed a positive correlation between relative AQP3-content and osmoadaptation during cryopreservation, which is a challenging process since sperm are exposed to significant osmolality changes. Moreover, AQP7 has been suggested to be related to sperm motility in humans (Saito et al., 2004), but not in mice (Sohara et al., 2007). As far as AQP9 is concerned, there is little evidence on its particular role, since despite having been observed in pig spermatozoa (Vicente-Carrillo et al., 2016), homozygous *Aqp9*$^{-/-}$ mice show preserved fertility and their spermatozoa are morphologically normal and motile (Rojek et al., 2007). Finally, and with regard to AQP11, while its relative content was found to be correlated with plasma membrane integrity and motility in pig spermatozoa (Prieto-Martínez et al., 2014), it was confirmed as a cryotolerance biomarker in cattle (Morató et al., 2018) but not in pig spermatozoa (Prieto-Martínez et al., 2017). It is worth mentioning that the specific role of each AQP appears to differ across species, and that the particular relevance of their functions evokes that certain members of the AQP family can be compensated by others. Nevertheless, since exposure to the female reproductive tract involves a major challenge to the ability of spermatozoa to adapt to drastic osmolality variations, the role of AQPs in osmoregulation is essential to ensure preservation of sperm function and the success of subsequent post-ejaculatory events, such as motility activation [reviewed by Yeste et al. (2017)].

Because of their exposure to the female reproductive tract, sperm cells meet constantly changing environments, from which they receive different chemical and thermal signals. This set of inputs drives a series of signaling events that are essential for sperm capacitation, which is the process that confers sperm the ability to fertilize an oocyte (Chang, 1951). Briefly, after entering the female tract, spermatozoa find higher bicarbonate and calcium levels, whose influx activates the cAMP-PKA pathway and increases tyrosine phosphorylation downstream, thus hyperactivating sperm motility (reviewed by Puga Molina et al., 2018). In addition, this ion flow through plasma membrane triggers lipid reorganization and cholesterol efflux; as a consequence, the sperm membrane is hyperpolarized and its fluidity rises, which is crucial to increase membrane fusogenicity (reviewed in Bailey, 2010). Thereafter, progesterone triggers the acrosome reaction through its interaction with a G protein-coupled receptor (GPCR) (Buffone et al., 2014). Given the importance of intracellular pH as a regulator of the sperm-specific, soluble adenylyl cyclase (sAC), which is the source of cAMP that allows the activation of the cAMP-PKA pathway, it is reasonable to posit that AQPs might have a relevant role during mammalian sperm capacitation.

High affinity inhibitors are a reasonably accurate strategy to study AQPs function, and transitional metals have been used as blockers of water permeability in different cell types (Haddoub et al., 2009). Different mercurial compounds were used at first to prove the existence of water channels in erythrocytes and renal proximal tubule cells (Smith and Agre, 1991), as well as in *Xenopus* oocytes (Preston et al., 1992). Silver compounds have also been used as AQP inhibitors (Niemietz and Tyerman, 2002), showing a higher affinity and specificity for this family of proteins. Finally, cooper was also identified as a reversible, rapid and specific inhibitor of AQP3 (Zelenina et al., 2004).

Considering all the aforementioned, this study aimed to elucidate the role of the different AQPs in mammalian sperm capacitation using the pig as a model, and through their inhibition with transition metal compounds.

MATERIALS AND METHODS

Animals and Ejaculates

A total of 32 ejaculates from separate Piétrain boars (n = 32) were used in this study. Boars were housed in a local farm (Grup Gepork SL, Masies de Roda, Spain) in controlled climatic conditions and fed with a standard diet. Sperm-rich fractions were manually collected and subsequently diluted to a final concentration of 33 × 10^6 sperm/mL in a commercial semen extender (Vitasem LD; Magapor SL, Zaragoza, Spain) and preserved at 17°C. Samples were transported to the laboratory within 2 h post-collection and, upon arrival, ejaculates were combined in pools of four for each experiment.

After that, each ejaculate pool was split into four different aliquots that were centrifuged (Universal 32R centrifuge; Hettich Zentrifugen; Tuttlingen, Germany) at 600 × *g* and 17°C for 5 min. Supernatants were discarded, and samples were then resuspended in pre-warmed, equilibrated capacitation medium [20 mM 4- (2-Hydroxyethyl) piperazine-1-ethanesulfonic acid (HEPES), 112 mM NaCl, 3.1 mM KCl, 5 mM glucose, 21.7 mM sodium L-lactate, 1 mM sodium pyruvate, 0.3 mM Na_2HPO_4, 0.4 mM $MgSO_4 \times 7H_2O$, 4.5 mM $CaCl_2 \times 2H_2O$, 5 mg/mL BSA and 15 mM bicarbonate; pH = 7.4 ± 0.1; osmolality = 0.300 Osm/Kg ± 0.01] to a final concentration of 25×10^6 sperm/mL. Thereafter, the corresponding inhibitors were added according to the treatment, and samples were kept in a Hera Cell 150 incubator at 38°C and 5% CO_2. In order to induce the acrosome reaction, progesterone (final concentration: 0.01 mg/mL) was added after 4 h of incubation and samples were incubated for an additional hour.

AQP Inhibitors

Three different AQP inhibitors were added to capacitation medium prior to incubation: cooper sulfate ($CuSO_4$; Sigma Aldrich; Saint Louis, MO, United States), mercury chloride ($HgCl_2$; Sigma Aldrich) and silver sulfadiazine (AgSDZ; Sigma Aldrich). The final concentrations of each inhibitor were set after preliminary experiments based on previous studies (Niemietz and Tyerman, 2002; Yeung et al., 2009; Reca et al., 2018). Each inhibitor was previously diluted in water. $CuSO_4$ (stock concentration: 400 mM) was added to samples at a final concentration of 100 μM; $HgCl_2$ (stock concentration: 40 mM) was added to a final concentration of 20 μM; and AgSDZ (stock concentration: 40 mM) was used at a final concentration of 5 μM.

Evaluation of Sperm Quality and Function

For the evaluation of sperm quality and function, sperm motility, flow cytometry, immunoblotting and ELISA analyses were performed after 0, 120, 240, 250, and 300 min of incubation in capacitation medium.

Motility

Sperm motility was assessed using a commercial computer-assisted sperm analysis (CASA) system, which consisted of a phase contrast microscope (Olympus BX41; Olympus, Tokyo, Japan) equipped with a video camera and ISAS software (Integrated Sperm Analysis System V1.0; Proiser SL, Valencia, Spain). With this purpose, a 5-μL drop of the sperm suspension was placed onto a Makler counting chamber (Sefi-Medical Instruments, Haifa, Israel) and observed under a negative phase-contrast field (Olympus 10 × 0.30 PLAN objective; Olympus). The following sperm motility parameters were recorded in each motility assessment: total motility (TMOT;%); progressive motility (PMOT,%); curvilinear velocity (VCL, μm/s); straight-line velocity (VSL, μm/s); average pathway velocity (VAP, μm/s); amplitude of lateral head displacement (ALH, μm); beat-cross frequency (BCF, Hz); linearity (LIN,%), that resulted from LIN = VSL/VCL × 100; straightness (STR,%), which was calculated as VSL/VAP × 100; and oscillation index (WOB,%), obtained from VAP/VCL × 100. A motile sperm was defined as having a VAP ≥ 10 μm/s, and a sperm cell was considered as progressively motile when its STR was at least 45%. In addition, the percentage of progressively motile spermatozoa among the population of motile sperm was calculated. For each sample, three replicates of at least 1,000 spermatozoa each were assessed. For each parameter, the corresponding mean and standard error of the mean (SEM) were calculated.

Flow Cytometry

Eight different parameters were assessed through flow cytometry in each time point and treatment: sperm plasma membrane integrity, membrane lipid disorder, acrosome membrane integrity, mitochondrial membrane potential (MMP), intracellular levels of calcium, superoxide ($O_2^{-}\bullet$) radicals and hydrogen peroxide (H_2O_2), and intracellular pH. All fluorochromes were obtained from ThermoFisher Scientific (Waltham, MA, United States) unless otherwise stated. Prior to the addition of the corresponding combination of fluorochromes, samples were diluted in phosphate-buffered saline (PBS) to a final concentration of 2×10^6 spermatozoa/mL. After staining, samples were incubated at 38°C in the dark. For each parameter, three replicates of at least 10,000 spermatozoa were assessed.

A Cell Lab Quanta^{TM} SC cytometer (Beckman Coulter; Fullerton; CA, United States) was used to analyze sperm samples. Samples were excited with an argon ion laser (488 nm) at a power of 22 mW. Cell diameter/volume was assessed using the Coulter principle, which measures electrical resistance changes caused by suspended, non-conductive particles in an electrolyte solution. In this system, forward scatter (FS) was replaced by electronic volume (EV) and for EV-channel calibration, 10-μm Flow-Check fluorospheres (Beckman Coulter) were positioned at channel 200 on the EV-scale.

For fluorescence detection, three different optical filters were used: FL1 (Dichroic/Splitter, DRLP: 550 nm, BP filter: 525 nm, detection width 505–545 nm); FL2 (DRLP: 600 nm, BP filter: 575 nm, detection width: 560–590 nm); and FL3 (LP filter: 670 nm/730 nm, detection width: 655–685 nm). FL1 was used to detect green fluorescence from SYBR-14, YO-PRO-1, fluorescein isothiocyanate (FITC)-conjugated peanut agglutinin (PNA; PNA-FITC), JC-1 monomers (JC-1_{mon}), Fluo-3, 2′,7′-dichlorofluorescein (DCF^+) and 2′,7′-Bis-(2-Carboxyethyl)-5-(and-6)-Carboxyfluorescein, Acetoxymethyl (BCECF). FL2 was used to detect orange fluorescence from JC-1 aggregates (JC-1_{agg}). Finally, FL3 was used to detect red fluorescence from propidium iodide (PI), merocyanine 540 (M540) and ethidium (E^+). The signal was logarithmically amplified, and photomultiplier settings were adjusted according to particular staining methods.

The sheath flow rate was set at 4.17 μL/min, and EV and side scatter (SS) were measured and linearly recorded for all particles. Subcellular debris (particle diameter < 7 μm) and cell aggregates (particle diameter > 12 μm) were excluded through the adjustment of the analyzer threshold on the EV channel, and the sperm-specific events were positively gated on the basis of EV/SS distributions. For each sample and

parameter, three different replicates of a minimum of 10,000 events were evaluated.

Data analysis was performed using Flowing Software (Ver. 2.5.1; University of Turku, Finland), following the recommendations of the International Society for Advancement of Cytometry (ISAC). According to Petrunkina et al. (2010), the percentage of non-sperm debris particles from the SYBR-14$^-$/PI$^-$ population was used to correct the events corresponding to double-negative particles in the other protocols. For each sample and parameter, the corresponding mean and SEM were calculated.

Sperm plasma membrane integrity

The assessment of plasma membrane integrity was performed using the LIVE/DEAD sperm viability kit (Molecular Probes; Eugene, OR, United States) following the protocol of Garner and Johnson (1995). Briefly, spermatozoa were incubated in the presence of SYBR-14 (final concentration: 100 nmol/L) for 10 min, and PI (final concentration: 12 μmol/L) was subsequently added prior to an additional incubation of 5 min. Three different sperm populations were identified in flow cytometry dot-plots: (1) viable, green-stained spermatozoa (SYBR-14$^+$/PI$^-$); (2) non-viable, red-stained spermatozoa (SYBR-14$^-$/PI$^+$); and (3) non-viable, green- and red-stained spermatozoa (SYBR-14$^+$/PI$^+$). In addition, unstained, non-sperm particles (SYBR-14$^-$/PI$^-$) were not included for the calculation of the final percentages of the three previously mentioned populations. SYBR-14 fluorescence spill over into FL3 channel was compensated (2.45%).

Membrane lipid disorder

Co-staining with M540 and YO-PRO-1 was used to evaluate sperm membrane lipid disorder, following the protocol from Rathi et al. (2001) with minor modifications (Yeste et al., 2014). This protocol is based on the intercalation of M540 in the outer monolayer of the sperm plasma membrane when packing order of phospholipids decreases. In brief, samples were co-stained with M540 (final concentration: 2.6 μmol/L) and YO-PRO-1 (final concentration: 25 nmol/L) and then incubated for 10 min. Four different sperm populations were identified in flow cytometry dot-plots: (1) viable spermatozoa with low membrane lipid disorder (M540$^-$/YO-PRO-1$^-$); (2) viable sperm with high membrane lipid disorder (M540$^+$/YO-PRO-1$^-$); (3) non-viable sperm with low membrane lipid disorder (M540$^-$/YO-PRO-1$^+$); and (4) non-viable sperm with high membrane lipid disorder (M540$^+$/YO-PRO-1$^+$). The percentage of SYBR-14$^-$/PI$^-$ particles corresponding to non-sperm debris was used to correct the percentages of viable spermatozoa with low membrane lipid disorder (M540$^-$/YO-PRO-1$^-$); percentages of the other sperm populations were recalculated. Data were not compensated. Membrane lipid disorder was assessed through the calculation of the percentage of viable sperm with low membrane lipid disorder (M540$^-$/YO-PRO-1$^-$ sperm) from the population of viable spermatozoa (YO-PRO-1$^-$ sperm).

Acrosome membrane integrity

Samples were co-stained with fluorescein isothiocyanate (FITC)-conjugated peanut agglutinin (PNA; PNA-FITC) and PI in order to evaluate acrosome membrane integrity following the protocol from Nagy et al. (2003). PNA-FITC binds specifically to the outer acrosomal membrane. In brief, samples were co-incubated in the presence of PNA-FITC (final concentration: 2.5 μg/mL) and PI (final concentration: 12 μmol/L) for 10 min. As spermatozoa were not permeabilized, four different sperm populations were identified in flow cytometry dot-plots: (1) spermatozoa with an intact plasma membrane (PNA-FITC$^-$/PI$^-$); (2) spermatozoa with a damaged plasma membrane and an outer acrosome membrane that could not be fully intact (PNA-FITC$^+$/PI$^+$); (3) spermatozoa with a damaged plasma membrane and a non-intact acrosome membrane (PNA-FITC$^-$/PI$^+$); and (4) spermatozoa a with damaged plasma membrane (PNA-FITC$^+$/PI$^-$). The percentage of SYBR-14$^-$/PI$^-$ particles corresponding to non-sperm debris was used to correct the percentages of viable sperm with intact acrosome (PNA-FITC$^-$/PI$^-$), and the percentages of the other sperm populations were recalculated. PNA-FITC fluorescence spill over into FL3 channel was compensated (2.45%).

Intracellular levels of calcium

Sperm samples were co-stained with Fluo-3 AM and PI for the evaluation of intracellular calcium levels following the protocol from Harrison et al. (1993). Fluo-3 stains calcium that is located in the mid-piece, but it also stains faintly the calcium present in the sperm head (Yeste et al., 2015). In brief, samples were co-incubated with Fluo-3 (final concentration: 1 μmol/L) and PI (final concentration: 12 μmol/L) for 10 min. Four different sperm populations were identified in flow cytometry dot-plots: (1) viable sperm with low intracellular levels of calcium (Fluo-3$^-$/PI$^-$); (2) viable sperm with high intracellular levels of calcium (Fluo-3$^+$/PI$^-$); (3) non-viable sperm with low intracellular levels of calcium (Fluo-3$^-$/PI$^+$); and (4) non-viable sperm with high intracellular levels of calcium (Fluo-3$^+$/PI$^+$). The percentage of SYBR-14$^-$/PI$^-$ particles corresponding to non-sperm debris was used to correct the percentages of viable sperm with low intracellular levels of calcium (Fluo-3$^-$/PI$^-$), and the percentages of the other sperm populations were recalculated. Fluo-3 fluorescence spill over into FL3 channel was compensated (2.45%). Intracellular levels of calcium were assessed through the calculation of the percentage of viable sperm with high intracellular levels of calcium (Fluo-3$^+$/PI$^-$ sperm) within the population of viable spermatozoa (PI$^-$ sperm).

Mitochondrial membrane potential

Samples were stained with JC-1 in order to evaluate mitochondrial membrane potential following the protocol of Ortega-Ferrusola et al. (2008) with minor modifications. JC-1 molecules (5,5′,6,6′-tetrachloro-1,1′,3,3′tetraethyl-benzimidazolylcarbocyanine iodide) remain as monomers (JC-1$_{mon}$) in the presence of low MMP and emit green fluorescence, whereas in the presence of high MMP, these molecules form aggregates (JC-1$_{agg}$) that present orange fluorescence. Briefly, samples were incubated with JC-1 (final concentration: 0.3 μmol/L) for 30 min. Flow cytometry dot-plots allowed the identification of three different populations: (1) sperm with mitochondria presenting low MMP (JC-1$_{mon}$; FL1$^+$/FL2$^-$); (2) sperm with mitochondria showing high MMP

($JC\text{-}1_{agg}$; $FL1^-/FL2^+$); and (3) sperm with heterogeneous mitochondria ($JC\text{-}1_{mon}$ and $JC\text{-}1_{agg}$; $FL1^+/FL2^+$). The percentage of $SYBR\text{-}14^-/PI^-$ particles corresponding to non-sperm debris was used to correct the percentages of sperm with mitochondria presenting low MMP ($JC\text{-}1_{mon}$; $FL1^+/FL2^-$), and the percentages of the other sperm populations were recalculated. The sum of populations (2) and (3) corresponded to high MMP-spermatozoa. MMP was also assessed through the calculation of the ratio of the intensity of fluorescence $JC\text{-}1_{agg}/JC\text{-}1_{mon}$ from each sperm population. $JC1_{mon}$ fluorescence spill-over into the FL2 channel was compensated (51.70%).

Intracellular levels of superoxide ($O_2^{-}\bullet$) radicals

Samples were co-stained with hydroethidine (HE) and YO-PRO-1 in order to evaluate the intracellular levels of superoxides ($O_2^{-}\bullet$) following the protocol from Guthrie and Welch (2006). In the presence of $O_2^{-}\bullet$ radicals, HE is oxidized into ethidium (E^+) and other products. Briefly, samples were incubated in the presence of HE (final concentration: 4 μmol/L) and YO-PRO-1 (final concentration: 25 nmol/L) for 20 min. As a result, flow cytometry dot-plots allowed the identification of four different sperm populations: (1) viable sperm with low intracellular levels of $O_2^{-}\bullet$ (E^-/YO-PRO-1^-); (2) viable sperm with high intracellular levels of $O_2^{-}\bullet$ (E^+/YO-PRO-1^-); (3) non-viable sperm with low intracellular levels of $O_2^{-}\bullet$ (E^-/YO-PRO-1^+); and (4) non-viable sperm with high intracellular levels of $O_2^{-}\bullet$ (E^+/YO-PRO-1^+). The percentage of $SYBR\text{-}14^-/PI^-$ particles corresponding to non-sperm debris was used to correct the percentages of viable sperm with low intracellular levels of $O_2^{-}\bullet$ (E^-/YO-PRO-1^-), and the percentages of the other sperm populations were recalculated. YO-PRO-1 spill-over into the FL3 channel was compensated (5.06%). Intracellular levels of superoxide radicals were assessed through the calculation of the percentage of viable sperm with high intracellular levels of superoxide (E^+/YO-PRO-1^- sperm) within the population of viable spermatozoa (YO-PRO-1^-sperm).

Intracellular levels of hydrogen peroxide (H_2O_2)

Intracellular levels of hydrogen peroxide (H_2O_2) were evaluated through co-staining with H_2DCFDA and PI following the protocol from Guthrie and Welch (2006). In the presence of H_2O_2, the non-fluorescent probe H_2DCFDA is intracellularly de-esterified and oxidized into highly fluorescent DCF^+. In brief, samples were co-incubated with H_2DCFDA (final concentration: 200 μmol/L) and PI (final concentration: 12 μmol/L) for 30 min. Four different sperm populations were identified in flow cytometry dot-plots: (1) viable sperm with low intracellular levels of H_2O_2 (DCF^-/PI^-); (2) viable sperm with high intracellular levels of H_2O_2 (DCF^+/PI^-); (3) non-viable sperm with low intracellular levels of H_2O_2 (DCF^-/PI^+); and (4) non-viable sperm with high intracellular levels of H_2O_2 (DCF^+/PI^+). The percentage of $SYBR\text{-}14^-/PI^-$ particles corresponding to non-sperm debris was used to correct the percentages of viable sperm with low intracellular levels of H_2O_2 (DCF^-/PI^-), and the percentages of the other sperm populations were recalculated. DCF^- spill-over into the FL3 channel was compensated (2.45%). Intracellular levels of hydrogen peroxide were assessed through the calculation of the percentage of viable sperm with high intracellular levels of peroxide (DCF^+/PI^- sperm) within the population of viable spermatozoa (PI^- sperm).

Intracellular pH

Intracellular pH was measured through staining with BCECF following the protocol from Pons-Rejraji et al. (2009) with minor modifications. BCECF is intracellularly modified by esterases, and its fluorescence excitation profile is pH-dependent. In brief, samples were incubated in the presence of BCECF (final concentration: 6 μmol/L) for 25 min. Data were not compensated. The intensity of fluorescence was measured for the different treatments and time points, and the intracellular pH was calculated as the variation compared to the control.

Immunoblotting

Tyrosine phosphorylation levels were assessed for the different treatments and time points through immunoblotting. With this purpose, samples were centrifuged at 600 × *g* and capacitation medium was discarded. Samples were subsequently stored at −80°C until analysis.

For cell lysis, samples were thawed on ice and resuspended in lysis buffer (xTractor® Buffer; Takara Bio, Mountain View, CA, United States) supplemented with 1% protease inhibitor cocktail, 1 mM sodium orthovanadate and 1 mM phenylmethanesulfonyl fluoride (PMSF). After incubation at 4°C for 30 min with shaking, samples were sonicated thrice for 30 s. Samples were then centrifuged at 4°C and 12,000 × *g* for 15 min, and supernatants were collected and stored at −80°C until analysis. Total protein was quantified by triplicate through a detergent compatible (DC) method (Bio-Rad, Hercules, CA, United States) using an Epoch™ microplate spectrophotometer (BioTek, Winooski, VT, United States).

For each sample, 10 μg of total protein was diluted in loading buffer, which consisted of 4 × Laemmli reductor (Bio-Rad) supplemented with 10% (v:v) 2-Mercaptoethanol. Then, samples were incubated at 95°C for 5 min and a total volume of 30 μL per sample was loaded onto a gradient (8–16%) polyacrylamide gel (Mini-PROTEAN® TGX Stain-Free™ Precast Gels, Bio-Rad). Electrophoresis ran at 150 V for approximately 1 h, and proteins from the gels were transferred onto polyvinylidene difluoride (PVDF) membranes using *Trans*-Blot® Turbo™ (Bio-Rad). Next, total protein content was visualized by UV exposition and acquisition using a G:BOX Chemi XL system (SynGene, Frederick, MD, United States). Membranes were subsequently incubated in blocking buffer [10 mM Tris, 150 mM NaCl, 0.05% (v:v) Tween-20 and 5% (w:v) bovine serum albumin (Roche Diagnostics, S.L., Basel, Switzerland); pH = 7.3] in agitation for 1 h at room temperature. Then, membranes were incubated overnight at 4°C with a 4G10® Platinum, Anti-Phosphotyrosine Antibody [mouse monoclonal cocktail IgG2b; Sigma Aldrich; 1:5,000; (v:v)]. Then, membranes were washed five times with TBS-Tween 20 1 × (10 mmol/L Tris, 150 mmol/L NaCl and 0.05% Tween-20; pH = 7.3) for 5 min before incubation with a rabbit anti-mouse, secondary antibody conjugated with HRP [ref. P0260; Agilent, Santa Clara, CA, United States; 1:10,000 (v:v)] for 1 h in agitation. Finally, membranes were

washed five times. For visualization, membranes were incubated in a chemiluminescence substrate (Immobilion^{TM} Western Detection Reagents, Millipore) for 5 min, and then revealed in G:BOX Chemi XL 1.4.

Two technical replicates per sample were evaluated, and band quantification was performed using the Image Studio^{TM} Lite Software (LI-COR Biosciences GmbH, Bad Homburg vor der Höhe, Germany). Band pattern quantifications were normalized using total protein values, and the corresponding mean ± SEM was calculated.

Enzyme-Linked Immunosorbent Assays

Concentrations of PKA in sperm samples were measured using a colorimetric activity kit (EIAPKA; Invitrogen, ThermoFisher Scientific) following the manufacturer's instructions. In brief, samples were centrifuged at 600 × *g*, capacitation medium was discarded and sperm cells were stored at −80°C until analysis. For cell lysis, samples were resuspended in cell lysis buffer, incubated for 30 min on ice with occasional vortexing, and then sonicated three times for 30 s each. After that, samples were centrifuged at 10,000 × *g* and 4°C for 10 min, and supernatants were recovered for analysis. Then, standards were diluted in kinase reaction buffer to obtain the standard curve (0.625, 1.25, 2.5, and 5 U/mL PKA), and samples were also diluted in this buffer (1:5,000). Then, 40 μL of the standards and diluted samples were added to the plate in duplicate, and 10 μL of ATP were also added to each well prior to a 90-min incubation at 30°C. After washing plate wells four times, 25 μL of the Donkey anti-Rabbit IgG HRP conjugate was added to each well followed by 25 μL of the Phospho PKA substrate antibody. Then, the plate was incubated at room temperature for 1 h. After washing the plate wells four times, 100 μL of TMB substrate was added to each well before incubating the plate at room temperature for 30 min. Finally, 50 μL of stop solution was added to all wells, and the plate was immediately read at 450 nm using an Epoch^{TM} microplate spectrophotometer (BioTek). Means were calculated for duplicate measurements of standards and samples, and average optical density from the blank was subtracted. The equation of the linear regression curve obtained through the interpolation of PKA concentration from absorbance reading was: (PKA) = 12.148 × Abs + 0.2793, R^2 = 0.9975 for one plate, and (PKA) = 6.5865 × Abs—0.0454, R^2 = 0.9962 for the other. This ELISA kit showed a sensitivity of 0.366 U/mL.

Concerning cAMP concentration, sperm samples were measured using a colorimetric competitive ELISA kit (ab133051; Abcam, Cambridge, United Kingdom) following the manufacturer's instructions. Briefly, samples were centrifuged at 600 × *g* to eliminate capacitation medium and sperm cells were stored at −80°C until analysis. Lysis buffer (0.1 mol/L HCl and 1% Triton X-100) was used to resuspend sperm cells, which were incubated at room temperature for 30 min with agitation. Next, samples were sonicated three times for 30 s and cell debris were pelleted through centrifugation at 10,000 × *g* and 4°C for 10 min. Supernatants were recovered for analysis. Then, standards were diluted in lysis buffer to obtain the standard curve (0.078, 0.312, 1.25, 5, and 20 pmol/mL cAMP), and samples were also diluted in this buffer (1:20; v:v). Then, acetylating reagent [acetic anhydride diluted and triethylamine; 1:2 (v:v)] was added to standards and samples [1:20 (v:v)] to achieve the maximum sensitivity of the kit (0.039 nmol/L). Apart from standards and samples, different controls were also loaded onto the plate: blank wells, that only contained pNpp substrate; total activity wells, which contained conjugate and pNpp substrate; non-specific binding control, with neutralizing reagent, lysis buffer, conjugate and substrate; and the zero standard, that contained neutralizing reagent, lysis buffer, conjugate, antibody and substrate. Fifty μL of neutralizing reagent was added to the plate wells, prior to the addition of 100 μL of standards and samples. After that, 50 μL of Cyclic AMP complete Alkaline Phosphatase conjugate was added, followed by 50 μL of cyclic AMP complete antibody. Thereafter, the plate was incubated at room temperature for 2 h with shaking. Next, 200 μL of pNpp substrate solution was added to every well and the plate was incubated at room temperature for 1 h. Finally, 50 μL of stop solution was added to every well and the plate was then read at 405 nm using an Epoch^{TM} microplate spectrophotometer (BioTek). Means were calculated for duplicate measurements of standards and samples, and average optical densities from the blank and the non-specific binding control were subtracted. The equation of the exponential regression curve obtained through the interpolation of cAMP concentration from absorbance reading was: (cAMP) $11.16942 \times e^{-11.30138 \times Abs}$, R^2 = 0.99001 for one plate, and (cAMP) = $29.322 \times e^{-24.69 \times Abs}$, R^2 = 0.9821 for the other.

Statistical Analyses

The results of this work were analyzed using a statistical package (IBM SPSS Statistics 25.0; Armonk, New York, United States). In order to assess the distribution of data and homogeneity of variances, Shapiro–Wilk and Levene tests were run, respectively. For each sperm parameter, a mixed model was subsequently conducted. The time point (i.e., 0, 120, 240, 250, or 300 min) was the intra-subjects factor, the treatment at a given concentration (i.e., control, CuSO, $HgCl_2$ or AgSDZ) was the fixed-effects factor (inter-subject), and the ejaculate pool (i.e., 1–8) was the random-effects factor. Pair-wise comparisons were evaluated through a *post hoc* Sidak test, and the level of significance was set at $P \leq 0.05$. Data are shown as mean ± standard error of the mean (SEM).

RESULTS

To determine the effects of AQP inhibitors during sperm capacitation, quality and function parameters of spermatozoa from the control and samples containing CuSO, $HgCl_2$ or AgSDZ were evaluated after 0, 120, 240, 250 and 300 min of incubation. No differences between treatments and the control ($P > 0.05$) were expected at 0 min for any parameter measured, since inhibitors were added immediately before starting incubation in capacitation medium. Therefore, sperm quality was exclusively measured in the control samples at 0 min (**Figures 1–6**).

Sperm Motility

Different motility and kinetics parameters were assessed in the presence of separate inhibitors and the control throughout

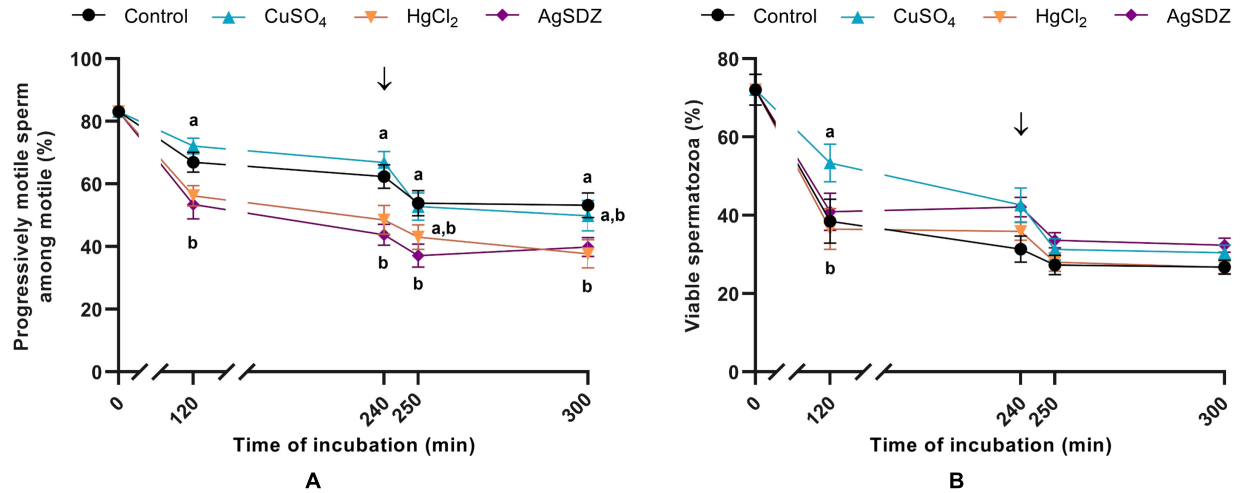

FIGURE 1 | Sperm motility and viability. **(A)** Percentages of progressively motile sperm within the population of motile cells (%) and **(B)** sperm viability measured as the percentage of spermatozoa with an intact plasma membrane (%) in samples exposed to the presence or absence of different AQP inhibitors in the capacitation medium: cooper sulfate ($CuSO_4$), mercury chloride ($HgCl_2$) and silver sulfadiazine (AgSDZ). Data were collected after 0, 120 and 240 min of incubation in capacitation medium. At this point, progesterone was added to capacitation medium (arrow) and data were collected after further 10 min and 60 min of incubation. Data are shown as mean ± SEM, and different letters (a,b) indicate significant differences ($P < 0.05$) between different treatments within a given time point.

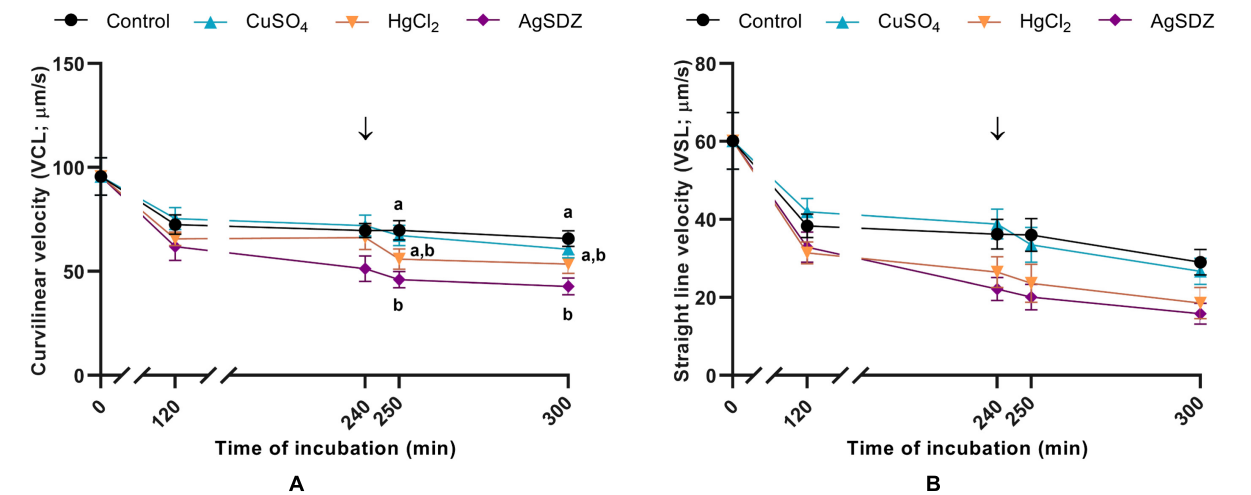

FIGURE 2 | Sperm kinetics parameters. **(A)** Curvilinear velocity (VCL, µm/s) and **(B)** straight-line velocity (VSL, µm/s) in samples exposed to the presence or absence of different AQP inhibitors in the capacitation medium: cooper sulfate ($CuSO_4$), mercury chloride ($HgCl_2$) and silver sulfadiazine (AgSDZ). Data were collected after 0, 120 and 240 min of incubation in capacitation medium. At this point, progesterone was added to capacitation medium (arrow) and data were collected after further 10 min and 60 min of incubation. Data are shown as mean ± SEM, and different letters (a,b) indicate significant differences ($P < 0.05$) between different treatments within a given time point.

incubation. From 120 min of incubation until the end of the period at 300 min, PMOT from the population of motile sperm (**Figure 1A**) was significantly lower in the treatments containing $HgCl_2$ and AgSDZ than in the control ($P < 0.05$). Nevertheless, TMOT was significantly lower than the control after 120 min of incubation only (**Table 1**).

Regarding kinetics parameters, VCL (**Figure 2A**) was significantly ($P < 0.05$) lower in the presence of AgSDZ than in control samples from 250 min of incubation in capacitation medium and until the end of the experiment. Similarly, samples containing AgSDZ presented lower ALH and BCF with respect to the control at 240, 250 and 300 min; whereas in the presence of $HgCl_2$ samples presented the same effect from 250 min of incubation ($P < 0.05$; **Table 1**). In addition, STR was lower than the control in the presence of $HgCl_2$ after 240 min and 300 min of incubation; in samples treated with AgSDZ, this effect was only observed after 300 min of incubation ($P < 0.05$; **Table 2**). Moreover, no significant differences between treatments/inhibitors and the control were observed in terms

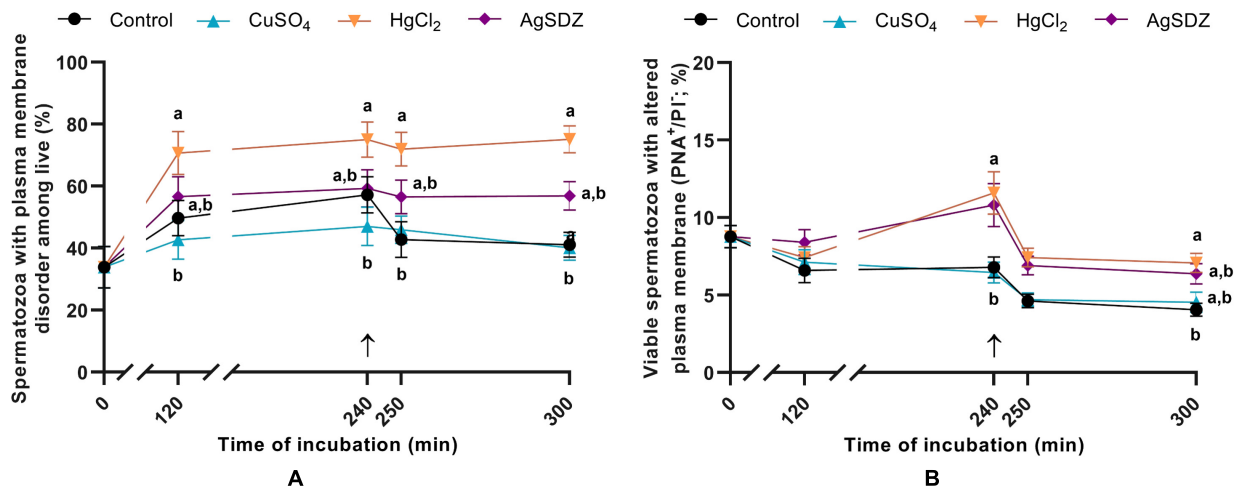

FIGURE 3 | Sperm plasma and acrosome membranes status. **(A)** Percentages of sperm cells with high membrane lipid disorder within the viable sperm population (%) and **(B)** percentages of viable spermatozoa with altered integrity of acrosome membrane (%) in samples exposed to the presence or absence of different AQP inhibitors in the capacitation medium: cooper sulfate ($CuSO_4$), mercury chloride ($HgCl_2$) and silver sulfadiazine (AgSDZ). Data were collected after 0, 120 and 240 min of incubation in capacitation medium. At this point, progesterone was added to capacitation medium (arrow) and data were collected after further 10 min and 60 min of incubation. Data are shown as mean ± SEM, and different letters (a,b) indicate significant differences ($P < 0.05$) between different treatments within a given time point.

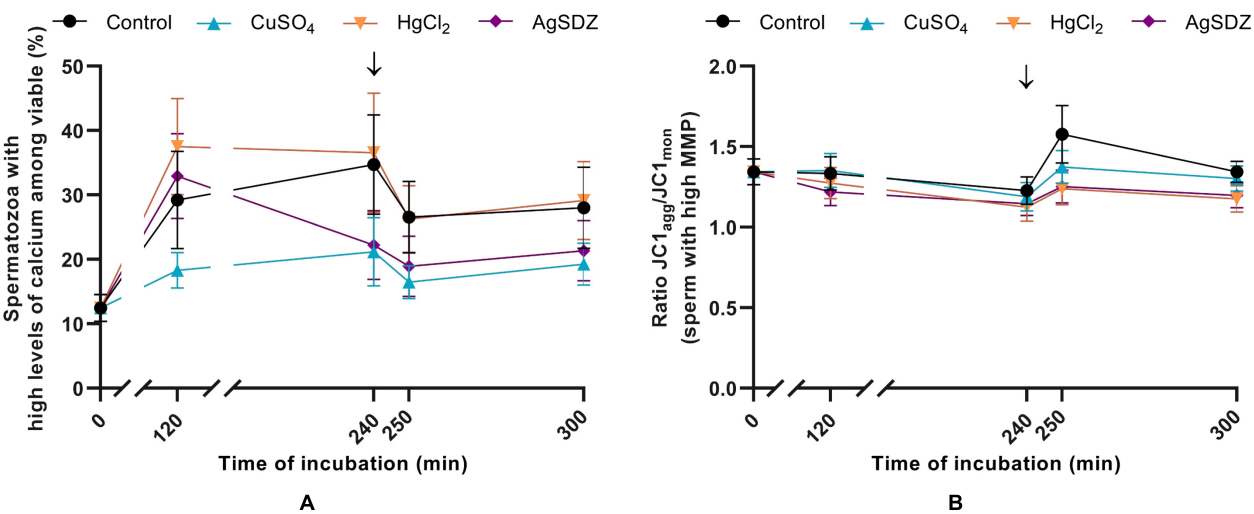

FIGURE 4 | Intracellular levels of calcium and mitochondrial membrane potential. **(A)** Percentages of spermatozoa with high levels of intracellular calcium within the viable sperm population (%) and **(B)** ratio of $JC1_{agg}/JC1_{mon}$ intensity of fluorescence in the population of spermatozoa with high MMP in samples exposed to the presence or absence of different AQP inhibitors in the capacitation medium: cooper sulfate ($CuSO_4$), mercury chloride ($HgCl_2$) and silver sulfadiazine (AgSDZ). Data were collected after 0, 120 and 240 min of incubation in capacitation medium. At this point, progesterone was added to capacitation medium (arrow) and data were collected after further 10 min and 60 min of incubation. Data are shown as mean ± SEM, and different letters (a,b) indicate significant differences ($P < 0.05$) between different treatments within a given time point.

of VSL (**Figure 2B**), VAP, LIN, or WOB ($P > 0.05$) at any time point (**Tables 1**, **2**).

Sperm Plasma Membrane Integrity and Membrane Lipid Disorder

As aforementioned, sperm plasma membrane integrity was evaluated through co-staining with SYBR-14 and PI in order to assess the effects of separate inhibitors at the different time points (**Figure 1B**). Sperm viability was higher in the presence of $CuSO_4$ than in the control after 120 min of incubation ($P > 0.05$).

Co-staining with M540 and YO-PRO-1 was used to evaluate the effects of the different inhibitors on plasma membrane lipid disorder during *in vitro* capacitation (**Figure 3A**). Percentages of spermatozoa exhibiting high levels of plasma membrane lipid disorder within the viable sperm population were significantly

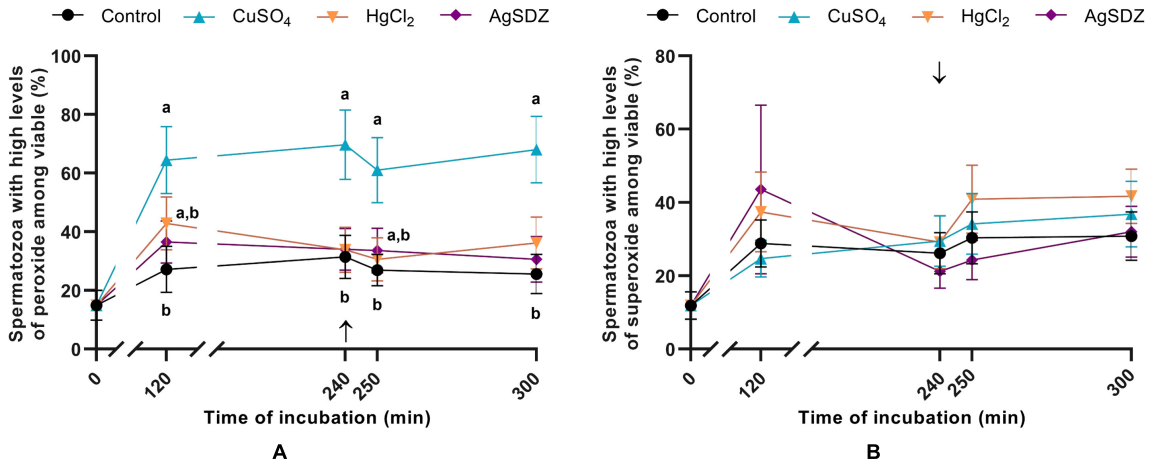

FIGURE 5 | Intracellular levels of ROS. **(A)** Percentages of spermatozoa with high intracellular levels of hydrogen peroxide within the viable sperm population (%) and **(B)** percentages of spermatozoa with high intracellular levels of superoxide within the viable sperm population (%) in samples exposed to the presence or absence of different AQP inhibitors in the capacitation medium: cooper sulfate ($CuSO_4$), mercury chloride ($HgCl_2$) and silver sulfadiazine (AgSDZ). Data were collected after 0, 120 and 240 min of incubation in capacitation medium. At this point, progesterone was added to capacitation medium (arrow) and data were collected after further 10 min and 60 min of incubation. Data are shown as mean ± SEM, and different letters (a,b) indicate significant differences ($P < 0.05$) between different treatments within a given time point.

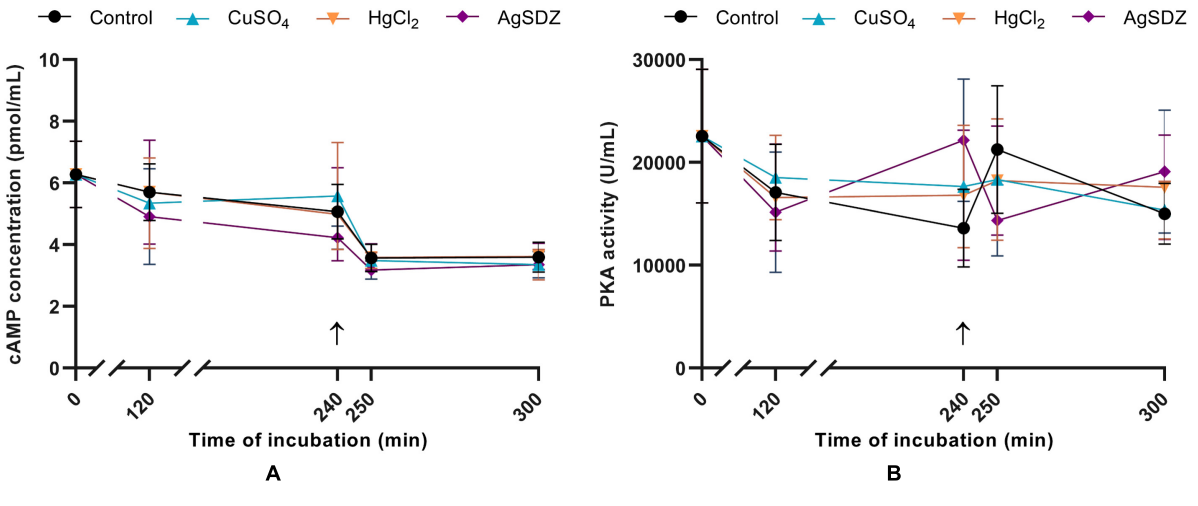

FIGURE 6 | Intracellular concentration of cAMP and PKA activity. **(A)** Intracellular concentration of cyclic AMP (cAMP) in sperm cells (pmol/mL) and **(B)** PKA intracellular activity (U/mL) in samples exposed to the presence or absence of different AQP inhibitors in the capacitation medium: cooper sulfate ($CuSO_4$), mercury chloride ($HgCl_2$) and silver sulfadiazine (AgSDZ). Data were collected after 0, 120, and 240 min of incubation in capacitation medium. At this point, progesterone was added to capacitation medium (arrow) and data were collected after further 10 and 60 min of incubation. Data are shown as mean ± SEM, and different letters (a,b) indicate significant differences ($P < 0.05$) between different treatments within a given time point.

higher in samples containing $HgCl_2$ than in the control after 250 and 300 min of incubation ($P < 0.05$). Nevertheless, a notable trend was observed from 120 min of incubation, since membrane lipid disorder was already higher in samples treated with $HgCl_2$ than in the control ($P = 0.062$).

Acrosome Membrane Integrity

Sperm were co-stained with PNA-FITC and PI to evaluate the effects of the different AQP inhibitors on acrosome membrane integrity during *in vitro* capacitation (**Figure 3B**). Samples treated with $HgCl_2$ and AgSDZ presented a higher percentage of spermatozoa with an altered plasma/acrosomal membrane after 240 min of incubation ($P < 0.05$). At the end of the experiment (300 min), this difference persisted in samples treated with $HgCl_2$ ($P < 0.05$).

Intracellular Levels of Calcium

Intracellular levels of calcium were evaluated through co-staining with Fluo-3 AM and PI in order to assess the effects of different AQP inhibitors during capacitation (**Figure 4A**). There were no

significant differences between the control and samples treated with inhibitors on the intracellular levels of calcium in the viable sperm population at any time point ($P > 0.05$).

Mitochondrial Membrane Potential

Mitochondrial membrane potential (MMP) was assessed through staining with JC1 in order to evaluate the effect of different inhibitors on this sperm function parameter during capacitation (**Figure 4B**). In the population of sperm with high MMP, the ratio of $JC1_{agg}/JC1_{mon}$ intensity presented no significant differences between the different treatments and the control at any time point ($P > 0.05$).

Intracellular Levels of ROS

The effects of different AQP inhibitors on the intracellular levels of ROS during capacitation were evaluated with two different co-staining protocols: H_2DCFDA/PI was used to assess peroxide levels and HE/YO-PRO-1 was used to determine $O_2^{-}\bullet$ levels. The addition of $CuSO_4$ to capacitation medium caused an increase in the percentage of viable spermatozoa with high intracellular levels of peroxides at any time point ($P < 0.05$; **Figure 5A**). No differences between the control and treated samples were observed in terms of $O_2^{-}\bullet$ levels at any time point ($P > 0.05$; **Figure 5B**).

Intracellular cAMP Levels and PKA Activity

Two different Enzyme-Linked Immunosorbent Assays were conducted to assess PKA intracellular activity and intracellular cAMP levels. No significant differences in terms of cAMP concentration (**Figure 6A**) or PKA activity (**Figure 6B**) were observed between the control and AQP inhibitors at any time point.

Intracellular pH

To assess the effects of inhibiting AQPs on intracellular pH, a BCECF staining protocol was used. The addition of AgSDZ caused a decrease in intracellular pH compared to the control after 250 min of incubation ($P < 0.05$; **Figure 7A**).

Tyrosine Phosphorylation

Levels of tyrosine phosphorylation were assessed through immunoblotting. A tyrosine phosphorylation band pattern was observed, and apart from total phosphorylation, four different bands were analyzed to assess the potential differences between

TABLE 1 | Sperm motility and kinetics parameters from direct measurement.

Time (min)	Control	$CuSO_4$	$HgCl_2$	AgSDZ
		TMOT (%)		
0	62.71% ± 2.33	62.71% ± 2.33	62.71% ± 2.33	62.71% ± 2.33
120	35.60% ± 3.73^{a}	40.13% ± 3.76^{a}	22.09% ± 2.05^{b}	19.29% ± 2.52^{b}
240	30.87% ± 3.15	35.27% ± 3.77	21.01% ± 2.81	13.54% ± 2.47
250	16.24% ± 2.28	17.11% ± 2.70	10.00% ± 1.15	7.67% ± 1.04
300	16.11% ± 2.64	14.96% ± 2.45	8.09% ± 1.07	7.65% ± 1.28
		VAP (μm/s)		
0	69.87 ± 8.56	69.87 ± 8.56	69.87 ± 8.56	69.87 ± 8.56
120	46.98 ± 3.64	50.00 ± 4.16	40.23 ± 3.08	40.45 ± 4.66
240	44.76 ± 3.90	46.83 ± 4.27	37.06 ± 3.98	29.24 ± 3.60
250	45.35 ± 4.32	42.77 ± 4.82	32.10 ± 4.75	27.63 ± 3.40
300	38.27 ± 3.31	35.48 ± 3.67	27.49 ± 4.04	22.49 ± 2.83
		ALH (μm)		
0	3.05 ± 0.15	3.05 ± 0.15	3.05 ± 0.15	3.05 ± 0.15
120	2.57 ± 0.09	2.61 ± 0.11	2.40 ± 0.11	2.17 ± 0.20
240	2.42 ± 0.07^{a}	2.51 ± 0.08^{a}	2.42 ± 0.20^{a,b}	1.84 ± 0.17^{b}
250	2.64 ± 0.11^{a}	2.41 ± 0.13^{a}	1.87 ± 0.12^{a,b}	1.53 ± 0.15^{b}
300	2.39 ± 0.10^{a}	2.04 ± 0.17^{a,b}	1.75 ± 0.18^{a,b}	1.46 ± 0.17^{b}
		BCF (Hz)		
0	11.06 ± 0.64	11.06 ± 0.64	11.06 ± 0.64	11.06 ± 0.64
120	9.92 ± 0.56^{a,b}	10.59 ± 0.47^{a}	8.44 ± 0.45^{a,b}	8.04 ± 0.74^{b}
240	9.18 ± 0.55^{a}	9.88 ± 0.52^{a}	7.97 ± 0.88^{a,b}	6.53 ± 0.89^{b}
250	9.12 ± 0.74^{a}	8.24 ± 0.63^{a}	5.33 ± 0.63^{b}	4.76 ± 0.63^{b}
300	7.98 ± 0.55^{a}	7.44 ± 0.74^{a}	4.75 ± 0.72^{b}	4.43 ± 0.68^{b}

Percentage of total motile spermatozoa (TMOT, %), average pathway velocity (VAP, μm/s), amplitude of lateral head displacement (ALH, μm) and beat-cross frequency (BCF, Hz) from samples exposed to the presence or absence of different AQP inhibitors in the capacitation medium: cooper sulfate ($CuSO_4$), mercury chloride ($HgCl_2$) and silver sulfadiazine (AgSDZ).

Data were collected after 0, 120, and 240 min of incubation in capacitation medium. At this point, progesterone was added to capacitation medium (arrow) and data were collected after further 10 min and 60 min of incubation.

Data are shown as mean ± SEM, and different letters (a,b) indicate significant differences ($P < 0.05$) between different treatments within a given time point.

TABLE 2 | Secondary sperm kinetics parameters.

Time (min)	Control	$CuSO_4$	$HgCl_2$	AgSDZ
		LIN (%)		
0	61.18 ± 3.02	61.18 ± 3.02	61.18 ± 3.02	61.18 ± 3.02
120	52.56 ± 2.28	55.43 ± 2.03	47.52 ± 3.05	49.28 ± 4.66
240	50.57 ± 3.82^{a,b}	53.45 ± 2.99^{a}	38.71 ± 4.69^{b}	41.22 ± 3.45^{a,b}
250	50.51 ± 3.62	47.81 ± 3.74	39.88 ± 4.78	41.98 ± 3.56
300	43.05 ± 3.47	42.47 ± 3.85	31.48 ± 4.79	33.51 ± 3.59
		STR (%)		
0	86.31 ± 1.09	86.31 ± 1.09	86.31 ± 1.09	86.31 ± 1.09
120	81.41 ± 1.52	84.26 ± 1.44	77.23 ± 1.74	75.04 ± 5.94
240	79.07 ± 2.34^{a}	82.30 ± 2.07^{a}	66.13 ± 4.46^{b}	71.72 ± 3.14^{a,b}
250	77.57 ± 2.54	76.27 ± 2.28	68.24 ± 3.15	69.08 ± 2.45
300	73.41 ± 2.62^{a}	72.58 ± 3.06^{a,b}	59.68 ± 4.45^{c}	62.38 ± 4.29^{b,c}
		WOB (%)		
0	70.69 ± 3.24	70.69 ± 3.24	70.69 ± 3.24	70.69 ± 3.24
120	64.34 ± 2.35	65.64 ± 2.03	60.92 ± 2.80	60.40 ± 5.31
240	62.93 ± 3.33	64.35 ± 2.65	52.17 ± 4.37	55.97 ± 3.14
250	61.00 ± 3.61	61.78 ± 3.31	55.87 ± 4.12	59.42 ± 3.25
300	57.40 ± 2.96	56.90 ± 3.21	48.47 ± 4.01	49.42 ± 3.11

Linearity (LIN, %), straightness (STR, %) and oscillation index (WOB, %) from samples exposed to the presence or absence of different AQP inhibitors in the capacitation medium: cooper sulfate ($CuSO_4$), mercury chloride ($HgCl_2$) and silver sulfadiazine (AgSDZ).

Data were collected after 0, 120, and 240 min of incubation in capacitation medium. At this point, progesterone was added to capacitation medium (arrow) and data were collected after additional 10 and 60 min of incubation.

Data are shown as mean ± SEM, and different letters (a,b) indicate significant differences ($P < 0.05$) between different treatments within a given time point.

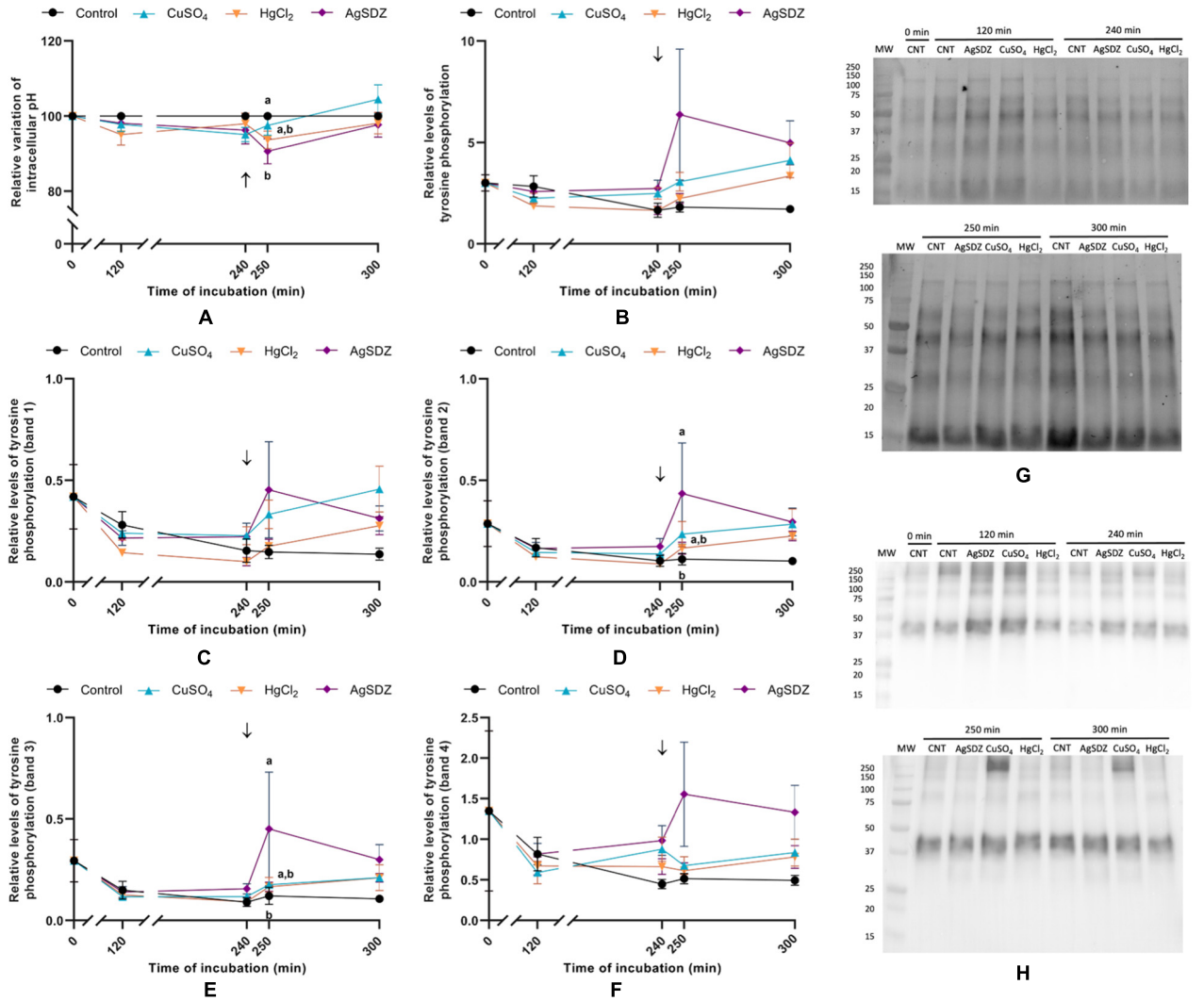

FIGURE 7 | Relative variation of pH and relative levels of tyrosine phosphorylation. **(A)** Intracellular variation of pH compared to the control sample; **(B)** relative levels of total tyrosine phosphorylation; **(C)** relative levels of total tyrosine phosphorylation from band 1 (~200 kDa); **(D)** relative levels of total tyrosine phosphorylation from band 2 (~175 kDa); **(E)** relative levels of total tyrosine phosphorylation from band 3 (~75 kDa); **(F)** relative levels of total tyrosine phosphorylation from band 4 (~40 kDa); **(G)** total protein measured through stain-free; and **(H)** immunoblotting showing the tyrosine phosphorylation pattern after the incubation with a 4G10® Platinum, mouse monoclonal Anti-Phosphotyrosine Antibody [1:5,000; (v:v)] and rabbit anti-mouse, secondary antibody conjugated with HRP [1:10,000; (v:v)]. All parameters were measured in samples exposed to the presence or absence of different AQP inhibitors in the capacitation medium: cooper sulfate ($CuSO_4$), mercury chloride ($HgCl_2$) and silver sulfadiazine (AgSDZ). Data were collected after 0, 120 and 240 min of incubation in capacitation medium. At this point, progesterone was added to capacitation medium (arrow) and data were collected after further 10 and 60 min of incubation. Data are shown as mean ± SEM, and different letters (a,b) indicate significant differences ($P < 0.05$) between different treatments within a given time point.

inhibitors and the control (**Figures 7B–H**). Despite no differences being observed in terms of total tyrosine phosphorylation of sperm proteins between different treatments and the control ($P > 0.05$), bands 2 and 3 from samples treated with AgSDZ presented a higher intensity than the control ($P < 0.05$), thus indicating higher levels of tyrosine phosphorylation.

DISCUSSION

Although several studies to address the function of ion channels during sperm capacitation were conducted (reviewed by Puga Molina et al., 2018), the potential role of water channels on this process is yet to be unveiled. Nevertheless, it is well known that soluble adenylate cyclase (sAC), which is regulated by pH, is crucial for the cAMP-PKA pathway triggered during capacitation (Chang and Oude-Elferink, 2014). Therefore, given the link between water flow and intracellular pH, it is reasonable to suggest that AQPs might be relevant in this process. For this reason, the aim of this study was to assess the role of the different groups of AQPs during mammalian sperm capacitation and acrosome reaction using the pig as a model. Three different salts of transition metals that have largely been demonstrated as AQP inhibitors (Haddoub et al., 2009)

were used: cooper sulfate ($CuSO_4$), mercury chloride ($HgCl_2$) and silver sulfadiazine (AgSDZ). $CuSO_4$ is a specific inhibitor of AQP3, since Cu^{2+} binds to three different extracellular residues of this protein, which correspond, in human AQP3, to Trp128, Ser152 and His241 (Zelenina et al., 2004). $HgCl_2$ is an unspecific and reversible inhibitor of AQPs; its blocking effect presumably occurs because of the Hg^{2+}-mediated, covalent modification of a Cys residue that is present in the pore of most AQPs. This modification either blocks the channel or causes conformational changes that avoid water transport (Hirano et al., 2010). Nevertheless, the fact that this Cys residue is not present in AQP7 could explain why previous studies demonstrated that AQP7 is Hg^{2+}-resistant (Ishibashi et al., 1997). Finally, AgSDZ is an unspecific, irreversible inhibitor of all AQPs, and is also thought to interact with this Cys residue of the AQP pore. Such an irreversibility suggests that its inhibitory mechanism might be different from that of Hg^{2+}. Niemietz and Tyerman (2002) surmised that, since the size of this ion (2.5 Å) matches the diameter of the AQP pore (2.8 Å), Ag^{2+} might block the AQP channel; thus, it is possible that this metal also inhibits AQP7 through that mechanism.

The effects of the aforementioned AQP inhibitors were evaluated in terms of sperm motility and kinetics parameters through a CASA system; flow cytometry was used to assess different sperm quality and function parameters; and tyrosine phosphorylation levels, PKA activity and intracellular levels of cAMP were evaluated as indicators of the intracellular pathways involved in capacitation. Briefly, the presence of $CuSO_4$ led to higher sperm viability than the control and increased intracellular levels of peroxides after 120 min of incubation; this effect persisted even after the addition of progesterone to trigger the acrosome reaction at 240 min. The addition of $HgCl_2$ augmented membrane lipid disorder from 120 min until the end of the experiment, caused a rise in the percentage of spermatozoa with an altered acrosome membrane from 240 min to the end of the experiment, and decreased progressive motility and other kinetics parameters from 120 min of incubation. Finally, the addition of AgSDZ caused a decrease in different parameters that evaluated sperm motility and kinetics during the entire incubation period, and the same effects on acrosome membrane integrity that were observed in the presence of $HgCl_2$. In addition, the presence of AgSDZ caused a decrease in intracellular pH, as well as an increase in tyrosine phosphorylation levels after the addition of progesterone (250 min of incubation).

Regarding the effects of $CuSO_4$, it became apparent from our results that AQP3 has not a key role in sperm capacitation or acrosome reaction. On the one hand, the higher percentages of sperm viability compared to the control after 120 min of incubation could be misleading. Considering the capacitation process leads to plasma membrane destabilization, it is possible that PI enters viable, membrane-destabilized sperm. Thus, while a population of sperm stained with both SYBR-14 and PI was observed, it could not be considered as strictly viable, since their viability was already compromised. In addition, the presence of $CuSO_4$ led to a lower (although not significant) membrane lipid disorder compared to the control. This could explain the higher rate of entrance of PI into live cells in the control compared to sperm treated with $CuSO_4$. These slight differences could lead to the small (but significant) difference in sperm viability between the control and the $CuSO_4$ treatment. On the other hand, the increase in intracellular levels of peroxides could be explained because of AQP3 permeability to this molecule (Miller et al., 2010). Therefore, AQP3-inhibition could block the outflow of peroxides to the extracellular medium, which would make them to accumulate intracellularly. In fact, Delgado-Bermúdez et al. (2019) also reported an increase of intracellular peroxides in pig spermatozoa in the presence of 1,3-propanediol, another inhibitor of AQPs. Surprisingly, and despite high extracellular peroxide levels having a detrimental effect upon sperm function (Laforenza et al., 2017), no sperm quality or function parameter was altered when peroxides were intracellularly accumulated. This suggests that sperm capacitation and acrosome reaction, at least in pigs, do not seem to be impaired by high intracellular H_2O_2 levels. Nevertheless, ROS have a central role as stimulators of capacitation that has been extensively described in other mammalian species (reviewed by Aitken, 2017). In fact, Rivlin et al. (2004) suggested that while relatively low concentrations of H_2O_2 are beneficial for sperm capacitation, too high ones inhibit that process. This report also concluded that H_2O_2 activates adenylyl cyclase to produce cAMP, leading to PKA-dependent protein tyrosine phosphorylation. In addition, H_2O_2 has been demonstrated to inhibit different tyrosine phosphatases (Hecht and Zick, 1992), and Aitken (2017) suggested that in sperm this inhibition could increase phosphorylation of cAMP-PKA pathway target proteins. In spite of this, in this work, high intracellular H_2O_2 levels did not seem to stimulate capacitation-associated changes, either in terms of acrosome membrane integrity or in terms of cAMP levels, PKA activity or tyrosine phosphorylation patterns. Therefore, it seems that the observed increase in intracellular peroxides was not sufficient either to impair or to enhance capacitation or acrosome reaction. Additional studies are needed to evaluate the relevance of H_2O_2 in pig sperm capacitation.

Concerning $HgCl_2$, it inhibits the different AQPs present in mammalian sperm except AQP7 (i.e., AQP3, AQP8, AQP9, and AQP11). Samples treated with $HgCl_2$ showed an increase in membrane lipid disorder and impaired kinetics parameters, which could result from cholesterol efflux and lipid reorganization, since this is a featured event that occurs during capacitation (reviewed by Aitken, 2017). In this context, one could posit that certain capacitation-associated events are enhanced when some AQPs are inhibited. Nevertheless, the absence of significant effects on acrosome membrane integrity and on intracellular calcium levels after the addition of progesterone suggests that plasma membrane alterations are not related to a higher sperm ability to elicit *in vitro* capacitation and the subsequent acrosome reaction. This is supported by the fact that neither tyrosine phosphorylation, nor cAMP levels or PKA activity were altered. Thus, while the presence of $HgCl_2$ seemed to induce an increase in membrane lipid disorder, likely increasing membrane fusogenicity, the observed changes were capacitation-like events that did not drive a proper, physiological sperm capacitation, as they did not lead to an increase in the percentage of spermatozoa undergoing the acrosome reaction. Considering all the aforementioned, these results suggest that AQP3 and AQP11 might exert some influence

on certain capacitation-associated changes, but do not have direct consequences on the ability of spermatozoa to undergo the acrosome reaction. A possible reason for the observed effects would be that the limitation of water flow through the plasma membrane resulting from AQPs blocking would compromise sperm osmoregulation ability, which is in turn crucial for the activation and maintenance of sperm motility (reviewed by Chen and Duan, 2011). In our experiment, blocking of AQPs during *in vitro* capacitation might have caused an alteration in sperm volume, which could have ended up with plasma membrane damage and motility impairment, without altering the intracellular pathways involved in sperm capacitation.

Finally, AgSDZ, an unspecific inhibitor of all AQPs had similar effects to those observed in the presence of $HgCl_2$. Nevertheless, an additional effect was observed, which suggests a relevant role of all AQPs as a whole during sperm capacitation and acrosome reaction. Samples treated with AgSDZ showed a lower intracellular pH compared to the control after the addition of progesterone to trigger the acrosome reaction, with a concomitant increase in tyrosine phosphorylation at the same time point (250 min of incubation). Nonetheless, cAMP levels and PKA activity were not impaired in the presence of this inhibitor. Therefore, either the concentration and activity changes were too subtle to be detected through the methods used in this study, or other signaling pathways were involved in the observed alteration of tyrosine phosphorylation patterns. According to Buffone et al. (2014), capacitation and acrosome reaction are driven through different signaling pathways. On the one hand, capacitation-associated changes are driven by phosphorylation of tyrosine residues as a downstream effect of the cAMP-PKA pathway, which relies upon cAMP synthesis by sAC. On the other hand, acrosome reaction is triggered by progesterone, which interacts with a GPCR coupled to a transmembrane adenylate cyclase (trAC) that is the source of the cAMP required in this process. It is important to highlight that, whilst sAC is regulated by pH, trAC activity does not. As the change in pH caused by the blockade of AQPs occurred after the addition of progesterone, it would be reasonable to suggest that sAC activity was unaltered, which would be in agreement with the lack of variations in PKA activity and cAMP levels. A potential candidate to explain the observed alteration in tyrosine phosphorylation levels would be PKC, which is involved in the intracellular signaling pathways that trigger the acrosome reaction (Teijeiro et al., 2017). Therefore, changes in osmoregulation during capacitation could induce latent alterations in sperm function that would become apparent upon triggering the acrosome reaction. The fact that these effects are only observed when all AQPs are inhibited as a whole might be the consequence of a functional compensation that is only possible when some AQPs remain unblocked. When a general inhibitor like AgSDZ is added and the function of all AQPs is suppressed, the absence of osmoregulation becomes an unbeatable challenge for the sperm cell that ends up altering its physiology, including the intracellular signaling pathways involved in the acrosome reaction. Additional experiments evaluating the mechanisms through which AQPs inhibition ends up with changes in intracellular pH and tyrosine phosphorylation patterns after triggering the acrosome reaction through progesterone are needed.

In conclusion, the relevance of AQPs during sperm capacitation is apparently related to their osmoregulatory ability. Whereas AQP3 is essential for H_2O_2 efflux, its inhibition does not seem to cause a toxic accumulation of this molecule at an intracellular level. Finally, the AQPs as a whole seem to have a relevant role for the intracellular signaling pathways involved in the acrosome reaction, thus suggesting that their blockade during the capacitation process has underlying effects that only become evident after the addition of progesterone.

DATA AVAILABILITY STATEMENT

The original contributions presented in the study are included in the article/supplementary material, further inquiries can be directed to the corresponding author/s.

AUTHOR CONTRIBUTIONS

AD-B and MY: conceptualization. AD-B, SR, and MY: methodology. AD-B, AS, and MY: formal analysis. AD-B, SR, ML, YM-O, AS, IB, and JR-M: investigation. MY: supervision and funding acquisition. AD-B: writing—original draft preparation and visualization. SR, ML, YM-O, AS, IB, JR-M, and MY: writing—review and editing. All authors have read and agreed to the published version of the manuscript.

FUNDING

This research was funded by the Ministry of Science and Innovation (Spain) (RYC-2014-15581, AGL2017-88329-R, and PRE2018-083488); and Regional Government of Catalonia, Spain (2017-SGR-1229).

ACKNOWLEDGMENTS

The authors would like to thank the technical support received from Jordi Soler (University of Girona, Spain).

REFERENCES

Aitken, R. J. (2017). Reactive oxygen species as mediators of sperm capacitation and pathological damage. *Mol. Reprod. Dev.* 84, 1039–1052. doi: 10.1002/mrd.22871

Bailey, J. L. (2010). Factors regulating sperm capacitation. *Syst. Biol. Reprod. Med.* 56, 334–348. doi: 10.3109/19396368.2010.512377

Bonilla-Correal, S., Noto, F., Garcia-Bonavila, E., Rodríguez-Gil, J. E., Yeste, M., and Miró, J. (2017). First evidence for the presence of aquaporins in stallion sperm. *Reprod. Domest. Anim.* 52, 61–64. doi: 10.1111/rda.13059

Buffone, M. G., Wertheimer, E. V., Visconti, P. E., and Krapf, D. (2014). Central role of soluble adenylyl cyclase and cAMP in sperm physiology. *Biochim. Biophys. Acta - Mol. Basis Dis.* 1842, 2610–2620. doi: 10.1016/j.bbadis.2014.07.013

Chang, J. C., and Oude-Elferink, R. P. J. (2014). Role of the bicarbonate-responsive soluble adenylyl cyclase in pH sensing and metabolic regulation. *Front. Physiol.* 5:42. doi: 10.3389/fphys.2014.00042

Chang, M. C. (1951). Fertilizing capacity of spermatozoa deposited into the fallopian tubes. *Nature* 168, 697–698. doi: 10.1038/168697b0

Chen, Q., and Duan, E. K. (2011). Aquaporins in sperm osmoadaptation: an emerging role for volume regulation. *Acta Pharmacol. Sin.* 32, 721–724. doi: 10.1038/aps.2011.35

Chen, Q., Peng, H., Lei, L., Zhang, Y., Kuang, H., Cao, Y., et al. (2011). Aquaporin 3 is a sperm water channel essential for postcopulatory sperm osmoadaptation and migration. *Cell Res.* 21, 922–933. doi: 10.1038/cr.2010.169

Delgado-Bermúdez, A., Llavanera, M., Fernández-Bastit, L., Recuero, S., Mateo, Y., Bonet, S., et al. (2019). Aquaglyceroporins but not orthodox aquaporins are involved in the cryotolerance of pig spermatozoa. *J. Anim. Sci. Biotechnol.* 10:77. doi: 10.1186/s40104-019-0388-388

Garner, D. L., and Johnson, L. A. (1995). Viability assessment of mammalian sperm using SYBR-14 and propidium Iodide1. *Biol. Reprod.* 53, 276–284. doi: 10.1095/biolreprod53.2.276

Guthrie, H. D., and Welch, G. R. (2006). Determination of intracellular reactive oxygen species and high mitochondrial membrane potential in Percoll-treated viable boar sperm using fluorescence-activated flow cytometry. *J. Anim. Sci.* 84, 2089–2100. doi: 10.2527/jas.2005-2766

Haddoub, R., Rützler, M., Robin, A., and Flitsch, S. L. (2009). "Design, synthesis and assaying of potential aquaporin inhibitors," in *Aquaporins. Handbook of Experimental Pharmacology*, ed. E. Beitz (Berlin: Springer-Verlag), 385–402. doi: 10.1007/978-3-540-79885-9_19

Harrison, R. A. P., Mairet, B., and Miller, N. G. A. (1993). Flow cytometric studies of bicarbonate-mediated Ca2+ influx in boar sperm populations. *Mol. Reprod. Dev.* 35, 197–208. doi: 10.1002/mrd.1080350214

Hecht, D., and Zick, Y. (1992). Selective inhibition of protein tyrosine phosphatase activities by H2O2 and vanadate *In vitro*. *Biochem. Biophys. Res. Commun.* 188, 773–779. doi: 10.1016/0006-291X(92)91123-8

Hirano, Y., Okimoto, N., Kadohira, I., Suematsu, M., Yasuoka, K., and Yasui, M. (2010). Molecular mechanisms of how mercury inhibits water permeation through aquaporin-1: understanding by molecular dynamics simulation. *Biophys. J.* 98, 1512–1519. doi: 10.1016/j.bpj.2009.12.4310

Ishibashi, K., Kuwahara, M., Gu, Y., Tanaka, Y., Marumo, F., and Sasaki, S. (1997). Cloning and functional expression of a new water channel abundantly expressed in the testis permeable to water glycerol, and urea. *J. Biol. Chem.* 272, 20782–20786. doi: 10.1006/bbrc.1998.8252

Laforenza, U., Pellavio, G., Marchetti, A., Omes, C., Todaro, F., and Gastaldi, G. (2017). Aquaporin-Mediated water and hydrogen peroxide transport is involved in normal human spermatozoa functioning. *Int. J. Mol. Sci.* 18:E66. doi: 10.3390/ijms18010066

Miller, E. W., Dickinson, B. C., and Chang, C. J. (2010). Aquaporin-3 mediates hydrogen peroxide uptake to regulate downstream intracellular signaling. *Proc. Natl. Acad. Sci. U S A.* 107, 15681–15686. doi: 10.1073/pnas.1005776107

Morató, R., Prieto-Martínez, N., Muiño, R., Hidalgo, C. O., Rodríguez-Gil, J. E., Bonet, S., et al. (2018). Aquaporin 11 is related to cryotolerance and fertilising ability of frozen–thawed bull spermatozoa. *Reprod. Fertil. Dev.* 30, 1099–1108. doi: 10.1071/rd17340

Nagy, S., Jansen, J., Topper, E. K., and Gadella, B. M. (2003). A triple-stain flow cytometric method to assess plasma- and acrosome-membrane integrity of cryopreserved bovine sperm immediately after thawing in presence of egg-yolk particles. *Biol. Reprod.* 68, 1828–1835. doi: 10.1095/biolreprod.102.011445

Niemietz, C. M., and Tyerman, S. D. (2002). New potent inhibitors of aquaporins: silver and gold compounds inhibit aquaporins of plant and human origin. *FEBS Lett.* 531, 443–447. doi: 10.1016/S0014-5793(02)03581-3580

Ortega-Ferrusola, C., Sotillo-Galán, Y., Varela-Fernández, E., Gallardo-Bolaños, J. M., Muriel, A., González-Fernández, L., et al. (2008). Detection of "Apoptosis-Like" changes during the cryopreservation process in equine sperm. *J. Androl.* 29, 213–221. doi: 10.2164/jandrol.107.003640

Petrunkina, A. M., Waberski, D., Bollwein, H., and Sieme, H. (2010). Identifying non-sperm particles during flow cytometric physiological assessment: a simple approach. *Theriogenology* 73, 995–1000. doi: 10.1016/j.theriogenology.2009.12.006

Pons-Rejraji, H., Bailey, J. L., and Leclerc, P. (2009). Cryopreservation affects bovine sperm intracellular parameters associated with capacitation and acrosome exocytosis. *Reprod. Fertil. Dev.* 21, 525–537. doi: 10.1071/RD07170

Preston, G. M., Carroll, T. P., Guggino, W. B., and Agre, P. (1992). Appearance of water channels in *Xenopus oocytes* expressing red cell CHIP28 protein. *Science* 256, 385–387. doi: 10.1126/science.256.5055.385

Prieto-Martinez, N., Morato, R., Muino, R., Hidalgo, C. O., Rodriguez-Gil, J. E., Bonet, S., et al. (2016). Aquaglyceroporins 3 and 7 in bull spermatozoa: identification, localisation and their relationship with sperm cryotolerance. *Reprod. Fertil. Dev.* 29, 1249–1259. doi: 10.1071/RD16077

Prieto-Martínez, N., Morató, R., Vilagran, I., Rodríguez-Gil, J. E., Bonet, S., and Yeste, M. (2015). Aquaporins in boar spermatozoa. Part II: detection and localisation of aquaglyceroporin 3. *Reprod. Fertil. Dev.* 29, 703–711. doi: 10.1071/rd15164

Prieto-Martínez, N., Vilagran, I., Morató, R., Rivera, del, Álamo, M. M., et al. (2017). Relationship of aquaporins 3 (AQP3), 7 (AQP7), and 11 (AQP11) with boar sperm resilience to withstand freeze-thawing procedures. *Andrology* 5, 1153–1164.

Prieto-Martínez, N., Vilagran, I., Morató, R., Rodríguez-Gil, J. E., Yeste, M., Bonet, S., et al. (2014). Aquaporins 7 and 11 in boar spermatozoa: detection, localisation and relationship with sperm quality. *Reprod. Fertil. Dev.* 28, 663–672. doi: 10.1071/rd14237

Puga Molina, L. C., Luque, G. M., Balestrini, P. A., and Marín-briggiler, C. I. (2018). Molecular basis of human sperm capacitation. *Front. Cell Dev. Biol.* 6:72. doi: 10.3389/fcell.2018.00072

Rathi, R., Colenbrander, B., Bevers, M. M., and Gadella, B. M. (2001). Evaluation of *in vitro* capacitation of stallion spermatozoa. *Biol. Reprod.* 65, 462–470. doi: 10.1095/biolreprod65.2.462

Reca, A., Szpilbarg, N., and Damiano, A. E. (2018). The blocking of aquaporin-3 (AQP3) impairs extravillous trophoblast cell migration. *Biochem. Biophys. Res. Commun.* 499, 227–232. doi: 10.1016/j.bbrc.2018.03.133

Rivlin, J., Mendel, J., Rubinstein, S., Etkovitz, N., and Breitbart, H. (2004). Role of hydrogen peroxide in sperm capacitation and acrosome reaction. *Biol. Reprod.* 70, 518–522. doi: 10.1095/biolreprod.103.020487

Rojek, A. M., Skowronski, M. T., Füchtbauer, E. M., Füchtbauer, A. C., Fenton, R. A., Agre, P., et al. (2007). Defective glycerol metabolism in aquaporin 9 (AQP9) knockout mice. *Proc. Natl. Acad. Sci. U S A.* 104, 3609–3614. doi: 10.1073/pnas.0610894104

Saito, K., Kageyama, Y., Okada, Y., Kawakami, S., Kihara, K., Ishibashi, K., et al. (2004). Localization of aquaporin-7 in human testis and ejaculated sperm: possible involvement in maintenance of sperm quality. *J. Urol.* 172, 2073–2076. doi: 10.1097/01.ju.0000141499.08650.ab

Smith, B. L., and Agre, P. (1991). Erythrocyte Mr 28,000 transmembrane protein exists as a multisubunit oligomer similar to channel proteins. *J. Biol. Chem.* 266, 6407–6415.

Sohara, E., Ueda, O., Tachibe, T., Hani, T., Jishage, K., Rai, T., et al. (2007). Morphologic and functional analysis of sperm and testes in aquaporin 7 knockout mice. *Fertil. Steril.* 87, 671–676. doi: 10.1016/j.fertnstert.2006.07.1522

Teijeiro, J. M., Marini, P. E., Bragado, M. J., and Garcia-Marin, L. J. (2017). Protein kinase C activity in boar sperm. *Andrology* 5, 381–391. doi: 10.1111/andr.12312

Vicente-Carrillo, A., Ekwall, H., Alvarez-Rodriguez, M., Rodriguez-Martinez, H., Álvarez-Rodríguez, M., and Rodríguez-Martínez, H. (2016). Membrane stress during thawing elicits redistribution of aquaporin 7 but not of aquaporin 9 in boar spermatozoa. *Reprod. Domest. Anim.* 51, 665–679. doi: 10.1111/rda.12728

Watson, H. (2015). Biological membranes. *Essays Biochem.* 59, 43–70. doi: 10.1063/1.2913788

Yeste, M., Estrada, E., Rivera Del, Álamo, M. M., Bonet, S., Rigau, T., et al. (2014). The increase in phosphorylation levels of serine residues of protein HSP70 during holding time at 17°C is concomitant with a higher cryotolerance of boar spermatozoa. *PLoS One* 9:e90887. doi: 10.1371/journal.pone.0090887

Yeste, M., Fernández-Novell, J. M., Ramió-Lluch, L., Estrada, E., Rocha, L. G., Cebrián-Pérez, J. A., et al. (2015). Intracellular calcium movements of boar spermatozoa during '*in vitro*' capacitation and subsequent acrosome exocytosis follow a multiple-storage place, extracellular calcium-dependent model. *Andrology* 3, 729–747. doi: 10.1111/andr.12054

Yeste, M., Morató, R., Rodríguez-Gil, J. E., Bonet, S., and Prieto-Martínez, N. (2017). Aquaporins in the male reproductive tract and sperm: functional implications and cryobiology. *Reprod. Domest. Anim.* 52, 12–27. doi: 10.1111/rda.13082

Yeung, C. H., Callies, C., Rojek, A., Nielsen, S., and Cooper, T. G. (2009). Aquaporin isoforms involved in physiological volume regulation of murine spermatozoa. *Biol. Reprod.* 80, 350–357. doi: 10.1095/biolreprod.108.071928

Yeung, C. H., Callies, C., Tüttelmann, F., Kliesch, S., and Cooper, T. G. (2010). Aquaporins in the human testis and spermatozoa - identification, involvement in sperm volume regulation and clinical relevance. *Int. J. Androl.* 33, 629–641. doi: 10.1111/j.1365-2605.2009.00998.x

Yeung, C. H., and Cooper, T. G. (2010). Aquaporin AQP11 in the testis: molecular identity and association with the processing of residual cytoplasm of elongated spermatids. *Reproduction* 139, 209–216. doi: 10.1530/REP-09-0298

Zelenina, M., Tritto, S., Bondar, A. A., Zelenin, S., and Aperia, A. (2004). Copper inhibits the water and glycerol permeability of aquaporin-3. *J. Biol. Chem.* 279, 51939–51943. doi: 10.1074/jbc.M407645200

Conflict of Interest: The authors declare that the research was conducted in the absence of any commercial or financial relationships that could be construed as a potential conflict of interest.

frontiers in Cell and Developmental Biology

ORIGINAL RESEARCH
published: 07 September 2021
doi: 10.3389/fcell.2021.694889

Canine IVM With SOF Medium, Insulin-Transferrin-Selenium, and Low O_2 Tension Improves Oocyte Meiotic Competence and Decreases Reactive Oxygen Species Levels

*Matteo Duque Rodriguez[1,2,3], Camila O. Cittadini[2], Gabriela M. Teplitz[4], Adrian De Stefano[2], Daniel M. Lombardo[4] and Daniel F. Salamone[2,3]**

[1] Facultad de Ciencias Agrarias, Politécnico Colombiano Jaime Isaza Cadavid, Medellin, Colombia, [2] Laboratorio Biotecnología Animal, Departamento de Producción Animal, Facultad de Agronomía, Universidad de Buenos Aires, Buenos Aires, Argentina, [3] Instituto de Investigaciones en Producción Animal, Universidad de Buenos Aires, Buenos Aires, Argentina, [4] Facultad de Ciencias Veterinarias, Instituto de Investigación y Tecnología en Reproducción Animal, Catedra de Histología y Embriología, CONICET-Universidad de Buenos Aires, Buenos Aires, Argentina

OPEN ACCESS

Edited by:
Ana Josefa Soler, University of Castilla-La Mancha, Spain

Reviewed by:
Zhonghua Liu, Northeast Agricultural University, China
Zhao-Jia Ge, Qingdao Agricultural University, China
Adel Moawad, Cairo University, Egypt

***Correspondence:**
Daniel F. Salamone
salamone@agro.uba.ar

Specialty section:
This article was submitted to Cell Growth and Division, a section of the journal Frontiers in Cell and Developmental Biology

Received: *13 April 2021*
Accepted: *03 August 2021*
Published: *07 September 2021*

Citation:
Duque Rodriguez M, Cittadini CO, Teplitz GM, De Stefano A, Lombardo DM and Salamone DF (2021) Canine IVM With SOF Medium, Insulin-Transferrin-Selenium, and Low O_2 Tension Improves Oocyte Meiotic Competence and Decreases Reactive Oxygen Species Levels. Front. Cell Dev. Biol. 9:694889. doi: 10.3389/fcell.2021.694889

Assisted reproductive technologies in canine species are limited due to the low efficiency of *in vitro* maturation (IVM). Unlike other mammals, bitches ovulate oocytes in the germinal vesicle stage and complete metaphase II (MII) after 48–72 h in the oviductal environment and become fertilizable. For this reason, we compared two different IVM media, synthetic oviductal fluid (SOF) supplemented with 8% bovine serum albumin (BSA) or a mixture of 8% BSA–2.5% fetal bovine serum (FBS) and TCM-199 with 10% FBS. Additionally, we evaluated the effect of supplementation with insulin-transferrin-selenium (ITS) and low O_2 tension in oocyte maturation, reactive oxygen species (ROS) levels, membrane integrity, and embryo development following parthenogenetic activation (PA). After 72 h of culture, SOF + BSA, SOF + BSA + FBS, and TCM-199 + FBS show 5, 7, and 4% of MII, respectively, without a statistical difference. However, SOF + BSA produced significantly higher degeneration rates compared to SOF + BSA + FBS (44 and 23%, respectively). Remarkably, supplementation with 1 μl/ml of ITS under high O_2 tension demonstrated a beneficial effect by improving maturation rates up to 20% compared to the other groups. Low O_2 tension increased maturation rates to 36.5%, although there were no statistical differences compared to high O_2 tension in the presence of ITS. Lower ROS levels and higher integrity of the cytoplasmic membrane were found in the presence of ITS despite no differences in maturation rates under low O_2 tension groups. Additionally, after PA, 1% development until the eight-cell stage was obtained after activation of *in vitro*-matured oocytes in the presence of ITS. Taken together, these results indicate that SOF supplemented with 8% BSA and 2.5% FBS is suitable for IVM of canine oocytes and ITS supplementation was beneficial for both high and low O_2 tension. Furthermore, the addition of ITS in the cultured system lowers ROS levels and increases membrane integrity in domestic dog oocytes after IVM.

Keywords: *in vitro* maturation, canine, oxygen tension, insulin-transferrin-selenium, SOF medium

HIGHLIGHTS

- Insulin-transferrin-selenium supplementation in high O_2 tension improves up to 20% MII of canine oocyte IVM from bitches of unknown age, breed, and stage of the estrous cycle.
- Low O_2 tension increased maturation rates to 36.5%, although there were no statistical differences compared to high O_2 with ITS.
- Higher integrity of the cytoplasmic membrane and lower reactive oxygen species (ROS) levels were found when COCs were cultured in the presence of ITS and low O_2 atmosphere.

INTRODUCTION

The low efficiency of *in vitro* maturation (IVM) in canine remains a real challenge for reproductive biologists (Van Soom et al., 2014). There are several aspects of the bitch's reproductive physiology that differ from that of other domestic females. The bitch ovulates an immature oocyte [germinal vesicle (GV)] that corresponds to the prophase of the first meiotic division. The germinal vesicle breakdown (GVBD) occurs in the oviduct under high progesterone concentrations at 48–96 h after ovulation (Luvoni et al., 2005; Reynaud et al., 2012). Canine oocytes reach 10% of metaphase II (MII) after IVM, while most oocytes (30–40%) degenerate (Farstad, 2000; Luvoni, 2000). Some authors such as No et al. (2018) have used coculture with oviduct epithelial cells to improve maturation rates and have achieved 13% of MII using oocytes recovered from bitches at diestrus and 47% of MII with bitches at estrus. Most reports on canine IVM have been focused on the supplementation of the medium with hormones, such as estrogen, progesterone, follicle-stimulating hormone (FSH), luteinizing hormone (LH), human chorionic gonadotropin (HCG), and L-carnitine (Moawad et al., 2021). The medium TCM-199 is the medium of choice for IVM of most domestic species. However, synthetic oviductal fluid (SOF) was formulated based on the sheep oviductal fluid composition (Tervit et al., 1972), and it is interesting to evaluate due to the different location of the oocyte maturation in the dog. Previous authors have reported the use of SOF media for canine IVM with different supplementation and results (Hewitt and England, 1999; Bolamba et al., 2002; Saikhun et al., 2008; Lange-Consiglio et al., 2017).

Another component of the medium that is still under discussion is supplementation with fetal bovine serum (FBS) or bovine serum albumin (BSA). Some studies suggested that the use of FBS is beneficial during canine IVM due to its vitamins, hormones, and growth factors that it contains (Eppig and Schroeder, 1986; Luvoni et al., 2005; Rota and Cabianca, 2005). Serum is also capable of neutralizing the effect of potential toxic substances such as reactive oxygen species (ROS) (Rodrigues and Rodrigues, 2006). BSA, on the other hand, is capable of reducing toxic metabolites and ROS while promoting the uptake of other components like steroids, vitamins, fatty acids, and cholesterol (Bavister, 1995). Oviductal secretions include enzymatic defenses against ROS as a classic catalase and the family of glutathione peroxidase (Lapointe and Bilodeau, 2003; Saint-Dizier et al., 2020). The major antioxidants that control *in vivo* ROS levels in the oviduct remain to be characterized in species like the dog (Lapointe and Bilodeau, 2003). Furthermore, oxidative stress and ROS affect canine oocytes probably due to the high concentration of lipid droplets in the ooplasm (Tesoriero, 1981). Insulin-transferrin-selenium (ITS) has been used in IVM media of several species, generating positive outcomes (Jeong et al., 2008; Guimarães et al., 2016). While insulin promotes the absorption of nutrients, transferrin, and selenium have antioxidant properties (Jeong et al., 2008).

The main objective of the present study was to compare two different IVM media, one based on oviductal composition (SOF) supplemented with 8% BSA or a mixture of 8% BSA–2.5% FBS and a TCM-199 + 10% FBS. Additionally, we evaluated the supplementation of ITS and lowering O_2 tensions.

MATERIALS AND METHODS

Reagents

Except otherwise indicated, all chemicals were obtained from Sigma Chemical Company (St. Louis, MO, United States). Medium was prepared weekly and filtered through 0.22-mm pores (#4192 Acrodisc; Pall Corp., Ann Arbor, MI, United States) into sterile tubes.

Experimental Design

Experiment 1: Media and Protein Supplementation Effect on Canine *in vitro* Maturation

We compared the ability of two different media to resume meiosis and reach MII stage of immature oocytes recovered after ovariectomy of bitches with unknown stage of the estrous cycle. The first medium consisted of TCM-199 supplemented with 10% v/v FBS (TCM-199 + FBS), and the second medium consisted of SOF supplemented with two different protein sources: 8% v/v BSA (SOF + BSA) or a mixture of 8% v/v BSA and 2.5% v/v FBS (SOF + BSA + FBS) based on our SOF media formulation (Buemo et al., 2016). For IVM, cumulus–oocyte complexes (COCs) were incubated in each maturation medium in an independent assay for 72 h (n = 237 COCs) and then 48 h (n = 96 COCs) on high O_2 tension in humidified air at 38.5°C. Three biological replicates were performed for this experiment.

Experiment 2: Insulin-Transferrin-Selenium Effects on Canine *in vitro* Maturation

The optimal medium determined in the first experiment (SOF + 8% BSA + 2.5% FBS) was supplemented with two concentrations of ITS. SOF + BSA + FBS in the absence of ITS was used as control. Maturation medium was supplemented with 1 and 10 μl/ml of ITS (41400045; Thermo Fisher Scientific; insulin: 0.1721763 mM, transferrin: 0.006875 mM, and selenium: 0.0038728325 mM). For IVM, COCs (n = 232) were incubated in each maturation medium for 72 h on high O_2 tension in humidified air at 38.5°C. Three biological replicates were performed for this experiment.

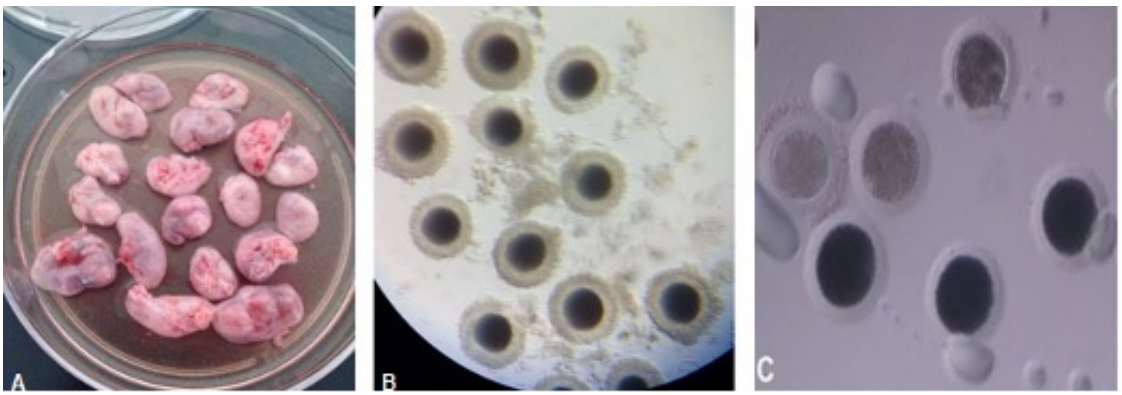

FIGURE 1 | (A) Bitch ovaries that were previously washed and freed from ovarian tissue. **(B)** Grade I cumulus–oocyte complexes (COCs) recovered from the ovaries by the slicing method. The COCs had dark and uniform cytoplasm, large size, and two or more layers of cumulus cells. **(C)** Denuded canine oocytes. The presence of pale-looking oocytes is observed after 72 h of *in vitro* maturation (IVM).

Experiment 3: The Effect of O_2 Tension and Insulin-Transferrin-Selenium Supplementation on Canine *in vitro* Maturation

To evaluate the effect of high (20%) and low (5%) O_2 tension and ITS supplementation, COCs (n = 245) were incubated in SOF + 8% BSA + 2.5% FBS in the presence (1 μl/ml) or absence of ITS in a controlled atmosphere with high or low O_2 tension. It was decided to perform IVM for 48 h instead of 72 h based on the optimum maturation time assessed in experiment 1. Four groups were selected: (A) SOF + BSA + FBS + high O_2; (B) SOF + BSA + FBS + 1 μl/ml of ITS + high O_2; (C) SOF + BSA + FBS + low O_2; and (D) SOF + BSA + FBS + 1 μl/ml of ITS + low O_2. After maturation with low O_2 tension in the presence or absence of ITS, oocytes were used to analyze ROS levels (n = 72), membrane integrity (n = 138), and parthenogenetic activation (PA) (n = 163) through dichlorodihydrofluorescein diacetate (DCHFDA) co-stained with propidium iodide (PI) and ionomycin and 6-dimethylaminopurine (6-DMAP) for activation. Three biological replicates were performed for this experiment.

Cumulus–Oocyte Complexes Collection and *in vitro* Maturation

In this study, a total of 197 ovaries were used from bitches of unknown age, breed, and stage of the estrous cycle. The ovaries were obtained from the Tigre Zoonotic Center (Tigre, Buenos Aires, Argentina) after routine ovariectomy. Ovaries were transported to the laboratory in Falcon tubes containing 10 ml of 4-(2-hydroxyethyl)-1-piperazineethanesulfonic acid (HEPES)-buffered Tyrode's medium containing albumin, lactate, and pyruvate [TALP-HEPES (Bavister and Yanagimachi, 1977)] at 20–25°C and were processed within 6 h after extraction. Once in the laboratory, the ovaries were extracted from the ovarian bursa and washed in TALP-HEPES medium at 38.5°C. Clean ovaries were processed as follows. First, a longitudinal cut with a scalpel followed by numerous punctures with needle and scraping of the ovarian surface was performed to release the COCs to the medium. COCs were selected based on previously established morphological criteria (Hewitt and England, 1999). Briefly, COCs that had a larger size, were surrounded by more than two layers of cumulus cells, had dark and uniform cytoplasm were selected and categorized as grade I (**Figure 1**). Oocytes that were small, fragmented or had a pale cytoplasm were discarded. For experiment 1, the first medium consisted of TCM-199 (31100-035; Thermo Fisher Scientific, Waltham, MA, United States) supplemented with 2.5 mM sodium pyruvate (P2256), 0.57 mM L-cysteine (C7352), 10 μg/ml FSH (NIH-FSH-P1; Folltropin, Athens, Georgia, United States), 10 ng/ml epidermal growth factor (EGF) (PHG0314, Thermo Fisher Scientific), 1% v/v antibiotic (15240-096; Thermo Fisher Scientific), and 10% v/v FBS (013/07; Internegocios S.A., Mercedes, Buenos Aires, Argentina). The second medium consisted of SOF (Tervit et al., 1972) supplemented with 10 μg/ml FSH, 10 ng/ml EGF, and two different protein sources: 8% BSA (A6003) or a mixture of 8% BSA and 2.5% FBS. Groups of up to 20 grade I COCs were incubated in 100-μl droplets of the selected medium, coated with mineral oil (M8410). Plates were incubated under high O_2 (5% CO_2) tension and humidified air at 38.5°C for 48 or 72 h (depending on the experiment). The medium was renewed every 24 h.

Evaluation of Nuclear Stage

After maturation, for nuclear stage assessment, oocytes were first denuded by repeated passages through a glass pipette with an appropriate diameter. Once denuded, oocytes were permeabilized by incubation in 0.3% Triton-X (T-9284) for 15 min and washed in TALP-HEPES. Following permeabilization, oocytes were incubated in 1% v/v Hoechst 33342 (B-2261) droplets for 20 min in darkness at room temperature. Oocytes were washed three times in TALP-HEPES and mounted on glass slides for observation under UV light (excitation and emission wavelengths of 350 and 461 nm, respectively). The glass slides were covered with a coverslip supported by four small droplets of paraffin in the corner in order to regulate

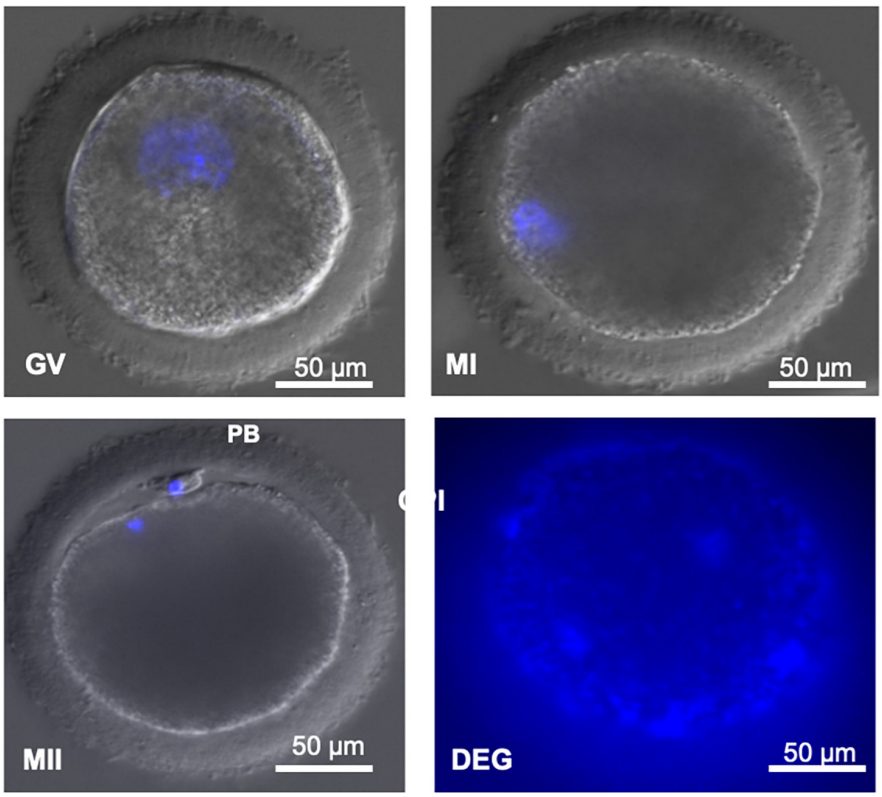

FIGURE 2 | (GV) Decondensed DNA contained in a large germinal vesicle. (MI) Condensed DNA. (MII) Condensed DNA and presence of the first polar body. (PB) First polar body. Degenerated (DEG) oocytes without identifiable material. Image obtained under confocal microscope (magnification ×400). Scale bar: 50 µm.

the distance between both glasses without breaking the oocytes. Nuclear stage assessment was scanned using an inverted confocal microscope (Olympus IX83 Spinning Disk Confocal System). Oocytes were classified based on the morphology of the nucleus as shown in **Figure 2** and based on previously established criteria (Hewitt and England, 1999).

Assessment of Reactive Oxygen Species Levels

Reactive oxygen species levels were measured by DCHFDA staining as described by Lorenzo et al. (2019). For ROS measurement by the DCHFDA method, COCs (n = 72) were denuded as previously described. Oocytes were incubated with 153 µM of DCHFDA (D6883) for 30 min in darkness at 37°C. Oocytes were mounted on glass slides for observation under an epifluorescent microscope (Leica DM4000B LED trinocular connected to a Leica DCC-380X camera). Images were captured using LAS version 4.2.0 microscope software (Leica) using excitation and emission wavelengths of 450–490 and 515–565 nm, respectively. The greater the intensity of green fluorescence, the greater the amount of ROS. Fluorescence intensity was determined by the transmittance variable measured by digital morphometry on images captured using Leica Qwin V3.1 software. The transmittance arbitrary units corresponded to levels between 0 and 256 for each of the Red–Green–Blue (RGB) channels for the pixels of the analyzed matrix. The mean transmittance of each experimental group was recorded and compared. ROS levels were measured in oocytes matured with SOF + BSA + FBS medium in the presence (1 µl/ml) or absence of ITS under low O_2 (5% CO_2, 5% O_2, and 90% N_2) tension in humidified air at 38.5°C for 48 h. Three biological replicates were performed.

Viability Assessment

Aside from the ROS level assessment, oocytes from the two groups described in the previous section were co-stained with PI in order to evaluate oocyte viability and membrane integrity. Briefly, COCs (n = 138) matured in SOF + BSA + FBS medium in the presence (1 µl/ml) or absence of ITS under low O_2 tension in humidified air at 38.5°C for 48 h were assessed. For co-staining, oocytes were incubated in a 1% v/v PI (P4170) solution for 5 min at 37°C. Oocytes were washed and placed between a glass slide with a coverslip and examined under epifluorescence microscope using excitation and emission wavelengths of 450–490 and 515–565 nm, respectively. Three biological replicates were performed.

Parthenogenetic Activation

Oocytes (n = 163) that had been previously exposed to the most optimal maturation conditions (SOF + BSA + FBS under low O_2 tension) for 48 h in the presence (1 µl/ml) or absence of

ITS were chemically activated. After IVM, oocytes were denuded and subjected to activation with ionomycin (I24222; Thermo Fisher Scientific) and 6-DMAP (D2629). Briefly, oocytes were incubated for 4 min in TALP-HEPES with 1 μl/ml ionomycin and then washed three times. Oocytes were then incubated in a 1% v/v 6-DMAP solution in SOF medium supplemented with 2.5% FBS for 4 h. Oocytes were then washed thoroughly in TALP-HEPES and cultured. Oocyte culture was performed in SOF droplets supplemented with 2.5% FBS (without hormones) in low O_2 tension in humidified air at 38.5°C. Seven days after activation, oocytes were evaluated for cleavage. Three biological replicates were performed.

Statistical Analysis

All data were analyzed by the Chi-square test using GraphPad Prism 6 software. To compare ROS levels between groups, an unpaired two-tailed *t*-test was performed, and to assess viability, a comparison of proportions (Fisher test) was performed using GraphPad Prism 6 software. Statistical significance was determined when the *p*-value was <0.05.

RESULTS

The experiments reported in this study were carried out over a period of 1 year. During this year, a total of 1,305 COCs were collected from bitches of unknown age, breed, and stage of the estrous cycle. It was possible to obtain information on the recovery rates per ovary during the different seasons of the year (**Table 1**). We found that the recovery rate of COCs grade I per ovary was 8.6 ± 1.7 in fall, 8.9 ± 2.1 in winter, 9.1 ± 1.1 in summer, and 6.3 ± 1.4 in spring. No significant differences were found between the different seasons.

Experiment 1: Media and Protein Supplementation Effect on Canine *in vitro* Maturation

After 72 h of culture, the maturation rates (MII) were low for the three media, 4% for TCM-199 + FBS, 5% for SOF + BSA, and 7% for SOF + BSA + FBS without significant differences between them. Most of the oocytes were arrested at the metaphase I (MI) stage or did not resume meiosis. Degeneration rates were higher than 20% in all cases, but in SOF + BSA medium, it was significantly higher (44%, $p \leq 0.05$; **Table 2**). For this reason, SOF + BSA was discarded for experiment 2. The rate of non-identifiable oocytes (NN) was higher in SOF + BSA + FBS, and this category corresponds to oocytes that could belong to any of the previous categories. Moreover, the presence of oocytes with unidentifiable nuclear material could be related to difficulties in the staining methods that is common in this species. The presence of oocytes with a pale or lightly pigmented cytoplasm after 72 h of culture is associated with degeneration (**Figure 1**). After 48 h of maturation in TCM-199 + FBS and SOF + BSA + FBS media, similar results to those of 72 h were found with no significant differences (**Table 2**). In addition, maturation rates did not change, supporting the hypothesis that a longer period of time during IVM contributes to degeneration of canine oocytes without improving maturation rates (**Table 2**).

TABLE 1 | Grade I COCs collected per ovary during different seasons of the year.

Season	No. ovaries	No. COCs grade I	Recovery rate per ovary
Spring	72	452	6.3 ± 1.4
Summer	18	160	9.1 ± 1.13
Fall	53	473	8.6 ± 1.7
Winter	27	220	8.9 ± 2.1
Total	170	1,305	–

In the same column, percentages without the same superscripts differed significantly (p-value < 0.05).
COC, cumulus–oocyte complex.

Experiment 2: Insulin-Transferrin-Selenium Effect on Canine *in vitro* Maturation

In order to evaluate the effect of antioxidant supplementation on canine IVM, maturation was performed using SOF + BSA + FBS medium in the presence of different concentrations of ITS for 72 h. It was found that supplementation with 1 μl/ml ITS significantly improved canine IVM, increasing the proportion of oocytes that reached the MII stage (20%). No significant differences were observed in the proportion of oocytes arrested at the GV and MI stages or in the proportion of oocytes with NN between groups (**Table 3**). It was observed that the proportion of degenerated (DEG) oocytes was significantly higher in 10 μl/ml ITS.

Experiment 3: The Effect of O_2 Tension and Insulin-Transferrin-Selenium Supplementation on Canine *in vitro* Maturation

After 48 h of IVM, it was observed that the maturation rate of SOF + BSA + FBS + high O_2 was significantly lower than those in the other groups (**Table 4**). It is important that excluding SOF + BSA + FBS + high O_2, maturation rates exceeded 20% without significant differences between them. On the other hand, it was observed that the proportion of oocytes arrested at the MI stage was greater than 30% in all groups. The number of oocytes in the GV stage was also higher than those in groups that had been cultured under high O_2 tension. These results indicate that low O_2 tension either in the presence or absence of ITS was able to resume meiosis more successfully. Finally, no significant differences were observed in the rate of DEG oocytes for any group, but it is an interesting fact that the degeneration rates were less than 10% in all cases.

Assessment of Reactive Oxygen Species Levels

Reactive oxygen species levels were measured for the most suitable treatment groups determined in the previous experiments (SOF + BSA + FBS medium in the presence or absence of 1 μl/ml of ITS under low O_2 tension). ROS

TABLE 2 | *In vitro* maturation of canine oocytes for 72 and 48 h in three different media under high O_2 atmosphere.

Group	Time IVM	No. oocytes	GV	MI	MII	DEG	NN
TCM-199 + FBS	72	73	16 (21.9%)^{a}	24 (32.8%)^{a}	3 (4.1%)^{a}	22 (30.1%)^{a,c}	8 (10.9%)^{a}
	48	41	8 (19.5%)^{a}	21 (51.2%)^{b}	4 (9.7%)^{a}	3 (7.3%)^{b}	5 (12.1%)^{a}
SOF + BSA + FBS	72	86	17 (19.7%)^{a}	23 (26.9%)^{a}	6 (6.9%)^{a}	20 (23.2%)^{c}	20 (23.2%)^{b}
	48	55	16 (29%)^{a}	27 (49%)^{b}	2 (3.6%)^{a}	5 (9%)^{b}	5 (9%)^{a}
SOF + BSA	72	78	16 (20.5%)^{a}	21 (26.9%)^{a}	4 (5.5%)^{a}	34 (43.5%)^{a}	3 (4.1%)^{a}

The percentages of oocytes in the germinal vesicle (GV), metaphase I (MI), metaphase II (MII), degenerated (DEG), and non-identifiable (NN) stages were recorded. In the same column, percentages without the same superscripts differed significantly (^{a-c}p-value < 0.05). The experiments were repeated three times (n = 3).
BSA, bovine serum albumin; FBS, fetal bovine serum; IVM, in vitro maturation; SOF, synthetic oviductal fluid.

TABLE 3 | The effect of ITS supplementation on canine IVM for 72 h under high O_2 atmosphere.

Group	No. oocytes	GV	MI	MII	DEG	NN
SOF + BSA + FBS	71	16 (22.5%)^{a}	37 (52.1%)^{a}	3 (4.2%)^{a}	7 (9.8%)^{a,b}	8 (11.2%)^{a}
SOF + BSA + FBS + 1 μl/ml ITS	81	16 (19.7%)^{a}	32 (39.5%)^{a}	16 (19.7%)^{b}	7 (8.6%)^{a}	10 (12.3%)^{a}
SOF + BSA + FBS + 10 μl/ml ITS	80	16 (20%)^{a}	29 (36.2%)^{a}	5 (6.2%)^{a}	17 (21.2%)^{b}	13 (16.2%)^{a}

SOF + BSA + FBS (control): COCs cultured in SOF + 8% BSA + 2.5% FBS; SOF + BSA + FBS + 1 μl/ml ITS: COCs cultured in SOF + 8% BSA + 2.5% FBS and 1 μl/ml ITS; and SOF + BSA + FBS + 10 μl/ml ITS: COCs cultured in SOF + 8% BSA + 2.5% FBS and 10 μl/ml ITS. The percentages of oocytes in the germinal vesicle (GV), metaphase I (MI), metaphase II (MII), degenerated (DEG), and non-identifiable (NN) stages was recorded. In the same column, percentages with different superscripts differed significantly ($^{a,b}p < 0.05$). The experiments were repeated three times (n = 3).
BSA, bovine serum albumin; COC, cumulus–oocyte complex; FBS, fetal bovine serum; ITS, insulin-transferrin-selenium; IVM, in vitro maturation; SOF, synthetic oviductal fluid.

TABLE 4 | *In vitro* maturation of canine oocytes in SOF + BSA + FBS medium for 48 h under two different O_2 tension atmospheres in the presence or absence of ITS.

Group	No. oocytes	GV	MI	MII	DEG	NN
SOF + BSA + FBS + high O_2	64	26 (40.6%)^{a}	27 (42.2%)^{a}	5 (7.8%)^{a}	6 (9.4%)^{a}	0 (0%)^{a}
SOF + BSA + FBS + 1 μl/ml ITS + high O_2	53	16 (30.2%)^{a,c}	20 (37.7%)^{a}	13 (24.5%)^{b}	2 (3.8%)^{a}	2 (3.8%)^{a}
SOF + BSA + FBS + low O_2	63	5 (7.9%)^{b}	32 (50.8%)^{a}	23 (36.5%)^{b}	1 (1.6%)^{a}	2 (3.2%)^{a}
SOF + BSA + FBS + 1 μl/ml ITS + low O_2	65	11 (16.9%)^{b,c}	34 (52.3%)^{a}	17 (26.2%)^{b}	2 (3.1%)^{a}	1 (1.5%)^{a}

The percentages of oocytes in the germinal vesicle (GV), metaphase I (MI), metaphase II (MII), degenerated (DEG), and non-identifiable (NN) stages were recorded. In the same column, percentages with different superscripts differed significantly ($^{a-b}p < 0.05$). The experiments were repeated three times (n = 3).
BSA, bovine serum albumin; FBS, fetal bovine serum; ITS, insulin-transferrin-selenium; IVM, in vitro maturation; SOF, synthetic oviductal fluid.

levels were found to be significantly higher in the absence of ITS (97.23 ± 19.49; n = 31) compared to 1 μl/ml of ITS (41.19 ± 5.32; n = 42) as evidenced by oocyte fluorescence intensity measurement in **Figure 3**.

Viability Assessment

Aside from the ROS level assessment, oocytes cultured in SOF + BSA + FBS medium in the presence (1 μl/ml) or absence of ITS under low O_2 tension were co-stained with PI in order to evaluate maturation and cell membrane integrity. Oocyte viability was significantly higher in the ITS-supplemented group (56.3 vs. 23.8%; **Table 5**). In this experiment, oocytes matured in SOF + BSA + FBS + 1 μl/ml of ITS had significantly higher maturation rates (25.3%) compared to that in the absence of ITS (11.9%; **Table 5**).

Parthenogenetic Activation and Embryo Development

Parthenogenetic activation was performed after oocyte maturation in SOF + BSA + FBS medium in the presence (1 μl/ml) or absence of ITS under low O_2 tension. After 7 days of culture, it was found that a high proportion of oocytes was DEG or had unidentifiable material (DEG + NN). This proportion was significantly higher in the group that had been matured in the absence of ITS compared to that in the 1-μl/ml ITS group (94.4 and 71.4%, respectively). Cleaved oocytes were obtained, being two oocytes from each group arrested at the 2- to 4-cell stage. A single oocyte from SOF + BSA + FBS + 1 μl/ml ITS + low O_2 tension was found at a more advanced stage of development, arrested at the eight-cell stage (**Figure 4**). Neither morula nor blastocysts were obtained. The cleavage rates were very low in both groups (2.8 and 3.3%, respectively); however, the only oocyte in the eight-cell stage was obtained in the group supplemented with 1 μl/ml of ITS.

DISCUSSION

We evaluated different strategies to improve IVM, including media compositions, ITS supplementation, and low O_2 tension. Most of the reproductive technologies that produced puppies as *in vitro* fertilization (IVF) and cloning were done using

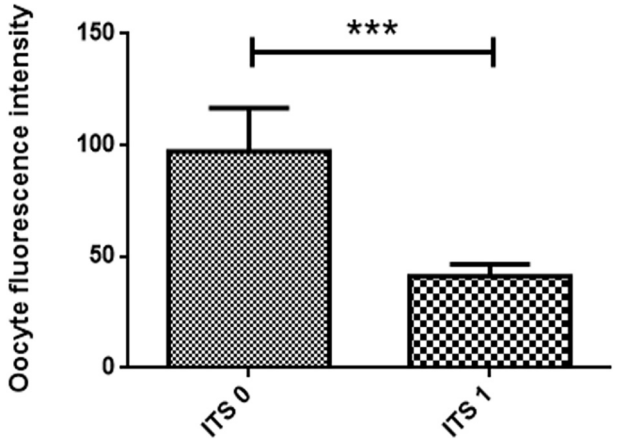

FIGURE 3 | Effect of insulin-transferrin-selenium (ITS) on oocyte reactive oxygen species level. Data show mean ± SEM. Oocyte fluorescence intensity (transmittance) in each experimental group after staining with 2′,7′-dichlorodihydrofluorescein diacetate (three replicates). ITS 0: oocytes matured in the absence of ITS; ITS 1: oocytes matured in the presence of 1 μl/ml of ITS. The meaning of "****" is that the statistical difference is significant.

in vivo-matured oocytes, which has several welfare- and cost-associated problems (Jang et al., 2010; Oh et al., 2018). Therefore, improvement of IVM in the dog would allow the use of oocytes obtained from regular ovariectomies in veterinary clinics, which would favor the development of reproductive technologies. Although several reports have been made to improve canine IVM performance, results are still suboptimal with less than 10% of matured oocytes (Luvoni, 2006; Nagashima et al., 2019).

Experiment 1 compared different media and sources of protein supplementation. Maturation rates were low for all the treatment groups without differences, but lower degeneration rates were found in SOF + BSA + FBS compared with SOF + BSA. Similar to our findings, previous reports also compared TCM-199 with SOF medium, with similar MII rates (<10%) (Rota and Cabianca, 2005; Evecen et al., 2009). Additionally, Lange-Consiglio et al. (2017) reported that 2.5% FBS in SOF medium also had similar degeneration rates to our results. It is clear that independent of the media and supplementation, *in vitro* meiotic resumption of dog oocytes is low. For this reason, in the next experiments, we tried to identify some of the lacking or detrimental components of the culture system.

Dog oocytes contain a large amount of intracellular lipids that are likely to be susceptible to oxidative stress. Results demonstrated that 1 μl/ml of ITS in high O_2 tension improved significantly the MII rates up to 20%, supporting the hypothesis that ITS is important for IVM of canine oocytes. The first report that used ITS in canine IVM using TCM-199 was Rota and Cabianca (2005), without significant improvement in MII rates with markedly low results (<3%). However, Saikhun et al. (2008), who compared different media using ITS in all of them, reported high MII rates in accordance with our results. Other authors showed in bovine and feline that ITS has a beneficial effect on embryo developmental competence (Moro et al., 2014; Guimarães et al., 2016) but not better maturation rates. Otherwise, in the dog, we determined that ITS under a high O_2 culture system duplicated MII rates.

Oxygen concentrations in the oviduct are one-third of the atmosphere and, for that reason, IVM in experiment 3 was performed in two different oxygen tensions (Rodrigues and Rodrigues, 2010). Canine and pig oocytes have the highest amount of lipid droplets and also longer maturation periods, making them more prone to oxidative stress due to lipid peroxidation with potential damage to the cell membrane (Bradley and Swann, 2019; Dalbies-Tran et al., 2020). Therefore, it would be reasonable to assume that by reducing or alleviating the effect of oxidative stress by antioxidant supplementation in an oxygen-depleted atmosphere improves canine IVM. We showed that lower O_2 tensions are beneficial for canine IVM, since higher maturation rates and lower degeneration rates were obtained when COCs were cultured in low O_2 tension in either the presence or absence of ITS. Salavati et al. (2012) also compared high and low O_2 tensions but with remarkably low results and without differences between treatments. These outcomes are in agreement with previous reports in other species that have shown beneficial effects of lowering O_2 tension to physiological levels during IVM (Salavati et al., 2012).

The optimal medium SOF + BSA + FBS and low O_2 tension in the presence or absence of ITS were further investigated for ROS levels, viability assay, and PA after 48 h of IVM. Although no differences in maturation rates were demonstrated, the presence of ITS and low O_2 tension decreased ROS levels considerably (**Figure 3**) and increased oocytes with membrane integrity after maturation. Transferrin constitutes a major protein component in follicular and ampullary fluids and also acts as a chelator of highly toxic hydroxyl radicals to limit oxidative stress (Das et al., 2014). Selenium protects the cells from oxidative damage by reducing free radical production and inhibiting lipid

TABLE 5 | Viability and IVM of canine oocytes in SOF + BSA + FBS medium for 48 h under low O_2 tension atmospheres in the presence or absence of ITS.

Group	No. oocytes	Viability	GV + MI	MII	NN
SOF + BSA + FBS + low O_2	67	16 (23.8%)^a	59 (88.1%)^a	8 (11.9%)^a	9 (13.4%)^a
SOF + BSA + FBS + 1 μl/ml ITS + low O_2	71	40 (56.3%)^b	53 (74.6%)^a	18 (25.3%)^b	10 (14.1%)^a

Viability and IVM of oocyte after co-staining with propidium iodide (PI) and Hoechst 33342 to determine maturation and cell membrane integrity. The percentages of oocytes in the germinal vesicle or metaphase I (GV + MI), metaphase II (MII), and non-identifiable (NN) stages were recorded simultaneously with cell membrane integrity evaluation after 48 h of IVM. In the same column, percentages with different superscripts differed significantly ($^{a,b}p < 0.05$). The experiments were repeated three times (n = 3).

BSA, bovine serum albumin; FBS, fetal bovine serum; IVM, in vitro maturation; ITS, insulin-transferrin-selenium; SOF, synthetic oviductal fluid.

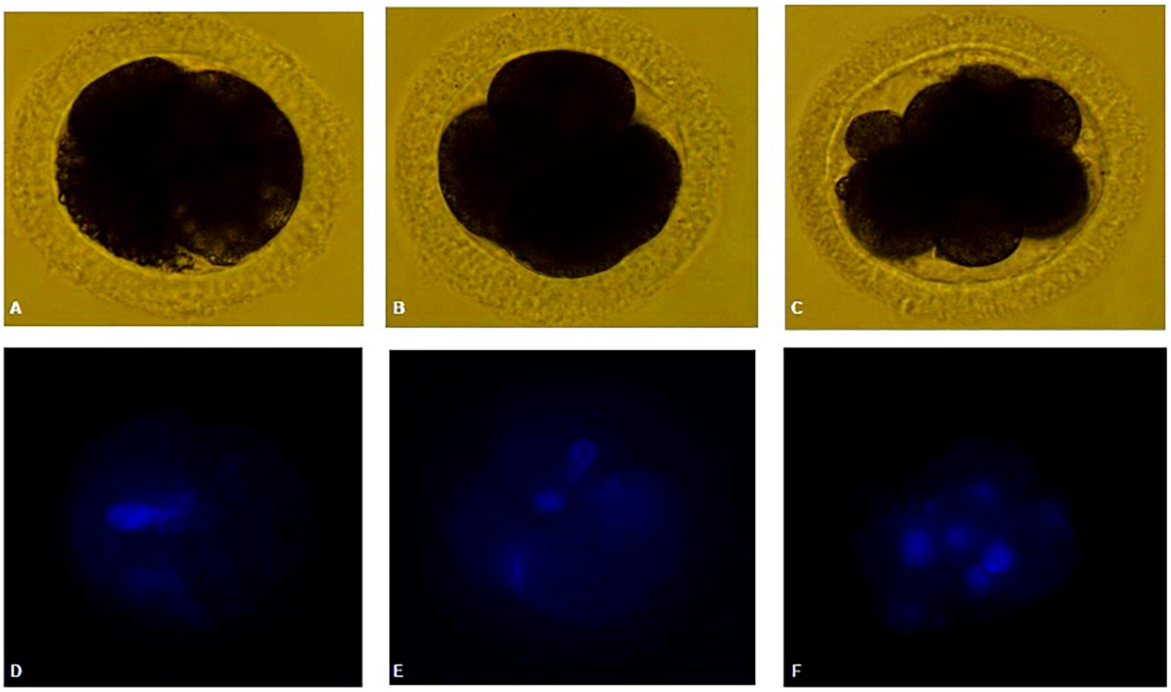

FIGURE 4 | (A,D) Canine oocyte at 2-cell stage. **(B,E)** Canine oocyte at four-cell stage. **(C,F)** Canine oocyte at eight-cell stage. Parthenogenetic embryos visualized by bright field and Hoechst staining.

peroxidation (Córdova et al., 2010). In addition, insulin is a key metabolic hormone influencing energy metabolism at different levels. It has been documented that insulin binds to its receptors in oocytes, granulosa cells, and both theca cells of healthy follicles, supporting the hypothesis that this hormone plays a role in oocyte maturation, follicular growth, and stroma cell function (Alvarez et al., 2019).

Finally, embryo development after PA was compared in the presence or absence of ITS supplementation under low O_2 tensions, and cleavage rates were low for both groups, and there were no statistical differences between them. Only one oocyte belonging to the 1-μl/ml ITS group was found at the eight-cell stage, while oocytes at the 2- to 4-cell stage could be obtained for both groups (**Figure 4**). To our knowledge, this is the first report of ionomycin and 6-DMAP PA of *in vitro*-matured oocytes and developed up to eight-cell stage. Comparison of different activation protocols using *in vivo*-matured oocytes has been reported, reaching 25% of eight-cell stage embryos with no blastocyst obtained using ionomycin and 6-DMAP for PA (Jang et al., 2008).

CONCLUSION

In summary, we could conclude that SOF with 8% BSA and 2.5% FBS is suitable for IVM, and ITS supplementation in high O_2 tension improves up to 20% MII of canine oocytes from bitches of unknown age, breed, and stage of the estrous cycle. Low O_2 tension increased maturation rates to 36.5%, although there were no statistical differences compared to high O_2 tension in the presence of ITS. Additionally, higher integrity of the cytoplasmic membrane and lower ROS levels were found when COCs were cultured in the presence of ITS. These findings will help to improve *in vitro* embryo production and the efficiency of assisted reproduction in canine species.

DATA AVAILABILITY STATEMENT

The original contributions presented in the study are included in the article/supplementary material, further inquiries can be directed to the corresponding author.

AUTHOR CONTRIBUTIONS

MD and CC: conceptualization, methodology, formal analysis, and writing—original draft. GT, AD, and DL: methodology and formal analysis. DS: supervision, project administration, writing, review and editing, and funding acquisition. All authors contributed to the article and approved the submitted version.

ACKNOWLEDGMENTS

We would like to thank the Tigre Zoonosis center for providing the ovaries needed to perform the experiments reported herein, especially the veterinarians Jennifer Kosiner and Rocio Longo for neutering the bitches and for ovary collection.

REFERENCES

Alvarez, G. M., Barrios Expósito, M. J., Elia, E., Paz, D., Morado, S., and Cetica, P. D. (2019). Effects of Gonadotrophins and Insulin on Glucose Uptake in the Porcine Cumulus-Oocyte Complex during IVM. *Reprod. Fertil. Dev.* doi: 10.1071/RD18321 [Epub ahead of print].

Bavister, B. D. (1995). Culture of Preimplantation Embryos: facts and Artifacts. *Hum. Reprod. Update* 1, 91–148. doi: 10.1093/humupd/1.2.91

Bavister, B. D., and Yanagimachi. (1977). The Effects of Sperm Extracts and Energy Sources on the Motility and Acrosome Reaction of Hamster Spermatozoa in Vitro. *Biol. Reprod.* 16, 228–237. doi: 10.1095/biolreprod16.2.228

Bolamba, D., Russ, K. D., Olson, M. A., Sandler, J. L., and Durrant, B. S. (2002). In Vitro Maturation of Bitch Oocytes from Advanced Preantral Follicles in Synthetic Oviduct Fluid Medium: serum Is Not Essential. *Theriogenology* 58, 1689–1703. doi: 10.1016/S0093-691X(02)01080-4

Bradley, J., and Swann, K. (2019). Mitochondria and Lipid Metabolism in Mammalian Oocytes and Early Embryos. *Int. J. Dev. Biol.* 63, 93–103. doi: 10.1387/ijdb.180355ks

Buemo, C. P., Gambini, A., Moro, L. N., Hiriart, M. I., Fernández-Martín, R., Collas, P., et al. (2016). Embryo Aggregation in Pig Improves Cloning Efficiency and Embryo Quality. *PLoS One* 11:e0146390. doi: 10.1371/journal.pone.0146390

Córdova, B., Morató, R., Izquierdo, D., Paramio, T., and Mogas, T. (2010). Effect of the Addition of Insulin-Transferrin-Selenium and/or L-Ascorbic Acid to the in Vitro Maturation of Prepubertal Bovine Oocytes on Cytoplasmic Maturation and Embryo Development. *Theriogenology* 74, 1341–1348. doi: 10.1016/j.theriogenology.2010.06.003

Dalbies-Tran, R., Cadoret, V., Desmarchais, A., Elis, S., Maillard, V., Monget, P., et al. (2020). A Comparative Analysis of Oocyte Development in Mammals. *Cells* 9, 1–27. doi: 10.3390/cells9041002

Das, Z. C., Gupta, M. K., Uhm, S. J., and Lee, H. T. (2014). Supplementation of Insulin-Transferrin-Selenium to Embryo Culture Medium Improves the in Vitro Development of Pig Embryos. *Zygote* 22, 411–418. doi: 10.1017/S0967199412000731

Eppig, J. J., and Schroeder, A. C. (1986). Culture Systems for Mammalian Oocyte Development: progress and Prospects. *Theriogenology* 25, 97–106. doi: 10.1016/0093-691X(86)90186-X

Evecen, M., Cirit, Ü, Demir, K., Karaman, E., Bakirer, G., Hamzaoðlu, A. I., et al. (2009). Comparison of Two Different Media for In Vitro Production of Dog Embryos. *Kafkas Univ. Vet. Fak. Derg.* 16, 897–902.

Farstad, W. (2000). Assisted Reproductive Technology in Canid Species. *Theriogenology* 53, 175–186. doi: 10.1016/S0093-691X(99)00250-2

Guimarães, A. L. S., Pereira, S. A., DIógenes, M. N., and Dode, M. A. N. (2016). Effect of Insulin-Transferrin-Selenium (ITS) and l-Ascorbic Acid (AA) during in Vitro Maturation on in Vitro Bovine Embryo Development. *Zygote* 24, 890–899. doi: 10.1017/S0967199416000228

Hewitt, D. A., and England, G. C. W. (1999). Synthetic Oviductal Fluid and Oviductal Cell Coculture for Canine Oocyte Maturation in Vitro. *Anim. Reprod. Sci.* 55, 63–75. doi: 10.1016/S0378-4320(98)00162-6

Jang, G., Kim, M. K., and Lee, B. C. (2010). Current Status and Applications of Somatic Cell Nuclear Transfer in Dogs. *Theriogenology* 74, 1311–1320. doi: 10.1016/j.theriogenology.2010.05.036

Jang, G., Oh, H. J., Kim, M. K., Fibrianto, Y. H., Hossein, M. S., Kim, H. J., et al. (2008). Improvement of Canine Somatic Cell Nuclear Transfer Procedure. *Theriogenology* 69, 146–154. doi: 10.1016/j.theriogenology.2007.08.022

Jeong, Y. W., Hossein, M. S., Bhandari, D. P., Kim, Y. W., Kim, J. H., Park, S. W., et al. (2008). Effects of Insulin-Transferrin-Selenium in Defined and Porcine Follicular Fluid Supplemented IVM Media on Porcine IVF and SCNT Embryo Production. *Anim. Reprod. Sci.* 106, 13–24. doi: 10.1016/j.anireprosci.2007.03.021

Lange-Consiglio, A., Perrini, C., Albini, G., Modina, S., Lodde, V., Orsini, E., et al. (2017). Oviductal Microvesicles and Their Effect on in Vitro Maturation of Canine Oocytes. *Reproduction* 154, 167–180. doi: 10.1530/REP-17-0117

Lapointe, J., and Bilodeau, J. F. (2003). Antioxidant Defenses Are Modulated in the Cow Oviduct During the Estrous Cycle1. *Biol. Reprod.* 68, 1157–1164. doi: 10.1095/biolreprod.102.007476

Lorenzo, M. S., Maruri, A., Cruzans, P. R., Teplitz, G. M., Tello, M. F., and Lombardo, D. M. (2019). The antioxidant dimethylthiourea improves IVF efficiency and decreases cumulus cell apoptosis in pigs. *Reprod. Fertil. Dev.* 31, 1607–1615. doi: 10.1071/RD19020

Luvoni, G. C. (2000). Current Progress on Assisted Reproduction in Dogs and Cats: in Vitro Embryo Production. *Reprod. Nutr. Dev.* 40, 505–512. doi: 10.1051/rnd:2000114

Luvoni, G. C. (2006). Gamete Cryopreservation in the Domestic Cat. *Theriogenology* 66, 101–111. doi: 10.1016/j.theriogenology.2006.03.012

Luvoni, G. C., Chigioni, S., Allievi, E., and Macis, D. (2005). Factors Involved in Vivo and in Vitro Maturation of Canine Oocytes. *Theriogenology* 63, 41–59. doi: 10.1016/j.theriogenology.2004.03.004

Moawad, A. R., Salama, A., Badr, M. R., and Fathi, M. (2021). Beneficial Effects of L-Carnitine Supplementation during IVM of Canine Oocytes on Their Nuclear Maturation and Development In Vitro. *Animals* 11:581. doi: 10.3390/ani11020581

Moro, L. N., Sestelo, A. J., and Salamone, D. F. (2014). Evaluation of Cheetah and Leopard Spermatozoa Developmental Capability after Interspecific ICSI with Domestic Cat Oocytes. *Reprod. Domest. Anim.* 49, 693–700. doi: 10.1111/rda.12355

Nagashima, J. B., Travis, A. J., and Songsasen, N. (2019). The domestic dog embryo: *in vitro* fertilization, culture, and transfer. *Methods Mol. Biol.* 2006, 247–267. doi: 10.1007/978-1-4939-9566-0_18

No, J., Zhao, M., Lee, S., Ock, S. A., Nam, Y., and Hur, T. Y. (2018). Enhanced in Vitro Maturation of Canine Oocytes by Oviduct Epithelial Cell Co-Culture. *Theriogenology* 105, 66–74. doi: 10.1016/j.theriogenology.2017.09.002

Oh, H. J., Ra, K., Kim, M. J., Kim, G. A., Setyawan, E. M. N., Lee, S. H., et al. (2018). The Promise of Dog Cloning. *Reprod. Fertil. Dev.* 30, 1–7. doi: 10.1071/RD17375

Reynaud, K., Fontbonne, A., Saint-Dizier, M., Thoumire, S., Marnier, C., Tahir, M. Z., et al. (2012). Folliculogenesis, Ovulation and Endocrine Control of Oocytes and Embryos in the Dog. *Reprod. Domest. Anim.* 47, 66–69. doi: 10.1111/rda.12055

Rodrigues, B. A., and Rodrigues, J. L. (2006). Responses of canine oocytes to *in vitro* maturation and *in vitro* fertilization outcome. *Theriogenology* 66, 1667–1672. doi: 10.1016/j.theriogenology.2006.02.017

Rodrigues, B. A., and Rodrigues, J. L. (2010). In Vitro Maturation of Canine Oocytes: a Unique Conundrum. *Anim. Reprod.* 7, 3–15.

Rota, A., and Cabianca, G. (2005). In Vitro Maturation Rates of Canine Oocytes from Anoestrous Bitches in Simple Media. *Reprod. Nutr. Dev.* 44, 89–98. doi: 10.1051/rnd

Saikhun, J., Sriussadaporn, S., Thongtip, N., Pinyopummin, A., and Kitiyanant, Y. (2008). Nuclear Maturation and Development of IVM/IVF Canine Embryos in Synthetic Oviductal Fluid or in Co-Culture with Buffalo Rat Liver Cells. *Theriogenology* 69, 1104–1110. doi: 10.1016/j.theriogenology.2008.01.024

Saint-Dizier, M., Schoen, J., Chen, S., Banliat, C., and Mermillod, P. (2020). Composing the Early Embryonic Microenvironment: physiology and Regulation of Oviductal Secretions. *Int. J. Mol. Sci.* 21, 1–21. doi: 10.3390/ijms21010223

Salavati, M., Ghafari, F., Zhang, T., and Fouladi-Nashta, A. A. (2012). Effects of Oxygen Concentration on in Vitro Maturation of Canine Oocytes in a Chemically Defined Serum-Free Medium. *Reproduction* 144, 547–556. doi: 10.1530/REP-12-0176

Tervit, H. R., Whittingham, D. G., and Rowson, L. E. (1972). Successful Culture in Vitro of Sheep and Cattle Ova. *J. Reprod. Fertil.* 30, 493–497. doi: 10.1530/jrf.0.0300493

Tesoriero, J. V. (1981). Early Ultrastructural Changes of Developing Oocytes in the Dog. *J. Morphol.* 168, 171–179. doi: 10.1002/jmor.1051680206

Van Soom, A., Rijsselaere, T., and Filliers, M. (2014). Cats and Dogs: two Neglected Species in This Era of Embryo Production in Vitro? *Reprod. Domest. Anim.* 49, 87–91. doi: 10.1111/rda.12303

Conflict of Interest: The authors declare that the research was conducted in the absence of any commercial or financial relationships that could be construed as a potential conflict of interest.

Publisher's Note: All claims expressed in this article are solely those of the authors and do not necessarily represent those of their affiliated organizations, or those of the publisher, the editors and the reviewers. Any product that may be evaluated in this article, or claim that may be made by its manufacturer, is not guaranteed or endorsed by the publisher.

Advantages of publishing in Frontiers

OPEN ACCESS
Articles are free to read for greatest visibility and readership

FAST PUBLICATION
Around 90 days from submission to decision

HIGH QUALITY PEER-REVIEW
Rigorous, collaborative, and constructive peer-review

TRANSPARENT PEER-REVIEW
Editors and reviewers acknowledged by name on published articles

Frontiers
Avenue du Tribunal-Fédéral 34
1005 Lausanne | Switzerland

Visit us: www.frontiersin.org
Contact us: frontiersin.org/about/contact

REPRODUCIBILITY OF RESEARCH
Support open data and methods to enhance research reproducibility

DIGITAL PUBLISHING
Articles designed for optimal readership across devices

FOLLOW US
@frontiersin

IMPACT METRICS
Advanced article metrics track visibility across digital media

EXTENSIVE PROMOTION
Marketing and promotion of impactful research

LOOP RESEARCH NETWORK
Our network increases your article's readership